

ACS SYMPOSIUM SERIES 981

Chemical Evolution across Space & Time

**From the Big Bang to
Prebiotic Chemistry**



EDITED BY
Lori Zaikowski and Jon M. Friedrich

Chemical Evolution across Space & Time

About the Cover

The cover art, entitled “Shining” was created by Elizabeth Zaikowski of San Diego, California. It is illustrative of the mandala theme seen in much of her artwork. Mandala is the Sanskrit word for circle, and mandalas are a symbolic representation of the macro and the micro; what lies within and without. The basic pattern of a circle in the center is common in nature and is seen in both physics and astronomy. “Shining” evokes a sense of order arising out of chaos, and embodies the theme of the book in which complex organization develops following the disarray of the Big Bang.

Mandala art has been used throughout the world as a process of self-expression, in the service of personal growth and spiritual transformation. Elizabeth creates each mandala using a combination of airbrush and acrylic paints, and by allowing it to develop in an organic manner, starting from the center and working outward. Through her art, she strives to create more balance in our sometimes chaotic world. Expressing the need for balance in life, her paintings are a reflection of the symmetrical nature of the universe. You can view more of her work at <http://www.elizabethzaikowski.com>.

ACS SYMPOSIUM SERIES **981**

Chemical Evolution across Space & Time

From the Big Bang to Prebiotic Chemistry

Lori Zaikowski, Editor
Dowling College

Jon M. Friedrich, Editor
Fordham University

**Sponsored by the
ACS Divisions of Chemical Education, Inc., Geochemistry,
Inc., and Nuclear Chemistry and Technology**



American Chemical Society, Washington, DC



Library of Congress Cataloging-in-Publication Data

Chemical evolution across space & time: from the Big Bang to prebiotic chemistry /
Lori Zaikowski, Jon M. Friedrich, editors.

p. cm.—(ACS symposium series ; 981)

Three day symposium “Chemical evolution I: Chemical change across space & time,”
held at the Spring 2007 American Chemical Society National Meeting in Chicago, IL.

ISBN 978-0-8412-7431-0 (alk. paper)

I. Cosmochemistry—Congresses. 2. Geochemistry—Congresses. III. Molecular
evolution—Congresses. 4. Life—Origin—Congresses. 5. Cells—Evolution—
Congresses

I. Zaikowski, Lori, 1964– II. Friedrich, Jon M. III. American Chemical Society.
Meeting (2007 : Chicago, Ill.)

QB450.C46 2007

523'.02—dc22

2007060562

The paper used in this publication meets the minimum requirements of
American National Standard for Information Sciences—Permanence of Paper
for Printed Library Materials, ANSI Z39.48–1984.

Copyright © 2008 American Chemical Society

Distributed by Oxford University Press

All Rights Reserved. Reprographic copying beyond that permitted by Sections
107 or 108 of the U.S. Copyright Act is allowed for internal use only, provided
that a per-chapter fee of \$36.50 plus \$0.75 per page is paid to the Copyright
Clearance Center, Inc., 222 Rosewood Drive, Danvers, MA 01923, USA.
Republication or reproduction for sale of pages in this book is permitted only
under license from ACS. Direct these and other permission requests to ACS
Copyright Office, Publications Division, 1155 16th Street, N.W., Washington,
DC 20036.

The citation of trade names and/or names of manufacturers in this publication is
not to be construed as an endorsement or as approval by ACS of the commercial
products or services referenced herein; nor should the mere reference herein to
any drawing, specification, chemical process, or other data be regarded as a
license or as a conveyance of any right or permission to the holder, reader, or
any other person or corporation, to manufacture, reproduce, use, or sell any
patented invention or copyrighted work that may in any way be related thereto.
Registered names, trademarks, etc., used in this publication, even without
specific indication thereof, are not to be considered unprotected by law.

PRINTED IN THE UNITED STATES OF AMERICA

Chemical Evolution
Chemical Change Across Space and Time

Edited by

Lori Zaikowski and Jon M. Friedrich

Proceedings of the American Chemical Society Symposium
Spring 2007 ACS National Meeting
Chicago, IL

DOWLING
COLLEGE



FORDHAM UNIVERSITY
THE JESUIT UNIVERSITY OF NEW YORK

The
Meteoritical
Society



Organizers and Sponsors

Symposium Organizers

Lori Zaikowski, Dowling College
Jon M. Friedrich, Fordham University

ACS Sponsoring Division

Chemical Education

ACS Co-sponsoring Divisions

Geochemistry

Nuclear Chemistry and Technology

ACS Division of Chemical Education Program Chair

Cathy Middlecamp, University of Wisconsin, Madison

ACS 233rd Meeting Co-Chairs, Division of Chemical Education

George M. Bodner, Purdue University

Wayne E. Jones, Jr., Binghamton University, SUNY

Special thanks to Cathy Middlecamp and Anna M. Wilson for support
and cooperation throughout the project.

Financial Support

Dowling College
Fordham University
The Meteoritical Society
The National Science Foundation

Table of Contents

Foreword	xi
Preface	xiii-xv
Preamble	xvii-xviii
<i>Introduction</i>	1
1 The Emergence of Chemical Complexity: An Introduction <i>Robert M. Hazen</i>	2-13
<i>Part I: Chemical Evolution in Astrophysics</i>	15
2 Chemical Origins: Nuclear Chemistry in the Early Universe <i>Keith A. Olive</i>	16-38
3 Origin of the Elements: Nucleosynthesis in Stars <i>Bradley S. Meyer</i>	39-60
4 Circumstellar Chemistry and Dust from Dead Stars in Meteorites <i>Katharina Lodders</i>	61-79
5 Chemical Evolution in the Interstellar Medium: Feedstock of Solar Systems <i>Louis J. Allamandola</i>	80-110
6 Identifying Molecules in Space: Exploring Astrochemistry through High-Resolution Spectroscopy <i>L. M. Ziurys</i>	111-128
<i>Part II: Geochemical Evolution: Solar System and Earth</i>	129
7 Chemical Diversity and Abundances across the Solar System <i>John S. Lewis</i>	130-140
8 Photochemistry in the Early Solar System <i>Robert N. Clayton</i>	141-152
9 Lessons from Meteorites <i>Michael E. Lipschutz</i>	153-186
10 Chemistry and Composition of Planetary Atmospheres <i>Laura Schaefer and Bruce Fegley, Jr.</i>	187-207
11 Hafnium—Tungsten Chronometry of Planetary Accretion and Differentiation <i>Thorsten Kleine</i>	208-230
<i>Part III: Prebiotic Chemistry</i>	231
12 Cosmic Carbon Chemistry P. Ehrenfreund and M. Spaans	232-245
13 Extraterrestrial Organic Chemistry as Recorded in Carbonaceous Chondrites <i>Oliver Botta</i>	246-260

14	Earth's Early Atmosphere, Biosphere, Lithosphere, and Hydrosphere <i>Douglas Rumble, III</i>	261-281
15	Prebiotic Organic Synthesis in Neutral Planetary Atmospheres <i>H. J. Cleaves, J. H. Chalmers, A. Lazcano, S. L. Miller, and J. L. Bada</i>	282-292
16	The RNA World Scenario for the Origins of Life <i>James P. Ferris and John W. Delano</i>	293-308
	<i>Summary: Systems Chemistry Sketches</i>	309
17	Systems Chemistry Sketches <i>Stuart A. Kauffman</i>	310-324
	<i>Part IV: Teaching Chemical Evolution</i>	325
18	Science and the Concept of Evolution: From the Big Bang to the Origin and Evolution of Life <i>Lori Zaikowski, Richard T. Wilkens, and Kurt Fisher</i>	326-342
19	Online Tools for Understanding Galactic Chemical Evolution <i>Allen Parker and Bradley S. Meyer</i>	343-348
20	Spectroscopy and the Cosmos: Applications in the Chemical Sciences <i>Lori Zaikowski, S. Russell Seidel, and Jon M. Friedrich</i>	349-362
21	Development of Laboratories for Teaching Chemical Principles Using Radio Astronomy <i>DeWayne T. Halfen, Aldo J. Apponi, and Lucy M. Ziurys</i>	363-377
22	Chemistry of Life: Chemical Evolution as a Theme for Teaching Undergraduate Chemistry <i>Bhawani Venkataraman</i>	378-388
	Afterword <i>Richard N. Zare</i>	389-390
	Glossary	391-397
	Indexes	399
	Author Index	401
	Subject Index	403-430
	Color Figure Inserts	C1-C18

Foreword

The ACS Symposium Series was first published in 1974 to provide a mechanism for publishing symposia quickly in book form. The purpose of the series is to publish timely, comprehensive books developed from ACS sponsored symposia based on current scientific research. Occasionally, books are developed from symposia sponsored by other organizations when the topic is of keen interest to the chemistry audience.

Before agreeing to publish a book, the proposed table of contents is reviewed for appropriate and comprehensive coverage and for interest to the audience. Some papers may be excluded to better focus the book; others may be added to provide comprehensiveness. When appropriate, overview or introductory chapters are added. Drafts of chapters are peer-reviewed prior to final acceptance or rejection, and manuscripts are prepared in camera-ready format.

As a rule, only original research papers and original review papers are included in the volumes. Verbatim reproductions of previously published papers are not accepted.

ACS Books Department

Preface

The concept of evolutionary change is a fundamental thread linking the sciences, and although the discipline of biology is the focus of attacks on teaching evolution, such attacks threaten the teaching of sound science in all disciplines. An evolutionary perspective can provide one framework for unifying and advancing the sciences, and chemistry has contributed much to our understanding of evolution. Chemists today use principles of evolution and take lessons from chemistry in nature to advance modern chemistry in areas such as agriculture, energy, new materials, and pharmaceuticals. This book presents chemical evolution from a chronological perspective, beginning with the simplest elements produced in the Big Bang and concluding with prebiotic molecules. The three day symposium *Chemical Evolution I: Chemical Change Across Space and Time*, held at the Spring 2007 American Chemical Society (ACS) National Meeting in Chicago, Illinois, explored the evolutionary nature of chemistry, the scientific evidence that supports it, and ideas for using these concepts in chemistry courses from the high school to graduate levels. The peer-reviewed proceedings of the sessions are presented here.

Our goal in the first three parts of the book is to provide current reviews of the chemical and physical processes in operation from the origin of the simplest elements to the development of precursors of life, as described by scientists who are leaders in their fields. The fourth part of the book provides peer-reviewed resources and ideas for teachers to integrate these topics into their courses, and hopefully to inspire the creation of new courses using the material presented in the first three parts.

As the reader browses through the volume, we invite you to keep in mind our objectives: (1) to follow the evolution of chemistry from the simplest elements to the molecular diversity and complexity present today; (2) to demonstrate how multidisciplinary applications of chemical principles and techniques are central to our understanding of the universe and its history; (3) to provide instructors with up-to-date information for teaching how chemistry has evolved over time and

shaped our world; (4) to foster the expansion and integration of new topics and approaches to chemistry into courses for majors and non-majors; and (5) to provide current reviews on chemical evolution for graduate students and the general scientific populace.

The sequel to this symposium is scheduled for the 235th National Meeting of the ACS in April 2008, and is entitled *Chemical Evolution II: From Origins of Life to Modern Society*. It will trace chemical evolution from the formation of complex prebiotic molecules in nature to the development of novel chemicals by humans. Additional teaching materials will be developed through a Chemical Evolution Workshop at the Spring 2008 ACS Mid-Atlantic Regional Meeting (MARM) at Queensborough Community College in New York from May 18–21, 2008.

Finally, we wish to acknowledge those who helped make the symposium and book possible. The symposium was sponsored by the ACS Division of Chemical Education, Inc., and we are grateful for the support and cooperation of Program Chair Cathy Middlecamp of University of Wisconsin at Madison, Treasurer Anna M. Wilson of Purdue University, and Meeting Cochairs George M. Bodner of Purdue University and Wayne E. Jones of Binghamton University. The Divisions of Geochemistry and Nuclear Chemistry and Technology co-sponsored the symposium, and we extend our thanks to their Chairs Martin Schoonen of Stony Brook University and Heino Nitsche of University of California at Berkeley. Financial support was provided by Dowling College, Fordham University, The Meteoritical Society, NSF Award No. 03–35799, and the ACS Division of Chemical Education, Inc. We are grateful for the efforts of Mr. and Mrs. Lewis of Lonesome Pine Productions as they were able to mobilize on short notice for travel and filming. We thank the acquisition editors and reviewers of our initial ACS Books proposal for their enthusiastic response to the prospectus and for providing insight that enhanced the scope and content of the book. We also appreciate the valuable comments on the draft chapters that were provided by dozens of reviewers.

Above all, our vision and goals could not have been achieved without the generous time and energy given by each of the speakers, and we would like to extend our heartfelt appreciation to each for taking time out of their busy schedules to consider our invitation, to participate in the symposium, and to author review chapters for the book. It is because of their diligent efforts and attention to timelines that the vision for this

project became a reality. We are fortunate to have worked with such a distinguished, dedicated, and cooperative group. Thank you.

We hope that this publication will benefit chemists, instructors, and students of chemistry, and all others with an interest in the evolution of the universe in which we live.

Lori Zaikowski

Department of Chemistry
Dowling College
Oakdale, NY 11769
ZaikowsL@dowling.edu

Jon M. Friedrich

Department of Chemistry
Fordham University
Bronx, NY 10458

Preamble

Niles Eldredge

**The American Museum of Natural History
New York, NY**

Everything in the cosmos has a history. The old dichotomy between the “historical” sciences (like geology, paleontology and evolutionary biology) and the (for want of a better term) “functional” sciences (like physics and chemistry—some would call them the “real sciences”) was always supposed to be that fields like physics study dynamic processes and discover immutable laws of interaction among particles composing the cosmos—while the historical sciences study, well, history—the supposed outcome of such interactions over time.

But the dichotomy was never so simple as that: within evolutionary biology itself, there has always been something of a split between those determined to understand the causes of evolutionary change, and those who prefer to reconstruct life’s history. Much the same distinction has always pervaded geology—a modern manifestation being plate tectonics—with, again, those who seek to understand the dynamics of plate interactions by and large forming a group distinct from those interested in the actual configuration of plates through geologic time.

That all this is nothing new is nicely embodied in one of my favorites quotes—from the Preface of paleontologist George Gaylord Simpson’s most original book, *Tempo and Mode in Evolution* (1944), written in two distinct phases and published during World War II. Simpson was asking rhetorically what a paleontologist could be expected to add to our understanding of the processes of biological evolution—and characterized the situation he faced in this wry little passage:

"Not long ago paleontologists felt that a geneticist was a person who shut himself in a room, pulled down the shades, watched small flies disporting themselves in bottles, and thought that he was studying nature. A pursuit so removed from the realities of life, they said, had no significance for the true

biologist. On the other hand, the geneticists said that paleontology had no further contributions to make to biology, that its only point had been the completed demonstration of the truth of evolution, and that it was a subject too purely descriptive to merit the name 'science.' The paleontologist, they believed, is like a man who undertakes to study the principles of the internal combustion engine by standing on a street corner and watching the motor cars whiz by." (Simpson, 1944, p. xv).

Simpson's larger point—one that still needs emphasis—is that any theory of process must be accountable to the known patterns of history supposedly generated by that process. Simpson thought there were elements to the history of life revealed in paleontological data that would not be evident to those who restricted their gaze to the short-term dynamics observed in fly bottles and rat cages in genetics labs. Logically, the two—study of process, study of history—are inter-related. You might be able to study history without thinking about process (though in my opinion this is a largely dull and incomplete enterprise); but your best grasp of process comes from checking your predictions based on your causal theory against your best estimate of what history has looked like.

And everything has a history. Even evanescent subatomic particles leaving their characteristic trails in cloud chambers have histories. Indeed, that is the very point: however brief and inconsequential their "lives" may be as independent objects, if you observe enough of them, you can characterize yet another class of cosmic objects.

The early days of science were fundamentally concerned with the description of the elements composing the universe—and the law-like regular interactions between them. There was a sense of stability and timelessness to this that seemed to speak of God's implacable eternity. To paraphrase my colleague Neil deGrasse Tyson, it took Darwin and his message of change through time mediated by natural law to help a true, historical *evolutionary* cosmology to be imagined and to emerge. For what is "evolution" in its most general sense but the history of a system, one that embodies change through time, brought about natural law that we can analyze and come to understand through the evidence of our senses: in other words, through science. Evolution pervades all science, as the contributions to this book make beautifully clear.

Introduction

Chapter 1

The Emergence of Chemical Complexity: An Introduction

Robert M. Hazen

**Geophysical Laboratory, Carnegie Institute of Washington,
Washington, DC 20015**

The ancient origins of stars, planets and life may be viewed as a sequence of emergent events, each of which added to the chemical complexity of the cosmos. Stars, which formed from the primordial hydrogen of the Big Bang, underwent nucleosynthesis to produce all the elements of the Periodic Table. Those elements were dispersed during supernova events and provided the raw materials for planets and all their mineralogical diversity. Chemical evolution on Earth (and perhaps countless other planets and moons) led to life through a sequence of steps: the formation of biomolecules, the assembly of those molecules into organized molecular systems, and ultimately the appearance of self-replicating collections of molecules. Today, chemical complexification occurs at an ever accelerating rate through the efforts of chemists and chemical engineers.

Introduction

The history of the universe has been one of inexorable, inevitable chemical complexification – a sequence of emergent evolutionary episodes from nucleosynthesis, to planet formation, to life. The collected essays of this volume review that epic 14 billion years of history and, in the process, touch on all of the natural sciences: physics, astronomy, geology, biology and, of course, chemistry. In short, this book retells the story of the emergence of everything (1).

Every step in this immense journey is an example of ordering by the process of emergence (Kauffman, this volume; 1,2). Emergent systems occur when energy flows through an assemblage of interacting particles, such as molecules, sand grains, cells or stars. Each individual object, or “agent” in the jargon of emergence, responds only to its environment, yet the behavior of the collective whole is distinct from that of any individual agent. A single sand grain cannot form a rippled surface, nor can a single neuron be conscious.

Emergent behavior appears in countless systems all around us, all the time, including the interactions of atoms, automobiles, or ants. As energy flows through a collection of agents, they tend spontaneously to become more ordered and to display new, often surprising behaviors. At first blush, such patterning might seem to violate the second law of thermodynamics, which dictates a universal tendency for increasing entropy. Yet, as local patterns arise, energy is dissipated more efficiently in accord with the second law of thermodynamics (3). It is easy to focus on this increase in local order, while missing the key fact that the global entropy of the system increases.

In this volume the emergence of chemical complexity has been divided into three evolutionary episodes: stellar evolution and the emergence of elemental diversity, planetary evolution and the emergence of mineralogical diversity, and prebiotic chemical evolution. All of these episodes depend on evolutionary processes that produce change over time under selective pressure (Zaikowski, this volume), and all of them continue to this day.

Stellar Evolution and the Origin of Elements

The periodic table boasts almost 100 naturally occurring chemical elements, but that diversity was not present during the earliest stages of the universe. The Big Bang gave rise to just three elements – predominantly hydrogen, with lesser amounts of helium and lithium. Big Bang nucleosynthesis occurred within the first few minutes of the moment of creation, and for the next million years or so those three elements represented all the chemical complexity of the cosmos (Olive, this volume).

As the universe expanded and cooled, atoms clumped into the first hydrogen-rich stars. The largest of these luminous masses underwent dramatic

sequences of nuclear fusion events, producing a cascade of heavier elements: beryllium, boron, carbon, nitrogen, oxygen, fluorine and more (Meyer, this volume). The fusion reactions of neon burning, oxygen burning and silicon burning produced more new elements, through atomic number 26 (iron). But iron, with the lowest energy per nucleon, is the end point of nuclear burning reactions. The largest stars, having exhausted their supply of nuclear fuel, underwent the rapid collapse and explosive rebound known as a supernova. Not only did this process generate all the other elements of the periodic table (primarily through neutron capture), but it also dispersed those elements into space (Parker & Meyer, this volume). In interstellar space, vast clouds of dust and gas concentrated as new generations of metal-rich stars and planets formed.

Mineralogical Evolution and the Origin of Planets

Life is perhaps the most dramatic example of chemical complexification, but the evolution of the mineral world represents an important precursor to life's origins. Earth today boasts almost 4300 known types of minerals, with as many as 50 new species recognized each year. Yet the mineralogical diversity now found at or near Earth's surface (< 3 km) was not present for much of the planet's history. Indeed, both the variety and relative abundances of near-surface minerals have evolved dramatically over 4.5 billion years of Earth history through a variety of physical, chemical and biological processes.

The early history of the solar system was marked by many processes of differentiation and fractionation. As the nascent Sun irradiated the protoplanetary environment, gradients in temperature and radiation led to significant chemical (Lewis, this volume) and isotopic (Clayton, this volume) fractionation.

Planetesimals of a protoplanetary environment form initially from a surprisingly small number of refractory condensed phases, such as corundum, spinel, graphite and SiC (Lodders, this volume). The most primitive materials to form Earth are represented by a class of meteorites called chondrites, which include a variety of stony meteorites that formed early in the history of the solar nebula. The most striking features of chondritic meteorites are chondrules, which are small spherical objects (typically << 1 cm diameter) that represent molten droplets formed in space by rapid heating and cooling in the nebula prior to accretion. Chondritic meteorites are simply accumulations of chondrules plus mineral grains and dust that have not been significantly altered by melting or differentiation, and thus represent the most primitive raw materials of the Solar System (Lipschutz, this volume).

Unaltered chondrites are characterized by extreme mineralogical parsimony, with no more than about twenty different mineral species (4). As planetesimal accretion progressed and chondrite parent bodies became larger, aqueous and thermal alteration led to new suites of minerals (5,6). Yet the total mineralogical

repertoire of chondritic meteorites is limited to approximately 100 different mineral species.

Mineralogical diversity increased with the advent of asteroid melting and differentiation – processes that resulted in the large-scale separation of stony and metallic components. Differentiated meteorites include several classes of stony achondrites, as well as stony-iron and iron meteorites. Nevertheless, no more than ~150 mineral species are known to occur in all types of meteorites. These minerals, dominated by magnesium silicates, provided raw materials for the accreting Earth.

The accretion and rapid differentiation of Earth at approximately 4.55 Ga (Kleine, this volume), as well as the Moon-forming impact at about 4.5 Ga, led to new near-surface mineralogical diversity. Much of that diversification resulted from volcanic outgassing and fluid-rock interactions associated with formation of the atmosphere and oceans (Fegley, this volume). Indeed, dynamic interactions among the early atmosphere, lithosphere and hydrosphere were the principal mechanisms for Hadean mineral diversification (Rumble, this volume). An immediate mineralogical consequence of these interactions would have been copious formation of hydrous silicates and oxides, including serpentinization and the first significant production of clay minerals and perhaps zeolites.

From their inception at least 4.3 Ga ago (7), oceans would have increased steadily in salinity [predominantly Na, Ca, Mg and Cl, though ratios may have varied significantly over time (8,9)]. Ocean concentrations of sulfate and nitrate would also have increased owing to photolytic and lightning-induced reactions in the atmosphere and subsequent ocean-atmosphere exchange. These compositional changes would also have led to the first significant evaporate deposits on Earth, and associated sulfate, nitrate, and halide minerals, although no traces of evaporate minerals have been found prior to about 3.4 Ga (10).

The earliest shallow crustal igneous rocks on Earth would have been basalts. However, fractional melting in the presence of aqueous fluids and crystal separation led to the familiar variety of igneous rocks, including andesite, diorite, gabbro and granite. Recent discoveries of sedimentary zircon grains dated to 4.4 Ga have been interpreted to indicate that granite production (and by extension the first assembly of continental crust) was active within 150 million years of accretion (11). An important mineralogical consequence of granite formation was the enrichment of more than a dozen rare “pegmatophile” elements in residual fluids and the production of hundreds of distinctive pegmatite minerals.

While the timing of the beginnings of plate tectonics, in particular the commencement of large-scale subduction processes and associated crustal reworking and arc volcanism, remains a matter of intense debate (12,13), most researchers conclude that at least some form of subduction was active prior to 3 Ga (14). Significant mineralogical consequences of subduction include base metal deposition and associated precious metal concentrations that result from magmatic and volcanogenic processes (15,16). Yet another mineralogical

consequence of plate tectonics was the uplift and subsequent exposure of regional metamorphic terrains – events which, for the first time, brought high-pressure mineral phases to near-surface environments.

Throughout Earth history, mineralogical evolution has been driven by cyclical selective processes: heating and cooling, melting and crystallization, burial and uplift, weathering and sedimentation, dissolution and precipitation. Each cycle modified preexisting mineral species and generated new physico-chemical niches. All new minerals thus arose from natural selective processing of older minerals.

The last billion years have witnessed a particularly dramatic increase in mineralogical diversity, primarily as a consequence of atmospheric oxygenation. To understand this Neoproterozoic and Phanerozoic acceleration in mineral evolution we must thus address another emergent chemical event – the origin of life.

Chemical Evolution and the Origin of Life

The origin of life may be modeled as a sequence of so-called “emergent” events, each of which added new structure and chemical complexity to the prebiotic Earth (1,2). The recognition and description of these varied emergent systems provides an important foundation for origins of life research, for life is the quintessential emergent phenomenon. From vast collections of interacting lifeless molecules emerged the first living cell.

The overarching problem with studying life’s origins is that even the simplest known lifeform is vastly more complex than any non-living components that might have contributed to it. What now appears as a great divide between non-life and life reflects the fact that the chemical evolution of life must have occurred as a stepwise sequence of successively more complex stages of emergence. The challenge, therefore, is to establish a progressive hierarchy of emergent steps that leads from a pre-biotic ocean enriched in organic molecules, to functional clusters of molecules perhaps self-assembled or arrayed on a mineral surface, to self-replicating molecular systems that copied themselves from resources in their immediate environment, to encapsulation and eventually cellular life (2).

The Emergence of Biomolecules

The first vital step in life’s emergence on Earth must have been the synthesis and accumulation of abundant carbon-based biomolecules. In the beginning, life’s raw materials consisted of water, rock, and simple volcanic gases – predominantly carbon dioxide and nitrogen, but with local concentrations of hydrogen, methane, ammonia and other species. Decades of experiments have

revealed that diverse suites of organic molecules can emerge from a variety of geochemical and cosmochemical environments.

The experimental pursuit of geochemical organic synthesis, arguably the best understood aspect of life's origin, began a half-century ago with the pioneering studies of University of Chicago graduate student Stanley Miller and his distinguished mentor Harold Urey (17,18). Together they established the potential role of organic synthesis that occurred in Earth's primitive atmosphere and ocean as they were subjected to bolts of lightning and the Sun's intense radiation (Bada et al., this volume).

Molecules formed in interstellar space represent another important source of life's building blocks (Ehrenfreund & Botta, this volume). A variety of organic species, including aromatic hydrocarbons, alcohols and sugars, represent a significant fraction of the more than 130 molecular species identified by radio astronomy (Ziurys, this volume; Halfen et al., this volume). These deep-space processes have been simulated in cryogenic laboratory experiments using UV radiation (Allamandola, this volume). The rich inventory of organic species brought to Earth in carbonaceous chondrite meteorites underscores the importance of extraterrestrial sources of biomolecules (Botta, this volume).

The discovery of deep-ocean ecosystems led to speculation that a hydrothermal vent, rather than earth's surface, might have been the site of life's origin (19-21). Recent experiments bolster this hypothesis. The most fundamental biological reaction is the incorporation of carbon atoms (starting with the gas carbon dioxide) into organic molecules. Many common minerals, including most minerals of iron, nickel, or copper, promote carbon addition under hydrothermal conditions (22-24). While deep-sea vents remain a highly speculative location for life's origins, mineral-rich hydrothermal systems did contribute to early Earth's varied inventory of bio-building blocks.

It now appears that anywhere energy and simple carbon-rich molecules are found together, a suite of interesting organic molecules is sure to emerge (25). In spite of the polarizing advocacy of one favored environment or another, experiments point to the likelihood that there was no single dominant source. By four billion years ago Earth's oceans must have become a complex, albeit dilute, soup of life's building blocks. Though not alive, this chemical system was poised to undergo a sequence of increasingly complex stages of molecular organization and evolution.

The Emergence of Organized Molecular Systems

Synthesizing biomolecules is relatively easy – some might argue too easy. Life's simplest molecular building blocks, including amino acids, sugars, lipids and bases, emerged inexorably through facile, inevitable chemical reactions in numerous prebiotic environments. Prebiotic processes also produced a bewildering diversity of seemingly useless molecules; most of the molecular

jumble played no obvious role. The emergence of concentrated suites of just the right mix thus remains a central puzzle in origin-of-life research.

Life requires the assembly of just the right combination of small molecules into much larger collections – “macromolecules” with specific functions. Making macromolecules is complicated by the fact that for every potentially useful small molecule in the prebiotic soup, dozens of other molecular species had no obvious role in biology. Life is remarkably selective in its building blocks, whereas the vast majority of carbon-based molecules synthesized in prebiotic processes have no obvious biological use. Consequently, a significant challenge in understanding life’s chemical emergence lies in finding mechanisms by which the right combination of small molecules was selected, concentrated and organized into the larger macromolecular structures vital to life.

The oceans formed a weak solution in which it would have been difficult for advantageous combinations of molecules to react in the chemical path to life. Two processes, self-selection and surface organization, are likely to have led to molecular selection.

Phospholipid molecules, the building blocks of cell membranes, are “amphiphiles” that possess contrasting regions that are attracted to, and repelled by, water. Consequently, these molecules spontaneously self-organize into tiny cell-like spheres when placed in water (26,27). Nevertheless, most water soluble molecules don’t self organize and must be selected by another means. Recent experiments demonstrate that chemical complexity can arise at mineral surfaces where different molecules congregate and interact (28). Once confined and concentrated, small molecules tend to undergo reactions to form larger molecular species that aren’t otherwise likely to emerge from the soup (Ferris et al., this volume). Evaporating tidal pools, where rock and water meet and cycles of evaporation concentrate stranded chemicals, provide another scenario for origin-of-life chemistry (29). Deep within the crust and in hydrothermal volcanic zones mineral surfaces may have played a similar role, selecting, concentrating and organizing molecules on their periodic crystalline surfaces (20,30).

The Emergence of Self-Replicating Molecular Systems

Four billion years ago the molecular building blocks of life had been synthesized, and these molecules must have become locally concentrated on surfaces and through self-selection as they assembled into vesicles and polymers of biological interest. Yet accumulations of organic molecules, no matter how highly selected and intricately organized, are not alive unless they also possess the ability to reproduce.

The simplest self-replicating system consists of one type of molecule that makes copies of itself (31). Under just the right chemical environment, such an isolated molecule will become 2 copies, then 4, then 8 molecules and so on in a geometrical expansion. Such an “autocatalytic” molecule must act as a template

that attracts and assembles smaller building blocks from an appropriate chemical broth. Although fascinating, single self-replicating molecules do not meet minimum requirements for life because they can't evolve.

More relevant to biological metabolism are systems of two or more molecules that form a self-replicating cycle or network (32-34). Living systems are distinguished from simple self-replicating collections of molecules because living systems must also incorporate a degree of sloppiness. Only through such mutability can the system experiment with new, more efficient reaction pathways and thus evolve.

Origin-of-life researchers focus primarily on two contrasting models of the first self-replicating system, metabolism and genetics. Metabolism is a cyclical chemical process in which chemicals react, thus releasing energy and manufacturing new useful molecules that reinforce the cycle. Metabolism requires a sequence of chemical reactions that work in concert. While a number of prominent researchers advocate a metabolism-first scenario (1,2,20,21,24), most origin experts favor a genetics-first scenario, with a self-replicating molecule that also passes information from one generation to the next – a genetic molecule like DNA or RNA (35-38). This so-called “RNA world” model rests on the dual ability of genetic material to catalyze reactions and transfer information. According to most versions of this hypothesis, metabolism emerged later as a means to make the RNA replication process more efficient.

The RNA world model is not without its difficulties. Foremost among these problems is the exceptional challenge in the prebiotic synthesis of RNA (39-40). Many of the presumed proto-metabolic molecules are easily synthesized in experiments that mimic prebiotic environments. RNA nucleotides, by contrast, have never been synthesized from scratch. Furthermore, even if a prebiotic synthetic pathway to nucleotides could be found, a plausible mechanism to link those nucleotides into an RNA strand has not been demonstrated. It is not obvious how useful catalytic RNA sequences would have formed spontaneously in any prebiotic environment. Perhaps, some scientists speculate, a simpler nucleic acid preceded RNA (41-42).

Whatever the scenario, metabolism first or genetics first, the origin of life required more than the replication of chemicals. For a chemical system to be alive, it must display evolution by the process of natural selection.

The Emergence of Natural Selection

Once a collection of molecules began to make copies of itself, natural selection was inevitable. Molecular selection, the process by which a few key molecules earned essential roles in life's origin, proceeded on many fronts. Some molecules were inherently unstable or highly reactive and so they quickly disappeared from the scene. Other molecules easily dissolved in the oceans and so were effectively removed from contention. Still other molecular species may

have sequestered themselves by bonding strongly to surfaces of chemically unhelpful minerals or clumped together into goeey masses of little use to emerging biology.

In every geochemical environment, each kind of organic molecule had its reliable sources and its inevitable sinks. For a time, perhaps for hundreds of millions of years, a kind of molecular equilibrium was maintained as the new supply of each species was balanced by its loss. Such an equilibrium features nonstop competition among molecules, to be sure, but the system does not evolve.

The first self-replicating molecules changed that equilibrium. Even a relatively unstable collection of molecules can be present in significant concentration if it learns how to make copies of itself. The first successful metabolic cycle of molecules, for example, would have proven vastly superior to its individual chemical neighbors at accumulating atoms and harnessing energy. But success breeds competition. Inevitable slight variations in the self-replicating cycle, triggered by the introduction of new molecular species or by differences in environment, initiated an era of increased competition. More efficient cycles flourished at the expense of the less efficient. Evolution by natural selection had begun on Earth.

Two common processes – variation and selection – provide a powerful mechanism for self-replicating systems to evolve. For a system to evolve it must first display a range of variations. Natural systems display random variations through mutations, which are undirected changes in the chemical makeup of key biomolecules. Most variations are neutral or they harm the organism and are doomed to failure. Once in a while, however, a random mutation leads to an improved trait – a more efficient metabolism, better camouflage, swifter locomotion, or greater tolerance for extreme environmental conditions. Such beneficial variations are more likely to survive in the competitive natural world – such variations fuel the process of natural selection.

Competition drives the emergence of natural selection. Such behavior appears to be inevitable in any self-replicating chemical system in which resources are limited and some molecules have the ability to mutate. Over time, more efficient networks of autocatalytic molecules will increase in concentration at the expense of less efficient networks. In such a competitive milieu the emergence of increasing molecular complexity is inevitable; new chemical pathways overlay the old. So it is that life has continued to evolve over the past four billion years of Earth history.

Chemical Education and the Future of Chemical Complexification

This volume examines three major evolutionary episodes of chemical complexification: stellar evolution and the emergence of elemental diversity,

planetary evolution and the emergence of mineralogical diversity, and prebiotic chemical evolution. The second volume in this series will consider the emergence and evolution of life. Have we come to the end of chemical complexity? Are we it?

The next volume will address this question by pointing to a fourth dramatic, ongoing episode of rapid chemical evolution – human engineering in the modern era. Physicists' deep understanding of nucleosynthesis and technological ingenuity has added more than a score of heavy elements to the periodic table. Naturalists' discoveries of the diversity of minerals and their distinctive physical and chemical properties have inspired the synthesis of countless thousands of new mineral-like compounds – many times the number of known natural species. Molecular biologists' deciphering of the genetic code and their development of genetic technologies has led to a growing number of genetically engineered lifeforms. And now, chemical complexification is accelerating as we learn more, and as we pass that knowledge on to our students.

These examples of highly accelerated, human-mediated evolution are more general examples of what Charles Darwin referred to as artificial selection [as opposed to the more gradual, undirected process of natural selection (43)]. Human knowledge and ingenuity can be used to design promising new configurations of elements and molecules, and then select the most successful products for further study and refinement.

The central driver of this continuing engineered complexification is effective chemical education, fostered by innovative ways of teaching chemistry (Halfen et al., this volume; Parker & Meyer, this volume; Venkataraman, this volume; Zaikowski et al., this volume). Armed with such powerful teaching aids, educators will continue to inspire a new generation of chemists to create new dimensions of chemical complexity.

References

1. Morowitz, H. J. *The Emergence of Everything*: Oxford University Press, New York, 2002.
2. Hazen, R. M. *Genesis: The Scientific Quest for Life's Origin*: Joseph Henry Press, Washington, DC, 2005.
3. Nicolis, G.; Prigogine, I. *Exploring Complexity: An Introduction*: W. H. Freeman and Company, New York, 1989.
4. Mason, B. The minerals in meteorites. *Researches on Meteorites* **1961**, 145-163.
5. Brearley, A. J.; Jones, R. H. Chondritic meteorites. *Reviews in Mineralogy and Geochemistry* **1998**, *36*, 3.1-3.398.
6. Zolensky, M. E.; Bodnar, R. J.; Gibson, E. K. Jr.; Nyquist, L. E.; Reese, Y.; Shih, C.-Y.; Weismann, H. Asteroidal water within fluid inclusion-bearing halite in an H5 chondrite, Monahans. *Science* **1999**, *285*, 1377-1379.

7. Mojzsis, S. J.; Harrison, T. M.; Pidgeon, R.T. Oxygen-isotope evidence from ancient zircons for liquid water at the Earth's surface 4,300 Myrs ago. *Nature* **2001**, *409*, 178-181.
8. Lowenstein, T.K.; Timofeeff, M. N.; Brennan, S. T.; Hardie, L. A.; Demicco, R. V. Oscillations in Phanerozoic seawater chemistry: Evidence from fluid inclusions. *Science* **2001**, *294*, 1086-1088.
9. Dickson, J.A.D. Fossil echinoderms as monitor of the Mg/Ca ratio of Phanerozoic oceans. *Science* **2002**, *298*, 1222-1224.
10. Tice, M.M.; Lowe, D. R. Photosynthetic microbial mats in the 3416-Myr-old ocean. *Nature* **2004**, *431*, 549-552.
11. Valley, J. W.; Cavosie, A. J.; Graham, C. M.; King, E. M.; Peck, W. H.; Wilde, S. A. Zircon evidence of the earliest Archean crust: 4.0-4.4 Ga. *Geochimica et Cosmochimica Acta* **2002**, *66*, A794.
12. Stern, R.J. Evidence from ophiolites, blueschists, and ultrahigh-pressure metamorphic terranes that the modern episode of subduction tectonics began in Neoproterozoic time. *Geology* **2005**, *33*, 557-560.
13. Cawood, P.A.; Kroner, A.; Pisarevsky, S. Precambrian plate tectonics: Criteria and evidence. *GSA Today* **2006**, *16*, 4-11.
14. Witze, A. The start of the world as we know it. *Nature* **2006**, *442*, 128-131.
15. Hutchinson, R.W. Volcanogenic sulfide deposits and their metallogenic significance. *Economic Geology* **1973**, *68*, 1223-1246.
16. Sangster, D.F. Precambrian volcanogenic massive sulfide deposits in Canada: A review. *Geological Survey of Canada Paper* **1972**, *72-22*, 1-43.
17. Miller, S. L. Production of amino acids under possible primitive earth conditions. *Science* **1953**, *117*, 528-529.
18. Miller, S. L.; Urey, H. C. Organic compound synthesis on the primitive earth. *Science* **1959**, *130*, 245-251.
19. Corliss, J. B.; Baross, J. A.; Hoffman, S. E. An hypothesis concerning the relationship between submarine hot springs and the origin of life on earth. *Oceanologica Acta* **1981**, *4* (supplement), 59-69.
20. Wächtershäuser, G. Groundworks for an evolutionary biochemistry: the iron-sulfur world. *Progress in Biophysics and Molecular Biology* **1992**, *58*, 85-201.
21. Russell, M. J.; Hall, A. J. The emergence of life from iron monosulphide bubbles at a submarine hydrothermal redox and pH front. *Journal of the Geological Society of London* **1997**, *154*, 377-402.
22. Blöchl, E.; Keller, M.; Wächtershäuser, G.; Stetter, K. O. Reactions depending on iron sulfide and linking geochemistry with biochemistry. *Proceedings of the National Academy of Sciences USA* **1992**, *89*, 8117-8120.
23. Heinen, W.; Lauwers, A. M. Organic sulfur compounds resulting from interaction of iron sulfide, hydrogen sulfide and carbon dioxide in an aerobic aqueous environment. *Origins of Life and Evolution of the Biosphere* **1996**, *26*, 131-150.

24. Cody, G. D.; Boctor, N. Z.; Brandes, J. A.; Filley, T. R.; Hazen, R. M.; Yoder, H. S. Jr. Assaying the catalytic potential of transition metal sulfides for prebiotic carbon fixation. *Geochimica et Cosmochimica Acta* **2004**, *68*, 2185-2196.
25. Chyba, C. F.; Sagan, C. Endogenous production, exogenous delivery, and impact-shock synthesis of organic molecules: an inventory for the origins of life. *Nature* **1992**, *355*, 125-132.
26. Luisi, P. L.; Varela, F. J. Self-replicating micelles: a chemical version of a minimal autopoietic system. *Origins of Life and Evolution of the Biosphere* **1989**, *19*, 633-643.
27. Segré, S.; Deamer, D. W.; Lancet, D. The lipid world. *Origins of Life and Evolution of the Biosphere* **2001**, *31*, 119-145.
28. Hazen, R. M. Mineral surfaces and the prebiotic selection and organization of biomolecules. *American Mineralogist* **2006**, *91*, 1715-1729.
29. Lahav, N.; White, D.; Chang, S. Peptide formation in the prebiotic era: Thermal condensation of glycine in fluctuating clay environments. *Science* **1978**, *201*, 67-69.
30. Gold, T. *The Deep Hot Biosphere: Copernicus*, New York, 1999.
31. Wilson, E. K. Go forth and multiply. *Chemical and Engineering News* **1998**, *76*(December 7, 1998), 40-44.
32. Eigen, M.; Schuster, P. *The Hypercycle: A Principle of Natural Self-Organization*: Springer-Verlag, Berlin, 1979.
33. Kauffman, S. A. *The Origins of Order: Self-Organization and Selection in Evolution*: Oxford University Press, New York, 1993.
34. Huber, C.; Eisenreich, W.; Hecht, S.; Wächtershäuser, G. A possible primordial peptide cycle. *Science* **2003**, *301*, 938-940.
35. Orgel, L. E. RNA catalysis and the origin of life. *Journal of Theoretical Biology* **1986**, *123*, 127-149.
36. Woese, C. R. *The Genetic Code*: Harper & Row, New York, 1967.
37. Crick, F. H. C. The origin of the genetic code. *Journal of Molecular Biology* **1968**, *38*, 367-379.
38. Orgel, L. E. Evolution of the genetic apparatus. *Journal of Molecular Biology* **1968**, *38*, 381-393.
39. Joyce, G. F. The rise and fall of the RNA world. *New Biology* **1991**, *3*, 399-407.
40. Orgel, L. E. Some consequences of the RNA world hypothesis. *Origins of Life and Evolution of the Biosphere* **2003**, *33*, 211-218.
41. Eschenmoser, A. The TNA-family of nucleic acid systems: Properties and prospects. *Origins of Life and Evolution of the Biosphere* **2004**, *34*, 277-306.
42. Nielsen, P. E. Peptide nucleic acid (PNA): a model structure for the primordial genetic material? *Origins of Life and Evolution of the Biosphere* **1993**, *23*, 323-327.
43. Darwin, C. *On the Origin of Species*: John Murray, London, 1859.

**Part I: Chemical Evolution
in Astrophysics**

Chapter 2

Chemical Origins: Nuclear Chemistry in the Early Universe

Keith A. Olive

William I. Fine Theoretical Physics Institute, University of Minnesota,
Minneapolis, MN 55455

Big bang nucleosynthesis (BBN), describes the production of the light elements in the early universe. The theoretical prediction for the abundances of D, ^3He , ^4He , and ^7Li is discussed and compared with their observational determination. The spectrum of anisotropies in the cosmic microwave background (CMB) now independently measures the baryon density to high precision. As a result, the CMB data test BBN. One finds that the CMB along with D and ^4He observations paint a consistent picture. This concordance stands as a major success of the hot big bang. On the other hand, ^7Li remains discrepant with the CMB-preferred baryon density; possible explanations are reviewed.

One of the most fundamental questions in science relates to the chemical origins of the elements and their nuclear isotopes. By far, most of the natural elements are synthesized in stars, but a handful trace their origins back to the first few minutes of the Universe. Big-bang nucleosynthesis (BBN) offers the deepest reliable probe of the early universe, being based on well-understood Standard Model physics. Predictions of the abundances of the light elements, D, ^3He , ^4He , and ^7Li , synthesized shortly after the big bang are in good overall agreement with the primordial abundances inferred from observational data, thus validating the standard hot big-bang cosmology (see [1, 2, 3]). This is particularly impressive given that these abundances span nine orders of magnitude — from $^4\text{He}/\text{H} \sim 0.08$ down to $^7\text{Li}/\text{H} \sim 10^{-10}$ (ratios by number). Thus BBN provides powerful constraints on possible deviations from the standard cosmology [4], and on new physics beyond the Standard Model [5].

The universe as described by the Big Bang theory began in an extremely hot, dense, and largely homogenous state. Today, the universe is nearly 14 billion years old, but at the time of the formation of the light elements, the universe had existed only minutes. The temperature of the universe refers to the temperature associated with the black body radiation known as the cosmic microwave background (CMB) which fills the universe. Today this black body is at a temperature of 2.7 K. Because the universe cools as it expands, the early universe was very hot and at the time of BBN, the temperature exceeded 10^{10} K. At these temperatures, there are no neutral atoms. Indeed, there are no nuclei besides the neutrons and protons coupled to the hot plasma. The density of neutrons and protons (collectively known as baryons¹) was about 10^{17} per cc when nucleosynthesis began. Though small when compared to terrestrial densities, it was far larger than the average density of normal matter in the universe today, 10^{-7} per cc. As will be described below, equilibrium processes, governed the production of the light nuclei as the universe cooled.

Indeed, the notion of a hot and dense early universe grew from the work of the Gamow, Alpher, and Herman, [6, 7], who were attempting to determine the origins of the elements in the Universe. By establishing the thermodynamic conditions needed for nucleosynthesis in the early universe, they were able to predict the existence of a present-day background radiation with temperature of order $T \sim 5$ K. This historic BBN–CMB connection has recently been deepened with the advent of high precision measurements of the CMB anisotropy [8]. The measurements have led to determinations of cosmological parameters with an unprecedented accuracy. These include the baryon density which is the sole parameter in standard BBN. As such, with all parameters fixed, BBN simply

¹ Baryons refer to the class of strongly interacting particles which are made up of 3 quarks. The only long lived baryons are the neutrons and the proton. All other baryons are very short lived and produced only in accelerators (or cosmic ray collisions).

makes definite predictions for the abundances of the light elements which can then be contrasted with their observational determinations [9]. This will be the approach taken in this review [10].

Big Bang Nucleosynthesis Theory

The standard model [1, 2, 3] of Big Bang nucleosynthesis is based on the relatively simple idea of including an extended nuclear network into a homogeneous and isotropic cosmology. The observed homogeneity and isotropy enable us to describe the overall geometry and evolution of the Universe in terms of two cosmological parameters accounting for the spatial curvature and the overall expansion (or contraction) of the Universe. These two quantities appear in the most general expression for a space-time metric with these symmetries known as the Robertson-Walker metric:

$$ds^2 = dt^2 - R^2(t) \left[\frac{dr^2}{1 - kr^2} + r^2 (d\theta^2 + \sin^2 \theta d\phi^2) \right] \quad (1)$$

where $R(t)$ is the cosmological scale factor and k is the curvature constant. By rescaling the radial coordinate, we can choose k to take only the discrete values $+1$, -1 , or 0 corresponding to closed, open, or spatially flat geometries.

The cosmological equations of motion are derived from Einstein's equations which describe the time rate of change of the scale factor, $\dot{R} = dR/dt$, and lead to

$$H^2 = \frac{\dot{R}^2}{R^2} = \frac{8\pi G_N \rho}{3} - \frac{k}{R^2} + \frac{\Lambda}{3} \quad (2)$$

and

$$\frac{\ddot{R}}{R} = \frac{\Lambda}{3} - \frac{4\pi G_N}{3} (\rho + 3p) \quad (3)$$

where $H(t)$ is the Hubble parameter and describes the relative rate of expansion of the universe. G_N is Newton's gravitational constant. Λ is the cosmological constant and may be important in accounting for the observed acceleration of the expansion today. Because the energy density ρ is proportional to R^{-3} in a matter (pressureless) dominated Universe, or is proportional to R^{-4} when the universe is dominated by radiation with $p = \rho/3$, at early times (small R), the curvature and cosmological constant contributions to H can be ignored. This is particularly true at the time of nucleosynthesis.

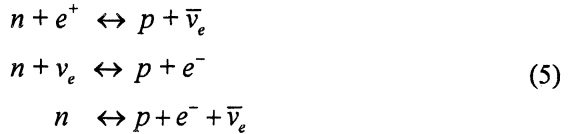
In the early universe, the energy density was dominated by radiation and relativistic particle species

$$\rho_{\text{rad}} = \frac{\pi^2}{30} \left(2 + \frac{7}{2} + \frac{7}{4} N_\nu \right) T^4 \equiv \frac{\pi^2}{30} g_* T^4 \quad (4)$$

which consists of photons, electrons and positrons, and N_ν neutrino flavors. At higher temperatures, other particle degrees of freedom should be included as well. This is just a generalized black body at high temperature. Time and temperature scale with the Hubble parameter as $t \sim 1/H \sim 1/T^2$, and in standard BBN (i.e., with $N_\nu = 3$), we roughly have $t/1 \text{ sec} \simeq (2.4/g_*)(1 \text{ MeV}/T)^2$. Units have been chosen such that $k_B = c = \hbar = 1$.

Apart from the input nuclear cross sections, the theory contains only a single parameter, namely the ratio of the number densities of baryons to photons, η . Because both densities scale as R^{-3} , their ratio is constant, barring any non-adiabatic processes. The theory then allows one to make predictions (with well-defined uncertainties) of the abundances of the light elements, D, ^3He , ^4He , and ^7Li .

The synthesis of the light elements is sensitive to physical conditions in the early radiation-dominated era at temperatures $T \lesssim 1 \text{ MeV}$, corresponding to an age $t \gtrsim 1 \text{ s}$. At these and higher temperatures, weak interactions rates $\Gamma_{\text{weak}} \gg H$ were rapid compared to the expansion rate, and thus the weak interactions were in thermal equilibrium. In particular, the processes which interconvert neutrons and protons through scatterings with electrons (e^-), positrons (e^+), electron neutrinos (ν_e) and electron anti-neutrinos ($\bar{\nu}_e$), namely



fix the ratio of the neutron and proton number densities to be $n/p = e^{-Q/T}$, where $Q = 1.293 \text{ MeV}$ is the neutron-proton mass difference. At $T \gg 1 \text{ MeV}$, $(n/p) \simeq 1$. As the temperature dropped, the neutron-proton inter-conversion rate, $\Gamma_{np} \sim G_F^2 T^5$, where G_F is the Fermi constant, fell faster than the Hubble expansion rate, $H \sim \sqrt{g_* G_N} T^2$. This resulted in breaking of chemical equilibrium (“freeze-out”) at $T_{fr} \sim (g_* G_N / G_F^4)^{1/6} \simeq 0.8 \text{ MeV}$. The neutron fraction at this time, $n/p = e^{-Q/T_{fr}} \simeq 1/6$ is thus sensitive to every known physical interaction, since Q is determined by both strong and electromagnetic interactions while T_{fr} depends on the weak as well as gravitational interactions. After freeze-out the neutrons were free to β -decay so the neutron fraction dropped to $\simeq 1/7$ by the time nuclear reactions began. A useful semi-analytic description of freeze-out has been given [11, 12].

The nucleosynthesis chain begins with the formation of deuterium in the process $p + n \rightarrow D + \gamma$. However, because of the large number of photons relative to nucleons (or baryons), $\eta^{-1} = n_\gamma/n_B \sim 10^{10}$, deuterium production is delayed past the point where the temperature has fallen below the deuterium binding energy, $E_B = 2.2$ MeV (the average photon energy in a blackbody is $\bar{E}_\gamma \approx 2.7T$). This is because there are many photons in the exponential tail of the photon energy distribution with energies $E > E_B$ despite the fact that the temperature or \bar{E}_γ is less than E_B . The degree to which deuterium production is delayed can be found by comparing the qualitative expressions for the deuterium production and destruction rates,

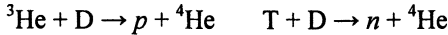
$$\begin{aligned}\Gamma_p &\approx n_B \sigma v & (6) \\ \Gamma_d &\approx n_\gamma \sigma v e^{-E_B/T}\end{aligned}$$

When the quantity $\eta^{-1} \exp(-E_B/T) \sim 1$, the rate for deuterium destruction ($D + \gamma \rightarrow p + n$) finally falls below the deuterium production rate and the nuclear chain begins at a temperature $T \sim 0.1$ MeV.

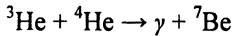
In addition to the $p + n \rightarrow D + \gamma$ reaction, the other major reactions leading to the production of the light elements tritium (T) and ^3He are:



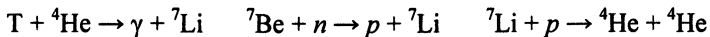
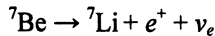
followed by the reactions producing ^4He :



The gap at $A = 5$ is overcome and the production and destruction of mass $A = 7$ are regulated by:



Followed by the decay of ^7Be



The gap at $A = 8$ prevents the production of other isotopes in any significant quantity. The nuclear chain in BBN calculations was extended [13] and is shown in Figure 1.

When nucleosynthesis begins, nearly all the surviving neutrons end up bound in the most stable light element ${}^4\text{He}$. Heavier nuclei do not form in any significant quantity both because of the absence of stable nuclei with mass number 5 or 8 (which impedes nucleosynthesis via ${}^4\text{He} + n$, ${}^4\text{He} + p$ or ${}^4\text{He} + {}^4\text{He}$ reactions) and the large Coulomb barriers for reactions such as the $T + {}^4\text{He} \rightarrow \gamma + {}^7\text{Li}$ and ${}^3\text{He} + {}^4\text{He} \rightarrow \gamma + {}^7\text{Be}$ reactions listed above. Hence the primordial mass fraction of ${}^4\text{He}$, conventionally referred to as Y_p , can be estimated by the simple counting argument

$$Y_p = \frac{2(n/p)}{1+n/p} \approx 0.25$$

There is little sensitivity here to the actual nuclear reaction rates, which are important in determining the other “left-over” abundances: D and ${}^3\text{He}$ at the level of a few times 10^{-5} by number relative to H, and ${}^7\text{Li}/\text{H}$ at the level of about 10^{-10} (when $\eta_{10} \equiv 10^{10}\eta$ is in the range 1–10). These values can be understood in terms of approximate analytic arguments [14, 12]. The experimental parameter most important in determining Y_p is the neutron lifetime, τ_n , which normalizes (the inverse of) Γ_{np} . (This is not fully determined by G_F alone since neutrons and protons also have strong interactions, the effects of which cannot be calculated very precisely.) The experimental uncertainty in τ_n has recently been reduced substantially. The Particle Data Group [15] world average is $\tau_n = 885.7 \pm 0.8\text{s}$.

Historically, BBN as a theory explaining the observed element abundances was nearly abandoned due its inability to explain *all* element abundances. Subsequently, stellar nucleosynthesis became the leading theory for element production [16]. However, two key questions persisted. 1) The abundance of ${}^4\text{He}$ as a function of metallicity² is nearly flat and no abundances are observed to be below about 23% as exaggerated in Figure 2. In particular, even in systems in which an element such as oxygen, which traces stellar activity, is observed at extremely low values (compared with the solar value of $\text{O}/\text{H} \approx 4.6 \times 10^{-4}$), the ${}^4\text{He}$ abundance is nearly constant. This is very different from all other element abundances (with the exception of Li as we will see below). For example, in Figure 3, the N/H vs. O/H correlation is shown [17]. As one can clearly see, the abundance of N/H goes to 0, as O/H goes to 0, indicating a stellar source for nitrogen. 2) Stellar sources can not produce the observed abundance of D/H. Indeed, stars destroy deuterium and no astrophysical site is known for the production of significant amounts of deuterium [18, 19, 20]. Thus we are led back to BBN for the origins of D, ${}^3\text{He}$, ${}^4\text{He}$, and ${}^7\text{Li}$.

Recently the input nuclear data have been carefully reassessed [21, 22, 23, 24, 25], leading to improved precision in the abundance predictions. The

² Metallicity refers to the abundance of all elements with $Z > 2$ collectively.

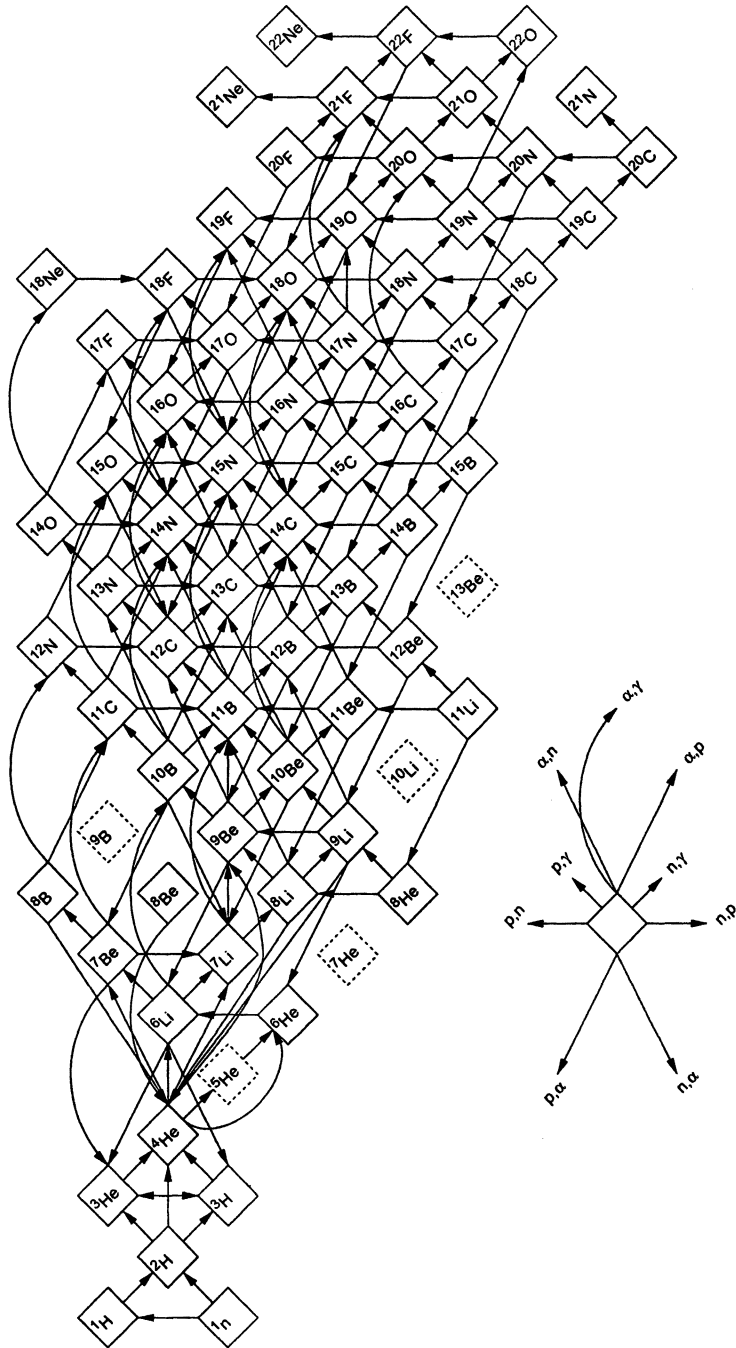


Figure 1. The nuclear network used in BBN calculations.

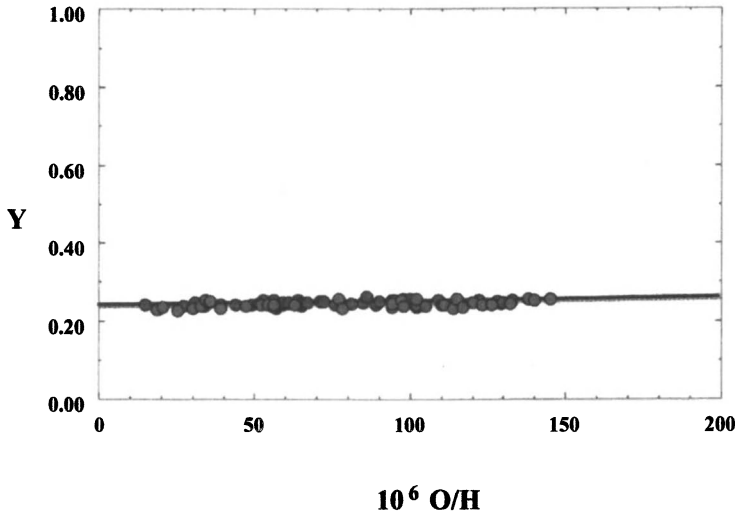


Figure 2. The ${}^4\text{He}$ mass fraction as determined in extragalactic H II regions as a function of O/H.

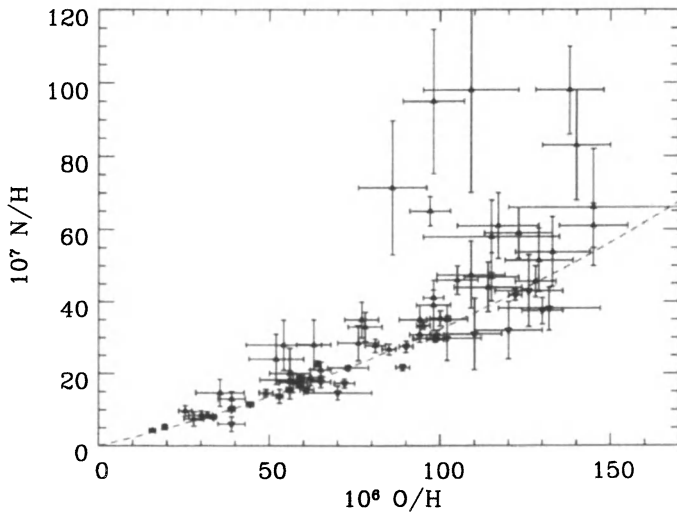


Figure 3. The nitrogen and oxygen abundances in the same extragalactic H II regions with observed ${}^4\text{He}$ shown in Figure 2.

Nuclear Astrophysics Compilation of Reaction Rates (NACRE) collaboration presented an updated nuclear compilation [24]. For example, notable improvements include a reduction in the uncertainty in the rate for ${}^3\text{He} + n \rightarrow p + \text{T}$ from 10% [26] to 3.5% and for $\text{T} + \alpha \rightarrow \gamma + {}^7\text{Li}$ from $\sim 23\text{--}30\%$ [26] to $\sim 4\%$. Since then, new data and techniques have become available, motivating new compilations. Within the last year, several new BBN compilations have been presented [27, 28, 29].

The resulting elemental abundances predicted by standard BBN are shown in Figure 4 as a function of η [22]. The left plot shows the abundance of ${}^4\text{He}$ by mass, Y , and the abundances of the other three isotopes by number. The curves indicate the central predictions from BBN, while the bands correspond to the uncertainty in the predicted abundances. This theoretical uncertainty is shown explicitly in the right panel as a function of η . The uncertainty range in ${}^4\text{He}$ reflects primarily the 1σ uncertainty in the neutron lifetime.

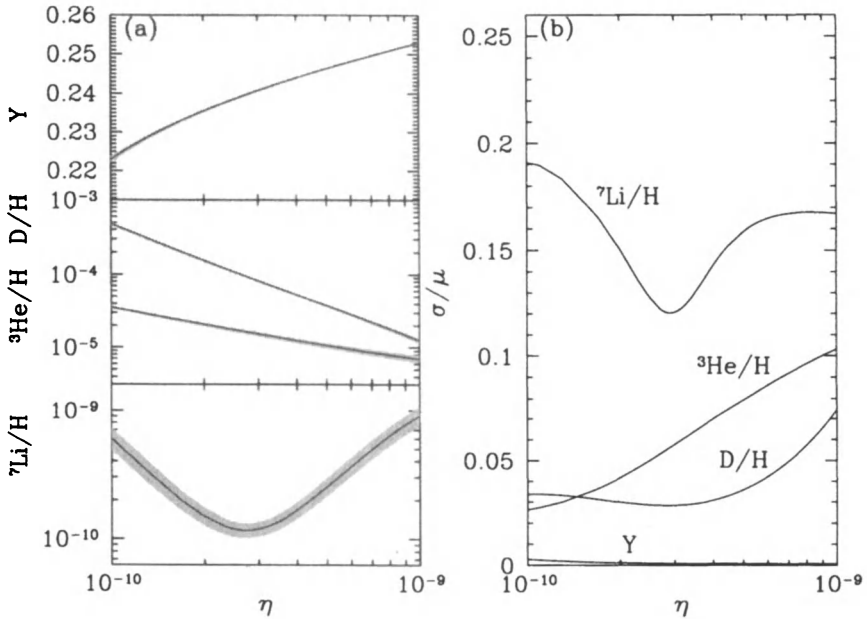


Figure 4. The predictions of standard BBN [22], with thermonuclear rates based on the NACRE compilation [24]. (a) Primordial abundances as a function of the baryon-to-photon ratio η . Abundances are quantified as ratios to hydrogen, except for ${}^4\text{He}$ which is given in baryonic mass fraction $Y_p = \rho_{\text{He}}/\rho_{\text{B}}$. The lines give the mean values, and the surrounding bands give the 1σ uncertainties. (b) The 1σ abundance uncertainties, expressed as a fraction of the mean value μ for each η .

In the standard model with $N_\nu = 3$, the only free parameter is the density of baryons which sets the rates of the strong reactions. Thus, any abundance measurement determines η , while additional measurements over-constrain the theory and thereby provide a consistency check. BBN has thus historically been the premier means of determining the cosmic baryon density.

With the increased precision of microwave background anisotropy measurements, it is now possible to use the CMB to independently determine the baryon density. The 3rd year WMAP data implies [8]

$$\eta_{10} = 6.12^{+0.20}_{-0.25} \quad (7)$$

Equivalently, this can be stated as the allowed range for the baryon mass density today expressed as a fraction of the critical density: $\Omega_B = \rho_B/\rho_{\text{crit}} \simeq \eta_{10}h^{-2}/274 = (0.02233^{+0.00072}_{-0.00091})h^{-2}$, where $h \equiv H_0 / 100 \text{ km s}^{-1} \text{ Mpc}^{-1}$ is the present Hubble parameter.

The promise of CMB precision measurements of the baryon density suggests a new approach in which the CMB baryon density becomes an input to BBN. Thus, within the context of the Standard Model (i.e., with $N_\nu = 3$), BBN becomes a zero-parameter theory, and the light element predictions are completely determined to within the uncertainties in η_{CMB} and the BBN theoretical errors. Comparison with light element observations then can be used to restate the test of BBN–CMB consistency, or to turn the problem around and test the astrophysics of post-BBN light element evolution [30]. Alternatively, one can consider possible physics beyond the Standard Model (e.g., with $N_\nu \neq 3$) and then use all of the abundances to test such models.

Light Element Observations and Comparison with Theory

BBN theory predicts the universal abundances of (D), ^3He , ^4He , and ^7Li , which are essentially determined by $t \sim 180$ s. Abundances are however observed at much later epochs, after stellar nucleosynthesis has commenced. The ejected remains of this stellar processing can alter the light element abundances from their primordial values, but also produce heavy elements such as C, N, O, and Fe (“metals”). Thus one seeks astrophysical sites with low metal abundances, in order to measure light element abundances which are closer to primordial. For all of the light elements, systematic errors are an important and often dominant limitation to the precision of the primordial abundances.

In recent years, high-resolution spectra have revealed the presence of D in high-redshift, low-metallicity quasar absorption systems (QAS), via its isotope-shifted Lyman- α absorption. These are the first measurements of light element abundances at cosmological distances. It is believed that there are no

astrophysical sources of deuterium [18, 19, 20], so any measurement of D/H provides a lower limit to primordial D/H and thus an upper limit on η . For example, the local interstellar value of $D/H = (1.56 \pm 0.04) \times 10^{-5}$ [31] requires that $\eta_{10} \leq 9$. In fact, local interstellar D may have been depleted by a factor of 2 or more due to stellar processing. However, for the high-redshift systems, conventional models of galactic nucleosynthesis (chemical evolution) do not predict significant D/H depletion [32, 33]; in this case, the high-redshift measurements recover the primordial deuterium abundance.

The six most precise observations of deuterium [34, 35, 36, 37, 38, 39] in QAS give $D/H = (2.83 \pm 0.26) \times 10^{-5}$, where the error is statistical only. These are shown in Figure 5 along with some other recent measurements [40, 41, 42].

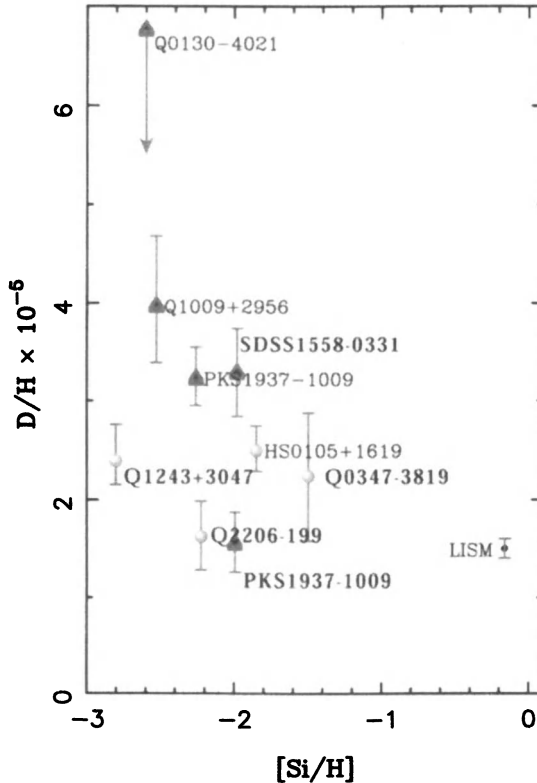


Figure 5. D/H abundances shown as a function of the log of the Si abundance relative to its solar value, $[Si/H]$. Labels denote the background QSO, except for the local interstellar value (LISM; [31]).

Inspection of the data shown in the figure clearly indicates the need for concern over systematic errors. Nevertheless, these measurements are clearly consistent with the CMB/BBN determined value of the primordial D/H abundance which is predicted to be:

$$(D/H)_p = 2.6 \pm 0.2 \times 10^{-5} \quad (8)$$

^4He is observed in clouds of ionized hydrogen (HII regions), the most metal-poor of which are in dwarf galaxies. There is now a large body of data on ^4He and carbon, nitrogen, and oxygen (CNO) in these systems [43, 44, 45]. The He abundance from this sample of 45 low metallicity HII regions, observed and analyzed in a uniform manner [43, 44, 45], is $Y_p = 0.244 \pm 0.002$. An analysis based on the combined available data as well as unpublished data yielded an lower value of 0.238 ± 0.002 with an estimated systematic uncertainty of 0.005 [46, 47]. An extended data set including 89 HII regions obtained $Y_p = 0.2429 \pm 0.0009$ [48]. However, the recommended value is based on the much smaller subset of 7 HII regions, finding $Y_p = 0.2421 \pm 0.0021$.

^4He abundance determinations depend on a number of physical parameters associated with the HII region in addition to the overall intensity of the He emission line. These include, the temperature, electron density, optical depth and degree of underlying absorption. A self-consistent analysis may use multiple ^4He emission lines to determine the He abundance, the electron density and the optical depth. In [43, 44, 45], five He lines were used, underlying He absorption was assumed to be negligible, and temperatures based on OIII data were used.

The question of systematic uncertainties was addressed in some detail in [49]. It was shown that there exist severe degeneracies inherent in the self-consistent method, particularly when the effects of underlying absorption are taken into account. The results of a Monte-Carlo reanalysis [50] of NCG 346 [51, 52] is shown in Figure 6. In the left panel, solutions for the ^4He abundance and electron density are shown (symbols are described in the caption). In the right panel, a similar plot with the ^4He abundance and the equivalent width for underlying absorption is shown. As one can see, solutions with no absorption and high density are often indistinguishable (i.e., in a statistical sense they are equally well represented by the data) from solutions with underlying absorption and a lower density. In the latter case, the He abundance is systematically higher. These degeneracies are markedly apparent when the data is analyzed using Monte-Carlo methods which generate statistically viable representations of the observations as shown in Figure 6. When this is done, not only are the He abundances found to be higher, but the uncertainties are also found to be significantly larger than in a direct self-consistent approach.

Recently a careful study of the systematic uncertainties in ${}^4\text{He}$, particularly the role of underlying absorption has been performed using a subset of the highest quality from the data of Izotov and Thuan [43, 44, 45]. All of the physical parameters listed above including the ${}^4\text{He}$ abundance were determined self-consistently with Monte Carlo methods [49]. Note that the ${}^4\text{He}$ abundances are systematically higher, and the uncertainties are several times larger than quoted in [43, 44, 45]. In fact this study has shown that the determined value of Y_p is highly sensitive to the method of analysis used. The result is shown in Figure 7 together with a comparison of the previous result. The extrapolated ${}^4\text{He}$ abundance was determined to be $Y_p = 0.2495 \pm 0.0092$. The value of η corresponding to this abundance is $\eta_{10} = 6.9_{-4.0}^{+11.8}$ and clearly overlaps with η_{CMB} . Conservatively, it would be difficult at this time to exclude any value of Y_p inside the range 0.232 – 0.258.

At the WMAP value for η , the ${}^4\text{He}$ abundance is predicted to be:

$$Y_p = 0.2485 \pm 0.0005 \quad (9)$$

This value is considerably higher than any prior determination of the primordial ${}^4\text{He}$ abundance, it is in excellent agreement with the most recent analysis of the ${}^4\text{He}$ abundance [50]. Note also that the large uncertainty ascribed to this value indicates that the while ${}^4\text{He}$ is certainly consistent with the WMAP determination of the baryon density, it does not provide for a highly discriminatory test of the theory at this time.

The systems best suited for Li observations are metal-poor stars in the spheroid of our Galaxy. These stars belong to a generation of stars labeled Pop II. Pop I stars are late stars which include the current generation of stars. Pop II stars are older and Pop III refer to the very first generation of stars. Observations have long shown [53, 54, 55] that Li does not vary significantly in Pop II stars with metallicities $\lesssim 1/30$ of solar — the “Spite plateau”. Recent precision data suggest a small but significant correlation between Li and Fe [56] which can be understood as the result of Li production from Galactic cosmic rays [57, 58]. Extrapolating to zero metallicity one arrives at a primordial value [59] $\text{Li}/\text{H}|_p = (1.23 \pm 0.06) \times 10^{-10}$.

Figure 8 shows the different Li components for a model with $({}^7\text{Li}/\text{H})_p = 1.23 \times 10^{-10}$. The linear slope produced by the model is independent of the input primordial value. The model of reference [60] includes in addition to primordial ${}^7\text{Li}$, lithium produced in Galactic cosmic-ray nucleosynthesis (primarily $\alpha + \alpha$ fusion), and ${}^7\text{Li}$ produced by the ν -process during core collapse supernovae. As one can see, these processes are not sufficient to reproduce the population I abundance of ${}^7\text{Li}$, and additional production sources are needed.

Recent data [61] with temperatures based on H α lines (considered to give systematically high temperatures) yields ${}^7\text{Li}/\text{H} = (2.19 \pm 0.28) \times 10^{-10}$. This

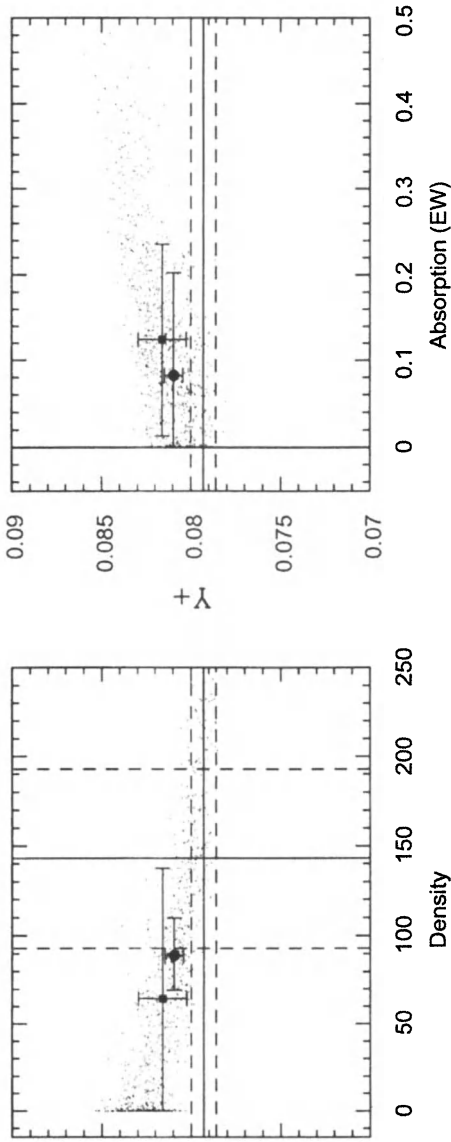


Figure 6. Results of modeling of 6 He I line observations of NGC 346 [51, 52]. The solid lines show the original derived values and the dashed lines show the 1σ errors on those values. The solid circles (with error bars) show the results of the χ^2 minimization solution (with calculated errors) [50]. The small points show the results of Monte Carlo realizations of the original input spectrum. The solid squares (with error bars) show the means and dispersions of the output values for the χ^2 minimization solutions of the Monte Carlo realizations.

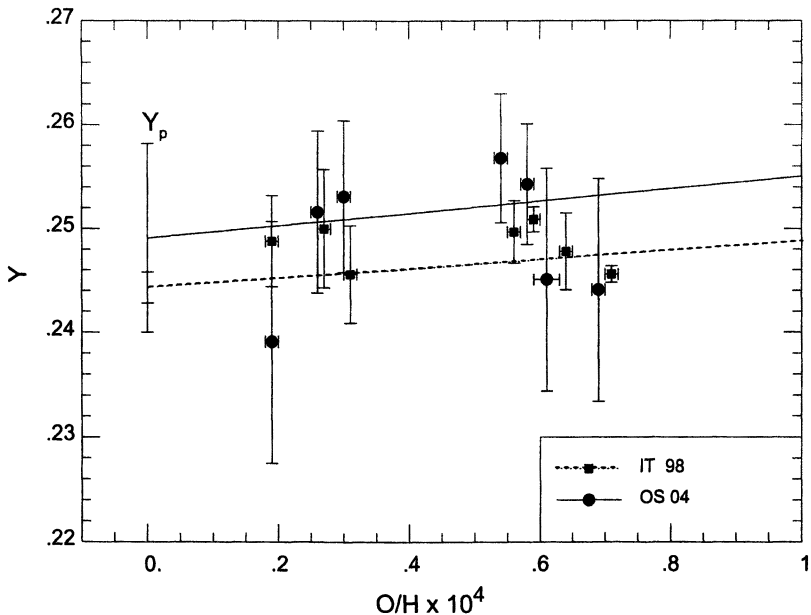


Figure 7. A comparison of the results for the best targets [43, 44, 45] and a re-analysis of the spectra for those targets [50].

result is based on a globular cluster sample (NGC 6397) and is consistent with previous Li measurements of the same cluster which gave ${}^7\text{Li}/\text{H} = (1.91 \pm 0.44) \times 10^{-10}$ [62] and ${}^7\text{Li}/\text{H} = (1.69 \pm 0.27) \times 10^{-10}$ [63]. A related study (also of globular cluster stars) gives ${}^7\text{Li}/\text{H} = (2.29 \pm 0.94) \times 10^{-10}$ [64].

The ${}^7\text{Li}$ abundance based on the WMAP baryon density is predicted to be:

$${}^7\text{Li}/\text{H} = 4.3 \pm 0.7 \times 10^{-10} \quad (10)$$

This value is in clear contradiction with most estimates of the primordial Li abundance. It is a factor of ~ 3 higher than the value observed in most halo stars, and just about 0.2 dex over the globular cluster value.

The quoted value for the ${}^7\text{Li}$ abundance assumes that the Li abundance in the stellar sample reflects the initial abundance at the birth of the star; however, an important source of systematic uncertainty comes from the possible depletion of Li over the $\gtrsim 10$ Gyr age of the Pop II stars. The atmospheric Li abundance will suffer depletion if the outer layers of the stars have been transported deep enough into the interior, and/or mixed with material from the hot interior; this

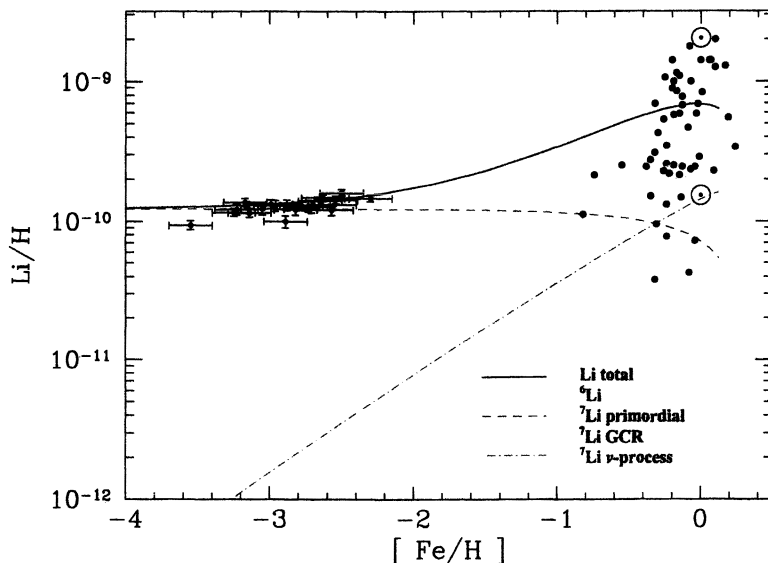


Figure 8. Contributions to the total predicted lithium abundance from the adopted GCE model of [60], compared with low metallicity stars and a sample of high metallicity stars. The solid curve is the sum of all components.

may occur due to convection, rotational mixing, or diffusion. Standard stellar evolution models predict Li depletion factors which are very small ($\sigma_{A(\text{Li})} < 0.05$ dex) in very metal-poor turnoff stars [65]. However, there is no reason to believe that such simple models incorporate all effects which lead to depletion such as rotationally-induced mixing and/or diffusion. Current estimates for possible depletion factors are in the range ~ 0.2 – 0.4 dex [66, 67, 68, 69]. As noted above, this data sample [56] shows a negligible intrinsic spread in Li leading to the conclusion that depletion in these stars is as low as 0.1 dex.

Another important source for potential systematic uncertainty stems from the fact that the Li abundance is not directly observed but rather, inferred from an absorption line strength and a model stellar atmosphere. Its determination depends on a set of physical parameters and a model-dependent analysis of a stellar spectrum. Among these parameters, are the metallicity characterized by the iron abundance (though this is a small effect), the surface gravity which for hot stars can lead to an underestimate of up to 0.09 dex if $\log g$ is overestimated by 0.5, though this effect is negligible in cooler stars. Typical uncertainties in $\log g$ are ± 0.1 – 0.3. The most important source for error is the surface

temperature. Effective-temperature calibrations for stellar atmospheres can differ by up to 150–200 K, with higher temperatures resulting in estimated Li abundances which are higher by ~ 0.08 dex per 100 K. Thus accounting for a difference of 0.5 dex between BBN and the observations, would require a serious offset of the stellar parameters. In fact, there has been a recent analysis [70] which does support higher temperatures, and the consequences of the higher temperatures on the inferred abundances of related elements such as Be, B, and O have also been explored [71].

Finally another potential source for systematic uncertainty lies in the BBN calculation of the ${}^7\text{Li}$ abundance. As one can see from Figure 4, the predictions for ${}^7\text{Li}$ carry the largest uncertainty of the 4 light elements which stem from uncertainties in the nuclear rates. The effect of changing the yields of certain BBN reactions was recently considered by Coc et al. [72]. In particular, they concentrated on the set of cross sections which affect ${}^7\text{Li}$ and are poorly determined both experimentally and theoretically. In many cases however, the required change in cross section far exceeded any reasonable uncertainty. Nevertheless, it may be possible that certain cross sections have been poorly determined. In [72], it was found for example, that an increase of the ${}^7\text{Be}(d,p)2{}^4\text{He}$ reaction by a factor of 100 would reduce the ${}^7\text{Li}$ abundance by a factor of about 3 in WMAP η range. This reaction has since been remeasured and precludes this solution [73].

The possibility of systematic errors in the ${}^3\text{He}(\alpha, \gamma){}^7\text{Be}$ reaction, which is the only important ${}^7\text{Li}$ production channel in BBN, was considered in detail in [74]. The absolute value of the cross section for this key reaction is known relatively poorly both experimentally and theoretically. However, the agreement between the standard solar model and solar neutrino data thus provides additional constraints on variations in this cross section. Using the standard solar model of Bahcall [75], and recent solar neutrino data [76], one can exclude systematic variations of the magnitude needed to resolve the BBN ${}^7\text{Li}$ problem at the $\gtrsim 95\%$ confidence level [74]. Thus the “nuclear fix” to the ${}^7\text{Li}$ BBN problem is unlikely.

Figure 8 also shows the evolution of the ${}^6\text{Li}$ abundance in a standard model of galactic chemical evolution. In the case of ${}^6\text{Li}$, new data [77, 78, 79, 80, 81, 82] lie a factor ~ 1000 above the BBN predictions [83], and fail to exhibit the dependence on metallicity expected in models based on nucleosynthesis by Galactic cosmic rays [84, 85, 86]. On the other hand, the ${}^6\text{Li}$ abundance may be explained by pre-Galactic Population-III stars, without additional over-production of ${}^7\text{Li}$ [87, 88]. Some exotic solutions to both lithium problems involving particle decays in the early universe have been proposed [89, 90, 91, 92, 93, 94, 95, 96, 97, 98], but that goes beyond the scope of this review.

Finally, we turn to ${}^3\text{He}$. Here, the only observations available are in the solar system and (high-metallicity) HII regions in our Galaxy [99]. This makes

inference of the primordial abundance difficult, a problem compounded by the fact that some stellar nucleosynthesis models for ${}^3\text{He}$ are in conflict with observations [100] though recent models invoking deep mixing [101] may alleviate this problem. Consequently, ${}^3\text{He}$ as a cosmological probe [102] carries substantial uncertainties. Instead, one might hope to turn the problem around and constrain stellar astrophysics using the predicted primordial ${}^3\text{He}$ abundance [103]. For completeness, we note that the ${}^3\text{He}$ abundance is predicted to be:

$${}^3\text{He}/\text{H} = 9.3 \pm 0.5 \times 10^{-6} \quad (11)$$

at the WMAP value of η .

Summary

In Figure 9, we show the direct comparison between the BBN predicted abundances given in eqs. (8), (9), and (10), using the WMAP value of η_{10} with the observations [104]. As one can see, there is very good agreement between theory and observation for both D/H and ${}^4\text{He}$. Of course, in the case of ${}^4\text{He}$, concordance is almost guaranteed by the large errors associated with the observed abundance. In contrast, as was just noted above, there is a marked discrepancy in the case of ${}^7\text{Li}$.

As cosmology moves into a new and high precision era, the utility of BBN is shifting from a test of the standard FRW model to one which is a sensitive probe of astrophysical processes which relate to the light element abundances as well as a sensitive probe of physics beyond the standard model. The parameters of the standard model as they relate to BBN are now well determined: $\eta_{10} = 6.12$ and $N_s = 3$. With these values, BBN is able to make very definite predictions for the primordial abundances of the light elements. These predictions are then contrasted with observational determinations of the abundances and reveal either our knowledge or ignorance of the astrophysical processes which affect the primordial abundances. In the case of ${}^4\text{He}$ and D/H , within the large uncertainties in the observational data, the concordance is excellent. ${}^7\text{Li}$ remains problematic though several possible (if not perfect) astrophysical solutions are available. Finally, as the data on the light element abundances improves, BBN will sharpen its ability to probe physics beyond the standard model. As such it remains the only available tool for which to examine directly the very early universe.

Acknowledgments

This work of was partially supported by DOE grant DE-FG02-94ER-40823.

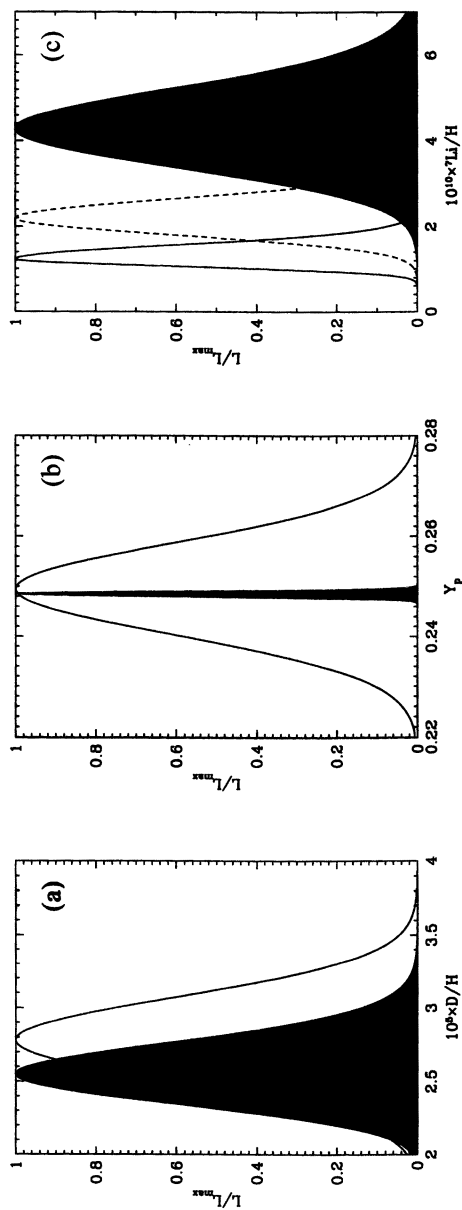


Figure 9. Primordial light element abundances as predicted by BBN and WMAP (dark shaded regions) [104]. Different observational assessments of primordial abundances are plotted as follows: (a) the light shaded region shows $D/H = (2.78 \pm 0.29) \times 10^{-5}$; (b) the light shaded region shows $Y_p = 0.249 \pm 0.009$; (c) the light shaded region shows ${}^7\text{Li}/H = 1.23^{+0.34}_{-0.16} \times 10^{-10}$ while the dashed curve shows ${}^7\text{Li}/H = (2.19 \pm 0.28) \times 10^{-10}$.

References

1. Walker, T. P.; Steigman, G.; Schramm, D. N.; Olive, K. A.; Kang, K. *Astrophys. J.* **1991**, 376, 51.
2. Olive, K. A.; Steigman, G.; Walker, T. P. *Phys. Rep.* **2000**, 333, 389.
3. Fields, B. D.; Sarkar, S. *J. Phys.* **2006**, G33, 220.
4. Malaney, R. A.; Mathews, G. J. *Phys. Rept.* **1993**, 229, 145.
5. Sarkar, S. *Rep. Prog. Phys.* **1996**, 59, 1493.
6. Gamow, G. *Nature* **1948**, 162, 680.
7. Alpher, R. A.; Herman, R. *Nature* **1948**, 162, 774.
8. Spergel, D. N. et al. [WMAP Collaboration], arXiv:astro-ph/0603449.
9. Cyburt, R. H.; Fields, B. D.; Olive, K. A. *Phys. Lett. B* **2003**, 567, 227.
10. Fields, B. D.; Olive, K. A. *Nucl. Phys. A*, **2006**, 777, 208.
11. Bernstein, J.; Brown, L. S.; Feinberg, G. *Rev. Mod. Phys.* **1989**, 61, 25.
12. Mukhanov, V. arXiv:astro-ph/0303073.
13. Thomas, D.; Schramm, D.; Olive, K. A.; Fields, B. *Astrophys. J.* **1993**, 406, 569.
14. Esmailzadeh, R.; Starkman, G. D., Dimopoulos, S. *Astrophys. J.* **1991**, 378, 504.
15. Yao, W. M. et al. *J. Phys.* **2006**, G33, 1.
16. Burbidge, E.M.; Burbidge, G.R.; Fowler, W.A.; Hoyle, F. *Rev. Mod. Phys.* **1957**, 29, 547.
17. Fields, B.D.; Olive, K.A. *Astrophys. J.* **1998**, 506, 177.
18. Reeves, H.; Audouze, J.; Fowler, W. A.; Schramm, D. N. *Astrophys. J.* **1973**, 179, 909.
19. Epstein, R. I.; Lattimer, J. M.; Schramm, D. N. *Nature* **1976**, 263, 198.
20. Prodanović, T.; Fields, B. D. *Astrophys. J.* **2003**, 597, 48.
21. Nollett, K. M.; Burles, S. *Phys. Rev. D* **2000**, 61, 123505.
22. Cyburt, R. H.; Fields, B. D.; Olive, K. A. *New Astron.* **1996**, 6, 215.
23. Coc, A.; Vangioni-Flam, E.; Cass'è, M.; Rabiet, M. *Phys. Rev. D* **2002**, 65, 043510.
24. Angulo, C.; et al. *Nucl. Phys.* **1999**, A656, 3.
25. Coc, A.; Vangioni-Flam, E.; Descouvemont, P.; Adahchour, A.; Angulo, C. *Astrophys. J.* **2004**, 600, 544.
26. Smith, M.; Kawano, L.; Malaney, R. A. *Astrophys. J. Supp.* **1993**, 85, 219.
27. Cyburt, R. H. *Phys. Rev. D* **2004**, 70, 023505.
28. Descouvemont, P.; Adahchour, A.; Angulo, C.; Coc, A. ; Vangioni-Flam, E. arXiv:astro-ph/0407101.
29. Serpico, P. D.; Esposito, S.; Iocco, F.; Mangano, G.; Miele, G.; Pisanti, O. *Int. J. Mod. Phys.* **2004**, A19, 4431.
30. Cyburt, R. H.; Fields, B. D.; Olive, K. A. *Astropart. Phys.* **2002**, 17, 87.
31. Linsky, J. L. ; et al. *Astrophys. J.* **2006**, 647, 1106.
32. Clayton, D. D. *Astrophys. J.* **1985**, 290, 428.

33. Fields B. D. *Astrophys. J.* **1996**, 456, 678.
34. Burles, S.; Tytler, D. *Astrophys. J.* **1998**, 499, 699.
35. Burles, S.; Tytler D. *Astrophys. J.* **1998**, 507, 732.
36. O'Meara, J. M.; Tytler, D.; Kirkman, D.; Suzuki, N.; Prochaska, J. X.; Lubin, D.; Wolfe, A. M. *Astrophys. J.* **2001**, 552, 718.
37. Kirkman, D.; Tytler, D.; Suzuki, N.; O'Meara, J. M.; Lubin, D. *Astrophys. J. Supp.* **2003**, 149, 1.
38. Pettini, M.; Bowen, D. V. *Astrophys. J.* **2001**, 560, 41.
39. O'Meara, J. M.; Burles, S.; Prochaska, J. X.; Prochter, G. E.; Bernstein, R. A.; Burgess, K. M. *Astrophys. J.* **2006**, 649, L61.
40. Kirkman, D.; Tytler, D.; Burles, S.; Lubin, D.; O'Meara, J. M. *Astrophys. J.* **1999**, 529, 655.
41. D'Odorico, S.; Dessauges-Zavadsky, M.; Molaro, P. *A.A.*, **2001**, 368, L21
42. Crighton, N.H.; Webb, J.K.; Ortiz-Gill, A.; Fernandez-Soto, A. *Mon. Not. Roy. Astron. Soc.* **2004**, 355, 1042.
43. Izotov, Y. I.; Thuan, T. X.; Lipovetsky, V. A. *Astrophys. J.* **1994**, 435, 647.
44. Izotov, Y. I.; Thuan, T. X.; Lipovetsky, V. A. *Astrophys. J. Supp.* **1997**, 108, 1.
45. Izotov, Y. I.; Thuan, T. X. *Astrophys. J.* **1998**, 500, 188.
46. Olive, K. A.; Steigman, G. *Astrophys. J. Suppl.* **1995**, 97, 49.
47. Olive, K. A.; Skillman, E. D.; Steigman, G. *Astrophys. J.* **1997**, 483, 788.
48. Izotov, Y. I.; Thuan, T. X. *Astrophys. J.* **2004**, 602, 200.
49. Olive, K. A.; Skillman, E. D. *New Astron.* **2001**, 6, 119.
50. Olive, K. A.; Skillman, E. D. *Astrophys. J.* **2004**, 617, 9.
51. Peimbert, M.; Peimbert, A.; Ruiz, M.T. *Astrophys. J.* **2000**, 541, 688.
52. Peimbert, A.; Peimbert, M.; Luridiana, V. *Astrophys. J.* **2002**, 565, 668.
53. Spite, F.; Spite, M. *Astron. Astrophys.* **1982**, 115, 357.
54. Molaro, P.; Primas, F.; Bonifacio, P. *Astron. Astrophys.* **1995**, 295, L47.
55. Bonifacio, P.; Molaro, P. *MNRAS* **1997**, 285, 847.
56. Ryan, S. G.; Norris, J. E.; Beers, T. C. *Astrophys. J.* **1999**, 523, 654.
57. Fields, B. D.; Olive, K. A. *New Astronomy*, **1999**, 4, 255.
58. Vangioni-Flam, E.; Cass'è, M.; Cayrel, R.; Audouze, J.; Spite, M.; Spite, F. *New Astronomy*, **1999**, 4, 245.
59. Ryan, S. G.; Beers, T. C.; Olive, K. A.; Fields, B. D.; Norris, J. E. *Astrophys. J. Lett.* **2000**, 530, L57.
60. Fields, B. D.; Olive, K. A. *Astrophys. J.* **1999**, 516, 797.
61. Bonifacio, P. ; et al. *Astron. Astrophys.* **2002**, 390, 91.
62. Pasquini, L ; Molaro, P. *Astron. Astrophys.* **1996**, 307, 761.
63. Thevenin, F. ; et al. *Astron. Astrophys.* **2001**, 373, 905.
64. Bonifacio, P. *Astron. Astrophys.* **2002**, 395, 515.
65. Deliyannis, C. P.; Demarque, P.; Kawaler, S.D. *Astrophys. J. Supp.* **1990**, 73, 21.
66. Vauclair, S.; Charbonnel, C. *Astrophys. J.* **1998**, 502, 372.

67. Pinsonneault, M. H.; Walker, T. P.; Steigman, G.; Narayanan, V. K. *Astrophys. J.* **1998**, *527*, 180.
68. Pinsonneault, M. H.; Steigman, G.; Walker, T. P.; Narayanan, V. K. *Astrophys. J.* **2002**, *574*, 398.
69. Korn, A. J.; et al., *Nature* **2006**, *442*, 657.
70. Melendez, J.; Ramirez, I. *Astrophys. J.* **2004**, *615*, L33.
71. Fields, B. D.; Olive, K. A.; Vangioni-Flam, E. *Astrophys. J.* **2005**, *623*, 1083.
72. Coc, A.; Vangioni-Flam, E.; Descouvemont, P.; Adahchour, A.; Angulo, C. *Astrophys. J.* **2004**, *600*, 544.
73. Angulo, C.; et al. *Astrophys. J.* **2005**, *630*, 105.
74. Cyburt, R. H.; Fields, B. D.; Olive, K. A. *Phys. Rev. D* **2004**, *69*, 123519.
75. Bahcall, J. N.; Pinsonneault, M. H.; Basu, S. *Astrophys. J.* **2001**, *555*, 990.
76. Ahmed, S. N.; et al. [SNO Collaboration] *Phys. Rev. Lett.* **2004**, *92*, 181301.
77. Smith, V. V.; Lambert, D. L.; Nissen, P. E. *Astrophys. J.* **1993**, *408*, 262.
78. Smith, V. V.; Lambert, D. L.; Nissen, P. E. *Astrophys. J.* **1998**, *506*, 405.
79. Hobbs, L. M.; Thorburn, J. A. *Astrophys. J. Lett.*, **1994**, *428*, L25.
80. Hobbs, L. M.; Thorburn, J. A. *Astrophys. J.* **1997**, *491*, 772.
81. Cayrel, R.; Spite, M.; Spite, F.; Vangioni-Flam, F. Cass' e, M.; Audouze, J. *Astron. Astrophys.* **1999**, *343*, 923.
82. Asplund, M.; Lambert, D. L.; Nissen, P. E.; Primas, F.; Smith, V. V. *Astrophys. J.* **2006**, *644*, 229.
83. Thomas, D.; Schramm, D. N.; Olive, K. A.; Fields, B. D. *Astrophys. J.* **1993**, *406*, 569.
84. Steigman, G.; Fields, B. D.; Olive, K. A.; Schramm, D. N.; Walker, T. P. *Astrophys. J.* **1993**, *415*, L35.
85. Fields, B. D.; Olive, K. A. *New Astronomy*, **1999**, *4*, 255.
86. Vangioni-Flam, E.; Casse, M.; Cayrel, R.; Audouze, J.; Spite, M.; Spite, F. *New Astronomy*, **1999**, *4*, 245.
87. Rollinde, E.; Vangioni-Flam, E.; Olive, K. A. *Astrophys. J.* **2005**, *627*, 666.
88. Rollinde, E.; Vangioni-Flam, E.; Olive, K. A. *Astrophys. J.* **2006**, *651*, 658.
89. Feng, J. L.; Rajaraman, A.; Takayama, F. *Phys. Rev. D* **2003**, *68*, 063504.
90. Feng, J. L.; Rajaraman, A.; Takayama, F. *Phys. Rev. D* **2004**, *70*, 063514.
91. Feng, J. L.; Rajaraman, A.; Takayama, F. *Phys. Rev. D* **2004**, *70*, 075019.
92. Ellis, J. R.; Olive, K. A.; Santoso, Y.; Spanos, V. C. *Phys. Lett. B* **2004**, *588*, 7.
93. Ellis, J. R.; Olive, K. A.; Vangioni, E. *Phys. Lett. B* **2005**, *619*, 30.
94. Jedamzik, K.; Choi, K. Y.; Roszkowski, L.; Ruiz de Austri, R. arXiv:hep-ph/0512044.
95. Jedamzik, K. *Phys. Rev. Lett.* **2000**, *84*, 3248.
96. Jedamzik, K. *Phys. Rev. D* **2004**, *70*, 063524.
97. Jedamzik, K. *Phys. Rev. D* **2004**, *70*, 083510.

98. Steffen, F. D. *JCAP* **2006**, *0609*, 001.
99. Balser, D.S.; Bania, T.M.; Rood, R.T.; Wilson, T.L. *Astrophys. J.* **1999**, *510*, 759.
100. Olive, K. A.; Schramm, D. N.; Scully, S. T.; Truran, J. W. *Astrophys. J.* **1997**, *479*, 752.
101. Eggleton, P. P.; Dearborn, D.S.P.; Lattanzio, J. C. arXiv:astro-ph/0611039.
102. Bania, T. M.; Rood, R. T.; Balser, D. S. *Nature* **2002**, *415*, 54.
103. Vangioni-Flam, E.; Olive, K. A.; Fields, B. D.; Casse, M. *Astrophys. J.* **2003**, *585*, 611.
104. Cyburt, R. H.; Fields, B. D.; Olive, K. A.; Skillman, E. *Astropart. Phys.* **2005**, *23*, 313.

Chapter 3

Origin of the Elements: Nucleosynthesis in Stars

Bradley S. Meyer

**Department of Physics and Astronomy, Clemson University,
Clemson, SC 29634-0978**

Over the 13.7 billion years since the Big Bang, stars have burned nuclear fuel to maintain pressure support against gravitational contraction. In doing so, they have converted the hydrogen and helium left over from the Universe's earliest moments into the heavier elements that make nearly all of chemistry possible. This paper briefly reviews the evolution of stars, the mainline stages of stellar burning, and the side reactions that make Nature's heaviest elements.

Introduction

As reviewed in the previous chapter, our Universe has been expanding since its birth 13.7 billion years ago. As it has expanded, it has cooled from unimaginably high temperatures in its initial moments to a mere 2.7 Kelvins above absolute zero today. In the first minutes and hours of this cooling, free neutrons and protons assembled into ${}^4\text{He}$ along with small amounts of ${}^2\text{H}$, ${}^3\text{He}$, ${}^6,7\text{Li}$, and negligible amounts of other isotopes. After a few hours, however, the universal temperature and density had dropped too low for further nuclear reactions to occur. The remaining 280 naturally-occurring isotopes in our Solar System had to be synthesized almost entirely in the fiery interiors of stars.

Figure 1 illustrates the relative production of elements from the Big Bang and from stars. Shown is the fractional abundance of each naturally-occurring element in the Solar System compared to the corresponding fractional abundance arising from a Big Bang nucleosynthesis calculation. Since the composition of our Solar System is the result of element formation by generations of stars, stellar nucleosynthesis has clearly produced the elements ranging from carbon, nitrogen, and oxygen up to lead, bismuth, and the long-lived actinides thorium and uranium.

While stars have created most of Nature's chemical elements, it is worth putting this accomplishment in perspective. Stars have burned for about 13 billion years, yet they have only succeeded in converting two percent of the mass of hydrogen and helium arising from the Big Bang into heavier nuclei. Of this mass of heavier species, roughly one percent is oxygen. The remaining carbon, nitrogen, phosphorous, calcium, iron (and all the other elements) make up about one percent of the mass of our Galaxy. On a cosmic scale, the elements so necessary for chemistry and for life are mere sprinklings of dust. It is the purpose of this chapter to review how stars have produced this small but crucial amount of "dust", of which, in Hamlet's eyes, we are the quintessence.

The Fuel of Stars

Stars shine. That distinguishing quality makes much of astronomy possible. It also means that stars must have finite lifetimes because they must tap some energy source to radiate away. Throughout nearly its entire life, a star is in hydrostatic equilibrium, which means it has found an internal balance between the two key forces at play in its interior: gravity and pressure. Gravity pulls all parts of the star towards the center. Pressure pushes in all directions, but, since the pressure in a star decreases with increasing distance from the star's core, it tends to push stellar layers outward. When gravity dominates, stars contract. This causes the pressure to rise, which counters further contraction. When the

outward pressure gradient dominates, stellar layers expand. This decreases the pressure, which stops further expansion. When a star shines, it loses energy from its interior. This generally lessens the pressure and leads to contraction. Without a way of replenishing the energy lost, stars cannot live more than several tens of millions of years.

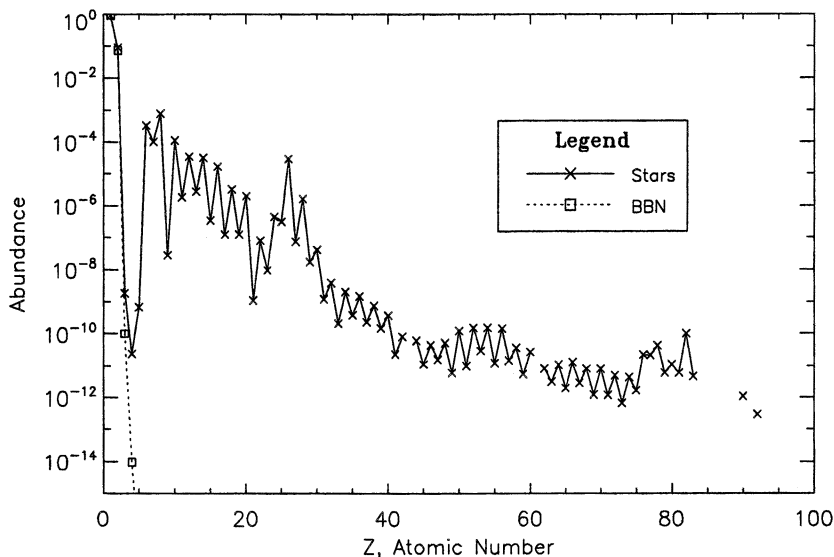


Figure 1. The fractional abundance of the elements in the Solar System from the Anders and Grevesse compilation (1) compared to that from a Big Bang nucleosynthesis calculation run with the Clemson University nucleosynthesis code (2).

To understand this point, it helps to imagine a hydrogen atom. Since a hydrogen atom is bound, its total energy is negative. This means one must put energy (at least 13.6 eV) into the atom to unbind it. On the other hand, if a proton captures an electron to become an atom, the atom must release 13.6 eV of binding energy, which it does by radiating away photons. Astronomers in the nineteenth century believed that the Sun's light arises similarly. In particular, the Sun is slowly contracting. To do so, it must radiate away gravitational binding energy, which is the light we see.

This was an accepted explanation for the source of the Sun's light until it was realized that this mechanism could only explain the Sun's luminosity for about 10 million years. Such a short timescale soon conflicted with mounting geological evidence for an Earth that was billions of years old. Some other

source of energy was needed that could last for such long times, and that source was the binding energy released in nuclear fusion reactions.

Nuclear fusion occurs when two or three light nuclei join together to make a heavier nucleus. For the reaction to succeed the heavier nucleus must be more bound than the fusing nuclei; thus, the reaction must release nuclear binding energy. Significantly, the binding energy released in nuclear reactions is millions of times greater than that released in chemical reactions. This means that relatively few nuclear fusion reactions are required to replenish the energy radiated away from a star's surface and thereby maintain the star's pressure.

How much energy is available in nuclear binding energy to fuel burning in stars? Because the hydrogen nucleus (mass number $A=1$) is not bound to any other nucleon, its nuclear binding energy is zero. The nuclear binding energy rises steeply to about 7 MeV per nucleon for ${}^4\text{He}$ and reaches a peak at 8.8 MeV per nucleon for ${}^{62}\text{Ni}$ before declining for larger mass nuclear species. The first stage of nuclear burning is to convert four hydrogen nuclei into one helium nucleus. This releases 7 MeV per hydrogen atom, which is about 10^{-12} J. The luminosity of the Sun is 4×10^{26} J/s, so the Sun is fusing an astonishing 4×10^{38} hydrogen nuclei every second. This is about 700,000,000 tons of hydrogen per second. Despite this large burn rate, the Sun has about 10^{57} hydrogen nuclei, so it has enough fuel for a life of more than 10 billion years!

We now know that as a star forms, it contracts from a loosely bound gas cloud. As the density of the star increases, its energy becomes increasingly negative, and this binding energy must be released. This is the star's initial collapse phase. However, once it attains central temperatures that allow it to fuse nuclei, it is no longer radiation of gravitational binding energy but rather nuclear binding energy that provides the star's luminosity. The nuclear fuel is sufficiently abundant to power the star for millions or billions of years.

The Mainline Stages of Stellar Burning and Their Products

Nuclear burning proceeds until the fuel is consumed and the pressure support can no longer be maintained. At this point, the star must contract. This causes the temperature to rise again until the ashes of the previous burning phase ignite. Stellar evolution is thus, in essence, a sequence of burning stages in which the ashes of one stage serve as the fuel for the next. We review these stages and their principal products.

Hydrogen Burning

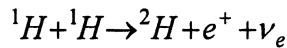
In the Hertzsprung-Russell Diagram, a graph of the luminosity of a star versus its surface temperature, most stars lie along a band known as the main

sequence. These stars, which include the Sun, are undergoing hydrogen burning, which is the first and longest hydrostatic burning stage in a star's life. There are two reasons why hydrogen burning is the first hydrostatic stellar burning stage. First, hydrogen is the most abundant matter in the cloud from which the star formed. Second, since hydrogen has charge unity, the fusion of two hydrogen nuclei has a relatively small Coulomb repulsion to overcome. This means that the burning can occur at the relatively low temperatures of roughly 10 to 30 million Kelvins.

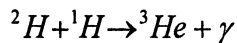
Hydrogen burning occurs in two key reaction sequences, the PP (or proton-proton) chains and the CNO (Carbon-Nitrogen-Oxygen) bi-cycle. Both sequences were first understood by Hans Bethe and his collaborators in the 1930s, for which work Bethe won the Nobel Prize in 1967 (3).

The PP Chains

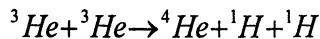
The PP chains dominate in stars with total mass about 1.2 times the mass of the Sun and lower. All PP reaction chains begin with the pp reaction:



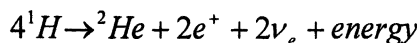
In this reaction, the e^+ is a positron and the ν_e is an electron-type neutrino. Significantly, this reaction depends on the weak force since it requires one of the two reacting protons to convert into a neutron in the brief moment the two protons are in close contact. This is rare, so the vast majority of proton-proton scatterings in a star do not result in deuterium production. The deuterium, that is, the ${}^2\text{H}$, produced by the pp reaction quickly captures a proton to become ${}^3\text{He}$:



where the γ represents the photon that carries away the binding energy of the ${}^3\text{He}$ and deposits it locally in the star. The next reaction steps distinguish the PPI, PPII, and PPIII reaction chains. The PPI chain closes when two ${}^3\text{He}$ nuclei interact to form ${}^4\text{He}$:

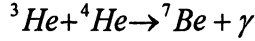


Because two ${}^3\text{He}$ are needed for this final reaction, the effective PPI reaction sequence is thus

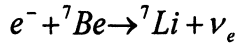


This reaction sequence liberates 7 MeV per reacting ${}^1\text{H}$. Roughly 0.3 MeV per reacting ${}^1\text{H}$ goes into the neutrinos, which immediately escape from the star because their interaction with the overlying material is so weak. The remaining 6.7 MeV per ${}^1\text{H}$ is deposited locally to maintain the star's pressure support.

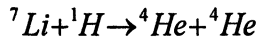
The PPII reaction chain occurs when ${}^3\text{He}$ produced in the first two PP reactions captures ${}^4\text{He}$:



The ${}^7\text{Be}$ then captures an electron from the plasma to become ${}^7\text{Li}$:

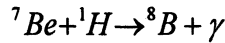


Finally, the ${}^7\text{Li}$ captures a proton to become two ${}^4\text{He}$:

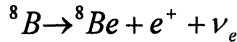


Again the effective reaction is four protons fuse to become one ${}^4\text{He}$ nucleus. The neutrino from electron capture on ${}^7\text{Be}$ carries away somewhat more energy than the PPI neutrinos, so the local energy deposition from PPII is slightly less than that in PPI.

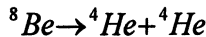
The final reaction chain is PPIII. In this chain, ${}^7\text{Be}$ produced by the ${}^3\text{He} + {}^4\text{He}$ reaction captures a proton to become ${}^8\text{B}$:



The ${}^8\text{B}$ then decays to ${}^8\text{Be}$ by positron emission:



Finally, ${}^8\text{Be}$ is unstable and decays to ${}^4\text{He}$:



Again the effective reaction sequence is four ${}^1\text{H}$ reacting to form ${}^4\text{He}$. As with PPII, the neutrino from ${}^8\text{B}$ decay has high energy, so the total local energy deposition from this reaction chain is slightly less than that in PPI.

In the Sun, the PPI, PPII, and PPIII reaction chains account for roughly 86%, 14%, and 0.11% of the nuclear energy generated, respectively. The proportions are dependent on the temperature, however. The central

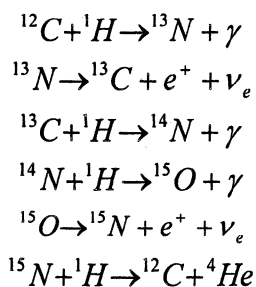
temperature of the Sun is about 15 million Kelvins. As the temperature increases above 15 million Kelvins, the PPII chain becomes more important, while above about 23 million Kelvins, the PPIII chain dominates.

Because neutrinos emitted by PP reactions provide insight into processes occurring in the Solar core, experimenters have carried out numerous campaigns to detect these elusive particles. Those experiments have shown that neutrinos are indeed produced by PP reactions in the Sun, as expected, but that some of these electron-type neutrinos convert into mu-type and tau-type neutrinos on their way to Earth (4). Such neutrino conversion lies outside the Standard Model of Particle Physics; thus, Earth-based neutrino detectors have not only provided stunning confirmation of the astrophysics of stars but also invaluable insights into the nature of fundamental particles (e.g., 5).

The CNO Bi-Cycle

The other reaction sequence giving rise to hydrogen burning in stars is the CNO bi-cycle. Because the cycles involve capture of protons by elements with charge six or larger, the Coulomb repulsion is greater than in the PP chains. This means that the CNO reactions require relatively high temperature so that the kinetic energy of the reactants can overcome this repulsion. Since higher mass stars require higher central pressures to support their high overlying weight, the CNO reactions become the dominant energy producers for stars more massive than about 1.2 times the mass of the Sun. For example, about 1.7% of the energy generated in the Sun comes from CNO reactions. For a star of roughly 1.5 solar masses or more, however, the energy generation is completely dominated by the CNO bi-cycle.

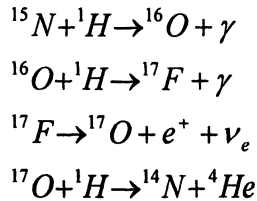
In CNO burning, the synthesis of ${}^4\text{He}$ is catalyzed by pre-existing isotopes of carbon, nitrogen, and oxygen, which were present in the star's starting composition. The CNO bi-cycle consists of two cycles operating simultaneously. In the CN cycle, the reaction sequence is the following:



This sequence is clearly a cycle since the last reaction restores the initial ${}^{12}\text{C}$.

The role of the C and N isotopes, then, is simply to catalyze the fusion of four protons into one ${}^4\text{He}$ plus two neutrinos and two positrons. Because the slow reaction in the CN cycle is the capture of a proton by ${}^{14}\text{N}$, the CN cycle tends to concentrate most C and N isotopes into this isotope. ${}^{14}\text{N}$ is, along with ${}^4\text{He}$, one of the principal products of hydrogen burning.

In some cases, ${}^{15}\text{N}$ arising in the CN cycle captures a proton to become ${}^{16}\text{O}$. This sets off the ON cycle:

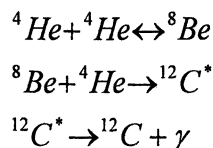


In the Sun, the ON cycle occurs about 25 times less frequently than the CN cycle, but this proportion varies with stellar temperature. It is also worth noting that when matter just starts to burn hydrogen in the ON cycle, the relative slowness of the ${}^{17}\text{O} + {}^1\text{H}$ reaction causes abundant ${}^{16}\text{O}$ to shift into ${}^{17}\text{O}$; thus, an enrichment of ${}^{17}\text{O}$ in the atmosphere of a star is a useful signature of dredge up by convective mixing of material that experienced partial hydrogen burning from the inner part of the star to the star's surface.

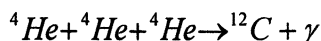
Helium Burning

Once a star has exhausted its hydrogen fuel, it contracts until the temperature rises to about 100 to 300 million Kelvins. At this point, reactions among ${}^4\text{He}$ nuclei can occur. This replenishes the pressure support, halts the contraction, and commences the helium burning stage of the star's life.

A crucial aspect of helium burning is that there is no stable mass eight isotope. This means when two ${}^4\text{He}$ nuclei combine to form a ${}^8\text{Be}$ nucleus, the ${}^8\text{Be}$ falls apart quickly into the two ${}^4\text{He}$ reactants. The consequence is that helium burning must proceed by a three-body reaction. In particular, if the ${}^8\text{Be}$ nucleus interacts with another ${}^4\text{He}$ before falling apart, an excited state of ${}^{12}\text{C}$, denoted ${}^{12}\text{C}^*$, may result. Decay of the excited ${}^{12}\text{C}^*$ nucleus to its ground state then finishes the so-called triple-alpha reaction. The reaction sequence is thus



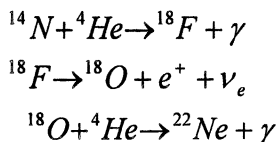
which effectively is the reaction



The two-stage nature of the triple-alpha reaction was recognized by Salpeter in the 1950s. Nevertheless, shortly after Salpeter's insight, Sir Fred Hoyle recognized the triple-alpha reaction would be too slow to explain the abundances of the heavy elements unless the reaction ${}^8\text{Be} + {}^4\text{He}$ occurred resonantly in stars. Hoyle pointed out that this required a 0^+ excited state (that is, a state with spin zero and positive parity) in ${}^{12}\text{C}$ at 7.6 MeV, and Cook, Fowler, and collaborators demonstrated the existence of this state experimentally (6). The prediction of the 7.6 MeV resonance and its subsequent experimental confirmation ranks as one of the great stories of modern science.

Once produced, ${}^{12}\text{C}$ can capture another ${}^4\text{He}$ to become ${}^{16}\text{O}$. The ${}^{16}\text{O}$ could capture another ${}^4\text{He}$ to produce ${}^{20}\text{Ne}$ except that the excited state of ${}^{20}\text{Ne}$ into which this would occur has the wrong parity and is thus invisible. This means that ${}^{16}\text{O}$ is the end point of helium burning and is, in fact the dominant product. Calculations show that the C/O ratio at the end of helium burning is typically 0.2, depending in large measure on the still uncertain ${}^{12}\text{C} + {}^4\text{He}$ reaction rate. Since the details of the evolution of stars after helium burning strongly depend on the C/O ratio after helium burning, there is an intense experimental effort to pin down the ${}^{12}\text{C} + {}^4\text{He}$ reaction rate.

The principal products of helium burning are thus ${}^{16}\text{O}$ and ${}^{12}\text{C}$. That these are the third and fourth most abundant isotopes in the Solar System (after ${}^1\text{H}$ and ${}^4\text{He}$) shows that helium burning is a significant player in the formation of the elements. Other key products of helium burning are ${}^{18}\text{O}$ and ${}^{22}\text{Ne}$ produced from ${}^{14}\text{N}$ left over from hydrogen burning:



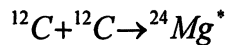
Also produced in helium burning are the s-process elements (see below).

Carbon Burning

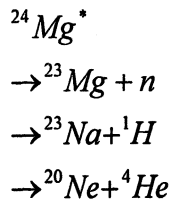
After helium is exhausted, the core of a star is composed mostly of carbon and oxygen, the principal products of helium burning. The star contracts again and the temperature and density rise. Carbon burning commences when the

temperature reaches about 600 million Kelvins. For stars with mass less than about eight times the mass of the Sun, however, electron degeneracy pressure becomes the dominant form of pressure before the carbon ignites. This halts the contraction. Thermal instabilities in helium burning shells outside the core expel the outer layers to produce a planetary nebula. The carbon/oxygen core is left behind as a white dwarf star, an object with a mass near that of the Sun but with the size of the Earth. This stellar cinder will slowly radiate its thermal energy over a long period of time and leave a cold, inert stellar remnant floating in the Galaxy.

For stars more massive than eight times the mass of the Sun, carbon ignites before degeneracy pressure becomes dominant. The key carbon burning reaction is



where $^{24}\text{Mg}^*$ is an excited state of ^{24}Mg . The excited state predominantly decays by one of three modes:

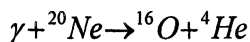


Much of the ^{23}Na and ^{23}Ne thus produced immediately capture light particles to become ^{24}Mg , so the principal products of carbon burning are ^{20}Ne , ^{23}Na , and ^{24}Mg . The ^{20}Ne channel is the dominant one, so this isotope is the leading product of carbon burning. The protons and alpha particles released during carbon burning can capture onto other particles leading to further nucleosynthesis, but these are side reactions in regards to energy generation.

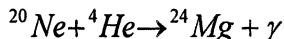
Neon Burning

A star with mass between about eight and ten times the mass of the Sun completes carbon burning but becomes degenerate before the next burning stage, neon burning, can occur. The fate of such a star, after it has expelled its outer layers in the planetary nebula phase, is to leave behind its core as an O/Ne/Mg white dwarf star. For stars more massive than ten times the mass of our Sun, however, contraction after carbon burning leads to neon burning, which commences at a temperature of about 1.2 billion Kelvins. Neon burning is a

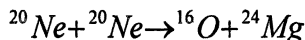
two-step process. The first step is the disintegration of one of the ^{20}Ne nuclei produced during the previous carbon burning



This reaction is endothermic, that is, it requires more energy than it releases; however, the ${}^4\text{He}$ so produced captures onto another ^{20}Ne to produce ^{24}Mg :



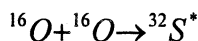
This second step releases more energy than the first consumes so that the effective reaction



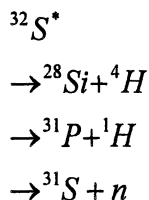
is exothermic and can deposit energy locally to maintain the pressure support. Neon burning produces ^{24}Mg and enhances the ^{16}O left over from the previous helium burning stage. Again, other side reactions occur during neon burning and alter the abundances of heavier species.

Oxygen Burning

The penultimate nuclear burning stage in the life of a star with mass more than ten times as large as our Sun is oxygen burning. The fuel is the ^{16}O primarily produced during helium burning. That ^{16}O has simply been a non-participating observer of the subsequent carbon and neon burning, although neon burning boosted the ^{16}O abundance about 10%. Oxygen ignites once the core contracts and the temperature rises to about 1.7 billion Kelvins. The key reaction is analogous to that in carbon burning:



where ${}^{32}\text{S}^*$ is an excited state of sulfur-32. The ${}^{32}\text{S}^*$ then decays by one of three channels:



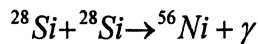
The ^{31}S decays quickly to ^{31}P , and most ^{31}P quickly captures light particles to become ^{32}S ; therefore, the key products of oxygen burning are ^{28}Si and ^{32}S .

It is significant that, at the conditions of oxygen burning, other reactions start to become sufficiently rapid that small clusters of isotopes with masses greater than that of silicon start to come into equilibrium under exchange of light particles (neutrons, protons, and alphas). This is the start of quasi-equilibrium nucleosynthesis that is even more pronounced in the next burning stage.

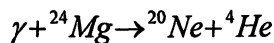
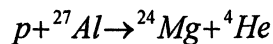
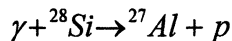
Silicon Burning

The final burning stage in a massive star is silicon burning, which occurs when the stellar core contracts and the temperature exceeds 2 billion Kelvins. The fuel for this stage is the ^{28}Si and ^{32}S produced in oxygen burning. These two species have equal numbers of neutrons and protons and are well bound with binding energies per nucleon of 8.45 MeV and 8.49 MeV, respectively. The nuclear species with the highest binding energy per nucleon with equal number of neutrons and protons is ^{56}Ni , with a value of 8.64 MeV. Silicon burning is thus the last gasp effort of the star to extract the last few tenths of an MeV of nuclear binding energy from the available fuel and prevent stellar collapse.

The effective reaction would be



However, the large Coulomb repulsion prevents this reaction from occurring directly. Instead what happens is that ^{28}Si begins to disintegrate via reactions such as



The disintegration can flow all the way to the point that a ^{28}Si is completely disintegrated into neutrons, protons, and alpha particles. Those light particles allow the remaining ^{28}Si to capture enough light particles to become ^{56}Ni . Roughly speaking, then, one ^{28}Si completely disintegrates and its constituents capture onto another ^{28}Si to produce ^{56}Ni . In fact the reaction flows are much more complicated with forward reaction flows (which increase the nuclear mass) competing with rapid disintegration flows (which decrease the nuclear mass). Many reactions become so rapid that the nuclear populations approach a full

equilibrium under exchange of light particles. In this sense, the nuclear dynamics is that of a “Darwinian” equilibrium in which nuclear species compete for abundance. Their “fitness” is their nuclear binding, and it is thus evident that the most bound nuclear species, the iron-group isotopes, are the winners.

Silicon burning predominantly produces isotopes from silicon to nickel. The so-called “alpha” isotopes, ones like ^{28}Si , ^{32}S , ^{36}Cl , and ^{40}Ca that can be thought of as made up of some number of ^4He nuclei, are relatively well bound and are, consequently, abundantly produced. Other key species are made as daughters of radioactive alpha-nucleus progenitors: ^{44}Ca (made as ^{44}Ti), ^{48}Ti (made as ^{48}Cr), and ^{52}Cr (made as ^{52}Fe). The primary product of silicon burning, however, is ^{56}Fe (made as ^{56}Ni). The importance of silicon burning is evident from Figure 1, which shows that ^{56}Fe and its immediate neighbors buck the trend of declining abundance with increasing element number. It is also apparent from the fact that ^{56}Fe is the sixth most abundant isotope by mass in the Solar System, beaten only by ^1H , ^4He , ^{16}O , ^{12}C , and ^{20}Ne !

Stellar Burning Lifetimes

To appreciate the lifetimes of stars, one needs to follow models of their evolution. Figure 2 illustrates the evolution of the temperature and density in the core of a model of a star 25 times the mass of our Sun. The labels H, He, C, Ne, and O in the figure indicate the conditions at which the H, He, C, Ne, and O burning phases start (Si burning was not followed in this model). Of course, each burning phase is shorter in duration than the previous one, and evolution occurs as the fuel for the previous phase is exhausted. In this stellar evolution model, hydrogen burning lasts about six million years, and the central temperature and density remain fairly constant during this epoch. The central temperature starts at about 32 million Kelvins at the beginning of core hydrogen burning and ends at about 55 million Kelvins while the central density begins at about 2.6 grams per cubic centimeter and ends at about 12 grams per cc. Once the central hydrogen is exhausted, the core contracts and heats to about 140 million Kelvins and a density of about 400 grams per cubic centimeter. At this point central helium burning ignites and lasts about 750,000 years. Following the core helium burning, the star contracts until core carbon burning begins at about 630 million Kelvins and a density of 45,000 grams per cubic centimeter.

In the model shown in Figure 2, core carbon burning lasts about 1,200 years. It is followed by core neon burning which commences at a temperature of about 1.3 billion Kelvins and a density of 2 million grams per cubic centimeter. Core neon burning lasts only a few years. Core oxygen burning in the model begins at a temperature near 1.7 billion Kelvins and a density of about 3 million grams per cc. This phase lasts less than a year. It is followed by silicon burning, at temperatures near 2-3 billion Kelvins and densities in excess of 200 million

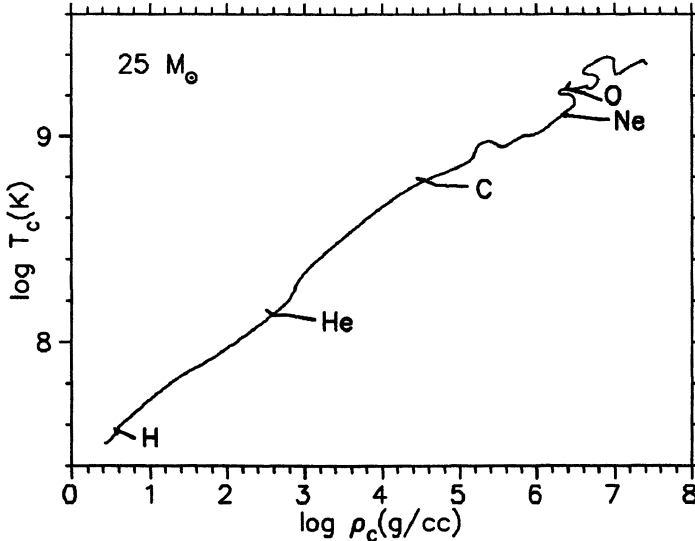


Figure 2. The base ten logarithm of the central temperature in Kelvins as a function of the base ten logarithm of the central density in grams per cubic centimeter in a model of the evolution of a star with mass twenty-five times greater than that of our Sun (7). The labels H, He, C, Ne, and O indicate the ignition of those burning phases in the star's life.

grams per cc. The silicon burning phase constitutes the last few days of the star's life.

It is worth noting that, following a core burning phase, a shell burning phase can follow in material outside the core. For example, after core hydrogen burning, a hydrogen burning shell can ignite in the hydrogen-rich layers surrounding the hydrogen-depleted core. Similarly, a helium burning shell can surround a carbon burning core. Core and shell burning both provide energy via release of nuclear binding energy and thereby support the star against gravitational contraction. Shell burning is ignited and extinguished in a complicated dance with core burning, and the final structure of the nuclear abundances in a star is complex as a result of this fascinating choreography.

It is also essential to note that stars of differing mass have different thermodynamic trajectories and therefore different lifetimes from that of the star described above. Stars more massive than 25 solar masses achieve even higher core temperatures, shine more brightly, and thus must exhaust their fuel even more rapidly than the model star discussed above. For example, a star with mass greater than 50 times the mass of our Sun will live for less than a million years! Stars less massive than 25 solar masses but still more than 10 solar masses run

through the same evolution sequence as shown in Figure 2 but on a longer timescale because they burn their nuclear fuel at a more modest rate. For example, a 15 solar mass star fuses nuclei into iron in its core but does so slowly enough to live for about 12 million years. Still lower mass stars live even longer times. Our Sun will live a total of 10 billion years (it has already been alive for about 5 billion years, so it is middle aged) while even lower mass stars live tens of billions of years, which is greater than the current age of our Universe!

Explosive Burning

For a massive star, silicon burning is the end point of its stable evolution. Once silicon burning has occurred, the star has no useful nuclear fuel left. At this point the stellar core loses pressure support and collapses. The inner core collapses subsonically until it reaches nuclear matter density. At this point, the nucleons touch and the pressure rises sharply. This halts the collapse, and a neutron star starts to form. Matter from the outer part of the stellar core rains down supersonically, however, and cannot get the signal to stop collapsing before it crashes onto the nascent neutron star. This highly non-adiabatic process generates a shock wave that, after a push from neutrinos escaping the hot baby neutron star, drives its way out through the outer layers and expels them into the interstellar medium. This violent explosion signals the death of the star in what is known as a core-collapse supernova. Only a neutron star or, if enough mass was left behind, a black hole remains.

As the shock wave passes through the outer layers of the star, it heats and compresses them. This causes further nuclear reactions. For example, when the shock passes through the silicon and sulfur-rich zones of the star, it heats them and causes explosive silicon burning. Oxygen-rich layers experience explosive oxygen burning, neon-rich layers experience explosive neon burning, etc. The ejecta from a massive star then enrich the interstellar medium with new elements.

Explosive nucleosynthesis also occurs in novae and thermonuclear supernovae. As reviewed above, stars with mass less than about eight times the mass of the Sun leave behind a carbon/oxygen white dwarf star, while stars with masses between eight to ten solar masses leave an oxygen/neon/magnesium white dwarf. For these objects, electron degeneracy, not thermal, pressure supports them against further contraction, so their evolution was halted before they had tapped all of their nuclear binding energy. Nevertheless, if a white dwarf star is a companion to a normal main-sequence star, it can be born again.

Novae occur when a white dwarf star accretes matter from its companion star. As the mostly hydrogen-rich material settles onto the dense white dwarf, it gets compressed and heated. This matter can then ignite violently, and the resulting outburst can eject small amounts of matter that experienced explosive hydrogen or even helium burning. Since the nova is like a bomb going off on the

surface of the white dwarf, the nova can also eject carbon/oxygen-rich or oxygen/neon/magnesium-rich matter from the underlying compact star. Observations of the chemical composition of nova ejecta can therefore tell us a great deal about the nature of the underlying white dwarf and the temperature and density reached in the nova explosion.

In considering novae, it is important to understand the nature of nuclear burning under degenerate conditions. When matter compressed on the surface of a white dwarf starts burning, the local environment is heated. In normal stars there is a feedback mechanism that prevents a thermal runaway: as the temperature rises, the pressure builds, and the material expands and cools, which counters the temperature rise. In this way, the star can reach a thermal balance. When electron degeneracy pressure dominates the thermal pressure, however, a significant rise in temperature does not lead to a large increase in pressure. Thus, as the burning raises the temperature, the temperature rise increases the burning. This is a runaway that only ceases once the temperature gets so high that the thermal pressure can eventually get large enough to expel matter from the surface of the white dwarf.

A thermonuclear supernova is an even more extreme version of this. If the mass accreted by a white dwarf star becomes sufficiently high, the central pressure and temperature rise to values high enough to ignite carbon burning. This leads to a thermonuclear runaway that is so violent that it disrupts the entire star. The temperatures reached in such events are high enough that the material can get close to nuclear equilibrium; thus, such supernovae are prodigious producers of iron-group elements. Models suggest that, over the course of the Galaxy's history, thermonuclear supernovae made about half of the Solar System's iron. Massive stars made the other half.

Supernova Classification

In discussing supernovae, one frequently encounters the terms Type Ia, Ib, and Ic and Type II supernovae. These are spectroscopic classifications. Type I supernovae do not have hydrogen in their spectra, while Type II do. The subclassification of Type I supernovae denotes whether they have silicon or helium in their spectra. Type Ia supernovae do not have hydrogen or helium in their spectra but do have silicon. Type Ib supernovae do not have hydrogen or silicon in their spectra, but do have helium. Type Ic's show no hydrogen, helium, or silicon in their spectra. The connection to core-collapse or thermonuclear supernovae discussed above is that Type Ia supernovae are probably thermonuclear explosions of white dwarf stars. Type II supernovae are probably core-collapse explosions of massive stars. Type Ib and Ic supernova are probably also core-collapse explosions but of massive stars that have lost

their hydrogen (Ib) or hydrogen and helium (Ic) envelopes via stellar winds prior to the supernova explosion.

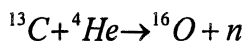
Type II supernovae also have subclassifications depending on their light curves (the optical afterglow from the explosion mostly arising from the decay of radioactive nickel and cobalt produced by explosive burning). Type II-L supernovae show a linear decline in luminosity with time after peak brightness. Type II-P supernova light curves have a plateau phase after peak brightness when the luminosity remains fairly constant in time. The interested reader may wish to consult the review by Filippenko (8) for more details on the classification of supernovae.

The Heaviest Elements

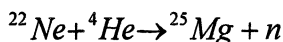
A rearrangement of lighter elements into elements heavier than iron or nickel leads to a decrease in nuclear binding energy per nucleon. This is the reason that iron and nickel are the end points of mainline stellar burning. Nevertheless, heavier elements can be made via side reactions to the mainline burning or in explosive burning when excess free nucleons allow capture beyond iron.

The s Process

The s process is the “slow” process of neutron capture. Slow refers to the fact that the neutron captures are generally slow compared to beta decays, the significance of which is described below. Such nuclear processing typically occurs during helium burning either in the cores of massive stars or the shells of low-mass stars. Carbon burning in massive stars also leads to some s processing. The principal neutron sources for the s process are ^{13}C , from incomplete CNO burning, and ^{22}Ne , which, as mentioned above, is produced in helium burning from abundant ^{14}N . The key reactions are



and



The neutrons thus produced capture on nuclei that the star inherited from its birth cloud. Nuclei capture neutrons until they become unstable to beta decay. Because the neutron density in the s process is low, beta decay typically occurs

before another neutron capture. This means that the s-process flow is always close to the stable isotopes. The neutron capture flow dams up at isotopes with a magic number¹ of neutrons, such as ⁸⁸Sr, ⁸⁹Y, ⁹⁰Zr, ¹³⁸Ba, and ²⁰⁸Pb, since these species have small neutron capture cross sections. These isotopes are all key s-process products.

The neutron fluence in massive stars is such that iron can capture neutrons up to Zr, but not much beyond that. This is the so-called weak component of the s process. In contrast, the region between the hydrogen and helium burning shells in an evolved low-mass star experiences a complex sequence of events that allows iron to capture all the way to Pb and Bi. Because the isotopes of Po are all unstable, however, s-process flow cannot continue to the actinides. This burning in low-mass stars provides what is known as the main component of the s process.

The r Process

The r process is the “rapid” neutron capture process. In this process, the neutron density is so high that neutron captures occur much more rapidly than beta decays. The result is that the isotopes of an element come into equilibrium under exchange of neutrons. Flow to the next element occurs as these isotopes then beta decay. Since the nuclei present are more neutron rich than the stable isotopes, the nuclear flow can reach up to the actinides. The limit on the extent of the flow may be that the heavy nuclei produced simply fission when they get too large.

Where possible, the r-process flow follows the magic neutron numbers. At these points, the nuclei present lie closer to beta stability than elsewhere in the flow. This means that the beta-decay rates decrease, which causes a “traffic jam” in the upward flow in nuclear mass; thus, there is an abundance build up for these nuclei. When the flux of neutrons ceases, the r-process nuclei decay back to stability. Because the r-process flow encounters the magic neutron numbers at nuclear masses less than the s-process flow, the resulting r-process abundance peaks lie lower in nuclear mass than the corresponding s-process peaks.

The source of the neutrons for the r process is not clear, nor, for that matter, is the r process’s astrophysical setting. A leading idea for the r process is that

¹ The magic numbers in nuclear physics are those numbers of neutrons or protons for which a nucleus is particularly strongly bound. The magic numbers are exactly analogous to closed electron shells in atoms. The typical magic numbers in nuclei are 2, 8, 14, 20, 28, 50, 82, 126, and 184, though these depend to some extent on the deformation of the nucleus. ⁴He, ¹⁶O, ²⁸Si, ⁴⁰Ca, ⁵⁶Ni, and ²⁰⁸Pb are strongly bound nuclei because they are doubly magic (that is, magic in both their number of neutrons and protons).

the last gasp material escaping from the nascent neutron star in a core collapse supernova becomes slightly neutron rich due to interactions with neutrinos. At the high temperatures present, the isotopes achieve an abundance equilibrium, but not all neutrons get incorporated into nuclei. As the material expands and cools, the reactions between charged particles cease. This leaves an abundance of nuclei and neutrons. The subsequent *r* processing then makes nuclei up to the actinides. An alternative idea is that neutron stars can occur in binary systems. Through the release of gravitational radiation, these stars eventually spiral into each other. The violent merger process might eject very neutron-rich matter which can then undergo an *r* process.

Whatever the site, we now know from astronomical observations of very old stars in our Galaxy that the *r* process occurred early. In particular, these stars are so old that they formed from Galactic gas that was enriched with matter from only one or a few *r*-process events. Remarkably, for *r*-process nuclei in the nuclear mass range from about $A = 130$ to $A = 195$, the abundance pattern in these stars is almost identical to that inferred in the Solar System, for which millions of *r*-process events have contributed. The rather astonishing implication is that the *r*-process mechanism is robust in the sense that its operation seems to have been fairly constant throughout the history of the Galaxy.

The *p* Process.

Thirty-five heavy isotopes lie on the proton-rich side of beta stability and cannot be made by neutron-capture processes. These are generally rather rare isotopes compared to their *s* and *r*-process counterparts. Their formation process is known as the *p* process, which was originally envisioned as a proton-capture process, hence the name. The leading idea for their production now is the so-called “gamma” process. The idea is that if pre-existing *r* and *s* process nuclei are exposed to high temperature, they will begin to “melt” towards iron. They first start disintegrating neutrons, then protons and alpha particles. If their environment expands and cools before the disintegration flow reaches iron, a distribution of proton-rich nuclei results. These nuclei decay to stability and produce the *p*-process nuclei. This process could occur in the oxygen/neon-rich layers of a massive star as the supernova shock wave passes or in the outer skin of a thermonuclear supernova where the temperature does not get quite high enough to drive all nuclei to iron.

The Next Steps

With the death of its stellar nursery, a newly-born nucleus commences its fascinating journey to our Solar System. It will first capture electrons to become

a neutral atom. It may then get locked up into a molecule or even solid dust grain, in which form it will travel through the medium between the stars until it becomes part of the cloud that formed the Solar System. Along the way, it may cycle back into a newly forming star in which it undergoes new nuclear reactions, changes its chemical identity, and restarts its journey to the Solar System in a new form. The subsequent chapters in this text review the next steps of the chemical journey of the elements begun in stars.

For Further Reading

The science of element formation in stars is a mature field. The first serious considerations date to the 1930s and 1940s (3,9). The 1950s saw the grand synthesis of the key ideas (10-12), while many details were worked out in the 1960s and 1970s (e.g., 13-18). Work continues today, motivated by exotic phenomena like x-ray bursts (e.g., 19), isotopic anomalies in primitive minerals (e.g., 20), and presolar stardust grains in meteorites (e.g., 21). Recently, a more complete understanding of the nuclear dynamics involved in explosive nucleosynthesis has afforded some surprises (e.g., 2).

Many useful reviews of stellar nucleosynthesis exist. Three fairly recent reviews are those by Wallerstein et al. (22), Busso, Gallino, and Wasserburg (23), and Woosley, Heger, and Weaver (24). Textbooks by Clayton (25) and Arnett (26) provide a useful, systematic approach to the topic, and Clayton's Handbook of the Isotopes in the Cosmos (27) is a very nice reference. Finally, it is worth mentioning that many resources are becoming available over the worldwide web. Many of the articles on stellar nucleosynthesis at wikipedia.org are well written and informative. Also, the JINA web site, at <http://www.jinaweb.org>, provides many useful resources for students, educators, and professionals. Finally, the web site <http://www.webnucleo.org>, developed at Clemson University, provides some interactive tools and codes of interest for study of stellar nucleosynthesis.

References

1. Anders, E.; Grevesse, N. Abundances of the elements - Meteoritic and solar. *Geochim. Cosmochim. Acta* **1989**, *53*, 197-214.
2. Jordan, G. C., IV; Meyer, B. S. Nucleosynthesis in Fast Expansions of High-Entropy, Proton-rich Matter. *Astrophys. J. Lett.* **2004**, *617*, 131-134.
3. Bethe, H. A. Energy Production in Stars. *Physical Review* **1939**, *55*, 434-456.

4. Ahmad, Q. R. et al. (The Sudbury Neutrino Observatory Collaboration) Direct Evidence for Neutrino Flavor Transformation from Neutral-Current Interactions in the Sudbury Neutrino Observatory. *Physical Review Letters* **2002**, *89*, 011301-1.
5. Aliani, P.; Antonelli, V.; Ferrari, R.; Picariello, M.; Torrente-Lujan, E. Determination of neutrino mixing parameters after SNO oscillation evidence. *Physical Review D* **2003**, *67*, 013006-1.
6. Cook, C. W.; Fowler, W. A.; Lauritsen, C. C.; Lauritsen, T. B¹², C¹², and the Red Giants. *Physical Review* **1957**, *107*, 508-515.
7. El Eid, M. F.; The, L.-S.; Meyer, B. S. Evolution of Massive Stars Up to the End of Central Oxygen Burning. *Astrophys. J.* **2004**, *611*, 452-465.
8. Filippenko, A. V. Optical Spectra of Supernovae. *Ann. Rev. Astron. Astrophys.* **1997**, *35*, 309-355.
9. Hoyle, F. The Synthesis of the Elements from Hydrogen. *Mon. Not. Roy. Astr. Soc.* **1946**, *106*, 343-383.
10. Hoyle, F. On Nuclear Reactions Occurring in Very Hot STARS.I. the Synthesis of Elements from Carbon to Nickel **1954**, *1*, 121-146.
11. Burbidge, E. M.; Burbidge, G. R.; Fowler, W. A.; Hoyle, F. Synthesis of the Elements in Stars. *Rev. Mod. Phys.* **1957**, *29*, 547-650.
12. Cameron, A. G. W. Nuclear Reactions in Stars and Nucleogenesis. *Pub. Astr. Soc. Pac.* **1957**, *69*, 201-222.
13. Hoyle, F.; Fowler, W. A. Nucleosynthesis in Supernovae. *Astrophys. J.* **1960**, *132*, 565-590.
14. Clayton, D. D.; Fowler, W. A.; Hull, T. E.; Zimmerman, B. A. Neutron Capture Chains in Heavy Element Synthesis. *Ann. Phys.* **1961**, *12*, 331-408.
15. Seeger, P. A.; Fowler, W. A.; Clayton, D. D. Nucleosynthesis of Heavy Elements by Neutron Capture. *Astrophys. J.* **1965**, *11*, 121-166.
16. Bodansky, D.; Clayton, D. D.; Fowler, W. A. Nuclear Quasiequilibrium During Silicon Burning. *Astrophys. J. Suppl.* **1968**, *16*, 299-371.
17. Howard, W. M.; Arnett, W. D.; Clayton, D. D.; Woosley, S. E. Nucleosynthesis of Rare Nuclei from Seed Nuclei in Explosive Carbon Burning. *Astrophys. J.* **1972**, *175*, 201-216.
18. Woosley, S. E.; Arnett, W. D.; Clayton, D. D.; The Explosive Burning of Oxygen and Silicon. *Astrophys. J. Suppl.* **1973**, *26*, 231-312.
19. Woosley, S. E. et al.; Models for Type I X-Ray Bursts with Improved Nuclear Physics. *Astrophys. J. Suppl.* **2004**, *151*, 75-102.
20. Meyer, B. S.; Krishnan, T. D.; Clayton, D. D. Theory of Quasi-Equilibrium Nucleosynthesis and Applications to Matter Expanding from High Temperature and Density. *Astrophys. J.* **1998**, *498*, 808-830.
21. Meyer, B. S.; Clayton, D. D.; The, L.-S. Molybdenum and Zirconium Isotopes from a Supernova Neutron Burst. *Astrophys. J. Lett.* **2000**, *540*, 49-52.

22. Wallerstein, G. et al. Synthesis of the elements in stars: forty years of progress. *Rev. Mod. Phys.* **1997**, *69*, 995-1084.
23. Busso, M.; Gallino, R. Wasserburg, G. J. Nucleosynthesis in Asymptotic Giant Branch Stars: Relevance for Galactic Enrichment and Solar System Formation. *Ann. Rev. Astr. Astrophys.* **1999**, *37*, 239-309.
24. Woosley, S. E.; Heger, A.; Weaver, T. A. The evolution and explosion of massive stars. *Rev. Mod. Phys.* **2002**, *74*, 1015-1071.
25. Clayton, D. D. *Principles of Stellar Evolution and Nucleosynthesis*; The University of Chicago Press: Chicago, IL, 1968.
26. Arnett, W. D. *Supernovae and nucleosynthesis*; Princeton University Press: Princeton, NJ, 1996.
27. Clayton, D. D. *Handbook of the Isotopes in the Cosmos*; Cambridge University Press, Cambridge, UK, 2003.

Chapter 4

Circumstellar Chemistry and Dust from Dead Stars in Meteorites

Katharina Lodders

**Department of Earth and Planetary Sciences and McDonnell Center for the
Space Sciences, Washington University, Saint Louis, MO 63130**

This chapter briefly introduces the chemistry in circumstellar envelopes (CSE) around old, mass-losing stars. The focus is on stars with initial masses of one to eight solar masses that evolve into red giant stars with a few hundred times the solar radius, and which develop circumstellar shells several hundred times their stellar radii. The chemistry in the innermost circumstellar shell adjacent to the photosphere is dominated by thermochemistry, whereas photochemistry driven by interstellar UV radiation dominates in the outer shell. The conditions in the CSE allow mineral condensation within a few stellar radii, and these grains are important sources of interstellar dust. Micron-sized dust grains that formed in the CSE of red giant stars have been isolated from certain meteorites and their elemental and isotopic chemistry provides detailed insights into nucleosynthesis processes and dust formation conditions of their parent stars, which died before the solar system was born 4.56 Ga ago.

Giant Star Evolution and the Circumstellar Environment

The evolution of low and intermediate mass stars to mass-losing giant stars and the associated processes creating and operating in circumstellar environments are reviewed in (1-10). The following summary serves to place the circumstellar chemistry into context. Table I gives some symbols and values frequently used in astronomy, and Table II some properties of the Sun and giant stars. Most dwarf stars near the Sun have elemental abundances similar to those in the solar photosphere, which are generally used as a reference composition (11). Low-mass dwarf stars like the sun burn H to He mainly through the proton-proton chain, but, with increasing mass, the CNO cycle, in which nitrogen is a by-product, becomes more important. As long as H-burning occurs in the core, elemental abundances on the stellar exterior remain practically unchanged. Dwarf stars with masses of ~ 1 to 8 solar masses (M_{\odot}) evolve into giant stars after hydrogen fuel is exhausted in their cores ($\sim 10^{10}$ years for the Sun). The first changes in surface composition appear in the red giant (RG) stage, when the N produced in the CNO cycle is mixed up from the stellar interior (the so-called first dredge-up). These stars then burn He to C and O in their cores.

After He is exhausted in their cores, stars alternately burn H and He in shells surrounding the electron-degenerate carbon-oxygen core. Stars $> 4 M_{\odot}$ can experience a second dredge up of CNO cycle products during this stage. The H- and He-shell-burning stars are located on the asymptotic branch moving off the main sequence defined by dwarf stars in the Hertzsprung-Russell diagram; hence, they are called asymptotic giant branch (AGB) stars. The AGB stars experience multiple thermal pulses when He-shell burning ignites every $\sim 10,000$ years. These thermal pulses are responsible for the “3rd-dredge-up” episodes, which bring ^{12}C , produced by previous He-shell burning, along with s-process elements up to the stellar surface (7). Many isotopes of elements heavier than Fe (e.g., Y, Zr, Sr, Ba) are primarily produced by *slow* neutron capture nucleosynthesis in AGB stars and are therefore referred to as “s-process elements”.

Table I. Useful Astronomical Quantities

<i>Quantity</i>	<i>Symbol</i>	<i>Unit Value</i>
Mass of Sun	M_{\odot}	1.99×10^{30} kg
Radius of Sun	R_{\odot}	6.96×10^8 m
Astronomical Unit (Earth-Sun distance)	AU	1.50×10^{11} m
Luminosity of Sun	L_{\odot}	3.83×10^{26} W
Mass-loss rate, dM/dt	M_{\odot}/yr	6.30×10^{22} kg/s
Stefan-Boltzmann constant	σ	5.67×10^{-8} W/(m^2K^4)
Gravitational constant	G	6.67×10^{-11} $\text{m}^3/(\text{kg s}^2)$

Table II. Properties of the Sun and Cool AGB Stars

<i>Property</i>	<i>Sun</i>	<i>M</i>	<i>S</i>	<i>C</i>
Effective Temp. (K)	5780	2600-3300	2300-3100	2200-3000
Radius, R_{\odot}	$\equiv 1$	160 – 370	270 – 530	400 – 560
Luminosity, L_{\odot}	$\equiv 1$	$100 - 10^4$	$2000 - 10^4$	$2000 - 10^4$
A(H)	$\equiv 12$	$\equiv 12$	$\equiv 12$	$\equiv 12$
A(C)	8.39	8.52	8.55	8.75
A(N)	7.83	8.28	8.77	7.78
A(O)	8.69	8.86	8.75	8.70
A(Fe)	7.45	7.37	7.36	7.36
C/O (atomic)	0.50	0.45	1.00	1.14
s-process elements	$\equiv 1$	$\sim 1-5$	$\sim 5 - 10$	$\sim 5 - 100$
dM/dt , M_{\odot}/yr	10^{-14}	$10^{-8} - 10^{-4}$	$10^{-8} - 10^{-6}$	$10^{-8} - 10^{-4}$
Dust seen in CSE	None	silicates, oxides	silicates SiC (rare)	SiC, carbon

NOTE: Abundances A(i) are given in the standard astronomical notation on a logarithmic scale where the number of H atoms is defined (\equiv) as $\log N(H) = 12$. For M, S, and C stars, average or characteristic values are listed.

SOURCE: Modified from (34)

The increased energy output from He-core burning, and subsequent H- and He-shell burning literally turns dwarfs into giants: RG stars have radii of ~ 10 -50 R_{\odot} and AGB stars ~ 100 -600 R_{\odot} (12) (the Sun-Earth distance is $\sim 215 R_{\odot}$). The effective temperatures (i.e. the temperature equivalent to an ideal blackbody) of giant stars (~ 2000 -3500 K) are lower than those of dwarf stars of similar mass. Thus, giant stars emit most of their radiation at red wavelengths. Red giant stars have luminosities ($L = 4\pi\sigma R^2 T_{\text{eff}}^4$) up to 10,000 times greater than the sun.

The atmospheres of low-mass dwarf stars are relatively tightly bound by gravitation, and mass loss from their outer atmospheres is very low; e.g., the Sun loses $\sim 10^{-14} M_{\odot}/yr$. For stars of the same mass, the surface gravity ($g = GM/R^2$) decreases with increasing radius. For example, the Sun's gravity (in cm/s^2 and logarithmic form as preferred by astronomers) is $\log g = 4.4$, whereas a 1 M_{\odot} AGB star with 215 R_{\odot} has $\log g \sim -0.2$. Then atmospheric pressure scale heights (H) are larger and required escape velocities are smaller. (The scale height is defined as $H = RT/\mu g$ where R is the gas constant and μ is the mean molecular weight). Relatively small radial oscillations may become sufficient to levitate the outer atmosphere enough to allow it to escape. The matter lost from the expanded atmospheres creates more or less spherical circumstellar shells, also called circumstellar envelopes (CSE). Observed mass-loss rates in RG stars are $\sim 10^{-7} M_{\odot}/yr$ or less, and range from 10^{-7} to $10^{-4} M_{\odot}/yr$ in AGB stars (13-15). Annual mass-loss for RG stars can be estimated from Reimers' formula $dM/dt = 4 \times 10^{-13} \eta LR/M$, where η is a constant between $\sim 1/3$

to ~ 3 , and L, R, and M are in solar units. However, mass-loss rates for AGB stars are typically underestimated by this equation.

The higher mass-loss rates in AGB stars are caused by stellar pulsation and grain condensation in their CSE (16-20). Many AGB stars are radially-pulsating variable stars with periodic changes in luminosity. They are either irregular (Lb) or semi-regular (SR) variables with periods of 50 – 300 days, or are Mira-type variables with regular periods of 100 – 1000 days (21). A periodic variation in stellar radii implies that mass can escape the star on regular cycles. Observed mass-loss rates and expansion velocities tend to correlate well with variability periods (14). The atmospheric pulsations produce shock waves that propagate into the CSE where they dissipate (22). Thus, the temperature, density, and, likely, the chemistry in the CSE are dynamically coupled to the stellar atmosphere with timescales similar to those of the luminosity variability periods. Detailed models of stellar atmospheres and circumstellar shells take these time-dependent variations into account (15, 22-25).

Figure 1 is an idealized sketch of a CSE around an AGB star to show the variations of temperature and density as a function of radial distance. A typical AGB star has a stellar radius (R_*) $\sim 3.5 \times 10^{15}$ cm $\sim 500 R_\odot$. Near the photosphere, the T and P structure is determined by hydrostatic equilibrium of the star (e.g., 25-28). In the transition zone, T and P drop due to adiabatic expansion and, to some extent, radiative cooling. Within ≤ 5 stellar radii, conditions in the CSE become favorable for dust condensation. Dust formation speeds up the loss of the stellar atmosphere through dust-driven winds (8, 16-20). Dust grains are accelerated by radiation pressure, and, through momentum transfer, the dust drags the surrounding gas outwards. This leads to terminal expansion velocities ranging from 5-25 km/s, with typical values around 10-15 km/s (13-15). The density (ρ) in the CSE is related to the mass-loss rate as $dM/dt = 4\pi R^2 \rho(R) v_{\text{exp}}(R)$, and temperatures follow $T(R) = T_0 (R_0/R)^\alpha$, where $\alpha = 0.6-0.8$ is a measure of the heating and cooling processes in the outflowing gas. The outer limit of the CSE is given by the duration of mass-loss, e.g., for $v_{\text{exp}} = 10$ km/s, the CSE grows by ~ 2 AU per year. Observed mass-loss rates correlate with expansion velocities, and dM/dt seems to increase with stellar luminosity as well as inverse effective temperature (14, 15), which is consistent with the idea that radiation pressure acting on grains is driving the mass-loss.

On longer timescales, such as the duration of the AGB stage, the mass-loss from giant stars is more or less continuous, but there is evidence for episodes of increased mass-loss for which the reasons are not entirely clear. Some objects show clumpiness in their CSEs, and several stars have detached shells or multiple circumstellar shells expanding at different speeds, indicating different ejection times of material. This may be related to the thermal pulses caused by ignition of He-shell burning (14, 29). Some objects with large mass-loss rates ($\sim 10^{-4} M_\odot/\text{yr}$) developed very thick circumstellar shells that obscure detection of the central stars at optical wavelengths. Several enshrouded objects were discovered first by infrared emission from their circumstellar shells (e.g., 30).

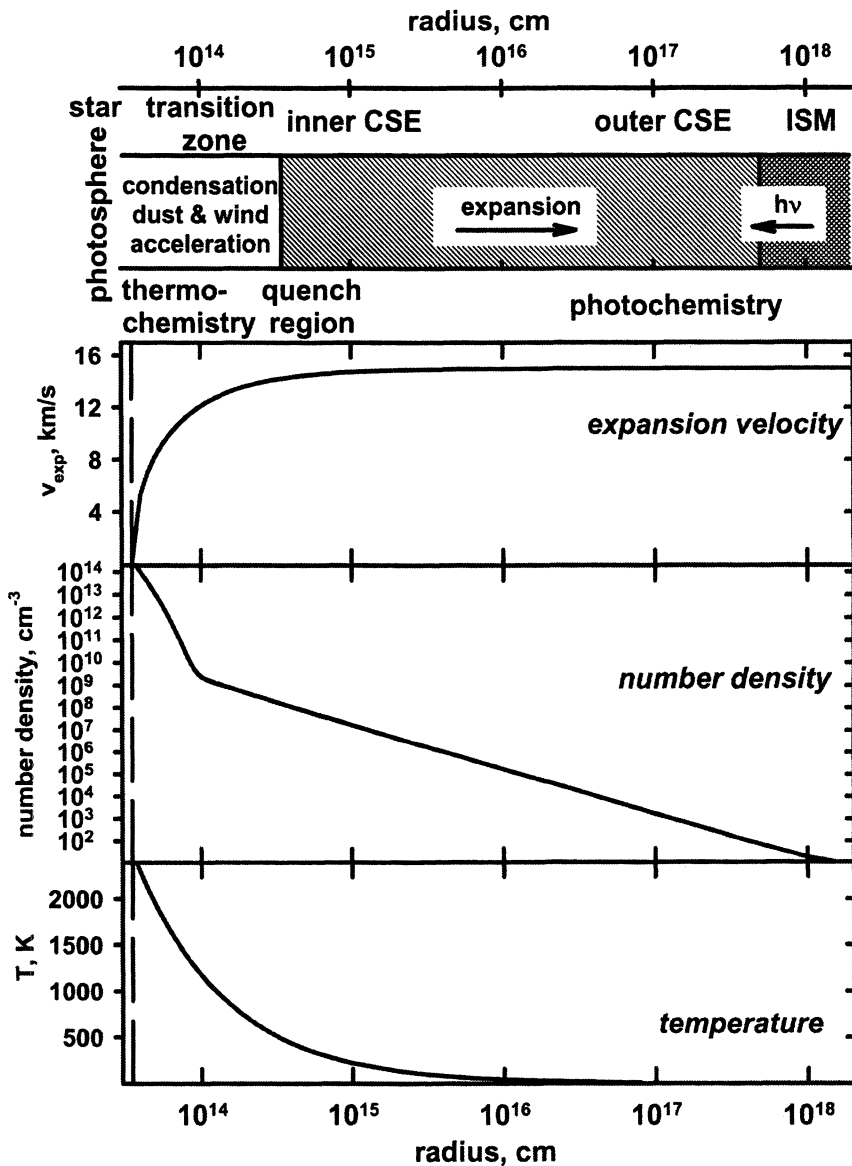


Figure 1. Approximate conditions in a circumstellar envelope around an AGB star of $\sim 500 R_{\odot}$ (3.5×10^{13} cm) and $1 M_{\odot}$

Dust-driven winds are thought to be the major cause for the complete loss of an AGB star's H- and He-rich atmosphere. Loss of the stellar envelope to the CSE limits the duration of the AGB stage to $\sim 10^5$ to 10^6 years. The last material leaves an AGB star in a fast superwind that shocks and ionizes the older, chemically processed CSE ejecta, which then appears as a so-called planetary nebula that surrounds a white dwarf – the remnant C-O-rich stellar core (31).

Elemental Abundances and Gas Chemistry

The major elements whose abundances are affected by nucleosynthesis in giant stars are C, N, and O (when compared to solar abundances). This affects the molecular speciation of many other elements in cool stellar atmospheres and their CSEs because C and O play a key role in determining the overall oxidation state. Stellar spectroscopy uses the changing molecular chemistry caused by an increase in C to classify cool RG stars into O-rich and C-rich stars. The carbon to oxygen (C/O) ratio in the sun is about 0.5. Figure 2 illustrates the calculated changes in gas chemistry for a few elements when the C/O ratio is increased by adding C to an otherwise solar composition gas at T and P conditions roughly representative of photospheric regions (see 32-35).

Elemental Abundance Classification of Stars: M, S, and C Stars

Cool O-rich giant stars with $C/O < 1$ (M stars) have elemental abundances comparable to those of the Sun, and the gas molecules identified in their photospheric spectra (e.g., CO, H₂O, TiO, VO, ZrO) are similar to those expected to form in a gas with solar elemental composition based upon thermochemical computations (Figure 2). The major C- and O-bearing gases in a solar gas are CO and H₂O. Essentially all C is locked up in the very stable CO molecule. Oxygen is twice as abundant, and most O is evenly distributed between CO and H₂O gas. The metal oxide abundances are limited by the total metal abundances, which are typically much less than that of oxygen, and metal distribution into other gases such as sulfides must be considered as well. The C/O ratio is not changed by much in cool red giant stars, and their gas chemistry is quite similar to that of a solar gas. Although the N abundances in red giant stars are higher due to the first dredge-up, an increase in N abundance does not affect the chemistry of other elements very much because nitrogen is mainly present as N₂ and atomic N.

The C/O ratio increases in the outer atmosphere during the AGB stage by continuous dredge-up of C from the stellar interior. Stars with C/O near unity are called S stars. They still show CO and oxides in their spectra, but, because more O is in CO, the abundances of other oxides drop. The abundances of neutral and ionized atoms and sulfides are not affected much by an increase in

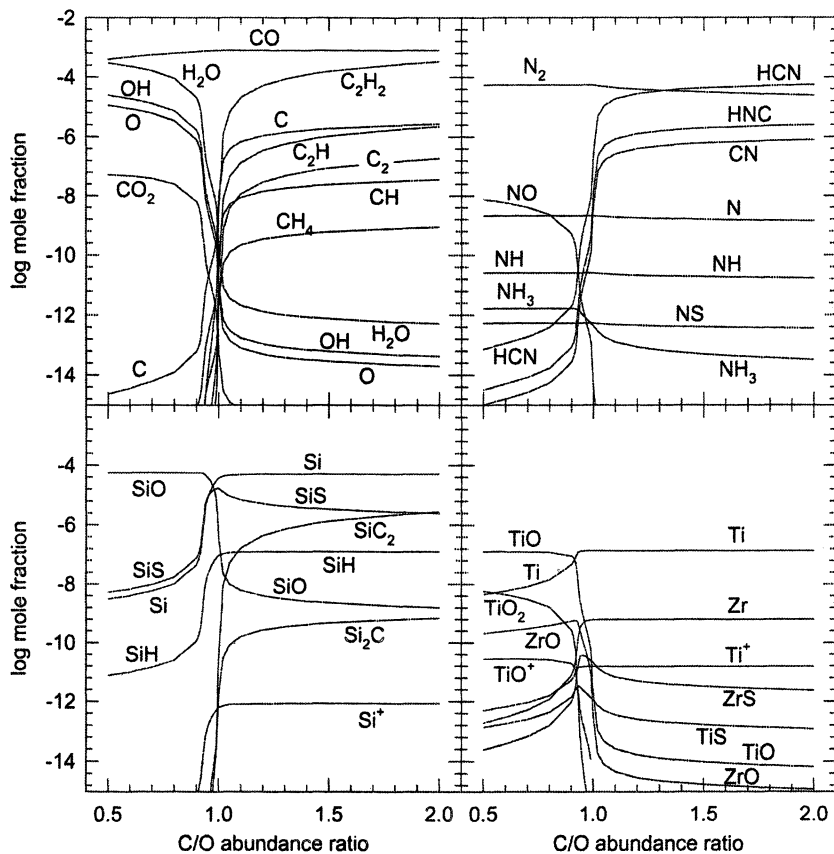


Figure 2. Thermochemical equilibrium abundances (mole fractions) as a function of C/O ratio at 2000 K and $P_{tot} = 10^{-5}$ bar. Only a few gases are shown to illustrate trends.

the C/O ratio. One characteristic of S stars is that they show stronger ZrO absorption bands than observed in M stars with comparable temperatures (36). This appears to be at odds with the expected trend of decreasing oxide abundances with increasing C/O ratio (Figure 2). However, Zr is produced by s-process nucleosynthesis and is dredged up to the surface of these AGB stars like many other s-process elements, which are more abundant in S stars than in M stars (36, 37). The presence of radioactive Tc, which has a relatively short half-life of 2×10^5 years and therefore must be made in the star where it is observed, is proof that nucleosynthesis is indeed responsible for the observed s-process element enrichments.

Stars with $C/O > 1$ are called carbon (C) stars. It was quickly recognized after their discovery in the 1860s that the presence of molecules such as C_2 requires reducing atmospheres (see (34) for a historical review). If C is more abundant than O, essentially all O is locked up in CO, and water is no longer a major gas. The C not tied up in CO is distributed among molecules such as C_2H_2 , CH, C_2H , C_2 , CN, HCN, and HNC (Figure 2). The metals that form oxides in M and S stars are instead present as atoms and sulfides in C stars, and carbide gases such as SiC_2 and Si_2C appear (32-35).

Some cool giants are heavily enshrouded by their CSE and are mainly detectable in the infrared. Oxygen-rich AGB stars with strong infrared brightness and OH maser emission are so-called OH/IR stars. The closest C-rich AGB star with a thick CSE is IRC +10216 at a distance of 100-200 parsec (330-650 light years). Its CSE is a fruitful observation ground where most organic molecules observed in circumstellar shells were discovered (see Table III).

Table III. Molecules Detected in Circumstellar Shells

<i>O & C rich shells</i>	<i>O-rich shells</i>	<i>C-rich shells</i>
CO, H ₂ O, OH	CO ₂	C _n (n=2-5), CH ₄ , C ₂ H ₂ , C ₂ H ₄ , C _n H (n=28), C _n H ₂ (n=3,4,6), C ₆ H ₆ , C ₃ O, H ₂ CO, HCO ⁺ , C ₆ H ⁺
HCN, HNC, CN, NH ₃		C ₃ N, C ₅ N, HC _n N (n=2-5,7,9,11), CH ₃ CN, HC ₂ NC
CS, SiO, SiS, H ₂ S	SO, SO ₂ , OCS	C ₂ S, C ₃ S, SiH ₄ , SiC _n (n=1-4), HSiC ₂ , SiN, SiNC, SiCN, HCl, NaCl, NaCN, KCl, MgCN, MgNC, AlF, AlCl, AlNC

Circumstellar Envelope Chemistry

Photosphere and Inner CSE: Dust Condensation and Thermochemistry

This chemistry occurs in the transition zone (Figure 1), where stellar winds drive hot gas from the photosphere into the circumstellar environment. Dust

condensation also occurs relatively close to the photosphere in the cooling, expanding gas. Observations indicate that dust forms within 3-5 stellar radii of the central star (38, 39). Several minerals become stable between 1000–2000 K. Figure 3 shows the types of condensates as a function of C/O ratio at a constant total pressure of 10^{-5} bar. The relative condensation sequence does not change much at different total pressures. Generally, condensation temperatures decrease with lower total pressures. The major point here is that the types of condensates change from refractory oxides, silicates, and metals at $C/O < 1$ to carbonaceous condensates such as graphite, carbides, and nitrides (such as AlN) at $C/O > 1$ (e.g., 33-35). The condensation temperatures decrease as C/O increases from 0.5 to 1 because CO consumes more O and less is available for oxide formation. Aside from O and C, the major condensate-forming elements are Si, Mg, and Fe. Their condensates should be the most abundant minerals, and M, S, and C stars should have different types of minerals in their CSEs.

The radiation from the central star heats the dust in the CSE to higher temperatures than the surrounding gas. This leads to thermal emission from the dust. The dust closer to the photosphere at 1500-1000 K emits in the near infrared (1-5 microns) and dust further out at 500 K emits at mid-infrared wavelengths (up to ~ 20 microns). Iron metal is infrared inactive and its predicted presence in CSEs is difficult to confirm. However, Mg-silicates, such as forsterite (Mg_2SiO_4 , an olivine) and enstatite ($MgSiO_3$, a pyroxene), have been detected by IR spectroscopy in M star CSEs. Infrared studies show that amorphous and crystalline pyroxenes and olivines are present and are typically Mg-rich, with minor, varying amounts of Fe substituting for Mg (e.g., fayalite Fe_2SiO_4 and ferrosillite $FeSiO_3$) (40). Carbon stars contain SiC and carbon in their CSEs, and the 11.3 micron infrared emission feature of SiC is a well-known characteristic of C stars (41). Another expected major mineral condensing at ~ 1020 K is MgS, which may be responsible for the 30 micron emissions in some C stars (42). Dust from AGB stars is not only studied by astronomical observations but also in the laboratory because genuine stardust from AGB stars is found in meteorites (see below).

The spatial extent of the circumstellar environment and outflow conditions such as expansion velocities and stellar mass-loss rates can be probed using circumstellar line emissions in infrared to radio wavelengths for many molecules (e.g., CO, OH, H_2O , CN, HCN, CS, SiO, SiS) (13-15, 20, 44-51). The abundances of the molecules CO, C_2H_2 , HCN, CS, SiO and SiS are thought to be established from equilibrium thermochemistry near the photosphere (Figure 2).

However, as temperatures and densities drop steeply in the circumstellar shell with increasing distance from the central star, reaction kinetics may no longer permit establishment of thermochemical equilibrium in the stellar outflow (4). Detailed and generally applicable discussions of the reaction kinetics relevant here can be found in (52, 53). Let us follow a parcel of hot atmospheric gas traveling away from the photosphere and assume that a certain gas is produced or destroyed by some reaction in the CSE. As long as chemical

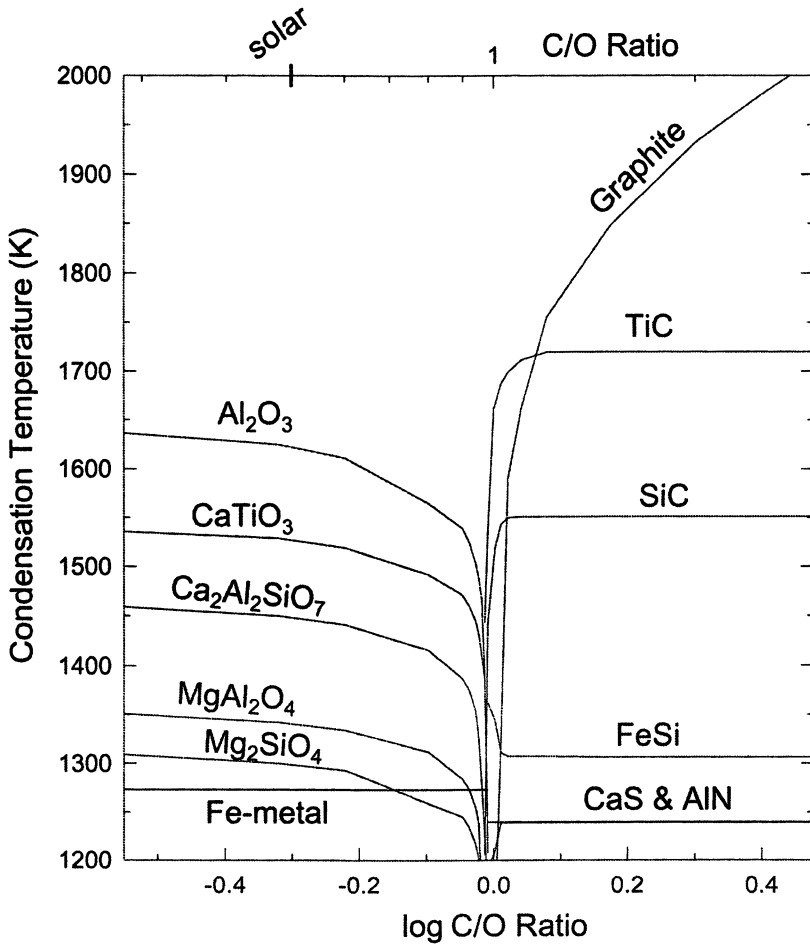


Figure 3. Major condensates and condensation temperatures as a function of C/O ratio at 10^{-5} bar total pressure. At $C/O > 1$, MgS condenses at $\sim 1020\text{K}$.

reaction times (τ_{chem}), which are different for different gases, are shorter than residence times determined by the expansion velocity in the CSE ($\tau_{\text{exp}}(R) = H/v_{\text{exp}}$), one should expect that the gas abundance can be modeled by thermochemical equilibrium. Fast reaction times are favored by high temperatures and high total pressures, so equilibrium conditions are best realized in the photospheric and adjacent shell regions. At the quench distance R_Q , where $\tau_{\text{exp}}(R) = \tau_{\text{chem}}$, the abundance of our sample gas becomes “frozen in”. At $R > R_Q$, the residence time of the gas parcel is shorter than the reaction time ($\tau_{\text{chem}} > \tau_{\text{exp}}$) required to reach reaction equilibrium at the given T and ρ conditions. As a rough guide, endothermic reactions with higher activation energies are quenched closer to the star than exothermic reactions, and reactions involving radicals are expected to operate at large distances from the star (4, 52, 53).

Chemical equilibrium abundances for many C-, N-, and O-bearing gases for $T = 500\text{-}2500\text{K}$ and $P = 10^{-7}\text{-}1000$ bars for a solar composition gas can be found in (54). Although these calculations were applied to brown dwarfs and giant planet atmospheres, the pressure conditions also include those appropriate for O-rich photospheres and their inner CSEs ($10^{-4} - 10^{-7}$ bars).

The very stable molecules CO (observed) and N_2 (not observable) are the major C-, O-, and N-bearing gases throughout the entire CSE, as expected from thermochemical equilibrium. Under the low total pressures in the CSE, conversions of CO to CH_4 or N_2 to NH_3 as the major C- or N-bearing gases does not occur. Even if pressure conditions were favorable, these reactions would not reach equilibrium because they are kinetically inhibited (these conversions are quenched even in the much denser giant planet atmospheres (e.g., 54)). This does not mean that CH_4 or NH_3 should be absent from the CSE; it only means that their abundances are likely less than that expected from thermochemical equilibrium. In O-rich CSE, most oxygen is evenly distributed between CO and H_2O , but CO_2 , produced by the rapid water gas reaction ($\text{CO} + \text{H}_2\text{O} = \text{H}_2 + \text{CO}_2$) is also an abundant gas (54) and has been observed.

Many investigations of circumstellar molecules have been done for C-rich CSE. Figure 4 shows observed abundance trends of several molecules as a function of radial distance in the thick CSE of the well-studied C star IRC+10216. The top shows gases whose abundances are determined by thermochemical equilibrium and quenching near the photosphere; the center panel shows molecules that seem to originate beyond $\sim 10R_*$ (within the CSE), and the bottom panel shows some of the mainly photochemically-produced gases.

The CO/H_2 ratio remains constant throughout the CSE because CO is always the most thermochemically and kinetically stable O-bearing gas. CO is only destroyed by photodissociation in the outer CSE. One can assume that N_2 , which is not observable, behaves similarly. Abundances of C_2H_2 , HCN, CS, SiO (50) and SiS (45) are controlled by thermochemical equilibria near the photosphere (within $\sim 1\text{-}3 R_*$), which includes quenching of gas-phase reactions and control of gas abundances by condensate formation. These “parent” molecules are sources for the chemistry in the middle and outer CSE.

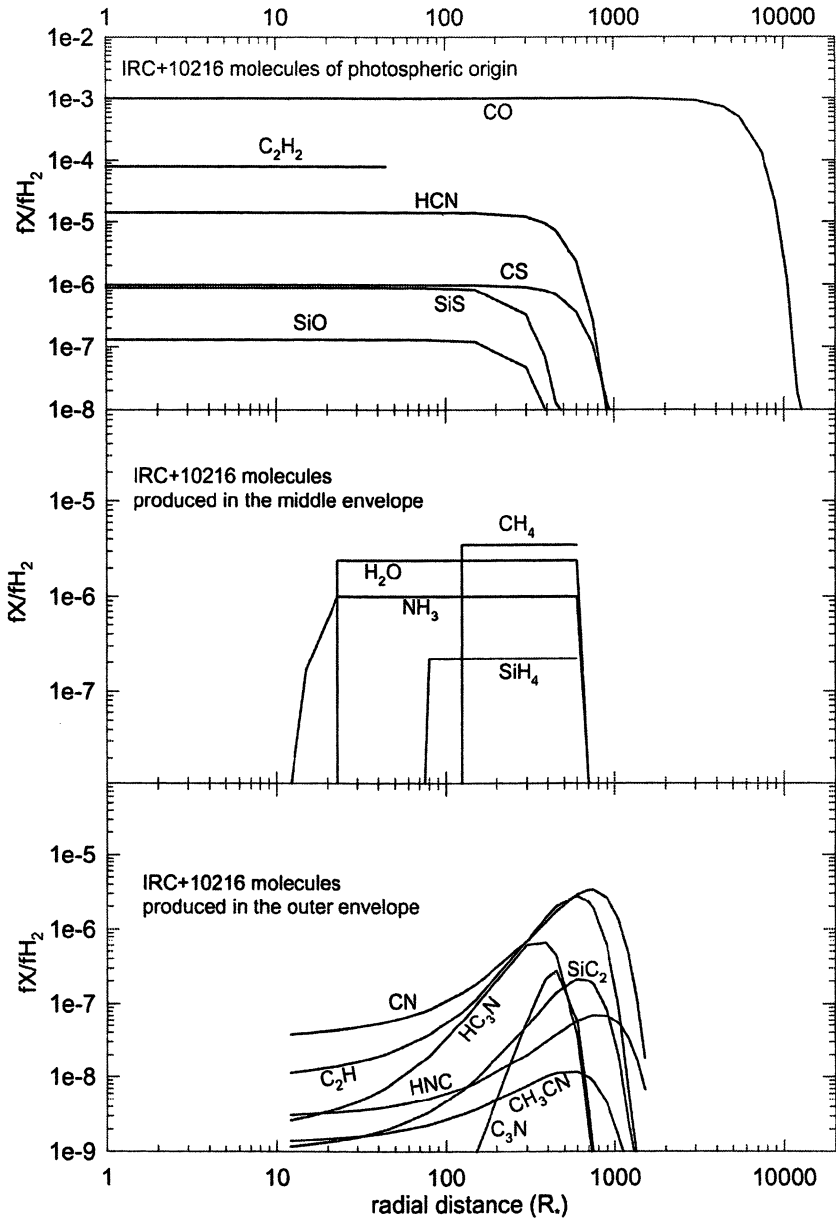


Figure 4. Abundance ratios (relative to hydrogen) of molecules and their emitting regions as a function of radial distance (in stellar radii) in the C-rich CSE of IRC+10216. See text for references.

Middle Envelope Region: Reaction Kinetics and Dust-Gas Reactions

Around 10 R_* , abundances of CH_4 (44), NH_3 (44, 55, 56), H_2O (56), and SiH_4 (44, 55) increase and remain until their likely photochemical destruction in the outer CSE. Their peak abundances are considerable, but do not exceed the maximum abundances of the photospheric molecules. They are, however, higher than expected from thermochemical equilibrium. The reaction pathways leading to the formation of CH_4 , NH_3 , H_2O , and SiH_4 are not clear, but grain-surface reactions are likely involved (44, 52). The presence of dust may foster several types of reactions. Neutral molecule gas-phase reactions may proceed through grain surface catalyses. An argument against surface-catalyzed reactions is that CH_4 , NH_3 , H_2O , and SiH_4 abundances should begin to increase within the grain condensation region much closer to the star, but they do not. However, dust temperatures closer to the star could simply be too high to allow efficient gas adsorption, so that only the cooler dust further out may be catalytically active (55).

Another possible dust-driven reaction is parent molecule destruction by collisions with dust grains, e.g., $\text{H}_2\text{O} + \text{dust} \rightarrow \text{OH} + \text{H} + \text{dust}$ (more relevant to O-rich CSE) and $\text{HCN} + \text{dust} \rightarrow \text{CN} + \text{H} + \text{dust}$. This may be a source for radicals to build new molecules through radical + neutral reactions (17, 52). The parent molecule for NH_3 production is not well known. Abundant HCN could be one source in C-rich CSE. However, NH_3 has also been observed in O-rich CSE (57), which have very low HCN abundances. This would argue against a production mechanism involving HCN (see Figure 2 for HCN abundances in O- and C-rich photospheres).

The increase of SiH_4 (silane) is roughly correlated with the decrease in SiS and SiO abundances, but it seems unlikely that SiH_4 is produced directly from either SiO or SiS gas. Silane is only known to occur in C-rich CSE, whereas SiO and SiS are present in both C and O-rich CSEs. The depletion of SiO and SiS (as well as CS) is likely related to the continuing condensation of SiC and MgS. In that case, other Si-bearing gases should also become depleted but not produced. The detection of relatively large amounts of H_2O in the C-rich CSE of IRC+10216 is unexpected because essentially all O is bound in CO, which is not yet photodissociated at the distances where H_2O is observed (56). Overall, convincing models explaining the observed abundances of CH_4 , NH_3 , H_2O , and SiH_4 are still lacking.

Outer Envelope Region: Photochemistry

The chemistry changes drastically when interstellar UV radiation can penetrate the more tenuous outer regions of the CSE, and photochemistry starts to control molecular abundances. Neutral molecule plus radical reactions and neutral molecule plus ion (“ion-molecule”) reactions are important for the

production of many organic molecules in the outer CSE, particularly in C-rich objects (e.g., 4, 52, 58-63).

Frequently employed tracers for photochemistry in CSE are CO, which photodissociates in the outer regions of the CSE, and CN and OH, which are photodissociation products of HCN and H₂O, respectively. Photodissociation of photospheric parent molecules (e.g., H₂O + $h\nu$ → OH + H; C₂H₂ + $h\nu$ → C₂H + H; HCN + $h\nu$ → CN + H) increases the radical abundances, and abundances of parent molecules start to decline. The distance in the CSE at which photodissociation begins is different for different parent molecules and reflects the distance where the CSE becomes transparent for the UV radiation to drive the photodissociation reaction.

Photoionization of neutral C to C⁺ and C₂H₂ to C₂H₂⁺ by UV photons and cosmic ray ionization of H₂ to H₃⁺ are the major ion sources for subsequent ion molecule reactions and dissociative recombination reactions (59). So far only two ions (HCO⁺, C₆H⁺(60)) have been observed in IRC+10216. Ion-molecule reactions involving C₂H₂⁺ can account for the abundances of several molecules produced in the outer CSE (e.g., C_nH, C_nS, C₃O, CH₃CN, HNC, C_nN, C₃H₂HC_{2n+1}N, etc.), but other reactions may also be required (59-64).

Neutral molecule plus radical reactions in the outer CSE are probably the major production channel of longer C-chain molecules such as C_{2n}H, and the cyanopolynes (HC_{2n+1}N). For example, the reaction channel C_{2n}H₂ + C₂H → C_{2n+2}H₂ + H and subsequent photodissociation: C₄H₂ + H → C₄H + H can build up C₄H and C₆H from the parent molecule C₂H₂ (62).

Dust Grains from AGB Stars in Meteorites

Primitive (i.e., thermally unaltered) meteorites are now known to contain nm to micron-size grains with substantially different isotopic compositions in C, N, O, and Si than other solar system materials. The isotopic compositions link the majority of these grains to AGB stars (>95%) and supernovae. Because such grains must predate the formation of our solar system, they are collectively called "presolar grains". Detailed reviews about presolar grains are given in (65, 66). The major known presolar minerals are refractory solids that condense at relatively high temperatures and are resistant to physical and chemical (laboratory) processing. Currently known presolar minerals include corundum (Al₂O₃), spinel (MgAl₂O₄), silicates of the pyroxene and olivine groups, graphite, diamond, and silicon carbide (SiC). Most of the oxide and silicate grains are ascribed to RG and O-rich AGB stars, and most of the SiC and graphite grains seem to come from C-rich AGB stars. Known minerals from supernovae include graphite, SiC, and Si₃N₄ (sinoite); however, these grains are rare, although supernovae are thought to be major dust producers. The origin of presolar nano-diamonds is not well known, in part because individual grains cannot be analyzed.

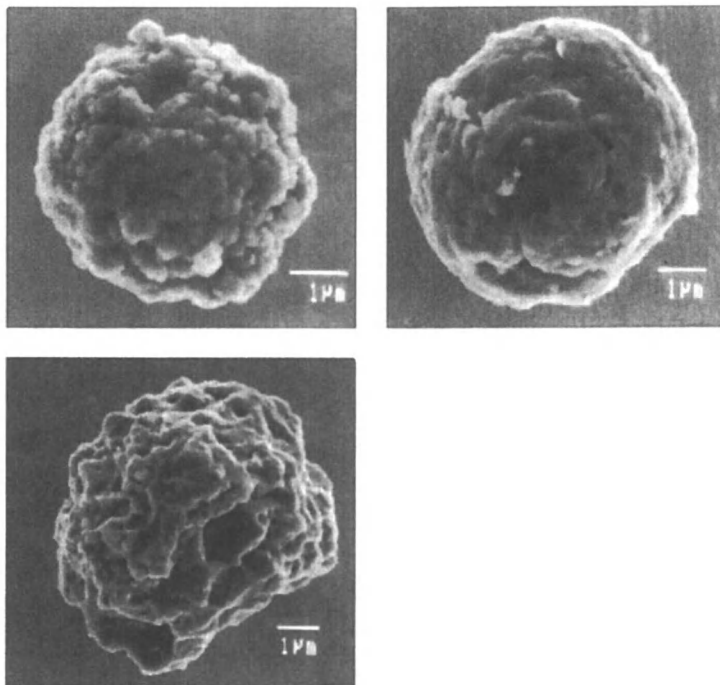


Figure 5. Scanning electron microscopic photographs of 2 circumstellar graphite grains (top) and a presolar SiC grain (bottom) isolated from meteorites. Photos courtesy of Sachiko Amari.

Examples of rarer but larger presolar graphite grains with “cauliflower” and “onion” morphology are shown in Figure 5. Some of the micron-size graphite grains contain sub-grains of 10-100 nanometer-size carbides; either pure TiC or (Ti,Zr,Mo)C from AGB stars, or TiC and metallic particles of varying Fe-Ni content from supernovae. Often the refractory carbides are located in or near the center of graphite grains, which indicates that they formed first and acted as nucleation seeds for the graphite (67). The elemental compositions of presolar grains are used to determine their stellar sources and the environmental conditions in which the grains formed. For example, the measured trace element abundances in SiC grains from AGB stars are well understood to result from fractional equilibrium condensation close to the photospheres of the stars (33, 34, 66). The measured isotopic compositions of trace elements also provide sensitive tests to nucleosynthesis models (see reviews 65, 66).

AGB stars return ~ 0.3 solar masses per year to the interstellar medium (ISM) in our galaxy (68), of which C stars contribute about 10–50% (14, 30). Thus, dust condensation in the circumstellar envelopes of C stars is a plausible source of the presolar C-bearing grains found in meteorites. Although

carbonaceous dust is observed in CSEs, neither SiC nor carbon dust has yet been detected in the interstellar medium; instead, only silicate dust is detected (e.g., 40). The reason for the apparently missing SiC in the ISM is still not clear. It has been suggested that SiC grains become coated with silicate mantles, and that such composite grains may prevent detection of the 11.3 μm SiC absorption feature (69). Such composite grains have not yet been discovered among presolar grains studied thus far. Still, if the theoretical predictions of grain processing in the ISM are correct, such grains should have been with those that traveled through the ISM from their parent stars to the molecular cloud from which the solar system formed.

Summary

Stars with initial masses of $\sim 1\text{-}8 M_{\odot}$ evolve into red giant stars and lose their outer atmospheres through stellar winds. The lost material creates huge circumstellar shells. The overall composition of a CSE is determined by the ongoing nucleosynthesis in the star. Most importantly, production and dredge-up of C in AGB stars changes the surface composition from oxygen rich ($C/O < 1$ in M stars) to carbon-rich ($C/O > 1$ in C stars). The C/O ratio determines the gas chemistry in the CSE and which condensates (e.g., silicates or carbides) appear.

The chemistry in the CSE depends on the distance from the star as temperatures and densities drop steeply with increasing distance. Equilibrium thermochemistry and condensation chemistry dominate in the photospheric and inner CSE regions ($< 3\text{-}5$ stellar radii). With increasing distance from the star, abundances become controlled by reaction kinetics. Abundances of important gases (CO , H_2O , C_2H_2 , HCN , $\text{SiO}\dots$) become frozen-in. Gas-grain reactions are probably important to explain the relatively large abundances of CH_4 , NH_3 , SiH_4 , H_2O that appear at low temperatures further from the central stars. Photochemistry produces many radicals and unsaturated gases in the outer CSE; e.g., C_nH ($n=2\text{-}8$), HC_{2n+1}N ($n=1\text{-}3$).

Genuine star dust is preserved in meteorites. Most of the presolar grains comes from RG and from O-rich and C-rich AGB stars. Dust from supernovae and novae has also been found. Elemental, isotopic, and structural analyses of this star dust gives details on stellar nucleosynthesis and dust formation conditions in the circumstellar environments.

Acknowledgements

This work was supported in part by NASA grant NNG04GG13G. I thank Bruce Fegley, Jon Friedrich, Hans Olofsson, Laura Schaefer, and Lori Zaikowski for comments on the manuscript.

References

1. Iben, I. Renzini, A. *Annu. Rev. Astron. Astrophys.* **1983**, *21*, 271
2. Lafon, J.P.J; Berruyer, N. *Astron. Astrophys. Rev.* **1991**, *2*, 249
3. Clegg, R.E.S.; Stevens, I.R.; Meikle, W.P.S. Circumstellar media in the late stages of stellar evolution, Cambridge Univ. Press, **1996**, pp. 345
4. Glassgold, A.E. *Annu. Rev. Astron. Astrophys.* **1996**, *34*, 241
5. Habing, H.J. *Astron. Astrophys. Rev.* **1996**, *7*, 97
6. Bernatowicz, T.J.; Zinner, E. Astrophysical implications of the laboratory study of presolar materials, AIP Conf. Proc. 402, **1997**, pp.750
7. Busso, M.; Gallino, R.; Wasserburg, G. J. *Annu. Rev. Astron. Astrophys.* **1999**, *37*, 239
8. Lamers, H.J.G.L.M.; Cassinelli, J.P. Introduction to stellar winds, Cambridge Univ. Press, **1999**, pp. 438
9. LeBertre, T.; Lebre, A; Waelkens, C. (eds.) Asymptotic giant branch stars, IAU symposium no. 191, **1999**, Astronomical Soc. Pacific, pp. 632
10. Habing, H.J. Olofsson, H. (eds.) Asymptotic giant branch stars, Springer, Berlin, **2003**, pp. 559.
11. Lodders, K. *Astrophys. J.* **2003**, *591*, 1220
12. van Belle, G.T.; Dyck, H.M.; Thompson, R.R.; Benson, J.A.; Kannappan, S.J. *Astron. J.* **1997**, *114*, 2150.
13. Loup, C.; Forveille, T.; Omont, A.; Paul, J.F. *Astron. Astrophys. Suppl.* **1993**, *99*, 291
14. Schoier, F.L.; Olofsson, H. *Astron. Astrophys.* **2001**, *368*, 969
15. Winters, J.N.; LeBertre, T.; Jeong, K.S.; Nyman, L.A.; Epchtein, N. *Astron. Astrophys.* **2003**, *409*, 715
16. Gilman, R. C. *Astrophys. J.* **1972**, *178*, 423
17. Goldreich, P.; Scoville, N. *Astrophys. J.* **1976**, *205*, 144
18. Jones, T.T.; Ney, E.P; Stein, W.A. *Astrophys. J.* **1981**, *250*, 324
19. Gail, H.P.; Sedlmayr, E. *Astron. Astrophys.* **1987**, *177*, 186
20. Habing, H.J.; Tignon, J.; Tielens, A.G.G.M. *Astron. Astrophys.* **1994**, *286*, 523
21. Hoffmeister, C.; Richter, R.; Wenzel, W. Variable stars, Springer, Berlin, **1985**, pp. 328
22. Bowen, G.H. *Astrophys. J.* **1988**, *329*, 299
23. Fleischer, A.J.; Gauger, A.; Sedlmayr, E. *Astron. Astrophys.* **1992**, *266*, 321
24. Höfner, S. Feuchtinger, M.U.; Dorfi, E.A. *Astron. Astrophys.* **1995**, *297*, 815
25. Jorgensen, U.G.; Hron, J.; Loidl, R. *Astron. Astrophys.* **2000**, *356*, 253
26. Lambert, D. L.; Gustafsson, B.; Eriksson, K.; Hinkle, K. H. *Astrophys. J. Suppl.* **1986**, *62*, 373
27. Tsuji, T.; Ohnaka, K.; Aoki, W. *Astron. Astrophys.* **1997**, *320*, L1
28. Ohnaka, K.; Tsuji, T.; Aoki, W. *Astron. Astrophys.* **2000**, *353*, 528

29. Olofsson, H.; Bergman, P.; Eriksson, K.; Gustafsson, B. *Astron. Astrophys.* **1996**, *311*, 587
30. Guglielmo, F.; Epchtein, N.; LeBertre, T; et al. *Astron. Astrophys. Suppl. Ser.* **1993**, *99*, 31
31. Kwok, S. *Annu. Rev. Astron. Astrophys.* **1993**, *31*, 63
32. Tsuji, T. *1973, Astron. Astrophys.* **1973**, *23*, 411
33. Lodders, K.; Fegley, B.; *Meteoritics* **1995**, *30*, 661
34. Lodders K, Fegley B.; *AIP Conf. Proc.* **1997**, *402*, 391
35. Ferrarotti, A.S.; Gail, H.P *Astron. Astrophys.* **2002**, *382*, 256
36. Smith; V.V.; Lambert, D.L. *Astrophys. J. Suppl.* **1990**, *72*, 387
37. Abia, C.; Dominguez, I; Gallino, R.; Busso, M.; Maserà, S.; Straniero, O.; de Laverny, P.; Plez, B.; Isern, J. *Astrophys. J.* **2002**, *579*, 817
38. Bergeat, J.; Lefevre, J.; Kandel, R.; Lunel, M.; Sibille, F. *Astron. Astrophys.* **1976**, *52*, 245
39. Danchi, W. C.; Bester, M.; *Astrophys. Space Sci.* **1995**, *224*, 339
40. Molster, F.; Kemper, C. *Space Sci. Rev.* **2005**, *119*, 3
41. van der Veen, W.E.C.J.; Habing, H.J. *Astron. Astrophys.* **1988**, *194*, 125.
42. Hony, S.; Waters, L.B.F.M.; Tielens, A.G.G.M. *Astron. Astrophys.* **2002**, *390*, 533
43. Jimenez-Esteban, F.M.; Agudo-Merida, L.; Engels, D.; Garcia-Lario, P. *Astron. Astrophys.* **2005**, *431*, 779
44. Keady, J.J.; Ridgway, S.T.; *Astrophys. J.* **1993**, *406*, 199
45. Biegging, H.H.; Tafalla, M.; *Astron. J.* **1993**, *105*, 576
46. Olofsson, H.; Eriksson, K.; Gustafsson, B.; Carlstrom, U.; *Astrophys. J. Suppl.* **1993**, *87*, 267
47. Olofsson, H.; Eriksson, K.; Gustafsson, B.; Carlstrom, U.; *Astrophys. J. Suppl.* **1993**, *87*, 305
48. Biegging, J.H.; Shaked, S.; Gensheimer, P.D. *Astrophys. J.* **2000**, *543*, 897
49. Lindqvist, M.; Schoier, F.L.; Lucas, R.; Olofsson, H.; *Astron. Astrophys.* **2000**, *361*, 1036
50. Woods, P.P.; Schoier, F.L.; Nyman, L.A.; Olofsson, H.; *Astron. Astrophys.* **2003**, *402*, 617
51. Gonzales Delgado, D.; Olofsson, H.; Kerschbaum, F.; Schöier, F.L.; Lindqvist, M.; Groenewegen, M.A.T. *Astron. Astrophys.* **2003**, *411*, 123
52. Lafont, S.; Lucas, R.; Omont, A. *Astron. Astrophys.* **1982**, *106*, 201
53. Prinn, R.; Fegley, B.; in *Origin and evolution of planetary and satellite atmospheres*, Univ. Arizona Press, 1989, pp. 89
54. Lodders, K.; Fegley, B. *Icarus* **2002**, *155*, 393
55. Monnier, J.D.; Danchi, W.C.; Hale, D.S.; Tuthill, P.G.; Townes, C.H. *Astrophys. J.* **2000**, *543*, 868
56. Hasegawa, T.I.; Kwok, S.; Koning, N.; Volk, K.; Justtanont, K.; Olofsson, H.; Schöier, F.L.; Sandqvist, A.; Hjalmarsen, A.; Olberg, M; Winnberg, A.; Nyman, L.A.; Frisk, U. *Astrophys. J.* **2006**, *637*, 791

57. Menten, K.M.; Alcolea, J. *Astrophys. J.* **1995**, *448*, 416
58. Huggins, P.J.; Glassgold, A.E. *Astron. J.* **1982**, *87*, 1828
59. Glassgold, A.E.; Lucas, R.; Omont, A. *Astron. Astrophys.* **1986**, *157*, 35
60. McCarthy, M.C.; Gottlieb, C.A.; Gupta, H.; Thaddeus, P. *Astrophys. J.* **2006**, *652*, L141
61. Nejad, L.A.M.; Millar, T.J. *Astron. Astrophys.* **1987**, *182*, 279
62. Howe, D.A.; Millar, T.J.; *Mon. Not. R. Astr. Soc.* **1990**, *244*, 444
63. Millar, T.J.; Herbst, E. *Astron. Astrophys.* **1994**, *288*, 561
64. Doty, S.D.; Leung, C.M. *Astrophys. J.* **1998**, *502*, 898
65. Zinner, E. in *Treatise on Geochemistry 1*, Elsevier, Oxford, 2004, pp. 17
66. Lodders, K.; Amari, S. *Chem. Erde* **2005**, *65*, 93
67. Bernatowicz, T.J.; Cowsik, R.; Gibbons, P.C.; Lodders, K.; Fegley, B.; Amari, S.; Lewis, R.S. *Astrophys. J.* **1996**, *472*, 760
68. Knapp, G.R.; Morris, M. *Astrophys. J.* **1985**, *292*, 640
69. Ossenkopf, V.; Henning, T.; Mathis, J.S. *Astron. Astrophys.* **1992**, *261*, 567

Chapter 5

Chemical Evolution in the Interstellar Medium: Feedstock of Solar Systems

Louis J. Allamandola

Astrochemistry Laboratory, NASA Ames Research Center, MS 245-6,
Mountain View, CA 94035-1000

Great strides have been made in our understanding of interstellar material thanks to advances in infrared and radio astronomy and laboratory astrophysics. Ionized polycyclic aromatic hydrocarbons (PAHs), shockingly large molecules by earlier astrochemical standards, are widespread and very abundant throughout much of the cosmos. In cold molecular clouds, the birthplace of planets and stars, interstellar atoms and molecules freeze onto dust and ice particles forming mixed molecular ices dominated by simple species such as water, methanol, ammonia, and carbon monoxide. The interplay between the gas and the dust leads to a very rich chemistry in these clouds. Within these clouds, and especially in the vicinity of star and planet forming regions, these ices and PAHs are processed by ultraviolet light and cosmic rays forming hundreds of far more complex species, some of biogenic interest. Eventually, these are delivered to primordial planets by comets and meteorites. The chemical context, highlights of this field from a chemist's perspective, and the astronomer's infrared toolbox will be reviewed.

Introduction

Throughout most of the last century it was believed that the chemical compounds in space are rather simple, with chemical complexity limited by harsh radiation fields and extremely low densities. Indeed, the only interstellar species known through most of the first half of the 20th century were the highly reactive CH, CH⁺, and CN (1). The picture of a chemically sterile universe was so ingrained that the discovery of interstellar OH in the early 1960's made headlines. This broke the spell and detections of interstellar NH₃, CO, and H₂CO followed over the next few years. The realization that deep space might harbor polyatomic molecules was so startling that the discoverers of interstellar H₂CO concluded their paper stating 'Polyatomic molecules containing at least two atoms other than H can form in the interstellar medium' (2).

We have come a long way from those early days of interstellar molecule detection in a very short time. Thanks to breakthrough developments in observational infrared (IR) and radio astronomy, combined with dedicated laboratory experiments, we now know that the cosmic chemical inventory is far richer than found in any chemistry department stockroom. Today the list of interstellar molecules in the gas phase numbers over 130 and includes exotic species such as the linear cyanopolyacetylene, HC₁₁N. Large, complex polycyclic aromatic hydrocarbons are ubiquitous throughout the modern Universe and there is mounting evidence that they were already present only a few billion years after the Big Bang. Furthermore, complex molecules, including some that are biologically interesting, are readily formed in realistic laboratory simulations of interstellar and Solar System ices. Consequently, it is entirely possible that the extraterrestrial evolution of chemical complexity may play a crucial - perhaps even a determinant - role in defining the early, chemical state of young planetary systems. Compelling evidence is mounting that a substantial fraction of the compounds incorporated into planets, their satellites, asteroids, and comets in developing planetary systems is in the form of complex organic molecules. Moreover, the relative cosmic abundances of O, C, and N underscore the fact that (ignoring the chemically inert helium) these elements are *by far* the most abundant chemically reactive elements after hydrogen, dwarfing the amounts of the next tier of elements including that of silicon. This implies that chemistry throughout the cosmos is most likely composed of these most abundant elements and therefore evinces a chemistry similar to our own.

The history of the elements heavier than Li begins with their nucleosynthesis deep within the interiors of late-type stars (3, and references therein). Once formed they become part of the repeating cycle shown in Plate 1. These elements are thrown off into the surrounding interstellar medium during the periods of intense mass-loss that occur during the late asymptotic giant branch, or Red Giant, phase (Plate 1). Densities are high enough in the stellar "atmosphere" to allow chemical reactions to occur and a wide array of materials are produced as these elements are ejected into the interstellar medium (ISM),

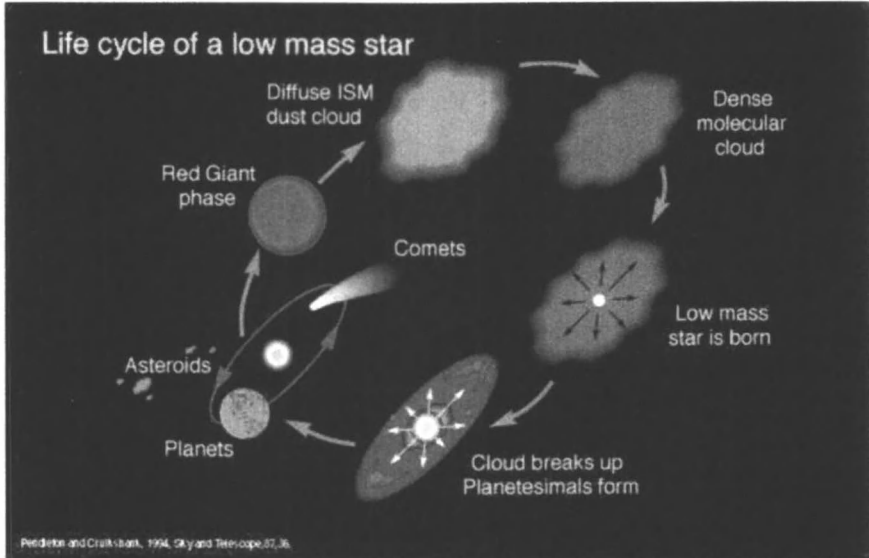


Plate 1. The chemical elements heavier than Lithium are produced by nucleosynthesis in Red Giant stars and injected into the interstellar medium during the Red Giant phase. Once in the interstellar medium, they participate in the chemistry at each stage of this cycle. These objects are not drawn to scale. A Red Giant can swell to sizes that engulf the inner planets of our Solar System. The diffuse ISM can be as vast as the space between the spiral arms of our Galaxy, The Milky Way, while molecular clouds measure from hundreds to hundreds of thousands of light years across. There are many star forming regions in molecular clouds, each several times the size of the Solar System. Plate reproduced with permission from (12). (See page 1 of color inserts.)

the space between the stars. For carbon-rich stars this includes simple radicals and molecules (<20 atoms) such as C_2 , acetylene, carbon monoxide, the polyacetylenes and cyanopolyacetylenes; large, robust molecules (tens to hundreds of atoms) such as polycyclic aromatic hydrocarbons (PAHs) and heterocyclics; and small (100-1000 Å, several thousands of atoms or more) amorphous carbon dust particles (4 and references therein). The ejecta for oxygen-rich stars includes molecular species such as H_2O , CO, OH etc.; mineral building blocks including silicon and magnesium oxides; and silicon rich dust particles. The vast surrounding diffuse ISM (Plate 1) is generally very tenuous. In the diffuse ISM, these compounds and particles are further modified through a variety of physical and chemical processes including: UV irradiation; cosmic ray bombardment; very low density gas-phase chemistry; some accretion and reaction upon grain surfaces; and destruction by shock waves generated by

supernova explosions. While refractory dust particles and large molecular species such as PAHs are relatively immune to photodestruction in the diffuse ISM, the simpler polyatomic molecules cannot withstand the harsh interstellar UV-radiation field and quickly dissociate.

However, the existence of interstellar matter is not limited to these tenuous, transparent regions. Much material is concentrated in large, relatively opaque, interstellar molecular clouds (Plate 1) (5-7). In contrast with the diffuse interstellar medium which is characterized by very low hydrogen number densities ($\sim 1-10$ H atoms cm^{-3}), the number densities in molecular clouds are much higher ($>10^4$ H atoms cm^{-3}). Astronomers often express measurements in terms of hydrogen because, as illustrated in Figure 1, it is the most abundant of the cosmic elements.

Hydrogen is some three to four orders of magnitude more abundant than C, N, and O, and has a number density that is roughly twelve orders of magnitude greater than that of the submicron sized dust particles. Although interstellar molecular cloud number densities correspond to the best vacuum achievable on Earth, and the optical path across any laboratory chamber at this pressure would be quite transparent, the background starlight that fills the diffuse ISM is strongly attenuated by dust particles in these "dense" clouds. This is because the clouds are hundreds to hundreds-of-thousands of light years across and, although their number densities are low, they are so large that the dust particles block out the starlight from the surrounding diffuse ISM.

This screening out of the UV-rich diffuse ISM radiation field permits simple, fragile molecules to form and flourish within these clouds through a rich network of gas phase reactions. Although a wide variety of these simple molecular species have been identified in the gas phase by extensive radio and infrared observations (8, and references therein) of their rotational and vibrational transitions, these represent only one aspect of the chemical inventory of these regions. At the low temperatures which characterize these dark molecular clouds ($\approx 10 - 50$ K), the majority of molecular species are expected to be frozen out upon the surfaces of cold, refractory grains (9). Thus, the molecular inventory of cold, dark interstellar clouds must be shaped by a *combination* of ion-molecule reactions in the gas phase and gas-grain surface reactions (6, 10). Moreover, the attenuated diffuse interstellar UV which penetrates dense clouds, as well as UV from internal sources and penetrating cosmic ray particles are sufficient to drive *in-situ*, solid-state reactions within the icy dust grain mantles leading to a variety of even more complex species (11). The chemistry in these dense, interstellar molecular clouds involves a complex interplay of these three processes.

It is within cold, dark molecular clouds such as this that new stars and planetary systems are born (Plate 1). Once part of a molecular cloud becomes unstable under its own gravitational field, it will begin to collapse, forming a protostar. As this collapse proceeds, the angular momentum possessed by the infalling material draws it into a disk. Planetary systems are thought to coalesce

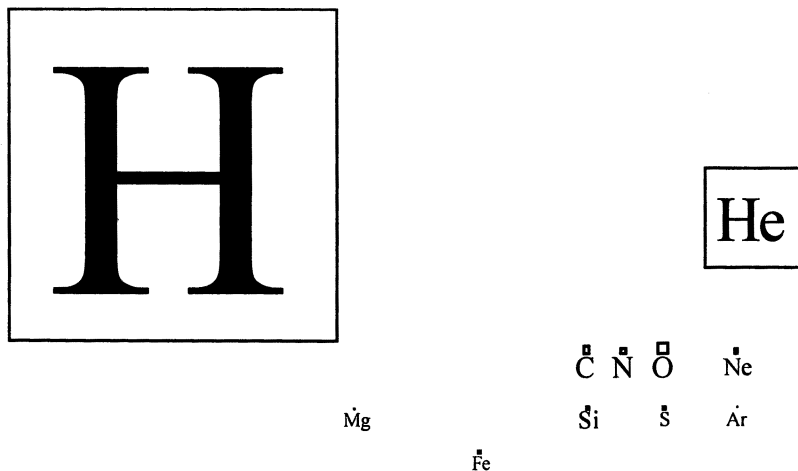


Figure 1. Astronomer's periodic table of the elements. The areas of the boxes illustrate the relative cosmic abundances of the most plentiful elements. Figure courtesy of Professor Ben McCall.

from the remnants of this protostellar accretion disk after the young star springs to life (the "Solar Nebula"). Thus, the raw material from which planetary systems form contains the elements in the same diverse states of molecular complexity found in the parent molecular cloud. Naturally, this material may also be modified to some extent by chemistry taking place during the collapse as well as in the accretion shock. Chemical processes at work during this epoch include equilibrium gas-phase reactions in the warmer regions of the nebula and non-equilibrium processes in colder regions and on coalescing planetessimals. Ultimately, the compounds present, whether produced or modified in the nebula or accepted unchanged from the ISM, are incorporated into the condensed matter that became the planets, satellites, asteroids, and comets. Once a terrestrial planet is sufficiently cool to retain volatile materials, cometary and meteoritic materials continuously pepper it with copious quantities of this complex chemical inventory. Eventually, the star exhausts its nuclear fuel, swells into a Red Giant swallowing many of its planets and moons, and its ejecta join the cycle. Thorough reviews of interstellar and solar nebula processes are given in references 5, 6, and 7.

The chemistry of dense, dark molecular clouds prior to planet formation is the topic of this paper. Dr. Ziurys has discussed the inventory and measurement of gas phase interstellar molecules associated with dense molecular clouds in the chapter, "Identifying Molecules in Space" (8). Here, the focus is on the chemistry in and on the ices and the interaction of these ices with species in the gas. Since these ices represent the largest repository of interstellar molecules in dense clouds, they tie up a large fraction of the chemical inventory in molecular

clouds. As this Chapter is intended for use as a guide book for the undergraduate chemistry student, many of the details presented here utilize material from the younger days of the field to present the foundational ideas. Current references are also included in each area for those interested in following specific topics further.

Infrared Spectroscopy of Molecular Clouds

Interstellar Ice

Before getting into the chemistry, it is important to understand how we determine what is out there and probe the chemistry that occurs thousands of light years away. It is easy to grasp how one can point a telescope at a visible star and, passing the captured ultraviolet and visible light through a spectrometer, identify some of the species comprising the star and the intervening diffuse ISM. This is how the elemental cosmic abundances illustrated in Figure 1 were initially determined. However, molecular clouds are dark. Probing the composition and chemistry within these clouds has come about thanks to fundamental advances in two areas, astrospectroscopy at infrared (IR) and longer wavelengths (Radio) and dedicated laboratory experimentation. Molecular clouds are not "dark" at these longer wavelengths. Experimentalists use modern laboratory tools to measure the IR and radio spectra of interstellar analog materials under simulated, realistic interstellar conditions and these laboratory spectra are used to interpret the astrospectra of molecular clouds.

Radio astronomy measures molecules in the gas phase. Transitions between the rotational states of most molecules that possess a permanent dipole moment absorb or emit electromagnetic radiation at wavelengths spanning the radio range. These observations and implied chemistry are reviewed in reference 8. Since molecules condensed on cold dust grains cannot rotate, they do not possess a rotational spectrum and are undetectable by observations at radio wavelengths. Infrared astronomy, which probes molecules in both the gas and solid phases, provides the rest of the story. The vibrations between atoms and subgroups that comprise a given molecule vibrate at specific, characteristic frequencies. Those vibrations that involve a change in dipole moment absorb or emit electromagnetic radiation at these bond-specific frequencies. Since these transitions fall in the mid-infrared region, chemists routinely use IR spectroscopy to characterize the chemical make-up of materials.

Plate 2 illustrates the dramatic difference between the visible and infrared image of the sky looking towards Orion. The infrared radiation that dominates the IR image of the constellation (colored red in the figure) comes from the blackbody radiation of the interstellar dust particles comprising what is known as

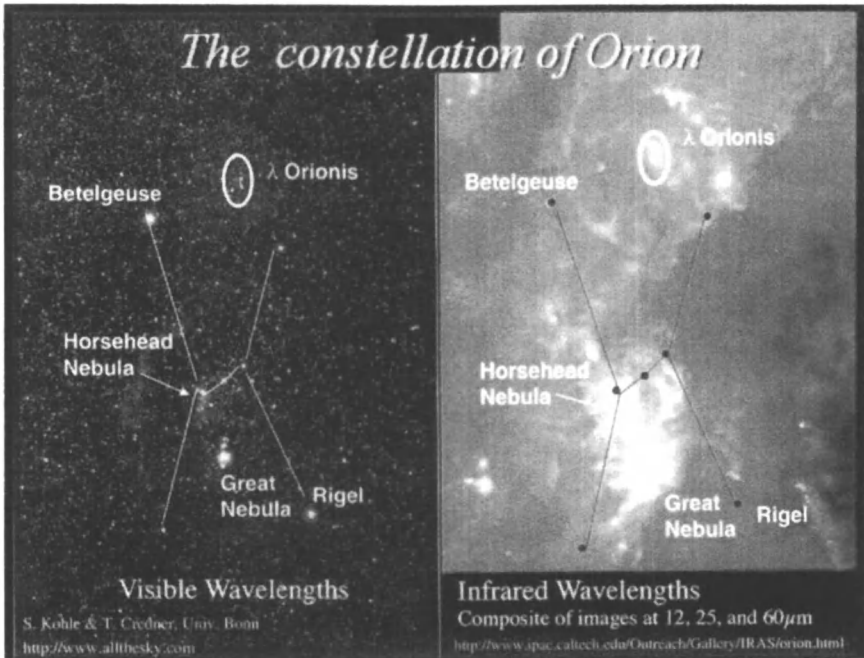


Plate 2. Visible and infrared images of the sky toward the Orion Constellation. Left: Visible Image. The white lines indicate the main stars of the well-known constellation. Right: The Infrared Astronomical Satellite IR image of the same region of the sky. The interconnected dark circles indicate the positions of the now invisible constellation stars. The reddish glow is from the dust in this enormous cloud which is many thousands of light years across. The yellow areas correspond to emission from the warmest dust, generally regions illuminated by light from nearby stars. Clouds such as these are the birthplace of stars and planets and are home to complex interstellar molecules. In this case the cloud is behind the stars that make up the constellation. Otherwise this would appear as a dark patch in the night sky. Plate courtesy of Dr. Andrew Mattioda (See page 2 of color inserts.)

the Orion Molecular Cloud which lies behind the stars we see. The IR hot spots (colored yellow) are associated with regions where intense UV radiation is striking the cloud.

Once a dense cloud is formed, thanks to the attenuation of the general interstellar radiation field, gas-phase and gas-grain chemistry leads to the production and sustaining of more complex species in the gas than possible in the diffuse ISM. At the same time, since the dust in a dense molecular cloud is

so cold (~20K), any polyatomic molecule striking a dust grain should condense (9), and one might expect grain composition to reflect gas composition. However, the simplest and most abundant gas-phase *polyatomic* molecules known from radio observations are orders of magnitude lower in abundance than their frozen counterparts (13). Thus, direct accretion of interstellar gas-phase species plays a very minor role in determining interstellar ice composition since the ice grains are chemical factories in their own right, generally harboring far greater amounts of material than the gas.

Interstellar ice compositions are revealed through their IR spectra. As illustrated in Plate 3, a star, fortuitously situated in or behind a molecular cloud, can provide a reasonably featureless, continuous mid-IR background spectrum much as a glow-bar does in a conventional laboratory spectrometer. As this radiation passes through the cold cloud, the intervening molecules in the gas and dust *absorb* at their characteristic vibrational frequencies. Since the diffuse ISM between the outer "edge" of the cloud and the Earth is far less dense, and the majority of interstellar polyatomic molecules are frozen on the grains, the IR absorption spectrum of objects obscured by molecular cloud material is mainly that of the dust in the dense molecular cloud. Since the ice features dominate these spectra, interstellar ice composition can be analyzed by directly comparing the astronomical data with the spectra of ices prepared in a laboratory which duplicate the salient interstellar conditions. This can be accomplished using a cryogenic sample chamber in which thin layers of mixed molecular ices are deposited on a cold (10 - 20 K), IR transparent sample window maintained under vacuum. Sample ice thickness is comparable to that of all the interstellar grain mantles along the line of sight. The infrared spectrum of the ice is then measured and compared directly with astronomical spectra. In a typical experiment, the spectrum of the sample would be measured before and after several periods of exposure to UV radiation and thermal cycles. A more detailed discussion of this approach is given in reference 14.

Figure 2 shows a collage of comparisons between the composite spectrum of W33A, a protostar deeply embedded within a molecular cloud, with the laboratory spectra of interstellar ice analogs (15-19). This spectrum of W33 is a combination of spectra measured at different telescopes. With the exception of the strong absorption near 10 μm for which the Si-O stretch from the silicate dust particles overwhelms the overlapping ice features (20), most of the absorptions in the spectrum of W33A are readily assigned to ice components. Excellent matches between the interstellar absorption features with laboratory spectra of the type shown in Figure 2 represent the basis of our knowledge of the composition of interstellar ice particles. Until quite recently, much more was known of interstellar ice grain composition - submicron sized particles hundreds of light years away - than of cometary ices in our own Solar System. This is still the case for most other icy objects in the Solar System!

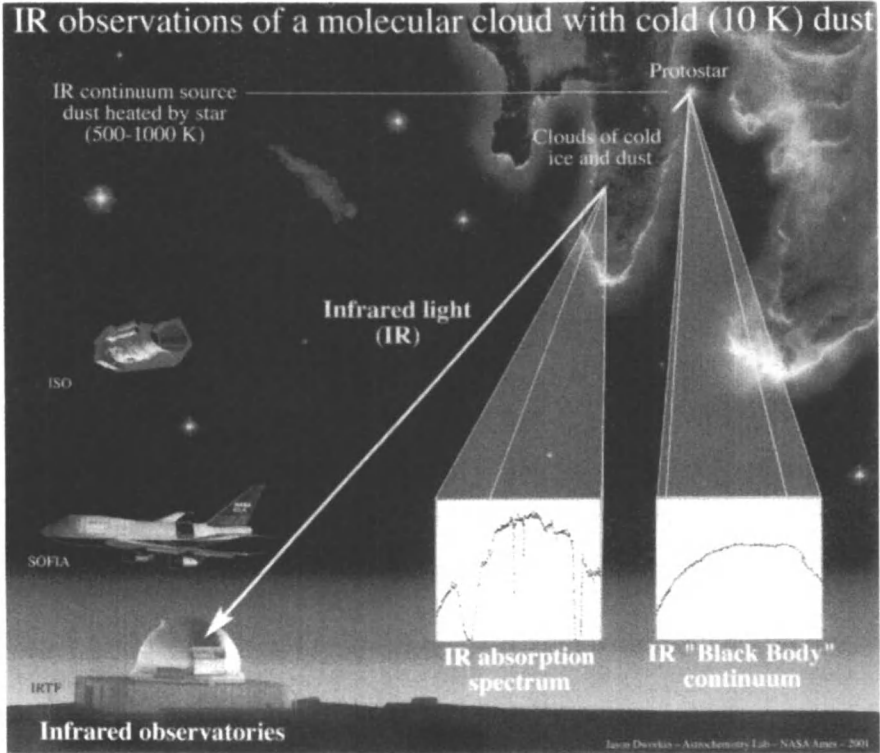


Plate 3. An illustration of how one measures the IR absorption spectra of interstellar clouds. A background star (protostar) serves as the IR source, the cloud is the sample, and the telescope gathers the light and sends it to a monochromator or spectrometer. The advent of airborne IR telescopes in the 70's and orbiting telescopes in the 80's made it possible to avoid IR absorptions by atmospheric H_2O , CO_2 , and so on, opening a new window into the Cosmos. Plate courtesy of Dr. Jason Dworkin. (See page 3 of color inserts.)

Over the past decade, deeper insight into the nature of interstellar ice and dust has been achieved through analysis of data from the European Space Agency's (ESA) Infrared Space Observatory (ISO) and NASA's Spitzer Space Telescope. These missions have enabled measurement of the complete mid-IR spectrum with one instrument, eliminating the need to piece together bits from different telescopes taken at different locations, under different atmospheric conditions and with different spectral parameters (Figure 3). The IR spectra obtained with these telescopes are pushing this field beyond analysis of the strongest spectral features, revealing important subtleties in the spectra that probe details of interstellar chemistry, grain evolution, and cloud development (6,7,21-23).

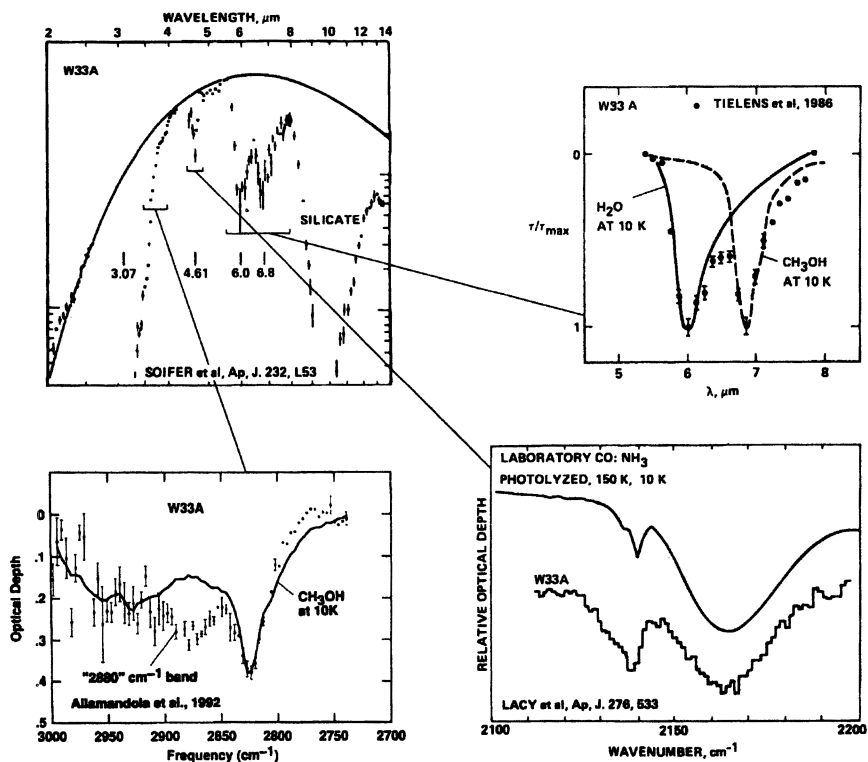


Figure 2. Comparisons of laboratory analog spectra with spectra from the object W33A, a protostar deeply embedded in a dense molecular cloud. Upper left: The dots trace out the interstellar spectrum and the solid line corresponds to the quasi-blackbody emission spectrum thought to be produced by the protostar. The strong absorption near $10\ \mu\text{m}$ is due to the silicate grains and the excess absorption labeled "2880 cm^{-1} Band" visible in the lower left-hand panel is thought to arise from interstellar microdiamonds in the cloud. All the remaining absorptions are produced by interstellar ices. These features are highlighted and compared to laboratory spectra on expanded scales in the surrounding frames. Lower left: The solid line is due to methanol in a laboratory ice. Lower right: The upper smooth line corresponds to a laboratory analog comprised of CO (sharp band) and OCN (XCN, broad band). Upper right: The solid and dashed lines correspond to spectra of H_2O and CH_3OH respectively. These data are presented and discussed in detail in references 15-19.

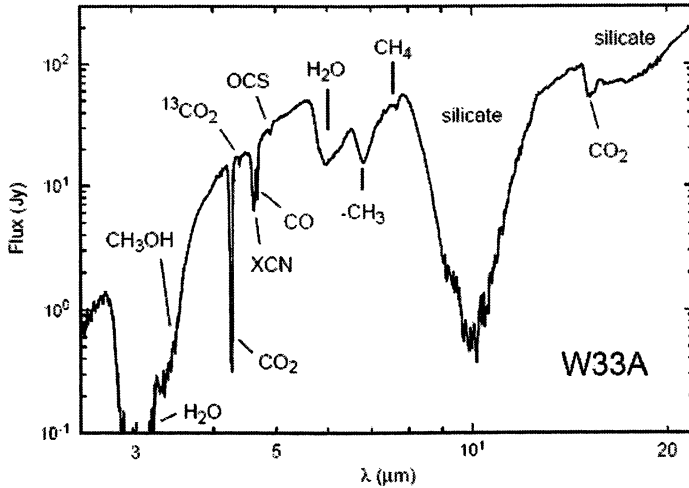


Figure 3. The complete mid-IR spectrum toward W33. The bands have all been identified as described here. This spectrum, measured with ISO, shows the full power of mid-IR astrospectroscopy (6, 21).

Table I. The main interstellar ice components (relative to H₂O) compared to that inferred for several comets. Cometary references: Halley (24), Hyakutake and Hale-Bopp (25). See Table 2 in Reference 6 for details.

Molecule	<u>Interstellar</u>	<u>Comet Parent Molecules</u>		
	<u>Ice</u>	Halley	Hyakutake	Hale-Bopp
	Abundance			
H ₂ O	100	100	100	100
CO _(polar ice)	1-10			
CO _(non-polar ice)	10-40	17	6-30	20
CH ₃ OH	<4-30	1.25	2	2
CO ₂	1-10	3.5	<7	6
OCN ⁻ (XCN)	1-10	---	---	---
NH ₃	5-10	1.5	0.5	0.7
CH ₄	~1	<0.8	0.7	0.6
H ₂ CO	1-4	3.8	0.2-1	1
OCS or CO ₃	few	0.2	0.1	0.3

Table I compares the dominant interstellar ice constituents with the inferred components from several comets and gives their abundance with respect to H₂O. Detailed reviews of this topic can be found elsewhere (6, 7).

Interstellar Polycyclic Aromatic Hydrocarbons

Since this chapter is intended for chemists and the goal is to focus on interstellar chemistry, it would be seriously remiss to omit discussion of the discovery that polycyclic aromatic hydrocarbons (PAHs), large, complex, chicken-wire structured, organic molecules, are ubiquitous and abundant throughout the cosmos (26, 27). This realization, also driven home by IR astrospectroscopy and dedicated laboratory analog studies, has shaken the astrochemist's view of the universe to its foundation. In a nutshell, an infrared *emission* spectrum is observed from a wide variety of galactic and extragalactic objects that is produced by vibrationally excited (hot) PAHs. The picture that has emerged is one in which the PAHs and nitrogen heterocycles (PANHs), which were formed during the Red Giant mass loss phase, survive the rigors of interstellar space because of their inherent chemical stability and participate in *every* stage of the cycle shown in Plate 1. The distribution of PAH emission from a spiral galaxy similar to our own is shown in Plate 4. The interstellar PAH IR emission features, shown in red in Plate 5, are obvious in many spectra of the cosmos. They are even implicated in the spectra of objects that appeared only a few billion years after the Big Bang. A thorough presentation of the cosmic PAH model, incorporating a chemist's perspective, is given in reference (28), and a recent review of the observations can be found in reference (29). The presence of such complex organic species, apparently widespread and abundant throughout the Universe, has come as quite a surprise, and the implications of this realization are yet to be understood.

Chemical Evolution within Dense, Dark, Molecular Clouds

The picture of mixed molecular interstellar ice described up to this point is supported by direct spectroscopic evidence (e.g. Figures 2, 3). The identities, relative amounts and absolute abundances of the ice species listed in Table I are sound (see references 6 and 7 and references therein for detailed discussions). However, this is not the entire story. Indeed, from a chemist's perspective, this is only the beginning of the story. As mentioned above, throughout the cloud's lifetime, processes such as accretion of gas phase species, simultaneous reactions on the surfaces involving atoms, ions, and radicals, as well as energetic processing within the body of the ice by ultraviolet photons and cosmic rays all combine to determine the ice mantle composition (5-7). Theoreticians are

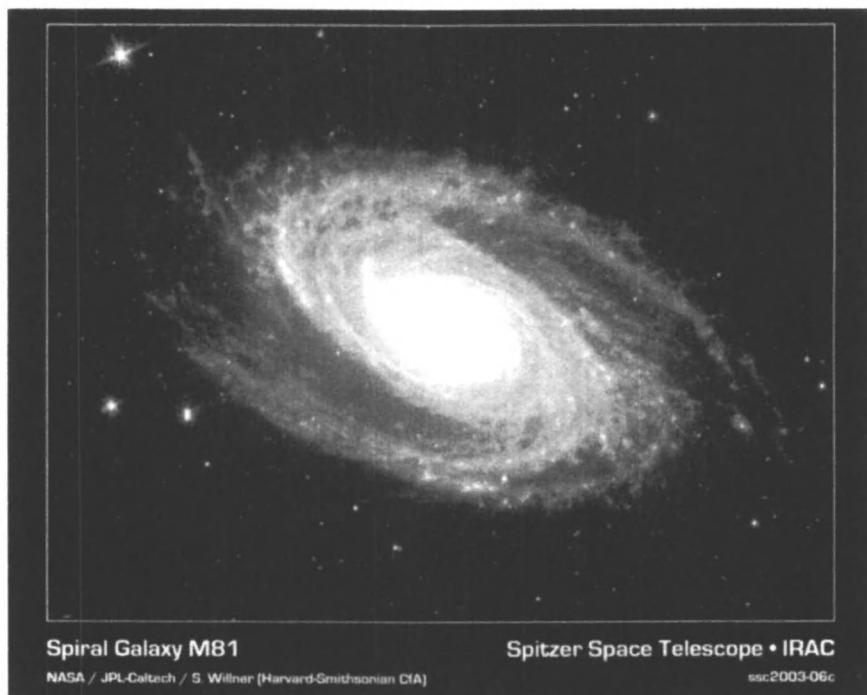


Plate 4. Spitzer Space Telescope IR image of M 81. The red color traces the strong PAH emission band between about 7 and 9 μm shown in Plate 5. (See page 4 of color inserts.)

continuously developing and improving models that attempt to describe this chemistry, account for the species observed, and predict their abundances (30-32). However, due to the range of the very different chemical processes posited, our poor understanding of the chemical processes involved, and the very limited amount of experimental kinetic data taken at the relevant temperatures and pressures, a detailed description of the chemistry is well beyond current capabilities. Consider the following; since hydrogen is 3 to 4 orders of magnitude more abundant than the next most abundant reactive elements such as C, N, and O, overall grain surface chemistry is strongly moderated by the H/H_2 ratio in the gas. In regions where this ratio is large, H atom addition (hydrogenation) dominates and species such as CH_4 , NH_3 and H_2O are expected to be prominent (33). If the H/H_2 ratio is substantially less than one, however, reactive heavy atoms such as O and N are free to interact with one another forming molecules such as CO, CO_2 , O_2 and N_2 . Thus, two qualitatively different types of ice mantle may be expected from grain surface reactions; one dominated by hydrogen-rich, polar molecules, capable of

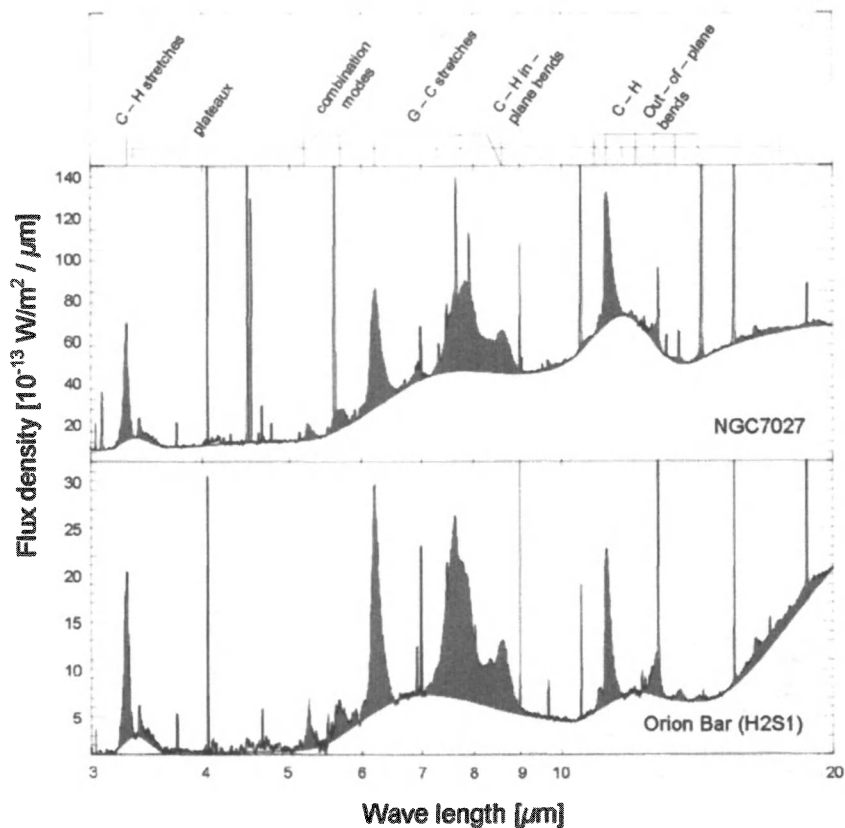


Plate 5. Two examples of the IR emission spectra from interstellar PAHs. The upper spectrum is of PAHs that were "freshly" ejected from a Red Giant. The lower spectrum is from the Great Nebula in the Orion molecular cloud (Figure 3, bottom, center, both panels) where it is exposed to the intense UV field from hot, young stars. The red features are all attributed to PAHs. The fundamental vibrations which produce the features are summarized across the top of the figure. The underlying broad structure is thought to arise from overlapping individual bands from PAHs and larger species. The variations between spectra reveal differences in the PAHs present in each object, reflecting the unique chemical history and conditions within the PAH emission region. Plate courtesy of Dr. Els Peeters, see reference (29). PAH structures are shown in Figure 8. (See page 5 of color inserts.)

hydrogen-bonding and the other dominated by hydrogen-poor, non-polar (or only slightly polar), highly unsaturated molecules. The different types of chemistry that polar and non-polar ice mantles promote are as different as the processes that can occur in oil versus those that can occur in water. Add to this the interplay between condensation of larger interstellar species from the gas phase, UV and cosmic ray bombardment, thermal cycling, etc. and the computational challenge is clear.

Interstellar Ice Photochemical Evolution

Experimentalists in several laboratories around the world have focused on the photochemical evolution of ice grain mantle analogs to shed some light on the chemistry that occurs when the ices in dense molecular clouds are irradiated by UV photons and cosmic rays, breaking and rearranging chemical bonds within the ice to form new species (14, 34-36). This chemistry is illustrated in Plate 6. Although the abundance of these new species is only a few percent, energetic processing is critically important since it can create remarkably complex molecules and chemical groups that cannot be made via gas phase and gas-grain reactions at the low temperatures and pressures characteristic of dense clouds. This is because the protection and ready availability of reaction partners in the solid phase favors chemical complexity and diversity while the energetics, radiation fields, and low densities of the gas phase favor simplicity.

The interstellar/precometary ice composition along the lines-of-sight to regions such as W33 where stars are developing is of particular relevance since these are places where new planets are also forming. The material *immediately* surrounding these star forming regions dominates the absorption spectrum because the volume concentration of gas and dust is many orders of magnitude greater here than it is along the rest of the line of sight. These are the regions in which the OCN⁻ (formerly XCN), CO₂, and CH₃OH bands are present. The evidence has been building for some time now that these species are tracers of grain reactions and *in-situ* energetic processing. The presence of methanol in these ices is of pivotal importance since it drives a rich interstellar ice photochemistry (14, 38-40) and plays an important role in gas phase chemistry (41). Furthermore, methanol has profound effects on the physical behavior of H₂O-rich ices (42). Since CH₃OH is often an abundant ice component in comets (Table I, cf. references 43 and 44), it may impact their structural, chemical, and vaporization behavior as well.

Figure 4 shows the spectral evolution of an interstellar ice analog comprised of H₂O:CH₃OH:CO:NH₃:C₃H₆ (100:50:10:10:10) as a function of UV photolysis. Except for the C₃H₆, this analog mixture reflects the major interstellar ice components associated with protostellar environments. The exposure to UV results in the destruction of several species (particularly

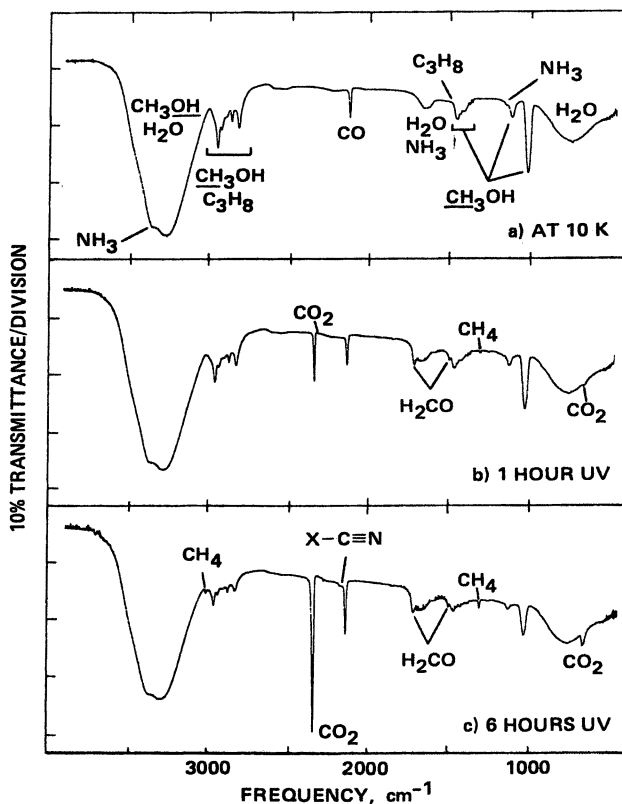


Figure 4. The photochemical evolution of an $\text{H}_2\text{O}:\text{CH}_3\text{OH}:\text{NH}_3:\text{CO}:\text{C}_3\text{H}_8$ (100:50:10:10:10) interstellar ice analog as traced by infrared spectra measured at 10 K. The spectra were taken before (a) and after 1 hour (b) and 6 hours (c) of UV irradiation. Note the ready formation of CO_2 , H_2CO , CH_4 , and XCN (now known to be OCN^-) at the expense of CH_3OH . Figure adapted from reference 14.

methanol) and the creation of others. The simplest and most abundant include the radical HCO , as well as the molecules H_2CO , CH_4 , CO , and CO_2 . As shown in Table I, almost all of these new species have been identified in interstellar ices and there is indirect evidence for HCO . The detection of these ice components in dense molecular clouds does not necessarily imply radiation processing is responsible for their production since many of these molecules can also be formed by gas-phase or gas-grain chemistry. So, at present, all we can say is that observations are consistent with energetic processing. To reiterate, the strongest evidence that energetic processing is important, at least in some locations within dense clouds, is provided by the OCN^- feature (XCN in Figures

2 and 3) and perhaps by CH_3OH and the ubiquity of CO_2 . While CO_2 is readily produced by UV photolysis, it can also be formed by reactions between CO and O on the ice surface (45). The OCN^- feature cannot be explained by any of the more abundant species predicted by gas-phase and gas-grain chemical models, but is readily made by the radiative processing of laboratory ices containing C, N and O. Excellent, detailed descriptions of the UV-induced chemical evolution of interstellar ice analogs can be found in the literature (14, 38, 46, 47). The role of methanol in the ice photochemistry discussed here is very critical to the kinds of compounds produced.

For the remainder of this paper we focus on the photochemical processing of the H_2O -rich, polar ices associated with the environments of high mass protostars. The ice chemistry so far considered involves the photoproduction of the most abundant, simple species in the solid state at 10 K. However, the full scope of the chemistry is much more complex. Upon warm-up to about 200 K under vacuum one observes that the parent compounds and most volatile ice constituents sublime, leaving a residual mixture of less volatile species on the substrate. Of the staggering array of compounds produced from even the simplest starting ice containing H_2O , CH_3OH , NH_3 , and CO, only a few have been identified. These are presented in Figure 5. In keeping with their expected low concentration and abundance, clear-cut IR spectroscopic evidence for these types of compounds in interstellar ices is presently lacking, although some of the weak spectral structure detected in the 2000-1250 cm^{-1} region by the ISO and Spitzer space telescopes is consistent with their presence. Additionally, spectral screening by the much more abundant, simpler ice species will likely represent an important, long-term obstacle. Higher quality astronomical spectra than those currently available will be needed to probe the species present at this level of concentration. Even then, identifications will likely be limited to chemical classes. As an aside, the abundance of many interstellar gas phase species, including NH_3 , H_2CO , and CH_3OH , is observed to increase in these warmer regions due to their sublimation from ice grain mantles.

The residue that remains after evaporation of the volatiles when the irradiated ice is warmed to room temperature under vacuum is also of interest since it is quite plausible that this type of material is closely related to that preserved in comets, meteorites and interplanetary dust particles (IDPs), and it is believed that these sources deliver between 12 and 30 *tons* of organic material to Earth monthly. During the period of great bombardment some 4 billion years ago, the amount of extraterrestrial organic material brought to the early Earth was many orders of magnitude greater. Thus, this type of material could have played an important role in steering the early chemistry on the primordial Earth. Now, let's consider more closely the molecules which are produced upon photolysis of *realistic* interstellar ice analogs. The word realistic is used to indicate that the laboratory ice composition reflects the interstellar polar ice composition shown in Table I. The standard ice we study has a starting composition of $\text{H}_2\text{O}:\text{CH}_3\text{OH}:\text{NH}_3:\text{CO}$ (100:50:1:1) or $\text{H}_2\text{O}:\text{CH}_3\text{OH}:\text{NH}_3:\text{CO}$

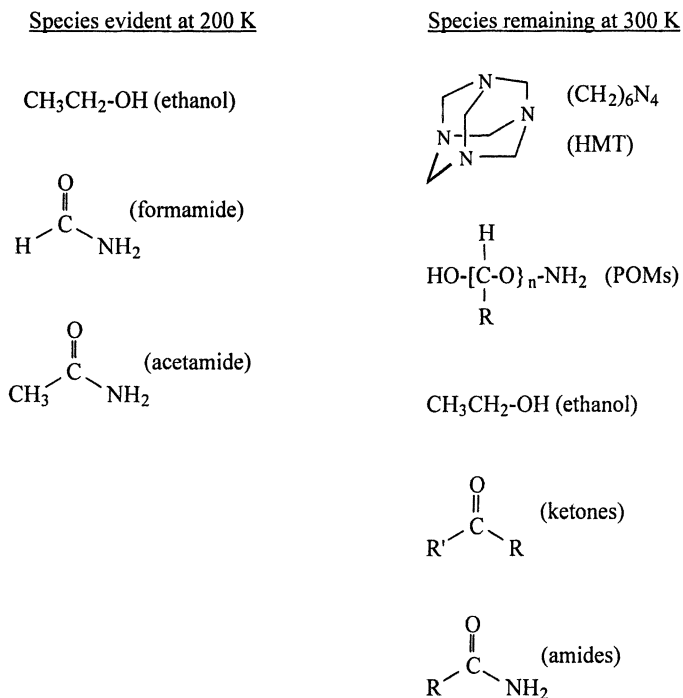


Figure 5. Identified compounds produced by the 10 K UV photolysis and subsequent warm-up of the realistic interstellar ice analogs $\text{H}_2\text{O}:\text{CH}_3\text{OH}:\text{NH}_3:\text{CO}$ (100:50:10:10) and (100:50:1:1)
Figure courtesy of Dr. Max Bernstein.

(100:50:5:5). As evident from Table I, these have slightly higher methanol concentrations ($\text{H}_2\text{O}/\text{CH}_3\text{OH} \sim 2/1$) than the maximum observed ($\text{H}_2\text{O}/\text{CH}_3\text{OH} \sim 3/1$). There is good reason for this experimental choice. Even with the higher methanol concentrations, to produce sufficient material for one analytical run requires between two to three months of constant sample preparation. Thus, using a single apparatus for sample preparation it is typically possible to do only four to five experiments *per year*. Reducing the yield would shift this from a very difficult project to one that is impossible given our current analytic capabilities. On the other hand, as the spectra of more molecular clouds become available, higher methanol concentrations are being detected.

Lastly, a comment is in order regarding the other abundant interstellar ice components CO_2 , OCN^- (XCN), CH_4 , and H_2CO listed in Table I. We are not concerned with their absence in the starting mixture because, as explained above (e.g. Figure 4) they are readily produced upon photolysis at concentrations consistent with the observations. As these are produced at the expense of

methanol (14), lowering that species concentration, *all the major interstellar ice ingredients known toward massive protostellar environments are represented in this experiment and at roughly the correct concentrations.*

Complex Organic Production in Ices without PAHs

While many of these new species sublime when the irradiated ice is warmed from 200K to room temperature under vacuum, a thick oily residue of non-volatile material remains. Among many other things, this residue is rich in the cage molecule hexamethylenetetramine (HMT, $C_6H_{12}N_4$) (38). This contrasts with the organic residues produced by irradiating mixed molecular ices which do not contain methanol (e.g. refs. 14, 38, 39) and those produced in thermally promoted polymerization-type reactions in non-irradiated realistic ice mixtures (48). In those experiments HMT is only a minor product in a residue dominated by a mixture of polyoxymethylene (POM) related species. Remarkably, POMs already start to form in these ices at temperatures as low as 40 K, temperatures at which most chemists would consider reaction between stable species impossible. Further, POM-like species have been suggested as an important organic component detected in the coma of Comet Halley (49). The synthesis of HMT by photolysis implies the presence of several other interesting intermediates in these ices as well. For example, there are a variety of secondary carbon and nitrogen containing species which are readily formed by HMT hydrolysis, thermalization, or photolysis, all processes which can occur during an interstellar ice grain, comet, or asteroid's lifetime. The HMT production pathway proposed in reference 38 involves the intermediate methylimine (CH_2N). Armed with this information, radioastronomers searched for and found methylimine to be widespread throughout the gas in many molecular clouds providing additional evidence for a connection between gas and grain chemistry (50). Beyond HMT and POMs, the non-volatile residue of photolyzed, methanol containing ices comprises lower concentrations of a bewildering array of organic compounds.

Due to the extreme complexity and analytical challenge posed by deeper analysis, and encouraged by recent interest in the application of these results to early earth biochemistry, effort has been redirected from solely establishing the chemical inventory of species produced in these interstellar/precometary ice analogs to searching for the presence of specific biogenically important species. This effort has involved High Performance Liquid Chromatography (HPLC) and laser desorption-laser ionization mass spectroscopy (L^2MS). Access to the latter technique has been made possible through a collaboration with Prof. R. Zare and his colleagues at Stanford University (51). While neither technique can provide an unequivocal identification directly, they are both particularly suited to microanalysis and give very valuable insight into the chemical properties of the compounds that make up the residue.

Figure 6 shows the HPLC chromatogram of one of the residues compared to the chromatogram of a soluble extract from the primitive meteorite Murchison. There are two conclusions to be drawn from this figure. First, since each peak represents a different compound, or more likely a different family of compounds, both the laboratory residue and meteoritic extract are complex chemical mixtures. Second, the similarity in peak distributions between the two samples indicates that the kinds of chemicals present in each sample are similar. This similarity raises the interesting question, "Do the families of compounds in carbonaceous meteorites have an interstellar ice/cometary heritage?"

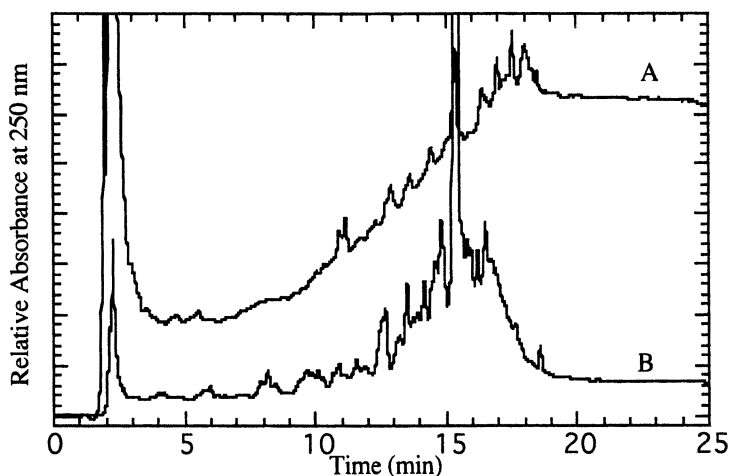


Figure 6. The high performance liquid chromatogram (HPLC) of (A) the room temperature residue produced by UV photolysis of an $\text{H}_2\text{O}:\text{CH}_3\text{OH}:\text{NH}_3:\text{CO}$ (100:50:1:1) ice (profile magnified 10x) and (B) mixed acid and base extracts of Murchison meteorite. Figure courtesy of Dr. Jason Dworkin. See (40)

Figure 7 shows the L^2MS of the residue from a photolyzed $\text{H}_2\text{O}:\text{CH}_3\text{OH}:\text{NH}_3:\text{CO}$ (100:50:1:1) ice. Mass spectra such as this provide us with further critical insight into the nature of the residue, showing that there are hundreds of compounds produced. Further, this shows that they are far more complex than the starting materials. The new materials produced are responsible for the envelope spanning the mass range from about 100 m/z to 350 m/z . (m/z is equivalent to an atomic mass unit). Given that none of the simple starting materials of $\text{H}_2\text{O}:\text{CH}_3\text{OH}:\text{NH}_3:\text{CO}$ has a mass greater than 32, nor do they contain a single CC bond, the complexity and extent of the photoproducts is staggering. Many of these compounds have molecular masses up to *ten times* larger than that of any of the starting materials. When this mass spectrum is compared with those of two interplanetary dust particles (IDPs) there is an

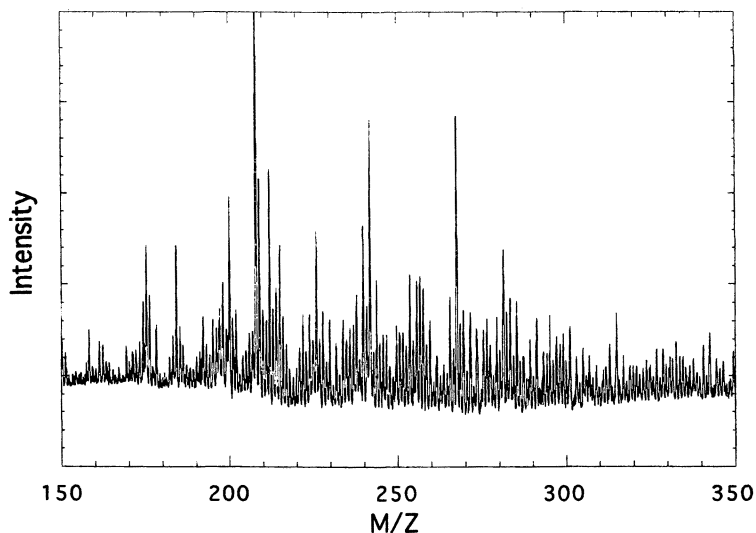


Figure 7. The laser desorption (L^2MS) mass spectrum of an interstellar ice analog residue produced by the photolysis of a $H_2O:CH_3OH:NH_3:CO$ (100:50:1:1) ice. The complexity of the interstellar ice analog residue is clearly evident (52). See also reference (53).

intriguing similarity between the mass envelope of the interstellar ice analog residue shown in Figure 7 and the mass envelopes in the IDP spectra (52). As with the HPLC results above, this resemblance between the laboratory ice residue and the extraterrestrial organics brought to Earth - this time in IDPs - again raises the question, "Do the compounds in IDPs have an interstellar ice/cometary heritage?" Since many IDPs are thought to originate in comets, the connection with interstellar cloud chemistry gets tighter.

Greenberg et al. (53) reported a fascinating study of residues produced by the photolysis of the somewhat different mixed molecular ices $H_2O:CH_3OH:NH_3:CO$ (100:20:20:100) and $H_2O:CH_4:NH_3:CO$ (100:40:40:40). These residues were placed in small sample chambers on the EURECA satellite and exposed to solar radiation through a UV-visible transparent MgF window. The residues were returned to Earth after a four month exposure. Subsequent analysis of these residues using the L^2MS technique showed a pattern reminiscent of the one presented in Figure 7, but now with mass peaks corresponding to the PAHs coronene, benzoperylene, pyrene, and phanthrene particularly strong.

Complex Organic Production in Ices with PAHs

As mentioned above, as a class, PAHs are among the most abundant interstellar polyatomic molecules known in the gas and are widespread throughout

the interstellar medium. As with all other polyatomic gas phase species in dense clouds, they should freeze out onto the grains and become part of the mixed molecular ice. Indeed, weak, broad absorption bands are evident in dense cloud spectra that are consistent with PAHs frozen in the ice mantles. However, the strong absorption bands of the main ice species screen out the weaker PAH features. The photochemical behavior of PAHs in H₂O ices has also been investigated in order to lay the foundation for a study of PAH photochemistry in realistic, multicomponent interstellar ice analogs.

While the UV photolysis of PAHs in interstellar ices likely modifies only a fraction of the interstellar PAH population, this change is significant in terms of interstellar chemistry and interesting from the prebiotic chemistry perspective. Upon photolysis in pure H₂O ice at 10 K, simple PAHs are not destroyed. Almost immediately upon irradiation, 70 to 80 % of the PAHs are readily ionized to the positively charged (cation) form (54). Remarkably, these PAH cations are not reactive in these ices at all until they are warmed above 100 K (55). Even above 100 K, the PAH cation reacts slowly with other species in the H₂O ice, ultimately producing the types of species shown in Figure 8 and discussed below (56). Some of these PAH ion charged ices are gently colored, raising the speculation that perhaps organic ion containing ices are responsible for some of the coloring of many icy objects in the Solar System, such as Saturn's icy moons and rings and the icy moons of Jupiter.

After warm-up to room temperature, we find that the PAHs in the residue have been partially oxidized and/or reduced (hydrogenated), forming structures as shown in Figure 8 (57). If deuterium is present in the ice, deuterated aromatics are also produced (58, 59). These alterations have significantly different effects on the chemical nature of the parent. Hydrogen atom addition transforms some of the edge rings into cyclic aliphatic hydrocarbons, thereby creating molecules with both aromatic and aliphatic character and decreasing the overall degree of aromaticity. Oxygenation produces ketones or aldehydes, changes which open up an entire range of possible chemical reactions that were not available to the parent PAH. Aromatic ketones are of particular interest since they are present in meteorites and closely related compounds are widely used in current living systems for electron transport across cell membranes. In view of PAH photochemistry in pure H₂O ice, it seems plausible that aromatic structures decorated with alkyl, amino, hydroxyl, cyano, carboxyl, and other interesting functional groups may be produced when mixed-molecular ices containing PAHs are photolyzed and warmed. Laboratory experiments have demonstrated that the aromatic structures decorated with alkyl, amino, hydroxyl, cyano, carboxyl, and other functional groups seen in meteorites are consistent with a pre-solar ice chemistry driven by UV photons and cosmic rays (60, 61).

Recently, we have also investigated the chemistry of polycyclic aromatic nitrogen heterocycles (PANHs) in interstellar ice analogs (62). PANHs are structurally similar molecules to PAHs, with one or more nitrogen atoms

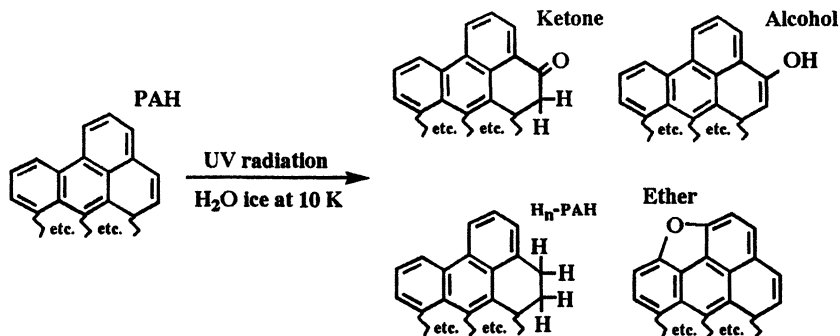


Figure 8. The types of PAH structures found in the residue that remains after PAHs are UV radiated in water ice at 10 K and the sample is warmed to room temperature under vacuum (57).

substituted for carbon in the molecular skeleton. These compounds are also believed to be present in the ISM (63) and should be present in interstellar ices. Experiments in which PANHs are photolyzed in water ice form species that are similar to those formed when PAHs are photolyzed in interstellar ice analogs. These too are found in the Murchison meteorite (64).

Interstellar PAHs, Ices, and Chemistry on the Early Earth

To better understand the role these interstellar/precometary residues might have played in the chemistry on the early Earth, we have also investigated both their bulk or collective chemical properties and searched for specific molecules such as amino acids. Examples of both will be given here.

We focused on collective chemical properties with Professor D. Deamer from the University of California, Santa Cruz. While much of the residue described above dissolves rapidly in liquid water or methanol, water-insoluble droplets are also formed (11, 40). Plate 7 shows a micrograph of these non-soluble droplets in water. Many of the droplets also show intriguing internal structures. Droplet formation shows that some of the complex organic compounds produced in these interstellar ice analogs are amphiphilic, i.e. they have both a polar and non-polar component, similar in structure to the molecules which comprise soap. These are also the types of molecules that make up cell membranes, and membrane production is considered a critical step in the origin of life. These droplets can encapsulate hydrophilic fluorescent dyes within their interior, demonstrating that they are true vesicles (hollow droplets) with their interiors separated from the surroundings by their lipid multilayer (see Figure 5

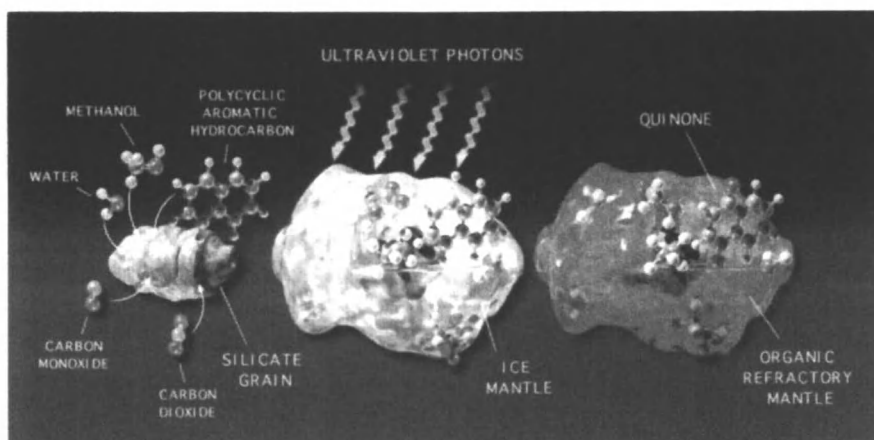


Plate 6. The Greenberg model of interstellar ice mantle formation and chemical evolution. The mantle grows by condensation of gas phase species onto the cold dust grains. Simultaneously, surface reactions between these species, ultraviolet radiation and cosmic ray bombardment drive a complex chemistry. These ice-mantled grains are thought to be micron sized at most. Plate reproduced with permission from (37). (See page 6 of color inserts.)

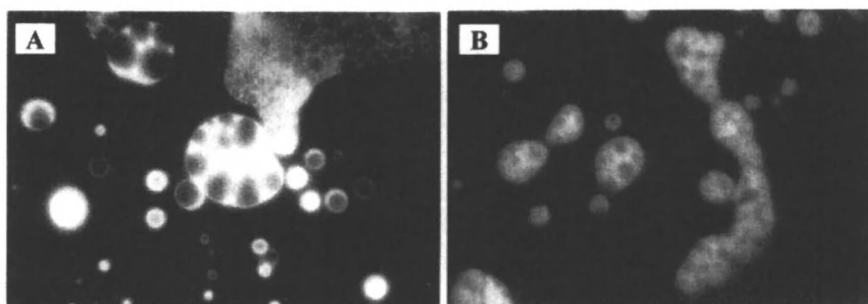


Plate 7. (A) Fluorescence micrograph of the water insoluble droplets formed from a Murchison meteorite extract (67) compared to (B) the fluorescent droplets produced from the photolysis residue of the interstellar/precometary ice analog: $H_2O:CH_3OH:NH_3:CO$ (100:50:1:1) at 10 K (40). The similarity between these vesicles is another indication of similarity between the laboratory ice residue and extraterrestrial organics in meteorites. (See page 6 of color inserts.)

in reference 40). Vesicle formation is thought critical to the origin of life since vesicles provide an environment in which life can evolve, isolating and protecting the process from the surrounding medium. For example, within the confines of a vesicle, pH can be moderated and held at a different value from that in the surrounding medium, and nutrients, catalysts, and other materials can be concentrated and held together. While it is uncertain where membrane formation falls in the sequence of events leading up to the origin of life, with some arguing that it must have been one of the first steps (65), and others that it occurred at a later stage (66), it is considered a very crucial step (68).

Plate 7 also shows that the membranes trap other, photoluminescent, molecules that are produced within the ice by UV irradiation (11, 40). Thus, not only are vesicle forming compounds produced from the simplest and most abundant interstellar starting materials, complex organics which absorb UV are also formed. The ability to form and trap energy receptors within these structures is considered another critical step in the origin of life as it provides the means to harvest energy available outside the system. Another class of potentially important organic molecules brought to the earth by meteorites are amino acids, the molecular building blocks of proteins and enzymes. That these amino acids in meteorites are extraterrestrial is demonstrated by their deuterium enrichments - the highest of any ever measured in a meteorite (69). The high abundances of deuterium suggested that these amino acids had a low temperature heritage (70). Consequently, it is widely held that meteoritic amino acids formed from interstellar precursors in liquid water in the asteroidal or cometary meteorite parent body within the forming solar nebula (71). However, since laboratory photolysis experiments of plausible presolar ice mixtures also produce amino acids (72), presolar ice photochemistry could also be a source of these amino acids.

The mounting evidence in favor of a strong connection between interstellar organic materials and the carbonaceous fractions of meteorites and IDPs (and by implication comets) strengthens the case for taking interstellar PAHs and ices into account when pondering an exogenous contribution to early Earth chemistry (see Figure 9).

Conclusion

Over the past thirty years tremendous strides have been made in our understanding of the complex chemistry in dense, dark, interstellar molecular clouds. This has come about because of fundamental advances in observational infrared astronomy and laboratory astrophysics. Thirty years ago the composition of interstellar dust was largely guessed at; the concept of ices in

dense molecular clouds ignored; and the notion of large, abundant, gas phase, carbon-rich molecules widespread throughout the interstellar medium considered impossible. Astronomical infrared spectroscopy and dedicated laboratory experimentation has changed all that. Today the composition of interstellar dust is reasonably well understood. Cold dust particles are coated with mixed molecular ices in molecular clouds and the signature of carbon-rich, large polycyclic aromatic hydrocarbons (PAHs), shockingly large molecules/particles by usual interstellar chemistry standards, is widespread throughout the Universe: even at cosmological distances.

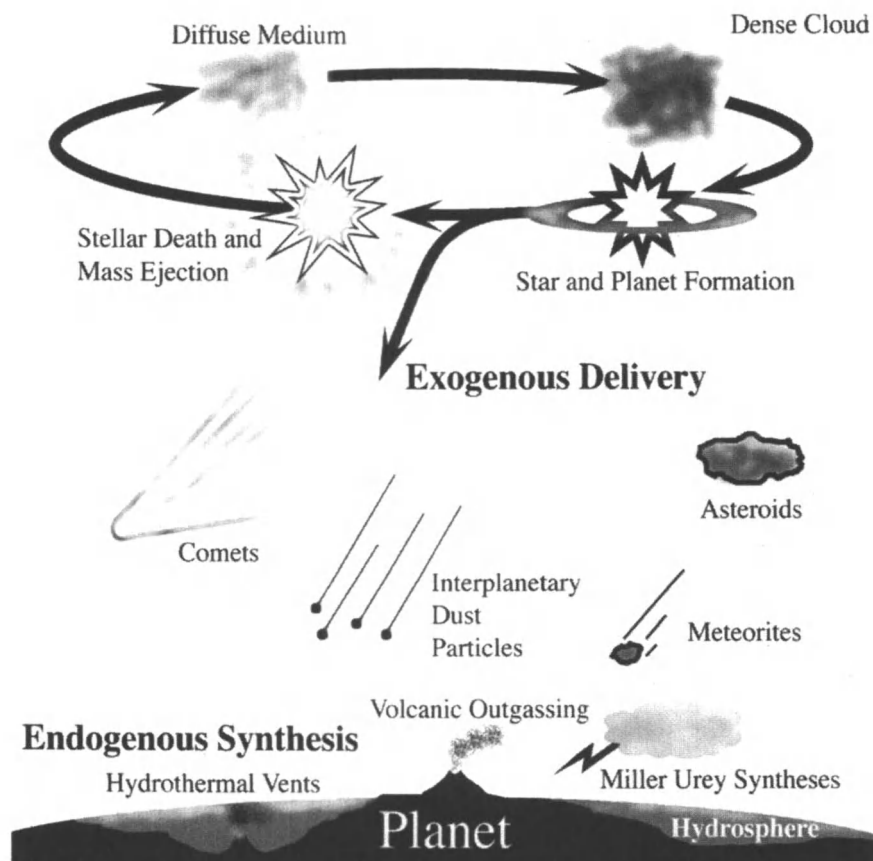


Figure 9. The cycle of stellar birth/death that leads to the production and evolution of organic compounds that can be delivered intact to and mixed with those produced on planetary surfaces (from reference 68).

Both these ice and PAH spectral features are now being used as new probes of the interstellar medium of our Galaxy, the Milky Way and other galaxies throughout the Universe. The ices probe chemical processes in dark clouds and planet forming regions and the PAH features reveal the ionization balance as well as the energetic and chemical history of the medium. This paper has focused on the role of ices in the formation of complex molecules that are part of the raw materials from which stars, planets, satellites, and comets form.

Cometary observations and meteoritic and IDP isotopic anomalies indicate that some interstellar material is delivered to planetary surfaces essentially unmodified. These results are driving a large change in our understanding of the materials that might fall on primordial planetary systems. Today we are in the midst of a major shift in our understanding of what contributed to the 'atmospheres' of the terrestrial planets. Instead of assuming that a planet's prebiotic chemistry had to 'start from scratch', evidence is building that a far more chemically complex interstellar broth was present right from the start.

Interstellar ice composition depends on local conditions. In areas associated with star, planet, and comet formation, ices comprised of simple, polar species and entrapped volatiles such as H_2O , CH_3OH , CO , CO_2 , and NH_3 , are most important. Energetic processing of these ices produces the simple species H_2 , H_2CO , CO_2 , CO , CH_4 , HCO as well as an extremely rich mixture of complex organic molecules. We now know that this prebiotic cocktail includes unsaturated fluorescent compounds; self-assembling, amphiphilic molecules; sugar precursors; and amino acids and we have just scratched the surface. These same lines of sight also show evidence for polycyclic aromatic hydrocarbons (PAHs), the organic molecules known from their characteristic emission to be widespread and abundant throughout the interstellar medium. Including PAHs in the irradiated ices adds PAH cations to the list of ice species, adds color, and, upon warm-up, additionally yields aromatic alcohols, ketones and ethers, species similar to those found in meteorites and having similar chemical properties to functionalized aromatic species used in living systems today. All of these compounds are readily formed and thus likely cometary constituents at the 0.1 to few percent level. Evidence is growing that this interstellar heritage did not become erased during the Solar Nebula phase, implying that some of the interstellar chemical inventory contributed to the chemistry on primitive Earth. The ready formation of these organic species from simple starting mixtures under general interstellar conditions, the ice chemistry that ensues when these ices are mildly warmed, and the observation that the more complex refractory photoproducts form fluorescent vesicles upon exposure to liquid water underscore the possibility that interstellar and cometary ices could have played a part in the origin of life.

Acknowledgements

While I am very grateful to my many colleagues whose work is represented here, I especially wish to acknowledge the major contributions of two people, Mayo Greenberg and Douglas Hudgins. Mayo's vision and steadfast persistence opened the field of solid state laboratory astrophysics. His model of interstellar ice mantle growth and energetic processing is now central to our understanding of astrochemistry. Doug, an exceptionally gifted experimental chemist, laid the solid foundation for the interstellar PAH model and contributed a professor's touch to this manuscript. The approach to many of the concepts, as well as specific topic treatments, are a direct outgrowth of our NATO Summer School chapter in Solid State Astrochemistry (13). I am also particularly grateful to NASA's Long Term Space Astrophysics, Exobiology, and Astrobiology programs for their continued support throughout this field's blossoming.

References

1. Herzberg, G.H. *Molecular Spectra and Molecular Structure I. Spectra of Diatomic Molecules*; Van Nostrand Reinhold: New York, NY, 1939; p 496.
2. Snyder, L. E.; Buhl, D.; Zuckerman, B.; Palmer, P. *Phys. Rev Lett.* **1969**, *22*, 679.
3. Meyer, B. S., this volume.
4. Lodders, K., this volume.
5. *Astrophysics of Dust*; Editors, Witt, A.N.; Clayton, G.C.; and Draine, B.T.; ASP Conf Ser. 309, Astronomical Society of the Pacific, San Francisco, CA, 2004.
6. Ehrenfreund, P.; Charnley, S., B. *Ann. Rev. Astron. Astrophys.* **2000**, *38*, 427.
7. van Dishoek, E.F. *Ann. Rev. Astron. Astrophys.* **2004**, *42*, 119.
8. Ziurys, L. M., this volume.
9. Sandford, S. A.; Allamandola L. J. *Astrophys. J.* **1993**, *417*, 815 and references therein.
10. Charnley, S. B. *Advances in Space Research* **2005**, *36*, 132.
11. Allamandola, L. J.; Bernstein, M. P.; Sandford, S. A. In *Astronomical and Biochemical Origins and the Search for Life in the Universe*, Editors, Cosmovici, C.B., Bowyer, S., Werthimer, D.; Editrice Compositori of the Italian Physical Society, Bologna, 1997, 23.
12. Pendleton, Y. J.; Cruikshank, D. P. *Sky and Telescope*, March **1994**, p 36.
13. Allamandola, L. J.; Hudgins, D. M. In *Solid State Astrochemistry*, Editors V. Pirronello, J. Krelowski, G. Manico eds., Kluwer, Dordrecht, ND, 2003, p 251.

14. Allamandola, L. J.; Sandford, S. A.; Valero, G. *Icarus* **1988**, 76, 225.
15. Willner, S. P.; *Astrophys. J.* **1977**, 214, 706.
16. Capps, R. W.; Gillett, F. C.; Knacke, R. F. *Astrophys. J.* **1978**, 226, 863.
17. Tielens, A. G. G. M.; Allamandola, L. J.; Bregman, J.; Goebel, J.; d'Hendecourt, L. B.; Witteborn, F. C. *Astrophys. J.* **1984**, 287, 697.
18. Lacy, J. H.; Baas, F.; Allamandola, L. J.; van de Bult, C. E. P. M.; Persson, S. E.; McGregor, P. J.; Lonsdale, C. J.; Geballe, T. R. *Astrophys. J.* **1984**, 276, 533.
19. Allamandola L. J.; Sandford S. A.; Tielens A. G. G. M.; and Herbst T. M. *Science*, **1993**, 260, 64.
20. Bowey, J. E.; Adamson, A. J.; and Whittet, D. C. B. *MNRAS*, **1998**, 298, 131.
21. Gibb, E.; Whittet, D. C. B.; Schutte, W. A.; Chiar, J.; Ehrenfreund, P. et al. *Astrophys. J.* **2000**, 536, 347.
22. Boogert et al., *Astrophys J. Supp. Ser.* **2004**, 154, 359.
23. Dartois, E.; Pontoppidan, K.; Thi, W. F.; Munoz Caro, G. M. *Astron. and Astrophys.* **2005**, 444, L57.
24. Altwegg, K.; Balsiger, H.; and Geiss, J. In *The Composition and Origin of Cometary Materials*, Editors Altwegg, K.; Ehrenfreund, P.; Geiss, J.; Huebner, W.; Kluwer Academic Pub., Dordrecht, 1999, p 3.
25. Crovisier, J.; and Bocklee-Morvan, D. In *The Composition and Origin of Cometary Materials*, Editors Altwegg, K.; Ehrenfreund, P.; Geiss, J.; Huebner, W. Kluwer Academic Pub., Dordrecht, 1999, p.19.
26. Allamandola, L.J.; Hudgins, D.M.; and Sandford, S.A. *Astrophys. J. (Letters)* **1999**, 511, L115.
27. Hudgins, D. M.; In *Astrophysics of Dust*, Editors Witt, A. N.; Clayton, G. C.; Draine, B. T. ASP Conf Ser. 309, Astronomical Society of the Pacific, San Francisco, CA, 2004, 665.
28. Allamandola, L. J.; Tielens, A. G. G .M.; Barker, J.R. *Astrophys. J. Suppl. Ser.* **1989**, 71, 733.
29. Peeters, E.; Allamandola, L. J.; Hudgins, D. M.; Hony, S.; and Tielens, A. G. G. M. In *Astrophysics of Dust*, Editors Witt, A. N.; Clayton, G. C.; Draine, B. T. ASP Conf Ser. 309, Astronomical Society of the Pacific, San Francisco, CA, 2004, 141.
30. Herbst, E.; Chang, Q.; Cuppen, H. M. *Journal of Physics: Conference Series*, **2005**, 6, 18.
31. Garrod, R. T.; Herbst, E. *Astron. Astrophys.*, **2006**, 457, 927.
32. Tielens, A. G. G. M. *The Physics and Chemistry of the Interstellar Medium*; Cambridge University Press; Cambridge, 2005; pp 101-114 and 364-393.
33. d'Hendecourt, L.B.; Allamandola, L.J.; and Greenberg, J.M. *Astronomy and Astrophysics*, **1985**, 152, 130.
34. Gerakines, P. A.; Schutte, W. A.; Ehrenfreund, P. *Astron. Astrophys* **1996**, 312, 289.

35. Gerakines, P. A.; Moore, M. H.; Hudson, R. L. *J. Geophys. Res.* **2001**, *106*, 33381
36. Loeffler, M. J.; Baratta, G. A.; Palumbo, M. E.; Strazzulla, G.; Baragiola, R. A. *Astron. Astrophys.* **2005**, *435*, 587
37. Bernstein, M. P.; Sandford, S. A.; Allamandola, L.J. *Scientific American*; July 1999, p 26
38. Bernstein, M. P.; Sandford S. A.; Allamandola L.J.; Chang S.; Scharberg M. A. *Astrophys. J.* **1995**, *454*, 327.
39. Elsila, J.; Allamandola, L. J.; Sandford, S. A. *Astrophys. J.* **1997**, *479*, 818.
40. Dworkin, J. P.; Deamer, D. W.; Sandford, S. A.; and Allamandola, L. J. *Pub. Nat. Acad.* **2001**, *98*, 815.
41. Charnley, S. B.; Tielens, A. G. G. M.; Millar, T. J. *Astrophys. J.* **1992**, *399*, L71.
42. Blake, D.; Allamandola, L. J.; Sandford, S. A.; Hudgins, D. M.; Freund, F. *Science*, **1991**, *254*, 548.
43. Mumma, M. J.; Stern, S. A.; Weissman, P. R., In *Protostars and Planets III*, Editors Levy, E. H.; Lunine, J. I.; Matthews, M. S.; University of Arizona Press, Tucson, AZ, 1993, p.1177.
44. Mumma, M.J. In *Astronomical and Biochemical Origins and the Search for Life in the Universe*, Editors, Cosmovici, C.B., Bowyer, S., Werthimer, D.; Editrice Compositori of the Italian Physical Society, Bologna, 1997, p.121.
45. Roser, J. E.; Vidali, G.; Manico, G.; Pironello, V. *Astrophys. J.* **2001**, *555*, L61.
46. Gerakines, P. A.; Schutte, W. A.; Ehrenfreundt, P. *Astron. and Astrophys.* **1995**, *312*, 289.
47. Briggs, R.; Ertem, G.; Ferris, J.P.; Greenberg, J. M.; McCain, P. J.; Mendoza-Gomez, C. X.; and Schutte, W. *Orig. Life Evol. Biosphere*, **1992**, *22*, 287.
48. Schutte, W. A.; Allamandola, L. J.; and Sandford, S. A. *Icarus*, **1993**, *104*, 118.
49. Huebner, W. F.; Boice, D. C.; Korth, A. *Adv. Space Res.*, **1989**, *9*, 29.
50. Dickens, J. E.; Irvine, W. M.; DeVries, C. H.; Ohishi, M. *Astrophys J.* **1997**, *479*, 307.
51. Clemett, S.; Maechling, C.; Zare, R.; Swan, P.; Walker, R. *Science* **1993**, *62*, 721.
52. Dworkin, J.P.; Gillette, J.S.; Bernstein, M.P.; Sandford, S.A.; Allamandola, L. J.; Elsila, J.E.; McGlothlin, R.M.; Zare, R.N. *Advances in Space Research*, **2004**, *33*, 67.
53. Greenberg, J.M. et al. *Astrophys. J.* **2000**, *531*, L71.
54. Gudipati, M. S.; Allamandola, L. J. *Astrophys. J.* **2003**, *596*, L195
55. Gudipati, M. S.; Allamandola, L. J. *Astrophys. J.* **2006**, *638*, 286.
56. Gudipati, M. S. *J. Phys. Chem. A* **2004**, *108*, 4412

57. Bernstein, M. P.; Sandford, S. A.; Allamandola, L. J.; Gillette, J. S.; Clemett, S. J.; Zare, R. N. *Science*, **1999**, *283*, 1135.
58. Sandford, S. A.; Bernstein, M. P.; Allamandola, L. J.; Gillette, J. S.; Zare, R.N. *Astrophys. J.* **2000**, *538*, 691.
59. Bernstein, M. P.; Dworkin, J. P.; Sandford, S. A.; Allamandola, L. J. *Met.&Planet.Sci.* **2001**, *36*, 351.
60. Bernstein, M. P.; Moore, M. H.; Elsila, J. E.; Sandford, S. A.; Allamandola, L. J.; Zare, R. N. *Astrophys. J.* **2003**, *582*, L25.
61. Bernstein, M. P.; Elsila, J. E.; Dworkin, J. P.; Sandford, S. A.; Allamandola, L. J.; Zare, R. N. *Astrophys. J.* **2002**, *576*, 1115.
62. Elsila, J. E.; Hammond, M. R.; Bernstein, M.P.; Sandford, S.A.; Zare, R.N. *Meteoritics & Planetary Science* **2006**, *41*, 785.
63. Hudgins, D. M.; Bauschlicher, Jr. C. M.; Allamandola, L. J. *Astrophys. J.* **2005**, *632*, 316.
64. Stoks P. G.; Schwartz A. W. *Geochimica et Cosmochimica Acta.* **1982**, *46*, 309.
65. Luisi, P.L. In *Astronomical and Biochemical Origins and the Search for Life in the Universe*, Editors, Cosmovici, C.B., Bowyer, S., Werthimer, D.; Editrice Compositori of the Italian Physical Society, Bologna, 1997,461.
66. DeDuve, C. (1997), In *Astronomical and Biochemical Origins and the Search for Life in the Universe*, Editors, Cosmovici, C.B., Bowyer, S., Werthimer, D.; Editrice Compositori of the Italian Physical Society, Bologna, 1997, 391.
67. Deamer, D. W. *Nature* **1985**, *317*, 792.
68. Deamer, D.; Dworkin, J. P.; Sandford, S. A.; Bernstein, M. P.; Allamandola, L. J. *Astrobiology* **2002**, *2*, 371.
69. Pizzarello, S. *Geochimica et Cosmochimica Acta*, **2005**, *69*, 5163.
70. Sandford, S. A.; Bernstein, M. P.; & Dworkin, J. P. *Meteoritics and Planetary Science*, **2001**, *36*, 1117.
71. Peltzer, E. T.; Bada, J. L.; Schlesinger, G.; Miller, S. L. *Adv. Space. Res.* **1984**, *4*, 69.
72. Bernstein, M. P.; Dworkin, J. P.; Sandford, S. A.; Cooper, G. W.; Allamandola, L. J. *Nature* **2002**, *416*, 401.

Chapter 6

Identifying Molecules in Space: Exploring Astrochemistry through High-Resolution Spectroscopy

L. M. Ziurys

Departments of Chemistry and Astronomy, Arizona Radio Observatory,
LAPLACE Center for Astrobiology, University of Arizona,
Tucson, AZ 85721

In the far reaches of interstellar space, over 130 different chemical compounds have been identified. These discoveries have been possible because of the nature of quantum mechanics and the “fingerprint” pattern that gas-phase molecules exhibit in high resolution spectra. These patterns can be measured very accurately in the laboratory, and then compared with radio telescope observations to seek out novel chemical species. A new view of the “molecular Universe” has emerged as a result.

For centuries, astronomers have focused on the study of stars and the hot, ionized nebulae that exist around them. The presence of molecules in space was in fact thought to be highly unlikely. The interstellar medium, i.e. the gas and dust between the stars, was presumed to be of such low density that any species more complicated than two atoms would be destroyed by ultraviolet radiation. It was not until the late 1960s, with the development of radio astronomy, that scientists began to realize that they were missing a large piece of the puzzle: the vast regions between the stars in fact contained giant gas clouds teeming with molecules that were invisible to optical telescopes. Some 30 years later, it is now estimated that 50% of the material in the inner 10 kpc of the Milky Way Galaxy is molecular in nature. As shown in Plate 1, molecular clouds exist throughout our Galaxy, and can occupy regions where there are no stars. Many of these clouds, some which contain as much as 10^6 solar masses of material, eventually collapse into stars and planetary systems. Our own solar system began, for example, as a molecular cloud. Similar clouds also exist in external galaxies, such as M31, the Andromeda galaxy (1).

In addition to the widespread presence of gas-phase molecular material, another unexpected surprise has been the degree of chemical complexity that has been found over the past few decades. At present, over 130 different chemical compounds have been securely identified in interstellar space, not including isotopic variants. The current list of known molecules, given in Table I (listed by number of atoms), illustrates this complexity, and also the "non-terrestrial" nature of interstellar chemistry. About 50% of the compounds found in the interstellar medium (ISM) are not stable under normal laboratory conditions, namely, they are free radicals and molecular ions. These species would be more common as reaction intermediates in terrestrial chemistry. On the other hand, many of these molecules are found in abundance on earth: H_2O , CH_3OH , $\text{CH}_3\text{CH}_2\text{OH}$, $(\text{CH}_3)_2\text{O}$, and even a simple sugar, glycolaldehyde (CH_2OHCHO). The presence of several "natural products" in interstellar space with common organic functional groups naturally leads to speculation on the ultimate complexity of interstellar chemistry. Can it lead to more complicated biogenic compounds such as ribose, or a phosphate ester, or amino acids? Such questions remain some of the major challenges for astrochemists.

Molecule Detection: A Basis in Quantum Mechanics

The key to interstellar identifications lies in quantum mechanics, as well as a knowledge of the physical conditions of the gas in which the molecules exist. Molecular clouds are generally quite cold, with gas kinetic temperatures in the range $T_k \sim 10 - 50$ K. If a hot, young star happens to be forming in these clouds, then the gas can be several hundreds of degrees. "Clouds" of gas also exist around old, highly evolved stars, which astronomers call *circumstellar envelopes*. These envelopes form because sufficiently massive stars at this stage

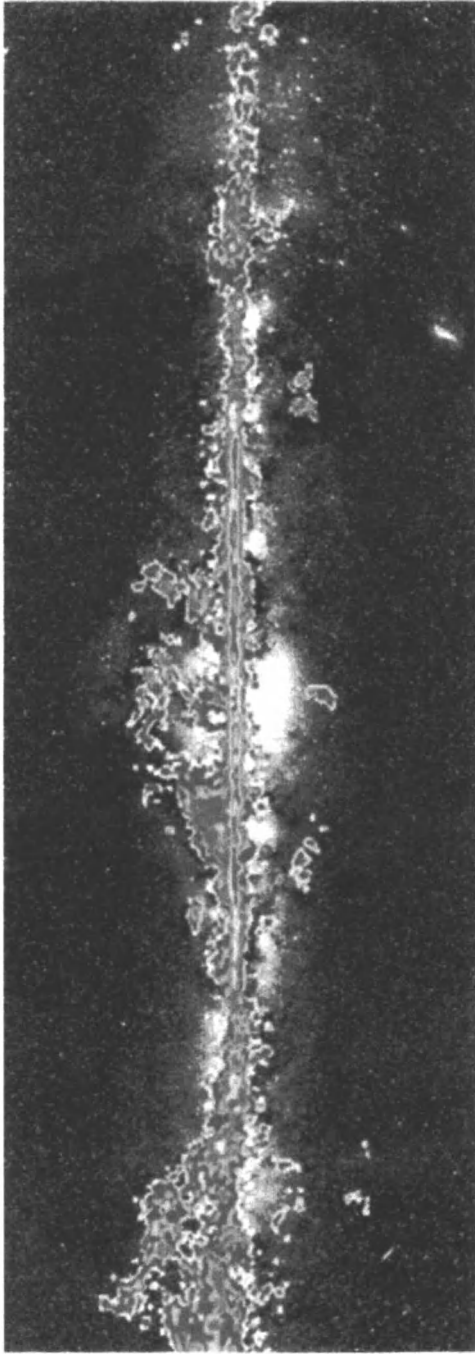


Plate 1. The distribution of molecular clouds in our Galaxy, as traced by emission of carbon monoxide at 115 GHz (CO: $J = 1 \rightarrow 0$ transition: colored contour; from Harvard CFA survey), superimposed over an optical image. (See page 7 of color inserts.)

of their evolution lose their outer atmosphere, which flows away from the star and then cools (see Plate 2). Circumstellar envelopes therefore exhibit fairly low temperatures ($T_k \sim 25 - 50$ K) throughout most of their extent, but remain quite hot very near the star. These regions are also important sources of interstellar dust, which condenses out of hot gas being blown off the stellar surface, as well as “heavy” elements such as carbon, aluminum, magnesium, and silicon (2).

Densities of molecular clouds fall in the range $10^3 - 10^6$ molecules cm^{-3} , corresponding to pressures of $10^{-15} - 10^{-12}$ torr at 10 K. Hence, while these objects are “dense” by interstellar standards, they are ultra-high vacuum in comparison with the terrestrial environment. For circumstellar envelopes, there is a density gradient, with $n \sim 10^{10}$ molecules cm^{-3} close to the star, but decreasing to about 10^5 molecules cm^{-3} at the outer edge.

Because interstellar compounds principally exist in cold, rarified gas, only some of their energy levels can be populated. Molecules have energy levels resulting from their rotation, vibration, and changes in electron configuration, as illustrated in Figure 1. The electronic energy levels, shown here for a diatomic molecule, depend on the internuclear distance and are represented by potential “wells.” Within each well are the vibrational energy levels, which arise from the spring motion of chemical bonds, as well as rotational energy levels, produced by end-over-end rotation of the molecule about its center of mass. A transition between two electronic energy levels requires an electron to change molecular orbitals; these changes correspond to the largest energy differences and therefore occur in the optical and ultraviolet regions of the electromagnetic spectrum. Transitions between vibrational energy levels occur in the infrared region, while those for rotation are in the millimeter and sub-millimeter radio regimes at frequencies of $\sim 30-300$ GHz. Given typical interstellar temperatures of $10 - 100$ K, usually only rotational energy levels of a given molecule are populated. Collisions with other molecules (primarily H_2) excite the higher rotational levels of a given species, which subsequently decay spontaneously back to the next lower level, following quantum mechanical selection rules. A photon is therefore emitted with an energy $E = h\nu$ (and thus with a characteristic energy frequency or wavelength), where E corresponds to the energy difference between the two levels.

The energies of molecular rotational levels, and hence energy differences, depend on the masses that are rotating: the heavy nuclei and their geometrical arrangement in space, i.e. the molecular “moments of inertia” I_x , I_y , and I_z (or I_a , I_b , and I_c , depending on the coordinate system). For a diatomic molecule of nuclear mass m_1 and m_2 , and internuclear distance r , the moment of inertia I is:

$$I = \mu r^2, \text{ where } \mu = \frac{m_1 m_2}{m_1 + m_2} \quad (1)$$

Table I. Known Interstellar Molecules Listed by Number of Atoms

2	3	4	5	6	7	8	9	10		
H ₂	CH ⁺	H ₂ O	C ₃	NH ₃	SiH ₄	CH ₃ OH	CH ₃ CHO	CH ₃ CO ₂ H	CH ₃ CH ₂ OH	CH ₃ COCH ₃
OH	CN	H ₂ S	MgNC	H ₃ O ⁺	CH ₄	NH ₂ CHO	CH ₃ NH ₂	HCO ₂ CH ₃	(CH ₃) ₂ O	CH ₃ C ₄ CN
SO	CO	SO ₂	NaCN	H ₂ CO	CHOOH	CH ₃ CN	CH ₃ CCH	CH ₃ C ₂ CN	CH ₃ CH ₂ CN	(CH ₂ OH) ₂
SO ⁺	CS	NNH ⁺	CH ₂	H ₂ CS	HC≡CCN	CH ₃ NC	CH ₂ CHCN	C ₇ H	H(C≡C) ₃ CN	
SiO	C ₂	HNO	MgCN	HNCO	CH ₂ NH	CH ₃ SH	H(C≡C) ₂ CN	H ₂ C ₆	H(C≡C) ₂ CH ₃	
SiS	SiC	SiH ₂	HOC ⁺	HNCS	NH ₂ CN	C ₃ H	C ₆ H	CH ₂ OHCHO	C ₈ H	
NO	CP	NH ₂	HCN	CCCN	H ₂ CCO	HC ₂ CHO	c-CH ₂ OCH ₂			
NS	CO ⁺	H ₃ ⁺	HNC	HCO ₂ ⁺	C ₄ H	CH ₂ =CH ₂	c-CH ₂ OCH ₂			
HCl	HF	NNO	AlNC	CCCH	c-C ₃ H ₂	H ₂ C ₄	H ₂ CC(OH)H			
NaCl	SH	HCO	SiCN	c-C ₃ H	CH ₂ CN	HC ₃ NH ⁺				
KCl	HD	HCO ⁺	SiNC	CCCO	C ₅	C ₃ N				
AlCl	CF ⁺	OGS	H ₂ D ⁺	C ₃ S	SiC ₄	C ₃ S?				
AlF	NH ₂	CCH	NH ₂	HCCH	H ₂ C ₃					
PN	HCS ⁺	KCN	HCNH ⁺	HCCNC						
SiN	c-SiCC	HCP	HCCN	HNCCC						
NH	CCO		H ₂ CN							
CH	CCS		c-SiC ₃							
			CH ₂ D ⁺ ?							

15 ions
 6 rings
 ~100 Carbon Molecules
 19 Refractory Species

H(C≡C)₄CN H(C≡C)₅CN

I1 I2

c- denotes cyclic structure.

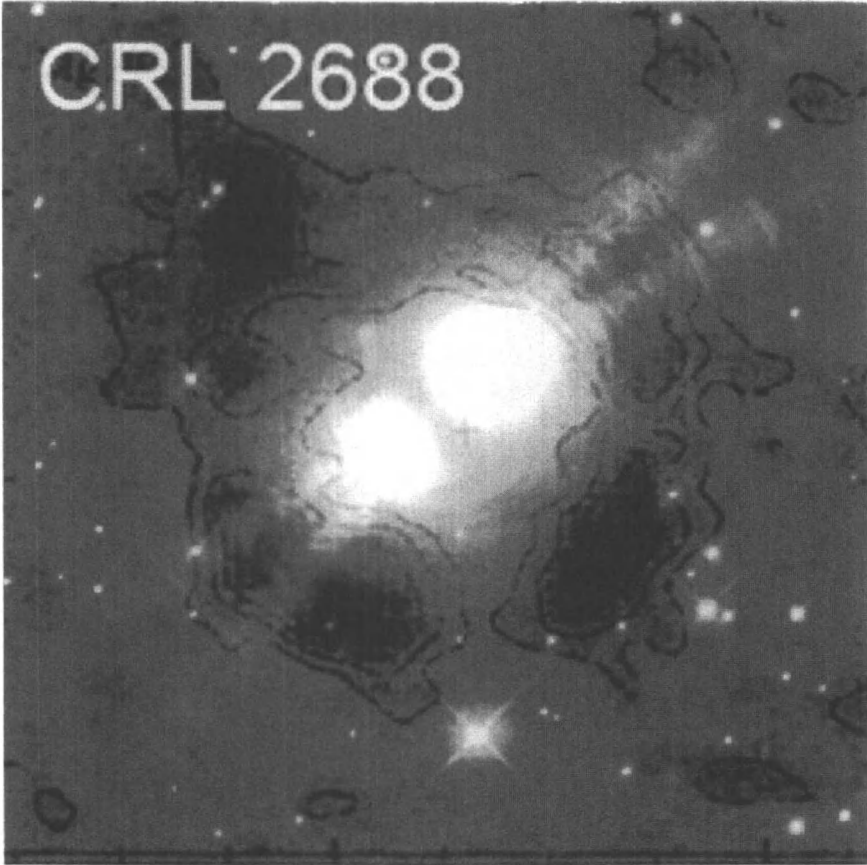


Plate 2. The circumstellar envelope of the evolved star CRL 2688, showing outflowing material (light blue: HST image) and resulting molecular shell (contours). (See page 8 of color inserts.)

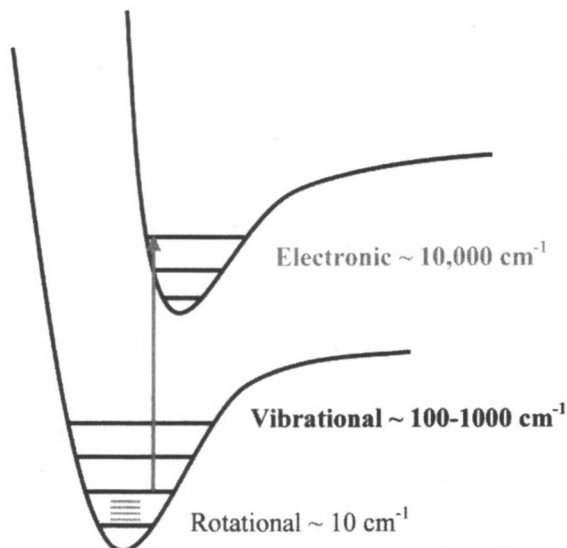


Figure 1. Energy levels of a diatomic molecule. The potential wells are individual electronic states. Within the wells lie vibrational and rotational levels.

A diatomic molecule has two axes around which it can physically rotate; see Figure 2. These axes are equivalent, and correspond to a single moment of inertia I . I determines the spacing of rotational energy levels of the molecule, and is used to define the “rotational constant” B , where $B = h/(8\pi^2I)$ and h is Planck’s constant. According to quantum mechanics, rotational energy levels can only take on certain discrete values, i.e. they are quantized, and we label them with a quantum number called J . The energies of the rotational levels are:

$$E_{\text{rot}} = B J (J+1) \quad (2)$$

where $J = 0, 1, 2, 3$, etc. The emitted photons correspond to the energy level differences, which follow the selection rule that the change in J must be ± 1 . The photon frequencies are the energy level differences divided by h , or

$$\nu = 2B (J+1) \quad (3)$$

As shown in Figure 3, rotational energy levels are thus spaced according to $E_{\text{rot}} = 0, 2B, 6B, 12B$, etc. Spectral lines corresponding to transitions between these levels occur at distinct frequencies of $\nu = 2B, 4B, 6B, 8B$, etc. Each molecule, depending on its mass and geometry, consequently has a unique rotational energy level diagram and associated rotational spectrum. As long as the rotational emission lines are sufficiently narrow in frequency that they

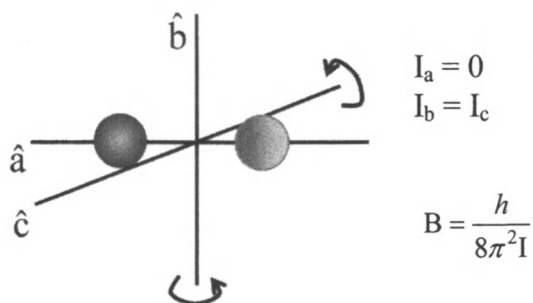


Figure 2. A diatomic molecule, its two equivalent rotational axes and corresponding moment of inertia, related to the rotational constant B .

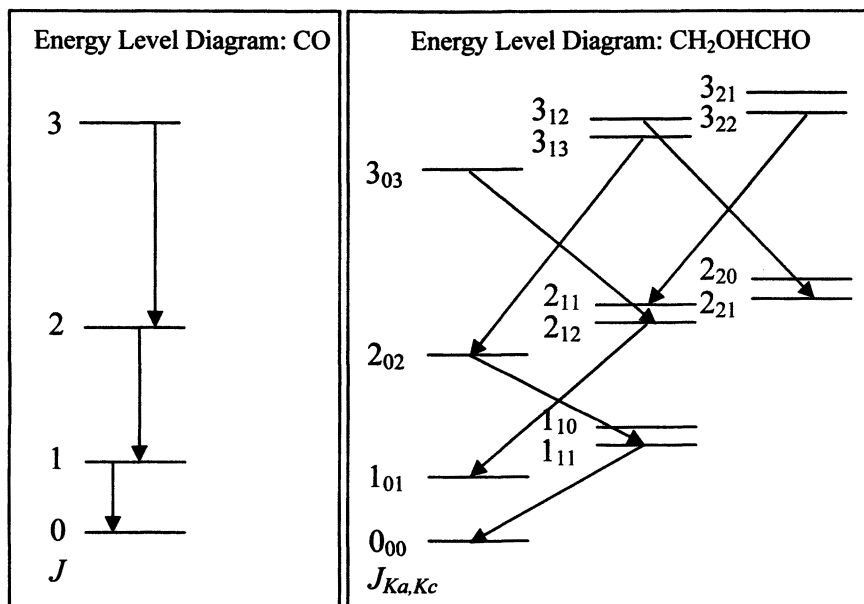


Figure 3. Rotational energy level diagrams for CO and CH₂OHCHO.

remain discrete features, which is the case in cold gas typical of the interstellar medium, then each molecule exhibits a unique “fingerprint.” Hence, if enough rotational lines are measured to identify a fingerprint, then the detection of a chemical species is *unambiguous*.

Diatomic molecules are the simplest cases, and polyatomic species naturally produce more complicated patterns defined by two or three differing moments of inertia (see Figure 3). These molecules, in spectroscopic language, are labeled “symmetric” and “asymmetric” tops. The principle, however, is the same. Another detail is that rotating molecules are subject to centrifugal force, causing bonds to lengthen as the speed of rotation increases. This effect necessitates a small correction to the energy, which depends on the quantum number J . A more correct energy level formula is thus (in units of frequency, Hz):

$$E_{\text{rot}} = BJ(J+1) - DJ^2(J+1)^2 \quad \text{and} \quad \nu = 2B(J+1) - 4D(J+1)^3 \quad (4)$$

Here D is the “centrifugal distortion” constant. Since we can measure the frequencies of spectral lines to one part in 10^7 , small corrections such as centrifugal distortion are absolutely necessary to identify any interstellar species.

The Critical Role of High Resolution Laboratory Spectroscopy

If the pure rotational spectrum of a molecule is known, in principle it can be identified in space. However, interstellar spectra can be quite complex, exhibiting emission from hundreds of lines, as shown in Figure 4. Therefore, it

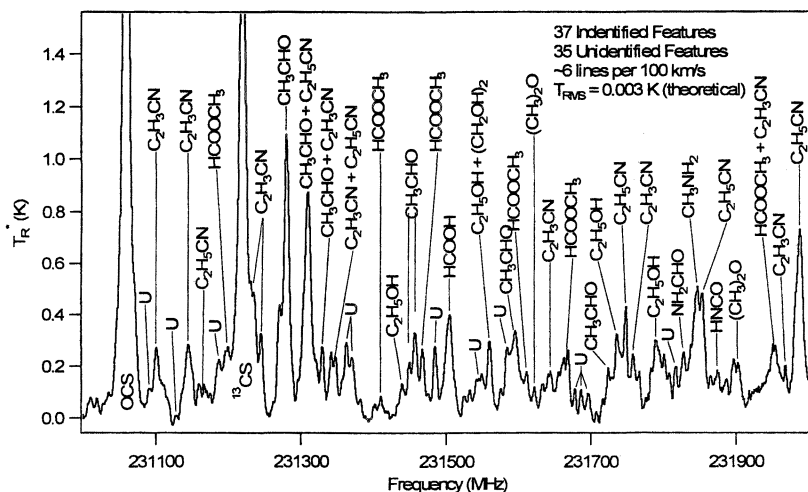


Figure 4. Spectra obtained towards a molecular cloud in the Galactic Center, Sgr B2(N), showing transitions of many different molecules, as well as unidentified features, labeled “U”.

is extremely important that the pure rotational spectrum be accurately measured, i.e. at least with an accuracy of one part in 10^6 , for example, 0.1 MHz in 100,000 MHz for a given transition. Such accuracies can only be realized by high resolution laboratory measurements done in the gas-phase: either a direct measurement of the transition of interest, or measurements of numerous transitions near-by in energy, from which spectroscopic constants can be obtained. From these constants, other transitions of interest can be predicted.

High resolution measurements of gas-phase rotational spectra are generally conducted with two types of experimental techniques: direct absorption or Fourier transform methods. Both techniques measure the energy differences, or frequencies, between rotational levels, as in Figure 3. The concept of direct absorption spectroscopy is in principle quite simple, as shown by the block diagram in Figure 5. The instrument consists of three basic parts: a tunable, stable source of radiation, a gas cell, and a detector. The radiation is focused through the gas cell and scanned in frequency. When a given frequency is coincident with a transition of a molecule contained in the cell, the radiation is absorbed. This absorption results in a decrease in power at the detector, hence the term, "direct absorption." A spectral line is created as a consequence, and the center of the line is at the exact transition frequency.

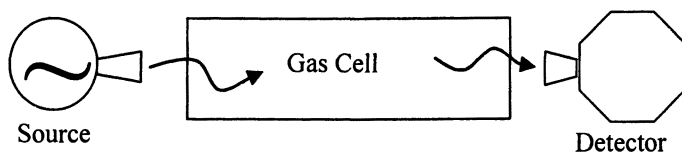


Figure 5. Schematic diagram of a direct absorption system showing the radiation source, gas cell and detector components. Spectra are recorded by scanning the source in frequency while simultaneously measuring the detector output.

The implementation of such a system in reality is far more complicated (3). Sophisticated electronics are required to keep the radiation source consistently at a given frequency, and the typical detector used for these instruments must be cooled to at least 4.2 K using liquid helium. To suppress background noise, an experimental technique called "phase-sensitive detection" is often employed, which requires a modulation scheme for the radiation source or the molecules. Because the wavelengths of the measurements are far longer than visible light, diffraction optics must be employed to properly collimate the radiation through the instrument. To make matters worse, these spectrometers are not commercially available at millimeter and sub-millimeter wavelengths.

Fourier transform microwave (FTMW) spectroscopy is very similar to nuclear magnetic resonance, except it probes rotational levels of molecules,

instead of those due to nuclear hyperfine interactions (4). These systems consist of a Fabry-Perot cavity created from two highly accurate spherical mirrors set in a confocal arrangement, which are contained in a large vacuum chamber (see Figure 6). The chemical compound of interest enters the cavity through a pulsed nozzle, creating a supersonic jet expansion. A fraction of a second later, these molecules are irradiated with a pulse of microwaves that have continuous frequency coverage over a small range. If any of the frequencies of the pulse correspond to the energy difference between two molecular energy levels, the radiation will be absorbed. The molecules will then spontaneously decay back to the initial level, and emit photons corresponding to the frequency of that energy level difference. These photons are detected by an amplifier as a function of time, creating the “free induction decay” or FID. Taking the Fourier transform of the FID creates a spectrum, as shown in Figure 7. Each experiment is complete in about 500 μ seconds; subsequent “shots” are averaged until the desired sensitivity level is achieved. Further frequencies can be probed by incrementing the microwave source. Eventually a whole spectrum covering several octaves is created, and multiple rotational transitions are measured.

Because so many interstellar molecules are reactive short-lived species, potential studies in the laboratory can be difficult. These chemical compounds cannot be obtained in bottles or gas cylinders, but have to be created inside the spectrometer reaction cell *in situ*, as they exist only for fractions of seconds. Their synthesis requires exotic gas-phase techniques employing DC or AC discharges, supersonic jets, as mentioned, and reactor-flow ovens (see Plate 3). There is no guarantee that a species of astrophysical interest can be created in sufficient quantities in the laboratory for spectroscopic studies.

Once the rotational spectrum of a molecule is obtained, it must be analyzed. Such an analysis insures that the transitions observed correspond to the correct energy level differences. The data is fit to a molecular model, the so-called “effective Hamiltonian”, which describes the quantum mechanical interactions in a given species, and spectroscopic constants are obtained. As mentioned, these constants can be used to predict rotational transitions that could not be measured. Naturally, the model must be extremely accurate for the constants to have predictive power to 1 part in 10^7 or 10^8 . A typical Hamiltonian for a radical species might be:

$$H_{\text{eff}} = H_{\text{rot}} + H_{\text{SO}} + H_{\text{SS}} + H_{\text{SR}} + H_{\text{hf}} + H_{\text{eQq}} \quad (5)$$

The interactions here describe molecular rotation, coupling of the spin and orbital angular momentum of any unpaired electrons, and hyperfine splittings, which result from the nuclei having spin. A more detailed discussion of these interactions can be found in (5). It should be recognized that analysis of molecular spectra can be very involved because of additional splittings in rotational levels due to electron and nuclear spins, i.e. relativistic effects.

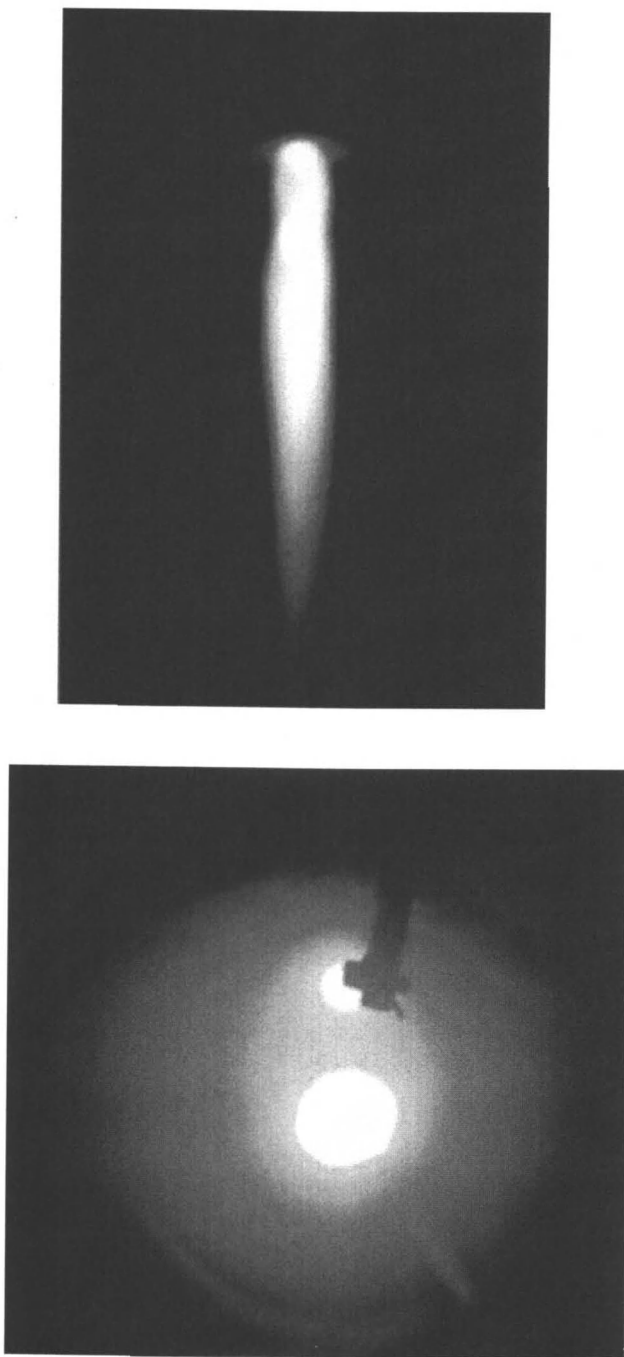


Plate 3. Molecular free radicals being created in DC discharges in a reactor flow oven (left) and a supersonic jet expansion (right). (See page 9 of color inserts.)

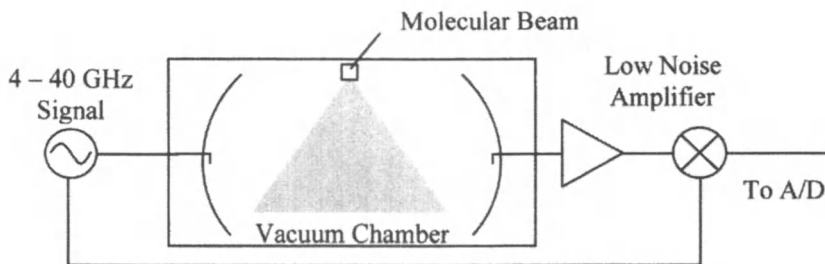


Figure 6. A simplified diagram showing the 4 basic parts of an FTMW spectrometer. The signal generator transmits a pulse of microwave radiation into the Fabry-Perot cavity. The molecules absorb the radiation through excitation of a rotational transition, and then spontaneously decay. The “echo” signal from the molecules is amplified and then detected as a function of time, creating the “FID.”

Radio Astronomy as an Analytical Tool

Despite the fact that signals from molecules may be coming from thousands of light years away, a quantitative analysis can be performed on interstellar gas through the use of radio telescopes and their remote sensing capabilities. Such telescopes at first glance may seem an odd tool for a chemist, but these instruments basically exploit fundamental principles of molecular spectroscopy in a manner similar, but not identical, to a laboratory spectrometer.

A radio telescope is basically a large satellite dish with an extremely accurate surface composed of aluminized panels. An average measure of the smoothness across the entire surface of typical millimeter telescope is between 15 to 70 microns. The telescope diameter, D , and the observing wavelength, λ , establishes the solid angle that the instrument subtends on the sky, known as the “beam size”, θ_b , where $\theta_b \approx 1.2 \lambda/D$ (in radians). As shown in Plate 4, the signal from the sky is focused from the “primary dish,” to the “secondary” mirror or “sub-reflector,” which in turn directs the signal through an opening in the primary. The signal is then focused into the detector, called a “receiver.”

The signals from interstellar space are very weak and must be amplified in order to be detected. Direct amplification of the space signals is ineffective, because millimeter-wave electronics generate too much random noise. Instead, the “super heterodyne” technique is used at millimeter telescopes. In this scheme, the radiation from space, ν_{sky} , is “mixed” (combined) in a solid state diode, the “mixer,” with a signal generated at the telescope, the so-called “local oscillator”, $\nu_{\text{L.O.}}$, or simply “LO”. The LO is produced by a semiconductor chip, usually a Gunn diode. The mixer generates an intermediate frequency, $\nu_{\text{I.F.}}$, by

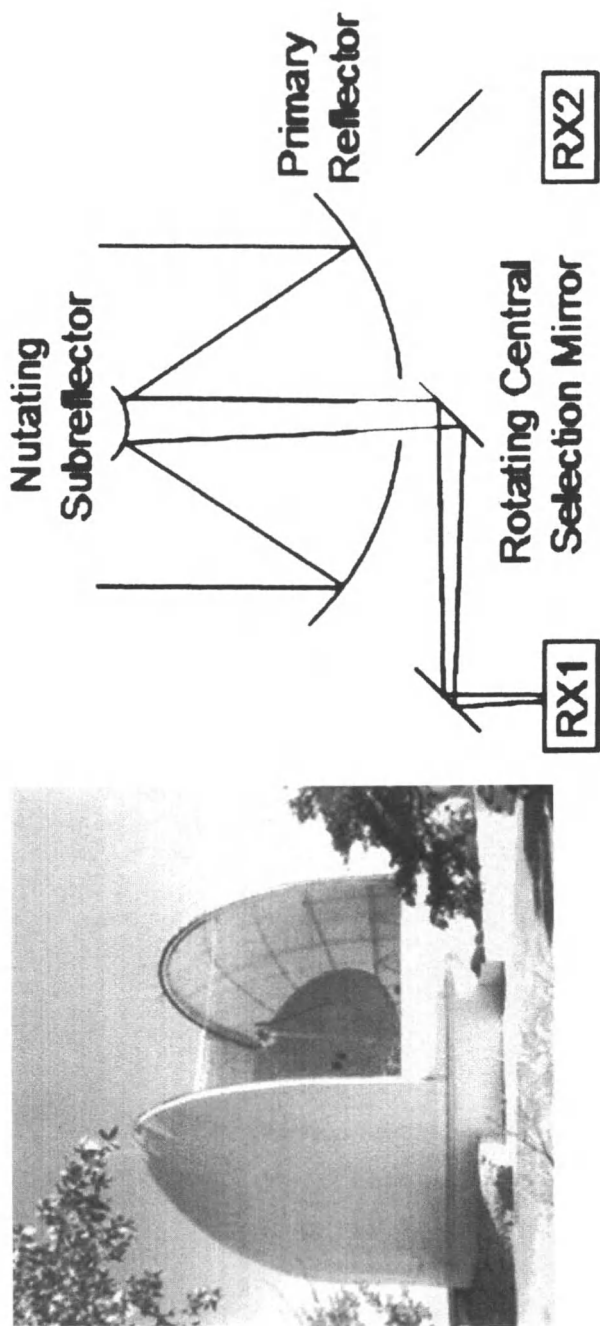


Plate 4. A millimeter radio telescope, the 12 m of the Arizona Radio Observatory (left), and its associated optics (right). (See page 6 of color inserts.) (See page 10 of color inserts.)

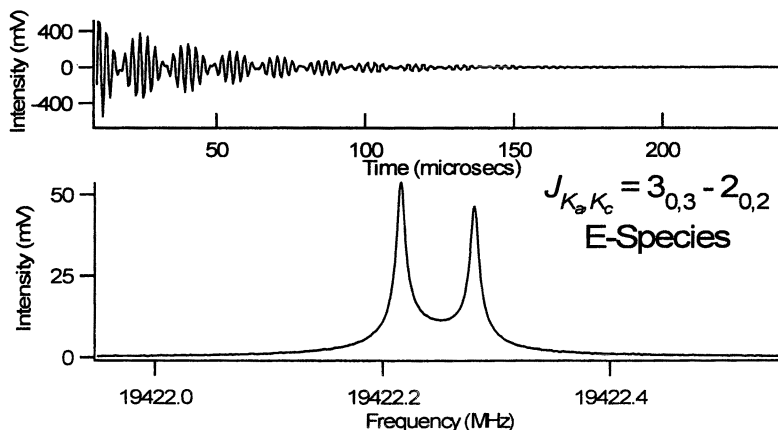


Figure 7. Spectrum obtained with an FTMW spectrometer. The top figure shows the FID of the $J=3_{0,3} \rightarrow 2_{0,2}$ E transition of acetol, while the lower one is the actual spectrum, the Fourier transform of the FID. The double peak of the spectrum is a result of the Doppler shift of the molecular beam.

multiplying the sky signal with the local oscillator signal, which is mathematically equivalent to producing sums and differences of the LO and the incoming sky frequency. In this way, the sky signal, for example, 115 GHz, is converted with a local oscillator frequency (113.5 GHz), to a much lower frequency (1.5 GHz). This intermediate frequency is sent to an ultra low-noise amplifier, available only at the lower frequencies, and then to a spectrometer. The amplifier is constructed to have finite bandwidth, and thus limits the overall frequency range of the spectrometer.

The use of the mixer and amplifier combination thus determines which sky frequency is observed. In practice, at a radio telescope, the value of the intermediate frequency is fixed (usually in the range 1.5 – 8 GHz), and the value of $\nu_{L.O.}$ is chosen to obtain the desired sky frequency according to the equation:

$$\nu_{L.O.} = \nu_{sky} - \nu_{I.F.} \quad (6)$$

However, mixers are relatively broadband devices, such that not just one, but a range of frequencies is observed simultaneously. The local oscillator signal must be extremely stable in frequency (to about 1 part in 10^9), because any drifting with time would cause the sky frequency also to change. This stabilization is accomplished using a “phase-lock loop,” an electronic circuit that continuously compares the LO signal with a very stable, lower frequency reference, and corrects any change as needed (6).

The spectrometer is the final device in the electronic processing of signals from space. The range of frequencies that pass through the IF amplifier have to

be separated to create a spectrum, i.e. signal as a function of frequency. Radio astronomy utilizes several types of spectrometers. A common type is a “filter bank”, in which individual channels are tuned to slightly different frequencies in order to create a spectrum. Each channel has a finite bandwidth, typically in the range 0.1 to 1.0 MHz. One channel bandwidth is used for an individual bank. In this way, a complete spectrum is obtained at once, a technique known as “multiplexing”. Unlike the laboratory, comparatively large frequency ranges can be studied without having to “scan” the instrument.

The signals from the spectrometer are subsequently sent to a computer disk and spectra are viewed on a computer screen. In order to reduce the noise in a measurement (i.e. increase the signal-to-noise ratio), the data from the sky is often signal-averaged, usually in a 5 – 6 minute integration period. These 5 minute “scans” are recorded to the disk with a unique scan number, which is used as an identifier for subsequent data reduction. Because the stability of the electronics is excellent at radio telescopes, a large number of individual scans can be averaged together in order to obtain a spectrum with a very high signal-to-noise ratio. The spectrum in Figure 4, for example, was created from about 20, 6 minute scans, or about 2 hours of total integration time.

The goal of signal-averaging is to minimize the rms noise level (T_{rms}) of a spectrum. This noise level can be described by the radiometer equation:

$$T_{rms}(1\sigma) = \frac{2T_{sys}}{\sqrt{B_w \tau}} \quad (7)$$

Here B_w is the bandwidth (or spectral resolution) of the individual channels of the spectrometer, τ is the total integration time, and T_{sys} is the “system temperature,” a measure of the noise from the detection electronics and the sky itself; both obscure the desired signal. The intensity scale in radio astronomy is often expressed in temperature units (K), the so-called antenna temperature. The signal is actually measured as a voltage. It is converted to a temperature scale because originally liquid nitrogen was used as a reference. The voltage (or temperature) is a measure of the incident energy flux (joules/m²/sec/Hz-of-bandwidth) falling on the antenna in the direction in which it is pointed. The system temperature can vary with time because sky conditions change.

Radio astronomical spectra trace more than just the chemical content of a given gas cloud. They also indicate the physical conditions and kinematic motions in a source. Rotational transitions arising from levels that are high in energy trace gas that is very hot, for example. Very narrow lines indicate cold, quiescent gas. Objects with gaseous outflows, such as circumstellar envelopes, have broader spectra. If the dispersing material comes from a hollow shell, such as in the case of the evolved star IRC+10216, the molecular lines can have a U-shape, as shown in Figure 8. The spectral shape may not look at all like what has been measured in the laboratory; however, it is essential that the center

frequency of the features be identical. The astronomical frequency is corrected for Doppler motions of the Earth and any motion of the source relative to the Earth, but these corrections are well-known.

Objects are targeted for astronomical searches based on past detections and a knowledge of their chemistry. Typical molecular clouds used in searches are Sgr B2(N), which is in the center of our Galaxy, or the Orion-KL region, which is relatively close to our solar system. Circumstellar envelopes such as IRC+10216 or CRL 618 are also known to be chemically rich. Because the spectra of these objects are usually dense in molecular lines, including a large percentage of unidentified features, it is critical that a sufficient number of internally-consistent rotational transitions be detected in a given object. The chance of a false coincidence is quite high, especially for the more complicated molecules that have a high density of energy levels and therefore transitions. For example, to confirm the identification of glycolaldehyde in Sgr B2(N), a total of 40 individual transitions were observed over a range of 65 – 170 GHz (7). All of the favorable lines (about 30) were detected, although some were obviously

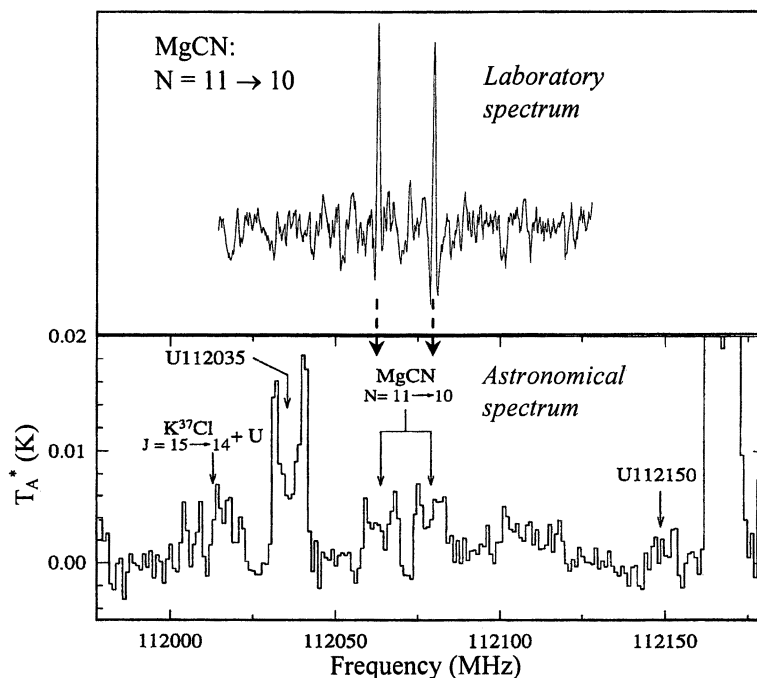


Figure 8. The end product of the effort: a transition of MgCN, measured in the lab, is found by a radio telescope in the circumstellar shell of the evolved star IRC+10216. The doublet structure, due to an unpaired electron in this species, is clearly visible in both spectra.

blended with features from other molecules. Unraveling interstellar spectra poses challenges; however, the presence of certain molecular splittings can be a useful aid (see Figure 8). Here the fine structure splitting of the free radical MgCN, due to its unpaired electron, is a certain “fingerprint” for identification. The doublet structure, which is 15 MHz wide, is present in every transition and can be resolved in both the laboratory and the astronomical spectra.

Conclusion

Over the past few decades, it has become increasingly obvious that interstellar space has a rich and varied chemistry. Quantum mechanics is the basis by which molecules are investigated in space. Rotational spectra obtained from accurate laboratory measurements allow for unambiguous identification of such molecules, combined with the remote-sensing capabilities of radio astronomy. This symbiotic relationship has led to a new chemical field: Astrochemistry.

References

1. Kwok, S. *Physics and Chemistry of the Interstellar Medium*; University Science Books: Sausalito, CA, 2007.
2. Ziurys, L.M. *PNAS*, **2006**, *103*, 12274.
3. Ziurys, L.M.; Barclay, W. L. Jr.; Anderson, M. A.; Fletcher D. A.; Lamb, J. *W. Rev. Sci. Instrum.* **1994**, *65*, 1517.
4. Balle, T.J.; Flygare, W.H. *Rev. Sci. Instrum.* **1981**, *52*, 33.
5. Carrington, A. *Microwave Spectroscopy of Free Radicals*; Academic Press: London, 1974.
6. Rohlfs, K.; Wilson, T.L. *Tools of Radio Astronomy*; Springer: Berlin, 1996.
7. Halfen, D.T.; Apponi, A.J.; Polt, R.; Wolf, N.J.; Ziurys, L.M. *Ap.J.* **2006**, *639*, 237.

**Part II: Geochemical Evolution:
Solar System and Earth**

Chapter 7

Chemical Diversity and Abundances across the Solar System

John S. Lewis

Department of Planetary Sciences and Lunar and Planetary Laboratory,
University of Arizona, Tucson, AZ 85721

Chemical zoning of the Solar System, first noted by Harrison Brown in 1950, displays three major compositional classes distinguished by volatility, ranging from rocky material close to the Sun through ice-rock mixtures in more distant small bodies, to massive gas-giant planets rich in “permanent gases”, notably hydrogen and helium. Spacecraft exploration of the Solar System, laboratory studies of asteroidal, lunar, and Martian materials, and theoretical studies of accretion, condensation, melting, differentiation and partitioning of rocky and icy materials combine to reveal many additional features of these categories. The oxidation state gradient of the terrestrial planets, the chemical complexity of planetary atmospheres and the asteroid belt, the spectra (indeed, the very existence!) of the Centaur and Trans-Neptunian Objects, and compositional zoning in Jovian satellite systems combine to provide a more detailed picture of genetic processes soon to be tested by observations of other stellar systems.

Introduction

Both conditions of origin and evolutionary pathways have profoundly shaped the material of Earth and other Solar System bodies. Our first datum, Earth, has provided us for over 2000 years with many ideas of what other worlds must be like; indeed, the literature on the “plurality of worlds”, the *απεροι κοσμοι* of Greek philosophy, saw a vast universe with Earthlike worlds at every star, whereas Aristotle held that Earth was the only world. But which of the features of Earth are universal, foreshadowing other worlds not yet discovered, and which are idiosyncratic, rare and possibly altogether absent on other worlds? When we see and begin to study other “Earth-like” worlds, such as Mercury, Mars, and Venus, their differences are attributed either to different circumstances of origin, or to divergent evolution from a common starting point. This cosmic version of the nature/nurture debate is at the heart of many current disputes about Solar System bodies and processes. As we shall see, such an “either-or” dichotomy has little value, since both conditions of origin and “evolutionary” paths are both closely linked to distance from the Sun. There is a further confusion inherent in the usage of the word “evolution” in astronomy and geology, where it is generally used to imply the ageing of specific single bodies rather than progressive change in a population of bodies. Thus the “chemical evolution of the Galaxy” makes sense, whereas the “evolution of Venus” does not. We would be better advised to speak of “historical chemical and structural changes” of Solar System bodies rather than their “evolution”. I shall call this “history” for the sake of conciseness.

The history of the material of the Solar System is illustrative of the all-pervading war between entropy (abetted by temperature) and enthalpy, in a sense that would be very familiar to J. Willard Gibbs. Raw preplanetary material, an inheritance from the interstellar medium, may have been chemically and physically rather uniform on centimeter scales and larger, but even that material hosted a wide variety of small grains with different astrophysical provenances and histories, and different chemical and isotopic compositions: although it was highly heterogeneous on the micrometer scale, it may well have been grossly homogeneous on macroscopic scales. The entropy of this mixture was very high. But even this limited degree of uniformity breaks down quickly as a shrinking interstellar cloud gives rise to an accretion disk with profound gradients of temperature, pressure, and density. In the inner part of the disk temperatures were high enough to allow a close approach to thermodynamic equilibrium. In the outer regions, species that condense at low temperatures may have approached equilibrium, but high-temperature condensate grains inherited from the protostellar cloud would survive with little equilibration. It is in this cloud that the history of the Solar System as a distinct entity finally begins.

That history can be considered to consist of three eras. The first, the nebular phase, transpires in a flattened, disk-shaped gas and dust cloud of interstellar

origin, surrounding the forming Sun. The second, accretionary, phase, comprises the physical and chemical processes associated with the assembly and growth of young planets. The third, which overlaps somewhat with the accretionary phase, is the differentiation and outgassing phase, during which heat sources such as accretion energy and radioactive decay melt planetary material and allow it to separate into layers of different density and composition, during which the minor and trace elements partition themselves between metals, sulfides, silicates and volatiles according to their chemical affinities.

The Nebular Phase

A young prestellar nebula, rich in gases and polyatomic molecules, has such high infrared opacity that most of it convects and circulates in its own gravitational field as an adiabatic mixture of gas and dust in which changes in gravitational potential (GM/r) govern the thermal energy of the gas (kT). In general, most of such a nebula, excepting only regions where the opacity is low and radiative processes control temperatures, displays a strong temperature gradient in which T varies closely with $1/r$.

Where radiative control dominates, the luminosity (L) of the proto-Sun soon provides a radiant flux that drops off according to an inverse square law ($L/4\pi r^2$), in which solid particles absorb that flux rather efficiently and re-radiate it in a steady state as thermal radiation (σT^4). In this radiatively controlled regime, T^4 varies as $1/r^2$, and T is therefore proportional to $1/r^{1/2}$, a much weaker dependence. Nonetheless, from the perihelion of Mercury (0.31 Astronomical Units from the Sun) to the aphelion of Mars (1.68 AU), the temperature must still have varied by a factor of 2.3. Since the vapor pressures of solids vary exponentially with $1/T$, this is a very significant difference.

The conclusion is inescapable: the raw materials available for planetary accretion varied strongly with location in the pre-solar accretion disk, from fully vaporized close to the Sun to thoroughly baked and equilibrated solids in the terrestrial planet region to weakly heated and poorly equilibrated solids in the outer half of the asteroid belt.

The main features predicted by chemical equilibrium models (which pertain directly to the inner disk) include successive condensation of refractory oxides and metals, metallic iron-nickel alloy, magnesium silicates, feldspars (aluminosilicates of Ca, Na, and K), FeS, FeO-bearing silicates, and -OH- and H₂O-bearing silicates. Departures from local equilibrium in newly accreted solid bodies could be caused by any of three major factors: imperfect gas-phase equilibrium due to kinetic inhibition of reactions such as the reduction of CO and N₂ to CH₄ and NH₃ at low temperatures, radial mixing of materials originating at different distances from the Sun, and relict presolar grains originally formed in distant astrophysical settings such as nova or supernova shells or mass outflow

from giant stars. Where temperatures are low and complete equilibration cannot be achieved, relict high-temperature grains survive nearly unaltered, as in the carbonaceous asteroids and comets, accompanied by organic matter, with low-temperature condensates such as water ice which are in equilibrium with the ambient gases. As a result, bulk composition and density closely follow the predictions of perfect equilibrium, whereas refractory relict grains may be far out of equilibrium with the gas and other neighboring grains. This chemistry is reflected in detail in meteorites.

The Accretionary Phase

Most discussions of the accretion history of the terrestrial planets are based on a series of models that begin with a population of 100-200 equal-mass moon-sized bodies in moderately eccentric 2-dimensional orbits (1, 2). Further refinement of this model, including its generalization to three dimensions (3, 4) led to Wetherill's (5) accretion models and Lewis's (6) condensation-accretion models for Mercury and the terrestrial region. A logical consequence of the initial conditions assumed for these models is that disruptive collisions between large bodies occur⁵, and that the absence of a substantial mass of smaller bodies removes the damping effects of accretion of small bodies on the migration of large bodies. Wide wandering of the growing planets occurs, largely erasing any initial gradient in composition, and leading to a high frequency of "pathological cases" in which the simulation produces "Mercuries" that may have originated nearly anywhere in the inner solar system. The effect of accretion of the vast numbers of smaller bodies omitted from these simulations may be simulated by using Gaussian accretion sampling models⁶ that allow for a substantial composition gradient across the terrestrial planet region. Such models predict a high-temperature, FeO-poor and volatile-poor composition for Mercury, similar to the highly reduced Mercury model proposed by Wasson (7).

The terrestrial planet region, in addition to these condensation and accretion processes, can be shaped by radial migration of growing planets under the combined influence of dynamical interaction with the gas disk and gravitational interactions with other planets, especially their (moving) orbital resonances, in much the same way as suggested by Malhotra for Pluto's orbit (8).

The Differentiation and Outgassing Phase

The accompanying review by Fegley discusses both the release of volatiles from planetary interiors during melting and density-dependent differentiation and their subsequent compositional evolution (9). The present composition of planetary atmospheres reflects a richly complex history.

Evidence From Across the Modern Solar System

1. The Terrestrial Planet Region

Different amounts of compositional information of different sorts are available for each terrestrial planet: the only two lines of evidence available for all of them are bulk density and oxidation state. The bulk densities, however, must be corrected to “zero pressure” (actually, 1 atmosphere) to remove the effect of internal self compression and afford a directly relevant measure of composition (see Table I).

Table I. Observed and Zero-Pressure Densities of Terrestrial Bodies

<i>Body</i>	<i>Observed density (Mg/m³)</i>	<i>Zero-Pressure Density (Mg/m³)</i>
Mercury	5.43	5.30
Venus	5.24	4.00
Earth	5.515	4.05
Mars	3.93	3.74
Moon	3.34	3.32
Phobos*	2.2	2.2
Deimos*	1.7	1.7
Io	3.57	3.54

*Phobos and Deimos are so small that they may contain substantial void space

These corrections are large for the terrestrial bodies with the largest masses and internal pressures, Venus and Earth, and smallest for the Moon and Mercury. Note that making precise corrections requires some prior knowledge of the compressibility, and hence the mineralogy and structure, of the interior. These estimates assume that the same basic minerals (Fe-Ni, FeS, and silicates) are present in each body and that all are fully differentiated.

The choice of models can be further narrowed by consideration of the reduced principal moment of inertia, I/Mr^2 which is close to that of a uniform sphere ($I/Mr^2 = 0.4$) for undifferentiated and uncompressed (low-mass) bodies. The Moon displays a very small degree of central mass concentration (*10*), with $I/Mr^2 = 0.3932 \pm 0.0002$ consistent with a metallic core with mass no greater than about 2.5 to 3% of the mass of the Moon, and possibly as low as 0.5%. Mars' value of $I/Mr^2 = 0.3650 \pm 0.0012$ (*11*), is small enough to require differentiation, but too large to fit models in which the core and mantle have the same uncompressed density as Earth's core and mantle. The easiest explanation of this difference is that much more of the iron in Mars is oxidized, lessening the

mass and density of the core and raising the mass and density of the mantle. Such a model is compatible with core sulfur contents up to pure FeS composition (12) An alternative explanation, that Mars is incompletely differentiated, is ruled out by the study of Martian surface rocks and dirt, Martian meteorites, and planetary thermal history models.

There is also direct evidence regarding the oxidation state of terrestrial bodies and a gradient in FeO content with distance from the Sun (Table II).

Table II. FeO Contents of Terrestrial Bodies

<i>Body</i>	<i>FeO Content</i>
Mercury	≈ 2%
Venus	7%?
Earth	8%
Moon	12%
Mars	18%

The FeO content of Mars given here is consistent with the geochemical models of Dreibus and Wänke (13) and with laboratory studies of Mars-derived SNC meteorites. Since FeO content is a sensitive marker of the temperature of origin, the original location of bulk lunar material appears to have been between the orbits of Earth and Mars. The FeO content of Mercury's crust is probably best quoted as $1.5 \pm 1.5\%$, since it remains without any firm detection, and its presence cannot be verified at the 3% level (14).

Temperatures in the solar accretion disk dropped off inversely with heliocentric distance ($T \sim 1/r$) reflecting the inter-conversion of gravitational potential energy, GM/r , and thermal energy, kT , in the turbulent gas disk. The thermodynamic activity of FeO varies according to $\log a_{\text{FeO}} \sim 1/T \sim r$.

2. The Asteroid Belt

Much of the progress in understanding the compositions of asteroids has come from comparing the spectra of known meteorite types and meteoritic mineral separates to astronomical spectra of asteroids. Over 20 spectrally distinct classes of asteroids have been found, ranging from the essentially FeO-free differentiated silicates of the E class (dominated by the FeO-free mineral enstatite, MgSiO_3) at the inner edge of the asteroid belt to black, highly oxidized and often water-rich carbonaceous C-, D-, and P-class material in the outer half of the belt, which are rich in polymeric organic matter made by the inability of CO and N_2 to equilibrate to NH_3 and CH_4 at low temperatures (15).

3. The Meteorite Connection

The approximately 50 known classes of meteorite, excluding those known to have originated from the Moon or Mars, span a wide range of compositions. Most meteorites are *stones*. The remaining classes of meteorites, the *irons* and the *stony-irons*, are products of melting and differentiation. They consist mainly of metallic iron-nickel alloys, sulfides, carbides, phosphides, and igneous silicates. (See the chapter by M. Lipschutz in this volume).

The *stone* meteorites, which constitute the overwhelming majority of those falling on Earth, fall into two general categories. First, there are the most abundant type of stones, which are fairly homogeneous mixtures of grains of silicate, oxide, sulfide, metal and other minerals with widely different densities and melting points, often far out of chemical equilibrium with each other, and showing no signs of melting and density-dependent differentiation. Since most of these meteorites contain small glassy spherules called *chondrules*, the meteorites themselves are called *chondrites*. In contrast, those stony meteorites that have undergone melting, equilibration, and density-dependent differentiation are called *achondrites*.

The chondrites are subdivided into about a dozen classes distinguished by their content of metal, FeO, water and other volatiles. Some, with very low volatile and FeO contents, are clearly of relatively high-temperature origin. Since their dominant silicate mineral (as in the E asteroids) is the FeO-poor silicate enstatite (MgSiO_3), they are termed *enstatite (E) chondrites*. Their low FeO content betrays a high-temperature origin. Certain other chondrites are rich in water-bearing minerals, organic compounds, magnetite (Fe_3O_4), and water-soluble salts. They are called *carbonaceous (C) chondrites*. (The D and P classes of asteroids, which appear to be “super-carbonaceous”, have no counterpart among the meteorites known on Earth.) The C chondrites, having formed at the lowest temperatures, contain the most complete inventory of volatile and moderately volatile elements. They are often referred to as the most “primitive” meteorites, meaning that they are closest to the parental solar material in composition. The word “primitive” does not imply that planetary bodies and the other meteorite classes are derived from or descended from them. Many workers, taking the word literally, have assumed that the planets were originally made of C-type material, which unfortunately is the class of chondrites that is the least similar to the present terrestrial planets, and have then expended heroic efforts trying to “evolve” C-type material into the present Earth.

Workers often speak of “chondritic” compositional models for the terrestrial planets, but some use the phrase to denote “C chondrites” and some take it to mean “a mix of chondrite classes” or “material mineralogically similar to chondrites, but not exactly the same as any single class”. This confusion is a perennial source of confusion. *Caveat lector*.

4. The Giant Planets

The four giant planets have hydrogen- and helium-rich compositions reminiscent of the Sun, but all of them clearly depart from strict solar composition in that their densities are too high and the few heavier elements whose tropospheric abundances can be measured all show clear evidence of enrichment. For all four giant planets we have spectroscopic compositional data on the few compounds that remain uncondensed in the visible portion of their atmospheres, above their main cloud layers. These include ammonia, methane, phosphine, and germane. For Jupiter, these volatile elements (C, N, S, P and Ge) are enriched relative to their solar abundances by about a factor of five. For Saturn, with no detection of germane, the enhancement of C, N, and P is about a factor of 10. For Uranus and Neptune the methane enrichment factor is at least 60, consonant with their much higher uncompressed densities.

The Galileo entry probe was sent to Jupiter to sound the atmosphere down through the main cloud layers, to profile the clouds and measure the abundances of the important cloud-forming condensates ammonia, water vapor and hydrogen sulfide in warm, upwelling, condensate-free air. Improbably, and unfortunately, it fell into and sampled a rare region of subsiding, cloud-free, and extremely dry stratospheric air.

5. Satellite Systems of the Giant Planets

The giant planets display “miniature solar systems” of close moons in low-eccentricity, low-inclination orbits, families of highly-inclined moons at intermediate distances, and vast swarms of small retrograde moons at greater distances. Clear evidence of radial compositional trends in the inner satellite system of Jupiter suggests a close analogy with composition gradients observed in the solar system at large. The inclined orbits of intermediate-distance moons and the retrograde outer moons resemble the transition from the coplanar inner Solar System to the inclined plutinos to the randomly-orbiting long-period comets in the Oort cloud.

6. Planetary Sub-nebulae: the Galilean Family

The four Galilean satellites of Jupiter show a strong density gradient. The closest of these satellites to Jupiter is Io (J1), which has a Moon-like size and density, suggestive of highly oxidized rocky material with no condensed ices. Io has a volcanically active surface dominated by sulfur volcanism in a trace atmosphere largely composed of SO₂. Hydrogen compounds are rare or absent. The next satellite outward from Jupiter, Europa (J2), has a lower density

suggestive of a surface layer of ice tens of kilometers thick. The surface has the visible and near-IR spectrum of water ice. Surface imaging of Europa by the *Voyager* flybys and the *Galileo* orbiter suggest a thin (10 km?), mobile ice crust floating on a deep (50 km?) aqueous ocean. The outermost Galilean satellites, Ganymede (J3) and Callisto (J4), have much lower densities suggestive of massive amounts of water ice, approximately in the proportions expected for full condensation of rock-forming elements and H₂O from a parent gas of approximately solar composition. Ganymede's surface displays convincing evidence of large-scale tectonic activity, whereas the smaller and more distant Callisto has a heavily cratered ancient surface and little suggestion of internal dynamics. Both, like Europa, have the spectrum of water ice.

7. Titan

Titan has recently been studied by the *Cassini* Saturn orbiter and the *Huygens* entry probe. Placing Titan in the context of the other regular Saturnian satellites is not easy, since all of them apparently formed at such low temperatures that ices, including water ice, ammonia hydrate, and methane clathrate hydrate were fully condensed, thus causing density and composition differences to be too small to be discerned. Titan itself has an atmosphere that is denser than Earth's, dominated by a nitrogen/methane meteorology that involves an evaporation/precipitation cycle, methane rain at least at higher latitudes, and mature drainage systems and lakes. Photochemical processing of the methane in Titan's atmosphere by solar UV must have produced a layer of condensed hydrocarbons and C-H-N compounds at least 100 m in thickness over the age of the Solar System. Titan serves as a test case for theories of the inorganic origin of organic matter.

Pluto, its largest moon Charon, and Neptune's largest moon Triton appear to be colder cousins of nitrogen- and methane-rich Titan. Their formation temperatures must have been low enough for retention of ammonia- or nitrogen-bearing ices.

8. Centaurs, Trans-Neptunian Objects and Comets

Centaurs have unstable orbits that cross those of the Jovian planets. It is reasonable to search for a source of bodies to replenish Centaurs as they are lost to planetary impacts and to violent orbital perturbations that may convert them into outer (retrograde; transient) planetary satellites or periodic comets, or even expel them from the Solar System. Our ability to identify genetic relationships between Centaurs, Kuiper-Belt Objects (KBOs; "iceteroids" that orbit beyond Neptune), the distant irregular and retrograde moons of the giant planets, Trojan

asteroids and periodic (“short-period”) comets is limited by the very small amount of compositional data we have on each of these classes. Comets are well established as mixtures of ices and small unequilibrated rocky particles, but their dynamically related cousins are poorly studied. It is clear that there are two broad spectral groups present among Centaurs, one group neutral or slightly red in color and the other very red. Although KBOs do not show a bimodal color pattern, those with perihelia beyond 40 AU and those with inclinations less than about 4.5° are all red. To date, no clear relationship between membership in these spectral groups and orbital parameters has been established for Centaurs. Therefore the significance of their color dichotomy is not understood.

9. Asteroids and Comets as Sources of Volatiles for Terrestrial Planets

Since Newton there have been countless suggestions of profound effects on Earth attendant upon comet impacts. Many have suggested that Earth’s water supply is a secondary feature introduced by late “veneering” with cometary material, which also should introduce a wide range of other volatile materials in grossly solar proportions. However, the serious mismatch between the observed isotopic (D:H) compositions of terrestrial and cometary water (all comets studied have had D:H ratios about twice as high as in terrestrial water) argues strongly against this explanation. The alternative carrier of water, the C-type and related classes of asteroids, seems increasingly plausible in light of the isotopic similarity to terrestrial water. The question of whether most of this water was brought in during the accretion phase or as a “veener” is unresolved; however, the presence of about 1% ferric iron in Earth’s mantle, which has a circulation time scale of about a billion years, could be attributed to oxidation of FeO by ancient water. The Fe_2O_3 content could also be attributed to high-pressure disproportionation of FeO into metallic iron and ferric iron near the core-mantle boundary. In any case, no single source of volatiles satisfies both the water and noble gas data, and more complicated scenarios must be considered.

Conclusions

The tendency to approach chemical equilibrium was a driving force in determining the composition of solid materials in the early Solar System. Equilibrium between gases and dust during the nebular phase could be closely approached at the high temperatures found close to the Sun, in the terrestrial planet region. However, reduction of the stable high-temperature gases N_2 and CO must have been kinetically inhibited at low temperatures far from the Sun where CH_4 and NH_3 are thermodynamically stable. Thus CO and N_2 were available for incorporation into ices, whereas the reduced gases were in limited

supply when cometary ices were condensed. At all distances beyond the heart of the asteroid belt the process of equilibration between preexisting grains and gases was very incomplete. Thus, outer Solar System bodies from carbonaceous asteroids through the Centaurs, TNOs, outer retrograde satellites, and Trojan bodies on the orbits of the giant planets are repositories of ancient presolar grains that bear the chemical signatures of their own condensation environment. The regular (inner) satellite systems of the giant planets, formed in low-entropy (much denser) subnebula around their parent planets, should bear the chemical evidence of much better equilibration, most notably abundant methane and ammonia, in their interiors.

References

1. Cox, L. P.; Lewis, J. S.; Lecar, M. *Icarus* **1978**, *34*, 415-425.
2. Cox, L.P.; Lewis J. S. *Icarus* **1980**, *44*, 706-717.
3. Wetherill, G. W.; Cox, L. P. *Icarus* **1984**, *60*, 40-55.
4. Wetherill, G. W.; Cox, L. P. *Icarus* **1985**, *30*, 290-303.
5. Wetherill, G. W. In *Mercury*; Vilas, F.; Chapman, C. R.; Matthews, M., Eds.; Univ. of Arizona Press: Tucson, AZ, 1988; pp. 670-691.
6. Lewis, J. S. In *Mercury*; Vilas, F., Chapman, C. R., and Matthews, M., Eds.; Univ. of Arizona Press: Tucson, AZ, 1988; pp. 651-666.
7. Wasson, J. In *Mercury*; Vilas, F.; Chapman, C. R.; Matthews, M., Eds.; Univ. of Arizona Press: Tucson, AZ, 1988; pp. 622-650.
8. Malhotra, R. *Astron. J.* **1995**, *110*, 420-429.
9. Fegley, Jr., B., this volume.
10. Konopliv, A. S.; Binder, A. B.; Hood, L. L.; Kucinskis, A. B.; Sjogren, W. L.; Williams, J. G. *Science* **1998**, *261*, 1476-1480.
11. Yoder, C. F.; Konopliv, A.; Folkner, W. M. AGU Fall Meeting, Abstract #G42C-04, **2003**.
12. Bertka, C. M.; Fei, Y. *J. Geophys. Res.* **1997**, *102*, 5251-5264.
13. Dreibus, G.; Wänke, H. *Meteoritics* **1985**, *20*, 367-381.
14. Robinson, M. S.; Taylor, G. J. *Meteoritics Planet. Sci.* **2001**, *336*, 841-847.
15. Lewis, J. S.; Prinn, R. G. *Astrophys. J.* **1980**, *238*, 357-365.

Chapter 8

Photochemistry in the Early Solar System

Robert N. Clayton

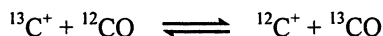
Enrico Fermi Institute, University of Chicago, Chicago, IL 60637

Isotope-selective photodissociation of gaseous carbon monoxide is a well-known process in molecular clouds. This process may have been important in the early solar system, with the nascent Sun as the source of ultraviolet radiation. The consequent self-shielding gives rise to the non-mass-dependent oxygen isotope variations observed in primitive meteorites. This model implies that the solar oxygen isotope ratios, $^{18}\text{O}/^{16}\text{O}$ and $^{17}\text{O}/^{16}\text{O}$, are about 5% smaller than those ratios in the Earth and other inner solar system bodies. A similar effect may also have occurred for nitrogen, through photolysis of N_2 . These photochemical processes lead to disequilibrium chemistry in the formation of solid bodies in the Solar System.

Introduction

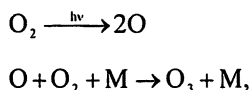
The importance of chemistry in astronomical settings has been increasingly recognized in recent years. This is especially true for the formation of stars (including our Sun) within dense molecular clouds. Molecular clouds have masses in the range 10^2 – 10^6 solar masses, densities on the order of 10^3 – 10^4 particles/cm³, and temperatures of 10–20 K. They are common birthplaces of

new stars, as is seen today in the Orion molecular cloud. Their principal molecules are H_2 and CO , reflecting the cosmic abundances of the elements H, C, and O, and the stability of these molecules. At the low temperatures of molecular clouds, only those exothermic reactions without activation energy can occur. These are ion-molecule reactions, with ionization produced by either stellar ultraviolet light and X-rays or by galactic cosmic rays. An example of a cosmochemically important ion-molecule reaction, with implications for isotopic variability, is as follows (1):



The difference in zero-point energy between ^{12}CO and ^{13}CO (288 J/mole) is similar in magnitude to the mean kinetic energy of molecules at 10 K (125 J/mole), so that the equilibrium constant for this reaction is 32, i.e., a substantial enrichment of ^{13}C in CO . However, a separate process also affects the $^{13}\text{C}/^{12}\text{C}$ ratio of CO in molecular clouds, acting in the opposite direction: isotope-selective photodissociation of CO by ultraviolet starlight. This process preferentially dissociates the less abundant species, ^{13}CO , due to the phenomenon of self-shielding (2), which will be discussed below in the context of formation of the solar system.

Photochemistry is also important in present-day planetary atmospheres. The best-known abiotic example is the production of ozone (O_3) in the Earth's stratosphere, initiated by the photodissociation of O_2 by ultraviolet sunlight:



resulting in a ratio of O_3/O_2 that is many orders of magnitude greater than the equilibrium value. On Venus, water vapor has been photodissociated, accompanied by hydrogen escape from the planet, resulting in a very dry atmosphere and a D/H ratio in hydrogen that is about 100 times greater than that on Earth. Photodissociation of N_2 in the atmosphere of Mars, with consequent preferential loss of ^{14}N , has produced a $^{15}\text{N}/^{14}\text{N}$ enrichment of more than 60% (3). In Jupiter and the other gas giant planets, the principal carbon reservoir is methane, but its photodissociation leads to production of other hydrocarbons, such as ethane and acetylene.

The examples in the previous paragraph all describe the effects of ultraviolet sunlight on planetary atmospheres. These chemical effects are largely confined to the atmospheres, since short-wavelength light is strongly absorbed by molecules. This same property has led to the view that ultraviolet photochemistry was probably not important in the much more massive solar nebula: the cloud of gas and dust from which the Sun and planets formed. As a

consequence, almost all published models of solar nebular chemistry are based on ordinary, thermally-activated reactions, governed by equilibrium chemical thermodynamics.

In this chapter, I wish to explore the possible role of photochemistry (an inherently disequilibrium process) in formation of the planets and smaller bodies in the solar system. As was seen in the planetary examples above, the small differences in chemical properties of the stable isotopes of abundant light elements, especially carbon, nitrogen, and oxygen, provide key information regarding nebular chemistry. The rapid attenuation of light in a cloud of dust and gas requires that the irradiation region be continuously replenished, so that chemistry and dynamics are intimately interrelated.

Meteorite Evidence

Oxygen

It is difficult to decipher early solar-system history from observations of the planets themselves, since most of their earliest records have been obliterated by subsequent processing. However, the meteorites, mostly derived from asteroids, have remained largely unchanged since their constituent minerals formed in the presence of the nebular gas, and thus provide the best information on early chemical and physical processes, such as evaporation and condensation, or chemical exchange between gas and condensed phases.

Probably the most informative objects in meteorites are the refractory, calcium-aluminum-rich inclusions (CAIs). They are sub-millimeter- to centimeter-sized objects found in all types of primitive (chondritic) meteorites. On the basis of their uranium/lead radiometric ages, they are believed to be the first-formed "rocks" in the Solar System (4). Their chemical compositions are consistent with equilibrium condensation as solids from a gas of solar composition at high temperatures (~ 1700 K). The major mineral phases are spinel (MgAl_2O_4), pyroxene (Mg, Ca, Al, Ti silicate), melilite (another Mg, Ca, Al silicate), and anorthite ($\text{CaAl}_2\text{Si}_2\text{O}_8$). They are enriched in refractory (less volatile) trace elements, such as the rare-earth elements, by a factor of 15–20 (5), reflecting their high temperature of condensation. The abundances of the three stable isotopes of oxygen exhibit a pattern not seen in any terrestrial rocks (6). On earth, ratios of abundances of isotopes, such as $^{17}\text{O}/^{16}\text{O}$ and $^{18}\text{O}/^{16}\text{O}$, vary by a few percent as a result of differences in bond energies caused by differences in isotopic mass. In such mass-dependent effects, variations in $^{18}\text{O}/^{16}\text{O}$ are accompanied by variations in $^{17}\text{O}/^{16}\text{O}$ of one-half the magnitude. In

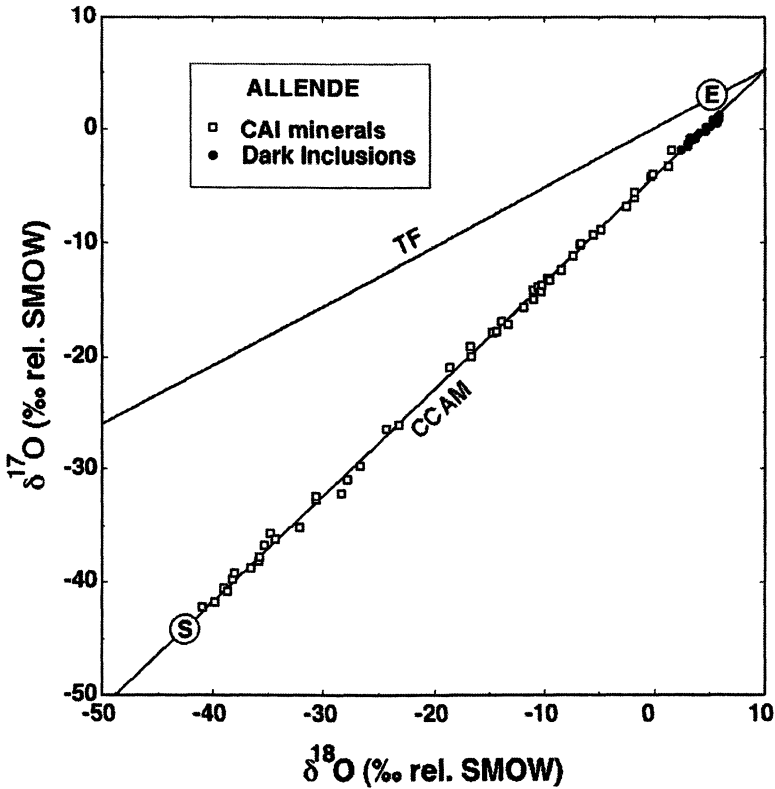


Figure 1. Oxygen three-isotope diagram showing isotopic compositions of minerals from Allende CAIs (CCAM = carbonaceous chondrite anhydrous minerals). The other line, labelled TF (terrestrial fractionation) is the locus of data points for terrestrial rocks and waters (data not shown). The bulk oxygen isotopic composition of the Earth is indicated by point E; the expected oxygen isotopic composition of the Sun is indicated by point S. The δ -notation on the axes is defined as:

$$\delta^x\text{O} = 1000 \left(\frac{R_x}{R_s} - 1 \right)$$

where $x = 17$ or 18 , and $R = \frac{x\text{O}}{^{16}\text{O}}$; standard s = Standard Mean Ocean Water, and is $(0,0)$ in this plot.

meteoritic CAIs and chondrules (less refractory spherules), the ratio $^{17}\text{O}/^{18}\text{O}$ remains almost constant, whereas $^{18}\text{O}/^{16}\text{O}$ and $^{17}\text{O}/^{16}\text{O}$ vary by several percent. The contrast between the meteoritic “non-mass-dependent” (NMD) fractionation and the terrestrial “mass-dependent” fractionation is illustrated in Figure 1.

The statistical mechanical theory underlying the well-known mass-dependent isotope effects was presented 60 years ago by Urey (7) and by Bigeleisen and Mayer (8). Some fundamentally different process is required in order to produce the NMD effects seen in primitive solar system materials. The first proposal was that CAIs had inherited excess ^{16}O derived from supernova nucleosynthesis (9), but this proposal failed due to the absence of related nuclear effects in magnesium and silicon, to which the “anomalous” oxygen is chemically bound. A second proposal was based on the experimental demonstration of NMD isotope effects in the synthesis of O_3 from O_2 (10). This phenomenon has been well documented both in the laboratory (10) and in the Earth’s atmosphere (11, 12). It has not yet been shown whether a similar NMD process may have been important in early solar system chemistry, although such a process has been proposed (13). The third proposal (14), currently under evaluation, is the isotope-selective photodissociation of CO, the most abundant oxygen-bearing species in molecular clouds, and probably in the solar nebula (15).

Ultraviolet photolysis of carbon monoxide occurs through absorption in narrow lines, corresponding to specific rotational and vibrational levels of several electronic transitions. The absorption wavelengths are isotope-dependent due to the effect of isotopic mass on the vibrational and rotational energies. As a consequence, the absorption lines due to $^{12}\text{C}^{16}\text{O}$, the most abundant isotopologue, do not overlap those due to $^{12}\text{C}^{17}\text{O}$ and $^{12}\text{C}^{18}\text{O}$. Because of the large differences in isotopic abundance ($^{16}\text{O}/^{17}\text{O} = 2500$; $^{16}\text{O}/^{18}\text{O} = 500$), the absorption lines of $^{12}\text{C}^{16}\text{O}$ become saturated (optically thick), while the absorption lines of $^{12}\text{C}^{17}\text{O}$ and $^{12}\text{C}^{18}\text{O}$ remain unsaturated. Therefore, the photodissociation of $^{12}\text{C}^{16}\text{O}$ occurs predominantly close to the light source (stars or Sun), while the dissociation of $^{12}\text{C}^{17}\text{O}$ and $^{12}\text{C}^{18}\text{O}$ predominates in the part of the gas cloud that is more remote from the light source. This process of “isotopic self-shielding” has been modelled quantitatively for molecular clouds (16), and has been directly observed (17).

In the case of molecular clouds, it has been assumed that a cloud is irradiated by ambient ultraviolet starlight, so that CO molecules in the periphery of the cloud are dissociated in proportion to their original isotopic abundances. However, photodissociation in the cloud interior favors the rarer, unshielded isotopic species: $^{13}\text{C}^{16}\text{O}$, $^{12}\text{C}^{17}\text{O}$, and $^{12}\text{C}^{18}\text{O}$. In the case of the solar nebula, three different irradiation geometries have been proposed:

1. direct inheritance from the parent cloud (18),

2. irradiation of the surface of the solar nebular disk, by the Sun and nearby stars, at a radial distance of tens of astronomical units ($1 \text{ AU} = 1.5 \times 10^8 \text{ km}$) from the Sun (19), and
3. irradiation by sunlight very near the young Sun ($\sim 0.05 \text{ AU}$) (14).

In the first two of these scenarios, it has been proposed that the rare-isotope-enriched atomic oxygen was quickly trapped by reaction with H_2 to form water ice, which was transported *sunward* to enrich the inner solar system reservoir in ^{17}O and ^{18}O . In the third scenario it was proposed that the rare-isotope-enriched atomic oxygen was quickly trapped by reaction with metals to form solid mineral grains, which were transported *outward* by a stellar wind (20).

Photochemical self-shielding of CO has two observable consequences: (1) the “anomalous” oxygen isotope patterns observed in chondrules and CAIs, and (2) the apparent overabundance of oxidized species (such as Fe^{2+} in silicates). The self-shielding model also leads to a striking prediction of the oxygen isotopic abundances in the present-day Sun. Self-shielding enhances the abundances of atomic ^{17}O and ^{18}O in the interior of the nebular cloud, with the implication that the initial isotopic composition must lie at the ^{16}O -rich end of the mixing line in Figure 1. Thus, it is expected that there is about a 5% deficit in the solar ratios $^{17}\text{O}/^{16}\text{O}$ and $^{18}\text{O}/^{16}\text{O}$ relative to the values in the Earth and other inner solar system bodies. Existing measurements of the solar isotopic composition are not precise enough to detect the predicted difference, but forthcoming analyses of the solar wind, made by the NASA Genesis mission, should resolve this effect.

Two attempts have been made to estimate the solar oxygen isotopic composition by measurement of solar wind atoms implanted in metal grains on the surface of the Moon, with conflicting results. Hashizume and Chaussidon (21), analyzing grains from an ancient lunar soil, found a composition enriched in ^{16}O relative to terrestrial compositions, whereas Ireland et al. (22), analyzing grains from a young lunar soil, found a composition depleted in ^{16}O . The reason for this difference is unknown.

The oxygen isotopic record in CAIs appears to reflect a two-stage history: (1) primary condensation from a gas of solar chemical and isotopic composition, corresponding to point S in Figure 1, and (2) a secondary exchange process, that is mineral-specific, moving the oxygen isotopic composition upward along the slope-1 line of Figure 1. Objects forming at lower temperatures, such as chondrules and planetary precursors, appear to have seen only this second environment, in which reactive ^{17}O and ^{18}O atoms have been enriched by the photochemical shielding.

The sequence in the preceding paragraph suggests a solution to the long-standing problem of understanding the oxidation state of primitive meteoritic materials. The CAIs are highly reduced, containing no primary Fe^{2+} , and containing Ti^{3+} (along with the more common Ti^{4+}) in pyroxene (23), consistent

with equilibrium with a hydrogen-rich solar gas. On the other hand, matrix olivine crystals in the same meteorite have compositions that are much more oxidized, containing abundant ferrous iron. This matrix is also greatly enriched in the rarer, heavy isotopes of oxygen, relative to the CAIs (and hence, relative to the solar composition). The oxygen isotope enrichment is clearly a disequilibrium phenomenon, which suggests that the oxidation of iron was also a disequilibrium process. An astrophysical model of the chemical effects of photodissociation of CO (24) showed that the abundances of oxygen-bearing molecules, such as OH and H₂O, may differ from equilibrium values by many orders of magnitude.

Nitrogen

If photodissociation was an important process for CO in the early Solar System, it may also have been important for N₂, an isoelectronic and isobaric molecule, which had an abundance in the gas phase lower than CO by only a factor of six. Nitrogen is less useful than oxygen as a tracer of Solar System chemistry, for a number of fundamental reasons: (1) it has only two stable isotopes, so that there is no simple way to distinguish between mass-dependent and abundance-dependent isotope effects; (2) the homonuclear character of the N₂ molecule renders it invisible to most astronomical observational techniques; (3) it is not chemically trapped as a major element in meteoritic minerals. Nitrogen is, however, a major constituent of many organic molecules, both in space (25) and in meteorites (26).

The range of ¹⁵N/¹⁴N observed in Solar System materials exceeds a factor of three (Figure 2), which is much larger than can be accounted for by low-temperature ion-molecule chemistry (25), and which therefore suggests that isotope-selective photochemistry may occur in N₂, as it does in CO.

As in the case of oxygen, the stable isotope ratio, ¹⁵N/¹⁴N, in the Sun is not yet well known. It will also be measured in the Genesis solar wind sample. If the isotopic self-shielding mechanism applies to nitrogen, the Sun should show a lower ¹⁵N/¹⁴N ratio than the Earth, but there is no obvious meteoritic sample of unfractionated solar composition, as there is for oxygen in the CAIs. A possible candidate for such a primitive sample is the refractory mineral osbornite (TiN) found in a primitive carbonaceous chondrite (27). This mineral has a ratio of ¹⁵N/¹⁴N = 2.36 × 10⁻³, 36% lower than the ratio in the terrestrial atmosphere. The Allende meteorite, from which many of the CAI oxygen data have come, does carry a nitrogen component that is depleted in ¹⁵N by at least 9% (28), but this is not likely to be carried within the CAIs. Similar nitrogen isotope ratios were observed in several types of iron meteorite (29). Two samples that may represent the Solar System's primordial nitrogen isotope abundances are:

(1) ammonia in the atmosphere of Jupiter, and (2) solar wind ions implanted into lunar mineral grains. The former (30), based on measurements of the Galileo Probe Mass Spectrometer, gave $\delta^{15}\text{N} = -380 \pm 80\text{‰}$ relative to Earth's atmosphere; the latter (31), based on ion microprobe measurements of correlated hydrogen and nitrogen isotope abundances in lunar soil minerals, gave $\delta^{15}\text{N} < -240\text{‰}$. The isotopic compositions of oxygen (Figure 1) and nitrogen (Figure 2) are given in the conventional δ -notation, as deviations in permil (‰, parts per thousand) in $^{17}\text{O}/^{16}\text{O}$, $^{18}\text{O}/^{16}\text{O}$, $^{15}\text{N}/^{14}\text{N}$ from the corresponding terrestrial standards (SMOW for oxygen, AIR for nitrogen). These values, coupled with the highest ratio seen in a bulk meteorite (32), show that the $^{15}\text{N}/^{14}\text{N}$ ratios in early Solar System materials varied by a factor of three, well beyond the range of any known chemical kinetic or equilibrium process.

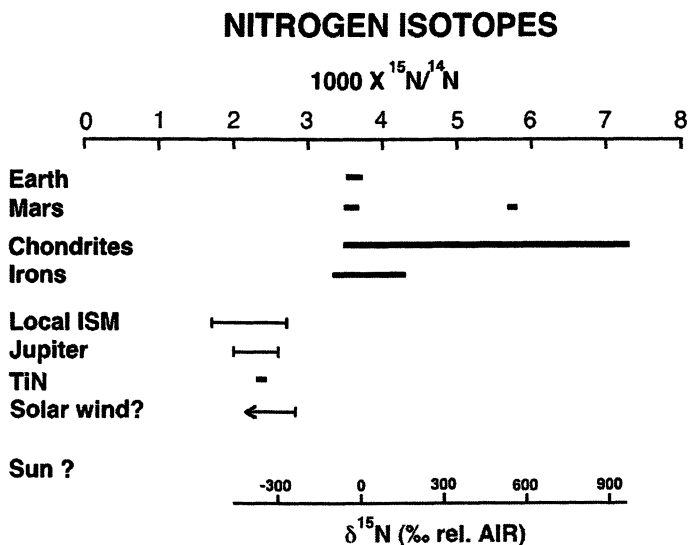


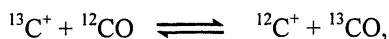
Figure 2. Nitrogen isotope abundances in solar system materials: upper scale gives absolute ratios; lower scale gives $\delta^{15}\text{N}$ relative to the terrestrial AIR standard. Heavy bars show observed ranges; light bars show measurement uncertainties.

If the Genesis solar wind analyses support the conjecture that the nitrogen isotope ratios in Jupiter and in the Sun are similar, whereas the $^{15}\text{N}/^{14}\text{N}$ ratios in the inner Solar System are much higher, there are major implications for the processes of planet formation, since such an observation would imply that the

gas giant planets formed from a gas of solar isotopic composition, whereas the inner, rocky planets formed from a photochemically processed nebula.

Carbon

If we attribute the “anomalous” isotope behavior of oxygen to the mechanism of photochemical self-shielding in the photolysis of CO, should we not expect similar effects in carbon isotopes? The ratio $^{12}\text{C}/^{13}\text{C}$ in solar system carbon is about 89, which is large enough to produce isotopic selectivity in photochemistry. However, no very large carbon isotope variations have been seen in meteoritic or planetary materials, except for the small contributions of ^{13}C -rich presolar grains (33). In the osbornite mentioned above under Nitrogen, the ratio of $^{12}\text{C}/^{13}\text{C}$ is 89, which is within the terrestrial range. The reason for the difference in behavior of carbon is shown in Table I, where it is seen that the ionization energy of carbon is below that of hydrogen (by far the most abundant element), whereas those of nitrogen and oxygen are above it. Thus atomic carbon is readily photo-ionized, leading to the rapid exchange reaction:



which removes the ^{13}C excess from the atomic carbon reservoir.

Table I. First Ionization Potentials of H, C, N, O

<i>Element</i>	<i>Ionization Energy (kJ/mole)</i>
H	1312.0
C	1086.5
N	1402.3
O	1313.9

Other elements

From the examples discussed above, a list of criteria can be made, in order to anticipate any additional examples of natural photochemical isotope effects:

1. the element should have two or more stable isotopes, at least one of which is of low abundance ($\leq 1\%$);
2. the element should form stable gaseous molecules, capable of photodissociation by visible or ultraviolet light;

3. the element's first ionization energy should be greater than that of hydrogen, if the process is to occur in a hydrogen-rich gas.

Magnesium fails criterion (2), as its stable vapor species is atomic Mg.

Silicon satisfies criterion (2), since SiO and SiS are both stable molecules in a gas of solar composition (34). However, silicon does not quite satisfy criterion (1) ($^{29}\text{Si}/^{28}\text{Si} = 0.051$; $^{30}\text{Si}/^{28}\text{Si} = 0.034$), and does not satisfy criterion (3). No large systematic NMD effects have been seen in meteoritic silicon (again, excepting the highly anomalous presolar SiC), although a few hints of effects $< 1\%$ have been observed (35).

Sulfur is a good candidate, with two of its four stable isotopes (^{33}S and ^{36}S) satisfying criterion (1), and several gaseous compounds satisfying criterion (2), notably SO_2 and H_2S . In a gas of solar composition, sulfur fails to satisfy criterion (3), and, in fact, NMD effects reports in meteorites are rare and very small (36). However, in the Earth's hydrogen-free atmosphere, NMD effects in sulfur, apparently due to photolysis of volcanic SO_2 , are well-established (37).

There are no other good candidates for photochemical isotope effects. For example, the halogens all fail criterion (1), and most metallic elements fail criterion (2).

Hydrogen, the most abundant element in the Solar System, has large isotopic variations in meteoritic and planetary materials, not all of which are well understood. Like nitrogen and carbon, hydrogen has only two stable isotopes, so that there is no simple way to distinguish between mass-dependent isotope effects and abundance-dependent effects. This problem is worse for hydrogen than for nitrogen, since mass-dependent effects in hydrogen may be very large, due to the factor of two difference in mass between D and H. In the case of hydrogen, measurement of the present-day D/H ratio in the Sun does not yield the primordial value, since deuterium has been destroyed in the Sun by nuclear reactions, as has been confirmed by measurements of solar wind implanted in lunar soils (38). A reasonable estimate of the primordial Solar System D/H ratio may be that measured by the Galileo Probe Mass Spectrometer in Jupiter (39). This measurement requires careful correction of the signal at $m/e = 3$ (HD^+) for contributions from isobaric ions, $^3\text{He}^+$ and H_3^+ . The resulting ratio is $(26 \pm 7) \times 10^{-6}$, compared with the terrestrial value of about 150×10^{-6} . Thus, the D/H ratio in Earth is about six times greater than that in Jupiter, and the ratio in the Mars interior is greater by an additional factor of at least two (40). In light of the evidence for a photochemical role in the isotopic variability in oxygen and nitrogen, it is desirable to consider whether isotope-specific photolysis of H_2 and/or H_2O may also have been an important process.

Conclusions

Although equilibrium chemical processes have been widely used to model the early evolution of the Solar System, there is growing evidence, particularly in isotopic abundances, that non-equilibrium chemistry was also important. The specific process of isotopic self-shielding in the photolysis of carbon monoxide may have played a major role. A key test of this hypothesis will be provided by laboratory-based isotopic analysis of the solar wind sampled in the NASA Genesis mission.

Quantitative modelling of the photochemical processes, in various astrophysical settings, is needed in order to address the question of their chemical consequences. In particular, the location of photochemical processes and the source of ultraviolet light are not yet well constrained, resulting in large differences among current proposed scenarios.

Photochemistry appears to be well established for oxygen and nitrogen in the early Solar System. Consideration should also be given to the possibility of analogous effects in hydrogen.

References

1. Langer, W. D.; Graedel, T. E.; Frerking, M. A.; Armentrout, P. B. *Astrophys. Jour.* **1984**, *277*, 581–604.
2. Bally, J.; Langer, W. D. *Astrophys. Jour.* **1982**, *255*, 143–148.
3. McElroy, M. B.; Yung, Y. L.; Nier, A. O. *Science* **1976**, *194*, 70–72.
4. Amelin, Y.; Krot, A. N.; Hutcheon, I. D.; Ulyanov, A. A. *Science* **2002**, *297*, 1678–1683.
5. Grossman, L. *Geochim. Cosmochim. Acta* **1973**, *37*, 1119–1140.
6. Clayton, R. N.; Grossman, L.; Mayeda T. K. *Science* **1973**, *182*, 485–488.
7. Urey, H. C. *J. Chem. Soc.* **1947**, 562–581.
8. Bigeleisen, J.; Mayer, M. G. *J. Chem. Phys.* **1947**, *15*, 261–267.
9. Clayton, R. N.; Onuma, N.; Grossman, L.; Mayeda, T. K. *Earth Planet. Sci. Lett.* **1977**, *34*, 209–224.
10. Thiemens, M. H.; Heidenreich, J. E. *Science* **1983**, *219*, 1073–1075.
11. Mauersberger, K. *Geophys. Res. Lett.* **1987**, *14*, 80–83.
12. Johnston, J.C.; Thiemens, M. H. *J. Geophys. Res.* **1997**, *102*, 25395–25404.
13. Thiemens, M. H. In *Chondrules and the Protoplanetary Disk*; Hewins, R. H.; Jones R. H.; Scott, E. R. D., Eds.; University of Arizona Press: Tucson, AZ, 1988, pp 107–118.

14. Clayton, R. N. *Nature* **2002**, *415*, 860–861.
15. Lewis, J. S.; Prinn R. G. *Astrophys. Jour.* **1980**, *238*, 357–364.
16. van Dishoeck, E. F.; Black, J. H. *Astrophys. Jour.* **1988**, *334*, 771–802.
17. Sheffer, Y.; Lambert, D. L.; Federman, S. R. *Astrophys. Jour.* **2002**, *544*, L171–L174.
18. Yurimoto, H.; Kuramoto, K. *Science* **2004**, *305*, 1763–1766.
19. Lyons, J.R.; Young, E.D. *Nature* **2005**, *435*, 317–320.
20. Shu, F.H.; Shang, H.; Gounelle, M.; Glassgold, A.E.; Lee, T. *Astrophys. Jour.* **2001**, *548*, 1029–1050.
21. Hashizume, K.; Chaussidon, M. *Nature* **2005**, *434*, 619–622.
22. Ireland, T. R.; Holden, P.; Norman, M. D.; Clarke, J. *Nature* **2006**, *440*, 776–778.
23. Simon, S. B.; Grossman, L. *Geochim. Cosmochim. Acta* **2003**, *67*, A437.
24. Sternberg, A.; Dalgarno, A. *Astrophys. Jour. Suppl.* **1995**, *99*, 565–607.
25. Terzieva, R.; Herbst, E. *Mon. Not. Roy. Astron. Soc.* **2000**, *317*, 563–568.
26. Gilmour, I. In *Treatise on Geochemistry*; Davis, A.M., Ed.; Elsevier: Oxford, UK, 2003; Vol. 1, pp 269–290.
27. Meibom, A.; Krot, A. N.; Mostefauoi, S.; Russell, S. S.; Petaev, M. I.; Gounell, M. *Lunar Planet. Sci. Conf. 38* **2007**, abstract #1256.
28. Thiemens, M. H.; Clayton, R. N. *Earth Planet. Sci. Lett.* **1981**, *55*, 363–369.
29. Prombo, C. A.; Clayton, R. N. *Geochim. Cosmochim. Acta* **1993**, *57*, 3748–3761.
30. Owen, T.; Mahaffy, P. R.; Niemann, H. B.; Atreya, S.; Wong, M. *Astrophys. Jour.* **2001**, *553*, L77–L79.
31. Hashizume, K.; Chaussidon, M.; Marty, B.; Robert, F. *Science* **2000**, *290*, 1142–1145.
32. Prombo, C. A.; Clayton, R. N. *Science* **1985**, *230*, 935–937.
33. Halbout, J.; Mayeda, T. K.; Clayton, R. N. *Earth Planet. Sci. Lett.* **1986**, *80*, 1–18.
34. Grossman, L. *Geochim. Cosmochim. Acta* **1972**, *36*, 597–619.
35. Clayton, R. N.; Hinton, R. W.; Davis, A. M. *Phil. Trans. Roy. Soc. Lond.* **1988**, *A325*, 483–501.
36. Rai, V. K.; Jackson, T. L.; Thiemens, M. H. *Science* **2005**, *309*, 1062–1065.
37. Baroni, M.; Thiemens, M. H.; Delmas, R. J.; Savarino, J. *Science* **2007**, *315*, 84–87.

Chapter 9

Lessons from Meteorites

Michael E. Lipschutz

**Department of Chemistry, Purdue University, West
Lafayette, IN 47907-2084**

Meteorites, which come mainly from various asteroids but also from Mars and our Moon, provide otherwise unobtainable information about objects in the inner Solar System in both space and time. The presence of meteorites on Earth allows application of the full gamut of instrumentation able to analyze materials from the asteroids (minor planets), Mars and the Moon with state of the art sensitivity and accuracy. Many meteorites include material that condensed and accreted in the primitive Solar nebula and were subsequently unaltered: some contain evidence for pre-Solar nuclear processes. Information in meteorites tracks the evolution of their parent bodies, both interiors and surfaces, the impacts that ejected them and the nuclear radiation history that occurred as they travelled Earthward. Meteoritic material also allows the dating of all of these episodes and determination of the composition of the Sun's surface and the particles streaming from it. This chapter is a brief tutorial outlining this information and indicating how it is obtained.

Introduction

The question routinely asked in basic geology courses - what kind of rocks exist on Earth? - is usually answered by "igneous, sedimentary, metamorphic". However, this list is incomplete because it omits meteorites: these objects of extraterrestrial origin include the only materials accessible to scientists on Earth that date back to Solar System genesis. Thus, many contain important, indeed unique, information on the planets' earliest formative stages. In the space available here, I can answer only the most basic questions. Why are meteorites important scientifically? What are meteorites? Where do they come from? How old are they? In answering these, much is omitted that I address in a very recent and more extended summary (1), to which I refer the reader: this also includes suggestions for further study, including the recent volume by Hutchison (2). I also cite here review chapters in this volume and that in which (1) appears.

Why are Meteorites Important Scientifically?

The importance of meteorites derives from the fact that many consist of parent material formed in the early Solar System, thus recording specific formative episodes and dating them (Figure 1), and allowing study of bodies' genesis and evolution in time and space. Some meteorites contain grains created before Solar System formation, allowing chemical characterization and establishment as to when the nucleosynthetic episodes occurred that produced its constituent elements (3,4). Differentiated meteorites - i.e. achondrites, irons and stony-irons - that formed in planetary interiors are the only accessible samples of such materials and record differentiation and crystallization processes in larger planetary bodies.

Meteorites come from more massive parents (mainly minor planets - i.e. asteroids - but also Mars and our Moon) and to get to Earth, their immediate predecessors - meteoroids - can only be excavated from its parent body by an explosive impact. This impact almost always generates short-lived but intense shock effects, results of which are present in many individual meteorites and groups of them (1) but which I do not discuss further here. The impact also provides the impulse necessary for the meteoroid to exceed the parent body's escape velocity; e.g. 5.4 km/s for Mars. Thus, meteoritic minerals provide barometers for shock pressures up to ~60 GPa (6×10^5 atm) corresponding to post-shock temperatures $>1250^\circ\text{C}$; at much higher pressures (temperatures), these materials vaporize. Incidentally, this explains why Earth receives meteorites from Mars but not Venus, which is closer: Venus' escape velocity is 10.4 km/s. One could write a book about this entitled "*Some Meteorites are from Mars: None are from Venus.*"

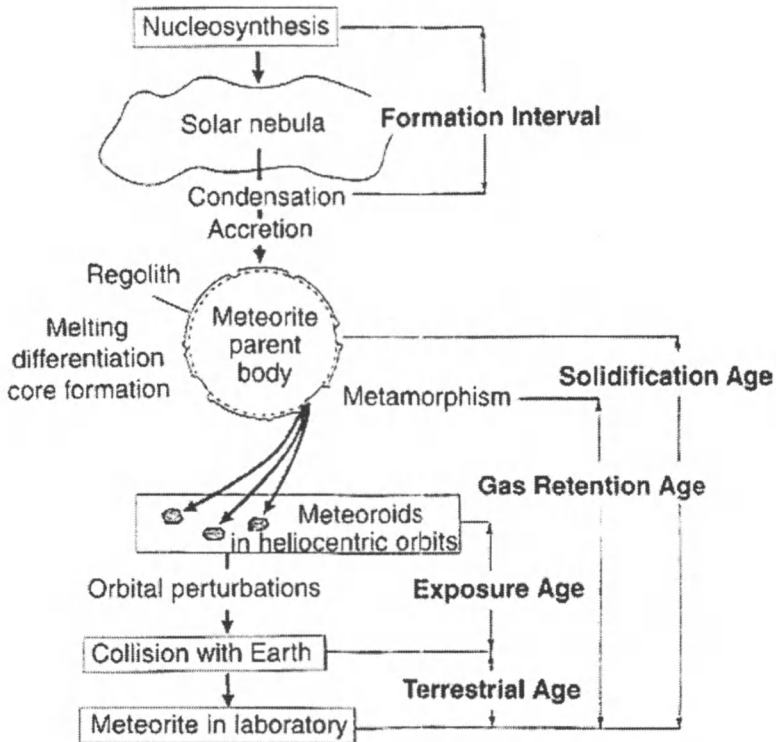


Figure 1. From nebula to meteorite: genetic processes and the corresponding age determinable for each process. Nuclides of nearly all elements were formed by nuclear reactions in interiors of large stars which then ejected them in very energetic events including supernovae. The protoplanetary nebula and disk formed by collapse of a dense cloud of dust and gas containing elements essentially in Solar proportions (but with some heterogeneities). In the disk, matter nucleated, condensed and accreted into primitive bodies. Source bodies for most meteorites were heated, causing solid state metamorphism or, at higher temperatures, differentiation involving separation of solids, liquids and gases. As a body evolved, it suffered numerous impacts and, if atmosphere-free, its surface was irradiated by Solar and galactic particles that embedded in the rims of small grains and/or caused nuclear reactions. Larger impacts ejected fragments which orbited the Sun. Subsequently, orbital changes caused by large-body gravitational attraction placed meteoroids into Earth-crossing orbits allowing their landing and immediate recovery (as a fall) or later (as a find). [Each process can alter elemental and/or isotopic contents. Which process(es) affected a given meteorite and the time elapsed since it/they occurred can be defined and determined.] (Reproduced with permission from reference 1.

Copyright 2006 Elsevier.)

In addition to acting as test systems for high-pressure shock events, meteorites record the effects of energetic nuclear bombardment. At parent body depths >1 m, matter is shielded from even the most energetic nuclear particles. When meter-sized meteoroids are ejected from their parent body by an impact, they are irradiated by cosmic rays (mainly protons and alpha particles) of Solar or galactic origin until they fall to Earth. Solar cosmic rays have a power law energy distribution; i.e. the particle flux increases rapidly with decreasing energy. Most Solar particles have energies <1 MeV and can only embed themselves in a grain rim on the very surface of the parent body. Galactic and some Solar particles have high energies (and velocities, from $E = 1/2 mv^2$) of hundreds of MeV to GeV that can induce nuclear reactions, producing cosmogenic radioactive or stable nuclides. In larger meteoroids, cosmogenic nuclear reactions occur only in the meter-thick outer shell penetrated by galactic cosmic ray primaries and secondaries - which differ compositionally and energetically from primaries. Nuclide levels produced during cosmic ray exposure (CRE) establish the duration of energetic particle bombardment, i.e. the CRE age, and the time spent by a meteoritic find on Earth, the terrestrial age (Figures 1, 2).

What are Meteorites?

General Properties

Meteorite parent bodies accreted from material condensed from the Solar nebula. Most meteorites - the chondrites - escaped post-accretionary alteration and their major-element composition is primary, i.e. just that established during nebular vapor-to-solid condensation (*I*). A few meteorites - achondrites, irons and stony-irons - are igneous, having crystallized from differentiated liquids generated from primary materials that were heated by various sources, especially radioactive decay, in more or less reducing environments in parent body interiors (Figure 3, Plate 1). Chondrites, the overwhelming majority, are undifferentiated polymineralic rocks derived from primitive asteroidal-sized parents which accreted from grains condensed in the early Solar nebula. Most grains formed as solids; others, e.g. chondrules, went through a very short-lived (minute-scale) liquid stage (*I*). Chondrules are more-or-less spherical, mm-sized droplets formed by very rapid partial or complete melting ($\geq 1600^\circ\text{C}$) of solids and quenching prior to incorporation into material that will form the matrix of undifferentiated meteorites.

Of the >7500 different meteorites in scientific collections, a few are of Lunar or Martian origin (31 and 32, respectively): thousands of others come

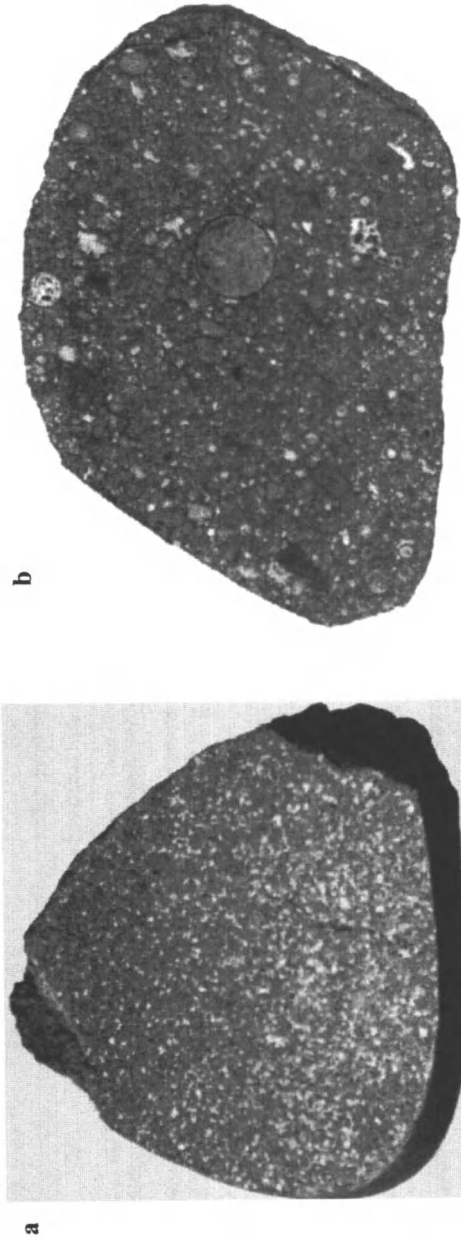
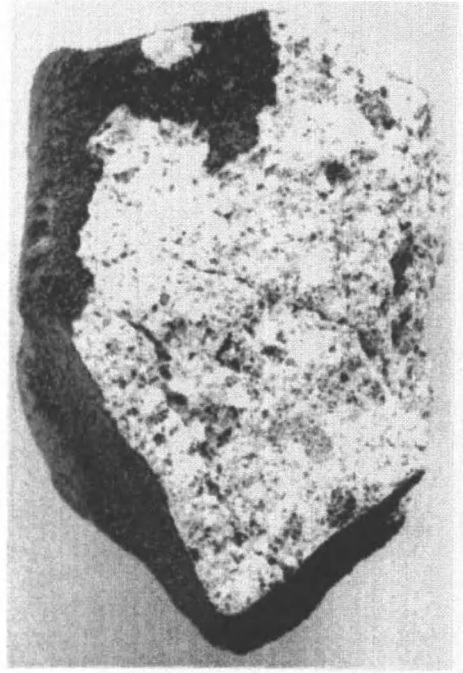
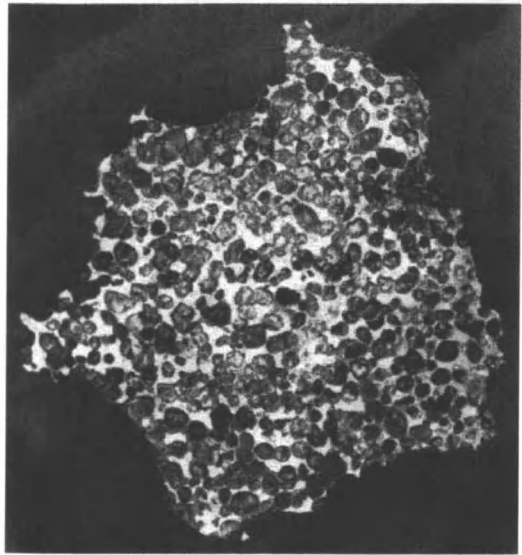


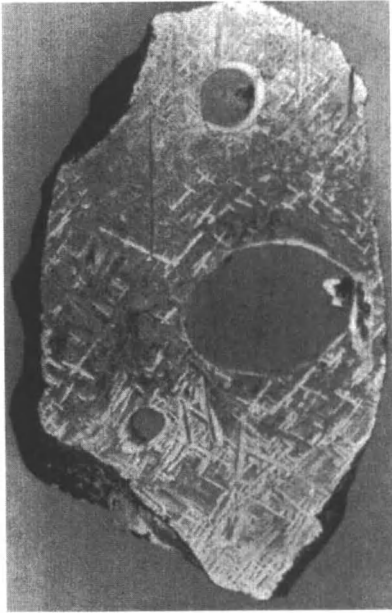
Plate 1. Common meteorite types (approximate longest dimensions): a) Whitman, H5 (6 cm); b) Allende; C3V (8 cm) – note 1 cm chondrule in center, c) Springwater pallasite (18 cm); d) Sioux Co. eucrite (8 cm); e) Sanderson III B medium octahedrite (13 cm) – note large FeS inclusions; f) Noblesville H chondrite – note that the fusion crust is thin and smooth (as it is on most meteorites) and has an usual dark brown color on top which grades to black on the other exposed surfaces (contrast with the Lafayette fusion crust in Plate 2). The broken surface next to the 1-cm cube shows the interior of this gas-rich regolith breccia. (Reproduced with permission from reference 1. Copyright 2006 Elsevier.) (See page 11 of color inserts.) Continued on next page.



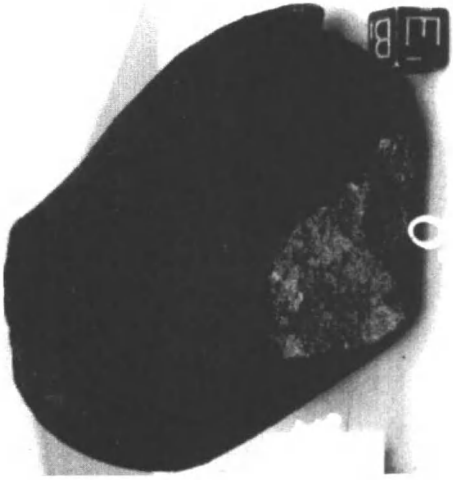
d



c



e



f

Plate 1. Continued. (See page 11 of color inserts.)

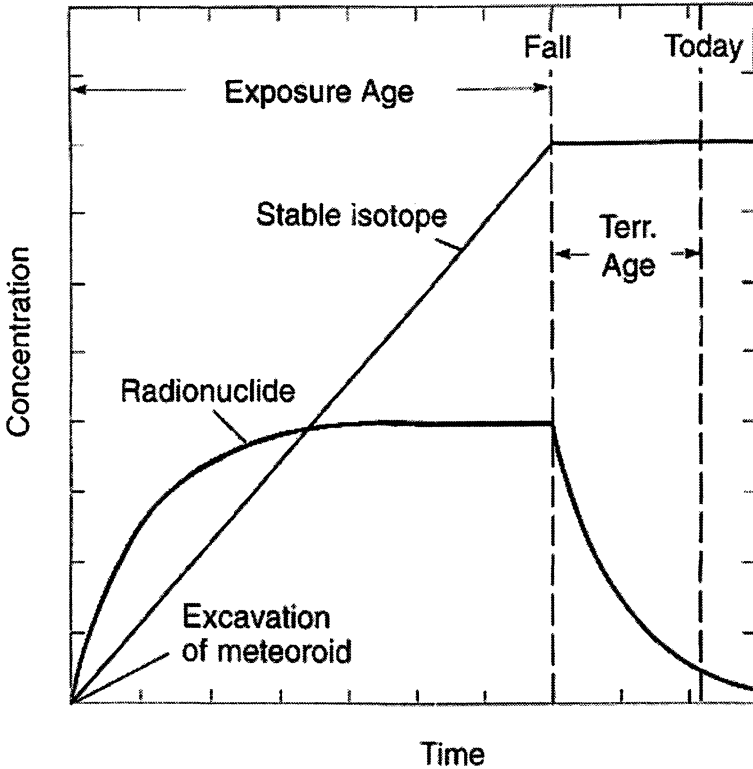


Figure 2. Concentrations of cosmic-ray-produced radioactive and stable nuclides during cosmic ray exposure and after the meteorite's fall on Earth. (Reproduced with permission from reference 1. Copyright 2006 Elsevier.)

from asteroids (4,5). All share one characteristic: they entered our atmosphere at 11-70 km/s (average 15 km/s) causing the meteoroid's surface to heat and ablate (losing ~90% of its mass) at similar rates. Thus, thermal alterations in meteorites reaching the Earth's surface, are only skin-deep (<1 mm) and the meteorite's interior remains cold. Apropos, it should be noted that although meteorites are depleted in carbon, hydrogen and nitrogen relative to the Solar photosphere, the most volatile-rich carbonaceous chondrites contain large amounts of preterrestrial organic matter: cf. (4) in this volume for a more complete discussion. Here, it is adequate to note that most organic compounds in meteorites can be altered or destroyed by even brief exposure to temperatures of 200-300°C. Thus, their presence in meteorites is an upper limit to postaccretionary heating temperatures during metamorphism, shock or atmospheric transit. If any biologic entities were generated on Mars, they should have already travelled here since we have Martian meteorites on Earth. This

CLASSIFICATION OF METEORITES

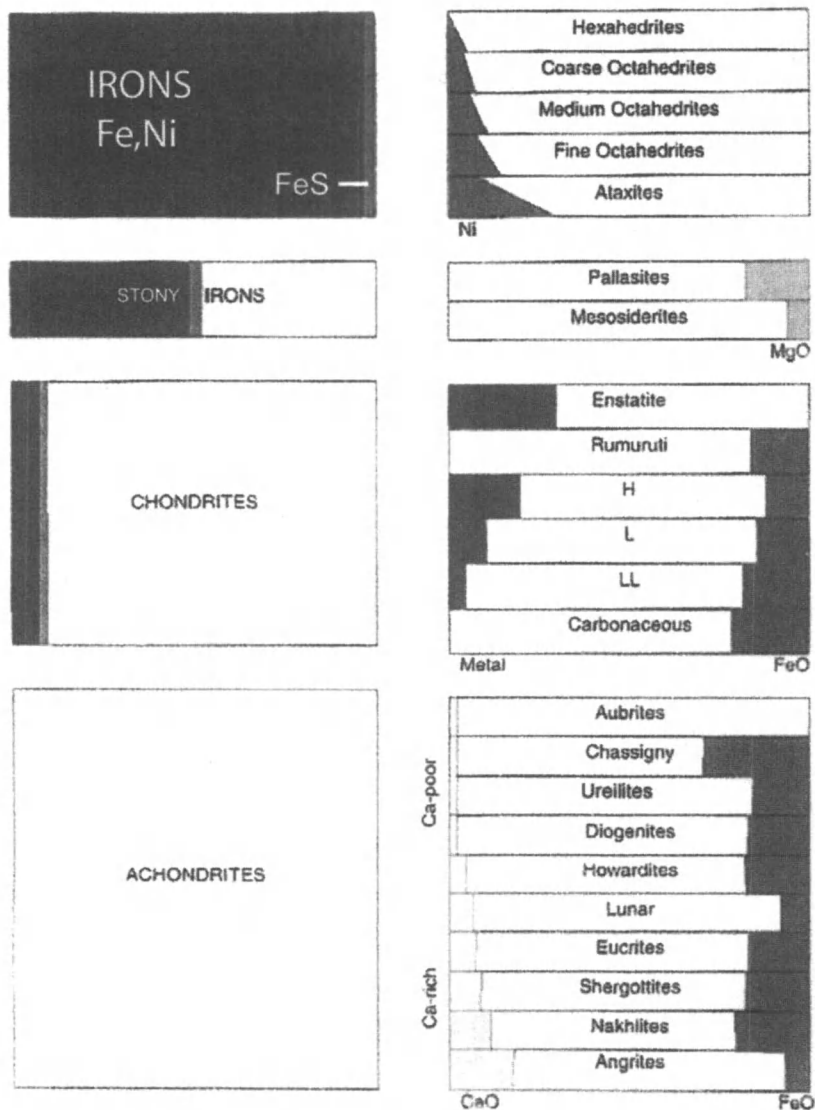


Figure 3. Classifications for the most common meteorites based upon Fe, Ni metal, FeS and silicate (white) on left and chemical criteria on right. (Reproduced with permission from reference 1. Copyright 2006 Elsevier.)

argues against the need to quarantine any Martian samples returned by future missions to Mars.

Ablative deceleration leaves a smoothed dark brown to black fusion crust on most meteorites (Plate 1f): translucent, pale crusts may occur on Fe-poor stony meteorites which may be olive-green on Lunar ones. Very rarely, an appropriately-shaped meteoroid may assume a quasi-stable orientation during late atmospheric traversal. In such a case, material ablated from the front can re-deposit as delicate droplets or streamlets on its sides and rear (Plate 2). The fusion crust is an unambiguous indicator that an object in question is a meteorite. Also, nearly all meteorites contain iron and will therefore attract a magnet; however, some terrestrial materials will too.

In view of current concerns about the hazards that asteroid impacts present to life here, we should briefly consider what can occur as a meteoroid enters our atmosphere to land anywhere on Earth. Large meteoroids – \geq decameters – are not decelerated much by atmospheric transit and, with an appropriate trajectory, may ricochet off the Earth's atmosphere or strike it at full geocentric velocity, >11 km/s (*I*). The latter case, i.e. an explosive, crater-forming impact, can do considerable damage. During such explosive impacts - whether on extraterrestrial bodies or on Earth - much of the projectile and immediate target volume vaporize. However, some of the projectile - particularly on the rear face - can survive, shock-heated to a greater or lesser extent, possibly causing volatile loss. The 1 km diameter Meteor Crater near Flagstaff, Arizona formed 50,000 years ago (i.e. 50 ka) by the impact of a 25-86 m meteoroid, yielded fragments now surviving as Canyon Diablo iron meteorites. At least 170, perhaps 300, terrestrial craters exhibit features thought to be produced only by explosive impact of a large meteoroid or comet nucleus (e.g. as in the 30 June 1908 event at Tunguska in Siberia). The 180-km diameter Chicxulub feature in Yucatan, Mexico marks the impact of an object ≥ 10 km in diameter: its impact-associated blast effects are accepted as having created the K-T die-off of dinosaurs and many other biota 65 Ma ago. Less massive observed "falls" (1 g to tens of kg recovered mass) have sometimes hit buildings, vehicles or people, without verifiably killing anyone. Despite this lack of lethality, the probability of dying in a meteoroid impact exceeds that of being killed in an airplane crash because the impact of a large meteoroid, small asteroid, or comet nucleus can be devastating, even causing the total extinction of life. Fortunately such impacts are infrequent.

An observed fall may generate remarkable light or sound effects or land silently, like Noblesville (Plate 1f), whose surface was at most slightly warm when picked up within a second or two of landing. Meteorites are named for the local post office or nearest physical feature to their recovery spot. Over 1000 falls are known (Table I). Sporadic "finds" (~1840, cf. Table 1) are recognized by some unique feature like fusion crust or iron's high density. The largest single



Plate 2. Fusion crust of Lafayette Martian meteorite. Lafayette exhibits very delicate, redeposited droplets on its sides, indicating an orientation with its front pointing Earthward late in its atmospheric traversal. (Reproduced with permission from reference 1. Copyright 2006 Elsevier.) (See page 12 of color inserts.)

piece find is a 60 metric ton iron meteorite found in 1920 on a Namibian farm where it remains.

Table I. Numbers of Classified Non-Antarctic Meteorite Falls and Finds, Including Those from Hot and Cold Deserts

	<i>Falls</i>	<i>Finds</i> [*]	<i>ANSMET</i> [†]
Chondrites	797	>814	2925
C1-6	40	20 (312)	109
E3-6	17	8 (307)	109
H3-6	316	405	<i>1048</i>
L3-7	350	350	<i>1140</i>
LL3-6	72	30	<i>574</i>
Achondrites	81	>73	184
Aubrites	9	3 (2)	7
HED	60	16 (276)	114
Lunar	0	1(22)	8
Martian	4	3 (17)	8
Irons	40	>690 (34)	47
Stony Irons	12	>61	13

^{*}Numbers in parentheses indicate fragments collected from hot deserts and Queen Maud Land Antarctica, uncorrected for pairing except for Lunar and Martian samples.

[†]Antarctic Search for Meteorites (ANSMET) recoveries from Victoria Land. Numbers in italics are estimated assuming 4 fragments per fall: those in normal type are corrected for pairing.

SOURCE: Reproduced with permission from reference 1. Copyright 2006 Elsevier.)

We are not certain about how many different meteorites are represented in collections on Earth. Some large meteoroids may fragment during atmospheric traversal resulting in a shower of meteorites which will form an ellipse whose long axis may extend for tens of km and the fragments can be associated ("paired") by their mineralogic/compositional similarities. For a non-cluster meteorite shower, its members are readily paired but such pairing is difficult for the very numerous meteorite pieces found clustered in hot (e.g. Saharan or Australian) or cold (Antarctic) deserts since 1969 (*J*). So far, starting in 1969, but mainly since 1976, Antarctica yielded over 31,000 fragments (16,500 collected by Japanese (JARE) and 13,907 by U.S. (ANSMET) –led teams and >677 by a European consortium, now an Italian-led effort). Hot desert-clusters in Australia, North Africa (mainly Algeria and Libya), China and the U.S. yielded >5,000 more to date. These discoveries in hot deserts are possible because dark meteorites are readily distinguished from the local, light-colored

terrestrial rocks. The 14 million km² ancient Antarctic ice sheet is a meteorite trove because the continent's unique topography and its effect on ice motion promotes the meteorites' collection, preservation, transportation and concentration. Assuming 4±2 fragments per meteoroid, Antarctic meteorites recovered thus far correspond to about 7,500 different impact events: more fragments/meteoroid are conceivable (Table I). To complicate matters, expeditions have taken two paths in characterizing their meteorite recoveries. ANSMET chooses to characterize each fragment by type. Other expeditions "cherry-pick" their collection for meteorites of rare type (which are thus of intrinsic interest) for more complete study: we include such meteorites in Table I. The "pairing" of even these samples, let alone the more common meteorites, in these other collections is not yet addressed (*1*).

Most falls are recent, generally having occurred during the last tens to hundreds of years. As noted earlier, nuclear reactions caused by CRE produce radionuclides in the outermost meter of a meteoroid. They allow determination of terrestrial age; the time elapsed since a meteoritic find landed on Earth. Terrestrial ages for non-cluster finds are typically a few thousand years while hot-desert meteorites range up to 50 ka (Figure 4). Finally, terrestrial ages for cold-desert (Antarctic) meteorites are older, usually ~10⁵ years, with a few at 2-5 Ma. Presumably because of differences in sub-ice topography and, thus, ice-sheet motion, terrestrial age ranges for meteorites vary with Antarctic recovery region with means at 100 ka and 300 ka for Queen Maud Land and Victoria Land respectively (*1*). Thus, each suite provides a different "age-window" sampling of near-Earth, meteorite-source populations.

Meteorite Classification

At the coarsest level, meteorites are described as irons, stones or stony-irons from their dominant constituent (Figure 1; Plate 1). Each can then be classified by a scheme with genetic implications (Figures 3, 5). Stones include the very numerous chondrites (Table I; Plates 1a,b) and the igneous achondrites (Plate 1d), irons (Plate 1e), and stony-irons (Plate 1c). Differentiated meteorites presumably formed from melted chondritic precursors by secondary processes in parent bodies (Figure 1). During melting, physical (and chemical) separation occurred, with high-density iron sinking to form pools ("nuggets") or a core inside the lower density achondritic parent magma. Ultimately, these liquids crystallized over a wide temperature range as parents of the differentiated meteorites. Stony-iron meteorites may represent metal-silicate interface regions. Pallasites (Plate 1c), having centimeter (cm)-sized rounded or angular olivines embedded in well-crystallized metal, resemble an "equilibrium" assemblage. They may have solidified within a few years, but cooled slowly; only a few degrees per million years (Ma). Mesosiderite structures - metal-silicate

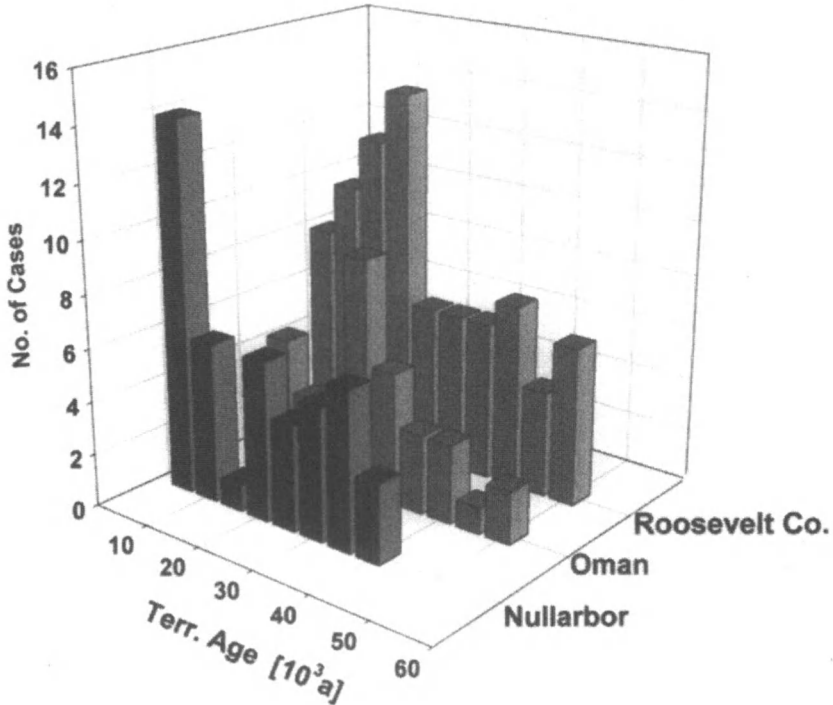


Figure 4. Terrestrial age distributions for meteorites found in three Hot Deserts.

mechanical mixtures or breccias - suggest more rapid and violent mixing, probably by impacts.

During differentiation, siderophilic elements accompany metallic iron during geochemical differentiation, being extracted into metallic melts. Such elements (for example, Ga, Ge, Au, Pt, Ni or Ir) are thus depleted in silicates and enriched in metal to concentrations well above those in precursor chondrites. Conversely, silicate magmas become enriched in lithophilic elements - like rare earth elements (REE), Ca, Cr, Al or Mg - above chondritic levels; concentrations of such elements approach zero in metallic iron. During substantial heating, noble gases and other atmophile elements - like carbon and nitrogen - are vaporized and lost from metallic or silicic regions of parent bodies. Chalcophilic elements that geochemically form sulfides like troilite - FeS - include Se, Te, Tl or Bi. Chalcophiles and a few siderophiles and lithophiles are also often quite easily mobilized (i.e. vaporized from solid or liquid matter) so that they may be enriched in sulfides in the parent body or lost from it. Concentrations of these elements in specific meteorites then depend in part on the fractionation histories of their parents and are markers of specific

heating event(s) - i.e. solid state thermal metamorphism, solid-liquid differentiation and/or shock heating - and their degree and duration.

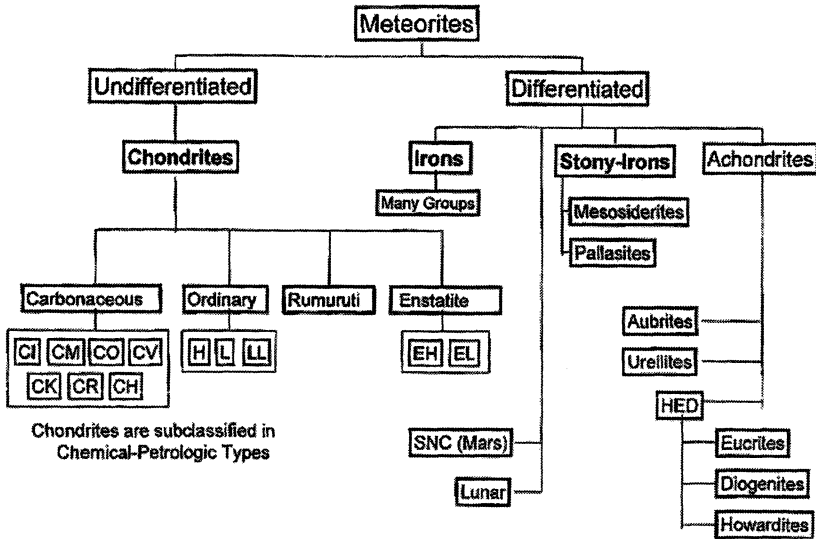


Figure 5. Associations between various meteorite classes.
(Reproduced with permission from reference 1. Copyright 2006 Elsevier.)

Meteorites "map" the Solar System by having specific oxygen isotopic compositions, a major element in all but the irons. Since its high chemical reactivity causes oxygen to form numerous compounds, it exists in many meteoritic minerals, even in silicate inclusions in iron meteorites. Elsewhere in this volume, Clayton (8) discusses meteoritic oxygen isotopic differences and processes that established these [cf. (1)].

Differentiated Meteorites

It is obvious, even to the naked eye, that most iron meteorites consist of large metallic iron crystals, which are usually single-crystal, body centered cubic α -Fe (kamacite) lamellae 0.2-50 mm thick with decimeter (dm) to meter lengths (Plate 1e). These relatively wide Ni-poor lamellae are bounded by thin, Ni-rich, face centered cubic γ -Fe (taenite). The solid-state nucleation and diffusive growth process by which kamacite grew at slow cooling rates from taenite previously nucleated from melt is quite well understood. The 1-atm Fe-Ni phase

diagram and measurement of Ni-partitioning between kamacite and taenite permit cooling rate estimation between ~900-400°C. These rates typically are a few degrees or so per Ma, depending on the specific iron meteorite group, consistent with formation in objects of asteroidal size. The Ni concentration in the melt determines the temperature of incipient crystallization and this, in turn, establishes kamacite orientation in the final meteorite which is revealed in the well-polished surface of an iron meteorite by brief acid etching.

Meteorites containing <6% Ni are called hexahedrites because they yield a hexahedral pattern of large, single-crystal (cm-thick) kamacite bordered by thin taenite on well-polished etched surfaces. Iron meteorites containing 6-16% Ni crystallize in an octahedral pattern, like that of Sanderson (Plate 1e), and hence are called octahedrites. Lower-Ni meteorites have the thickest kamacite lamellae (>3.3 mm) and yield the very coarsest Widmanstätten etch pattern while those highest in Ni are composed of very thin (<0.2 mm) kamacite lamellae and are very fine octahedrites. [Iron meteorites that contain >16% Ni nucleate kamacite at such low temperatures that large single crystals of kamacite could not form over the 4.57 Ga of Solar System history. Thus, they lack a Widmanstätten pattern and are called Ni-rich ataxites (i.e. without structure).] The Ni-poor ataxites are generally hexahedrites or octahedrites reheated in massive impacts, or artificially after they fell on Earth.

As noted earlier, when primitive parent bodies differentiated, siderophilic elements were extracted into molten metal. During melt crystallization, fractionation or separation of siderophiles could occur. About 50 years ago, Ga and Ge contents of iron meteorites were found to be clustered, not continuous, and they could then be used to classify irons into chemical groups denoted I to IV. Originally, these Ga-Ge groups – which correlate well with Ni content and Widmanstätten pattern – were thought to sample core materials from a very few parent bodies. Subsequent studies of many additional meteorites and some additional elements, especially Ni and Ir, modified this view. At present, the chemical groups suggest that iron meteorites sample perhaps 100 parent bodies although many, if not most, irons derive from but 5 parents.

Igneous achondrites, formed at high-temperatures, contain essentially no metal or sulfide and are enriched in refractory, i.e. non-volatile lithophiles like REE which, with their constituent minerals, allow classification into specific groups (Figures 3, 5). Most groups are named for a specific prototypical meteorite: others – howardites, eucrites and diogenites (HED meteorites) – were named non-systematically. At least 10 achondrite groups can be distinguished from their oxidized iron and calcium contents (FeO and CaO). Some apparently were associated in the same parent body but derive from different regions: the HED and the SNC (Shergottites-Nakhlites-Chassigny) associations. The HED meteorites are thought to come from 4 Vesta, and/or other V class asteroids

produced from it (see below). The evidence that the 32 SNC meteorites come from Mars is so strong that these are often called Martian meteorites, not SNCs.

Chondrites

Most meteorites are chondrites, so-called because almost all contain spherical mm- to cm-sized chondrules or their fragments early in the Solar System's history. Cooling rates for some were $\sim 1000^\circ\text{C/hr}$, and $10\text{-}100^\circ\text{C/hr}$ for others. Rapid heating and cooling are easily done in the laboratory but difficult on a Solar System scale. Yet, large volumes of chondrules must have existed in the Solar System because chondrites are numerous (Table I). Chondrites (and many achondrites) date to the Solar System's formation - indeed provide chronometers for it and represent accumulated primary nebular condensate and accretionary products. Some condensate formed from the hot nebula as mm-sized Ca- and Al-rich inclusions (CAI), mineral aggregates predicted as vapor-deposition products by thermodynamic calculations. These CAI, found mainly in chondrites rich in carbonaceous (organic) material (1,4), exhibit many isotopic anomalies and contain atoms with distinct nucleosynthetic histories. Other inclusions (like SiC and extremely fine diamond) are relict presolar material, as reviewed elsewhere in this volume (7). Other condensates formed at much lower temperatures. Some are enriched in isotopically heavy Mg and Si, and CAI may be refractory residues. Others, the fine-grained CAIs, condensed from vapor, with higher-temperature solid or liquid phases partially equilibrating with other such phases formed at lower temperatures.

Although most chondrites contain the same minerals, the proportions of these and their compositions differ among the 6 or 7 principal chondritic chemical groups. The primary bases for chondrite classification involve proportions of iron as metal and silicate (in which oxidized iron - expressed as FeO - may be present), and total iron (from Fe, FeO, and FeS) content (Figure 3). Total iron (Figure 6) defines meteorites with high and low contents of total iron and metal (H and L, respectively) or even lower levels of total iron and metal as LL chondrites. Numbers of H, L and LL chondrites are so large (Table I) that these are called the ordinary chondrites: these constitute 35%, 38% and 8%, respectively, i.e. $>80\%$ of all falls. Obviously, chondrite compositions with elements apportioned by chemical form are not continuous but, rather, quantized. Elsewhere (1) I list major element ratios diagnostic of specific chondritic groups. The total iron in some enstatite (E) chondrites - i.e. those in which the ferromagnesian silicate pyroxene (and the other low-Ca one, olivine) is Fe- and Ca-free MgSiO_3 - exceeds that in the H group of ordinary chondrites, denoting them as EH chondrites: the EL chondrite designation is self-evident.

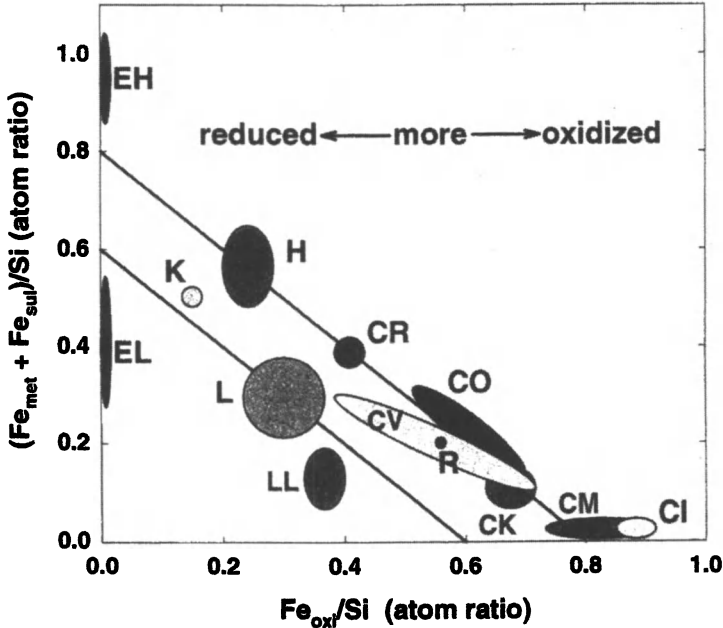


Figure 6. Silicon-normalized contents of Fe as metal and in FeS (ordinate) vs. Fe in ferromagnesian silicates (abscissa) in various chondritic groups: each diagonal defines constant total iron content. (Reproduced with permission from reference 1. Copyright 2006 Elsevier.)

What are the Meteorite Parent Bodies?

Large Bodies

Even before lunar meteorites were identified on Earth (1), a Martian source for SNC meteorites was suspected from their low gas-retention ages (Figure 1). Radioactive decay of long-lived U and Th isotopes produces ^4He while ^{40}K ($t_{1/2} = 1.27$ Ga) produces ^{40}Ar . These radiogenic gases can be lost if the body is hot; as it cools, ^4He and ^{40}Ar retention starts gas-retention-age "clocks". Small, asteroidal-sized bodies have high surface/volume ratios, cooling quickly to begin gas retention and yielding gas retention ages as long as 4.57 Ga. Large bodies like Mars and the Moon have low surface/volume ratios, thus lowering the cooling rate to yield short gas-retention ages ≤ 250 Ma.

Most SNC meteorites have short gas-retention ages, implying a large-body origin. Mars was "fingered" as their source when atmospheric gases implanted by shock into two, EET A79001 and Zagami, proved to be a mixture of Martian atmosphere (as measured by Viking missions in 1976) and terrestrial atmosphere. Later additional data have essentially confirmed this (9).

The first Lunar meteorite, found in 1981 in Antarctica, was immediately identified as such by its fusion crust and mineralogic and chemical resemblance to samples returned by the Apollo program. The properties of the 31 Lunar meteorites are more characteristic of the whole Moon, because they are random samples, than are the Apollo samples which derive from Lunar sites mainly selected for landing safety reasons (10).

Asteroids

Prior to discussing specific meteorite-asteroid (minor planet) links, we note that while $>10^5$ asteroids have been discovered, the spectral reflectances of only 1000-2000 are known. As white (Solar) light impinges on an asteroid's surface, its constituent minerals differ in reflectivity. Thus, the wavelength-reflectance dependence indicates the asteroid's major surficial constituent minerals and allows the asteroid to be classified by spectral type. The distribution of asteroid spectral type roughly varies with distance from the Sun [cf. (1, 5, 6)]. The same spectrometer can be used to determine the spectral reflectance of a meteorite on Earth and asteroid/meteorite spectra can be compared (11).

Besides long gas retention ages, three lines of evidence link all undifferentiated and most differentiated meteorites to asteroids: mineralogy; spectral reflectance; and the orbits of nine meteorite falls.

1. The nature of specific minerals found in meteorites, and their chemical compositions, as well as the cooling rates determined for irons and stony irons indicate that high hydrostatic pressures did not exist. The temperature profiles are consistent with those that asteroids (≤ 1000 km diameter) would have had over the 4.57 Ga history of the Solar System (1). These minerals include those formed during primary nebular condensation and accretion into primitive parent bodies and those formed by secondary processes - thermal metamorphism and/or differentiation - during alteration of primitive bodies into evolved ones.
2. Spectral reflectances of some meteorites match those of some asteroid types: irons or E chondrites with M type; enstatite achondrites with E type; the unique carbonaceous chondrite Tagish Lake with D type; HED achondrites with V type; stony-irons with most S type; thermally metamorphosed carbonaceous chondrites (see below) with C, G, B and F types. (Relative

frequencies with which asteroids of a given spectral type occur, vary with distance from the Sun. Thus, asteroid spectral type distributions in the Solar System reflect primary nebular condensation-accretion, perhaps somewhat modified by planetary gravitational perturbation over time.) However, the most common meteorites, ordinary chondrites, are matched with only rare asteroids, Q, or a small subset of the S type. Spectra of the most common asteroid types match those of only uncommon meteorites. This asteroid-meteorite paradox is attributed to "space weathering", i.e. the alteration and chemical reduction of asteroidal surface minerals by energetic Solar particles.

3. Finally, nine meteorites (all ordinary chondrites) have been recovered while their calculated orbits were determined from photographic observations from two or more widely separated locations during the meteoroids' atmospheric traversal. All nine (Plate 3) had aphelia (maximum orbital distance from the Sun) in the Asteroid Belt (*I*).

At this point, it is adequate to note that oxygen isotopic data (δ) suggest that at least eight major chondritic groups (H, L, LL, CH, CI, CM, CR and E) and a minor one (R), acapulcoites and brachinites, the two achondrite associations (SNC and HED), ureilites (U) and the silicate inclusions in group IAB iron meteorites derive from different "batches" of nebular material (*I*). The HED region also includes data for most pallasites and many mesosiderites suggesting derivation from a common parent body. Extrapolation of the HED trend-line passes through the isotopic region of the oxygen-containing silicate inclusions from IIIAB irons, suggesting that they, too, may be related to the HED association. Perhaps these irons come from deeper in the HED parent body but this would imply more complete disruption than V-class asteroids, like 4 Vesta exhibit.

Oxygen isotopic data hint that some meteorite groups derive from a common nebular region but these links are not as solid as those listed in the previous paragraph, primarily because the data are limited. These tentative links involve: silicate inclusions in IIE irons with H chondrites; silicates in IVA irons with L or LL chondrites; aubrites with E chondrites; winonaites (primitive meteorites modified at high-temperatures) with silicates from IAB and IIICD irons; and the very rare, highly-metamorphosed – even melted – primitive acapulcoites and lodranites.

One implication of the oxygen data is that the Solar System was isotopically inhomogeneous, since each "batch" of nebular matter seems to have its characteristic initial isotopic composition. Isotopic homogenization of gases is more facile than is chemical homogenization, so that oxygen isotopic differences (and more recent ones involving refractory Nd and Sm) imply that the Solar System condensed and accreted from a chemically inhomogeneous presolar nebula (Figure 1).

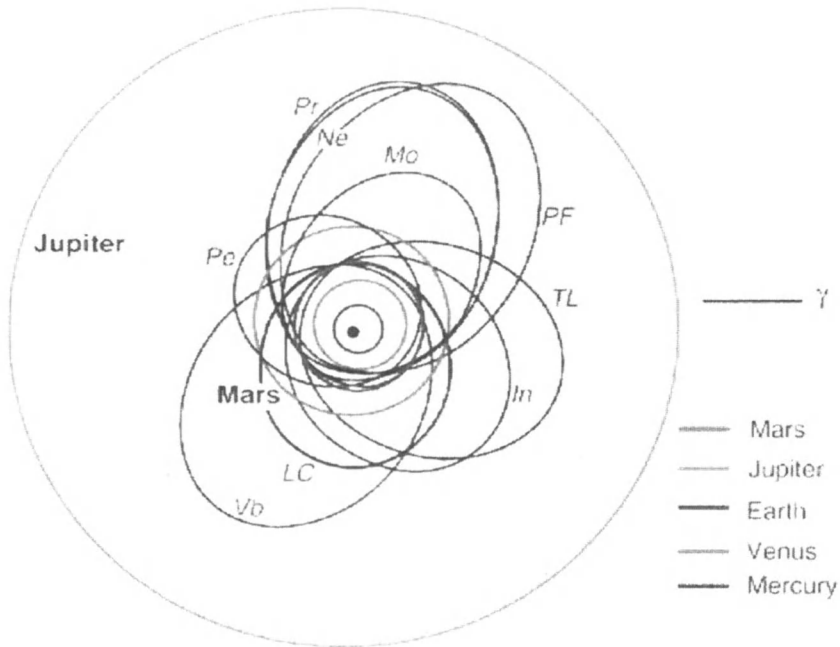


Plate 3. Orbits determined from overlapping camera coverage for nine recovered chondrite falls. Pr–Pribram (H5, 7 Apr. 1959); LC–Lost City (H5, 3 Jan. 1970); In–Innisfree (L5, 5 Feb. 1977); Pe–Peekskill (H6, 9 Oct. 1992); TL–Tagish Lake (C, 18 Jan. 2000); Mo–Moravka (H5-6, 6 May 2000); Ne–Neuschwanstein (EL6, 6 Apr. 2002); PF–Park Forest (L5, 26 Mar. 2003); Vb–Villalbeto de la Peña (L6, 4 Jan. 2004). The orbits shown are projections onto the ecliptic plane (orbits of the terrestrial planets and Jupiter in color are included with γ , the vernal equinox). Pribram and Neuschwanstein had identical orbits, but are of different chondritic types. (Reproduced with permission from reference 1. Copyright 2006 Elsevier.) (See page 12 of color inserts.)

The available data suggest that heat sources for melting primitive bodies (presumably chondritic in chemical composition and texture) that yielded differentiated meteorites were within rather than external to parent bodies. Important sources no doubt include impact shock-heating and radioactive heating from radionuclides – both extant (^{40}K , ^{232}Th , ^{235}U and ^{238}U) and extinct (e.g. ^{26}Al) – that were then more abundant in the early Solar System. Calculations show that ^{26}Al was important in heating small (a few km) primitive parents and other heat sources were effective in differentiating larger ones. Electrical inductive heating driven by dense plasma outflow along strong magnetic lines of force associated with the very early, pre-main sequence (T-Tauri stage) Sun is possible but unproven.

Major element and/or oxygen isotope data demonstrate that differences between parent materials of the various chondritic chemical groups (i.e., e.g. H, CM or EH) are of primary origin, i.e. those involving nebular condensation and accretion. Postaccretionary heating does not necessarily melt the entire parent body so that an intermediate region may exist between the primitive surface and the differentiated interior. Properties of many chondrites support this expectation and suggest that solid-state alteration of primary chondritic parent material like carbonaceous and the unequilibrated ordinary chondrites or UOC (i.e. those in which ferromagnesian olivine and pyroxene grains separated by a mm or so have variable Fe/Mg ratios) occurred during secondary heating. Eight characteristics observed during petrographic study of optically thin sections serve to estimate the degree of thermal metamorphism experienced by a chondrite and to categorize it into the major 3-6 types (Table II). The absence of chondrules and the presence of abnormally large (≥ 100 micrometer (μm)) feldspar characterize the very rare type 7. These pigeon-holes approximate a chondritic thermal metamorphic continuum. Petrographic properties (as well as bulk carbon and water contents) suggest increasing aqueous alteration at 0-100°C of type 3 material into types 2 and 1.

Two of these characteristics are illustrated in Plate 4: the opaque matrix and distinct chondrules of the type 3 chondrite, Sharps (H3), should be contrasted with the recrystallized matrix and poorly defined chondrules of extensively metamorphosed type 6 Kernouve (H6). As noted above, the Fe^{2+} contents (or Fe/Mg ratios) of the ferromagnesian silicates are almost completely random in a chondrite like Sharps and quite constant in one like Kernouve. Chondrites of higher numerical types could acquire their petrographic characteristics (Table II) by extended thermal metamorphism of a more primitive, i.e. lower type, chondrite of the same chemical group. Temperature ranges estimated for formation of types 3 through 7 are 300-600°, 600-700°, 700-750°, 750-950°, and >950°C, respectively.

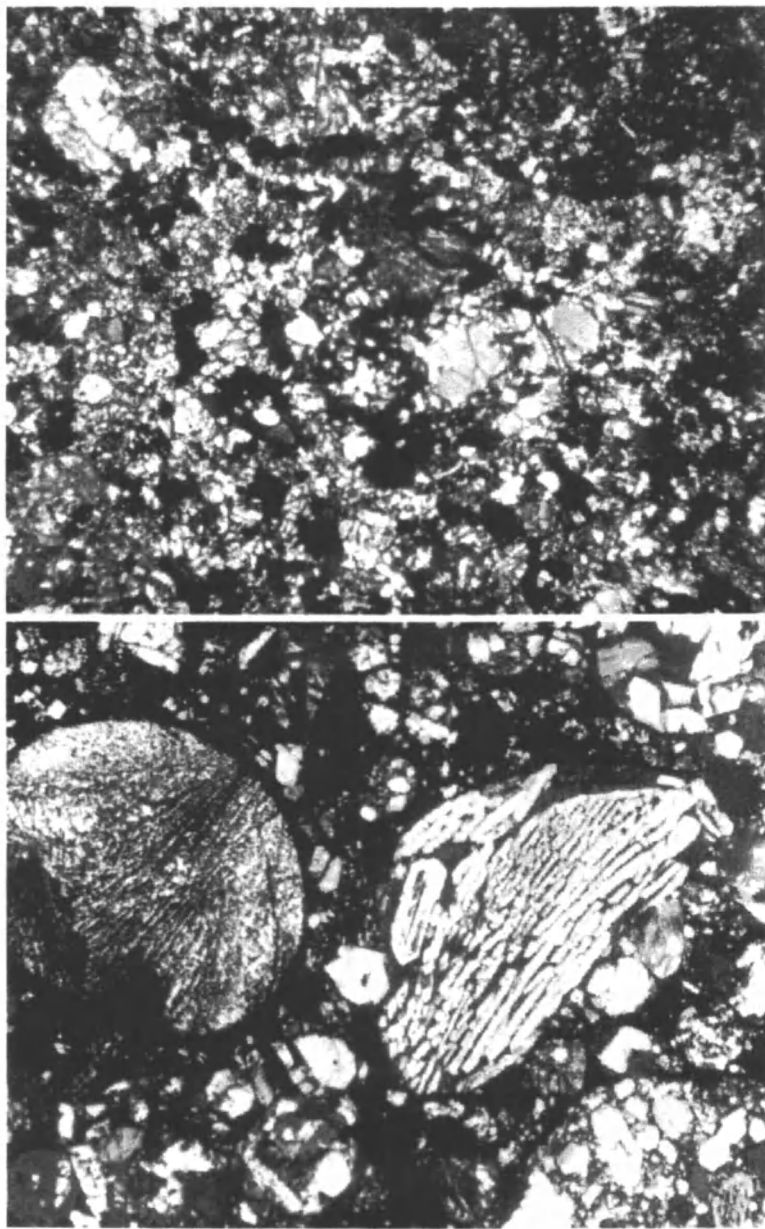


Plate 4. Petrographic (2.5 mm wide) thin sections in polarized transmitted light. Partial large chondrules are obvious in the H3 chondrite Sharps (left) but barely recognizable in the H6 chondrite Kernouve (right). (Reproduced with permission from reference 1. Copyright 2006 Elsevier.) (See page 13 of color inserts.)

Evolution of Asteroids: Chondritic Chemical Abundances

Chemical changes involving loss of a constituent, like carbon or water in chondrites, require an open system: other changes in Table II could occur in open or closed systems. It should be emphasized that thermal metamorphism can only affect secondary (parent body) characteristics – those listed horizontally in Table II – not primary ones. Postaccretionary processes by which H chondrite-like material can form from L or *vice versa* are unknown. Achondrites, from melted and differentiated parent bodies - including planets (e.g. Martian meteorites like Nakhla) - have petrologies indicative of igneous processing at temperatures $\gg 1000^\circ\text{C}$.

Since properties of a given chondrite reflect both its primary and its subsequent histories, a chondritic classification scheme reflecting both is used. No ordinary (or enstatite) type 1 or 2 chondrites is known. The UOC vary the most among themselves and from chondrites of other petrographic types. Within UOC, the chemical heterogeneity of ferromagnesian silicates and thermoluminescence (TL) sensitivity subdivide UOC into subtypes 3.0 to 3.9. [A similar subclassification of CO chondrites also exists.] Contents of highly volatile trace elements (mainly Cd, Bi, Tl, In and noble gases) are very much higher in UOC than in ordinary chondrites of types 4-6.

Many properties of ordinary chondrites demonstrate that each group has its own special history, even in something so simple as the numbers of each chemical-petrographic type (Table I). For example, proportions of H3 or L3 are low, 1-2%, while 13% of LL falls are LL3. Proportions of more evolved chondrites also differ (Table I). The plurality, 44% of H falls are H5, while type 6 dominates L and LL chondrites - 68% and 49%, respectively. Non-desert-cluster chondrite finds generally exhibit similar trends. This hints at smaller H chondrite parent(s) than L or LL.

Most chondrites are readily classified, but a few consist of two or more meteorite sorts, each readily identifiable in the lithified breccia, (2). Some of these, the regolith breccias (1) - either one chondritic type in another, like Plate 1f, or in an achondritic host - contain unique information on the history of Solar wind (12) particulates embedded in their constituent grains. A regolith is a fragmental (brecciated) layer from the surface of a parent body like an asteroid or our Moon that had no atmosphere. This formed by the breakup and mixing ("gardening") of rocks by repeated meteoroid impacts. Surfaces of fine grains with regolith breccias contain gases, mainly Solar particles of keV-MeV energies, implanted in 4π geometry. Analysis of these gases provides a time-window to past Solar particle ejection history. How implanted Solar gases can be distinguished from those introduced into a meteorite by other processes are described elsewhere (1, 2).

The only known type 1 or 2 chondrites are carbonaceous chondrites, nearly all non-Antarctic observed falls. They record hydrolysis - the action of liquid

water e.g. at 0-100°C (in the nebula or on parent bodies) - that altered pre-existing grains, producing various hydrated, clay-like minerals. These chondrites' petrography and the decidedly non-terrestrial $^2\text{H}/^1\text{H}$ ratios in water from them show that this hydrolysis was preterrestrial. As described by Clayton (8), oxygen isotopic compositions of hydrated minerals demonstrate that the two groups derive from different batches of nebular matter: thus, C1 (or CI) could not form C2 (or CM) by thermal metamorphism nor could C1 have formed by hydrolysis of C2 parent material. Thus, some specialists prefer the CM designation: others prefer a hybrid classification like C2M or CM2 since other C2-like chondrites exist.

While C1 chondrites contain *no* chondrules (Table II), their obvious compositional and mineralogic similarities to chondrule-containing C2 meteorites prompts this classification. Compositionally, C1 (or CI) chondrites closely resemble the Solar photosphere. Indeed, elemental abundance and isotopic data listed in "cosmic abundance tables" are largely those of C1 chondrites. However, a few differences between C1 abundances and Solar photospheric values exist (cf. 3). These involve elements depleted in C1 chondrites relative to the Sun's surface, like hydrogen, helium or carbon, which are gaseous or easily form volatile compounds that largely remained as vapor in the nebular region where C1 chondrite parent material condensed and accreted. Other elements - e.g. lithium, beryllium and boron - are easily destroyed by low-temperature nuclear reactions during pre-main-sequence stellar evolution: thus they are depleted in the Solar photosphere relative to C1 chondrites and cosmic abundance tables adopt the C1 values (3).

Comparison of eleven highly mobile trace elements, particularly Zn, In, Bi, Tl and Cd, in C1-C3 chondrites and similar samples heated artificially indicate that about a dozen were thermally metamorphosed in their parent bodies in open systems. Metamorphic temperatures, 400-900°C, estimated in this way agree with estimates provided by mineralogic-petrologic studies. Contents of these trace elements in E5 and E6 chondrites, whether EH or EL, indicate that these meteorites also experienced open-system thermal metamorphism in their parent(s).

How Old are Meteorites?

A unique answer to this question is not possible since an "age" is a time interval between two events and an age may depend on the specific chronometer used. An accurate chronometer must involve a mechanism operating on a predictable, but not necessarily constant rate. The "clock" starts by an event beginning the time interval and its end must be clearly and sharply recorded. Chronometers used in modern geo- and cosmo-chronology usually involve long-lived, naturally occurring radioactive isotopes such as the U-isotopes, ^{87}Rb or

⁴⁰K. Radioactive decay allows calculation of an age if the concentrations of both parent and daughter nuclide are known, the beginning of the time interval is defined and the system is not disturbed (i.e. it is a "closed system") during the time interval. Some chronometers involve production of particular stable or radioactive nuclides, or decay of the latter. Typically, the chronometer half-life should be comparable with the time interval being measured.

Meteorites yield a variety of ages, each reflecting a specific episode in their histories. Some of these "ages" are indicated in Figure 1: the end of nucleosynthesis in a star (3); the first formation of solids in the Solar system (7); melt crystallization in parent bodies (13); excavation of meteoroids from these bodies; and the meteorite's fall to Earth. Other events, like volcanism or metamorphism on parent objects can be established by gas retention as can formation intervals (based on extinct radionuclides) measuring the time between the last production of new nucleosynthetic material and mineral formation in early Solar System materials (14). In the following sections we discuss some of these ages and the information that they convey.

Cosmic Ray Exposure (CRE)

In principle, measurements of a cosmogenic radionuclide (or its decay product) and of a stable nuclide are needed to establish a CRE age. In practice, however, production rates of stable cosmogenic noble gas nuclides in stony meteorites are well-known and it usually suffices to measure just their concentrations. Absent contrary evidence, irradiation by cosmic rays of Solar and galactic origin is assumed simple, i.e. that the meteoroid was completely shielded (buried in a parent body) until an impact ejected it as a meter-sized object, remaining essentially undisturbed until collision with Earth. Some stones (e.g. the H4 chondrite Jilin) and irons (e.g. Canyon Diablo) exhibit complex irradiation histories involving preirradiation on the parent body surface, or secondary collisions in space that fractured the meteoroid and exposed new surfaces to CRE. In such a complex irradiation history, different samples of a meteorite exhibit different CRE ages. Meteoroids approaching the Sun to within 0.5 AU are warmed, causing diffusive loss of gases, especially ³H (a contributor to ³He production) from iron. Such cases are recognized by low isotopic ratios, particularly ³He/⁴He or ³He/²¹Ne, or low natural thermoluminescence. If unrecognized, CRE ages based on ³He contents would be erroneously low for these meteorites. On the other hand, for some studies it is useful to know that a meteorite's perihelion was unusually close to the Sun.

The data for ordinary chondrites in Figure 7 show that all groups have CRE ages ranging up to 90 Ma, but the distributions differ markedly. For H chondrites, there is at least one major peak, at ~7 Ma and a smaller one at 33

Ma. For L chondrites, major peaks are not obvious, but clusters occur at 20-30 Ma and 40 Ma, with a smaller one at 5 Ma. For LL chondrites, the major peak at 15 Ma includes ~30% of all measured samples and another is at 30 Ma. Major peaks correspond to major collisional breakups on/of chondrite parent bodies. Contrary to the H-chondrite situation, nearly 2/3 of the L chondrites have CRE ages >10 Ma. Further information on CRE ages for stony meteorites is summarized elsewhere (1).

Attempts to develop a reliable CRE age method for iron meteorites yielded inconsistent results except in one case which is a difficult, tedious, and no longer-practiced technique involving ^{40}K and stable ^{39}K and ^{41}K . About 70 iron meteorites were dated by the $^{40}\text{K}/^{41}\text{K}$ method and their resulting ages range from 100 Ma to 1.2 Ga. That CRE ages for iron meteorites greatly exceed those of stones, is attributed to the greater resistance of iron meteoroids to destructive collisions (so-called "space erosion") in space. CRE exposure age peaks are evident for but two chemical groups. For group IIIAB, 13 of 14 meteorites have a CRE age of 650 ± 60 Ma. This age is also exhibited by 3 of 4 measured IIICD meteorites, suggesting a major collisional event involving the parent of the chemical group III iron meteorites. The IVA irons also exhibit a CRE age peak: 7 of the 9 dated samples have an age of 400 ± 60 Ma. These iron meteorite groups are the two most numerous ones and contain the highest proportions of strongly shocked members. Either the parent asteroids of these groups were unusually large (requiring unusually large and violent breakup events) and/or the Earth preferentially sampled collisional fragments that had been strongly shocked (thus acquiring the significant shock-induced impulse required to send them Earthward).

Gas Retention Age

As discussed earlier, decay series initiated by the long-lived ^{232}Th , ^{235}U , and ^{238}U yield 6, 7 and 8 α -particles, respectively, while long-lived ^{40}K produces ^{40}Ar . Thus, from measurements of U, Th, and radiogenic ^4He or of ^{40}K and radiogenic ^{40}Ar , one can determine the time elapsed since a meteorite sample cooled sufficiently low to completely retain these noble gases (cf. 2 for specific references). A radiogenic age could record primary formation of the meteorite's parent material but in most cases, subsequent heating (metamorphic and/or shock) were accompanied was so severe that it partially or completely degassed the primary material. A variant of the K/Ar age, the ^{40}Ar - ^{39}Ar method involves conversion of some stable ^{39}K to ^{39}Ar by fast-neutron bombardment, i.e. $^{39}\text{K}(n,p)^{39}\text{Ar}$, followed by stepwise heating and mass-spectrometric analysis. From the $^{39}\text{Ar}/^{40}\text{Ar}$ ratio in each temperature step, it is possible to correct for

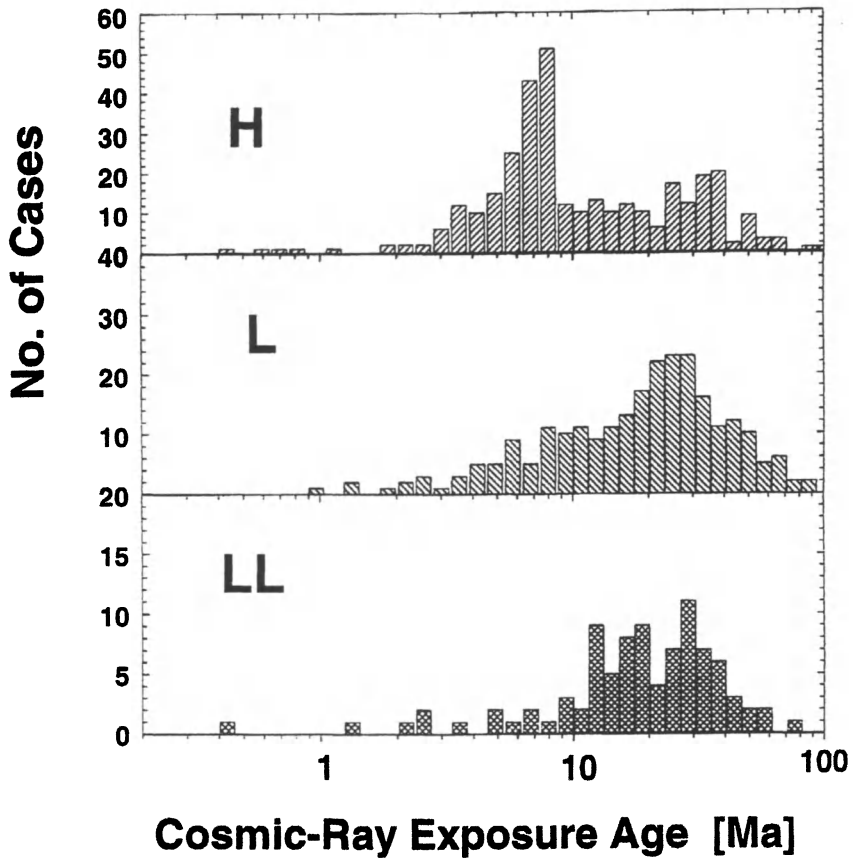


Figure 7. Cosmic ray exposure ages for ordinary H, L and LL chondrites. Peaks in the histograms indicate major collisional events on parent bodies that generated many meter-sized fragments. (Reproduced with permission from reference 1. Copyright 2006 Elsevier.)

later gas loss. This variant even permits analysis of small, inhomogeneous samples with a pulsed laser heat source.

Gas retention ages of many chondrites, achondrites and even silicate inclusions in iron meteorites range up to about 4.6 Ga. Many meteorites, particularly L chondrites, have young gas retention ages, ~500 Ma, while H chondrites cluster at higher ages (Figure 8). Meteorites with young gas retention ages generally exhibit petrographic evidence for strong shock-loading, implying diffusive gas loss from material having had quite high residual temperatures generated in major destructive collisions. Almost always, meteorites having young K-Ar or ^{40}Ar - ^{39}Ar ages have lower U, Th-He ages: this occurs because He is more easily lost from most minerals than is Ar. Diffusive loss of ^{40}Ar , incidentally, is much more facile than is loss of trapped ^{36}Ar or ^{38}Ar , enhancing its value as a chronometer. Preferential ^{40}Ar loss occurs because most is sited in feldspars and in K-rich minerals which are associated with radiation damage that provides a ready diffusive escape path. Highly mobile trace elements are lost more readily than is even ^{40}Ar so that L chondrites with young gas retention ages have lower contents of such elements than do those with old ages. The similarity in the CRE age of group III iron meteorites and the gas retention age of L chondrites may be coincidental perhaps or resulted from a particularly massive collision of their parent(s).

The number of fossil meteorites discovered in ordinary limestone beds in Swedish quarries imply that the meteorite flux on Earth ~480 Ma ago was 100x higher than the contemporary flux. Chromite grains (highly resistant to weathering) from fossil L chondrites have CRE ages of 0.1-1.2 Ma. This implies that these L chondrites arrived on Earth within 100-200 ka after the major collisional breakup that produced contemporary L chondrite falls.

As discussed below, solidification ages for most Martian meteorites are ~1.3 Ga, implying the existence of parent magmas as recently as this. The ^{40}Ar - ^{39}Ar ages of essentially unshocked nakhlites accord with the 1.3 Ga age but shergottites, which are heavily shocked, have gas retention ages probably indicating their parent materials' partial degassing ≤ 250 Ma ago, consistent with Rb-Sr internal isochrons for shergottites at 180 Ma as discussed below.

Solidification Age

Solidification ages establish the time elapsed since the last homogenization of parent and daughter nuclides, normally by rock or mineral crystallization (12, 13). Nuclides used to establish solidification ages are isotopes of non-gaseous elements insensitive to events that might affect gas retention. Some techniques, such as the Pb/Pb method that involves the ultimate decay products of ^{235}U , ^{238}U and ^{232}Th (^{207}Pb , ^{206}Pb and ^{208}Pb , respectively) depend upon relatively mobile Pb that is more readily redistributed than is the ^{147}Sm - ^{143}Nd dating pair (cf, 1, 2,

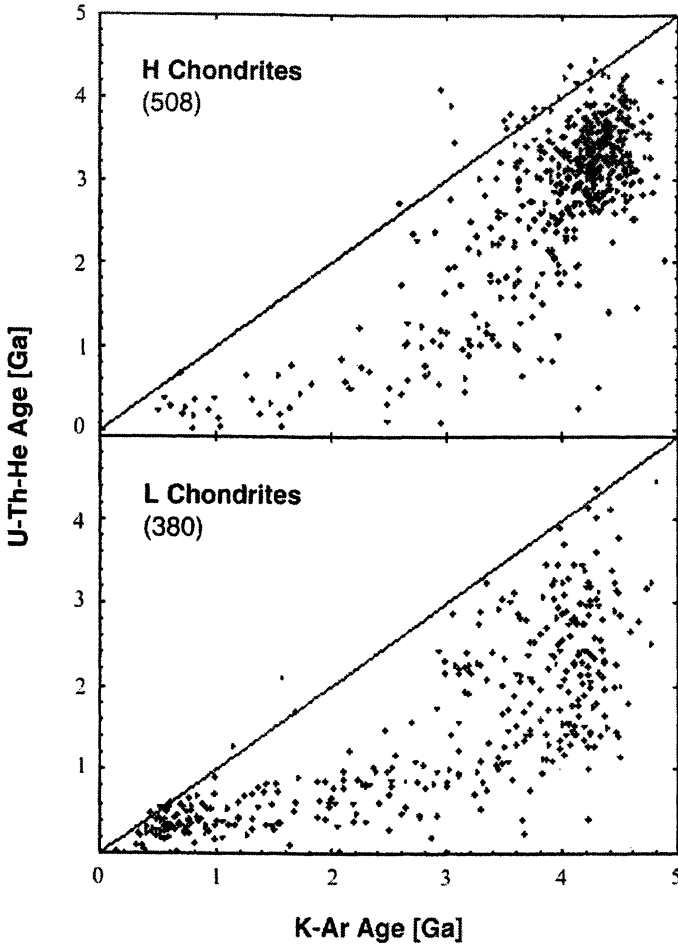


Figure 8. Gas retention ages of 508 H and 380 L chondrites. Data from the U, Th–He and K–Ar methods are plotted against each other. These data assume cosmogenic (${}^4\text{He}/{}^3\text{He}$) = 5, K concentrations of 800 and 900 ppm for H and L, respectively, U concentrations of 13 and 15 ppb, respectively and $(\text{Th}/\text{U}) = 3.6$. The 45° line represents concordant ages. The two major chondrite types exhibit strong thermal history differences. The dominant concordant long ages of H chondrites suggest that their parent(s) generally remained thermally unaltered since formation 4–4.5 Ga ago. The concentration of data defining concordant short ages of L chondrites suggests strong shock-heating in a major collision(s) 0.1–1.0 Ga ago. Nearly all discordant meteorites lie below the 45° lines because radiogenic ${}^4\text{He}$ is lost far more easily than is radiogenic ${}^{40}\text{Ar}$. (Reproduced with permission from reference 1. Copyright 2006 Elsevier.)

11). Hence, in principle, a sample dated using different chronometers might yield somewhat different ages depending upon a sample's post-formation thermal history.

Common techniques found to yield useful solidification ages include: the Pb-Pb method; ^{147}Sm ($t_{1/2} = 106$ Ga) - ^{143}Nd ; ^{87}Rb ($t_{1/2} = 48$ Ga) - ^{87}Sr ; and ^{187}Re ($t_{1/2} = 41$ Ga) & ^{187}Os (cf. 1, 2, 11, 15). Generally, methods used to determine solidification ages depend upon data depicted in isochron diagrams, for example, in which enrichment of radiogenic ^{87}Sr is proportional to the amount of ^{87}Rb , with ^{86}Sr being taken for normalization. The slope of such a line yields an "internal isochron" for a meteorite or a single inclusion of a meteorite, if minerals having various $^{87}\text{Rb}/^{86}\text{Sr}$ ratios are measured. The y-intercept provides the initial $^{87}\text{Sr}/^{86}\text{Sr}$ ratio - a relative measure of the time that nucleosynthetic products were present in the system prior to solidification - i.e. how "primitive" the system is. Clearly, the lower the $^{87}\text{Sr}/^{86}\text{Sr}$ ratio, the less radiogenic (or evolved) was the source material. For some time, basaltic achondrites (e.g. HED meteorites) and the angrite Angra dos Reis competed as the source containing the most primitive (least radiogenic) Sr. More recently, Rb-poor CAI inclusions in the CV3 chondrite, Allende, have become "champions" in this category, with $^{87}\text{Sr}/^{86}\text{Sr} = 0.69877 \pm 2$.

Solidification ages for most meteoritic samples are "old", i.e. close to 4.56 to 4.57 Ga (Figure 9). The results obtained by different methods agree quite well, although some "fine-structure" can be detected. A large number of chondrites studied by the Pb-Pb, Rb-Sr and Nd-Sm techniques yield results consistent with an age of about 4.56 Ga. The U/Pb method used to date phosphates from ordinary chondrites (Figure 9) produces ages for H6 chondrites exhibiting small, but significant, differences in Pb-Pb ages from H4 and H5 chondrites. These data suggest 4.563 Ga as the oldest ordinary chondrite solidification age with metamorphism requiring 60-70 Ma. The results are consistent with a stratified ("onion-shell") model for the H chondrite parent body, and suggestive of simple, progressive metamorphic alteration with increasing depth in it.

While most meteorites have solidification ages around 4.56 Ga, there is clear evidence of more recent disturbances of chronometric systems - particularly Pb-Pb and Rb-Sr - in many meteorites. For example, Rb-Sr internal isochrons for E chondrites (believed to have experienced open-system thermal metamorphism) were disturbed 4.3-4.45 Ga ago. Of course, chronometers in heavily shocked L chondrites show clear evidence for late disturbance.

Four techniques (^{40}Ar - ^{39}Ar , Rb-Sr, Pb-Pb and Sm-Nd) yield an age for nakhlites of 1.3 Ga implying their derivation from a large planet, Mars (cf. 2, 11). The heavily-shocked shergottites seem to have derived from several magma reservoirs and Rb-Sr internal isochrons suggest a major shock-induced disturbance 180 Ma ago, before the Martian meteoroids were ejected from their parent planet.

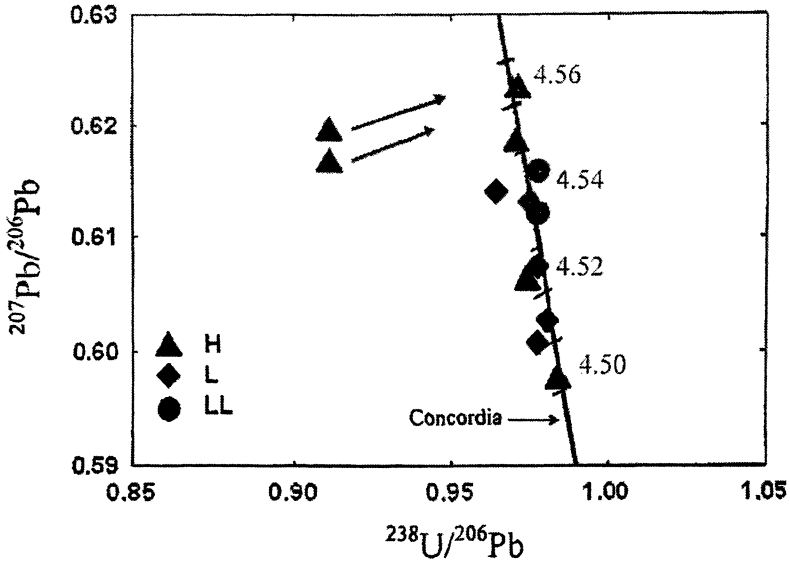


Figure 9. U-Pb ages of phosphates from ordinary chondrites. Numbers on the Concordia line are in Ga. The oldest solidification age (for H chondrites) is ~ 4.563 Ga ago and thermal metamorphism occupied the next 60-70 Ma. (Reproduced with permission from reference 1. Copyright 2006 Elsevier.)

Measurements of decay products of extinct radionuclides do not provide absolute dates in the sense discussed earlier but they do permit relative chronologies on time-scales comparable with the radionuclide's half-life. Thus far, clear positive evidence exists in meteorites or their constituent minerals (cf. 1, 2, 11) for the presence in the early Solar System of: ^{41}Ca ($t_{1/2} = 110$ ka); ^{26}Al ($t_{1/2} = 730$ ka); ^{10}Be ($t_{1/2} = 1.5$ Ma); ^{60}Fe ($t_{1/2} = 1.5$ Ma); ^{53}Mn ($t_{1/2} = 3.7$ Ma); ^{107}Pd ($t_{1/2} = 6.5$ Ma); ^{129}I ($t_{1/2} = 15.7$ Ma); ^{244}Pu ($t_{1/2} = 82$ Ma) and ^{146}Sm ($t_{1/2} = 103$ Ma). In most cases, relative ages are calculated from 3-isotope plots involving decay products of the extinct radionuclide. However, in some cases, the relative chronologic information can be combined with data for absolute ages, allowing small time differences in the early Solar System to be established. For example, combining the $^{53}\text{Mn}/^{55}\text{Mn}$ ratio measured in the Omolon pallasite with the absolute Pb-Pb age of the LEW 86010 angrite, yields an absolute age of 4557.8 ± 0.4 Ga for Omolon. Implications of solidification age and extinct radionuclide studies are many and varied, and the interested reader should consult other reviews (12-15) for discussions of these topics.

Summary

Not only do meteorites give us information on genetic and evolutionary processes of and in their parent bodies, some meteorites contain materials predating Solar System formation. Thus meteorites contain unique information on pre-Solar conditions, condensation processes within the Solar System, in the inner part where liquid water could have existed, and the present-day status of the Sun and its planets and satellites. Meteorites are unique in that they contain chronometers that allow the various genetic episodes that affected them to be dated.

The most important lessons that meteorites teach are the following. Formation of primitive bodies in the Solar System was quite rapid after its accretion began and times when important genetic events occurred can be established from meteorites. Evolution of these primitive bodies occurred quite rapidly. The nature of these evolutionary processes can be readily determined from mineralogic, petrologic and chemical compositional changes. Gas retention ages for nearly all meteorites are much larger than their CRE and terrestrial ages. Perhaps the most important lesson is that meteorites provide a selective, quite possibly biased, sampling of the minor planets and it is conceivable that this sampling varied with time, as well as space.

The lessons in the meteoritic record can be read best in an interdisciplinary light. Results of one type of study – say, trace element chemical analysis – provide insight to another – orbital dynamics, for example. Early experience gained from meteorite studies guided proper handling, preservation, and analysis of the manned U.S. Apollo and unmanned Russian Luna sample-return missions from our Moon. Studies of these samples, in turn, led to the development of extremely sensitive techniques now being used to analyze meteorites and microgram-sized interplanetary dust particles of probable cometary origin collected in Antarctica. Undoubtedly, this experience will prove invaluable as samples from other planets, their satellites, and small Solar System bodies are brought to Earth for study. The lessons that we learn give a zeroth-order approximation of other extant Solar Systems.

Previous studies of meteorites have yielded an enormous amount of knowledge about the Solar System, and there is no indication that the scientific growth curve in this area is beginning to level off. Predictions about future developments are very hazardous but we can expect surprises, probably from desert meteorites which seem to include so many peculiar objects. As has been said in another connection, those who work with meteorites don't pray for miracles, they absolutely rely on them.

Acknowledgement

This review is based on a chapter that I authored in the *Encyclopedia of the Solar System* 2nd Edition published by Elsevier and reproduced with permission from reference 1. Copyright 2006. I also thank Prof. Ludolf. Schultz for Figure 4.

References

1. Lipschutz, M. E.; Schultz, L. In *Encyclopedia of the Solar System*, 2d Edn., Weissman, P., McFadden, L. A., Johnson, T. V. Eds. Elsevier, New York, 2006, pp. 251-282.
2. Hutchison, R. *Meteorites A Petrologic, Chemical and Isotopic Synthesis*; Cambridge University Press: Cambridge, U.K., 2004.
3. Meyer, B. S., this volume.
4. Botta, O., this volume.
5. McFadden, L. A.; Binzel, R. P. In *Encyclopedia of the Solar System*, 2d Edn., Weissman, P., McFadden, L. A., Johnson, T. V. Eds. Elsevier, New York, 2006, pp. 283-300.
6. Britt, D. T.; Lebofsky, L. In *Encyclopedia of the Solar System*, 2d Edn., Weissman, P., McFadden, L. A., Johnson, T. V. Eds. Elsevier, New York, 2006, pp. 349-364.
7. Lodders, K., this volume.
8. Clayton, R. N., this volume.
9. Golombek, M. P., McSween H. Jr. In *Encyclopedia of the Solar System*, 2d Edn., Weissman, P., McFadden, L. A., Johnson, T. V. Eds. Elsevier, New York, 2006, pp. 331-348.
10. Taylor, S. R. In *Encyclopedia of the Solar System*, 2d Edn., Weissman, P., McFadden, L. A., Johnson, T. V. Eds. Elsevier, New York, 2006, pp. 227-250.
11. Lipschutz, M. E.; Gaffey, M. J.; Pellas, P. In *Asteroids II*, Binzel, R. P., Gehrels, T., Matthews, M. S. University of Arizona Press, Tucson AZ, 1989, pp. 740-777.
12. Gosling, J. T. In *Encyclopedia of the Solar System*, 2d Edn., Weissman, P., McFadden, L. A., Johnson, T. V. Eds. Elsevier, New York, 2006, pp. 99-116.
13. Kleine, T., this volume.
14. Halliday, A. N.; Chambers, J. E. In *Encyclopedia of the Solar System*, 2d Edn., Weissman, P., McFadden, L. A., Johnson, T. V. Eds. Elsevier, New York, 2006, pp. 29-53.
15. Lipschutz, M. E.; Wolf, S. F.; Culp, F. B.; Kent, A. J. R. *Anal. Chem.* **2005**, *77*, 3717-3736.

Chapter 10

Chemistry and Composition of Planetary Atmospheres

Laura Schaefer and Bruce Fegley, Jr.

Planetary Chemistry Laboratory, Department of Earth and Planetary Sciences, Washington University, St. Louis, MO 63130

This chapter summarizes atmospheric chemistry and composition for the seven planets in our solar system that have significant atmospheres. The terrestrial planets (Venus, Earth, and Mars) have secondary atmospheres that originated by the outgassing of volatile-rich material during and/or after planetary accretion. The gas giant planets (Jupiter, Saturn, Uranus, and Neptune) have primary atmospheres that were captured from the solar nebula. Some of the important chemical cycles that presently operate in planetary atmospheres are illustrated. Thermochemistry controls the atmospheric composition on Venus and in the deep atmospheres of the gas giant planets. In contrast, photochemistry dominates atmospheric chemistry on Mars and in the upper atmospheres of the gas giants. Biochemistry is the key process on Earth, with photochemistry also playing an important role. Some speculations about atmospheric chemistry and composition on extrasolar Earth-like planets are also presented.

Introduction

The planets in our solar system display a range of atmospheric compositions. Earth's atmosphere is oxygen-rich, those of Venus and Mars are mainly carbon dioxide, and the gas giant planets have hydrogen-rich atmospheres. Titan, the largest satellite of Saturn has a dense N₂-rich, CH₄-bearing atmosphere with a surface pressure of about 1.5 bar (1). A variety of tenuous atmospheres exist on Mercury, Pluto, and several planetary satellites. Mercury's rarified atmosphere of monatomic H, He, O, alkalis and alkaline earths has a surface pressure of less than 10⁻¹² bars and arises from the solar wind, surface sputtering, outgassing, and vaporization of impactors (2). Pluto has an atmosphere containing N₂, CH₄, and possibly other gases. Its 40 K surface temperature corresponds to an N₂ pressure of 5.8 × 10⁻⁵ bar (3). Neptune's largest satellite Triton has an N₂-rich, CH₄-bearing atmosphere with a surface pressure of 1.6 × 10⁻⁵ bar (4). Io, the innermost Galilean satellite of Jupiter has a volcanically produced SO₂-rich atmosphere with an average pressure of about 10⁻⁸ bars. The erupted volcanic gases also contain SO, S₂ vapor, S, NaCl, Na, and K. Theoretical models predict that O, O₂, and S₂O are also present (5). The other three Galilean satellites have rarified atmospheres of O₂ (Europa), O₂ and CO₂ (Callisto), and monatomic O and H (Ganymede) arising from charged particle bombardment and solar UV light irradiation of their icy surfaces (5).

This chapter reviews atmospheric chemistry and composition for the seven planets having significant atmospheres and is organized as follows. We first present some basic data about the nature and structure of planetary atmospheres. Next we describe the atmospheres of the terrestrial planets Venus, Earth, and Mars. Then we discuss atmospheric chemistry for the gas giant planets Jupiter, Saturn, Uranus, and Neptune. We close with some speculations about atmospheric chemistry on extrasolar Earth-like planets. Throughout the chapter we summarize the different processes responsible for producing and destroying atmospheric gases on each planet.

Basic Information and Definitions

Before discussing the compositions of planetary atmospheres, it is helpful to define the units in which they are described. The most common is the volume-mixing ratio (or simply mixing ratio), which is a dimensionless quantity given by the ratio of the gas partial pressure (P_i) to the total pressure (P_T). It is also commonly referred to as the mole (or volume) fraction of the gas. Mixing ratios are given in terms of percent (%), parts per million (ppmv), parts per billion (ppbv), and parts per trillion (pptv) by volume.

Table I. Physical Properties of Planetary Atmospheres

<i>Planet</i>	$T_{surface}$ (K)	$P_{surface}$ (bars)	g ($m\ s^{-2}$)	μ^a ($g\ mole^{-1}$)	H^b (km)	σ^c (cm^{-2})
Venus	740	95.6	8.870	43.45	15.96	1.49×10^{27}
Earth	288	1.013	9.820	28.97	8.42	2.14×10^{25}
Mars	214	6.36×10^{-3}	3.727	43.34	11.02	2.37×10^{23}
Jupiter ^d	165	1 ^e	25.376	2.33	23.20	1.02×10^{26}
Saturn ^d	134	1 ^e	10.443	2.32	45.99	2.49×10^{26}
Uranus ^d	76	1 ^e	8.85	2.64	27.05	2.58×10^{26}
Neptune ^d	71.5	1 ^e	11.14	2.53 ^f	21.09 ^f	2.14×10^{26f}

^aMean formula weight. ^bPressure scale height. ^cColumn density. ^dProperties given at the 1 bar pressure level. ^eObserved P-T profiles are adiabatic below the tropopause. ^fassuming $X_{H_2} = 0.80$, $X_{He} = 0.19$, and $X_{CH_4} = 0.01$.

Gas abundances are frequently given in terms of number density and column density (or column abundance). The number density of gas i is written as $[i]$ and has units of particles (atoms + molecules) per unit volume (particles cm^{-3}). It is calculated via the ratio $P_i N_A / RT$, where N_A is Avogadro's number, R is the ideal gas constant, and T is temperature in Kelvin. The column density of a gas is the number of gas particles throughout an atmospheric column and is found using the integral of $[i]dz$ from a given altitude z_0 (e.g. planetary surface) to the top of the atmosphere. It has dimensions of particles per unit area (particles cm^{-2}) and can be calculated from the ratio $P_i N_A / \mu g$, where μ is the mean formula weight of the gas and g is the acceleration due to gravity as a function of altitude.

The pressure scale height H is defined as the altitude change over which the atmospheric pressure decreases by a factor of e and is calculated from the ratio $RT/\mu g$. The change in pressure with altitude can be expressed through the barometric equation: $P = P_0 \exp(-z/H)$, which is valid in isothermal regions. In areas where temperature varies, the change in pressure with altitude is written as $P = P_0 (T/T_0)^{-\beta}$, where $\beta = \mu g / R T$ and $\Gamma = (dT/dz)$, the atmospheric temperature gradient (K/km)

Table I compares physical parameters of the planetary atmospheres discussed below. We separate these into two groups: (1) the terrestrial planets (Venus, Earth, and Mars), and (2) the gas giant planets (Jupiter, Saturn, Uranus, and Neptune). Properties for the terrestrial planets are given at the observed surface conditions. Properties for the gas giant planets, which do not have observable solid surfaces, are given at the 1 bar atmospheric level.

Atmospheres of the Terrestrial Planets

We discuss the atmospheres of the three terrestrial planets Venus, Earth, and Mars together. The atmospheres of these three planets are secondary in origin, i.e. volatiles outgassed from the interior of the planets during and/or after planetary accretion. Primary atmospheres captured from the solar nebula would be rich in H_2 and He, the two most abundant gases in solar composition material. Even after loss of these two gases, primary atmospheres would not show large relative depletions of the rare noble gases (Ne, Ar, Kr, Xe) with respect to chemically reactive volatiles; however, this is exactly what is observed. For instance, the Ne/ N_2 molar ratios in the atmospheres of Venus, Earth, and Mars are 9.1×10^{-5} , 1.1×10^{-5} , 4.2×10^{-5} times smaller than the Ne/ N_2 ratio in a primary atmosphere captured from the solar nebula, respectively. This indicates that any gas initially captured from the solar nebula was lost, and the current atmospheres are the result of planetary outgassing.

The Earth's bulk chemical composition is similar to that of the ordinary chondritic meteorites (6). Figure 1 shows the calculated composition of an outgassed atmosphere for an Earth-like planet composed of average ordinary chondritic material. High temperature volcanic outgassing of the volatile elements H, C, N, O, F, Cl, and S produces an atmosphere dominated by $CH_4 + H_2$ (7). Stanley Miller and Harold Urey proposed that a similar atmosphere on the early Earth would create large amounts of organic compounds (e.g., the prebiotic soup), leading to the genesis of life (8, 9). Subsequent modification of the outgassed atmospheres of the terrestrial planets by various processes (e.g. thermochemistry, photochemistry, biochemistry, atmospheric escape, etc.) has altered them to their current states. On Venus and Mars, photochemical oxidation of CH_4 to CO_2 and loss of hydrogen has led to CO_2 -rich atmospheres. On Earth, active tectonism and the presence of liquid water at the surface prevent a massive CO_2 build-up in the atmosphere because much of the carbon on the planet is sequestered in marine sediments, primarily carbonates. Photosynthetic life forms produce the O_2 -rich disequilibrium atmosphere of today (10). Below we discuss the important volatile cycles and processes for the atmospheres of Venus, Earth, and Mars in turn.

Venus

Table II gives the chemical composition of Venus' atmosphere, which is dominantly CO_2 with 3.5% of N_2 and smaller amounts of SO_2 , H_2O , CO, and many reactive trace gases. The probable major sources and sinks for each gas are given in Table II. The gas abundances are taken primarily from (11), with new values for H_2SO_4 (12) and NO (13). Chemistry in Venus' lower atmosphere is driven by high temperatures (740 K) and pressures (95 bars) generated by the

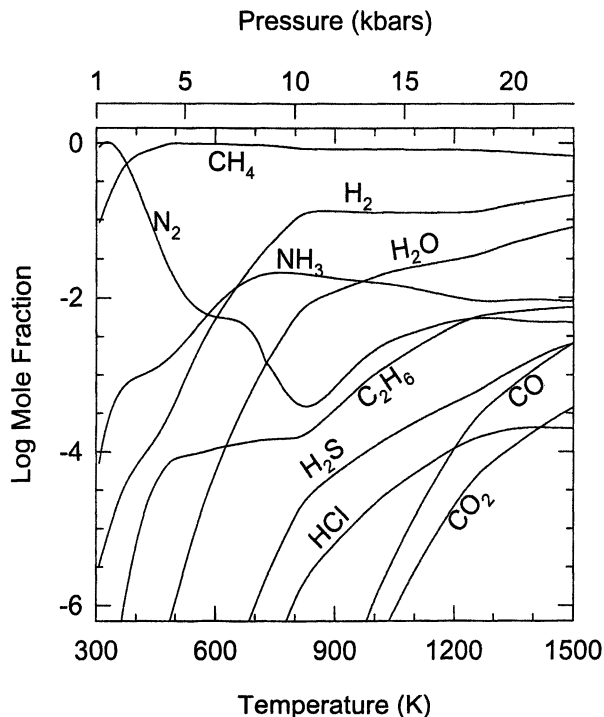


Figure 1. Chemical equilibrium composition of volatiles outgassed from average H-chondritic material as a function of temperature for the T-P profile of an Earth-like planet. Modified from (7).

massive CO₂ greenhouse effect. Venus is shrouded by global sulfuric acid clouds, and less than ~11% of the incident sunlight reaches its surface, making photochemistry in the lower atmosphere negligible. Rather, the high temperatures and pressures at the surface force the rock-forming elements C, S, Cl, and F into the atmosphere where their abundances are controlled by reactions with minerals at the surface. For instance, the CO₂ pressure on Venus is buffered by formation of carbonates on the surface through the reaction:



Carbon dioxide is only a minor gas in the Earth's atmosphere with a column abundance of $5.32 \times 10^{21} \text{ cm}^{-2}$, in comparison to Venus ($1.42 \times 10^{27} \text{ cm}^{-2}$) and Mars ($2.23 \times 10^{23} \text{ cm}^{-2}$). Most of Earth's surface carbon inventory is found in the crust, primarily as carbonates, with a total carbon abundance similar to that of CO₂ in Venus' atmosphere ($0.7 \times 10^{27} \text{ cm}^{-2}$). Despite this similarity, we do

Table II. Chemical Composition of the Atmosphere of Venus

<i>Gas</i>	<i>Abundance</i>	<i>Source(s)</i>	<i>Sink(s)</i>
CO ₂	96.5±0.8%	outgassing	UV photolysis, carbonate formation
N ₂	3.5±0.8%	outgassing	NO _x formation by lightning
SO ₂ ^a	150±30 ppm (22–42 km) 25–150 ppm (12–22 km)	outgassing & reduction of OCS, H ₂ S	H ₂ SO ₄ formation, CaSO ₄ formation
H ₂ O ^a	30±15 ppm (0–45 km)	outgassing and cometary impacts	H escape, Fe ²⁺ oxidation
⁴⁰ Ar	31 ⁺²⁰ ₋₁₀ ppm	outgassing (⁴⁰ K)	—
³⁶ Ar	30 ⁺²⁰ ₋₁₀ ppm	primordial	—
CO ^a	28±7 ppm (36–42 km)	CO ₂ photolysis	photooxidation to CO ₂
⁴ He ^b	0.6–12 ppm	outgassing (U, Th)	escape
Ne	7±3 ppm	outgassing, primordial	—
³⁸ Ar	5.5 ppm	outgassing, primordial	—
OCS ^a	4.4±1 ppm (33 km)	outgassing, sulfide weathering	conversion to SO ₂
H ₂ S ^a	3±2 ppm (<20 km)	outgassing, sulfide weathering	conversion to SO ₂
HDO ^a	1.3±0.2 ppm (sub-cloud)	outgassing	H escape
HCl	0.5 ppm (35–45 km)	outgassing	mineral formation
H ₂ SO ₄	0.1 – 10 ppm (35–50 km)	SO ₂ photolysis	cloud formation
⁸⁴ Kr	25 ⁺¹³ ₋₁₈ ppb	outgassing, primordial	—
SO ^a	20±10 ppb (cloud top)	photochemistry	photochemistry
S _{1–8} ^a	20 ppb (<50 km)	sulfide weathering	conversion to SO ₂
HF	4.5 ppb (35–45 km)	outgassing	mineral formation
NO	5.5±1.5 ppb (sub-cloud)	lightning	conversion to N ₂
¹³² Xe	<10 ppb	outgassing, primordial	—
¹²⁹ Xe	<9.5 ppb	outgassing (¹²⁹ I)	—

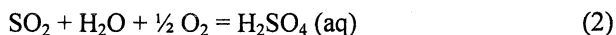
^aAbundances are altitude dependent. ^bThe He abundance in Venus' upper atmosphere is 12⁺²⁴₋₆ ppmv (14). The value listed above is a model-dependent extrapolation to lower altitudes.

not know if all CO₂ on Venus has been degassed and resides in the atmosphere. However, geological evidence summarized by (11) suggests that carbonates are present on Venus and that CO₂ is not completely degassed.

Hydrogen chloride and HF are present in terrestrial volcanic gases, and volcanism is probably the source of atmospheric Cl and F on Venus. The HCl and HF abundances are regulated by reaction with minerals such as sodalite (Na₄[AlSiO₄]₃Cl) and fluorophlogopite (KMg₃AlSi₃O₁₀F₂) at the surface of Venus. The HCl and HF abundances in Venus' atmosphere are present at concentrations significantly higher than in the terrestrial troposphere. Most of the Cl and F in Earth's atmosphere are present as synthetic chlorofluorocarbon (CFC) gases due to anthropogenic emissions. Most of the 1 ppbv HCl and 25 pptv HF in Earth's atmosphere are also anthropogenic. Some HCl originates from sea salt, and volcanic gases provide localized HCl and HF. The bulk of the Earth's surficial Cl content is found dissolved in the oceans, and essentially all F is found in the crust. The terrestrial crustal inventories of Cl and F are larger than the abundances of HCl and HF in Venus' atmosphere, indicating that these elements have been only partially degassed on Venus.

Sulfur dioxide is the third most abundant gas in Venus' atmosphere with an abundance of ~150 ppm in the middle atmosphere. It is produced primarily through volcanic outgassing and oxidation of volcanically outgassed reduced sulfur gases such as OCS and H₂S. In contrast, all sulfur gases are much less abundant in the Earth's atmosphere. Carbonyl sulfide (OCS) is the most abundant sulfur gas in Earth's troposphere but is present at only a few hundred pptv. On Earth, the reduced sulfur gases (OCS, H₂S, CS₂, (CH₃)₂S, etc.) are mainly produced biologically. The volcanic sources of OCS and H₂S are smaller than their biological sources. Most of the SO₂ in the terrestrial atmosphere is anthropogenic, with volcanic emissions being much less important.

The SO₂ abundance in Venus' atmosphere decreases at high altitudes due to the formation of the global sulfuric acid cloud layer (45-70 km), which is produced through SO₂ photolysis via the net photochemical reaction:



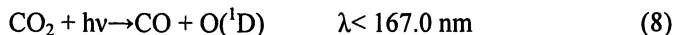
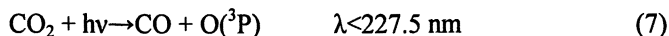
This reaction efficiently removes H₂O and SO₂ from the upper atmosphere above the global cloud layer. At lower altitudes (<22 km), some SO₂ is thermochemically converted into OCS gas. Reaction of SO₂ with calcite (CaCO₃) on the surface to form anhydrite (CaSO₄) plus CO gas irreversibly removes SO₂ from the atmosphere. This net thermochemical reaction would completely remove SO₂ from Venus' atmosphere in ~1.9 Myr, unless it is replenished by volcanic outgassing.

The CO₂ in Venus' atmosphere is continually converted by UV sunlight (hν) to CO and O atoms in their ground (³P) and electronically excited (¹D) states:

Table III. Catalytic Chlorine Cycle in Venus' atmosphere

$\text{CO} + \text{Cl} + \text{M} \rightarrow \text{COCl} + \text{M}^a$	(3)
$\text{COCl} + \text{O}_2 + \text{M} \rightarrow \text{ClCO}_3 + \text{M}$	(4)
$\text{ClCO}_3 + \text{O} \rightarrow \text{CO}_2 + \text{O}_2 + \text{Cl}$	(5)
$\text{CO} + \text{O} \rightarrow \text{CO}_2$	Net Reaction (6)

^aM is any third body.



The direct recombination of oxygen atoms and CO is much slower than oxygen atom recombination to form O₂. Therefore, photolysis would completely destroy all CO₂ in Venus' atmosphere in 5 Myr and would produce observable amounts of O₂ (which are not observed) in ~5 yr unless CO₂ is reformed by another route. Gas phase catalytic re-formation of CO₂ by H, Cl, or N gases has been proposed to solve this problem. For example, the reaction



is important at H₂ levels of tens of ppmv. At intermediate H₂ levels of ~0.1 ppmv, the reaction



precedes reaction 9, which then recycles CO to CO₂.

At very low H₂ levels of ~0.1 ppbv, reaction 9 is no longer important and catalytic cycles such as that shown in Table III, made possible by the large HCl abundance in Venus' atmosphere, recycle CO to CO₂. An analogous Cl cycle for O₃ destruction on Earth is made possible by anthropogenic emissions of CFCs.

Earth

The composition of the Earth's atmosphere, given in Table IV, is controlled by biological processes, with additional influences from photochemistry and human activities. The abundances in Table IV are taken from (15), with updated abundances for the chlorofluorocarbons (CFCs), hydrochlorofluorocarbons (HCFCs), hydrochlorocarbons (HCCs), and perfluorocarbons (PFCs) (16).

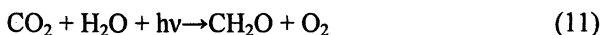
Table IV. Chemical Composition of the Terrestrial Troposphere

<i>Gas</i>	<i>Abundance^a</i>	<i>Source(s)</i>	<i>Sink(s)</i>
N ₂	78.084%	denitrifying bacteria	nitrogen fixing bacteria
O ₂	20.946%	photosynthesis	respiration & decay
H ₂ O	<4%, varies	evaporation, transpiration	condensation
Ar	9340 ppm	outgassing, ⁴⁰ K decay	—
CO ₂	377 ppm	respiration, decay, combustion	photosynthesis, oceanic dissolution, weathering
Ne	18.18 ppm	outgassing	—
⁴ He	5.24 ppm	outgassing (U, Th)	atmospheric escape
CH ₄	1.7 ppm	biological, agricultural	oxidation by OH
Kr	1.14 ppm	outgassing	—
H ₂	0.55 ppm	photochemistry, biology, combustion	uptake in soils, oxidation by OH
N ₂ O	~320 ppb	anthropogenic, biological	stratospheric photolysis
CO	125 ppb	photochemistry	photochemistry
Xe	87 ppb	outgassing	—
O ₃	~10–100 ppb	photochemistry	photochemistry
NMHCs ^b	≤ 80 ppb	foliar emissions, combustion, anthropogenic	photooxidation
HCl	~1 ppb	derived from sea salt	rainout
H ₂ O ₂	~0.3–3 ppb	photochemistry	photochemistry
NH ₃	0.1–3 ppb	biology	wet & dry deposition
HNO ₃	~0.04–4 ppb	photochemistry (NO _x)	rainout
Reduced S-gases ^c	≤500 ppt	biology, anthropogenic	photodissociation, photooxidation
NO _x	~30–300 ppt	combustion, biology	photooxidation
CFCs ^d	1013 ppt	anthropogenic	stratospheric photolysis
HCCs ^e	772.5 ppt	anthropogenic	reaction with OH
HCFCs ^f	154.6 ppt	anthropogenic	reaction with OH
PFCs ^g	83 ppt	anthropogenic	photolysis (upper atm.)
CH ₃ Br	22 ppt	ocean, marine biota	reaction with OH
SO ₂	20–90 ppt	combustion	photooxidation
CH ₃ I	~2 ppt	ocean, marine biota	photolysis (troposphere)
CClF ₂ Br	3.8 ppt	anthropogenic	stratospheric photolysis

^aAbundances by volume in dry air (non-urban troposphere). ^bNon-methane hydrocarbons: alkanes, alkenes, alkynes, aromatics, sterols. ^cOCS, H₂S, CS₂, (CH₃)₂S. ^dCF₂Cl₂, CFCl₃, C₂Cl₃F₃, C₂Cl₂F₄, C₂ClF₅, CClF₃, CCl₄. ^eCH₃Cl, CH₃CCl₃, CH₂Cl₂, CH₂ClCH₂Cl, CHCl₃, C₂H₅Cl, CHClCCl₂. ^fCHClF₂, CHCl₂F, C₂H₃Cl₂F, C₂H₃ClF₂. ^gCF₄, C₂F₆.

The major source of N₂ is the denitrifying bacteria in soils and oceans, which convert ammonium and nitrate compounds into N₂. Major sinks for N₂ are nitrogen-fixing bacteria in soils and oceans, lightning, and combustion. These sources and sinks result in an atmospheric lifetime of ~17 Myr for N₂ on Earth. In the absence of biological sinks, the atmospheric lifetime of N₂ would be a minimum of ~80 Myr, possibly as long as 1 Gyr in the absence of oxygen produced by photosynthesis.

The major oxygen-bearing species are O₂, H₂O, and CO₂. The abundance of water vapor is controlled by evaporation-precipitation. Atmospheric O₂ and CO₂ are biologically controlled by photosynthesis and respiration/decay. Photosynthesis is represented by the net photochemical reaction:



where CH₂O represents complex carbohydrates. The CO₂ destroyed by photosynthesis is restored by respiration and decay. However, the bulk of the carbon at the surface of the Earth is locked up in sedimentary rocks in the form of carbonates and organic carbon in roughly a 4:1 ratio (17). Photosynthetic production of O₂ began prior to 2.7 Gyr ago, but significant amounts of O₂ were not present in the atmosphere until ~2.3 Gyr ago (18). Build up of O₂ in the atmosphere may have been caused by gradual oxidation of the Earth's surface environment (crust and atmosphere) through H loss to space due to CH₄ photolysis (19). Most of the oxygen produced on Earth over time resides in Earth's crust and only a few percent is present as O₂ in the atmosphere.

Terrestrial stratospheric chemistry is closely linked to the ozone (O₃) layer at 15-35 km, which shields the Earth's surface from harmful UV sunlight ($\lambda < 300$ nm) and dissipates the absorbed solar energy as heat. The abundance of O₃ in the stratosphere is a balance between production, destruction, and lateral transport. Production and destruction of O₃ in the absence of other perturbing influences is described by the Chapman cycle given in Table V.

Reaction 15 in the Chapman cycle is kinetically slow, and several natural and anthropogenic trace gases in the earth's atmosphere catalyze ozone destruction more rapidly. Three important examples are the HO_x, NO_x and halogen (Cl, Br, I) oxide cycles, also shown in Table V. The HO_x and NO_x cycles involve naturally occurring species: OH radicals produced by reaction of electronically excited oxygen (¹D) with water vapor, and NO_x gases produced from nitrous oxide (N₂O) transported upward from the troposphere. However, the halogen oxide cycle involves halogens and halogen oxide radicals produced primarily through solar UV photolysis of anthropogenically emitted halocarbons (including CFCs, HCFCs, HCCs, and PFCs), many of which are used as refrigerants, e.g. freon-12 (CF₂Cl₂). Modeling of stratospheric chemistry shows that the NO_x, HO_x, ClO_x, and Chapman cycles account for 31-34%, 16-29%, 19-20%, and 20-25% respectively of O₃ destruction. The relative importance of the

Table V. Cycles for Ozone Depletion in Earth's Atmosphere

<i>Chapman Cycle</i>		
$O_2 + hv \rightarrow O + O$	$(\lambda = 180 - 240 \text{ nm})$	(12)
$O + O_2 + M \rightarrow O_3 + M$		(13)
$O_3 + hv \rightarrow O(^1D) + O_2$	$(\lambda = 200-300 \text{ nm})$	(14)
$O + O_3 \rightarrow O_2 + O_2$		(15)
$O_3 \rightarrow O + O_2$	Net Reaction	(16)
<i>Catalytic Cycle (X = H, OH, NO, Cl)</i>		
$X + O_3 \rightarrow XO + O_2$		(17)
$XO + O \rightarrow X + O_2$		(18)
$O + O_3 \rightarrow O_2 + O_2$	Net Reaction	(15)

Chapman reactions and the various catalytic cycles varies with altitude and with the concentration of NO_x , HO_x , and halogen oxide gases.

Mars

The chemical composition of the Martian atmosphere is given in Table VI, along with plausible sources and sinks. The abundances are taken primarily from (15), with new abundances for He (20), H_2 and HD (21), H_2O_2 (22, 23), and CH_4 (24). The Martian atmosphere is dominantly CO_2 , which is continually converted to O_2 and CO by solar UV light. However, as on Venus, the observed abundances of CO_2 , O_2 , and CO cannot be explained simply by the direct recombination of CO and O atoms to CO_2 because this reaction is too slow to maintain the high CO_2 and low CO and O_2 abundances. Instead, OH radicals produced from atmospheric water vapor by UV photolysis or by reaction with electronically excited O atoms enter into catalytic cycles such as that shown in Table VII, which recombine CO and O atoms to CO_2 .

Another catalytic cycle involves photolysis of hydrogen peroxide:



The HO_x radicals also regulate the O_3 level in the Martian atmosphere via catalytic cycles analogous to those in the terrestrial stratosphere. However, on Venus catalytic cycles involving chlorine for the re-combination of CO_2 are required because the hydrogen abundance is too low for catalytic cycles involving OH to be as efficient as they are on Mars.

Table VI. Chemical Composition of the Atmosphere of Mars

<i>Gas</i>	<i>Abundance^a</i>	<i>Source(s)</i>	<i>Sink(s)</i>
CO ₂	95.32%	outgassing, sublimation	condensation
N ₂	2.7%	outgassing	escape as N
Ar	1.6%	outgassing (40K), primordial	—
O ₂	0.13%	CO ₂ photolysis	photoreduction
CO	0.08%	CO ₂ photolysis	photooxidation
H ₂ O ^b	0.03%	evaporation, desorption	condensation & adsorption
NO	~100 ppm (at 120 km)	photochemistry (N ₂ , CO ₂)	photochemistry
H ₂	15±5 ppm	H ₂ O photolysis	escape
He	10±6 ppm	solar wind, outgassing,	escape
Ne	2.5 ppm	outgassing, primordial	—
HDO	0.85±0.02 ppm	evaporation, desorption	condensation & adsorption
Kr	0.3 ppm	outgassing, primordial	—
Xe	0.08 ppm	outgassing, primordial	—
O ₃ ^b	~(0.04–0.2) ppm	photochemistry (CO ₂)	photochemistry
H ₂ O ₂	20–50 ppb	H ₂ O photolysis	photochemistry
HD	11 ± 4 ppb	H ₂ O photolysis	escape
CH ₄	10 ± 3 ppb	outgassing	photochemistry

^aThe mixing ratios, but not the column densities, of noncondensable gases are seasonally variable as a result of the annual condensation and sublimation of CO₂.

^bSpatially and temporally variable.

Table VII. Catalytic CO₂ Cycle in the Martian Atmosphere

OH + CO → CO ₂ + H	(20)
H + O ₂ + M → HO ₂ + M	(21)
HO ₂ + O → OH + O ₂	(22)
CO + O → CO ₂	Net reaction (23)

Table VIII. Chemical Composition of the Atmospheres of Jupiter and Saturn

<i>Gas</i>	<i>Jupiter^a</i>	<i>Saturn</i>
H ₂	86.4 ± 0.3%	88 ± 2%
⁴ He	13.6 ± 0.3%	12 ± 2%
CH ₄	(1.81 ± 0.34) × 10 ⁻³	(3.8 ± 1.1) × 10 ⁻³
NH ₃	(6.1 ± 2.8) × 10 ⁻⁴	(1.6 ± 1.1) × 10 ⁻⁴
H ₂ O	520 ⁺³⁴⁰ ₋₂₄₀ ppm	2–20 ppb
H ₂ S	67 ± 4 ppm	<0.4 ppm
HD	45 ± 12 ppm	110 ± 58 ppm
¹³ CH ₄	19 ± 1 ppm	~51 ppm
C ₂ H ₆	5.8 ± 1.5 ppm	7.0 ± 1.5 ppm
PH ₃	1.1 ± 0.4 ppm	4.5 ± 1.4 ppm
CH ₃ D	0.20 ± 0.04 ppm	0.39 ± 0.25 ppm
C ₂ H ₂	0.11 ± 0.03 ppm	0.30 ± 0.10 ppm
HCN	60 ± 10 ppb	<4 ppb
C ₂ H ₄	7 ± 3 ppb	~0.2 ppb ^b
CO ₂	5–35 ppb	0.3 ppb
CH ₃ C ₂ H	2.5 ⁺² ₋₁ ppb	0.6 ppb
CO	1.6 ± 0.3 ppb	1.4 ± 0.7 ppb
GeH ₄	0.7 ^{+0.4} _{-0.2} ppb	0.4 ± 0.4 ppb
C ₄ H ₂	0.3 ± 0.2 ppb	0.09 ppb
AsH ₃	0.22 ± 0.11 ppb	2.1 ± 1.3 ppb

^a ³He 22.6±0.7 ppm, Ne 21±3 ppm, Ar 16±3 ppm, Kr 8±1 ppb, Xe 0.8±0.1 ppb. ^b assuming a total stratospheric column density of 1.54×10²⁵ cm⁻².

Atmospheres of the Gas Giant Planets

The atmospheres of the gas giant planets Jupiter, Saturn, Uranus, and Neptune are primary atmospheres composed of gases captured from the solar nebula, mainly H_2 and He. We separate them into two groups based on composition. Jupiter and Saturn are closer to solar composition, although both planets are generally enriched in elements heavier than He. Jupiter is depleted in oxygen relative to solar composition (25), and Saturn is less enriched in oxygen than other heavy elements (26). Their atmospheric compositions are given in Table VIII (15, 27-34). Abundances of the minor species PH_3 , GeH_4 , AsH_3 , and CO in the upper atmospheres of Jupiter and Saturn are larger than predicted from thermochemical equilibrium in the regions where these gases are observed. This indicates that they are transported upward from deeper levels where they are more abundant (27). Photochemistry (discussed below) and mass influx, e.g. the Shoemaker-Levy 9 (SL9) impact into Jupiter's upper atmosphere, affect stratospheric chemistry. The observed CO_2 and H_2O in Jupiter's stratosphere are believed to have formed from H_2O and CO delivered by SL9 (31).

Uranus and Neptune are smaller and denser than Jupiter and Saturn due to much larger enrichments of elements heavier than He. Oxygen is highly enriched on these planets and the net thermochemical reaction



produces 1,000 times more CO than on Jupiter or Saturn in the deep atmospheres of Uranus and Neptune (35). The compositions of their observable atmospheres are shown in Table IX (15, 36) and are seen to be significantly enriched in methane and deuterium relative to Jupiter and Saturn. Water, NH_3 , H_2S , and other condensable gases are not observed because they are removed by cloud condensation hundreds of kilometers below the observable atmospheric regions. Photochemistry plays a major role in the chemistry of the atmospheres of all four gas giant planets. In particular, methane and ammonia photochemistry produces many of the minor species observed in the stratospheres of these four planets, as discussed below.

Methane Photochemistry – Jupiter, Saturn, Uranus, and Neptune

Methane is photolyzed by UV sunlight with wavelengths $\lambda < 160$ nm to $^3\text{CH}_2 + 2\text{H}$ (51%), $^1\text{CH}_2 + \text{H}_2$ (41%), and $\text{CH} + \text{H} + \text{H}_2$ (8%). $^3\text{CH}_2$ is the triplet (electronic ground) state of methylene, and $^1\text{CH}_2$ is the singlet (electronic excited) state of methylene. Many higher hydrocarbons are formed from the

Table IX. Chemical Composition of the Atmospheres of Uranus and Neptune

<i>Gas</i>	<i>Uranus</i>	<i>Neptune</i>
H ₂	~82.5 ± 3.3%	~80 ± 3.2 %
He	15.2 ± 3.3 %	19.0 ± 3.2 %
CH ₄	~2.3 %	~1-2 %
HD	~148 ppm	~192 ppm
CH ₃ D	~8.3 ppm	~12 ppm
H ₂ Sa	<0.8 ppm	<3 ppm
NH ₃ ^a	<100 ppb	<600 ppb
CO	<40 ppb	0.65 ± 0.35 ppm
C ₂ H ₆	10 ± 1 ppb	1.5 ^{+2.5} _{-0.5} ppm
C ₂ H ₂	~10 ppb	60 ⁺¹⁴⁰ ₋₄₀ ppb
CH ₃ CN	--	<5 ppb
HCN	<15 ppb	0.3 ± 0.15 ppb
HC ₃ N	<0.8 ppb	<0.4 ppb
CH ₃ C ₂ H	0.25 ± 0.03 ppb	--
C ₄ H ₂	0.16 ± 0.02 ppb	--
CO ₂	40 ± 5 ppt	--

^aConverted to a mixing ratio using an H₂ column abundance of 400 km amagat. (1 km amagat = 2.69 × 10²⁴ cm⁻²)

products of methane photolysis. As an example, Table X shows the series of elementary reactions for the formation of ethane (C₂H₆) from methane. The methyl radical, which is important in ethane formation, has been observed in the stratospheres of Saturn and Neptune at column abundances of (1.5 – 7.5) × 10¹³ cm⁻² (37) and 1.6^{+1.2}_{-0.9} × 10¹³ cm⁻² (38), respectively. It has also been observed in the atmosphere of Jupiter (39) although its abundance has not been determined (40). There has been no detection of the methyl radical in Uranus' atmosphere, but an upper limit of .05 ppbv has been set (40).

Similar formation schemes can be written for the other observed hydrocarbons. Ethylene (C₂H₄) is formed by reaction of a methyl radical (CH₃)

Table X. Ethane Formation from Methane

$2(\text{CH}_4 + h\nu \rightarrow {}^1\text{CH}_2 + \text{H}_2)$	(25)
$2({}^1\text{CH}_2 + \text{H}_2 \rightarrow \text{CH}_3 + \text{H})$	(26)
$\text{CH}_3 + \text{CH}_3 + \text{M} \rightarrow \text{C}_2\text{H}_6 + \text{M}$	(27)
$\text{H} + \text{H} + \text{M} \rightarrow \text{H}_2 + \text{M}$	(28)
$2\text{CH}_4 \rightarrow \text{C}_2\text{H}_6 + \text{H}_2$	Net Reaction (29)

and a ${}^3\text{CH}_2$ radical, or by reaction of CH radicals with methane. Acetylene (C_2H_2) forms through reaction of 2 methylene radicals. All of these C_2 hydrocarbons undergo further photochemical reactions to a greater (C_2H_4) or lesser (C_2H_6) extent depending on the UV shielding provided to them by methane. Only a minor fraction of C_2H_6 is photolyzed via



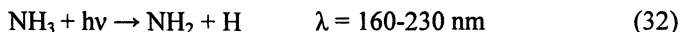
and most C_2H_6 is removed by vertical transport into the hot, lower atmospheres of the gas giant planets where CH_4 reforms via the net thermochemical reaction



Ultimately, downward mixing into the hot, lower atmospheres of the Jovian planets reconverts all higher hydrocarbons back to CH_4 via hydrogenation reactions.

NH_3 Photolysis on Jupiter, Saturn, Uranus, and Neptune

Ammonia condenses out of Jupiter's atmosphere forming a cloud of NH_3 ice particles at 138 K and 0.46-0.53 bars pressure (41). It is photolyzed by UV sunlight in the 160 – 230 nm region in Jupiter's upper troposphere. Shorter wavelength light is absorbed at higher altitudes by H_2 , CH_4 , and C_2H_6 while longer wavelength light does not destroy NH_3 . Almost all NH_3 photolyzes via the reaction:



Most of the NH_2 radicals form N_2 via the pathway given in Table XI. Some of the N_2H_4 (hydrazine) formed in reaction 34 condenses out of the upper atmospheres of the gas giants forming thin haze layers. However, most of the photolyzed NH_3 is recycled via photochemical reactions such as 36 and by

Table XI. Reaction Cycle for N₂ Formation in Gas Giants

$4(\text{NH}_3 + h\nu \rightarrow \text{NH}_2 + \text{H})$	(33)
$2(\text{NH}_2 + \text{NH}_2 + \text{M} \rightarrow \text{N}_2\text{H}_4)$	(34)
$2(\text{N}_2\text{H}_4 + h\nu \rightarrow \text{N}_2\text{H}_3 + \text{H})$	(35)
$\text{N}_2\text{H}_3 + \text{N}_2\text{H}_3 \rightarrow 2\text{NH}_3 + \text{N}_2$	(36)
$3(\text{H} + \text{H} + \text{M} \rightarrow \text{H}_2 + \text{M})$	(37)
$2\text{NH}_3 = \text{N}_2 + 3\text{H}_2$	Net Reaction (38)



Ultimately the N₂ and N₂H₄ produced by NH₃ photolysis are reconverted back to NH₃ via thermochemical reactions exemplified by



in the hot, deep atmospheres of the gas giant planets.

Extrasolar Earth-like Planets

To date, 215 extrasolar planets have been detected. Of these, two recent detections seem to be terrestrial-sized extrasolar planets, Gliese 876d ($7.5M_{\text{Earth}}$) (42) and OGLE-2005-BLG-390Lb ($5.5M_{\text{Earth}}$) (43). This begs the question: what kind of atmospheres should we expect to find around such planets. These planetary atmospheres will be affected by myriad variables including: the stellar environment (type of parent star, orbital location, tidal locking, planetary companions, etc.), the planet's size (tectonically active or not), its composition (wet or dry, volatile inventory), stage of evolution, presence of a biosphere, etc. Given the number of possible variables, the atmospheric compositions of extrasolar terrestrial-type planets will surely be more varied than we can possibly predict.

Spacecraft missions are being planned by both NASA (the Terrestrial Planet Finder) and ESA (Darwin) to search for Earth-like planets around other stars and to take spectra of their atmospheres and surfaces (44, 45). These missions are designed to detect planets located in the habitable zones (HZ) of other stars. The

HZ is defined as the orbital area around a star where a planet can sustain liquid water at the surface. Several studies have attempted to define the HZ as a function of stellar type (e.g. F, G, K, M dwarf stars) and time (see e.g. 46, 47, and references therein). The HZ is of interest because it is widely believed that liquid water is necessary for the genesis of (recognizable) life. The particular emphasis of the planned space missions is to search for signs of life on extrasolar Earth-like planets via spectroscopy. Atmospheric compounds such as O_2 , O_3 , N_2O , CH_4 , and CH_3Cl are considered biomarkers, and their spectroscopic detection in a terrestrial-type atmosphere, particularly O_2 or O_3 found together with a reduced gas such as CH_4 , would suggest life (48, 49). Detection of CO_2 would indicate that the planet is indeed a terrestrial-type planet (50).

Summary

There are two broad types of planetary atmospheres: primary and secondary. The gas giant planets have primary atmospheres, which consist of gas captured from the solar nebula. These atmospheres are composed of H_2 and He with lesser amounts of CH_4 and NH_3 . Photochemistry strongly affects the upper atmospheres of the gas giant planets, whereas thermochemistry dominates in their interiors. The terrestrial planets (Venus, Earth, and Mars) either lost or never had primary atmospheres. Rather, they have secondary atmospheres derived from volatiles outgassed from their rocky interiors. The atmospheres of Venus and Mars are dominantly CO_2 and N_2 . Thermochemistry is the dominant process controlling atmospheric composition on Venus due to the high surface temperature and pressure, whereas photochemistry dominates in the cold, thin atmosphere of Mars. Earth is significantly different from either Venus or Mars with an atmosphere composed primarily of N_2 and O_2 . The composition of Earth's atmosphere is controlled by biological processes, with photochemistry also playing a significant role, particularly in the generation of the ozone layer. Extrasolar planets may have atmospheres similar to those observed in our solar system. The compositions of extrasolar planetary atmospheres will help us to infer details about the planets such as the type of planet, processes operating on the planet, and whether or not the planet could support life.

Acknowledgments

This work was supported by the McDonnell Center for the Space Sciences and the NASA Astrobiology Program Grant NNG04G157A.

References

1. Niemann, H. D.; et al. *Nature* **2005**, *438*, 779-784.
2. Hunten, T. M.; Morgan, T. H.; Shemansky, D. E. In *Mercury*; Vilas, F.; Chapman, C. R.; Matthews, M. S., Eds.; Univ. of Arizona Press: Tucson, AZ, 1988; pp. 561-612.
3. Brown, M. E. *Annu. Rev. Earth Planet. Sci.* **2002**, *30*, 307-345.
4. *Neptune and Triton*; Cruikshank, D. P., Ed.; Univ. of Arizona Press: Tucson, AZ, 1995; pp. 1249.
5. McGrath, M. A.; Lellouch, E.; Strobel, D. F.; Feldman, P. D.; Johnson, R. E. In *Jupiter: the planet, satellites and magnetosphere*; Bagenal, F.; Dowling, T.; McKinnon, W., Eds.; Cambridge Univ. Press: Cambridge, UK, 2004; pp 457-483.
6. Larimer, J. W. *Geochim. Cosmochim. Acta* **1971**, *35*, 769-786.
7. Schaefer, L.; Fegley, Jr., B. *Icarus* **2007**, *186*, 462-483.
8. Miller, S. L. *J. Am. Chem. Soc.* **1955**, *77*, 2351-2361.
9. Miller, S. L.; Urey, H. C. *Science* **1959**, *130*, 245-251.
10. Kasting, J. F. *Precamb. Res.* **2005**, *137*, 119-129.
11. Fegley, Jr., B. In *Meteorites, Comets, and Planets*; Davis, A. M., Ed.; *Treatise on Geochemistry Vol. 1*; Turekian, K. K.; Holland, H. D., Eds.; Elsevier-Pergamon: Oxford, UK, 2004; pp 487-507.
12. Jenkins, J. M.; Kolodner, M. A.; Butler, B. J.; Suleiman, S. H.; Steffes, P. G. *Icarus* **2002**, *158*, 312-328.
13. Krasnopolsky, V. A. *Icarus* **2006**, *182*, 80-91.
14. Von Zahn, U.; Kumar, S.; Niemann, H.; Frinn, R. In *Venus*; Hunten, D. M.; Colin, L.; Donahue, T. M.; Moroz, V. I., Eds.; Univ. of Arizona Press: Tucson, AZ, 1983; pp 299-450.
15. Lodders, K.; Fegley, Jr., B. *The Planetary Scientist's Companion*; Oxford Univ. Press: New York, NY, 1998.
16. Ehhalt, D.; Prather, M.; et al. In *Climate Change 2001: The Scientific Basis*; Houghton, J. T.; Meira Filho, L. G.; Callander, B. A.; Harris, N.; Kattenberg, B.; Maskell, K., Eds.; Cambridge Univ. Press: Cambridge, UK, 2001; pp 239-287.
17. Schidowski, M. *Annu. Rev. Earth Planet. Sci.* **1987**, *15*, 47-72.
18. Rye, R.; Holland, H. D. *Am. J. Sci.* **1998**, *298*, 621-672.
19. Catling, D. C.; Zahnle, K. J.; McKay, C. P. *Science* **2001**, *293*, 839-843.
20. Krasnopolsky, V. A.; Gladstone, G. R. *Icarus* **2005**, *176*, 395-407.
21. Krasnopolsky, V. A.; Feldman, P. D. *Science* **2001**, *294*, 1914-1917.
22. Encrenaz, Th.; Bézard, B.; Greathouse, T. K.; Richter, M. J.; Lacy, J. H.; Atreya, S. K.; Wong, A. S.; Lebonnois, S.; Lefevre, F.; Forget, F. *Icarus* **2004**, *170*, 424-429.
23. Clancy, R. T.; Sandor, B. J.; Moriarty-Schieven, G. H. *Icarus* **2004**, *168*, 116-121.

24. Krasnopolsky, V. A.; Maillard, J. P.; Owen, T. C. *Icarus* **2004**, *172*, 537-547.
25. Lodders, K. *Astrophys. J.* **2004**, *611*, 587-597.
26. Visscher, C.; Fegley, Jr., B. *Astrophys. J.* **2005**, *623*, 1221-1227.
27. Fegley, B., Jr.; Lodders, K. *Icarus* **1994**, *110*, 117-154.
28. Visscher, C.; Fegley, B., Jr. *Astrophys. J.* **2005**, *623*, 1221-1227.
29. Lodders, K. *Astrophys. J.* **2004**, *611*, 587-597.
30. Atreya, S. K.; Mahaffy, P. R.; Niemann, H. B.; Wong, M. H.; Owen, T. C. *Planet. Space Sci.* **2003**, *51*, 105-112.
31. Lellouch, E.; Bézard, B.; Strobel, D. F.; Bjoraker, G. L.; Flasar, F. M.; Romani, P. N. *Icarus* **2006**, *184*, 478-497.
32. de Graauw, Th.; et al. *Astron. Astrophys.* **1997**, *321*, L13-L16.
33. Greathouse, T. K.; Lacy, J. H.; Bézard, B.; Moses, J. I.; Richter, M. U.; Knez, C. *Icarus* **2006**, *181*, 266-271.
34. Sada, P. V.; Bjoraker, G. L.; Jennings, D. E.; Romani, P. N.; McCabe, G. H. *Icarus* **2005**, *173*, 499-507.
35. Lodders, K.; Fegley, Jr., B. *Icarus* **1994**, *112*, 368-375.
36. Burgdorf, M.; Orton, G.; van Cleve, J.; Meadows, V.; Houck, J. *Icarus* **2006**, *184*, 634-637.
37. Bézard, B.; Feuchtgruber, H.; Moses, J. I.; Encrenaz, Th. *Astron. Astrophys.* **1998**, *334*, L41-L44.
38. Bézard, B.; Romani, P. N.; Feuchtgruber, H.; Encrenaz, Th. *Astrophys. J.* **1999**, *515*, 868-872.
39. Kunde, V. G.; et al. *Science* **2004**, *305*, 1582-1586.
40. Burgdorf, M.; Orton, G.; van Cleve, J.; Meadows, V.; Houck, J. *Icarus* **2006**, *184*, 634-637.
41. Atreya, S. K.; Wong, M. H.; Owen, T. C.; Mahaffy, P. R.; Niemann, H. B.; de Pater, I.; Drossart, P.; Encrenaz, Th. *Planet. Space Sci.* **1999**, *47*, 1243-1262.
42. Rivera, E.; Lissauer, J.; Butler, P.; Marcy, G.; Vogt, S.; Fischer, D.; Brown, T.; Laughlin, G.; Henry, G. *Astrophys. J. Lett.* **2005**, *634*, 625-640.
43. Beaulieu, J.-P. et al. *Nature* **2006**, *439*, 437-440.
44. Beichman, C. A.; Woolf, N. J.; Lindensmith, C. A. *The Terrestrial Planet Finder (TPF): A NASA Origins Program to Search for Habitable Planets*; JPL Publication 99-3: NASA Jet Propulsion Laboratory, Pasadena, CA, 1999.
45. Léger, A. *Space Res.* **2000**, *25*, 2209-2223.
46. Kasting, J. F.; Catling, D. *Annu. Rev. Astron. Astrophys.* **2003**, *41*, 429-463.
47. Tarter, J. C.; et al. *Astrobiol.* **2007**, submitted (arxiv preprint).
48. Segura, A.; Krelove, K.; Kasting, J.F.; Sommerlatt, D.; Meadows, V.; Crisp, D.; Cohen, M.; Mlawer, E. *Astrobiol.* **2003**, *4*, 689-707.

- Segura, A.; Kasting, J.; Meadows, V.; Cohen, M.; Scalo, J.; Crisp, D.; Butler, R. A. H.; Tinetti, G. *Astrobiol.* **2005**, *5*, 706-725.
49. Des Marais, D. J.; Harwit, M. O.; Jucks, K. W.; Kasting, J. F.; Lin, D. N. C.; Lunine, J. I.; Schneider, J.; Seager, S.; Traub, W. A.; Woolf, N. J. *Astrobiol.* **2002**, *2*, 153-181.

Chapter 11

Hafnium–Tungsten Chronometry of Planetary Accretion and Differentiation

Thorsten Kleine

Institute for Isotope Geochemistry and Mineral Resources, Department of Earth Sciences, ETH Zurich, Zurich, Switzerland

The formation and earliest history of many planetary bodies in the inner solar system involved heating and melting of planetary interiors, causing differentiation into silicate mantles and metal cores. A record of these earliest stages of planetary evolution is preserved in the W isotopic composition of meteorites as well as lunar and terrestrial rocks. Hafnium-tungsten chronometry reveals that the early thermal and chemical evolution of asteroids is controlled by the decay of ^{26}Al . This nuclide was sufficiently abundant to melt early-formed planetesimals (iron meteorite parent bodies) but could not raise the temperatures in the late-formed chondrite parent asteroids high enough to cause differentiation. Larger bodies such as the Earth grew over longer timescales and the energy required for differentiation was mainly delivered by large impacts. Formation of the Earth was largely completed by the impact of a Mars-sized body that led to the formation of the Moon between 4.53 and 4.47 billion years ago.

Planetary Accretion and Core Formation

The starting place for the accretion of the Earth and other planetary bodies is the solar nebula. This circumstellar disk of gas and dust formed by the gravitational collapse of a localized dense region of an interstellar molecular cloud. Within the inner region of the solar nebula, dust grains collide and stuck together to form a large population of meter- to kilometer-sized objects. Gravity and gas drag causes these planetesimals to collide and form increasingly larger bodies in a period of runaway growth, the products of which include numerous Moon- to Mars-sized planetary embryos. Collisions among these bodies mark the late stages of accretion culminating in the formation of a few terrestrial planets that sweep up all the other bodies. The Moon probably formed during this period, and involved a 'giant impact' of a Mars-sized body with Earth at the very end of Earth's accretion (1).

Planetary accretion is intimately linked with heating and subsequent melting of the planetary interiors. As a consequence, all major bodies of the inner solar system and also many smaller bodies are chemically differentiated into a metallic core and a silicate mantle. Presumably the planetary embryos began as relatively homogeneous objects, similar to the undifferentiated planetesimals observed today. However, the decay of short-lived radioactive isotopes, especially ^{26}Al ($t_{1/2}=0.73$ Myr), caused the planetary interiors to heat up (2). Furthermore, collisions among the planetary embryos resulted in temperature increases during growth. At some critical size, melting will have started within the planetary embryo, causing separation and segregation of a metallic core (3). Whether or not a planetary object differentiated, however, does not only depend on its size but also on the time of its accretion. For instance, the largest asteroid Ceres (diameter = 913 km) remained undifferentiated, whereas smaller asteroids like Vesta (diameter = 512 km) underwent widespread melting and core formation. As will be discussed in more detail below, this most likely reflects differences in the time of accretion and hence the amount of ^{26}Al present at the time of accretion (2, 4-6)

Melting in the interior of a planetary object permits the denser components to migrate towards the center, thereby forming a core. Metallic iron melts at lower temperatures as silicates, such that core formation occurs either by migration of molten metal through solid silicate matrix or by separation of metal droplets from molten silicate. The latter process probably is appropriate for core formation in Earth, where giant impacts cause the formation of widespread magma oceans. Once differentiation begins it proceeds rapidly. The downward motion of dense metal melts results in the release of potential energy and hence further heating, which further triggers differentiation (3).

The segregation of dense, Fe-rich alloy from Mg-rich silicates causes a strong chemical differentiation of a planet. Those elements that preferentially

partition into metal (the so-called 'iron-loving' or siderophile elements) will be concentrated in the core, whereas elements with a strong affinity to silicates (the so-called 'silicate-loving' or lithophile elements) will be concentrated in the mantle. Owing to this elemental fractionation the chemical composition of a bulk differentiated planet cannot be measured directly but it can be inferred by studying chondrites. These meteorites derive from asteroids that stayed undifferentiated. The relative abundances of elements having a high condensation temperature (the so-called refractory elements) are more or less constant among the chondrites. It is therefore assumed that almost all planetary objects of the inner solar system have chondritic relative abundances of refractory elements (the Moon is an important exception because of its overall depletion in siderophile elements). In contrast, elements having relatively low condensation temperatures (the so-called volatile elements) are strongly fractionated among the chondrite parent asteroids and other planetary objects.

Hf-W Chronometry of Planetary Accretion and Differentiation

The Extinct ^{182}Hf - ^{182}W System

The decay of ^{182}Hf to ^{182}W is well suited to date core formation in planetary objects mainly for three reasons. First, owing to the ^{182}Hf half-life of ~ 9 Myr, detectable W isotope variations can only be produced in the first ~ 60 Myr of the solar system. This timescale is appropriate for the formation of the Earth and Moon in particular and to planetary accretion and differentiation in general. Second, both Hf and W are refractory elements such that there is only limited fractionation of Hf and W in the solar nebula or among different planetary bodies (see above). The Hf/W ratio of the bulk Earth therefore can be assumed to be chondritic and hence can be measured today. Third, Hf is a lithophile and W is a siderophile element such that the chondritic Hf/W ratio of the Earth is fractionated internally by core formation. If core formation took place during the effective lifetime of ^{182}Hf , the metal core (Hf/W ~ 0) will develop a deficit in the abundance of ^{182}W whereas the silicate mantle, owing to its enhanced Hf/W, will develop an excess of ^{182}W (7-9).

The abundance of ^{182}W at time t can be subdivided in an initial component (i.e., ^{182}W atoms present at the time the sample formed) and a radiogenic component (i.e., ^{182}W atoms produced by ^{182}Hf decay after formation of the sample):

$$\left(^{182}\text{W}\right)_t = \left(^{182}\text{W}\right)_i + \left(^{182}\text{W}\right)^* \quad (1)$$

where $(^{182}\text{W})_i$ is the abundance of ^{182}W at the time a sample formed and $(^{182}\text{W})^*$ is the amount of ^{182}W produced by radioactive decay of ^{182}Hf . The radiogenic ^{182}W component is given by:

$$(^{182}\text{W})^* = (^{182}\text{Hf})_i - (^{182}\text{Hf})_t \quad (2)$$

where $(^{182}\text{Hf})_i$ is the abundance of ^{182}Hf at the start of the solar system (i.e., 4567.2 ± 0.6 (10) or 4568.5 ± 0.5 (11) million years (Ma) ago) and $(^{182}\text{Hf})_t$ is the abundance of ^{182}Hf at the time a sample formed. The number of radioactive ^{182}Hf atoms that remain at any time t of an original number of atoms $(^{182}\text{Hf})_i$ is given by:

$$(^{182}\text{Hf})_t = (^{182}\text{Hf})_i \times e^{-\lambda t} \quad (3)$$

where $\lambda = 0.078 \text{ Myr}^{-1}$ is the decay constant. From equations 1 to 3 it follows:

$$(^{182}\text{W})_t = (^{182}\text{W})_i + (^{182}\text{Hf})_i \times (1 - e^{-\lambda t}) \quad (4)$$

Equation 4 can be modified by dividing each term by the number of ^{184}W atoms, which is constant because this isotope is stable and not produced by the decay of a naturally occurring isotope of another element:

$$\left(\frac{^{182}\text{W}}{^{184}\text{W}} \right)_t = \left(\frac{^{182}\text{W}}{^{184}\text{W}} \right)_i + \left(\frac{^{182}\text{Hf}}{^{184}\text{W}} \right)_i \times (1 - e^{-\lambda t}) \quad (5)$$

At the present day all ^{182}Hf had decayed to ^{182}W and the present-day value of $^{182}\text{Hf}/^{184}\text{W}$ is 0, such that this ratio is replaced by $(^{182}\text{Hf}/^{180}\text{Hf}) \times (^{180}\text{Hf}/^{184}\text{W})$:

$$\left(\frac{^{182}\text{W}}{^{184}\text{W}} \right)_t = \left(\frac{^{182}\text{W}}{^{184}\text{W}} \right)_i + \left(\frac{^{182}\text{Hf}}{^{180}\text{Hf}} \right)_i \times \left(\frac{^{180}\text{Hf}}{^{184}\text{W}} \right) \times (1 - e^{-\lambda t}) \quad (6)$$

Owing to the short half-life of ^{182}Hf , the present-day value of $e^{-\lambda t} \sim 0$, and it follows:

$$\left(\frac{^{182}\text{W}}{^{184}\text{W}} \right)_t = \left(\frac{^{182}\text{W}}{^{184}\text{W}} \right)_i + \left(\frac{^{182}\text{Hf}}{^{180}\text{Hf}} \right)_i \times \left(\frac{^{180}\text{Hf}}{^{184}\text{W}} \right) \quad (7)$$

In a plot of $^{182}\text{W}/^{184}\text{W}$ vs. $^{180}\text{Hf}/^{184}\text{W}$ samples that formed from a common reservoir at the same time but have different $^{180}\text{Hf}/^{184}\text{W}$ ratios will plot on a line (the isochron) whose slope corresponds to the $^{182}\text{Hf}/^{180}\text{Hf}$ at the time of formation.

Due to the small variations observed in nature, W isotope ratios are usually reported in ϵ_{W} units, which are defined as follows:

$$\epsilon_{\text{W}}(0) = \left\{ \frac{\left(\frac{^{182}\text{W}}{^{184}\text{W}} \right)_j^0}{\left(\frac{^{182}\text{W}}{^{184}\text{W}} \right)_{\text{std}}^0} - 1 \right\} \times 10^4 \quad (8)$$

For modeling purposes it is useful to express the $^{182}\text{W}/^{184}\text{W}$ of a reservoir relative to the chondritic value:

$$\Delta\epsilon_{\text{W}}(t) = \left\{ \frac{\left(\frac{^{182}\text{W}}{^{184}\text{W}} \right)_j^t}{\left(\frac{^{182}\text{W}}{^{184}\text{W}} \right)_{\text{CHUR}}^t} - 1 \right\} \times 10^4 \quad (9)$$

Figure 1 illustrates how the Hf-W system can be used to date core formation. Tungsten isotope evolution curves are shown for the mantles and cores of three planetary bodies that underwent core formation at 10, 30, and 50 Myr, respectively. As expected, an early core formation will result in larger ^{182}W anomalies than a late core formation. If core formation occurred more than ~ 50 Myr after the beginning of the solar system, no resolvable W isotope variation would evolve because most ^{182}Hf would have already decayed away.

An age of core formation can be determined by calculating the time at which the mantle or core had the same $^{182}\text{W}/^{184}\text{W}$ ratio than chondrites. The following equation is obtained by equating equation 7 for a reservoir j (i.e., mantle or core) and chondrites (which are representative for the W isotope evolution of the bulk planet) and combining this with equation 3:

$$t = \frac{1}{\lambda} \times \ln \left\{ \frac{\left[\left(\frac{^{182}\text{Hf}}{^{180}\text{Hf}} \right)_i \times \left[\left(\frac{^{180}\text{Hf}}{^{184}\text{W}} \right)_j - \left(\frac{^{180}\text{Hf}}{^{184}\text{W}} \right)_{\text{CHUR}} \right] \right]}{\left(\frac{^{182}\text{W}}{^{184}\text{W}} \right)_j^0 - \left(\frac{^{182}\text{W}}{^{184}\text{W}} \right)_{\text{CHUR}}^0} \right\} \quad (10)$$

where CHUR denotes Chondritic Uniform Reservoir. Equation 10 illustrates the importance of the Hf-W systematics of chondrites for calculating core formation

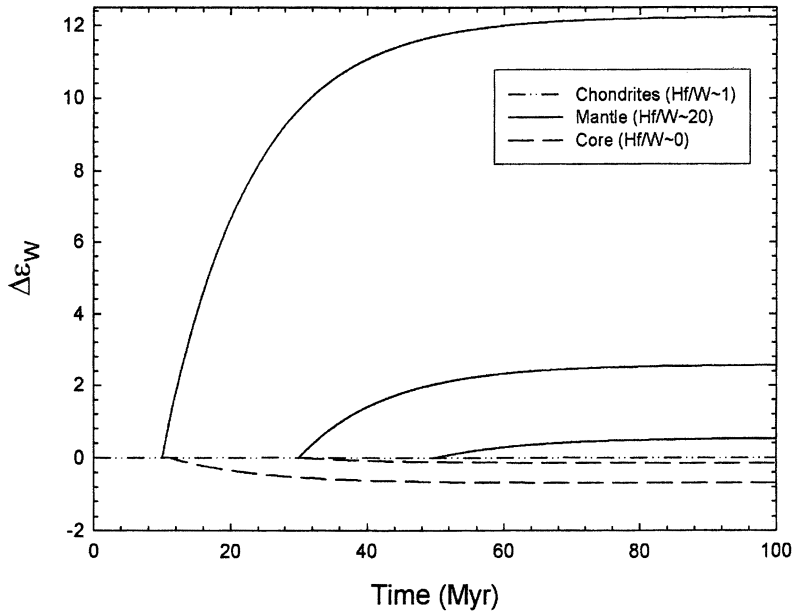


Figure 1. W isotope evolution in chondrites as well as mantle and core of a differentiated planet. Shown are hypothetical core formation events at 10, 30, and 50 Myr. For the 50 Myr event the evolution curve for the core is close to zero and not shown here. Note that the $\Delta\epsilon_W$ of chondrites is always zero. The $^{182}W/^{184}W$ ratio of the metal core does not change over time but its $\Delta\epsilon_W$ value evolves to more negative values over time (equation 9). Note the differences in ^{182}W anomalies that would develop depending on the time of core formation.

ages. Chondrites represent the W isotope evolution of the bulk planet and as such the reference for Hf-W core formation ages. The W isotope evolution of chondrites is defined by their present day $^{182}\text{W}/^{184}\text{W}$, their Hf/W ratio ($^{180}\text{Hf}/^{184}\text{W}=1.14 \times \text{Hf}/\text{W}$) and the initial $^{182}\text{Hf}/^{180}\text{Hf}$ of the solar system.

Hf-W Evolution of Chondrites

The first W isotope data for chondrites were presented by Lee and Halliday (1995, 1996) and were found to be identical to the terrestrial standard. In 2002, however, three groups independently showed that chondrites exhibit a small but resolvable ^{182}W deficit relative to the terrestrial standard (12-14). Figure 2 summarizes Hf-W data for chondrites and their components that define the ^{182}Hf - ^{182}W evolution of chondrites.

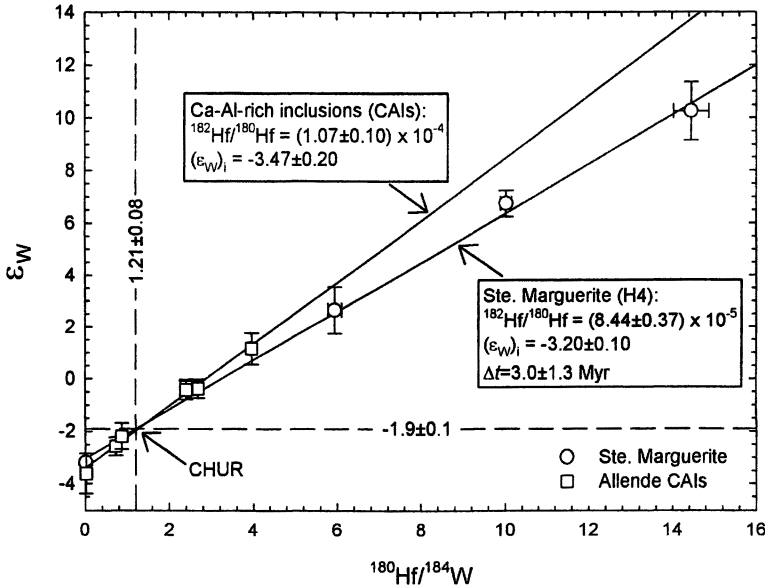


Figure 2. Hf-W data for chondrites and their components. The present-day $^{182}\text{W}/^{184}\text{W}$ and $^{180}\text{Hf}/^{184}\text{W}$ of the solar system is based on data from (12-14). The initial $^{182}\text{Hf}/^{180}\text{Hf}$ and $^{182}\text{W}/^{184}\text{W}$ ratios of the solar system are defined by the Hf-W isochron for CAIs. Note that the age difference between the Ste. Marguerite and CAI isochrons is consistent with the age difference between these two samples obtained from Pb-Pb systematics. Hf-W data for Ste. Marguerite from (12) and for CAIs from (5, 14).

Equation 7 illustrates that in a plot of $^{182}\text{W}/^{184}\text{W}$ vs. $^{180}\text{Hf}/^{184}\text{W}$ the slope of a linear regression corresponds to the $^{182}\text{Hf}/^{180}\text{Hf}$ at the time of formation. Thus, using a Hf-W isochron for a sample of independently known age, the $^{182}\text{Hf}/^{180}\text{Hf}$ at the start of the solar system can be calculated. The most direct approach to determine this value is to obtain a Hf-W isochron for Ca-Al-rich inclusions (CAIs) because these are the oldest objects that formed in the solar system. Their absolute age is usually taken as the age of the solar system. Hafnium-tungsten data for Allende CAIs define the initial $^{182}\text{Hf}/^{180}\text{Hf}$ of the solar system as $(1.07 \pm 0.10) \times 10^{-4}$ (5). The ordinary chondrite Ste. Marguerite has been dated with the ^{53}Mn - ^{53}Cr and ^{207}Pb - ^{206}Pb methods to be 3-4 Myr younger than CAIs (11, 15). The $^{182}\text{Hf}/^{180}\text{Hf}$ obtained for Ste. Marguerite (16) is lower than the $^{182}\text{Hf}/^{180}\text{Hf}$ of CAIs, indicating an age difference of 3.0 ± 1.3 Myr (calculated using equation 2). This is consistent with ages obtained from the ^{53}Mn - ^{53}Cr and ^{207}Pb - ^{206}Pb methods. Based on these data the solar system initial $^{182}\text{Hf}/^{180}\text{Hf}$ is well constrained to be $\sim 1 \times 10^{-4}$ and hence clearly lower than an earlier estimate of $\sim 2.75 \times 10^{-4}$ (17).

Model Ages for Instantaneous Core Formation

Once the W isotope evolution of chondrites is defined, the core formation age of a planetary body can be calculated from the $^{182}\text{W}/^{184}\text{W}$ and Hf/W ratios of its core or mantle (equation 10). Samples from the metal cores and silicate mantles from several differentiated bodies are available in the meteorite collections, such that core formation ages can be obtained for a range of different objects including several asteroids, Mars, the Moon and Earth.

Iron meteorite parent bodies

Magmatic iron meteorites are thought to be samples from the metal cores of differentiated asteroids (18) and as such are ideally suited for application of Hf-W chronometry. Iron meteorites contain virtually no Hf (i.e., Hf/W \sim 0), such that the timing of core formation in their parent bodies can be calculated from their $^{182}\text{W}/^{184}\text{W}$ alone. Tungsten isotope data are now available for a vast number of iron meteorites and their $^{182}\text{W}/^{184}\text{W}$ ratios are similar to or slightly lower than the initial $^{182}\text{W}/^{184}\text{W}$ of Allende CAIs. Taken at face value this would indicate that core formation in the iron meteorite parent bodies predated the formation of CAIs but the W isotope composition of many iron meteorites has been altered due to prolonged exposure to cosmic rays. The interaction with thermal neutrons produced by the cosmic rays affects the W isotopes to varying degrees because their neutron capture cross sections for thermal neutrons are different. Model

calculations show that the $^{182}\text{W}/^{184}\text{W}$ ratio of iron meteorites will decrease with an increasing thermal neutron flux (Figure 3). Iron meteorites with the longest exposure times have the lowest $^{182}\text{W}/^{184}\text{W}$ ratios, indicating that $^{182}\text{W}/^{184}\text{W}$ ratios lower than the initial value for Allende CAIs reflect ^{182}W burnout (Figure 3). Tungsten isotope data nevertheless permit dating of core formation in their parent bodies, either by correcting for the effects of ^{182}W burnout or by choosing samples having short exposure times.

Hafnium-tungsten ages for iron meteorites indicate that core formation in their parent bodies occurred within the first ~ 1.5 Myr of the solar system (5, 19, 20) and hence predated the formation of chondrules and chondrite parent bodies, which occurred between ~ 2 and ~ 5 Myr after the formation of CAIs [based on Al-Mg and Pb-Pb ages for chondrules (10, 21, 22)].

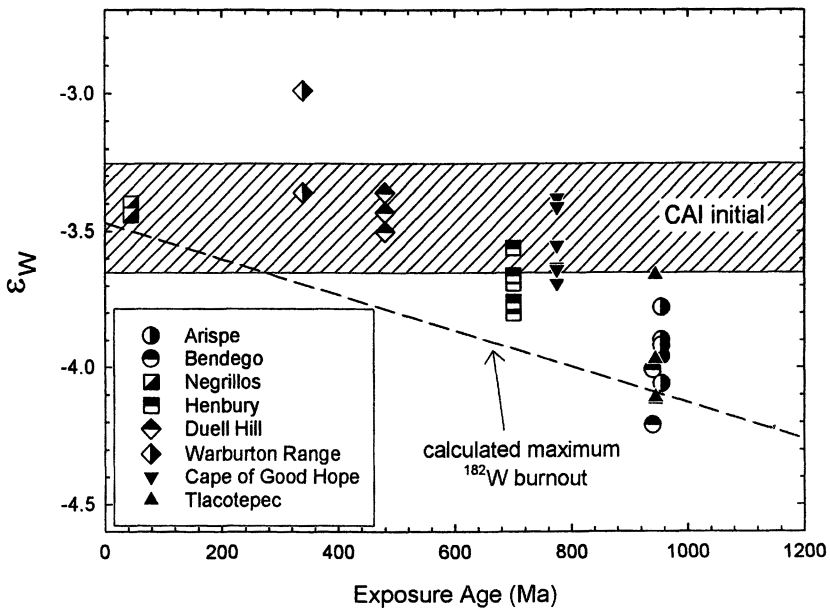


Figure 3. ϵ_W vs. exposure age for various iron meteorites. Iron meteorites having the oldest exposure ages also have the lowest ϵ_W values. The dashed line shows the maximum extent to which the ϵ_W values of iron meteorites can be lowered by interaction with thermal neutrons produced during cosmic-ray exposure (23). The hatched area indicates the initial ϵ_W of the solar system as determined from Hf-W data for Allende CAIs. Tungsten isotope data for iron meteorites are from (5, 19, 20, 24) and exposure ages are from (25).

This result is inconsistent with the standard model for asteroid formation, in which chondrites represent the precursor material from which asteroids accreted and then differentiated. The Hf-W ages for iron meteorites reveal that the opposite is the case, i.e., differentiated asteroids are the oldest planetesimals and undifferentiated asteroids (the chondrite parent bodies) formed later. This most likely reflects different abundances of ^{26}Al at the time of parent body accretion. Early formed bodies were heated by the decay of abundant ^{26}Al and could melt and differentiate into core and mantle, whereas later formed bodies remained undifferentiated because they contained too little ^{26}Al to cause melting and differentiation.

Vesta, Mars, Earth and Moon

Determining core formation ages for samples from planetary mantles is more complicated because the Hf/W ratio and in most cases also the $^{182}\text{W}/^{184}\text{W}$ ratio of the bulk mantle cannot be measured directly. The problem is that the Hf/W ratio of mantle-derived rocks (such as eucrites, lunar basalt or Martian meteorites) are the product of complex melting histories. During igneous processes, W is more incompatible (it goes into melts more readily) than Hf, resulting in Hf-W fractionation during partial melting (26). Melts have lower Hf/W ratio than their residues, such that the measured Hf/W ratios of igneous rocks are distinct from the Hf/W ratio of the bulk mantle of their parent body. Such Hf-W fractionations during igneous processes will result in variations in the $^{182}\text{W}/^{184}\text{W}$ ratios if they occurred during the lifetime of ^{182}Hf . Determining core formation ages based on samples from planetary mantles therefore requires estimates regarding the Hf/W and $^{182}\text{W}/^{184}\text{W}$ ratios of the bulk mantle.

Hf/W ratio of bulk planetary mantles

The Hf/W ratio of a bulk planetary mantle must be inferred by comparing the W concentrations with another element that behaves similarly during silicate melting (i.e., has a similar incompatibility), tends to stay in the mantle and whose abundance relative to Hf is known. The latter two conditions are met by refractory lithophile elements (RLE) because their relative abundances in bulk planetary mantles are chondritic (see above). This is because they are neither fractionated by core formation (because they are lithophile) nor by volatile element depletion (because they are refractory). The Hf/W ratio of a bulk planetary mantle can thus be calculated as follows:

$$\left(\frac{\text{Hf}}{\text{W}}\right)_{\text{mantle}} = \left(\frac{\text{RLE}}{\text{W}}\right)_{\text{mantle}} \times \left(\frac{\text{Hf}}{\text{RLE}}\right)_{\text{CHUR}} \quad (11)$$

where the subscript CHUR denotes chondritic uniform reservoir.

To infer the Hf/W ratio of a bulk planetary mantle it is thus critical to find a refractory lithophile element whose incompatibility is similar to that of W. Trace element studies on lunar and terrestrial basalts as well as eucrites show that La, Th, and U have similar incompatibilities as W (27, 28). From these studies the Hf/W ratios of the mantles of Earth, Moon, Mars and Vesta can be estimated to be ~ 20 , ~ 26 , ~ 4 , and ~ 35 , respectively.

$^{182}\text{W}/^{184}\text{W}$ ratios of bulk planetary mantles

Variations in $^{182}\text{W}/^{184}\text{W}$ ratios due to igneous Hf-W fractionations are observed for lunar samples, Martian meteorites and basaltic eucrites (16, 29-31). The $^{182}\text{W}/^{184}\text{W}$ of the bulk mantle of these planetary objects can be inferred using different approaches. The Hf-W data for basaltic eucrites form a linear array in a plot of $^{182}\text{W}/^{184}\text{W}$ vs. $^{180}\text{Hf}/^{184}\text{W}$ (i.e., a Hf-W isochron). From this array the initial $^{182}\text{W}/^{184}\text{W}$ and $^{182}\text{Hf}/^{180}\text{Hf}$ ratios for the eucrites can be calculated, and using equation 7 the $^{182}\text{W}/^{184}\text{W}$ of Vesta's mantle can be calculated from its Hf/W ratio of ~ 35 (16).

The $^{182}\text{W}/^{184}\text{W}$ ratios of Martian meteorites mainly fall into two groups (shergottites with $\epsilon_{\text{W}} \sim 0.2-0.4$ and nakhlites with $\epsilon_{\text{W}} \sim 2-3$). The shergottites appear to best represent the W isotope composition of the bulk Martian mantle because their $^{142}\text{Nd}/^{144}\text{Nd}$ ratios are close to the chondritic value. Neodymium-142 is the decay product of ^{146}Sm ($t_{1/2} \sim 103$ Myr) and igneous Hf-W fractionations in the source area of the shergottites during the lifetime of ^{182}Hf would be accompanied by Sm-Nd fractionations and, hence, deviations of the $^{142}\text{Nd}/^{144}\text{Nd}$ ratio from the chondritic value. This is not observed for the shergottites but is the case for nakhlites, such that the elevated $^{182}\text{W}/^{184}\text{W}$ of nakhlites can be attributed to igneous Hf-W fractionation within the Martian mantle (16, 31).

The $^{182}\text{W}/^{184}\text{W}$ ratios of lunar rocks have been difficult to determine because there is significant ^{182}W production via neutron-capture of ^{181}Ta during prolonged cosmic-ray exposure of the lunar surface (30, 32). This problem has now been overcome by analyzing metals from lunar basalts (30). These metals contain no Ta and hence no cosmogenic ^{182}W . Touboul et al. (33) obtained W isotope data for metals from a comprehensive set of lunar rocks and showed that probably all lunar samples have ϵ_{W} values of ~ 0 . Hence, the lunar and terrestrial mantles have identical W isotope compositions.

The $^{182}\text{W}/^{184}\text{W}$ ratio of the bulk silicate Earth is by definition $\epsilon_{\text{W}}=0$. No W isotope variations have yet been found in terrestrial samples, except the possibility for low $^{182}\text{W}/^{184}\text{W}$ ratios in a few Archean metasediments from Greenland that were attributed to incorporation of meteoritic material into these sediments (34).

Core formation model ages for Vesta, Mars, Earth and Moon

The Hf-W systematics of the metal cores (represented by magmatic iron meteorites, see above) and silicate mantles (represented by eucrites) of differentiated asteroids as well as of the Martian, lunar and terrestrial mantles are summarized in Figure 4. The model ages for core formation calculated from these parameters and equation 7 are shown in Figure 5.

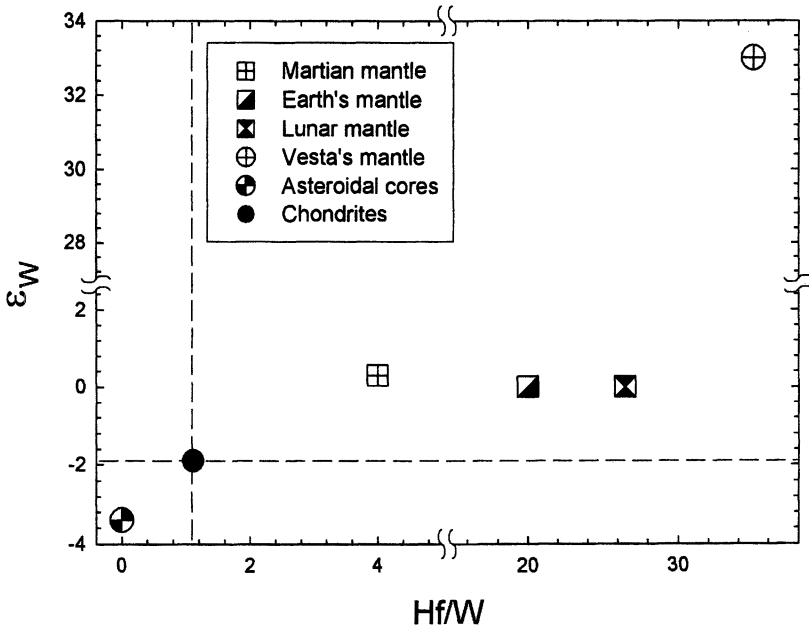


Figure 4. Hf/W fractionation and W isotope anomalies of mantles and cores of differentiated planetary bodies. The Hf-W systematics of bulk planets is represented by chondrites. Data from (5, 16, 19, 20, 29, 31).

Small objects such as the parent bodies of differentiated meteorites underwent core formation early, in less than a few Myr after formation of the solar system. Over these timescales the decay of ^{26}Al was a major heat source for differentiation. Accretion and differentiation of larger bodies such as Mars and Earth appear to have taken much longer, such that the energy required for differentiation was largely provided by collisions among planetary embryos. These Hf-W ages are consistent with numerical simulations that predict an early forma-

tion of planetesimals and planetary embryos and a more protracted accretion of terrestrial planets involving late-stage collisions (*I*).

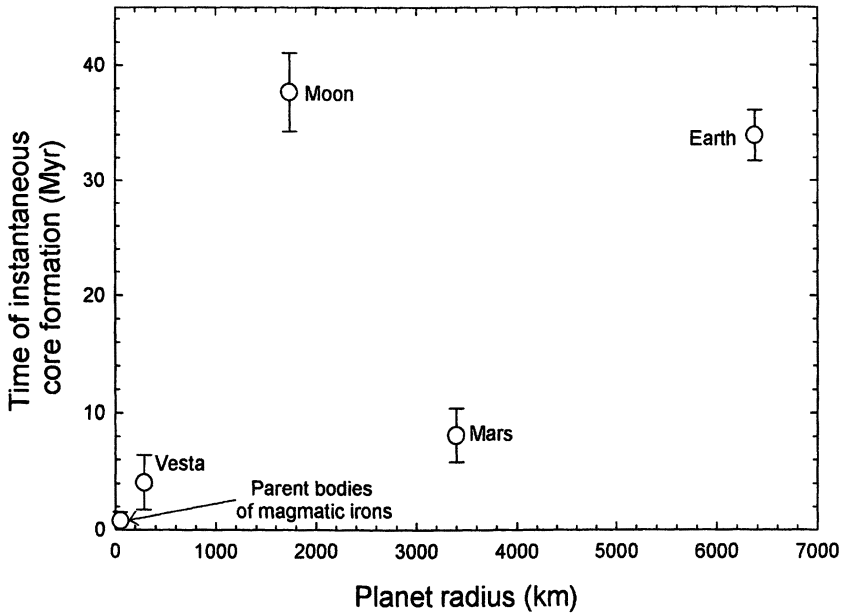


Figure 5. Model ages for instantaneous core formation in planetary bodies as a function of parent body size. Given the small size of the Moon, the W model age of the Moon is relatively young. This suggests that the Moon formed by a unique process, consistent with the giant impact hypothesis for the origin of the Moon.

The W model ages for core formation calculated using equation 7 assume that core formation occurred instantaneously. For differentiated asteroids this assumption probably is valid because accretion and differentiation occurred rapidly. For larger bodies like the Earth, however, accretion and differentiation occurred over longer timescales, such that the assumption of instantaneous core formation is not justified. For the Earth, the model age calculated using equation 7 would only date core formation if during this event the entire core was first remixed and homogenized with the entire mantle before segregating again. This seems physically implausible (35-37). The instantaneous core formation model ages nevertheless provide important age constraints. They assume that Earth's mantle had a chondritic W isotope composition at the time of its formation. This corresponds to the minimum $^{182}\text{W}/^{184}\text{W}$ Earth's mantle could have had at any time, such that the instantaneous core formation model ages correspond to the

earliest time core formation could have ceased (35). In other words, the earliest time the Earth's core could have been completely segregated is ~ 34 Myr after the start of the solar system.

Tungsten Isotopes and the Age of the Earth and Moon

Exponentially Decreasing Accretion with Concomitant Core Formation

For bodies the size of Earth, core formation did not occur as one single event but took place continuously during planetary growth. To determine realistic core formation ages for bodies like the Earth the W isotope evolution during continuous core formation must be considered (8, 35-38). During protracted accretion with concomitant core formation, the $^{182}\text{W}/^{184}\text{W}$ ratio of Earth's mantle reflects the contribution of two processes: (i) radiogenic ingrowth in the high Hf/W mantle; (ii) mixing with newly accreted material. The Hf-W data for differentiated meteorites provide evidence that Earth largely accreted from planetesimals already differentiated into mantle and core. Accretion of a differentiated object to Earth involves addition of the mantle of this object to Earth's mantle and addition of the core of the newly accreted object to the Earth's core. The W isotope composition of Earth's mantle after this event will largely depend on how much of the newly accreted core material first re-mixed and equilibrated with Earth's mantle before entering Earth's core. The $^{182}\text{W}/^{184}\text{W}$ ratio of Earth's mantle can therefore be expressed as a mixture of three components as follows:

$$\left(\frac{^{182}\text{W}}{^{184}\text{W}}\right)_{\text{BSE}}^{t_2} = \left\{ m_{\text{BSE}}^i \times [\text{W}]_{\text{BSE}} \times \left(\frac{^{182}\text{W}}{^{184}\text{W}}\right)_{\text{BSE}}^{t_1} + m_{\text{IM}} \times [\text{W}]_{\text{IM}} \times \left(\frac{^{182}\text{W}}{^{184}\text{W}}\right)_{\text{IM}} + F \times m_{\text{IC}} \times [\text{W}]_{\text{IC}} \times \left(\frac{^{182}\text{W}}{^{184}\text{W}}\right)_{\text{IC}} \right\} / \left\{ m_{\text{BSE}}^i \times [\text{W}]_{\text{BSE}} + m_{\text{IM}} \times [\text{W}]_{\text{IM}} + F \times m_{\text{IC}} \times [\text{W}]_{\text{IC}} \right\} \quad (12)$$

where BSE denotes bulk silicate Earth, IM and IC are impactor mantle and core, $[\text{W}]$ is concentration of W, and F is the fraction of the impactor's core that first equilibrates with the Earth's mantle before entering Earth's core.

The W isotope evolution of Earth's mantle during protracted accretion with continuous core formation can be calculated using equations 6 and 12 and assuming an accretion rate for the growth of Earth. A reasonable assumption is that the accretion of Earth took place at an exponentially decreasing accretion rate, such that

$$\frac{m}{M_E} = 1 - e^{-\frac{t}{\tau}} \quad (13)$$

where m/M_E is the cumulative fractional mass of the Earth at time t and τ is the accretionary mean life (i.e., the inverse of the time constant of accretion $\lambda=1/\tau$).

Figure 6 shows the growth curve of Earth calculated by assuming accretionary mean-lives τ of 11 and 22 Myr. Using these growth curves and equations 6 and 12 the $^{182}\text{W}/^{184}\text{W}$ evolution of Earth's mantle can be calculated for each value of τ . Thus, in principle, the accretion rate of Earth can be determined by finding the τ value that yields the present day $^{182}\text{W}/^{184}\text{W}$ ratio of Earth's mantle.

This is illustrated in Figure 6 where the W isotope evolution curves for the Earth's mantle and core as well as for the planetesimals that accrete to Earth are shown. In this calculation it is assumed that the planetesimals differentiated at T_0 (i.e., the start of the solar system) and that the Hf/W ratio in their mantles always was the same than the present-day Hf/W ratio of the Earth's mantle. Furthermore it is assumed that the metal cores of newly accreted planetesimals always entirely re-equilibrated with Earth's mantle before entering Earth's core (i.e., $F=1$ in equation 9). With these assumptions, the present-day $\Delta\epsilon_W$ of Earth's mantle of +1.9 can be produced if Earth accreted with an accretionary mean-life τ of 11 Myr. Using equation 13 this corresponds to 63% growth at 11 Myr (14) and to 99% growth at ~53 Myr (35).

How well are these assumptions justified? Hafnium-tungsten data for differentiated meteorites indicate that accretion and differentiation of their parent bodies occurred very early (see above). Bodies that formed so early would have melted and differentiated due to accumulation of radiogenic heat produced by decay of abundant ^{26}Al . Earth therefore most likely accreted from pre-differentiated planetesimals. The other assumptions, i.e., constant Hf/W ratios and complete metal-silicate re-equilibration, are less well constrained. The effects that changes in these two parameters have on the W isotope evolution of Earth's mantle are shown in Figure 7.

Metal-silicate re-equilibration during accretion and core formation serves to reduce the ^{182}W excess in Earth's mantle that built up due to ^{182}Hf decay. Consequently, a decreasing degree of metal-silicate re-equilibration (i.e., decreasing F values) will, for a given accretion rate, result in an increasingly radiogenic W isotope composition of Earth's mantle. Thus, to match the present-day W isotope composition of Earth's mantle, a decreasing degree of metal-silicate re-equilibration must be accompanied by longer accretion timescales (Figure 7).

Similar effects are observed if it is assumed that the Hf/W ratio in the mantles of newly accreting planetesimals was different from the value observed in Earth's mantle today. This is likely because the metal-silicate distribution coefficient for W is sensitive to many variables such as pressure, temperature, melt

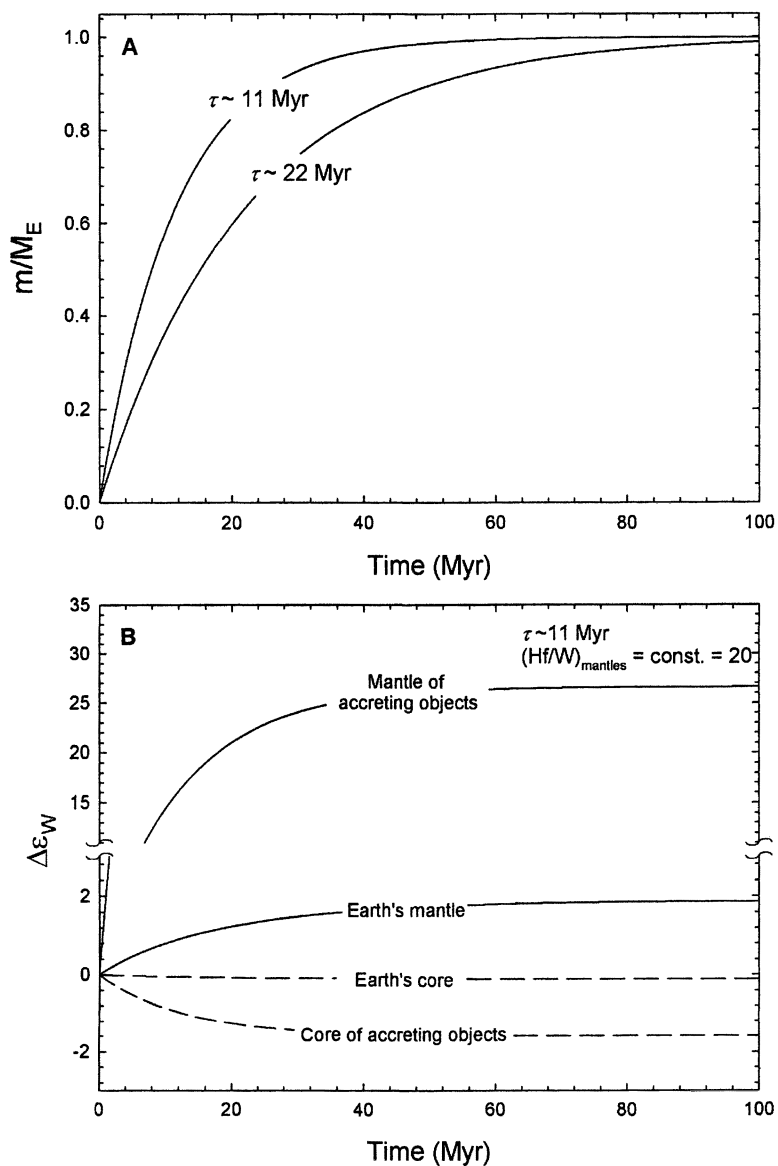


Figure 6. A. Growth curves for the Earth calculated using equation 12 and assuming $\tau = 11$ and $\tau = 22$ Myr. B. W isotope evolution for Earth's mantle and core and for the planetesimals that accrete to Earth. For details see text.

compositions, and particularly oxygen fugacity (39). These parameters likely were different in the various objects that combined to form Earth and also probably changed over time, such that considerable variability in the mantle Hf/W ratios is expected. A mantle with a relatively low Hf/W ratio will never develop a large ^{182}W excess, such that, upon accretion of such an object to Earth, the W isotope composition of Earth's mantle can stay at a relatively low value even without significant metal-silicate re-equilibration. Thus, changes in the Hf/W ratios of the mantles of newly accreting objects and different values of F have similar effects on the W isotope evolution of the Earth's mantle. For instance, assuming $F=1$ and $\text{Hf}/\text{W}=20$ in the mantles of the accreting planetesimals yields the same result as assuming $F=0.7$ and $\text{Hf}/\text{W}=4$ (Figure 7).

The Effects of Giant Impacts

In the models discussed above, it is assumed that accretion of the Earth occurred at an exponentially decreasing accretion rate. The real accretion process however likely involved several large impacts (*I*). Giant impacts bring in large core masses at once and therefore significantly affect the W isotope evolution of Earth's mantle. To illustrate the effects of giant impacts on the calculated core formation ages, W isotope evolution curves for two accretion scenarios are shown in Figure 8. In both models, 82% of the metal cores of newly accreted planetesimals re-equilibrated with Earth's mantle (i.e., $F=0.82$) and the Hf/W ratios in the mantles of the Earth and the newly accreting planetesimals were constant. In the first model however, Earth accreted at an exponentially decreasing rate with no giant impacts, whereas in the second model the final mass of Earth was reached by a giant impact at ~ 40 Myr. In both models the present-day $\Delta\epsilon_{\text{W}}$ value of Earth's mantle is obtained, but in the first model Earth reaches 99% of its mass at ~ 61 Myr, whereas in the second model 99% of Earth is accreted at ~ 40 Myr. Therefore, different assumptions regarding the mechanisms of accretion cause significant changes in the calculated core formation ages (35-38).

The Age of the Moon and W Isotope Constraints on the Mechanisms of Terrestrial Core Formation

The calculation of core formation ages based on Hf-W observations is strongly model-dependent. The W isotope evolution of Earth's mantle does not only depend on the timescale of accretion and core formation, but also on the degree of re-equilibration between the metal cores of newly accreted planetesimals, the W isotope composition in the mantles of the newly accreted objects, and on the mechanisms of accretion. Hence, Hf-W chronometry alone cannot

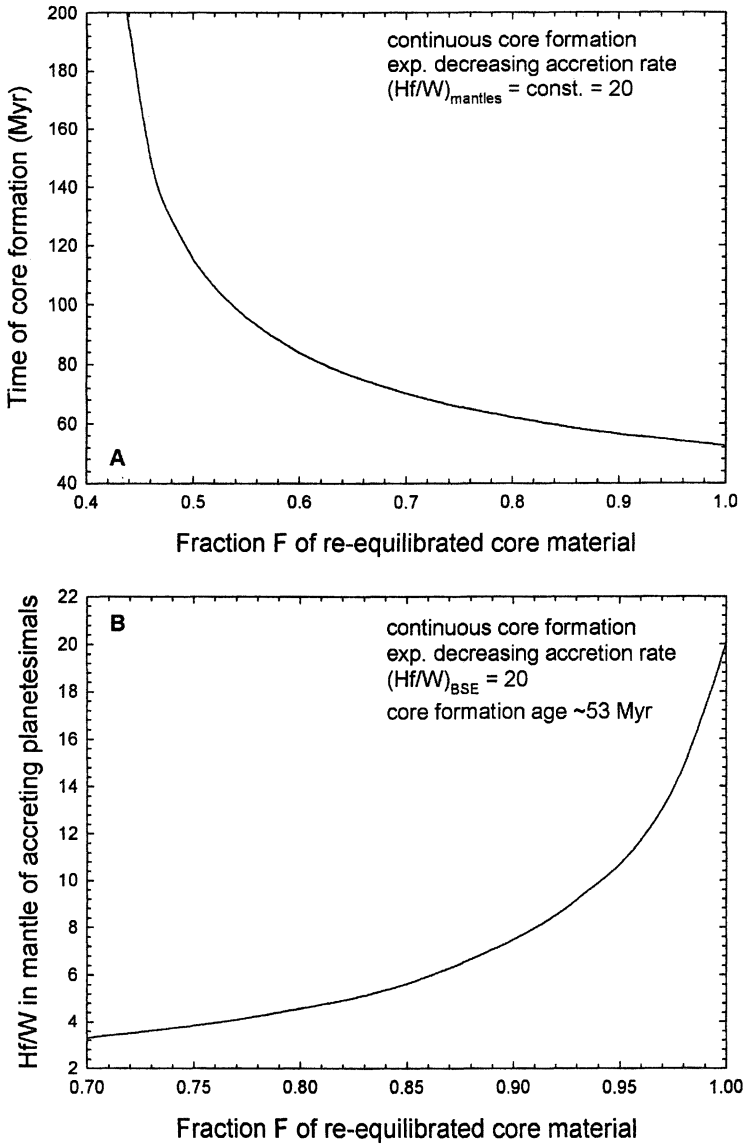


Figure 7. A. Core formation ages (corresponding to 99% growth) as a function of the assumed degree of metal-silicate re-equilibration during core formation. B. Relation between Hf/W ratio in the mantle of accreting planetesimals and the degree of metal-silicate re-equilibration during core formation.

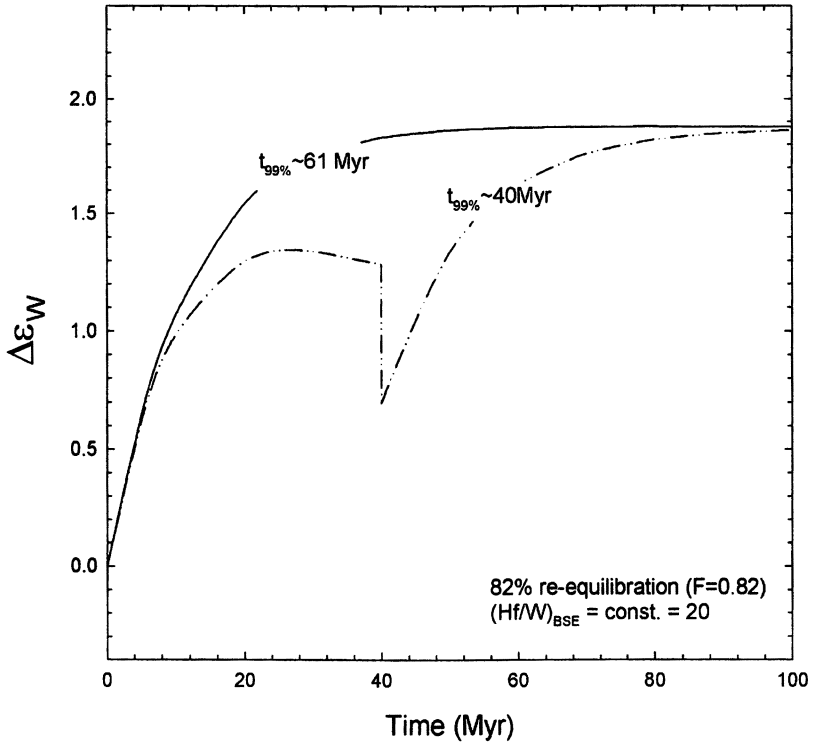


Figure 8. *W* isotope evolution of Earth's mantle in two different accretion scenarios. Exponentially decreasing accretion where 99% of Earth's mass is reached at ~ 61 Myr results in the same present-day *W* isotope composition of Earth's mantle as does accretion involving a large impact at ~ 40 Myr

provide an exact age of the Earth. Conversely, if independent age constraints for the formation of the Earth are available, the W isotope composition of Earth's mantle might be used to constrain the processes of accretion and core formation.

Most numerical simulations of the Moon-forming impact indicate that the Moon formed at the very end of Earth's accretion (40). The age of the Moon therefore can provide an independent constraint on the age of the Earth. The time of the giant impact has yet not been dated directly, but the oldest ages thus far reported for lunar samples provide a lower age limit for the formation of the Moon. Several chronometers applied to lunar samples date the formation of a particular sample (in most cases its crystallization from a melt) or large-scale differentiation within the lunar mantle (e.g., crystallization of the lunar magma ocean). The oldest dated lunar rocks are ferroan anorthosites, which exhibit ages ranging from 4.56 to 4.29 billion years (Ga) (41-43). Most estimates for the minimum age of the Moon are between 4.42 and 4.45 Ga (44). Using I-Pu-Xe dating, Swindle et al. (45) estimated the age of the Moon to 63 ± 42 Myr after the start of the solar system. These age estimates indicate that the Moon, and by inference the Earth's core, cannot have formed later than ~ 100 Myr after the start of the solar system (i.e., ~ 4.47 Ga).

Using a ~ 100 Myr age of the Earth, W isotopes can be used to constrain the mechanisms and conditions of terrestrial core formation. The ~ 100 Myr age in conjunction with the accretion models outlined above (Figures 7 and 8) reveals that there are two endmember interpretations of the W isotope record. Either the degree of metal-silicate re-equilibration during core formation was high (35) or Earth largely accreted from objects having relatively low Hf/W ratios in their mantles (36). The latter would imply relatively oxidizing conditions (because the siderophile character of W decreases with increasing oxygen fugacity) but most accretion scenarios predict that the conditions during accretion started off reducing and became more oxidizing with time (46, 47). Hence, the ^{182}W record of Earth's mantle seems to require that more than $\sim 50\%$ of the metal cores of newly accreted planetesimals first re-equilibrated with Earth's mantle before entering the core. This probably can only be achieved if the metal cores become highly fragmented and emulsified in the magma ocean, such that small metal droplets could rapidly equilibrate with the surrounding silicate melt.

Conclusions

Hafnium-tungsten chronometry, thermal modeling of asteroids, numerical simulations of planetary accretion, and experimental petrology combine to provide a consistent picture for the formation and early evolution of planetary bodies in the inner solar system. Thermal modeling indicates that heating by ^{26}Al decay will cause planetesimals that accreted within the first ~ 1 Myr of the solar

system to melt and differentiate (48). Owing to its short half-life, the abundance of ^{26}Al decreases rapidly and planetesimals that formed later than ~ 2 Myr did not contain sufficient ^{26}Al to cause melting and differentiation. Later-formed asteroids should therefore remain undifferentiated. Hafnium-tungsten chronometry shows that this is exactly what happened. Iron meteorites derive from asteroids that accreted and differentiated within less than ~ 1.5 Myr after the start of the solar system, whereas chondrites derive from asteroids that remained undifferentiated because they formed later than ~ 2 Myr.

The evolution of larger bodies such as the Earth was different from those of the meteorite parent bodies, mainly because large collisions were important in the evolution of the former. The formation of the Earth occurred over more than ~ 34 Myr, such that decay of ^{26}Al cannot have been an important heat source for differentiation. Large collisions instead released sufficient energy to cause melting and the formation of magma oceans, in which silicate and metal melts could separate efficiently. Both, the abundances of moderately siderophile elements (46, 47, 49) and the W isotope composition of Earth's mantle indicate a high degree of metal-silicate equilibration during core formation. This can only have been achieved in a magma ocean. The Moon probably formed at the very end of Earth's accretion and the age of this event would also provide the best estimate for the age of the Earth. The age of the Moon, however, has yet not been determined directly but this may become possible with further analytical developments.

Acknowledgements

I thank K. Mezger and H. Palme for their constant support and L. Zaikowski and J. Friedrich for inviting me to write this review. Thorough and constructive reviews by L. Zaikowski and H. Palme improved the manuscript. This work was supported by the Deutsche Forschungsgemeinschaft as part of the research priority program "Mars and the terrestrial planets" and by a EU Marie Curie post-doctoral fellowship to Thorsten Kleine.

References

1. Chambers, J.E. *Earth Planet. Sci. Lett.*, **2004**, *223*, 241-252.
2. Walter, M.J.; Tronnes, R.G. *Earth Planet. Sci. Lett.*, **2004**, *225*, 253-269.
3. Stevenson, D.J., *Fluid dynamics of core formation*, in *Origin of the Earth*, H.E. Newsom and J.E. Jones, Editors. 1990, Oxford University Press: New York. p. 231-249.
4. Grimm, R.E.; McSween, H.Y. *Science*, **1993**, *259*, 653-655.

5. Kleine, T.; Mezger, K.; Palme, H.; Scherer, E.; Münker, C. *Geochim. Cosmochim. Acta*, **2005**, *69*, 5805-5818.
6. Bizzarro, M.; Baker, J.A.; Haack, H.; Lundgaard, K.L. *Astrophys. J.*, **2005**, *632*, L41-L44.
7. Harper, C.L.; Volkening, J.; Heumann, K.G.; Shih, C.Y.; Wiesmann, H. *Lunar Planet. Sci.*, **1991**, *XXII*, 515-516.
8. Harper, C.L.; Jacobsen, S.B. *Geochim. Cosmochim. Acta*, **1996**, *60*, 1131-1153.
9. Lee, D.C.; Halliday, A.N. *Nature*, **1995**, *378*, 771-774.
10. Amelin, Y.; Krot, A.N.; Hutcheon, I.D.; Ulyanov, A.A. *Science*, **2002**, *297*, 1678-1683.
11. Bouvier, A.; Blichert-Toft, J.; Moynier, F.; Vervoort, J.D.; Albarede, F. *Geochim. Cosmochim. Acta*, **2007**, *71*, 1583-1604.
12. Kleine, T.; Münker, C.; Mezger, K.; Palme, H. *Nature*, **2002**, *418*, 952-955.
13. Schoenberg, R.; Kamber, B.S.; Collerson, K.D.; Eugster, O. *Geochim. Cosmochim. Acta*, **2002**, *66*, 3151-3160.
14. Yin, Q.Z.; Jacobsen, S.B.; Yamashita, K.; Blichert-Toft, J.; Telouk, P.; Albarede, F. *Nature*, **2002**, *418*, 949-952.
15. Polnau, E.; Lugmair, G.W. *Lunar Planet. Sci.*, **2001**, *XXXII*, 1527.pdf.
16. Kleine, T.; Mezger, K.; Münker, C.; Palme, H.; Bischoff, A. *Geochim. Cosmochim. Acta*, **2004**, *68*, 2935-2946.
17. Lee, D.C.; Halliday, A.N. *Chem. Geol.*, **2000**, *169*, 35-43.
18. Scott, E.R.D.; Wasson, J.T. *Rev. Geophys.*, **1975**, *13*, 527-546.
19. Markowski, A.; Quitté, G.; Halliday, A.N.; Kleine, T. *Earth Planet. Sci. Lett.*, **2006**, *242*, 1-15.
20. Schersten, A.; Elliot, T.; Hawkesworth, C.; Russell, S.S.; Masarik, J. *Earth Planet. Sci. Lett.*, **2006**, *241*, 530-542.
21. Kita, N.T.; H., N.; Togashi, S.; Morishita, Y. *Geochim. Cosmochim. Acta*, **2000**, *64*, 3913-3922.
22. Kunihiro, T.; Rubin, A.E.; McKeegan, K.D.; Wasson, J.T. *Geochim. Cosmochim. Acta*, **2004**, *68*, 2947-2957.
23. Leya, I.; Wieler, R.; Halliday, A.N. *Geochim. Cosmochim. Acta*, **2003**, *67*, 529-541.
24. Lee, D.C. *Earth Planet. Sci. Lett.*, **2005**, *237*, 21-32.
25. Voshage, H.; Feldmann, H. *Earth Planet. Sci. Lett.*, **1979**, *45*, 293-308.
26. Righter, K.; Shearer, C.K. *Geochim. Cosmochim. Acta*, **2003**, *67*, 2497-2507.
27. Palme, H.; Rammensee, W. *Proc. 12th Lunar Planet. Sci. Conf.*, **1981**, 949-964.
28. Palme, H.; Rammensee, W. *Lunar Planet. Sci.*, **1981**, *XII*, 796-798.
29. Lee, D.C.; Halliday, A.N. *Nature*, **1997**, *388*, 854-857.
30. Kleine, T.; Palme, H.; Mezger, K.; Halliday, A.N. *Science*, **2005**, *310*, 1671-1674.

31. Foley, C.N.; Wadhwa, M.; Borg, L.E.; Janney, P.E.; Hines, R.; Grove, T.L. *Geochim. Cosmochim. Acta*, **2005**, *69*, 4557-4571.
32. Leya, I.; Wieler, R.; Halliday, A.N. *Earth Planet. Sci. Lett.*, **2000**, *175*, 1-12.
33. Touboul, M.; Kleine, T.; Bourdon, B.; Palme, H.; Wieler, R. *Geochim. Cosmochim. Acta*, **2007**, *71*, in press.
34. Schoenberg, R.; Kamber, B.S.; Collerson, K.D.; Moorbath, S. *Nature*, **2002**, *418*, 403-405.
35. Kleine, T.; Mezger, K.; Palme, H.; Scherer, E.; Münker, C. *Earth Planet. Sci. Lett.*, **2004**, *228*, 109-123.
36. Halliday, A.N. *Nature*, **2004**, *427*, 505-509.
37. Nimmo, F.; Agnor, C.B. *Earth Planet. Sci. Lett.*, **2006**, *243*, 26-43.
38. Jacobsen, S.B. *Annual Reviews in Earth and Planetary Science Letters*, **2005**, *33*, 531-570.
39. Walter, M.J.; Thibault, Y. *Science*, **1995**, *270*, 1186-1189.
40. Canup, R.M.; Asphaug, E. *Nature*, **2001**, *412*, 708-712.
41. Carlson, R.W.; Lugmair, G.W. *Earth Planet. Sci. Lett.*, **1988**, *90*, 119-130.
42. Alibert, C.; Norman, M.D.; McCulloch, M.T. *Geochim. Cosmochim. Acta*, **1994**, *58*, 2921-2926.
43. Borg, L.E.; Norman, M.; Nyquist, L.; Bogard, D.; Snyder, G.; Taylor, L.; Lindstrom, M. *Geochim. Cosmochim. Acta*, **1999**, *63*, 2679-2691.
44. Wasserburg, G.J.; Papanastassiou, D.A.; Tera, F.; Huneke, J.C. *Phil. Trans. Roy. Soc. London*, **1977**, *285*, 7-22.
45. Swindle, T.D.; Caffee, M.W.; Hohenberg, C.M.; Taylor, S.R., *I-Pu-Xe dating and the relative ages of the Earth and Moon*, in *Origin of the Moon*, W. Hartmann, R. Phillips, and G.J. Taylor, Editors. 1986, Lunar and Planetary Institute: Houston. p. 331-357.
46. Righter, K. *Ann. Rev. Earth Planet. Sci.*, **2003**, *31*, 135-174.
47. Wade, J.; Wood, B.J. *Earth Planet. Sci. Lett.*, **2005**, *236*, 78-95.
48. Hevey, P.J.; Sanders, I.S. *Met. Planet. Sci.*, **2006**, *41*, 95-106.
49. Rubie, D.C.; Melosh, H.J.; Reid, J.E.; Liebske, C.; Righter, K. *Earth Planet. Sci. Lett.*, **2003**, *205*, 239-255.

Part III: Prebiotic Chemistry

Chapter 12

Cosmic Carbon Chemistry

P. Ehrenfreund¹ and M. Spaans²

¹Leiden Institute of Chemistry, Astrobiology Laboratory, P.O. Box 9502,
2300 RA Leiden, The Netherlands

²Kapteyn Astronomical Institute, P.O. Box 800, 9700 AV Groningen,
The Netherlands

The complexity of carbonaceous molecules and their abundance and timescale of formation in our evolving universe are crucial questions within cosmic chemistry. Interestingly, the organic chemistry in space seems to follow common pathways throughout space and time. Carbonaceous molecules in the gas or solid state, refractory or icy, are observed in similar abundances and composition in our and distant galaxies. Observations of galaxies at high red-shift, probes into the early universe, show carbonaceous molecules and dust formation. The largest fraction of carbon in the universe is incorporated into aromatic molecules such as gaseous polycyclic aromatic hydrocarbons as well as solid aromatic structures. Molecular clouds are the birthplace of stars, planets and small bodies. Therefore, a lineage between carbon reservoirs in the interstellar medium and in the solar system is expected. We attempt to compile the current knowledge on the connection between interstellar and solar system material, based on observations of interstellar dust and gas, cometary volatiles, simulation experiments, and the analysis of extraterrestrial matter. Those combined results are used to investigate the most abundant and stable carbonaceous material that was delivered to young planets and probably used to build life.

Introduction

Carbon is found in space in all its allotropic forms: diamond, graphite and fullerene (1). Astronomical observations in the last decade have shown that carbonaceous compounds (gaseous molecules and solids) are ubiquitous in our own as well as far distant galaxies (2). This indicates that pathways leading to the formation of carbon-based molecules and macromolecules proceed in similar ways throughout the universe. The first chemical enrichment of the universe may likely be connected to old stars that can no longer be observed. Carbon in space was first produced in stellar interiors in fusion reactions and was later expelled in interstellar and intergalactic space during stellar collapse and supernova explosions. In the denser regions of interstellar space, the so called interstellar clouds, active chemical pathways form simple and complex carbon molecules from carbon atoms. Circumstellar envelopes are regarded as the largest factories of carbon chemistry in space.

Interstellar matter provides the raw material for the formation of stars and planets. Approximately 4.6 billion years ago the collapse of an interstellar cloud led to the formation of our solar system made of planets and small bodies such as comets and asteroids. Volatile and robust carbon compounds residing in interstellar clouds were recycled during solar system formation. The carbonaceous inventory of our solar system therefore contains highly processed material that was exposed to high temperature and radiation, newly formed compounds and some relative pristine material with strong interstellar heritage. Organic compounds observed or sampled from our solar system such as planetary surfaces/atmospheres, comets and interplanetary dust hold the clue to processes that occurred during the origin of our solar system (3,4).

In the inner solar system where planets like Earth formed, only rocky material could stand the great heat. Ices were sublimed and existing carbon material (volatile and refractory) was combusted. Therefore, organic molecules found on terrestrial planets must have formed after the planetary surface had cooled down, or were delivered via impacts from random floating small bodies in the young solar system. Part of this material may have been important starting material for life (5). As our knowledge of the composition of interstellar dust and gas, comets, asteroids and meteorites grows, we can determine more accurately the molecular inventory of material that was transported to young planets by exogenous delivery. How elements are formed, how complex carbonaceous molecules in space are, what their abundance is and on what timescales they form are crucial questions within cosmochemistry. In this paper we review the individual steps of cosmic carbon chemistry from element formation to life's start-up material. Figure 1 shows the cycle of carbon chemistry in space.

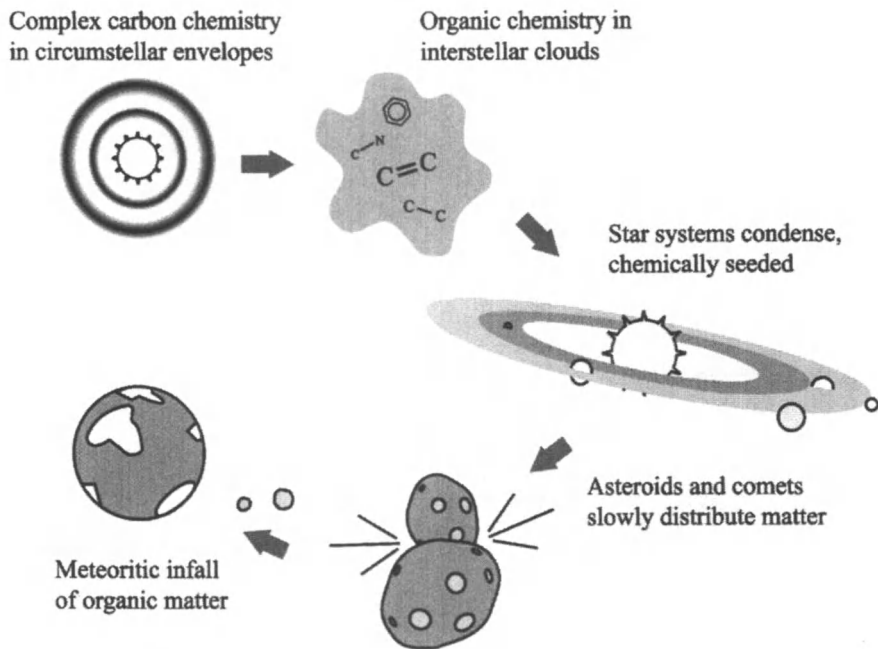


Figure 1. The carbon pathways between interstellar and circumstellar regions and the forming solar system.

Formation of the Elements – The First Stars

The universe is estimated to be approximately 13.7 billion years old. During big bang nucleosynthesis, only H and He and traces of a few other light nuclei such as D, T, Li and Be were formed. Since the universe was expanding, cooling and decreasing in density, heavier elements could not be formed during its early history, up to 100 million years after the big bang. Carbon, the basis of organic chemistry, is produced by the so-called triple- α process ($3 \times {}^4\text{He} \rightarrow {}^{12}\text{C}$) in the cores of stars. Today, stars more massive than half a solar mass form carbon after they have fused a significant fraction of their core hydrogen into helium. In the same cores, some carbon is further processed to the principal isotope of oxygen by ${}^{12}\text{C} + {}^4\text{He} \rightarrow {}^{16}\text{O}$. During the stellar burning cycle, contraction and heating of the stellar core alternates with a cycle of expansion and cooling. In this way heavier elements (until ${}^{56}\text{Fe}$) are produced in more massive stars. ${}^{56}\text{Fe}$ has the greatest nuclear binding energy and is unable to fuse with other nuclei to produce energy. The accumulation of ${}^{56}\text{Fe}$ in the stellar core

destabilizes the star and triggers stellar collapse. All elements heavier than iron are formed during the final evolutionary period of stars dominated by mass loss, core degradation and stellar explosions. When a star has exhausted its fuel and explodes as a nova or supernova it enriches interstellar gas with the elements that it has formed. The cosmic (or solar) abundances of the chemical elements are summarized in Table I. Note that it is common practice in astronomy to refer to elements heavier than helium as 'metals'.

Fundamental to the existence of a carbon chemistry then is the synthesis and dispersal of carbon by stars. Recent cosmological simulations indicate that the formation of the first stars (so called population III or zero metallicity stars) may have occurred as early as 200 million years after the big bang (8). These very

Table I. Solar abundances of Selected Elements

<i>Element</i>	<i>Solar Abundance</i>
H	1.0
D	1.5×10^{-5}
He	7.5×10^{-2}
C	4.0×10^{-4} a)
^{13}C	7.8×10^{-6}
O	8.3×10^{-4}
^{18}O	1.7×10^{-6}
N	1.0×10^{-4}
Cl	1.1×10^{-7}
S	1.7×10^{-5}
Si	4.3×10^{-5}
P	2.8×10^{-7}
Na	2.1×10^{-6}
Li	2.2×10^{-9}
Ca	2.2×10^{-6}
Mg	4.2×10^{-5}
Fe	4.3×10^{-5}
Mn	2.6×10^{-7}
Al	3.1×10^{-6}
K	1.3×10^{-7}
Ti	1.2×10^{-7}
Cr	4.4×10^{-7}
Ni	1.7×10^{-6}
Zn	4.0×10^{-8}
Rb	4.0×10^{-10}
Co	7.9×10^{-8}

Abundances scaled to H, taken from Reference (6) and a) Reference (7)

massive stars (probably several hundred solar masses) are born from gravitationally contracting gas clouds dominated by the elements hydrogen and helium in dark matter halos. Trace amounts of molecular hydrogen, formed through $H + e \rightarrow H^-$ and $H^- + H \rightarrow H_2 + e^-$, allow clouds of gas to cool and contract from temperatures of more than 10,000 K to about 200 K, as follows. The kinetic energy involved in collisions between H and H₂ causes molecular hydrogen to be excited rotationally. Spontaneous decay then yields mid-infrared photons that escape the cloud and carry away heat. It is this ability to cool down gas that allows gravity to form high density, $\sim 10^3$ - 10^4 cm⁻³, compact cores, of about 100-1,000 solar masses. The masses of population III stars are high since the ability of the primordial gas to cool is much smaller than that for a gas enriched in metals. Consequently, the Jeans mass (above which gravitational collapse becomes very likely) is large, up to 1,000 solar masses (9). The formed core then experiences a collapse to form an object/star with densities more than 200 g cm⁻³ and temperatures more than 20 million K that are even higher than inside our sun. These supermassive stars can no longer be observed because they explode after less than 30 million years and often leave a black hole as a remnant. As they explode large amounts of 'metals', in particular carbon and oxygen, are distributed. Subsequently dust is synthesized and dispersed throughout the universe (10).

The recent detection of hyper metal-poor stars (HMPs) provides important constraints for these early star formation processes (11, 12). The observed HMP stars have a Fe/H ratio less than 1/100,000 of the solar ratio. They have an overabundance in C and O relative to Fe, and are slightly less massive than the sun. Their modest masses allow them to exist for longer than 10 billion years, and thus to act as "fossil" records. Investigations of those stars may provide clues regarding the properties of the initial generation of stars and supernovae that distributed the first heavy elements in the early universe. Carbon appears to be favored as a formation product of the first generation of stars.

The cycle of birth and death of stars that is initiated by population III stars constantly increases the abundance of heavy elements in the interstellar medium, a crucial prerequisite for terrestrial (rocky) planet formation and subsequently for the origin of life (13). 'Metals' dispersed in the interstellar gas or incorporated into micron-sized dust particles and molecules like CO and water, have the ability to cool the interstellar gas much more efficiently than molecular hydrogen does for population III stars. These elements and molecules are also excited through atomic and molecular collisions and their return to lower lying energy levels releases energy via far-infrared and sub-millimeter radiation below 1,000 K. Unlike H₂, metals and molecules can cool interstellar gas down to 10 K. In turn, this more efficient cooling of the interstellar gas influences cloud fragmentation because low temperatures yield low pressures and thus less mass is needed for gravitational collapse to ensue. This metal enhanced fragmentation

triggers the formation of low-mass stars like our sun (14,15). Low-mass stars have long life spans (e.g. the sun has a stable lifetime of ~10 billion years) that allow sufficient time to form terrestrial planets and allow life to evolve. High mass stars typically live for less than 500 million years.

With the existence of 'metals' and dust, one expects the efficient formation of molecules like CO, water, hydrides and carbon chains (16). Indeed, high excitation CO emissions from the most distant quasar currently known at redshift $z = 6.419$ have been detected, indicating that CO, an important coolant of interstellar gas, has been present in the universe since approximately 800 millions years after the big bang (17). Clearly, an active chemistry was occurring already in the earliest epochs of the universe. That this one object with a significant amount of carbon is not a fluke, is shown in Figure 2, where the relative amount of carbon is presented as a function of redshift. In this, redshifts of 1 and 6 mean 35% and 7% of the present age of the universe. Clearly, carbon and thus star formation was already very much present in the young universe (18). Understanding the early universe is extremely relevant to the question of terrestrial planet formation and consequently life. Observations and theory in the last decade indicate that star formation and heavy element enrichment occurred much earlier than previously thought (19).

From Elements to Molecules

The step from atoms to molecules occurs in the more dense regions of interstellar clouds and circumstellar envelopes. Those regions can be regarded as nurseries for complex molecules and siliceous and carbonaceous micron-sized dust particles. H_2 is by far the most abundant molecule in these clouds. CO is the most abundant carbon-containing species, with $CO/H_2 \sim 10^{-4}$. More than 140 gas-phase molecules, have been identified in interstellar and circumstellar space (20). Spectroscopic evidence derived from astronomical observations indicates the presence of amorphous carbon, hydrogenated amorphous carbon, diamonds, and a more refractory organic component that could resemble carbonaceous networks such as coal, soot, graphite, quenched-carbonaceous condensates (21,22). How are those compounds formed?

The interstellar medium constitutes ~10 % of the mass of the galaxy. It can be subdivided into environments with very low-density hot gas, environments with warm intercloud gas, and regions with denser and colder material (23). H and He gas are the major components of interstellar clouds; molecules and submicron dust particles are only present in small concentration (22). Through gas phase reactions and solid-state chemistry, gas-grain interactions can build up complex organic molecules. Silicate and carbon-based micron-sized dust particles provide a catalytic surface for a variety of reactions when they are dispersed in dense molecular clouds (24). In cold clouds such dust particles

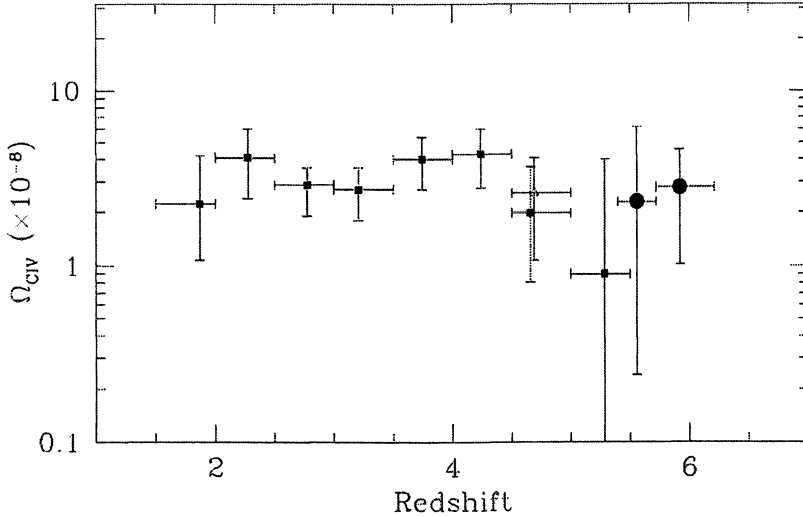


Figure 2. The evolution of the intergalactic ion C IV (C^{3+}) abundance as a function of redshift, in units of its contribution to the closing density. The constancy of the curve indicates that vigorous star formation was already underway when the universe was only 7% (where redshift is 6) of its present age. Credit: Robert A. Simcoe (18).

adsorb ice mantles of water, CO_2 , CO and CH_3OH , with smaller admixtures of CH_4 , NH_3 , H_2CO and HCOOH . Observations at infrared, radio, millimeter, and sub-millimeter frequencies show that a large variety of organic molecules are present in the dense interstellar gas (20). These include organics such as nitriles, aldehydes, alcohols, acids, ethers, ketones, amines, and amides, as well as long-chain hydrocarbons. The effective shielding of UV radiation by dust in such high-density regions enables complex gas-grain chemistry in the so-called “hot-core” regions close to the forming star that allows the formation of many organic molecules, including precursor molecules for life as we know it (25).

Carbon chemistry occurs most efficiently in circumstellar and diffuse interstellar clouds. The circumstellar envelopes of carbon-rich stars are the heart of the most complex carbon chemistry that is analogous to soot formation in candle flames or industrial smoke stacks (26). There is evidence that chemical pathways, similar to combustion processes on Earth, form benzene, polycyclic aromatic hydrocarbons (PAHs) and subsequently soot and complex aromatic networks under high temperature conditions in circumstellar regions (27,28). Molecular synthesis occurs in the circumstellar environment on timescales as short as several hundred years (29). Acetylene (C_2H_2) appears to be the

precursor for the synthesis of hexagonal aromatic rings of carbon atoms. The detection of the simple aromatic species, benzene, in circumstellar environments implies that larger PAHs can also be formed in such regions. Benzene has limited photostability in the interstellar medium, but when sufficiently shielded in circumstellar envelopes from protons and UV photons it can act as the seed for aromatic carbon chemistry. Benzene chemistry is the first step in the formation of polycyclic aromatic hydrocarbons (PAHs), fullerene-type material and larger aromatic macromolecular material (28).

Interstellar Carbon Compounds and their Abundance

Polycyclic aromatic hydrocarbons (PAHs) are observed in galactic and extragalactic regions and represent the most abundant carbonaceous gas phase molecules in space (30,31). Laboratory studies and theoretical calculations have provided important insights into their size and charge state distribution (32), see examples in Figure 3. All three isoforms of carbon: diamond, graphite and fullerene, have been identified in space environments (2). Diamonds were proposed to be the carriers of the 3.4 and 3.5 μm emission bands (33) observed in planetary nebulae. Graphite has not been unambiguously identified in the interstellar medium, but is present in low abundances in meteorites (34). The third isoform of carbon is the polyhedral C_{60} fullerene geometry first discussed by Kroto et al. (35). Rietmeijer et al. (36) showed that cosmic soot analogs consist of close packed metastable C_{60} and giant fullerenes. Fingerprints of the C_{60}^+ ion were discovered in the near-infrared spectra of stars crossing the material of diffuse interstellar clouds (37,38).

The remarkable stability of the cage structure makes fullerenes important candidates for survival and wide distribution in space. Fullerenes of astronomical origin have been detected in meteorites and in and around an impact crater on the Long Duration Exposure Facility spacecraft (39). Laboratory simulations in combination with interstellar observations support the idea that the predominant fraction of carbon in space is present as solid macromolecular carbon (40) or amorphous and hydrogenated amorphous carbon (41).

Cosmic abundances in the interstellar medium are derived by measuring elemental abundances in stellar photospheres, the atmospheric layer just above the stellar surface. Such measurements indicate the amount of elements available for the formation of molecules and particles. Cosmic dust models indicate that up to 80% of the carbon in the photon-dominated diffuse interstellar medium is incorporated into solid aromatic macromolecules and gaseous polycyclic aromatic hydrocarbons (41,30). CO gas and C-based ice species (such as CO, CO_2 , CH_3OH and others) may be responsible for up to ~25 % of the carbon in cold dense interstellar regions.

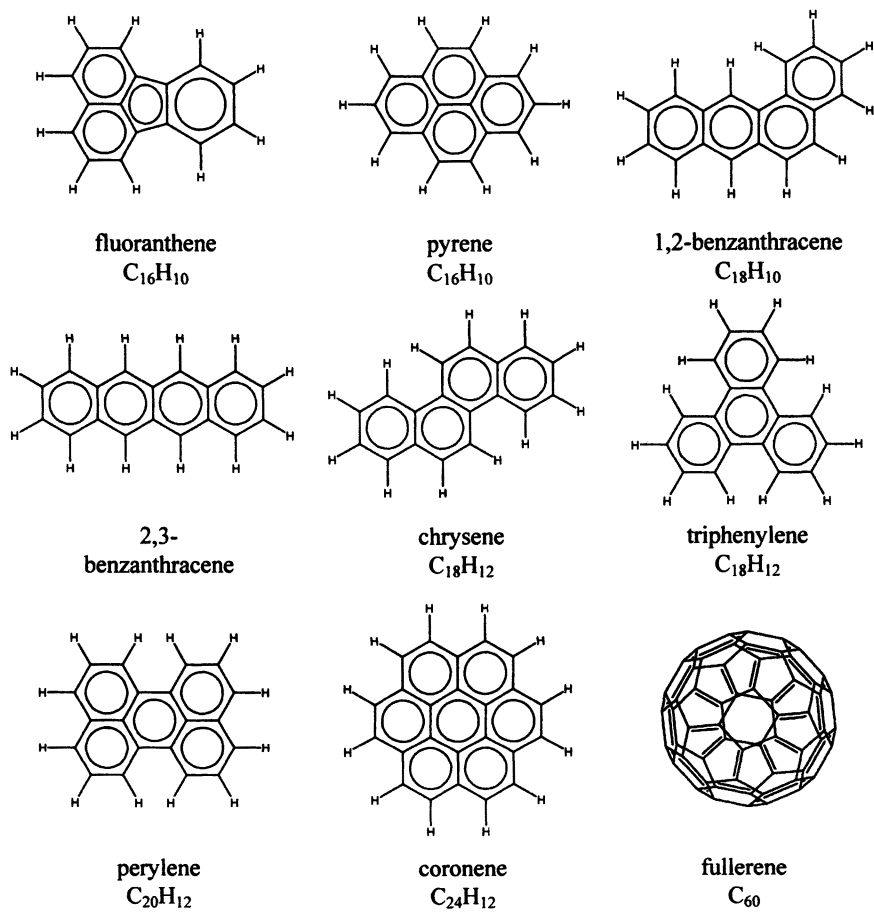


Figure 3. Examples of a variety of Polycyclic Aromatic Hydrocarbons (PAHs) and the fullerene C_{60} . PAHs containing 5-ring structures, heteroatoms, catacondensed and open structures are expected to reside in interstellar space.

From the Interstellar Medium to Planet Formation

Interstellar gas and icy or refractory dust composed of silicates and carbonaceous material provide the raw material for the formation of stars and planets. More than 4 billion years ago, the gravitational collapse of an interstellar cloud led to the formation of a protosolar disk (the solar nebula) with a central condensation developing into our sun (42,43). Clumps of small particles in the solar nebula grew bigger, accreted more and more material, eventually forming planets or moons.

During the formation of our solar system, interstellar gas and dust were mixed, processed and partly destroyed according to the distance from the forming star (44). Radiation chemistry involving X-rays and UV light acted on upper disk layers. Turbulent motions led to radial mixing of the products within the disk (45). Recent data from the stardust mission confirmed large-scale mixing in the solar nebula. Within the solar nebula, dust assembled into fluffy grains, which in turn assembled into boloids and ultimately into km-sized planetesimals that interact gravitationally (46,47). The key steps in this assembly process are still a mystery, but once self-gravitation begins, planetesimals grow by collision to form terrestrial planets (48). Many planetesimals formed in such a manner could not be integrated into planets and their ultimate fate was dependent on their location within the nascent solar system. The giant planets played an important role in stabilizing the structure of the solar system by trapping remnant bodies within defined regions such as the asteroid belt, or by ejecting them into outer solar system regions (Kuiper belt) and beyond (Oort cloud). The deflection of small bodies in the inner solar system led to large impacts on the forming terrestrial planets.

Carbon compounds in the solar system can be traced in planetary atmospheres, on planetary surfaces, comets, asteroids, meteorites and in the interplanetary medium. Gas and solid state chemistry within the solar nebula was responsible for new organic material (49,50). Many organic compounds have been identified on outer solar system bodies, some of them originating in the surface ices through energetic processing (4).

Small Bodies and Extraterrestrial Delivery

Comets are principally formed in the region beyond Jupiter. They are predominantly icy bodies containing some silicates and refractory organic material (51). More than 50 molecules have been identified in cometary comae (52). Many small organic molecules observed in cometary comae probably originate wholly or partially from the decomposition of larger molecules or particles, indicating that large polymers such as polyoxymethylene and HCN-polymers are present in comets (53). Carbonaceous meteorites contain a

substantial amount of carbon (up to 3 % by weight) and exhibit evidence of thermal and aqueous alteration believed to have occurred on their parent bodies (50, 54).

The NASA Stardust comet sample return mission visiting comet Wild-2 provided important new information on large-scale mixing in the solar nebula. Most of the $> 5\mu\text{m}$ solid particles collected by the mission are mineral grains or assemblages of high temperature minerals that condense at 1400K or above. Stardust data provide evidence for radial transport of large solid grains from the center of the solar nebula to the Kuiper belt (55).

Comets probably contributed most of the carbonaceous compounds during the heavy bombardment phase 4.5-4 billion years ago (3). Fragments of asteroids and comets such as interplanetary dust particles (IDPs) and carbonaceous meteorites were probably among the other major extraterrestrial contributors of carbon (56). The large quantities of extraterrestrial material delivered to young terrestrial planetary surfaces in the early history of our solar system may have provided the material necessary for the emergence of life. Conditions on the early Earth were hostile for life to emerge. Impacts, radiation and strong geological activity may have provided conditions alternating between glaciation and hot or even evaporating oceans. Material arriving from outside (carbon and nitrogen compounds as well as water) may have been crucial for the evolution of carbon chemistry and subsequently life.

Summary

To understand the emergence of carbon and how molecular complexity proceeds in star-forming regions is crucial to the investigation of star and planetary formation and solar nebula chemistry. Our universe provided carbon and dust in large amounts as early as 500 million years after the big bang through the supernova explosions that ended the lives of the first very massive stars. The enrichment of interstellar gas with 'metals' like carbon and oxygen facilitates the formation of many more stars and in particular stars with low masses and long lifetimes, like our sun. The variety of interstellar cloud environments offers many chemical pathways leading to the formation of gaseous and solid carbon compounds. The most abundant interstellar carbon fraction, in the form of macromolecular carbon, is produced in circumstellar envelopes of carbon stars. Substantial mixing and processing of interstellar and solar nebula material led to the current inventory of carbonaceous compounds in our solar system. The large quantities of extraterrestrial material delivered to young terrestrial planetary surfaces in the early history of our solar system may have provided the material necessary for the emergence of life.

References

1. Cataldo, F. *Astrobiology: Future Perspectives*, Ehrenfreund, P. et al. Eds.; Astrophysics and Space Science Library, Vol. 305, Kluwer Academic Publishers: Dordrecht, The Netherlands, **2004**, pp. 97–126.
2. Ehrenfreund, P.; Rasmussen, S.; Cleaves, J.H.; Chen, L. *Astrobiology* **2006**, *6/3*, 490.
3. Ehrenfreund, P.; Irvine, W.; Becker, L.; Blank, J.; Brucato, J.; Colangeli, L.; Derenne, S.; Despois, D.; Dutrey, A.; Fraaije, H.; Lazcano, A.; Owen, T.; Robert, F. *Rep. Prog. Phys.* **2002**, *65*, 1427–1487.
4. Roush, T.; Cruikshank, D. *Astrobiology: Future Perspectives*, Ehrenfreund, P. et al. Eds.; Astrophysics and Space Science Library, Vol. 305, Kluwer Academic Publishers: Dordrecht, The Netherlands, **2004**, pp. 149–165.
5. Chyba, C.; Sagan, C. *Nature* **1992**, *355*, 125–132.
6. Anders, E.; Grevesse, N. *Geochimica et Cosmochimica Acta* **1989**, *53*, 197–214.
7. Cardelli, J.A.; Mathis, J.S.; Ebbets, D.C.; Savage, B.D. *Astrophys. J.* **1993**, *402*, L17–L20.
8. Abel, T.; Bryan, G.L.; Norman, M.L. *Science* **2002**, *295*, 93–98.
9. Bromm, V.; Coppi, P.S.; Larson, R.B. *Astrophys. J.* **2002**, *564*, 23–51
10. Scannapieco, E.; Schneider, R.; and Ferrara, A. *Astrophys. J.* **2003**, *589*, 35–52.
11. Iwamoto, N.; Umeda, H.; Tominaga, N.; Nomoto, K.; Maeda, K. *Science* **2005**, *309*, 451–453.
12. Beers, T.C.; Christlieb, N. *Ann. Rev. Astron. & Astrophys.* **2005**, *43*, 531–580.
13. Spaans, M. *Astrobiology: Future Perspectives*, Ehrenfreund, P. et al. Eds.; Astrophysics and Space Science Library, Vol. 305, Kluwer Academic Publishers: Dordrecht, The Netherlands, **2004**, pp. 1–16.
14. Scalo, J.; Biswas, A. *Monthly Notices R. Astron. Soc.* **2002**, *332*, 769–776.
15. Spaans, M.; Silk, J. *Astrophys. J.* **2005**, *626*, 644–648.
16. Norman, C.A.; Spaans, M. *Astrophys. J.* **1997**, *480*, 145–154.
17. Bertoldi, F.; Cox, P.; Neri, R.; Carilli, C.L.; Walter, F.; Omont, A.; Beelen, A.; Henkel, C.; Fan, X.; Strauss, M.A.; Menten, K.M. *Astron. Astrophys.* **2003**, *409*, L47–L50.
18. Simcoe, R.A. *Astrophys. J.* **2006**, *653*, 977–987.
19. Daigne, F.; Olive, K.; Vangioni-Flam, E.; Silk, J.; Audouze, J. *Astrophys. J.* **2004**, *617*, 693–706.
20. Charnley, S.; Ehrenfreund, P.; Kuan, Y. *Physics World* Oct **2003**, 35–38.
21. Henning, T.; Salama, F. *Science* **1998**, *282*, 2204–2210.
22. Ehrenfreund, P.; Charnley, S.B. *Annu. Rev. Astron. Astrophys.* **2000**, *38*, 427–483.

23. Wooden, D.; Charnley, S.; Ehrenfreund, P. *COMETS II*, Festou, M.; Keller, H.U.; Weaver, Eds.: University of Arizona Press: Tucson, 2004, pp. 33–66.
24. Ehrenfreund, P.; Fraser, H. *Solid State Astrochemistry, NATO ASI Series: Pirronello, V.; Krelowski, J. Eds.: Kluwer Academic Publishers: Dordrecht, The Netherlands, 2003, pp. 317–356.*
25. Kuan, Y.; Charnley, S.B.; Huang, H.; Tseng, W.; Kisiel, Z. *Astrophys. J.* **2003**, *593*, 848–867.
26. Henning, Th.; Mutschke, H. *Astrophysics of Dust*, Witt, A.W.; Clayton, G.C.; Draine, B.T. Eds.: ASP Conference Series, Vol. 309, **2004**, p.603
27. Schnaiter, M.; Henning, Th.; Mutschke, H.; Kohn, B.; Ehbrecht, M.; Huiskens, F. *Astrophysical J.* **1999**, *519*, 687–696.
28. Frenklach, M.; Feigelson, E.D. *Astrophys. J.* **1989**, *341*, 372–384.
29. Kwok, S. *Nature* **2004**, *430*, 985–991.
30. Tielens, A.G.G.M.; Hony, S.; van Kerckhoven, C.; Peeters, E. *The Universe as Seen by ISO*, Cox, P., Kessler, M.F., Eds.; ESA SP 427: The Netherlands, **1999**, pp. 579–588.
31. Allamandola, L.J.; Hudgins, D.M.; Sandford, S.A. *Astrophys. J.* **1999**, *511*, 115–119.
32. Ruitenkamp, R.; Cox, N.L.J.; Spaans, M.; Kaper, L.; Foing, B.H.; Salama, F.; Ehrenfreund, P. *Astron. Astrophys.* **2005**, *431*, 515–529.
33. Guillois, O.; Ledoux, G.; Reynaud, C. *Astrophys. J.* **1999**, *521*, 133–136.
34. Nuth, J.A. *Nature* **1985**, *318*, 166–168.
35. Kroto, H.W.; Heath, J.R.; O'Brien, S.C.; Curl, R.F.; Smalley, R.E. *Nature* **1985**, 162–163.
36. Rietmeijer, F.J.M.; Rotundi, A.; Heymann, D. *Fullerenes Nanotubes Carbon Nanostruct.* **2004**, *12*, 659–680.
37. Foing, B.H.; Ehrenfreund, P. *Nature* **1994**, *369*, 296–298.
38. Foing, B.H.; Ehrenfreund, P. *Astron. Astrophys.* **1997**, *317*, 59–62.
39. Becker, L.; Bunch, T.E. *Meteoritics* **1997**, *32*, 479–487.
40. Pendleton, Y.; Allamandola, L. *Astrophys. J. Suppl.* **2002**, *138*, 75–98.
41. Mennella, V.; Colangeli, L.; Bussoletti, E.; Palumbo, P.; Rotundi, A. *Astrophys. J.* **1998**, *507*, 177–180.
42. *Protostars and Planets IV*, Mannings, V.; Boss, A.; Russell, S.S., Eds.; University of Arizona Press: Tucson, **2002**.
43. Boss, A.P. *COMETS II*, Festou, M.; Keller, H.U.; Weaver, Eds.: University of Arizona Press: Tucson, 2004, pp. 67–80.
44. Chick, K.; Cassen, P. *Astrophys. J.* **1997**, *477*, 398–409.
45. Markwick, A.; Charnley, S.B. *Astrobiology: Future Perspectives*, Ehrenfreund, P. et al. Eds.; Astrophysics and Space Science Library, Vol. 305, Kluwer Academic Publishers: Dordrecht, The Netherlands, **2004**, pp. 33–66.
46. Weidenschilling, S.; Cuzzi, J. *Protostars and Planets III*, Levy, E.; Lunine, J., Eds.; University of Arizona Press: Tucson, 1993, pp. 1031–1060.

47. Ormel, C.W.; Spaans, M.; Tielens, A.G.G.M. *Astron. Astrophys.* **2007**, *461*, 215–232.
48. Blum, J. Grain growth and coagulation. *Astrophysics of Dust*, Witt, A.W.; Clayton, G.C.; Draine, B.T. Eds.: ASP Conference Series, Vol. 309, **2004**, pp. 369–392.
49. Hill, Hugh G. M.; Nuth, Joseph A. *Astrobiology* **2003**, *3*, 291–304.
50. Sephton, M.A. *Nat. Prod. Rep.* **2002**, *19*, 292–311.
51. Greenberg, J. *Astron. Astrophys.* **1998**, *330*, 375–380.
52. Crovisier, J. *Astrobiology: Future Perspectives*, Ehrenfreund, P. et al. Eds.; Astrophysics and Space Science Library, Vol. 305, Kluwer Academic Publishers: Dordrecht, The Netherlands, **2004**, pp.179–204.
53. Ehrenfreund, P.; Charnley, S.B.; Wooden, D.H. *COMETS II*, Festou, M.; Keller, H.U.; Weaver, Eds.: University of Arizona Press: Tucson, 2004, pp. 115-133
54. Botta, O., this volume
55. Brownlee, D. et al. *Science* **2006**, *314*, 1711-1716.
56. Chyba, C.; Thomas, P.; Brookshaw, L.; Sagan, C. *Science* **1990**, *249*, 366–373.

Chapter 13

Extraterrestrial Organic Chemistry as Recorded in Carbonaceous Chondrites

Oliver Botta

International Space Science Institute, Bern, Switzerland

Meteorites are ancient objects originating in the asteroid belt that have recorded a succession of chemical processes, starting from reactions in the interstellar medium, followed by reactions that accompanied the formation and evolution of the early solar system, and culminated with reactions during aqueous alteration in the meteorite parent bodies. One of the challenges in meteorite research is to decipher this record and to learn about interstellar formation processes as well as to conditions in the early solar system. The rare carbonaceous chondrites contain up to 3 weight-% of organic carbon, more than 80 percent of which is locked in an insoluble macromolecular material with the rest present in the form of extractable organic compound classes such as carboxylic acids, amino acids (including some with enantiomeric excesses) and polycyclic aromatic hydrocarbons (PAH). Both the components of the macromolecular material and the soluble organic compounds exhibit molecular and isotopic characteristics of abiotic synthetic processes that must have occurred in extraterrestrial environments. A combination of interstellar surface and gas-phase reactions, thermal and shock processes in the accretionary disk and alterations inside the asteroid parent body lead to the mixture of organic compounds observed in meteorites.

Introduction

The Solar System is comprised of planets and dwarf planets as well as smaller objects such as asteroids, Trans-Neptunian Objects (TNOs) and comets. Due to their small sizes and masses, the majority of these objects has never experienced “planetary” processes such as core formation, volcanism or plate tectonics, and therefore has retained geological, geochemical and chemical signatures dating back to the formation of the Solar System and even beyond. Most of these signatures are contained in micro-morphological, elemental, mineralogical, isotopic and molecular composition of these objects and are not accessible by remote-sensing techniques. In recent years, several spacecraft have visited some of these objects and determined major element compositions using for example γ -ray spectrometers. The most primitive objects are comets. Since the first spacecraft encounter of *Giotto* with comet Halley in 1986, several mission have been visiting cometary objects, for example *Deep Space 1*, *Deep Impact* and *Stardust*. The last mission collected dust and gas from the comet tail and returned these samples to the Earth for laboratory analysis (1). Despite the success of this first sample return from outside the Earth-Moon system, the amount of material available for analysis is not more than a few milligrams. Such amounts are sufficient for elemental, mineralogical and morphological analyses, but at the edge of the current capabilities of traditional organic analyses (2).

There is another possibility, though, to obtain samples from Solar System objects, and these samples have been constantly delivered to the Earth over its entire existence. Although the recognition of meteorites as being extraterrestrial material was only accepted about 200 years ago, the investigations of these samples have provided insights into the physical and chemical processes that occurred at the earliest stages of formation of the Solar System. Most meteorites are pieces of asteroids, although a few examples have been found to originate on the Moon and on Mars (interestingly, there seems to be a lack of cometary meteorites, but it is not clear if they don't exist, or if we have not recognized them yet).

Meteorites are grouped into three major classes: irons, stones and stony-irons. Based on compositional dissimilarities, stony meteorites are subdivided into chondrites and achondrites. Chondrites are the most primitive meteorites based on their near-solar volatile composition and radiometric ages of 4.566 billion years, reflecting their formation during, or shortly after, the birth of the Solar System (3). Within the chondrites, there exists a carbonaceous subclass that contains up to 3 weight-% of organic carbon, a characteristic that contributes to a generally dark appearance. Carbonaceous chondrites themselves are subdivided into CM, CI, CV and other classes based on a combination of their

(primary) chemical composition (with the second letter being the first letter of a prototype specimen) and of their levels of secondary (aqueous and thermal) processing (Figure 1) (4,5). The chemistry and mineralogy of carbonaceous chondrites suggests that any organic matter they contain should be ancient, predating the origin of life on Earth, and represent a perfect example of abiotic chemical evolution. The understanding of the organic composition of these meteorites, as well as that of comets and interplanetary dust particles (IDP), is highly relevant since these objects have delivered a significant amount of organic material to the early Earth (6) that may have played a major role in the origin of life, perhaps as the original feedstock of organic compounds and/or as catalysts.

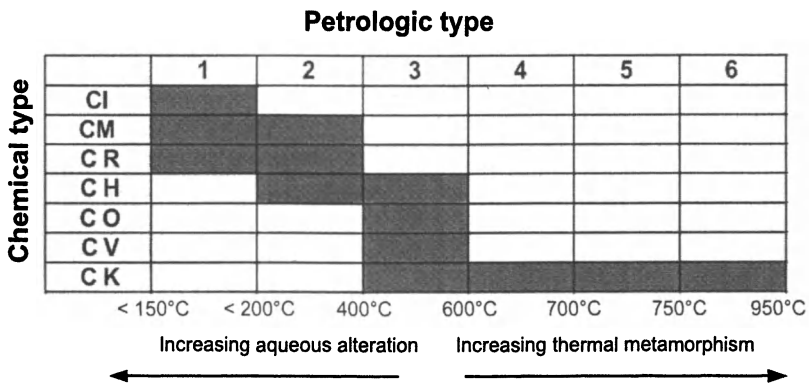


Figure 1. The classification of carbonaceous chondrites based on their primary elemental (chemical) composition and levels of secondary (aqueous and thermal) processing. (Adapted from References 4 and 5.)

By far the most meteorites have been recovered in Antarctica during international expeditions dedicated to the search of meteorites (7). More than 26,000 specimens have been recovered from there since systematic collections programs began about 30 years ago, providing a unique collection of extraterrestrial material accreting on the Earth. However, the most studied meteorites has been a carbonaceous chondrite that fell near the village of Murchison, Australia, on September 28, 1969 (a representative of CM2 class, Figure 2), the famous Orgueil meteorite (CI1), which fell in France in 1864, and the CM2 meteorites Murray (Kentucky, USA, 1950) and Cold Bokkeveld (South Africa, 1838). Yet the information derived from Murchison greatly surpasses that from the preceding carbonaceous chondrite falls because it was quickly delivered to several laboratories that had painstakingly developed methods to search for indigenous organic compounds in the Apollo lunar samples (8).



1.5 cm

Figure 2. A piece of the carbonaceous chondrite Murchison.

The Organic Compounds in Carbonaceous Chondrites

The organic matter in carbonaceous chondrites is heterogeneously dispersed throughout the matrix. This lithology is in a non-equilibrium state, which is apparent in the coexistence of high- and low-temperature minerals as well as oxidized and reduced species and the juxtaposition of hydrated and unhydrated minerals (9). The organic carbon can be divided into a non-soluble component, which makes up more than 80% of the total amount. This insoluble fraction is composed of macromolecular matter that is commonly referred to as “kerogen-like”. (Kerogen is *terrestrial* insoluble macromolecular organic matter, operationally defined as the organic residue left after acid demineralization of a rock. It should be noted that meteoritic kerogen is significantly different than terrestrial kerogen.) The rest is composed of material that is soluble in water or organic solvents and that contain complex mixtures of discrete organic compound classes such as amino acids and hydrocarbons. This heterogeneity requires different protocols and techniques to access the molecular, chiral and isotopic information present in this material.

Insoluble Organic Matter (IOM)

Analytical Protocols and Separation techniques

The analysis of the insoluble organic component (IOM) in carbonaceous chondrites is based on the techniques developed for coal, oil shales and petroleum source rocks. In order to analytically access the organic material the mineral phase of the meteorite is dissolved using a mixture of HCl and HF (9), leaving behind an organic residue that can be either processed further or used directly for analysis.

Early studies involved pyrolysis of this residue and revealed the presence of aromatic ring systems such as benzene, naphthalene, their alkyl derivatives as well as higher aromatic hydrocarbons. Today, GC-MS analyses of super-critical fluid extracts of hydrous pyrolysates (11), H₂-pyrolysis products (12) as well as solid-state ¹³C-NMR spectroscopy (13) of meteorite organic residues are applied to provide insight into the structure of the macromolecular carbon. Most recent, hydrothermal treatment (300 °C at 10 MPa) of demineralized IOM of the Murray meteorite has yielded in the release of a wide variety of carboxylic acids and heteroaromatic compounds including C₃-C₁₇ alkyl carboxylic acids and N-, O- and S-containing hydroaromatic and aromatic compounds (14).

Data obtained from a combination of pyrolysis-based techniques with compound specific GC-Combustion-Isotope Ratio-MS (GC-C-IRMS) have provided important insight into the formation of this material.

Molecular and Isotopic Characteristics

NMR analysis (13) has revealed the following characteristics for the Murchison IOM:

- 61 to 66 % of the carbon atoms in the Murchison macromolecular material are bound in aromatic components.
- The aromatic molecules in the organic residue are highly substituted.
- The bulk hydrogen content (H/C) ranges from 0.53 to 0.63.
- The aliphatic carbon chains are highly branched.

The GC-MS analyses of Murchison, Orgueil and Cold Bokkeveld macromolecular material indicate that the macromolecular materials in different meteorites are qualitatively very similar (e.g. made up of the same units) (11). In addition, oxygen-, sulfur- and nitrogen-containing moieties such as phenols, thiophenes and benzonitrile have also been detected in the pyrolysates. The H₂-pyrolysis further demonstrated that the refractory component probably consists of a network dominated by at least five- or six-ring PAH units that are crosslinked together (13).

The compound-specific isotope values of aromatic compounds liberated from the macromolecular material exhibit that $\delta^{13}\text{C}$ values of low molecular weight compounds increase with increasing carbon number, while $\delta^{13}\text{C}$ values for high molecular weight compounds decrease, indicating that bond formation and destruction was important during the formation of the macromolecular material (4).

Soluble Organic Compounds

Analytical Protocols and Separation techniques

The soluble fraction of the organic matter in carbonaceous chondrites can be accessed by extracting powdered meteorite samples with solvents of varying polarity. These extracts contain complex mixtures of discrete organic compounds that can then be purified further, for example by charcoal filtration, ion-exchange chromatography or sublimation, before analysis.

The determination of the concentrations of soluble organic compounds in meteorites is based on chromatography combined with techniques that detect the eluting compounds. Depending on the exact nature of the compounds and the goal of the study, the choice is between several methods:

- GC-MS: Gas chromatography-mass spectrometry is the most versatile method. It can be used for pyrolysates (see above), but also for the detection of PAHs in extracts. In combination with commercially available derivatization protocols, amino acids can be analyzed as well. If chiral columns are used, enantiomeric separation of chiral compounds is possible. Usually, either quadrupole or ion trap mass spectrometers are used as detectors, but Time-of-flight (ToF) MS can also be used.
- HPLC-FD: High-performance liquid chromatography combined with fluorescence detection has been used for the first analyses of nucleobases in carbonaceous chondrites (15). More recently, pre-column derivatization of amino acid with *o*-phthaldialdehyde/*N*-acetyl-L-cysteine (OPA/NAC) has allowed the detection and enantiomeric separation of a few pmol of amino acids (16).
- LC-FD/ToF-MS: Potential problems with co-elutions of compounds has led to the application of a combination of the high sensitivity of LC-FD with the mass resolution of ToF-MS in meteorite research (17), allowing the identification of unknown peaks in the chromatogram.
- CE: The analysis of meteorite samples with capillary electrophoresis was achieved as a proof of concept for a future Mars science instrument (18). The sensitivity is higher than for HPLC-FD, and the hardware can be highly miniaturized.
- GC-C-IRMS: The combination of a gas chromatograph with a combustion cell and an isotope ratio mass spectrometer allows the determination of compound-specific isotope ratios, which for some compound classes such as the nucleobases is the only method to determine whether they are indigenous to the meteorite or terrestrial contamination (5).

Bulk Molecular and Isotopic Characteristics of Soluble Organic Compounds

Carbonaceous chondrites, and in particular the Murchison meteorite, have a rich organic inventory, including carboxylic acids, amino acids, sulphonic acids dicarboximides and dicarboxylic acids, aliphatic and aromatic hydrocarbons and other classes of organic molecules (Table I) (for detailed reviews see (4, 19, 20)). Some of these classes of compounds, such as amino acids and nucleobases are essential in terrestrial biochemistry. For example, amino acids are integral components of proteins and enzymes, and nucleobases are components of DNA and RNA. Others, such as carboxylic acids and sugar-related molecules (21), have been detected in the interstellar medium (22).

Table I. Abundances of a selection of soluble organic compounds found in the Murchison meteorite.

<i>Compound Class</i>	<i>Abundance (in parts per million)</i>
Mono-carboxylic acids	332
Sulphonic acids	67
Amino acids	60
Dicarboximides	> 50
Dicarboxylic acids	> 30
Aromatic hydrocarbons	15-28
Aliphatic hydrocarbons	12-35
Sugar-related compounds	~ 24
Hydroxycarboxylic acids	15
N-heteroaromatic compounds	1.3

SOURCE: Adapted from References 4, 5 and 19.

There are several signatures in the molecular and isotopic composition of these compounds in the meteorites that combined provide unambiguous evidence for an extraterrestrial origin:

1. The high abundances of amino acids such as *α-aminoisobutyric acid* (AIB) and isovaline, which are not among the 20 amino acids that are translated from the genetic code and which are therefore very rare on Earth. However, AIB is the second most abundant amino acid in Murchison (after glycine).
2. For a given carbon number, all possible isomers are observed in most classes of compounds, at least among the lower homologs. This *complete structural diversity* suggests synthesis by random processes, involving carbon-containing free radicals and ions). This is in accordance to the observed *decline of concentrations with increasing carbon number in homologous series* as well as the *predominance of branched-chain isomers* over straight-chain isomers for a given carbon number.
3. Racemic or close-to-racemic enantiomeric ratios of chiral compounds indicate an abiotic origin of these molecules.
4. All soluble organic compounds show isotopic enrichments in carbon, nitrogen and hydrogen.

Detailed analysis of the carbon isotopic distribution of α -amino acids in Murchison has shown that the ^{13}C -enrichment declines with increasing chain length (23). This trend, which was also observed for carboxylic acids, points to chemical synthetic processes that are kinetically controlled, thus forming higher homologs from lower ones.

Enantiomeric Excesses in Meteoritic Amino Acids

Enantiomeric excesses (*ee*) in chiral molecules in natural products are usually associated with biochemical processes. Initially, all chiral amino acids in meteorites were found to be racemic, a finding that had helped to establish their abiotic (and therefore extraterrestrial) origin (8). More recently, a sub-group of α -amino acids, the α -dialkyl- α -amino acids, which are unknown in the terrestrial biosphere, was found to possess L-*ee* of up to 15 % in the Murchison and Murray (CM2) meteorites, while all the α -H-amino acids were present as racemic mixtures (24, 25).

There has been a lot of speculation about the origin of this enantiomeric excess, but so far no appropriate explanation has been brought forward (see (26) for a summary), but so far this feature has eluded experimental proof for its origin. However, even small enantiomeric excesses may have been instrumental in prebiotic synthesis via asymmetric catalysis, provided the necessary conditions such as concentration and temperature were achieved in the environment of the early Earth (27).

Extraterrestrial Organic Chemistry: Formation and Evolution of Complex Molecules in Space

The molecular and isotopic analysis of the organic component of meteorites provides valuable insights into the processes that occurred before and during the formation of the solar system. The composition of this material is the product of a combination of different processes that occurred in very different physical conditions over different periods of time. These processes can be divided into three types:

- Pre-solar processes occurring either in the interstellar or circumstellar medium.
- Processes that occurred during the formation of the solar system, e.g. in the accretionary disk environment.
- Parent body processes that occurred on the parent asteroid of the meteorite

Interstellar and Circumstellar Processes

The interstellar medium (ISM) contains different environments showing large ranges in temperature between 10 K in dense clouds and up to 200 K in warm circumstellar envelopes and densities between 100 to 10^8 hydrogen atoms cm^{-3} . Dense clouds are characterized by very low temperatures (10-30 K) and

relatively high densities (10^{4-8} hydrogen atoms cm^{-3}) that constrain the reaction mechanisms that are possible under these conditions. For example, one important consequence is that at these low densities all chemical reactions have to be binary in nature (28). Also, the low temperatures in most dense clouds pose an even stronger constraint in the sense that endothermic reactions and exothermic reactions with even small activation barriers are too slow to be competitive. Under these conditions, cold gas phase chemistry can efficiently form simple species such as CO, N_2 , O_2 , C_2H_2 , HCN, as well as simple carbon chains (28). Chemical reactions in dense clouds are driven by UV radiation from nearby young stellar objects (YSOs) or, more efficiently, induced by cosmic ray particles that penetrate into the cloud and excite H_2 , which then decays under UV emission (29).

Dust particles with sizes of about $0.1 \mu\text{m}$ make up about 1 % of the mass in a dense cloud and are important chemical catalysts. Surface reactions driven by UV radiation lead to the formation of molecules such as H_2O , CH_4 , and NH_3 , but also to more complex compounds such as CH_3OH , effectively forming mantles of ice (“interstellar ices”) around these grains. These grain surface processes are responsible for the high deuterium fractionations observed in specific molecules such as HDO, DCN D_2CO etc. The compounds formed in these processes are returned to the gas phase via selective desorption and mantle explosions, where they can react further (or may be destroyed by the UV-field) (29). This can occur for example in Hot Molecular Cores (HMC), which are regions of early star formation processes. These regions are particularly rich in complex organic molecules (29).

Another important region for the production of organic compounds are massive circumstellar envelopes (CSEs) of giant stars that are in the transition to become a protoplanetary nebula (PPNe). These so-called Asymptotic Giant Branch (AGB) stars can either be O- or C-rich and provide the dust and refractory material. Carbon-rich stars show strong emission signals from PAHs, suggesting that these molecules are intermediate steps for the production of carbon dust (soot) (30, 31). This carbonaceous dust may show a strong diversity and may include amorphous carbon, coal, diamonds and other components. However, most of these compounds are probably very stable in the interstellar UV-field and during solar system formation, and are probably incorporated into objects such as asteroids and comets without much further modification.

Processing During Solar System Formation

The formation of stars occurs through the gravitational collapse of individual galactic molecular cloud cores within dense clouds. As cold interstellar gas and ice-mantled dust grains collapsed onto the protosolar nebula,

they were heated by radiation and gas-grain drag. Also, infalling matter passes through a shock associated with the accretion, which can also lead to significant processing. However, far from the protosun, the lower nebular densities and slower shock periods resulted in less processing of interstellar material, limited primarily to dissociation and recondensation of the ices (32). Particularly in the outer regions of the solar system, where comets formed, and after the initial large-scale accretion had ended, some of the interstellar material may have entered the solar nebula relatively unscathed. This may even be true for meteorites, which formed much closer to the sun, as evidenced by the detection of PAHs associated with presolar grains in the Murchison meteorite (33). Such marginally processed material is probably found in cometary nuclei, and a first glimpse at such material was made possible by the *Stardust* mission (1,2), and future space missions such as *Rosetta* will allow a more thorough analysis of the composition of cometary material. A more detailed discussion about comets can be found in (34).

Parent Body Processing

Mineralogical evidence from silicate material in meteorites provides strong evidence for the presence of liquid water inside their asteroidal parent bodies for at least a few millions of years after accretion. Temperature estimates for this aqueous alteration phase range from about 20 °C in CMs to about ~50 °C in CIs (35), with a pH between 6 and 8 (36). Energy sources for this processing were both the radioactive decay of short-lived isotopes like ²⁶Al and ⁶⁰Fe as well as low-energy impacts on the asteroid. Under these conditions, extraterrestrial organic chemical reactions in the condensed phase, completely different from the ones occurring in the interstellar medium, could occur and lead to new secondary products. It should be noted that there is currently no evidence for this sort of secondary processing to have ever occurred on cometary nuclei, again indicating that a signature of pristine organic material is most probably to be found on comets (34).

Example 1: Macromolecular Material

Although the macromolecular material has been found to be qualitatively very similar between the Murchison, Cold Bokkeveld and Orgueil meteorites variations in the ratios between one-ring aromatic hydrocarbons (benzene and alkylated derivatives), two-ring aromatic hydrocarbons and phenols exist between these meteorites (11). Phenol abundances increase in the order Orgueil < Cold Bokkeveld < Murchison, while the one-ring aromatic compounds show the opposite trend. These characteristics may be explained by the effect of aqueous

alteration, during which ether linkages in the macromolecular material were cleaved during that period, leading to higher phenol abundances. On the other hand, the higher abundances of the one-ring aromatic hydrocarbons may be an indication of a relatively open (less condensed) organic structure, which would result from limited interaction of the reactive aromatic network with water-derived hydrogen (11). A variety of NMR studies of the IOM in the CR2 Elephant Moraine (EET) 92042, Murchison, Orgueil and the unique Tagish Lake meteorite have revealed variations in the abundances and types of sp^3 bonded carbon between these samples (37). These data indicate that chemical oxidation accompanied the aqueous alteration and that it has also significantly modified and chemically degraded the macromolecular material.

Example 2: Amino Acids

The molecular and isotopic characteristics of meteoritic mono-carboxylic and amino acids indicate a synthesis of these molecules, or their precursors, by random addition of single-carbon donors, clearly pointing to an interstellar origin. However, early analyses of the Murchison meteorite have also shown the presence of the corresponding α -hydroxy acids in the same relative homolog distribution as the α -amino acids, indicating a common synthetic pathway for these two classes of molecules (38, 39). Most likely, this common route is the Strecker-cyanohydrin synthesis, which, depending on the ammonia concentration in the solution, yields an equilibrium mixture of cyanonitriles and aminonitriles (Figure 3). These intermediates then undergo irreversible hydrolysis in aqueous solution to form α -amino- and α -hydroxy acids, respectively. Therefore, the diversity of hydroxy- and amino acids observed in the meteorites is not a product of secondary processing, but is inherited from the variety of the carbonyl compounds available in the parent body. Although this is a very reasonable hypothesis for the synthesis of α -amino acids, other amino acids such as β - and γ -amino acids are not products of the Strecker-cyanohydrin synthesis. For example, β -amino acids can be synthesized through Michael-addition of ammonia to substituted α,β -unsaturated nitriles, followed by reduction/hydrolysis, with potential precursor molecules such as acrylonitrile and cyanoacetylene that were detected in the interstellar medium (40).

The detection of diamino acids in the Murchison meteorite (41) has stirred up the speculation that these compounds are perhaps direct products of interstellar synthesis processes. In particular, laboratory experiments aimed at the ultraviolet (UV)-irradiation of interstellar ice analogs leads to the formation of refractory material which, after hydrolysis with 6 M HCl, has been shown to contain mono-amino acids as well as diamino acids (42). Although it is evident that some organic compounds that were formed in the interstellar medium, either in the gas phase or in interstellar grains, survived exposure to the interstellar

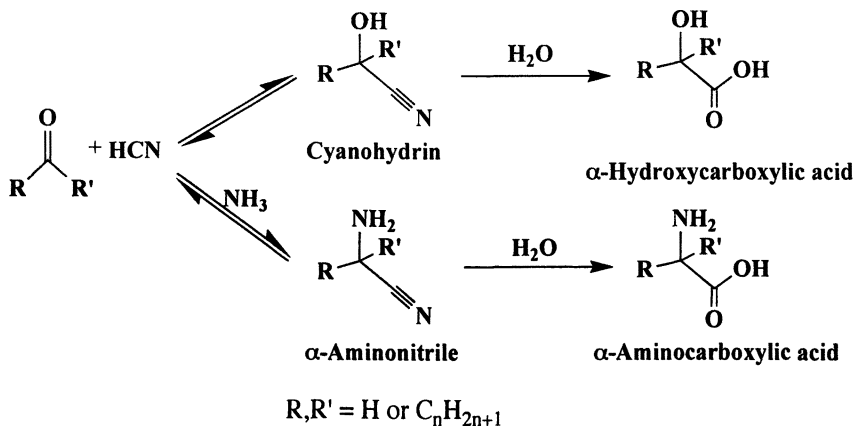


Figure 3. The Strecker-cyanohydrin synthetic pathway. This reaction may have produced the meteoritic α -hydroxy and α -amino acids during aqueous alteration on the asteroid parent body.

UV-field and the formation of the solar system, it is difficult to imagine how amino acids, which were shown to be destroyed by UV radiation (43), could have been incorporated intact into asteroids (the parent bodies of the meteorites). It is more likely that either simple interstellar precursors, such as the starting compounds for the Strecker synthesis, or a complex and heterogeneous macromolecular material formed in the gas and/or solid phases in the ISM that served as starting material for the secondary processing that inevitably occurred on the meteorite parent body.

Amino acid analyses have also been carried out on other carbonaceous chondrites, including Murray, the Antarctic meteorites Lewis Cliffs (LEW) 90500, Alan Hills (ALH) 83100 (16), the CM1s ALH 88045, Meteorite Hills (MET) 01070, LaPaz (LAP) 02277 (44) and the CI1s Orgueil and Ivuna (45). Absolute and relative amino acid abundances indicate that there are differences in the amino acid distributions between meteorite classes that may best be explained by abundance differences in the source regions of their parent bodies in combination with decomposition processes of amino acids during extended parent body aqueous alteration (44).

Summary

Carbonaceous chondrites contain a significant amount of a suite of organic compounds, both soluble and insoluble, that have recorded in their molecular

and isotopic characteristics the results of a variety of chemical processes. These processes have occurred both in the gas and solid phases of the interstellar medium as well as in the solar system during and shortly after its formation. Organic analyses using classical chemical extraction and separation techniques combined with chromatographic methods, including GC-MS, GC-C-IRMS, HPLC (with both absorbance/fluorescence and mass spectrometric detection) and capillary electrophoresis (CE) have led to the identification of a wide variety of compounds, some of which have essential functions in terrestrial biochemistry. These results from experiments are continuing not only to shed light on the physical and chemical conditions in the interstellar medium and in the early Solar System under which these compounds formed, but they will also be highly important for current and future space missions that will attempt to detect organic matter on planets and other objects like comets (2). The understanding of the extent of abiotic chemical evolution outside the Earth and the recognition of the corresponding molecular and isotopic signatures will enable scientists to discriminate between biogenic and abiogenic materials (46).

References

1. Brownlee, D. *et al.*, *Science* **2006**, *314*, 1711.
2. Sandford, S. A. *et al.*, *ibid.*, 1720.
3. Allègre, C. J; Manhès, G.; Göpel; Ch. *Geochim. Cosmochim. Acta* **1995**, *59*, 1445.
4. Sephton, M. A. *Nat. Prod. Rep.* **2002**, *19*, 292.
5. Martins, Z. Ph.D. thesis, Leiden Institute of Chemistry, Leiden, 2007.
6. Chyba, C. F.; Sagan, C. *Nature* **1992**, *355*, 125.
7. Harvey, R. P. *Chem. Erde* **2003**, *63*, 93.
8. Kvenvolden, K. *et al.*, *Nature* **1970**, *228*, 923.
9. Kerridge, J. F. *Space Sci. Rev.* **1999**, *90*, 275-288.
10. Robl, T. L; Davis, B. H. *Org. Geochem.* **1993**, *20*, 249.
11. Sephton, M. A.; Pillinger, C. T.; Gilmour, I., *Geochim. Cosmochim. Acta* **2000**, *64*, 321.
12. Cody, G. D.; Alexander, C. M. O'D.; Tera, F. *Geochim. Cosmochim. Acta* **2002**, *66*, 1851.
13. Sephton, M. A. *et al.*, *Geochim. Cosmochim. Acta* **2004**, *68*, 1385.
14. Yabuta, H. *et al.*, *Meteorit. Planet. Sci.* **2007**, *42*, 37.
15. Stoks, P. G.; Schwartz, A. W. *Geochim. Cosmochim. Acta* **1981**, *45*, 563.
16. Zhao, M; Bada, J. L. *J. Chromatogr. A* **1995**, *690*, 55.
17. Glavin, D. P. *et al.*, *Meteorit. Planet. Sci.* **2006**, *41*, 889.
18. Hutt, L. D. *et al.*, *Anal. Chem.* **1999**, *71*, 4000.
19. Botta, O.; Bada, J. L. *Surv. Geophys.* **2002**, *23*, 411.

20. Pizzarello, S.; Cooper, G. W.; Flynn, G. J. In *Meteorites and the Early Solar System II*; Lauretta, D. S.; McSween, H. Y., Eds.; University of Arizona Press: Tucson, AZ, 2006; pp. 625-651.
21. Cooper, G. W. *et al.*, *Nature* **2001**, *414*, 879.
22. Hollis *et al.*, *Astrophys. J.* **2004**, *613*, L45.
23. Pizzarello, S.; Huang, Y.; Fuller, M. *Geochim. Cosmochim. Acta* **2004**, *68*, 4963.
24. Cronin, J. R.; Pizzarello, S. *Science* **1997**, *275*, 951.
25. Pizzarello, S.; Cronin, J. R. *Geochim. Cosmochim. Acta* **2000**, *64*, 329.
26. Pizzarello, S.; *Acc. Chem. Res.* **2006**, *39*, 231.
27. Pizzarello, S.; Weber, A. L. *Science* **2004**, *303*, 1151.
28. Herbst, E.; *Chem. Soc. Rev.* **2001**, *30*, 168.
29. Ehrenfreund, P.; Charnley, S. B. *Annu. Rev. Astron. Astrophys.* **2000**, *38*, 427.
30. Frenklach, M.; Feigelson, E. D. *Astron. Astrophys.* **1989**, *341*, 372.
31. Cherchneff, I.; Barker, J. R.; Tielens, A. G. G. M. *Astrophys. J.* **1992**, *401*, 269.
32. Lunine, J. I. In *The Formation and Evolution of Planetary Systems*; Weaver, H. A.; Danly, L., Eds.; Cambridge University Press: New York 1989; pp. 213-242.
33. Messenger, S. *et al.*, *Astrophys. J.* **1998**, *502*, 284.
34. Ehrenfreund, P.; Charnley, S. B.; Wooden, D. In *Comets II*; Festou, M.; Keller, H. U.; Weaver, H. A., Eds.; University of Arizona Press: Tucson, AZ, 2004; pp. 115-133.
35. Leshin, L. A.; Rubin, A. E.; McKeegan, K. D. *Geochim. Cosmochim. Acta* **1997**, *61*, 835.
36. DuFresne, E. R.; Anders, E.; *Geochim. Cosmochim. Acta* **1962**, *26*, 1085.
37. Cody, G. D.; Alexander, C. M. O'D. *Geochim. Cosmochim. Acta* **2005**, *69*, 1085.
38. Peltzer, E. T.; Bada, J. L., *Nature* **1978**, *272*, 443.
39. Peltzer, E. T.; Bada, J. L.; Schlesinger, G.; Miller, S. L. *Adv. Space Sci.* **1984**, *4*, 69.
40. Irvine, W. M.; *Origins Life Evol. Biosphere* **1998**, *28*, 365.
41. Meierhenrich, U. J. *et al.*, *Proc. Natl. Acad. Sci. USA* **2004**, *101*, 9182.
42. Muñoz-Caro G. M. *et al.*, *Nature* **2002**, *416*, 403.
43. Ehrenfreund *et al.*, *Astrophys. J.* **2001**, *550*, L95.
44. Botta, O.; Martins, Z.; Ehrenfreund; P. *Meteorit. Planet. Sci.* **2007**, *42*, 81.
45. Ehrenfreund *et al.*, *Proc. Natl. Acad. Sci. USA* **2001**, *98*, 2138.
46. Sephton, M. A.; Botta, O.; *Astrobiology* **2005**, *4*, 269.

Chapter 14

Earth's Early Atmosphere, Biosphere, Lithosphere, and Hydrosphere

Douglas Rumble, III

**Geophysical Laboratory, Carnegie Institute of Washington,
Washington, DC 20015**

Reconstructions of ancient ecological interactions rely upon information found in rocks deposited at Earth's surface billions of years ago. Geologic and geochemical evidences of the nature of early Earth are widely dispersed in isolated outcrops across the globe and are imperfectly preserved. In addition to the impediments to understanding imposed by a fragmentary historical record, knowledge must be gained from studying modern environments in order to interpret evidence gleaned from Earth's oldest rocks. The application of data measured on modern samples to decipher clues hidden in ancient rocks necessitates extrapolating several billion years in time, a problematical exercise at best. There is an inevitable logical circularity in accepting the present as the key to the past: But, what other benchmark does one have? This presentation will explain how geological and geochemical evidence is used to constrain hypotheses for the evolution of Earth's atmosphere, biosphere, hydrosphere, and lithosphere, prior to 2.5 billion years ago.

Introduction

What is the most difficult research job in all of science? It is the task of deducing the history of Earth's evolution in its first two billion years, during the Hadean eon from 4.5 to 4.0 Ga (1Ga = 10^9 years before present) and the Archean eon from 4.0 to 2.5 Ga. Detectives of ancient rocks are faced with a lack of clues to investigate. Most of Earth's surface is covered by water. The cores of the continents are probably underlain by rocks older than 2.5 Ga but they are hidden by a veneer of younger sediments. Even in localities where Hadean-Archean rocks are readily available, alteration by subsequent geologic events has obscured the record of conditions under which they were formed. It is revealing to compare and contrast the detailed information available in a textbook of Earth's modern ecologies with the sparse collection of facts accepted by disciplinary consensus for the Hadean-Archean eras.

Geologists approach the mysteries of ancient Earth in the spirit of Sherlock Holmes, as detectives deprived of direct knowledge of the events under study and furnished with ambiguous clues. As with Holmes, the logical method of working multiple hypotheses is employed in the expectation that objective testing will leave only a single, unfalsified theory remaining, no matter how seemingly improbable it may be. Geologists rely upon observations of processes molding modern Earth and analysis of the products of those processes to calibrate interpretations of ancient deposits. The phrase "the present is the key to the past" sums up the geological approach. The earliest geologists used their eyes and brains to understand present day erosion, volcanic eruptions, and earthquakes and apply the results to interpreting the past. Implicit in their interpretations of the past was the assumption that if an ancient deposit looks like a modern one, it must have formed in the same way. But what looks like a beautiful volcanic surge deposit to one eye may be regarded by another as sediment from a river's catastrophic flooding. Just because I say those strange shapes in a rock resemble living organisms doesn't make it necessarily so that they are fossils of the same creature.

Anyone reading this far would be correct to conclude that there is a great deal of argument about the nature of the Hadean-Archean Earth. There is also an abundance of discerning science that has advanced understanding enormously. Geochemistry was invented to settle arguments about the origin of ancient deposits. Geochronologists now measure the age of rocks and minerals in billions of years to astonishing precision. Organic geochemists find biogenic molecules in improbably old sediments. Geochemists measure the stable isotopes of hydrogen and oxygen and deduce the nature of previous meteoric water cycles to reconstruct ancient climates. A skeptic might say that we have substituted the mass spectrometer for the eye in a search for quantitative comparisons of new and old, but the same logic of our 19th century colleagues remains in use. And

another skeptic might inquire how is it possible to recognize a uniquely ancient process or environment if all our references date from modern times?

Four questions whose answers exemplify a current understanding of Earth's most ancient past will be considered in turn. Asking "simple" questions exposes all the more clearly the difficulties in answering them. The four questions are:

- When did a solid crust first cover Earth?
- When did liquid water first appear on Earth's surface?
- When did life first appear on Earth?
- When did Earth's atmosphere first become oxygenated?

It is no accident that each of the questions begins with the word "when". Geology, distinct from other sciences, is necessarily historical in its quest for understanding.

When Did a Solid Crust First Cover Earth?

The oldest known rocks on Earth are 4.03 to 3.94 Ga (1 Ga = 10^9 years) in age (1). They outcrop in a 10 km by 10 km area along the Acasta River in a remote area of northwestern Canada, 300 km east of Great Bear Lake (Figure 1). The rocks are igneous rocks that crystallized from molten silicate liquids themselves formed by melting still older progenitors. Only a faint glimpse can be gleaned of their predecessors but it is likely that a history even older than 4.03 Ga remains to be discovered (3). The ages of Acasta rocks are known with confidence because of careful measurements with mass spectrometers of the child/parent ratios of the radioactive decay of ^{235}U to ^{207}Pb and of ^{238}U to ^{206}Pb .

If one held a sample of Acasta rocks in hand it would be impossible to guess its age as Earth's oldest based on mineralogy and texture alone. The mineralogical composition of Acasta rocks falls into two groups: a darker-colored group consists of hornblende, plagioclase, quartz and biotite with minor amounts of alkali-feldspar, zircon, titanite, apatite, and garnet; a lighter-colored rock group contains quartz, alkali-feldspar, plagioclase, and biotite with zircon, titanite, and apatite. Open drawers at random in the rock collection of an undergraduate teaching geology laboratory and rocks indistinguishable in appearance will be found. Present day crustal processes produce Acasta look-alikes in the cores of active mountain ranges such as the Himalaya or the Southern Alps of New Zealand and they are exposed in the eroded roots of the Appalachian Mountains.

The oldest known sedimentary rocks are 3.8 Ga in age (4). They are at Isua, 120 km NE of Nuuk, western Greenland, adjacent to the retreating Greenland ice sheet (Figure 1). Sedimentary rocks outcrop in a narrow, hook-shaped belt 35-

km long, embedded in 3.6 to 3.8 Ga quartz-feldspar igneous rocks, similar to the lighter-colored rocks along the Acasta River. The simple existence of sedimentary rocks implies the prior existence of a solid crust from which they were eroded and upon which they were deposited. Both turbidite and banded-iron-formation sediments are present (5). Turbidite sediments consist of rock and mineral fragments that drop to the ocean bottom from sediment-laden density currents flowing down submarine slopes. Density currents may be generated by earthquakes shaking over-steepened sediment accumulations on sloping ocean floors. Banded Iron Formations are thinly laminated precipitates of fine-grained quartz, magnetite, hematite, siderite, dolomite-ankerite, greenalite, stilpnomelane and riebeckite that are most abundant in the time interval from 3.5 to 1.8 Ga (6). At Isua, the rocks have been deeply buried, and sedimentary minerals were converted to metamorphic minerals including assemblages of quartz, magnetite, grunerite, actinolite, and ripidolite (7).

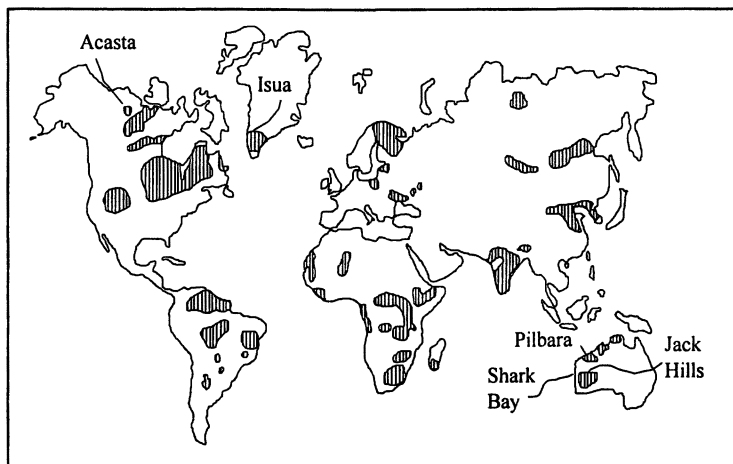


Figure 1. Locations of rock outcrops (shaded) older than 2.5 Ga ($1\text{Ga} = 10^9$ years (re-drawn from (2))).

The sediments of Isua illustrate the problems of relying upon the dictum “the present is key to the past”. Turbidite sediments are known from both modern and ancient times. Rapidly sequential breaks in submarine trans-Atlantic telephone cables following a 1929 earthquake are attributed to an accelerating density current flowing off the Grand Banks into deeper water. Deep-sea core samples taken from the path of the current show sedimentary grains sorted by size as they settled from the turbid water. The size-sorted sediments of the Atlantic abyssal plain have their ancient counterparts in the graded beds of 3.8 Ga rocks in Isua. In contrast, Banded Iron Formations are restricted in their

distribution throughout geologic time. Their absence from modern deposits makes it more difficult to understand their origin because their mechanism of formation cannot be observed.

The oldest minerals known on Earth are older than the oldest rocks. Zircon crystals ranging in age from 4.4 to 4.0 Ga occur as detritus in conglomeritic sediments from the Jack Hills, Western Australia (8) (Figure 1, Figure 2). Cores of the zircons preserve the oldest ages; rimming overgrowths form an onion-skin like envelope as young as 2.6 Ga. The mineral zircon, which crystallizes from molten silicate melts, resists physical abrasion and chemical exchange with its environment. Released by weathering and erosion from their parental rocks, zircon mineral grains persist as a permanent record of their growth conditions.

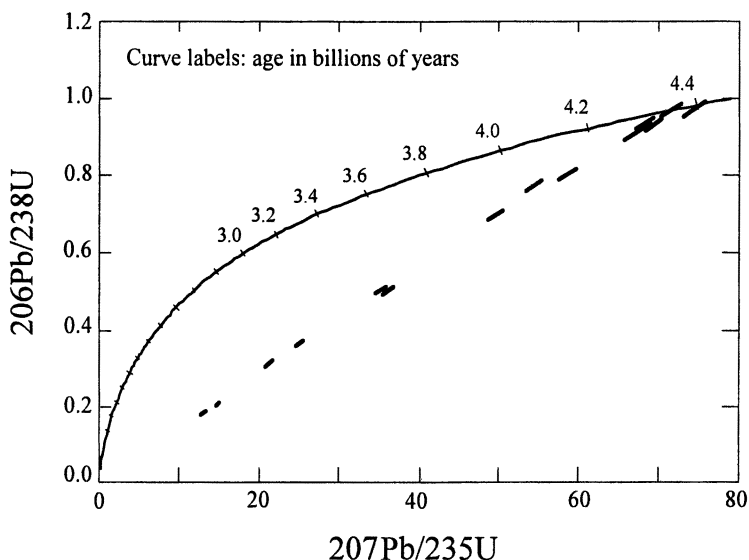


Figure 2. U-Pb isotopic data for some of Earth's oldest zircon crystals. The solid line shows the evolution of child/parent ratios, $^{206}\text{Pb}/^{238}\text{U}$ vs. $^{207}\text{Pb}/^{235}\text{U}$, as radioactive decay proceeds. The data points near 4.4 Ga give the age at which zircon first became closed in respect to exchange of U-Pb with its surroundings (re-drawn from (13)).

In consequence, it is a common trace mineral in rocks such as sandstone and conglomerate that are composed of rock and mineral fragments deposited from flowing water. Host sediments may have been deposited hundreds of million years after the cooling and solidification of igneous rocks that crystallized zircon, but the zircon mineral grains themselves record the age at which they nucleated from magma.

Earth's oldest rocks and oldest minerals record the presence of igneous processes: melting of older rocks and crystallization of molten silicate melts during 4.4 to 4.0 Ga. These are processes characteristic of the terrestrial crust today. It is important to establish to what extent ancient crustal processes may have resembled modern ones. Estimates of the conditions under which ancient igneous processes took place have been made by measuring the solubility of titanium dioxide in Hadean zircon crystals (9). Experiments measured the solubility of titanium in zircon crystallizing from either aqueous solutions or molten silicate liquids as a function of temperature, pressure, and TiO_2 saturation. The combined results show the crystallization temperatures of 180 Hadean zircons to be $688 \pm 23^\circ\text{C}$. Such a relatively low temperature with its accompanying narrow range of variation is symptomatic of water-saturated melting of typical crustal rocks. Melting temperatures of crustal rocks vary not only with mineralogical composition, with quartz-feldspar rocks being the lowest melting, but also are lowered in the presence of water because water partitions preferentially into molten silicate, thus stabilizing liquid phases at the expense of melting minerals.

Study of Earth's oldest rocks and minerals reveals not only ancient rocks closely resembling recent deposits, but also the operation of processes currently active in the crust. The present *seems to be* key to the past. But, not so fast: the unbalanced distribution of Banded Iron Formations across the vast span of geologic time serves as a warning flag that a hasty search for reassuring similarities may obscure the reality of significant differences between our time and the Archean.

There is an important qualification to answering the question "When did a solid crust first cover Earth?" In every outcrop studied to date, there are hints of still older crustal cycles. The age estimates for Earth's oldest rocks provide a constraint on the timing of crustal formation embodied in the statement "Earth's first crust formed at the same time or earlier than the age of its oldest known rocks".

When Did Liquid Water First Appear on Earth's Surface?

The oldest geologic evidence of the presence of liquid water on Earth's surface are "pillow basalts" outcropping in the 3.8 Ga Isua terrain of West Greenland (Figure 1, Figure 3) (10). The term "pillow" refers to rounded, ellipsoidal, one-meter masses of the volcanic rock basalt heaped on the ocean floor after an eruption. Pillow basalts are formed when basaltic lavas flow directly into water before solidifying. The long-standing eruption of the Hawaiian volcano Pu'u'O'o into the Pacific Ocean provides memorable examples of incandescent streams of low viscosity, liquid lava arching into the sea. Daring undersea photography has captured pillow-shaped, meter-sized pods

of basalt forming as a thin skin of glassy lava rock cools in contact with cold water, inflates like a balloon, and is punctured by extruding hot lava to form another pillow. The origin of pillow structures is sufficiently unique that their presence, alone, can be taken as proof of the existence of standing liquid water. The US Geological Survey provides excellent information on pillow basalts (11).

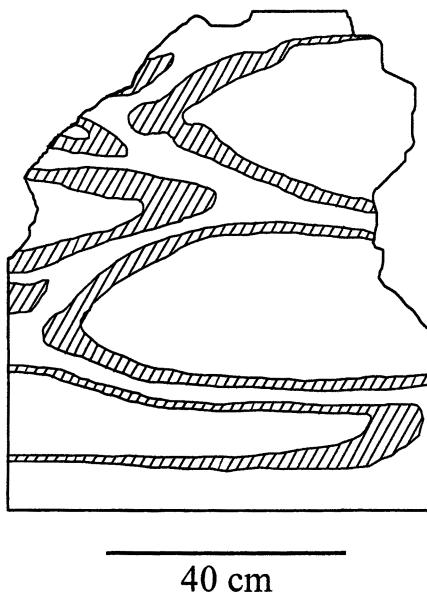


Figure 3. Outline sketch of pillow lavas exposed in glacially polished cross-sections at Isua, West Greenland. Shading highlights chilled margins that form when molten basalt pours into standing water. Pillows were flattened during burial by weight of younger deposits and their composition was transformed to minerals stable at higher temperature by geothermal heating (re-drawn from (10)).

There is indirect geochemical evidence for the presence of liquid water on Earth's surface during the Hadean. Analyses of the oxygen isotope ratios, $^{18}\text{O}/^{16}\text{O}$, of 3.96 Ga Acasta rocks give a $\delta^{18}\text{O}$ value of +8.9 ‰ relative to ocean water (see below for definition of "δ" notation) (12). Hadean zircons from western Australia average 7.3 ± 2 ‰ in $\delta^{18}\text{O}$ (13, 14, see *S-isotope discussion, below*, and R.N. Clayton, *this volume*). Values of $\delta^{18}\text{O} > 7.5$ measured on igneous rocks indicate weathered surface deposits were incorporated during melting. The Acasta and higher zircon values of $\delta^{18}\text{O}$ are consistent with surface weathering in the presence of liquid water at Earth's surface, followed by burial

of surface deposits, heating, melting and then subsequent cooling and solidification to produce igneous rocks with elevated values of $\delta^{18}\text{O}$.

Interpreting evidence for Earth's oldest surface water relies upon the present as key to the past. It is assumed that pillow basalts formed in the past as they are observed today. The known crustal cycle of surface weathering, burial, heating, partial melting, intrusion and solidification of molten rock as identified by its oxygen isotope signature is assumed to have operated more than 4 billion years ago. There is no strong reason to doubt the estimate for the time at which liquid water first appeared on Earth's surface but one should be aware of the assumptions underlying the estimate.

When Did Life First Appear on Earth?

Of all the questions to be asked about Early Earth history the one that is the most emotionally charged, and at the same time the most difficult to answer, is that of the age of first life. The dead remains of living organisms are quite fragile and especially so when the organism has no hard parts such as a protective shell or a skeleton. Complex organic molecules produced by living metabolisms are vulnerable to chemical and thermal degradation. The existing record of earliest life remains controversial despite decades of dedicated and competent investigation. Interpretations of fossil morphological evidence for ancient life inevitably rest upon "the present is key to the past" logic: "If it looks like the remains of a known organism then it must be a fossil of a similar, ancient life form". But these "looks like" interpretations have been challenged repeatedly. Investigations of Earth's earliest life are increasingly strengthened by new geochemical data. The geochemical present is key to the past: modern metabolic processes are known to produce unique chemical and isotopic signatures. Found in ancient deposits, with or without look-alike fossils, the geochemical signatures are accepted as evidence of the presence of ancient life.

Discoveries of microstructures in Archean rocks that resemble the forms of modern microbes have sparked a continuing debate about their origin: are they *bona fide* fossils or do they merely bear an accidental likeness to living organisms (15, 16)? A list of the growing body of geochemical data measured on rocks associated with those containing such microstructures demonstrates supporting evidence of active metabolisms. The following investigations were conducted in the Pilbara region of Western Australia, in 3.5 Ga rocks that have all experienced similar geological histories (Figure 1). *In-situ* Raman spectroscopy of Archean microstructures reveals the presence of insoluble carbonaceous matter that may be derived from thermal and chemical degradation of ancient living tissue (15). Sulfur isotope fractionations spanning a range in

$\delta^{34}\text{S}$ of 21 ‰ are consistent with the reduction of aqueous sulfate by microbes (17). The presence of ^{13}C -depleted, insoluble organic residues in silica dikes suggests the presence of thermophilic microbes living in a seafloor hot-springs environment (18). The same silica dikes contain 1-15 micron gas bubbles sealed in quartz and filled with methane even more strongly depleted in ^{13}C than insoluble organic residues, consistent with the vital effects of methanogenic microbes (19). Remember, the 3.5 Ga rocks of Pilbara contain not only putative microfossils and stromatolites but also geochemical evidence of microbial isotope fractionations. With such a body of evidence, one can sense a tilting in favor of the hypothesis that life was flourishing on Earth as early as 3.5 Ga.

Stromatolites are millimeter- to meter-sized “attached, lithified sedimentary growth structures, accretionary away from a point or limited surface of initiation” (20). This terse, accurate definition does not convey the beauty and variety of stromatolites observed throughout the geologic record. The contemporary, domal stromatolites of Shark Bay, Western Australia, initiate as cm-sized mounds on the Bay floor, grow upward and laterally until they resemble a half-meter tall, precariously balanced, upside-down bowling pin (Plate 1A). Closely spaced individual stromatolites are stabilized by lateral growth, first by bridging to adjacent neighbors then by in-filling to form a massive reef. Generations of geologists mapped ancient stromatolite reefs back in time into the Archean era, in rocks as old as 3.4 Ga, and accepted them as naked-eye evidence of the presence of living organisms (Plate 1B, 1C) (21). Like stromatolites in Shark Bay, ancient microorganisms trapped and bound sediment in their mucilaginous filaments, providing the glue that held the structure together until burial preserved them. The carbonate mineral constituting the stromatolite structure itself is not secreted directly by organisms, as a snail grows its own shell, for example. But the microorganisms provide the indispensable environmental conditions under which stromatolite growth is favored. The certainty with which stromatolites were interpreted as indisputable evidence of life processes of ancient microorganisms has been rocked by the discovery that non-biological processes may produce stromatolite look-alikes (22). Physical-mathematical models have been devised that call upon inorganic chemical precipitation of carbonate minerals at sediment-water interfaces to amplify existing cm-scale seafloor topography to produce stromatolitic structures.

The evidence for or against the presence of Archean life remains contentiously debated (23). One cannot fail to notice, however, that for every objection that is raised against the evidence for ancient life, a new piece of geochemical data is presented in support of the existence of microbial life as early as 3.5 Ga.



Plate 1A. Stromatolites growing today on the floor of Shark Bay, Western Australia (Figure 1). The bulbous, top-heavy individual stromatolite in left foreground will eventually join the massive reef to the right by bridging laterally towards other individuals such as the smaller one in center foreground. Largest stromatolites are approximately 0.5 meter in height (underwater photo by author). (See page 14 of color inserts.)



*Plate 1B. Outcrop cross-section of 1.9 Ga stromatolites exposed in Duck Creek Gorge, Western Australia. Stromatolites nucleate as isolated individuals then grow upward and laterally, bridging to adjacent individuals to form massive reefs. Note new stromatolite growing on a substrate of old stromatolites in upper right. Cross-sections show same bulbous, top-heavy form seen at Shark Bay. Hammer handle 25 cm in length (photo by author).
(See page 15 of color inserts.)*

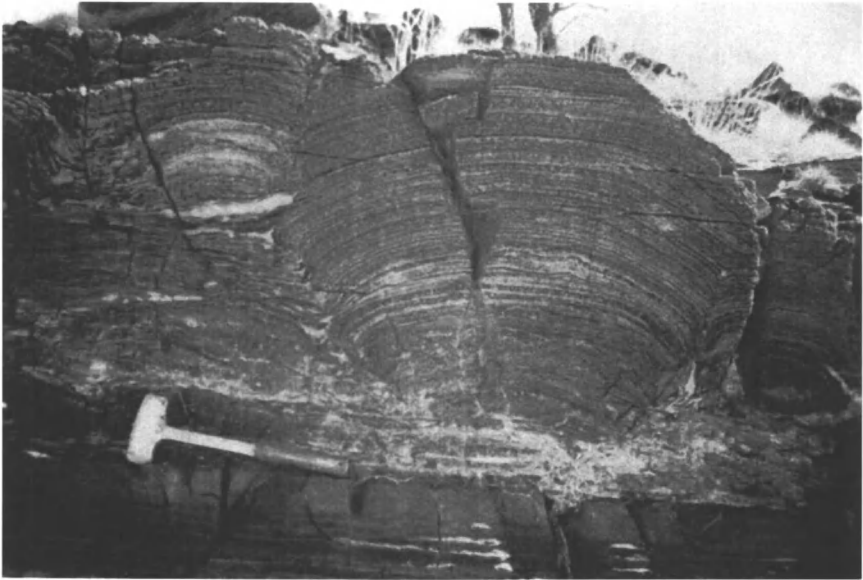


Plate 1C. Outcrop cross-section of 2.7 Ga stromatolites exposed near Redmont, Western Australia. See Plate 1B caption. Hammer handle 35 cm in length (photo by author). (See page 16 of color inserts.)

When Did the Earth's Atmosphere Become Oxygenated?

Study of the evolution of Earth's oxygenated atmosphere, a composition unique among the terrestrial planets, has proceeded at a different pace and by different methods than that of the history of its crust or of earliest life. Geologists have always had direct access to samples of ancient rocks. As the capabilities of modern science grew, geologists acquired an ever-deepening understanding of Earth's history by applying each new generation's improved analytical technologies to readily available rock samples. The study of atmospheric evolution presents a quite different problem, however. There are no direct samples of Hadean or Archean atmospheres. Faced with the seemingly insuperable obstacle of nothing to study, geologists began to search for chemical or isotopic signatures that could be uniquely attributed to some aspect of atmospheric chemistry. These tell-tale clues of the operation of ancient processes are termed "proxies". The quantitative mineralogical, chemical or isotopic parameter measured in rocks or minerals substitutes, or proxies, for direct observation of processes that otherwise left no trace behind.

Geologists have recognized a number of proxies that imply anoxic Archean conditions followed by oxygenation of the atmosphere beginning at 2.5 Ga (24). There are Archean conglomerates with pebbles of uraninite and pyrite, minerals that oxidize rapidly in an oxygenated atmosphere, but a lack of these minerals in younger detrital deposits. A spike in abundance of Banded Iron Formations prior to 2.5 Ga contrasts with sporadic occurrences in later times. Highly oxidized deposits of manganese ores and "red beds", sediments with red-colored, oxidized iron minerals, appear after 2.5 Ga but are absent from older rocks. Each of these proxies has its own value in suggesting the atmosphere gained oxygen after 2.5 Ga, but questions arise as to whether each is a uniquely definitive signature of atmospheric composition. Mineralogical proxies of atmospheric chemistry lack the force of a logically sufficient proof because one can almost always think of alternative explanations for them. Mineralogical proxies lack uniqueness because they are proxies of proxies: they are not direct deposits of atmospheric processes.

The search for definitive proxies of atmospheric chemistry had its first big success in recognizing a unique isotopic signature in ozone. Analyses of samples collected by high-altitude balloons found large enrichments in ^{17}O and ^{18}O in ozone (25). Laboratory experiments confirmed that it was the ozone-forming reaction, itself, that confers a measurable excess of ^{17}O and ^{18}O on ozone (26).

The search for surface deposits that preserve anomalous oxygen isotope fractionations led from improbable sites such as the hyper-arid, super-hot Atacama Desert, Chile, to super-cold sampling pits dug in snow at the South Pole. The proxy dragnet focused on these remote sites because aridity and freezing are two viable methods for preserving water-soluble, direct products of atmospheric chemistry for detailed investigations. Anomalously fractionated

oxygen is deposited at Earth's surface in the form of sulfuric and nitric acid aerosol particles (27, 28). Reactions between acid aerosols, wind blown sea salt, and calcite dust produce minerals such as anhydrite (CaSO_4) and nitratine (NaNO_3). The minerals preserve isotopic anomalies for as long as the minerals, themselves, persist. Oxygen isotope anomalies do not endure indefinitely in rocks, however. The minerals archiving oxygen isotope fractionation anomalies are water-soluble. They survive in arid deserts but are vulnerable to chance rainstorms.

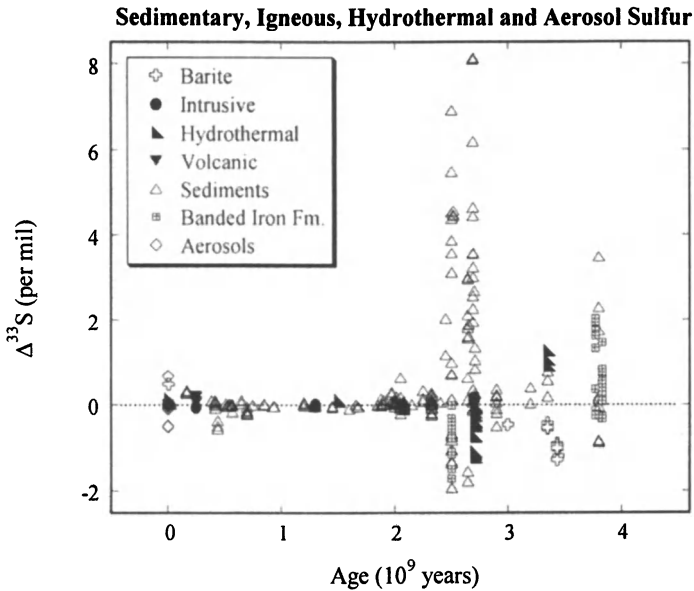


Figure 4. Sulfur isotope anomalous fractionations (see text) plotted vs. age in Ga. Sharp change in magnitude of anomalies at 2.5 Ga is found worldwide in rocks from Australia, Canada, India, and South Africa (29, 30, 31, 32, 33, 34, 35)

The discovery of large anomalous fractionations in sulfur isotopes, ^{32}S - ^{33}S - ^{34}S - ^{36}S , present in the minerals pyrite (FeS_2) and barite (BaSO_4) in rocks older than 2.5 Ga, presented geochemists with the prospect of a durable proxy for atmospheric chemistry (29). Storage of isotope anomalies in insoluble minerals such as pyrite or barite that persist indefinitely throughout geologic eons guarantees a robust atmospheric proxy. Interpretation of the significance of the isotope anomalies is based on their age distribution. There is a sharp change in the magnitude of anomalous fractionations (measured as $\Delta^{33}\text{S}$ in parts per thousand, see below) from a total range of variation of 10 per mil before 2.3 Ga

to a range of 2 per mil afterwards (Figure 4). The sharp change is not a localized phenomenon but is observed world-wide in Australia, Canada, India, and South Africa. The timing of the decrease in magnitude of sulfur isotope anomalies coincides with that of the traditional date proposed for atmospheric oxygenation, based on indirect proxies of atmospheric chemistry.

The production of anomalous fractionations by ultraviolet light was confirmed in laboratory experiments (36). Experimental irradiation of SO₂ gas, an abundant constituent of volcanic emissions, demonstrated that exposure to ultraviolet light generated anomalous isotope fractionations. The presence of molecular oxygen in a pre-2.5 Ga atmosphere, and the inevitable formation of ozone by UV photolysis, would have shielded volcanic SO₂ from the Sun's UV light and, thus, prevented the production of sulfur isotope anomalies. An oxygen-bearing atmosphere, furthermore, would not preserve sulfur isotope anomalies because fractionated products would have been homogenized by oxidation. Measured sulfur isotope anomalies indicate the presence of an oxygen-free atmosphere prior to 2.5 Ga with unrestricted UV photolysis followed by oxygenation and suppression of anomalies.

Discussion of atmospheric isotope proxies requires definitions of the quantities used by geochemists to report measured isotope ratios. Sulfur has four stable isotopes ³²S, ³³S, ³⁴S, and ³⁶S (³⁶S is ignored to simplify the text). Samples are prepared for analysis by laser heating sulfur-bearing minerals in the presence of F₂ gas, producing the working gas SF₆. Isotope ratios are measured in gas source, electron impact mass spectrometers with simultaneous collection of SF₅⁺ ion beams with m/e 127, 128, 129, and 131 in Faraday cups. The isotope ratios are measured by comparing unknown samples to standard SF₆ gas prepared from a reference material whose composition is given in respect to troilite (FeS) from the Canyon Diablo meteorite (Canyon Diablo Troilite, CDT). The Greek "delta" notation is used to report analytical data in units of "per mil", ‰.

$$\delta^{33}\text{S}_{\text{V-CDT}} = [({}^{33}\text{S}/{}^{32}\text{S})_{\text{sample}}/({}^{33}\text{S}/{}^{32}\text{S})_{\text{V-CDT standard}} - 1] * 1000$$

$$\delta^{34}\text{S}_{\text{V-CDT}} = [({}^{34}\text{S}/{}^{32}\text{S})_{\text{sample}}/({}^{34}\text{S}/{}^{32}\text{S})_{\text{V-CDT standard}} - 1] * 1000$$

The magnitude of anomalous fractionations of sulfur isotopes is given by the formula

$$\Delta^{33}\text{S} = \delta^{33}\text{S} - 1000 * [(1 + \delta^{34}\text{S}/1000)^\lambda - 1] \quad (1)$$

in units of "per mil", ‰, where λ is typically 0.515 for a variety of terrestrial samples. As originally interpreted, a non-zero value of $\Delta^{33}\text{S}$ in equation (1)

denoted anomalous isotope fractionation caused by atmospheric chemistry. It is now known, however, that in the fractionation of sulfur isotopes by microbes the value of λ is not necessarily equal to 0.515 (32). The magnitude of $\Delta^{33}\text{S}$ is governed not only by values of $\delta^{33}\text{S}$ and $\delta^{34}\text{S}$ but also by changes in λ .

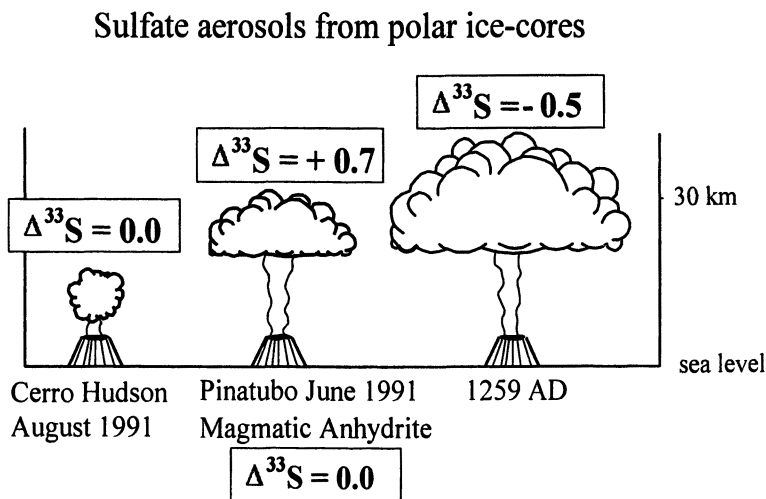


Figure 5. Sulfur isotope compositions of sulfuric acid aerosols in South Pole ice core samples. Aerosols from two eruptions, Pinatubo and AD 1259 that injected SO_2 into the stratosphere have anomalously fractionated ^{32}S - ^{33}S - ^{34}S (39).

Modern volcanic eruptions and their catastrophic impact on atmospheric chemistry appear to be remote from the problem of deducing the nature of Earth's earliest atmosphere. But it is Nature's experiments in atmospheric chemistry as exemplified by the injection of large amounts of SO_2 into the stratosphere by gigantic eruptions that validates sulfur isotope anomalies as proxies for ancient atmospheric chemistry. Isotopic records of the rapid oxidation of volcanic SO_2 at high altitude unshielded from UV light are preserved in sulfuric acid aerosol particles. Larger aerosol particles eventually fall as sediment on Earth's surface and thus offer opportunities for study by geochemists. If they fall in humid regions, aerosols are diluted by rainwater and disappear. If they fall in arid deserts, acidic aerosols react with windblown calcite (CaCO_3) dust, forming mineral salts (such as the mineral anhydrite, CaSO_4) and are preserved at least until the next rainstorm. And if aerosols fall on glacier ice and are frozen in snow, they are preserved until the ice melts.

Violent eruptions such as that of Mt. Pinatubo, Philippine Islands, in June 1991, inject millions of tons of microscopic glass particles (termed "ash") into the atmosphere. The most violent eruptions propel towering ash clouds into the stratosphere. In one famous incident, a trans-polar passenger jet liner was forced to land in Anchorage, Alaska, after flying through an ash cloud from an Aleutian volcano when the heated, internal surfaces of its engines became coated with melted glass. Explosive eruptions emit, in addition to ash, megatons of SO_2 gas into the troposphere, and in especially violent eruptions, into the stratosphere. Sulfur-bearing volcanic gases are oxidized to water-soluble sulfate by such powerful atmospheric oxidants as OH-radicals, ozone, and hydrogen peroxide (37). The resulting sulfuric acid, with its relatively low vapor pressure and high surface tension, forms droplets termed "aerosol particles". The Pinatubo eruption deposited 20 Terragrams of SO_2 into the stratosphere in a single day. Rapid oxidation yielded 30 Terragrams of aerosol particles. Clouds of Pinatubo aerosols circumnavigated the globe westward within 22 days. The eruptive clouds crossed the equator from North to South within a few weeks and a portion of the ash and aerosol particles fell upon snow in Antarctica.

A growing body of data on Antarctic ice cores shows that the history of volcanic eruptions is resolvable year-by-year (38). The record includes dated explosive events such as Cerro Hudson in 1991, Pinatubo-1991, Agung-1963, Krakatoa-1883, Tambora-1815, and a 1259 AD eruption of unknown location. Analysis of the oxygen and sulfur isotope composition of aerosol particles frozen in the polar refrigerator provides a proxy of atmospheric chemistry applicable to early Earth. Aerosols from Cerro Hudson, the smallest of the explosive eruptions, have normal sulfur isotope compositions with no anomalous fractionation of ^{32}S - ^{33}S - ^{34}S (39). Cerro Hudson's eruption cloud did not break through the tropopause into the stratosphere. Sulfate aerosols collected near the crater of Masaya volcano, Nicaragua, which has been quietly releasing SO_2 gas at low altitude without explosive eruptions for decades, have no sulfur isotope anomalies (40). Aerosol particles deposited from the largest eruptions, Mt. Pinatubo, Agung, and 1259 AD, have anomalies in $\Delta^{33}\text{S}$ ranging from -1 to +1.4 ‰ (39, 41). The eruptions differed not only in volume of emissions but also in the heights to which their ash and gas clouds rose. Mt. Pinatubo's SO_2 plume was initially concentrated in the stratosphere between 20 and 27 km altitude (37), Agung's cloud rose to 25 km (42). The height of the 1259 eruptive plume is not known but the enormous size of the sulfate chemical anomaly in ice cores suggests that it must have reached as high as those of Pinatubo and Agung. The SO_2 emitted in the largest eruptions rose to such a height that it was exposed to the Sun's UV light, above the ozone shield. Eruptive clouds restricted to the troposphere were protected from UV exposure by the ozone shield.

Do present-day volcanic eruptions provide a key to understanding Earth's ancient atmosphere? Eruptive clouds of volcanic SO_2 penetrating into the

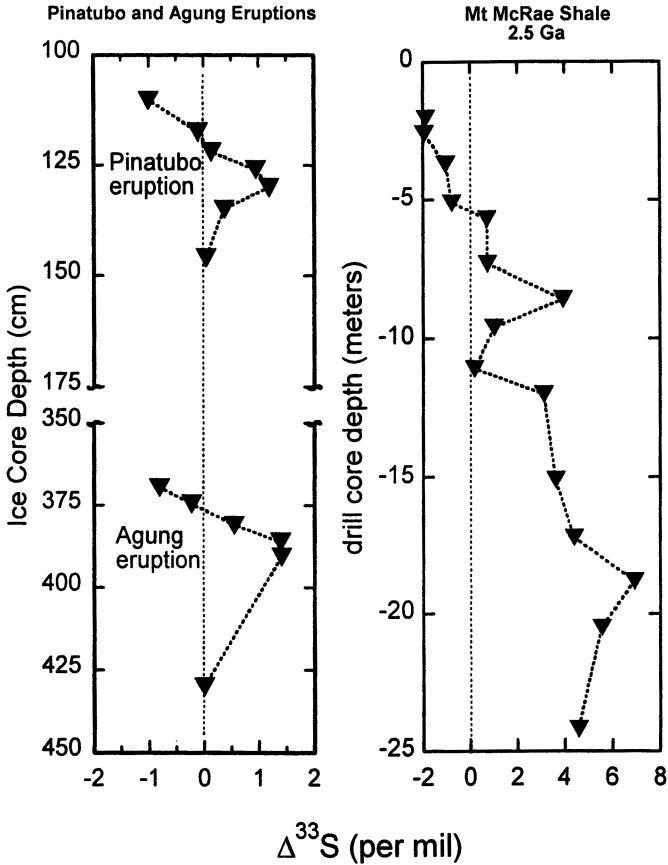


Figure 6. Comparison of ice core record of volcanic eruptions with sulfur isotope data from 2.5 Ga Mt. McRae shale, Western Australia. Range of sulfur isotope anomalies in Mt. McRae shale is 5 times bigger than in snow samples. Note 100-fold difference in depth scale (34, 41).

stratosphere acquire anomalous sulfur isotope fractionations despite the observation that sulfate crystallizing from molten lava has no anomaly (note composition of magmatic anhydrite in Figure 5). A side-by-side comparison of recent polar ice cores with 2.5 Ga rock drill samples shows a striking similarity in their zig-zag patterns of changing $\Delta^{33}\text{S}$ with elapsed time (Figure 6). Considered together with laboratory simulations, the key factor in producing anomalous isotope fractionations is exposure to ultraviolet light. An anoxic Archean atmosphere provides optimal conditions for producing and preserving

sulfur isotope fractionation anomalies. The smaller size of anomalies measured in modern ice cores compared to Archean rocks highlights just how difficult it is to preserve the full magnitude of fractionations in today's oxygenated atmosphere. In the Archean, it is likely that sulfate-reducing microbes performed the vital task of facilitating the precipitation of sulfate as the insoluble mineral pyrite (FeS_2). In the modern world, the anomalies are vulnerable to immediate erasure and are preserved only under fortuitous and ephemeral circumstances in ice cores.

Earth's Earliest Crust, Ocean, Life and Atmosphere

I would like to be able to report that geologists have reached a discipline-wide consensus on the environments of Early Earth. The rock record affords glimpses into the past revealing a planet recognizable as the Earth we live on today, extant since the beginning of the Archean eon. Nevertheless disagreements remain on vitally important questions: When did life first appear on Earth? What type of organisms were they? How did Earth's atmosphere evolve into its present day composition? The difficulties in answering these questions are exposed above. It is not merely the problem of interpreting an imperfect rock record but also of devising objective, calibrated proxies to obtain information on ancient environments and ecological relationships. The search for understanding of Early Earth demonstrates the radically inclusive perspective required to envision and validate environmental proxies. Disciplines as widely divergent as atmospheric photochemistry, microbiology, volcanology, geochemistry, paleontology, and geology must be embraced to discern interactions between atmosphere, biosphere, hydrosphere, and lithosphere. And the ultimate limitation to understanding lies in our logic: we have only the present to guide exploration of the past.

Acknowledgements

I am grateful to Drs. Lori Zaikowski (Dowling College) and Jon M. Friedrich (Fordham University) for the invitation to participate in the symposium "Chemical Change Across Space and Time". Dr. Bruce Watson (Rensselaer Polytechnic Institute) gave a constructive review of the manuscript. Thanks are due to Mr. Ross Mack, marine protection officer with the Department of Environment and Conservation of the Western Australian Government, who provided guided access to the stromatolites shown in Plate 1A. Drs. Yuichiro Ueno and Tsuyoshi Komiya, Tokyo Institute of Technology, introduced the author to the Archean geology of Western Australia. Profs. Don Lowe (Stanford University) and Gary Byerly (Louisiana State University) led an informative field trip to the Archean Outcrops of Barberton Mountain Land,

South Africa. Prof. Nicholas Beukes (University of Johannesburg) guided an excellent field trip to the Witwatersrand Basin, South Africa. The support of Dr. West Huntress, Director of the Geophysical Laboratory, Carnegie Institution of Washington, the National Science Foundation, EAR-0003276, and the National Aeronautics and Space Administration, NAG5-12948, is gratefully acknowledged.

References

1. Bowring, S. A.; Williams, I. S. *Contributions to Mineralogy and Petrology* **1999**, *134*, 3.
2. Valley, J. W. *Elements* **2006**, *2*, 201.
3. Iizuka, T.; Horie, K.; Komiya, T.; Maruyama, S.; Hirata, T.; Hidaka, H.; Windley, B. F. *Geology* **2006**, *34*, 245.
4. Moorbath, S.; O'Nions, R. K.; Pankhurst, R. J. *Nature* **1973**, *245*, 138.
5. Rosing, M. T.; Rose, N. M.; Bridgewater, D.; Thomsen, H. S. *Geology* **1996**, *24*, 43.
6. Klein, C. *American Mineralogist* **2005**, *90*, 1473.
7. Dymek, R. F.; Klein, C. *Precambrian Research* **1988**, *39*, 247.
8. Compston, W.; Pidgeon, R. T. *Nature* **1986**, *321*, 766.
9. Watson, E. B.; Harrison, T. M. *Science* **2005**, *308*, 841.
10. Komiya, T.; Maruyama, S.; Masuda, T.; Nohda, S.; Okamoto, K. *Journal of Geology* **1999**, *107*, 515.
11. URL at <http://volcanoes.usgs.gov/Products/Pglossary/PilowLava.html>
12. Muehlenbachs, K.; Bowring, S. A. *EOS* **1992**, *73*, 325.
13. Wilde, S. A.; Valley, J. W.; Peck, W. H.; Graham, C. M. *Nature* **2001**, *409*, 175.
14. Mojzsis, S. J.; Harrison, T. M.; Pidgeon, R. T. *Nature* **2001**, *409*, 178.
15. Schopf, J. W.; Kudryavtsev, A. B.; Agresti, D. G.; Wdowiak, T. J.; Czaja, A. D. *Nature* **2002**, *416*, 73.
16. Brasier, M. D.; Green, O. R.; Jephcoat, A. P.; Klepepe, A. K.; Van Kranendonk, M. J.; Lindsay, J. F.; Steele, A.; Grassineau, N. V. *Nature* **2002**, *416*, 76.
17. Shen, Y.; Buick, R.; Canfield, D. E. *Nature* **2001**, *410*, 77.
18. Ueno, Y.; Yoshioka, H.; Maruyama, S.; Isozaki, Y. *Geochimica et Cosmochimica Acta* **2004**, *68*, 573.
19. Ueno, Y.; Yamada, K.; Maruyama, S.; Isozaki, Y. *Nature* **2006**, *440*, 516.
20. Grotzinger, J. P.; Knoll, A. H. *Annual Reviews of Earth and Planetary Sciences* **1999**, *27*, 313.
21. Alwood, A. C.; Walter, M. R.; Kamber, B. S.; Marshall, C. P.; Burch, I. W. *Nature* **2006**, *441*, 714.
22. Grotzinger, J. P.; Rothman, D. H. *Nature* **1996**, *383*, 423.

23. Schopf, J. W. *Philosophical Transactions of the Royal Society B* **2006**, 361, 869.
24. Canfield, D. E. *Annual Reviews of Earth and Planetary Sciences* **2005**, 33, 1.
25. Mauersberger, K.; Lammerzahl, P.; Krankowsky, D. *Geophysical Research Letters* **2001**, 28, 3155.
26. Mauersberger, K.; Erbacher, B.; Krankowsky, D.; Gunther, J.; Nickel, R. *Science* **1999**, 283, 370.
27. Bao, H.; Thiemens, M. H.; Farquhar, J.; Campbell, D. A.; Lee, C. C.-W.; Heine, K.; Loope, D. B. *Nature* **2000**, 406, 176.
28. Michalski, G.; Scott, Z.; Kabling, M.; Thiemens, M. H. *Geophysical Research Letters* **2003**, 30, 1870.
29. Farquhar, J.; Bao, H.; Thiemens, M. H. *Science* **2000**, 289, 756.
30. Bekker, A.; Holland, H. D.; Wang, P.-L.; Rumble III, D.; Stein, H. J.; Hannah, J. L.; Coetzee, L. L.; Beukes, N. J. *Nature* **2004**, 427, 117.
31. Hu, G.; Rumble, D.; Wang, P.-L. *Geochimica et Cosmochimica Acta* **2003**, 67, 3101.
32. Johnston, D. T.; Wing, B. A.; Farquhar, J.; Kaufman, A. J.; Strauss, H.; Lyons, T. W.; Kah, L. C.; Canfield, D. E. *Science* **2005**, 310, 1477.
33. Mojzsis, S. J.; Coath, C. D.; Greenwood, J. P.; McKeegan, K. D.; Harrison, T. M. *Geochimica et Cosmochimica Acta* **2003**, 67, 1635.
34. Ono, S.; Eigenbrode, J. L.; Pavlov, A. A.; Kharecha, P.; Rumble III, D.; Kasting, J. F.; Freeman, K. H. *Earth and Planetary Science Letters* **2003**, 213, 15.
35. Papineau, D.; Mojzsis, S. J.; Coath, C. D.; Karhu, J.; McKeegan, K. D. *Geochimica et Cosmochimica Acta* **2005**, 69, 5033.
36. Farquhar, J.; Savarino, J.; Airieau, S.; Thiemens, M. H. *Journal of Geophysical Research* **2001**, 106, 32829.
37. McCormick, M. P.; Thomason, L. W.; Trepte, C. R. *Nature* **1995**, 373, 399.
38. Cole-Dai, J.; Mosley-Thompson, E.; Thompson, L. G. *Journal of Geophysical Research* **1997**, 102, 16761.
39. Savarino, J.; Romero, A. B.; Cole-Dai, J.; Bekki, S.; Thiemens, M. H. *Geophysical Research Letters* **2003**, 30, (21), 2131.
40. Mather, T. A.; McCabe, J. R.; Rai, V. K.; Thiemens, M.; Pyle, D. M.; Heaton, T. H. E.; Sloane, H. J.; Fern, G. R. *Journal of Geophysical Research* **2006**, 111, D18205.
41. Baroni, M.; Thiemens, M.; Delmas, R. J.; Savarino, J. *Science* **2007**, 315, 84.
42. URL at <http://www.volcano.si.edu/>

Chapter 15

Prebiotic Organic Synthesis in Neutral Planetary Atmospheres

H. J. Cleaves¹, J. H. Chalmers¹, A. Lazcano², S. L. Miller³,
and J. L. Bada^{1,*}

¹Scripps Institution of Oceanography, University of California at San Diego, La Jolla, CA 92093–0212

²Facultad de Ciencias, UNAM, 04510 Mexico D.F., Mexico

³Department of Chemistry and Biochemistry, University of California at San Diego, La Jolla, CA 92093–0314

*Corresponding author: jbada@ucsd.edu

It is now widely held that the early Earth's atmosphere was likely neutral, dominated by N₂ and CO₂. The synthesis of organic compounds by the action of electric discharges on neutral gas mixtures has been shown to be much less efficient than with reducing gas mixtures. We show here that contrary to previous findings, significant amounts of amino acids are produced under these conditions. The low yields found previously were likely the result of oxidation of the organic compounds during hydrolytic workup by nitrite and nitrate produced in the reactions. Addition of oxidation inhibitors prior to hydrolysis results in the recovery of several hundred times more amino acids than reported previously. Organic synthesis from neutral atmospheres may thus have depended as much on oceanic conditions as on the characteristics of the primitive atmosphere itself. These findings imply the need for a critical re-evaluation of the importance of such syntheses on the primitive Earth and other planetary bodies that, like Mars, may have been endowed with CO₂ and N₂-rich atmospheres throughout most of their history.

Introduction

Today, organic compounds are so pervasive on the Earth's surface that it is hard to imagine the Earth devoid of organic material. However, during the period immediately after the Earth first formed some 4.5 Ga (billion years ago), there would have likely been no reservoir of organic compounds present. This was because soon after accretion, the decay of radioactive elements heated the interior of the young Earth to the melting point of rocks. Volcanic eruptions expelled molten rock and hot scorching gases out of the juvenile Earth's interior creating a global inferno. In addition, the early Earth was also being peppered by mountain-sized planetesimals, the debris left over after the accretion of the planets. Massive volcanic convulsions, coupled with the intense bombardment from space, generated surface temperatures so hot that the Earth at this point could very well have had an "ocean" of molten rock, i. e., a "magma ocean".

Although temperatures would have slowly decreased as the infall of objects from space and the intensity of volcanic eruptions declined, elevated temperatures likely persisted for perhaps a hundred million years or longer after the formation of the Earth. During this period, temperatures would have probably been too hot for organic compounds to survive. Without organic compounds, life as we know could not have existed. However, based on data from ancient zircons, by approximately 4 Ga (or perhaps even earlier) the Earth's surface must have cooled down to the point that liquid water could exist and global oceans began to form (1). It was during this period that organic compounds would have first started to accumulate on the Earth's surface, as long as there were abiotic processes by which they could be synthesized or delivered intact to the Earth. This in turn would have marked an important transition in the chemistry of the early Earth since a reservoir of organic compounds is considered to be necessary for the origin of life.

At the turn of the 20th century, some scientists began to seriously tackle the seemingly intractable problem of how life started on Earth and where the necessary organic compounds may have come from. In the 1920s, publications of Oparin and Haldane (2), as well as others suggested that life on Earth arose from an abiotic mixture of organic compounds produced by natural geochemical reactions. Based on an evolutionary analysis of metabolism and the then fledgling knowledge of the primitive Earth and planetary atmospheres, a detailed stepwise sequence of the events leading from the synthesis and accumulation of organic compounds to primordial life-forms whose maintenance and reproduction depended on external sources of reduced carbon.

According to the modern version of the prebiotic soup theory for the origin of life (3) organic compounds derived from "home grown" chemical synthetic reactions directly on the Earth and the infall of organic rich material from space accumulated in the primordial oceans. These compounds then underwent further reactions in the primal broth producing ones with increasing molecular complexity. Some of these reactions took place at interfaces of mineral deposits

with primitive ocean water, while others occurred when the primitive ocean constituents were concentrated by various mechanisms such as evaporation in shallow water regions or the formation of eutectic brines produced during the freezing of parts of the oceans.

Organic Compounds from Space

Exogenous delivery of organic matter by asteroids, comets and interplanetary dust particles (IDPs) could have played a significant role in seeding the early Earth with the compounds considered to be necessary for the origin of life (4). This conclusion was based on knowledge of the organic composition of meteorites. Carbonaceous chondrites, a class of stony meteorites, have a high abundance of organic carbon, more than three percent by weight in some cases. Many of these types of meteorites have been extensively analyzed for organic compounds. The organic matter is dominated by a hot water insoluble fraction. Although present in lesser amounts, the hot water soluble organic matter has been found to consist of polycyclic aromatic hydrocarbons (PAHs), aliphatic hydrocarbons, carboxylic acids, fullerenes and amino/hydroxy acids (5). The purines adenine, guanine, xanthine and hypoxanthine have also been detected, as well as the pyrimidine uracil in concentrations of 200 to 500 parts per billion (ppb).

The importance of exogenous delivery of organic matter to the early Earth is critically dependent on the survivability of organic compounds during the delivery process. It is presently unclear exactly how much organic material would escape destruction during asteroid, comet and interplanetary dust particle infall to the Earth's surface.

“Home-Grown” Prebiotic Syntheses

It was not until the advent of organic chemical syntheses that processes could be studied that may have been involved in the direct synthesis of organic compounds on the early Earth. Friedrich Wöhler's report in 1828 on the synthesis of urea from silver cyanate and ammonium chloride represented the first synthesis of an organic compound from inorganic starting materials (3). Although it was not immediately recognized as such, a new era in chemical research had been begun: in 1850, Adolph Strecker achieved the laboratory synthesis of alanine from a mixture of acetaldehyde, ammonia and hydrogen cyanide (3). This was followed by the experiments of Alexandr M. Butlerov (3) showing that the treatment of formaldehyde with strong alkaline catalysts, such as sodium hydroxide (NaOH), leads to the synthesis of sugars.

The laboratory synthesis of biochemical compounds was soon extended to include more complex experimental settings. By the end of the 19th century a large

amount of research on organic synthesis had been performed, and had led to the abiotic formation of fatty acids and sugars using electric discharges with various gas mixtures (3). This work was continued into the 20th century by Klages (3) and Ling and Nanji (3), who reported the formation of glycine from formaldehyde and potassium cyanide. In addition, Löb, Baudish, and others worked on the synthesis of amino acids by exposing wet formamide (CHO-NH_2) to a silent electrical discharge (3) and to UV light (3).

There is no indication that any of these researchers had any interest in the question of how life began on Earth, or in the synthesis of organic compounds under possible prebiotic conditions. This is not surprising. Since it was generally assumed that the first living beings had been autotrophic, plant-like organisms, the abiotic synthesis of organic compounds did not appear to be a necessary prerequisite for the emergence of life. These organic syntheses were not conceived as laboratory simulations of Darwin's warm little pond, but rather as attempts to understand the autotrophic mechanisms of nitrogen assimilation and CO_2 fixation in green plants.

The situation changed at the start of the 1950s when several noted chemists were drawn towards the origin of life. Driven by his interest in evolutionary biology, Melvin Calvin attempted to simulate the synthesis of organic compounds under primitive Earth conditions using high-energy radiation sources. He and his group had limited success: the irradiation of solutions of CO_2 with the Crocker Laboratory 60-inch cyclotron led only to formic acid, albeit in fairly good yields (3).

The biggest breakthrough took place in 1953 when Stanley Miller, working in the laboratory of Harold Urey, first presented convincing evidence for the synthesis of important biochemical compounds under what was considered at the time plausible early Earth conditions. In this now classic experiment, Miller using a gas mixture of H_2 , CH_4 and NH_3 and a spark discharge as an energy source (to mimic lightning and coronal discharges on the early Earth) was able to demonstrate the transformation of almost 50% of the original carbon present as methane into a wide variety of organic compounds (6). Although almost all of the synthesized organic material was an insoluble tar-like solid, amino acids and other simple organic compounds were identified in the reaction mixture. Glycine, the simplest amino acid, was produced in 2% yield (based on the original amount of methane carbon), whereas alanine, the simplest amino acid with a chiral center, was produced in a yield of 1%.

Possible processes involved in the endogenous production of organic compounds were soon extensively investigated by a number of researchers. It has now been demonstrated that the action of an electric discharge and other energy sources on reduced gas mixtures such as H_2O , CH_4 and NH_3 (or N_2) results in the production of copious amounts of many types of biologically important organic compounds such as amino acids (6).

Although amino acids and other biochemical monomers are readily produced from reduced gas mixtures (6), the prebiotic relevance of these model atmospheres

has been questioned. It is now thought that the Earth's early atmosphere was likely composed of CO_2 (1-100 bar) along with ~ 1 bar N_2 , traces of CO , CH_4 , and water vapor (2), though some H_2 may have been present (7). Previous simulations of prebiotic atmospheric synthesis using CO_2/N_2 and energy sources such as high-energy plasmas, spark discharges and UV light did not produce significant amounts of organic compounds (8,9,10). Atmospheric synthesis under non-reducing conditions has thus been assumed to be a minor contributor to the prebiotic organic inventory on the early Earth and other planetary bodies.

Abiotic Syntheses in Neutral Atmospheres

We have reinvestigated abiotic synthesis from model neutral atmospheres ($\text{CO}_2/\text{N}_2/\text{H}_2\text{O}$) and found that amino acid yields are much higher than previously reported. As discussed here, our results suggest that the previously reported low yields were likely the result of both the experimental conditions and the analytical procedures.

In our experiments, 100 mL water, 100 mm CO_2 and 100 mm N_2 were subjected to the action of an electric discharge (generated by an Electrotechnics BD-50 Tesla coil) in a 3.1 liter flask for 48 hours at 23°C (8,9). The apparatus used in the experiments (Plate 1) was the same one used previously in studies of prebiotic syntheses using reducing gas mixtures (8,9). Detectable amounts of urea, HCN , NH_3 , HCHO , CH_3CHO , HOCCHO and HOCCO_2H were produced, but only negligible yields of amino acids were obtained when analyzed by standard methods (11) after acid hydrolysis to convert amino nitriles, polymeric materials and other precursors to free amino acids (Table I). Amino acid yields were $\sim .01\%$ based on input N_2 , similar to those found previously (8,9). Spark discharges acting on CO_2/N_2 gas mixtures produce large amounts of HNO_2 and HNO_3 (10). In the absence of a buffer, the pH of the aqueous phase after sparking was 3.2, likely due to the dissolved nitric and nitrous acids produced. Low pH inhibits the Strecker synthesis of amino acids, as it depends on the nucleophilicity of ammonia and cyanide anion (both pK_a 's ~ 9.2). The self-condensation of HCN to purines and amino acid precursors (9) is also inhibited because it proceeds optimally near its pK_a .

When the reaction was buffered with solid CaCO_3 , the pH of the aqueous phase after sparking was 7.1 and amino acid yields were increased 2-15 fold. Moreover, it was found that direct acid hydrolysis of the reaction mixtures gave dramatically lower amino acid yields than when an oxidation inhibitor was added prior to hydrolysis. When hydrolysis is carried out in the presence of ascorbic acid, which is typically added to natural water samples to inhibit oxidation by nitrate and nitrite (12), recoveries are increased a factor of 10-100 fold (Table I). Thus, the yield of amino acids from the neutral gas mixture with the addition of ascorbic acid prior to acid hydrolysis is comparable to that obtained from a reducing gas mixture (Table I).

Table 1. Yields of Amino Acids and other Small Molecules from Neutral Atmospheres.

Experiment	$pH_{initial}$ pH_{final}	NH_3	HCN	NO_2^-	NO_3^-	HCHO	THAA -	THAA +
CO_2/N_2 Control	~6 ~5	$<10^{-3}$	$<10^{-5}$	$<10^{-4}$	$<10^{-4}$	$<10^{-6}$	$<10^{-6}$	$<10^{-6}$
$CO_2/N_2/CaCO_3$ Control	7.3 7.3	$<10^{-3}$	$<10^{-5}$	$<10^{-4}$	$<10^{-4}$	$<10^{-6}$	$<10^{-6}$	$<10^{-6}$
CO_2/N_2	~6 3.2	0.26	0.26	0.008	0.02	3×10^{-4}	0.005	0.1
$CO_2/N_2/CaCO_3$	7.3 7.1	0.21	0	1.04	0.21	7×10^{-4}	0.002	1.2
$CH_4/NH_3/H_2$	8.7 ?	in starting mixture	2.8	ND	ND	0.0	~5.5	ND
$CO_2/N_2/O_2 + CaCO_3$	7.3 7.1	ND	ND	ND	ND	ND	8×10^{-5}	2×10^{-4}

Yields (%) are calculated based on input N_2 or CO_2 (for HCHO) from 100 mm CO_2 , 100 mm N_2 and 100 mL H_2O with or without 2 mmoles $CaCO_3$ in a 3.1 L flask at 23° C. Also included is an experiment with 10 mm of O_2 added to the gas mixture. The results with a reducing atmosphere (% yields based on starting carbon in the form of methane) are given for comparison [taken from (3, 4)]. Yields of THAA (Total Hydrolyzable Amino Acids labeled in plate 2) are shown after hydrolysis in the absence (-) or presence (+) of ascorbate. The controls are not sparked and represent blanks. ND = not determined.

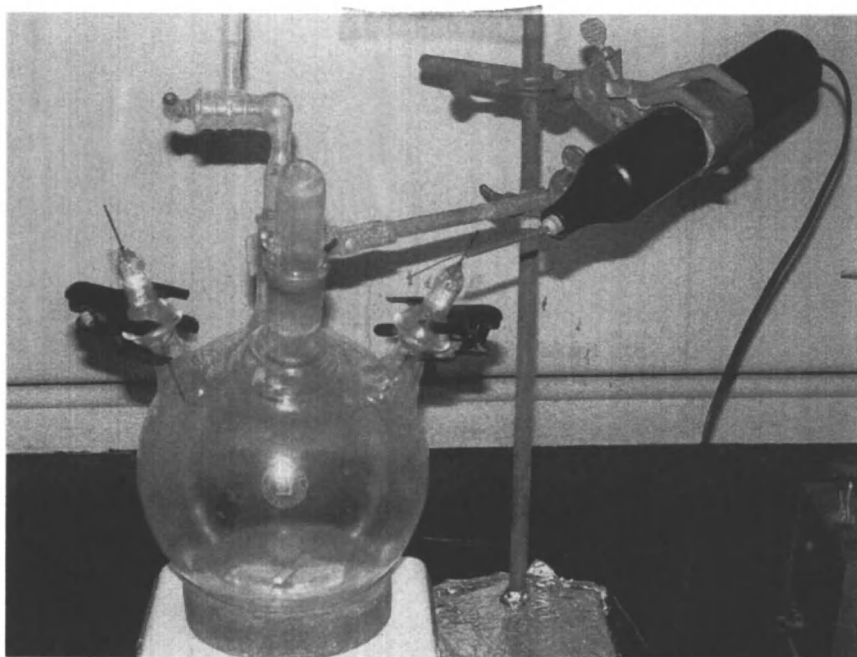
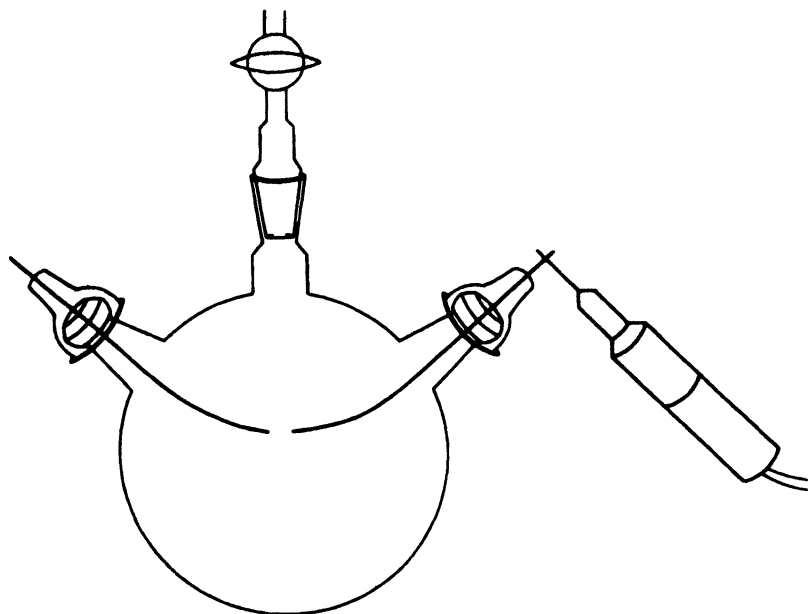


*Plate 1. Spark discharge apparatus used in these experiments.
(See page 17 of color inserts.)*

The main amino acid products were serine, glutamic acid, glycine and alanine, along with traces of aspartate, β -alanine, γ -amino butyric acid and α -aminoisobutyric acid (Figure 1). The alanine is racemic within experimental error demonstrating that it is not derived from contamination. Few amino acids are detected before acid hydrolysis, and the amounts of free cyanide, aldehydes and ammonia are low, suggesting that these intermediates may be bound as nitriles. The observed amino acids may have formed via the Strecker synthesis, or by the related Bucherer-Bergs pathway, which involves ammonium carbonate (13). Alternatively, the intermediates could be part of a polymer, which upon hydrolysis yields the observed amino acids. This latter possibility is supported by the similarity of the types and relative amounts amino acids detected here with those found when oligomers formed by the self-condensation of HCN in aqueous solution are hydrolyzed (14).

To show that the source of the amino acids in our experiments was not the result of the reaction of the various nitrogen species produced in the reaction with ascorbic acid, we reacted ascorbate individually and in combination with ammonia, hydrazine, nitrite, and nitrate. Very low traces of amino acids were produced in these reactions, indicating that the amino acids detected are in fact produced from the electric discharge reaction. While ascorbic acid is not likely to have been an abundant prebiotic species, oxidation could have been inhibited by other available chemical species such as sulfides and reduced metal ions.

We also evaluated the ability of various potentially prebiotic oxidation inhibitors to protect against oxidation during hydrolytic work-up. 1.5×10^{-4} moles (~ 100 fold molar excess over total nitrite + nitrate present in the solutions) each of FeCl_2 , Na_2S , Na_2SO_3 , FeSO_4 , pyrites, or NaCOOH per 1 mL discharge solution was dried under vacuum at room temperature, then HCl vapor-hydrolyzed and desalted. Only FeS and FeSO_4 were found to be able to protect against degradation to a significant degree using this molar ratio of reactants. Although the exact composition of primitive seawater is uncertain, it has been suggested that the pH was close to neutral (15), total dissolved carbonate concentrations were higher (15), NaCl concentrations may have been twice present values (15), and there were low but significant concentrations of Fe^{2+} and SO_4^{2-} (2,16,17). It seems reasonable that there was a significant excess of ferrous iron over nitrate/nitrite on the primitive Earth (16), and in fact, the reaction of nitrite with ferrous iron may have been an important source of ammonia in the primitive seas (17).

Finally, it is generally held that amino acid synthesis is impossible in the presence of O_2 . To test this we sparked a mixture containing 2 mmol CaCO_3 , 100 mL H_2O , 100 mm each CO_2 and N_2 , and 10 mm O_2 for 48 hours. To our surprise a small quantity of amino acids (Table I), consisting almost entirely of DL- alanine and glycine, were still produced. Since the early Earth's atmosphere was probably devoid of significant levels of oxygen until roughly 3 billion years ago (2,18), direct abiotic syntheses of compounds such as amino acids may have still taken place even after the origin of life and during the early rise of atmospheric O_2 .

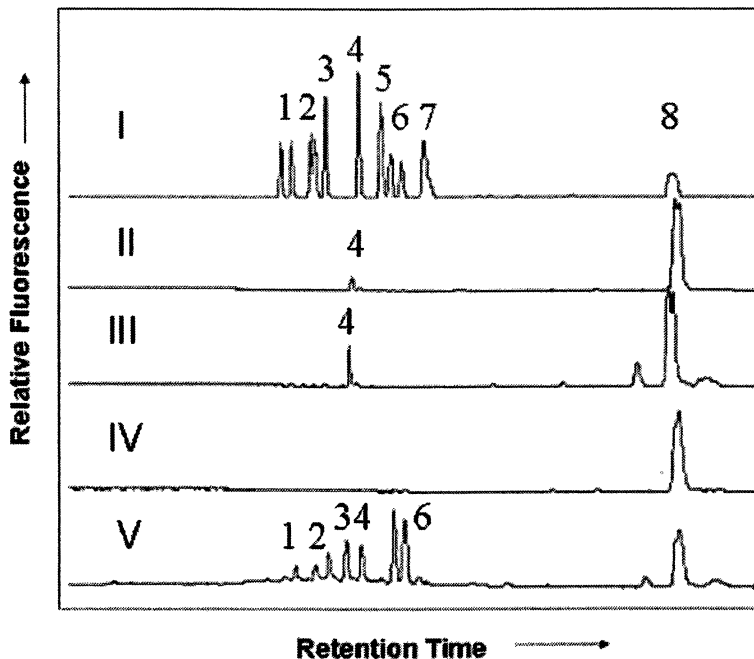


Figure 1. Typical HPLC chromatograms of the OPA-NAC (11) derivitized amino acids detected from the spark discharge reactions. Chromatograms labeled with roman numerals: I.) Amino acid standard, II.) CO_2/N_2 not sparked, III.) $\text{CO}_2/\text{N}_2 + \text{CaCO}_3$, sparked, hydrolyzed – ascorbate. IV.) CO_2/N_2 , sparked, hydrolyzed - ascorbate V.) CO_2/N_2 , sparked + CaCO_3 , hydrolyzed + ascorbate. Amino acids: 1.) DL aspartic acid 2.) DL glutamic acid 3.) DL serine 4.) glycine 5.) β -alanine 6.) DL alanine 7.) α -amino isobutyric acid 8.) DL norleucine (internal standard). The D and L enantiomers of glutamic acid and serine are not separated under these chromatographic conditions.

Conclusions

The results presented here suggest that neutral atmospheres can provide a variety of biochemical monomers in much higher yields than previously thought. While the Earth may have harbored a reducing atmosphere very early in its history, neutral conditions likely soon prevailed (2). Our findings suggest that organic molecules might still have been abundantly produced via prebiotic atmospheric syntheses, depending on oceanic pH and the presence of chemicals capable of protecting against oxidation. Experiments with slightly reducing model atmospheres (8,9) suggest that the addition of traces of methane and/or hydrogen in our simulations would enhance the production of amino acids.

Using the estimates provided by Sagan and Chyba for the sources of prebiotic compounds on the primitive Earth (4), atmospheric synthesis in neutral atmospheres may have been competitive with exogenous delivery and possible hydrothermal sources of organic compounds, although all of these sources likely would have contributed to the inventory of organic molecules. This work may also be relevant to other planets such as Mars, as the Martian atmosphere has likely been composed mainly of CO₂ and N₂ since soon after its formation (19). The results presented here thus have important implications for the synthesis of organic compounds throughout the history of Mars and may be detectable with instrumentation now in development (20).

Acknowledgments

This work was supported the University of California Institute for Mexico and the United States (UC MEXUS) program and the NASA Specialized Center of Research and Training in Exobiology. The authors would like to thank Andrew Aubrey for photographing the spark discharge apparatus and Lee Gardner Dewey for assistance with the Plates.

References

1. Wilde, S. A.; Valley, J. W.; Peck W. H.; Graham, C. M. Evidence from detrital zircons for the existence of continental crust and oceans on the Earth 4.4 Gyr ago. *Nature* **2001**, *409*, 175-178.
2. Kasting, J.F.; Catling, D. Evolution of a habitable planet. *Ann. Rev. Astron. Astrophys* **2003**, *41*, 429-463.
3. Lazcano, A.; Bada, J. L. The 1953 Stanley L. Miller Experiment: Fifty Years of Prebiotic Organic Chemistry. *Origins of Life Evol. Biosphere* **2003**, *33*, 235-242.
4. Chyba, C.; Sagan, C. Endogenous production, exogenous delivery and impact-shock synthesis of organic molecules: an inventory for the origins of life. *Nature* **1992**, *355*, 125-132.
5. Botta, O.; Bada, J. L. Extraterrestrial organic compounds in meteorites. *Surv. Geophys.* **2002**, *23*, 411-467.
6. Miller, S. A production of amino acids under possible primitive Earth conditions. *Science* **1953**, *117*, 528-529.
7. Tian, F.; Toon, O.; Pavlov, A.; De Sterck, H. A hydrogen-rich early Earth Atmosphere. *Science* **2005**, *308*, 1014-1017.
8. Schlesinger, G.; Miller, S. Prebiotic synthesis in atmospheres containing CH₄, CO and CO₂. I. Amino Acids. *J. Mol. Evol.* **1983**, *19*, 376-382.

9. Schlesinger, G.; Miller, S. Prebiotic synthesis in atmospheres containing CH₄, CO and CO₂. II. Hydrogen Cyanide, Formaldehyde and Ammonia. *J. Mol. Evol.* **1983**, *19*, 383-390.
10. Folsome, C.; Brittain, A.; Smith, A.; Chang, S. Hydrazines and carbonylhydrazides produced from oxidized carbon in Earth's primitive environment. *Nature* **1981**, *294*, 64-65.
11. Zhao, M.; Bada, J. L. Determination of α -Dialkylamino Acids and Their Enantiomers in Geological Samples by High Performance Liquid Chromatography After Derivatization with a Chiral Adduct of O-Phthalaldehyde. *J. Chromat. A* **1995**, *690*, 55-63.
12. Robertson, K.; Williams, P.; Bada, J. Acid hydrolysis of dissolved combined amino acids in seawater: a precautionary note. *Limnol. Oceanog.* **1987**, *32*, 996-997.
13. Bucher, H. Th.; Lieb, V. A.; Über die Bildung substituierter Hydantoine aus Aldehyden und Ketonen: Synthese von Hydantoinen (II. Mitteilung). *Journal für praktische Chemie N. F.* **1934**, *141*, 5-43.
14. Ferris, J. F.; Joshi, P. C.; Edelson, E. H.; Lawless, J. G. HCN: a plausible source of purines, pyrimidines and amino acids on the primitive Earth. *J. Mol. Evol.* **1978**, *11*, 293-311.
15. Morse, J. W.; Mackenzie, F. T. Hadean ocean carbonate geochemistry. *Aquatic Geochem.* **1998**, *4*, 301-319.
16. Walker, J. C.; Brimblecombe, P. Iron and sulfur in the pre-biologic ocean. *Precambrian Res.* **1985**, *28*, 205-222.
17. Summers, D. P. Sources and sinks for ammonia and nitrite on the early Earth and the reaction of nitrite with ammonia. *Origins of Life Evol. Biosphere* **1999**, *29*, 33-46.
18. Catling, D. C.; Claire, M. W. How Earth's atmosphere evolved to an oxic state: a status report. *Earth Planet. Sci. Letts.* **2005**, *237*, 1-20.
19. Jakosky, B. M.; Phillips, R. J. Mars' volatile and climate history. *Nature* **2001**, *412*, 237-244.
20. Bada, J. L.; Sephton, M. A.; Ehrenfreund, P.; Mathies, R. A.; Skelley, A. M.; Grunthaner, F. J.; Zent, A. P.; Quinn, R. C.; Josset, J.-L.; Robert, F.; Botta, O.; Glavin, D. P. New strategies to detect life on Mars. *Astronomy & Geophysics* **2005**, *46*, 626-627.

Chapter 16

The RNA World Scenario for the Origins of Life

James P. Ferris¹ and John W. Delano²

¹Department of Chemistry and Chemical Biology, Rensselaer Polytechnic Institute, Troy, NY 12180

²Department of Earth and Atmospheric Sciences, The University at Albany, Albany, NY 12222

RNA was proposed to have been the most important biopolymer in the first Life on Earth in 1968 by Crick and Orgel. The finding by Cech and Altman in 1982 that RNA can catalyze reactions as well as store genetic information supported this hypothesis. More recent experimental findings concerning this postulate for the origins of life will be discussed.

Introduction

“How and where did life on Earth arise” was highlighted as one of 25 top science questions in 2005 in *Science* (1) and one of the six top questions in “What Chemists Want to Know” in 2006 in *Nature* (2). Origins of life studies are one of the more interdisciplinary fields in science. It requires that astronomers, physicists, geologists, chemists and biologists collaborate to determine the sources and reactions of organic compounds that initiated the first life. Some of the areas of interaction in these investigations include: the search for interstellar organic compounds by astronomers; physicists modeling the formation of solar systems; geologists investigating the organic and inorganic compounds in meteorites and in ancient rock formations on Earth; chemists

simulating the reactions of organics in simulated prebiotic environments and analyzing the organics in meteorites; and biologists studying ancient life forms to gain insight into the nature of early life on Earth. Data from these and other sources are central to the development of scenarios of the steps leading to the compounds that initiated the first life on Earth.

At the time of this writing there is no hypothesis that is generally accepted in the scientific community that explains how life may have originated on Earth. Actually it is not known if life originated on Earth or if it was delivered here from some other location like Mars. Meteorites have been found on Earth that clearly came from Mars. It is likely that they were blasted off Mars by the impacts of large meteorites and traveled in highly elliptical orbits that eventually intersected the Earth's orbit. The high levels of radiation in the interplanetary medium suggest that life may not have survived a lengthy trip to Earth, a finding that supports the view that life originated on Earth, but does not totally preclude the possibility that Earth was seeded with life from another source.

In the study of the origin of life one must decide what are the most important properties of life. One answer is catalysis and replication with change. Information storage is essential so that the early life can be maintained by replication while change is required so the simplest life can evolve to the more efficient life forms we have on the Earth today. This simple model does not require a complex structure for the first life. A group of replicating polymers bound to the surface of a mineral, dubbed "life on the rocks" by Leslie Orgel, would do the trick (3).

A more complex system is favored by those who propose that the first life must be able to generate the compounds essential for life (metabolism) and this life is protected from the environment inside a "container", a structure similar to a cell membrane, so the integrity of the life can be protected from a changing environment. The spontaneous formation of a metabolic system appears to have been too complicated to occur on the primitive Earth, so we favor the "life on the rocks" scenario.

The RNA World

The RNA world scenario may provide a route to the origin of life. In this hypothesis it is claimed that RNA was the key biopolymer in the first life because RNA can serve both as a catalyst as well as repository of genetic information (4, 5). Later the RNA world evolved into the protein/DNA world that is the basis of life on Earth today. Evolution of the RNA world to the protein/DNA world was likely because protein is a more versatile catalyst than RNA. DNA is a more stable structure than RNA and hence is a better storehouse

of genetic information. The basic structure of RNA is similar to that of DNA except it has an extra hydroxyl group in the 2'-position on its 5-membered ring and a uracil in place of the thymine (Figures 1a and 1b).

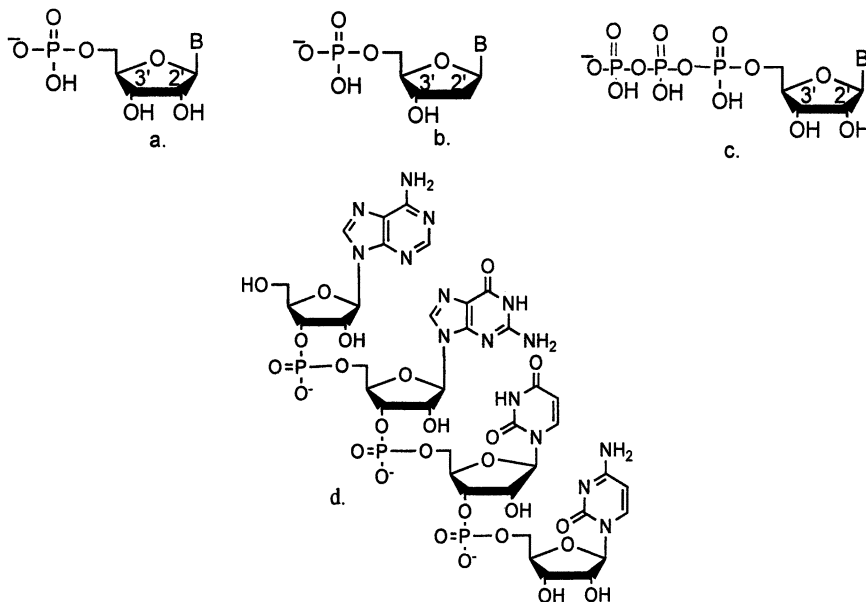


Figure 1. Structures of RNA and DNA (a) ribonucleic acid (RNA) monomers with B= adenine, guanine (G), cytosine (C) and uracil (U), (b) deoxyribonucleic acid monomer with B= adenine (A), guanine (G), cytosine (C), thymine (T), and (c) 5'-triphosphate of RNA (d) the structure of a 4 mer of RNA.

The synthesis of RNA and DNA in biological systems requires the presence of the high-energy triphosphate-activating group at the 5'-position of the monomers (Figure 1c) because hydrolysis of the phosphodiester bond of RNA and DNA is favored over its formation in the presence of water. Hence, the prebiotic synthesis of RNA also requires an activating group on the 5'-phosphate of the RNA monomers for the synthesis to occur. Imidazole and 1-methyladenine are used as activating groups in our proposed prebiotic synthesis of RNA oligomers. These activated nucleotides are abbreviated ImpN and MeadpN, respectively where Im is imidazole and Mead is 1-methyladenine. A tetramer of RNA, linked by 3', 5'-phosphodiester bonds is shown in Figure 1(d).

Status of the Prebiotic Synthesis of RNA Monomers

Purine and Pyrimidine Bases

Meteorites from the asteroid belt are a potential source of some of the purine bases present in RNA. As asteroids travel in their orbits between Mars and Jupiter they collide with each other and pieces are broken off that vary in size from large bodies (potential meteorites) to dust particles. If the energy of the collision is great enough, this material is propelled out of its orbit into the interplanetary medium and some of the material eventually reaches the Earth. Approximately 10^{21} kg of asteroidal material reached the primitive Earth's surface (6). This corresponds to a layer of material weighing 2×10^6 kg/m² if spread uniformly over the surface of the Earth. The carbon content of the soluble organics present (1%) is equivalent to a layer of carbon compounds 25 m thick on the primitive Earth. Since meteorites contain about 1 ppm of purines and pyrimidines, then about 10^{15} kg of these compounds were on the primitive Earth.

The purine and pyrimidine bases may have also been formed on the primitive Earth. The so-called "HCN polymer", formed by the self-condensation of liquid HCN or concentrated solutions of HCN (7), yields purines, pyrimidines and amino acids when hydrolyzed (Figure 2) (8).

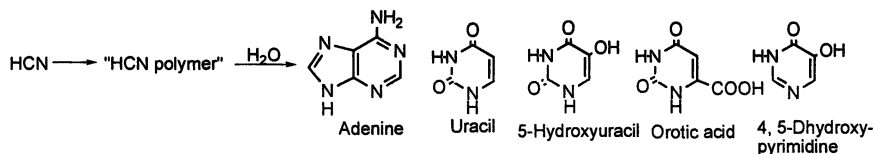


Figure 2. Formation of adenine and pyrimidines by hydrolysis of the "HCN polymer".

An alternative route to purines is via the self-condensation of dilute solution (>0.01 M) of HCN at pH 9 to a tetramer of HCN. Photolysis of the HCN tetramer yields 4-aminoimidazole-5-carbonitrile (9,10). This aminoimidazole reacts with HCN to generate adenine. Other purine bases are also formed by the reaction of the aminoimidazole carbonitrile with other one or two carbon compounds (8).

Pyrimidines are also formed by the reaction of cyanoacetylene and cyanoacetaldehyde with guanidine, cyanate and urea under a variety of reaction conditions (11, 12). The observation of several potential sources of purines and

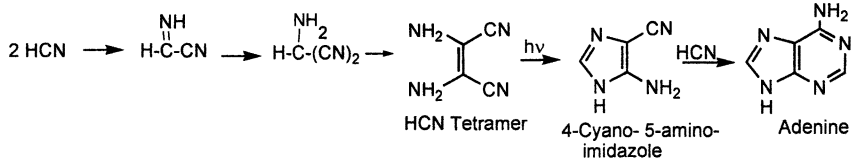


Figure 3. Adenine is formed stepwise by the reaction of 0.1 M HCN.

pyrimidines suggests that they were likely to have been present on the primitive Earth.

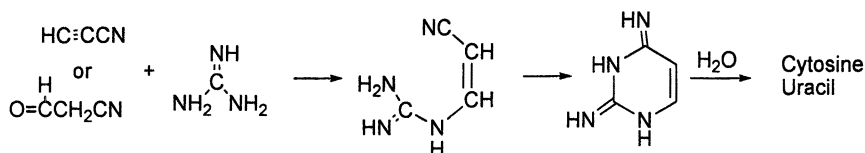


Figure 4. Pyrimidines are formed from cyanoacetylene or its hydrolysis product cyanoacetaldehyde.

Ribose

The sugar ribose is the backbone of RNA monomers (Figure 1a). Initially it was proposed that the self-condensation of formaldehyde was a prebiotic route to ribose. This pathway is out of favor because about thirty other sugars besides ribose are formed in this reaction with the yield of ribose being in the 1-2% range (13). Since most of these sugars have similar reactivity, it is not clear why the ribose in this mixture would react selectively with purines and pyrimidines to form nucleosides. Several new routes to ribose have been proposed in the last 15 years. Of particular interest are convergent syntheses that result in the formation of the four pentoses of sugars, one of which is ribose (Figure 5). In these syntheses it is possible to form the pentoses from sugars that have either lower or higher molecular weight than ribose (14, 15). Other prebiotic ribose syntheses have been reported (16, 17). The variety of routes to ribose suggests that it was present on the primitive Earth.

Nucleosides, Nucleotides And Activated Nucleotides

A major problem with the RNA world scenario is the absence of a convincing prebiotic synthesis of nucleosides (Figure 1). Dry heating of a

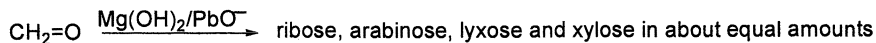


Figure 5. Metal ion catalysis of the conversion of formaldehyde to pentose sugars.

mixture of ribose, sea salt and adenine gives a 4% yield of the β -anomer of adenosine, and with guanine a 9% yield of the β -anomer of guanosine (18). α -anomers are among the other products (Figure 6a). No nucleosides were formed when mixtures of the pyrimidines, uracil, cytosine and thymine, were reacted together with ribose under the same conditions used to generate nucleosides from purine bases (18). The absence of a convincing prebiotic synthesis of nucleosides is a deficiency of the RNA world scenario for the origin of life.

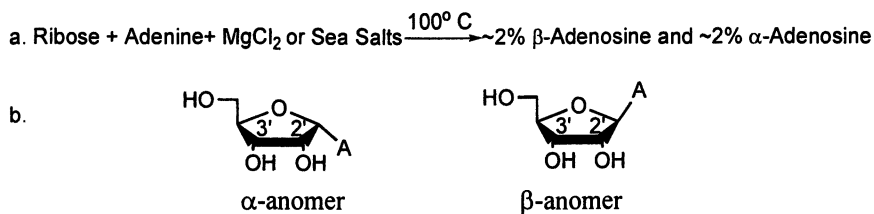


Figure 6. α - and β -Adenosine formation (a) by dry heating adenine with salts and ribose with the formation of (b) α - and β -anomers among other products.

The formation of nucleotides from nucleosides was more successful. Heating uridine in the presence of $\text{NH}_4\text{H}_2\text{PO}_4$ with an excess of urea yields uridine nucleotides that have phosphate groups at the 2', 3' or 5'-positions of nucleosides together with lower yields of products that have two or more attached phosphate group (19). When the mineral struvite ($\text{MgNH}_4\text{PO}_4 \cdot \text{H}_2\text{O}$) is used in place of $\text{NH}_4\text{H}_2\text{PO}_4$ in the synthesis a 25% yield of the 5'-pyrophosphate of uridine is obtained. (20)

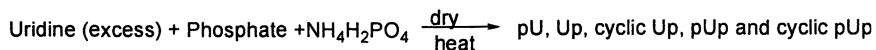


Figure 7. Phosphorylation of uridine to nucleotides

Catalysis of RNA Oligomer Formation

Metal Ion Catalysis

Both lead (Pb^{2+}) and some lead minerals catalyze the formation of up to 10 mers starting from the 5'-phosphorimidazolide of adenosine (5'-ImpA). (21, 22) The oligomers are linked mainly by 2', 5'-phosphodiester bonds. Uranyl ion (UO_2^{2+}) is a more efficient catalyst of the reaction of the activated nucleotides of A, U, and C. (23) Chain lengths 16, 10, and 10 monomer units (mers), respectively are formed that are linked mainly by 2', 5'-phosphodiester bonds. When the Pb^{2+} reaction is performed in the eutectic phase of water at -18°C for 20-40 days, oligomers as long as 17 mers are formed in yields of 80-90% (24, 25). Most of the water is present as ice crystals so the higher yields may be due to the slower rate of hydrolysis the imidazole activating groups at the lower temperature and/or the higher concentrations of the activated monomers in the liquid phase.

Montmorillonite Catalysis

The observation that montmorillonite clay was a weak catalyst for the formation of the 2', 3'-cyclic phosphates from 3'-nucleotides (26) prompted our investigation of the formation of RNA oligomers from 5'-imidazole activated nucleotides. Initial studies demonstrated that some montmorillonites were "excellent" catalysts for oligomer formation if they were converted to the Na^+ form by the procedure of Banin (29, 30). In this procedure the montmorillonite is treated with cold HCl to generate the acidic form of the montmorillonite and then converted to the Na^+ form by treatment with NaCl. Oligomers that contained up to 10 mers were formed from ImpA (Figure 7a) (27, 28). It was possible to attain 40-50 mers by the reaction of ImpA with a decameric primer in the presence of montmorillonite in a "feeding" reaction (32,33). The latest advance in the formation of long oligomers is the synthesis of 40-50 mers in one day using 1-methyladenine as the activating group and a modified reaction procedure (Figure 7b)(32, 33). This is important because it is now possible to generate large amounts of the long oligomers so it easier to probe their properties.

Most of the RNA in contemporary life is linked by 3', 5'-phosphodiester bonds while the oligomers formed by montmorillonite catalysis have both 3', 5'- and 2', 5'-phosphodiester bonds (Figure 8). The proportions of each type of

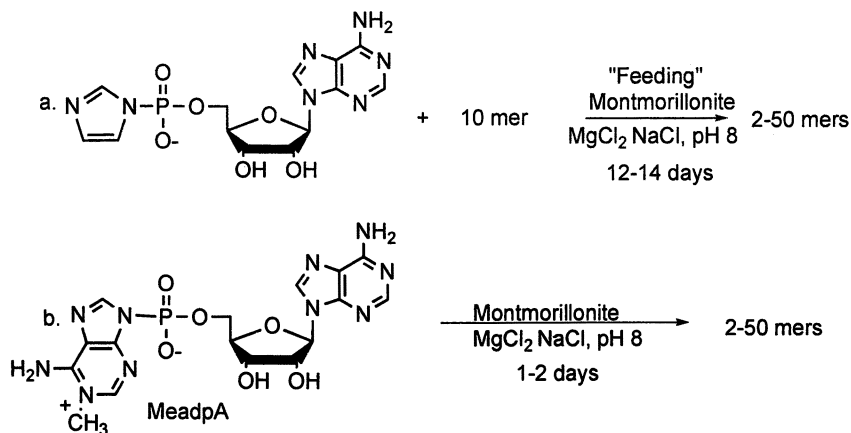


Figure 8. Formation of oligomers by (a) elongation of a 10 mer primer and (b) use of 1-methyladenine as the activating group.

linkage can be determined by enzymatic hydrolysis where the enzyme cleaves only the 3', 5'-phosphodiester bond. (28) The monomers joined by 2', 5'-links remain bonded together as dimers, trimers, tetramers etc. The respective quantities of 2', 5'- and 3', 5'-linked monomers can be determined from the relative areas of the monomers and oligomers HPLC peaks.

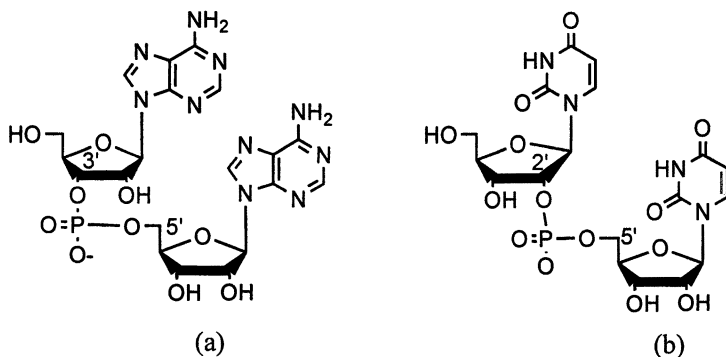


Figure 9. Dimers with (a) 3', 5'- phosphodiester bond and (b) 2', 5'-phosphodiester bond.

Catalysis of Template-Directed Synthesis

Metal Ion Catalysis

RNA is formed by template-directed synthesis where an RNA strand directs the formation of the complementary RNA from activated monomers. For example, a poly(C) template directs the formation of poly(G) oligomers from ImpG. The template may be considered to be a catalyst and in some cases metal ions also catalyze the reaction. Pb^{2+} catalysis of the poly(C) directed reaction of ImpG yields up to 40 mers that are linked mainly by 2', 5'-linked oligomers. The formation of oligo(A)s on poly(U) templates is less efficient with 7 mers being the longest oligomers formed. Here 75% of the phosphodiester bonds are 3', 5'-linked. Zinc ion (Zn^{2+}) also catalyzes the reaction of ImpG on a poly(C) template to give 30 mers where 75% of the bonds are 3', 5'-linked, but Zn^{2+} does not catalyze the formation of oligo(A)s.

It was observed that a poly(C) template catalyzes the formation of 30 mers of oligo(G)s when 2-methylimidazole is used as the activating group in place of imidazole(34). It is proposed that the methyl group of the methylimidazole orients the activated monomers on the poly(C) template so they are lined up in the optimal orientation to form 3', 5'-phosphodiester bonds. This suggests that the role of the metal ion catalyst in the reaction of ImpN is to bind to the activated monomer and/or template so that the activated monomers are orientated to form phosphodiester bonds between the monomers (35).

Selectivity in Oligomers Formed by Template-Directed Catalysis

The structures of the oligomers formed depend on the bases present in each monomer. In the absence of montmorillonite, only low yields of dimers and trimers are formed that are linked mainly by 2', 5'-phosphodiester bonds. In the montmorillonite-catalyzed reaction of ImpA, 67% of the phosphodiester bonds are joined by 3', 5'-links. ImpU yields oligomers in which 20% of the bonds are 3', 5'-links. It is proposed that the difference in regiospecificity between purine and pyrimidine activated monomers is due to differences in the orientation of activated monomers on the montmorillonite surface (33, 36).

Investigation of the binding of ImpA and ImpU to montmorillonite shows that ImpA binds more strongly than ImpU. The difference, due to Van der Waals forces, is consistent with the variation in orientations of the purine and pyrimidine activated nucleotides on the surface of the clay particles (33-40).

This, in turn, accounts for the difference in the regioselectivity of phosphodiester bond formation.

The reaction products vary with the pH of the reaction solution (41). Formation of dinucleoside pyrophosphate (AppA), where A= adenosine, occurs in the pH 1-6 range, together with the hydrolysis of the activated monomers. Slow hydrolysis occurs with neutral and basic conditions and oligomer formation occurs in the pH 6-10 range (Figure 10).

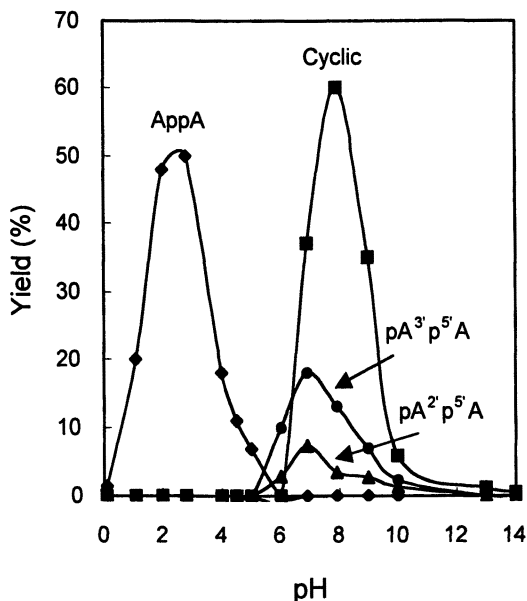
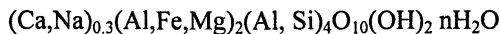


Figure 10. Variation of dimeric reaction products of *ImpA* with pH. Reproduced from Miyakawa et al. (41) with kind permission of Springer Science and Business Media.

Chemical Compositions of Montmorillonites

Studies have been performed on the montmorillonites with the objective of learning about the mechanism of their catalysis and their potential role in the prebiotic synthesis of RNA. Montmorillonites are 2:1 layer silicates having the following general formula:



Layer charge in montmorillonites is the result of substitution of lower valence cations (e.g., Mg^{2+} for Al^{3+} in the octahedral site; Al^{3+} for Si^{4+} in the tetrahedral site). The negative layer-charge is balanced by mono- and divalent cations between the layers (Na^+ ; Ca^{2+}). Montmorillonites are stable phases within a limited range of pressure and temperature. Burial to depths greater than 4 km (~1 kilobar) at temperatures of 75-100°C transforms the montmorillonites to illites (41) that have low cation exchange capacities and poor catalytic activity.

The ability of 18 different montmorillonites to catalyze the oligomerization of the 5'-phosphorimidazolidine of adenosine (ImpA) was explored (28). Those montmorillonites found to generate oligomers 8 mers or longer were designated "excellent catalysts". Five of these 18 montmorillonites are excellent catalysts and are in the 'Wyoming' class of montmorillonites. They all have similar elemental analyses and were obtained from deposits in South Dakota and Wyoming.

Environments That Produced Catalytically Active Montmorillonites

Explosive volcanism in western North America ~95 million years ago (Late Cretaceous age (42); spread volcanic ash downwind to the east of the volcanoes. Upon deposition, the volcanic ash was chemically altered (e.g., devitrification of volcanic glass) to form bentonite, in which montmorillonite is the dominant mineral. In addition, the Late Cretaceous bentonites contain low abundances of magmatic minerals (e.g., quartz, alkali-rich feldspar, zircon, biotite) that were quenched during the volcanic eruption (43, 44) and entrained in the volcanic ash. The explosive volcanic events are known to have produced ash having a granitic composition (40).

The five catalytically active montmorillonites are classified as '*Wyoming-type*' montmorillonites (44, 50-52) due to their having high cation exchange capacities, and their being composed of Na-rich smectites found in Wyoming, Montana, and South Dakota (46). The volcanic ash that was chemically altered to form the Na-rich, catalytic montmorillonites was deposited in a shallow, saline ocean (Mowry Sea) that existed throughout much of the western interior of North America during the Late Cretaceous (46, 53, 54).

It is considered likely that the catalytic Na-rich, '*Wyoming-type*' montmorillonites are distinctive not because of the composition of the original volcanic ash, but rather due to the saline-rich waters into which the volcanic ash was deposited and subsequently altered during shallow burial.

Environments on the Primitive Earth

Chemical and isotopic analyses of zircons (ZrSiO_4) having ages $>3,900$ million years (i.e., Hadean Eon) have provided geochemical constraints that bear importantly on whether catalytically active montmorillonites would have been present on the ancient Earth, and thereby played a role in the formation of biopolymers. For example, as previously noted, the catalytically active 'Wyoming-type' montmorillonites are the alteration products of explosive, airfall deposits of volcanic debris having granitic compositions. The Earth at 4,400-4,500 million years in the past may have already developed a significant mass of continental crust having a broadly granite-like composition (55). If the tectonic processes that generated that continental crust in the Hadean are similar to those that are known to have operated on the Earth for at least the last 3,000 million years, the Earth appears to have arrived at its current, large-scale chemical zonation (i.e., crust, mantle, core) ≤ 100 million years after planetary formation. Indeed, strong geochemical and isotopic evidence has emerged in support of that view. (56-63) In addition, Watson (61) reported major evidence in support of the Earth having produced granitic magmas 4,300-4,400 million years ago. Although data do not currently exist showing whether any granitic magmas were explosively erupted into the Earth's ancient atmosphere to form airfall deposits, the fact that that physico/chemical processes on the Hadean Earth were capable of generating magmas with the required compositions is important.

The catalytically active, 'Wyoming-type' montmorillonites are inferred to have developed their distinctive, high-Na smectite-rich compositions following deposition of granitic volcanic ash into a shallow, saline ocean during the Late Cretaceous. Oxygen isotopic data from Hadean zircons have been interpreted as indicating that oceans may have been present on the Earth by as early as 4,300-4,400 million years ago (62-63). While current evidence provides no information on the composition of the hypothesized Hadean seawater, the existence of oceans on the Hadean Earth is a necessary environment on the ancient Earth if catalytically active montmorillonites formed.

Although uncertainty remains, the environments required for the formation of 'Wyoming-type' montmorillonites (i.e., explosive eruptions of volcanic ash; granitic compositions; deposition of volcanic ash into saline water; shallow burial) may conceivably have been present on the prebiotic Earth. Formation of RNA oligomers would have proceeded from activated monomers if the aqueous environment had a pH in the neutral to mildly basic range (40).

The Current Status of the RNA World Scenario

The RNA world is one of several hypotheses for the origins of life. Another hypothesis proposes that life originated near deep-sea hydrothermal systems

where simple organics may be formed on the deposits of the reduced metal ions and sulfides found there (64). So far, only small molecules have been formed in laboratory experiments designed to simulate these reducing environments in the laboratory.

Autocatalytic systems have been proposed to be instigator of the first life. In this example the autocatalytic replication of nucleic acids generates the nucleic acid template for its own reproduction (65); in this case a hexadeoxynucleotide replicates. In the optimal case the autocatalytic system replicates exponentially resulting in a very rapid build up of the nucleotide. Exponential growth has not been attained in autocatalytic systems proposed to initiate the first life (66).

The RNA world scenario has been developed to a greater extent than most of the other approaches to the origin of the first life. This does not mean it is correct but rather that the positive and negative aspects of this scenario are more clearly defined. Problems with this approach start with the absence of a plausible prebiotic synthesis of nucleosides from the RNA bases and ribose. After the nucleoside formation issues are solved, there is no obvious route to the activated monomers that are required for the formation of oligomers. Since the activated monomers undergo relatively rapid hydrolysis in aqueous solution, their rates of synthesis would have had to be faster than their rates of hydrolysis. Other unaddressed problems include formation of RNAs that catalyze the replication of other RNAs, and the catalysis of the ligation of these same RNA oligomers.

Non-enzymatic template-directed synthesis is a positive aspect of the RNA world scenario (67). One problem with this is that the only effective non-enzymatic template-directed synthesis is that of 2-methylImpG on a poly(C) template. Additional catalysts may be needed to provide RNAs that contain all the nucleotides required for the establishment of the genetic code.

Other plausible aspects of the RNA world scenario include the montmorillonite catalysis of RNA oligomers that are long enough to be catalysts and to store genetic information. In addition, it has been possible to propose a plausible scenario for the formation of catalytic montmorillonite on the primitive Earth based on our studies of the geochemistry of the montmorillonite that we use in our current studies and the current models of the Earth based on the analysis of zircons that were formed 4200-4400 million years ago.

References

1. Zimmer, C. *Science* **2005**, *309*, 89.
2. Bell, P. *Nature* **2006**, *442*, 500-502.
3. Hill Jr., A. R.; Böhler, C.; Orgel, L. E., *Origins Life Evol. Biosphere* **1998**, *28*, 235-243.

4. Kruger, K.; Grabowski, P. J.; Zaug, A. J.; Sands, J.; Gottschling, D. E.; Cech, T. R. *Cell* **1982**, *31*, 147-157.
5. Guerrier-Takada, C.; Gardiner, K.; Marsh, T.; Pace, N.; Altman, S. *Cell* **1983**, *35*, 849-857.
6. Vokrouhlicky, D.; Farinella, P. *Nature* **2000**, *407*, 606-608.
7. Oro, J. *Biochem. Biophys. Res. Commun.* **1960**, *2*, 407-412.
8. Ferris, J. P.; Hagan, W. J., Jr. *Tetrahedron* **1984**, *40*, 1093-1120.
9. Ferris, J. P.; Orgel, L. E. *J. Am. Chem. Soc.* **1966**, *88*, 1074.
10. Sanchez, R.; Ferris, J.; Orgel, L. *J. Mol. Biol.* **1968**, *38*, 121-128.
11. Ferris, J. P.; Sanchez, R. A.; Orgel, L. E. *J. Molec. Biol.* **1968**, *33*, 693-704.
12. Ferris, J. P.; Zamek, O. S.; Altbuch, A. M.; Freiman, H. *J. Molec. Evol.* **1974**, *3*, (4), 301-309.
13. Decker, P.; Schweer, H.; Pohlmann, R. *J. Chromatog.* **1982**, *244*, 282-291.
14. Zubay, G. *Origins Life Evol. Biosphere* **1998**, *28*, 13-26.
15. Ricardo, A.; Carrigan, M. A.; Olcott, A. N.; Benner, S. *Science* **2004**, *303*, 196.
16. Springsteen, G.; Joyce, G. F. *J. Am. Chem. Soc.* **2004**, *126*, (31), 9578-9583.
17. Müller, D.; Pitsch, S.; Kittaka, A.; Wagner, E.; Wintner, C. E.; Eschenmoser, A. *Helvetica Chimica Acta* **1990**, *73*, 1410-1468.
18. Fuller, W. D.; Sanchez, R. A.; Orgel, L. E. *J. Mol. Biol.* **1972**, *67*, 25-33.
19. Osterberg, R.; Orgel, L. E.; Lohrmann, R. *J. Mol. Evol.* **1973**, *2*, 231-234.
20. Handschuh, G. J.; Lohrmann, R.; Orgel, L. E. *J. Mol. Evol.* **1973**, *2*, 251-262.
21. Sawai, H. *J. Am. Chem. Soc.* **1976**, *98*, 7037-7039.
22. Sleeper, H. L.; Orgel, L. E. *J. Mol. Evol.* **1979**, *12*, 357-364.
23. Sawai, H.; Higa, K.; Kuroda, K. *J. Chem. Soc. Perkin I* **1992**, 505-508.
24. Kanavarioti, A.; Monnard, P.-A.; Deamer, D. W. *Astrobiology* **2001**, *1*, (3), 271-281.
25. Monnard, P.-A.; Apel, C. L.; Kanavarioti, A.; Deamer, D. W. *Astrobiology* **2002**, *2*, (2), 139-152.
26. Ferris, J. P.; Hagan, W. J., Jr. *Origins Life Evol. Biosphere* **1986**, *17*, 69-84.
27. Ferris, J. P.; Ertem, G. *Science* **1992**, *257*, 1387-1389.
28. Ferris, J. P.; Ertem, G. *J. Am. Chem. Soc.* **1993**, *115*, 12270-12275.
29. Banin, A. Quantitative ion exchange process for clays. US Patent 3,725,528, 1973.
30. Banin, A.; Lawless, J. G.; Mazzurco, J.; Church, F. M.; Margulies, L.; Orenberg, J. B. *Origins Life Evol. Biosphere* **1985**, *15*, 89-101.
31. Ferris, J. P.; Hill, A. R., Jr.; Liu, R.; Orgel, L. E. *Nature* **1996**, *381*, 59-61.
32. Ferris, J. P., *Origins Life Evol. Biosphere* **2002**, *32*, 311-332.
33. Huang, W.; Ferris, J. P., *Chem. Commun.* **2003**, 1458-1459.
34. Huang, W.; Ferris, J. P. *J. Am. Chem. Soc.* **2006**, *128*, 8914- 8919.

35. Inoue, T.; Orgel, L. E. *J. Am. Chem. Soc.* **1981**, *103*, 7666-7667.
36. Birdson, P. K.; Orgel, L. E. *J. Mol. Biol.* **1980**, *144*, 567-577.
37. Joshi, P. C.; Pitsch, S.; Ferris, J. P. *Orig. Life Evol. Biosph.* **2007**, *37*, 3-26.
38. Lailach, G. E.; Thompson, T. D.; Brindley, G. W. *Clays Clay Min.* **1968**, *16*, 285-293.
39. Kawamura, K.; Ferris, J. P. *Origins Life Evol. Biosphere* **1999**, *29*, (6), 563-591.
40. Ertem, G.; Ferris, J. P. *Origins Life Evol. Biosphere* **2000**, *30*, 411-422.
41. Miyakawa, S.; Joshi, P. C.; Gaffey, M. J.; Gonzalez-Toril, E.; Hyland, C.; Ross, T.; Rybji, K.; Ferris, J. P. *Origins Life Evol. Biosphere* **2006**, *36*, 343-361.
42. Eberl, D. D. The hydrothermal strategy. In *Clay minerals and the origin of life*, Cairns-Smith, A. G.; Hartman, H., Eds.; Cambridge University Press: Cambridge, 1986; p 193.
43. Obradovich, J. D. A Cretaceous time scale. In *Evolution of the Western Interior Basin*, Caldwell, W. G. E., Kauffman, E.G., Eds. 1993; Vol. 39, pp 379-396.
44. Grim, R. E.; Guven, N. *Bentonites: Geology, Mineralogy, Properties, and Use*; Elsevier: Amsterdam, 1978; Vol. 24, p 256.
45. Knectel, M. M.; Patterson, S. H. *U. S. Geological Survey Bulletin* **1962**, 1082-M, 893-1030.
46. Kiersch, G. A.; Keller, W. D. *Economic Geology* **1955**, *50*, 469-494.
47. Moll, W. F., Jr. *Clays Clay Minerals* **2001**, *49*, 374-380.
48. Murray, H. *Industrial Clays Case Study. Mining, Minerals, and Sustainable Development*; 2002; Vol. 64, p 9.
49. Rath, D. L. In *Origin and characteristics of Wyoming bentonite deposits, Metallic and Non-Metallic Deposits of Wyoming and Adjacent Areas*, 1983; Geol. Wyoming Survey Pub. Info. Circ.1983; pp 84-90.
50. Smellie, J. *Swedish Nuclear Fuel and Waste Management Technical Report* **2001**, TR-01-26, 22.
51. Slaughter, M.; Earley, J. W. *Geol. Soc. Amer. Spec. Paper* **1965**, *83*, 95.
52. Kirshbaum, M. A.; Roberts, L. N. A. Stratigraphic framework of the Cretaceous Mowry Shale, Frontier Formation, and adjacent units, southwestern Wyoming Province, Wyoming, Colorado, and Utah. In *Petroleum Systems and Geologic Assessment of Oil and Gas in the Wyoming Province, Wyoming, Colorado, and Utah.*; Geol. Survey Digital Data Series DDS-69-D: 2005; p 35.
53. Merewether, E. A. *Stratigraphic and tectonic implications of Upper Cretaceous rocks in the Powder River Basin, northeastern Wyoming and southeastern Montana*; 1996; Vol.917-T, p 90.
54. Beyers, C. W.; Larson, D. W. *Amer. Assoc. Petrol. Geol. Bulletin* **1979**, *63*, 354-375.

55. Merewether, E. A.; Gautier, D. L. *Composition and depositional environment of concretionary strata of Early Cenomanian (early Late Cretaceous) age, Johnson County, Wyoming*; 2000; 1917-U, p 33.
56. Harrison, T. M.; Blichert-Toft, J.; Muller, W.; Albarede, F.; Holden, P.; Mojzsis, S. J. *Science* **2005**, *310*, 1947-1950.
57. Allegre, C. J.; Staudacher, T.; Sarda, P. *Earth Planet. Sci. Lett.* **1987**, *81*, 127-150.
58. Amelin, Y.; Halliday, A. N.; Pidgeon, R. T. *Nature* **1999**, *399*, 252-255.
59. Caro, G.; Bourdon, B.; Birck, J.-L.; Moorbath, S. *Nature* **2003**, *423*, 428-431.
60. Kleine, T.; Munke, C.; Mezge, R. K.; Palme, H. *Nature* **2002**, *418*, 952-955.
61. Schoenberg, R.; Kamber, B. S.; Collerson, K. D.; Eugster, O. *Geochim. Cosmochim. Acta* **2002**, *66*, 3151-3160.
62. Watson, E. B.; Harrison, T. M. *Science* **2005**, *308*, 841-844.
63. Wilde, S. A.; Valley, J. W.; Peck, W. H.; Graham, C. M. *Nature* **2001**, *409*, (6817), 175-178.
64. Mojzsis, S. J.; Harrison, T. M.; Pidgeon, R. T. *Nature* **2001**, *409*, (6817), 178-181.
65. Holm, N. G.; Andersson, E. M.; Hydrothermal systems. In *The Molecular Origins of Life*; Brack, A., Ed.; Cambridge University Press: Cambridge, 1998; pp 86-99.
66. von Kiedrowski, G. *Ang. Chem. Int. Ed. Engl.* **1986**, *25*, (10), 932-935.
67. Burmeister, J. Self-replication and autocatalysis. In *The Molecular Origins of Life*; Brack, A., Ed.; Cambridge University Press: Cambridge, 1998; pp 295-311.
68. Inoue, T.; Orgel, L. *Science* **1983**, *219*, 859-862.

Summary: Systems Chemistry Sketches

Chapter 17

Systems Chemistry Sketches

Stuart A. Kauffman

**Institute for Biocomplexity and Informatics, University of Calgary,
Calgary, Alberta, Canada**

Systems Chemistry, the study of very complex chemical reaction systems, is just emerging. In part, this is fueled by the emergence of Systems Biology, itself spawned by the genome project and powerful computers. In a human cell, some 25,000 genes and their products, which, due to alternative splicing, may number in the hundreds of thousands, coordinate their dynamical behavior, carry out work cycles linking spontaneous and non-spontaneous chemical and physical processes, and build rough copies of themselves. Organisms are interlinked chemically and in other ways in the entire persistently coevolving biosphere. Perhaps the most complex chemistry occurs in the biosphere. The other obvious candidates for complexity are the giant molecular clouds in interstellar space. Since reproduction and natural selection applies to the biosphere but presumably does not for giant molecular clouds, the features of their chemical complexity presumably differ dramatically.

A new area of chemistry that might be called Systems Chemistry is emerging and deals with very complex reaction networks, and the growth of chemical diversity in the universe and biosphere. I briefly discuss five topics: 1) the potential behavior of a small number of atoms on a very large chemical reaction graph, where the concept of chemical equilibrium may prove questionable, fluctuations may not damp out, and the detailed behavior may not be “lawful”, if by “law” one means a compact description beforehand of the regularities of the process. 2) Possible routes to the emergence of molecular reproduction, with a focus on DNA and peptide collectively autocatalytic sets and the testable theory of such sets. 3) The emergence of “agency” in the biosphere – the capacity of entities to act on their own behalf – a frank use of teleological language. 4) A confusing topic of the “propagating organization of process” that philosopher Kant worried about over 200 years ago. Here work is the constrained release of energy into a few degrees of freedom, but it typically takes work to construct those very constraints on the release of energy. Cells propagate work and constrain construction, together with “information” – a vexed concept – to reproduce themselves as collectively autocatalytic systems that do actual work. 5) The apparent incapacity to prestate the evolution of the biosphere by Darwinian preadaptations, which, if true, implies that we cannot write down equations for the evolution of the biosphere at the level of whole organisms, which again may be “lawless” in its detailed unfolding, but drives the vast increase in chemical complexity of the biosphere.

Vast and Atomically Under-populated Chemical Reaction Graphs

I begin with a largely unexplored topic – vast chemical reaction graphs that have very little matter reacting on them.

Consider a set of all possible molecules up to some maximum number of atoms per molecule that can be made from some initial set of atoms. As a biologist, I will pick carbon, hydrogen, nitrogen, oxygen, phosphorus, and sulphur, (CHNOPS), the building blocks of organic chemistry. To be concrete, consider all possible molecules of these with up to, say, 10,000 atoms per molecule. Proteins with a thousand amino acids in their primary sequence surpass this number.

I now want to define a chemical reaction graph. Figure 1 shows a simple chemical reaction graph in which two monomers, A and B, can undergo only cleavage and ligation reactions to form linear polymers. I represent a reaction by lines leading from the ‘substrates’ to a box representing the reaction, and an arrow leading to the product. The arrow direction is for convenience only, the direction of actual flow across any given reaction depends upon the direction of displacement from equilibrium.

Next, consider the truly vast reaction graph among all molecules comprised of CHNOPS, up to 10,000 atoms per molecule – an arbitrary limit as noted. Define the reaction conditions, temperature, pressure, and so forth, and write down, in principle, all the one substrate one product, one substrate two product, two substrate one product, and two substrate two product reactions among these molecules. Higher order reactions could be considered. The resulting reaction graph defines the reactions that can actually occur under the defined conditions.

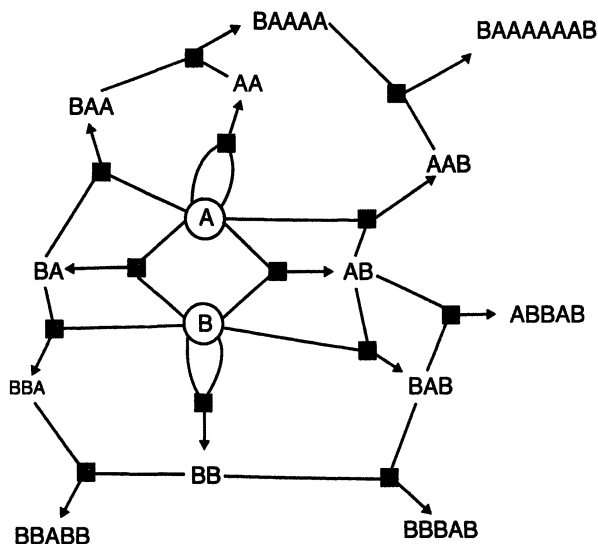


Figure 1. In this hypothetical network of chemical reactions, called a reaction graph, smaller molecules (A and B) are combined to form larger molecules (AA, AB, etc.) which in turn are combined to form still larger molecules (BAB, BBA, BABB, etc.). Simultaneously, these longer molecules are broken down into simple substrates again. For each reaction, a line leads from the two substrates to a square denoting the reaction, an arrow leads from the reaction square to the product. (Since reactions are reversible, the use of arrows is meant to distinguish substrates from products only in one direction of the chemical flow.) Since the products of some reactions are substrates of further reactions, the result is a web of interlinked reactions. (Reproduced with permission from reference 9. Copyright 2000 Oxford University Press.)

No one knows how many molecular species are in this reaction graph, to my knowledge, for counting them is an enormous problem in itself. However, it is safe to say that the number is enormous, and vastly larger than the estimated 10 to the 80th particles in the known universe as I show next.

I now want to suggest that at high levels of chemical molecular complexity, the flow of reactions on the graph above is almost certainly non-ergodic. Consider proteins with a length of 200 amino acids. There are twenty kinds of amino acids, hence 20 raised to the 200th power, or 10 to the 260th power possible proteins length 200. With some effort, we can synthesize any one of them. Now suppose that the universe was using its 10 to the 80th particles — ignoring space-like separation — and producing different proteins length 200, each requiring a femtosecond for synthesis. Stunningly, it would required 10 to the 67th repetitions of the history of the universe to make all the possible proteins length 200 once. If the processes happened at the Planck time scale of 10 to the -43rd seconds, it would take 10 to the 39th power repetitions of the universe to make all proteins length 200 once.

Thus, the universe has made only an infinitesimal fraction of all possible proteins. Moreover, the flow of chemical reactions forming proteins is vastly non-ergodic with respect to the set of possible proteins. The universe is on a unique trajectory in this chemical reaction space

Returning to our hypothetical CHNOPS vast reaction graph, I believe no one knows virtually anything about the flow of a small amount of matter, say a few moles of CHNOPS, on such a vast reaction graph. I want to suggest that it may be very much worth studying this problem.

Let me define the chemical “Actual”, and “Adjacent Possible”. Consider a set of N molecular species in a volume and the associated reaction graph. Call this set the “Actual”. Now let the molecules react. It may be that new molecular species, reachable in a single reaction step from the N, arise. Call these novel molecules the “Adjacent Possible”. The union of the Actual with this first Adjacent Possible creates a new Actual with a new Adjacent Possible. At issue is the flow of material from any initial Actual.

A number of issues arise here:

First, what does the concept of chemical equilibrium mean in the case considered? The normal concept of chemical equilibrium considers a few molecular species, say 2, X and Y, where X forms Y and Y forms X, with very many X and Y molecules, say millimoles or greater, and equilibrium is defined when the net rate of synthesis of X from Y and Y from X is equal, except for square root N fluctuations which dissipate.

But, as a guess before the actual analysis of mass underpopulated enormous reaction graphs is done, what would we expect to happen on our vast reaction graph with a few moles of CHNOPS? Perhaps nothing, for the atoms of CHNOPS might be distributed in such a way, for example, that atoms or molecules occur only as substrates to two substrate two product reactions, but in each case only one of the two substrates is present. The reactions could not proceed.

More generally, initial material may flow persistently into a possibly ever novel Adjacent Possible. Indeed, suppose a reaction couple with one or two substrate species, each having one molecule present, and two product species,

neither of which are present. Then the reaction is shifted to the left, with a real chemical potential driving the system towards the products, which may ultimately arise and then flow further on the graph.

Does the concept of chemical equilibrium make sense in this context? It is not clear that the concept of equilibrium makes sense, even for a closed thermodynamic system. Matter might flow persistently across the reaction graph for the lifetime of the universe non-ergodically, without ever reaching an equilibrium distribution.

A second issue that arises is whether chemical fluctuations “damp out”. In sharp contrast to the X Y equilibrium system with dissipating square root N fluctuations, my guess is that here typically fluctuations do not damp out. My guess, again prior to detailed analysis of such reaction systems, is that at points in the reaction graph where more than one reaction might occur, it will be a matter of chance – quantum or otherwise – which reaction occurs, and that matter will flow in some poorly predictable way on the graph. Then fluctuations may not damp out. The detailed distribution of matter on the graph may be deeply historically contingent on the previous evolution of matter on the graph from its initial Actual distribution.

A third issue is whether we can foretell how matter will distribute itself in detail on the graph. My bet is that we cannot in general. If a law is a compact description ahead of time of the regularities in the process, as Murray Gell-Mann argues at the Santa Fe Institute, then in this sense the overall pattern of flow of matter may not be law governed, despite following perfectly the laws of quantum or classical chemistry at each reaction step. Hopefully, at least there are statistical regularities that are law-like.

I end this section of the article with a plea to the chemists to study very complex reaction graphs. Quite new concepts are likely to arise. Furthermore, as a non-chemist I find myself wondering what is occurring chemically in the giant molecular clouds in the universe, that form grains that aggregate up to planetessimals. Presumably each modest size grain is molecularly unique in the universe. Its surface should therefore have a structure which may help catalyze new reactions, some of which add to the unique growth of the grain itself. While such systems are open to photons and other sources of energy, what diversity of molecular species would we detect if we could see down to a very small number of molecules of any given molecular species?

The Theory of Collectively Autocatalytic Sets and the Origin of Molecular Reproduction

The biosphere is the stunning example of molecular complexity with which we are most familiar. In this section I will briefly review five views of the origin of life, none known to be true.

- The first theory is that life started as a self replicating RNA single strand, that lined up free nucleotides and ligated sequentially in proper 3'-5' phosphodiester bonds, then the two strands would separate and cycle. This theory, obviously driven by the symmetry of double stranded DNA and RNA helices, has not yet worked (1).
- The second theory is the RNA World hypothesis, driven by the discovery that RNA can both carry genetic information, and act catalytically as a ribozyme. Here the hope has been to synthesize an RNA ribozyme polymerase that can copy any RNA single stranded molecule, including itself. Some success, using applied molecular evolution selection from about 10 to the 15th random RNA sequences, has been achieved in finding a molecule that can add about 13 nucleotides to a single stranded RNA (2). The approach is exciting and may work. However, it faces the problem, still unanalyzed, that if the RNA ribozyme polymerase made error copies of itself, they would presumably be more error prone, hence a runaway error catastrophe might arise that would overwhelm selection.
- The third view is the vesicle first theory, where the vesicle is either a micelle, or a something like a liposome. Luisi has created self reproducing liposomes, and micelles (3, 4).
- The fourth view is a metabolism first view. Harold Morowitz points out that the reverse TCA cycle is autocatalytic (5). In a lecture at the Systems Chemistry conference in December 2006 in Barcelona, Albert Eschenmoser suggested that collectively autocatalytic (as defined just below) metabolic systems may be possible (6).
- The fifth theory is that of collectively autocatalytic sets, first proposed for peptides by myself (7-10) and Freeman Dyson (11). The theory however, is broader than peptides alone, and might include a variety of polymers and metabolites (10, 12).

A collectively autocatalytic set is a set of molecules, say A and B, both say polymers, where A catalyzes the formation of B out of B fragments, while B catalyzes the formation of A out of A fragments. It is important to stress that in such a system, no molecule catalyzes its own formation. The set as a whole achieves catalytic "closure", such that each molecule in the system whose formation requires catalysis, has a last step in its synthesis catalyzed by some member of the set.

It is critical that two experimental examples of collectively autocatalytic sets have been achieved. Von Kiederowski made two single stranded DNA hexamers, each of which catalyzed the formation of the other out of two single stranded DNA timers (13). More astonishingly, after showing that a single 32 amino acid long zinc finger alpha helix coiled coil could catalyze its own formation by forming a peptide bond between 15 and 17 long fragments of itself (14) thus showing decisively that molecular reproduction need not be based on

polynucleotides, Ghadiri and colleagues (15) have made a collectively autocatalytic peptide set.

Thus, collectively autocatalytic sets have been demonstrated experimentally for DNA and peptide systems. The next point to make is that a cell is a collectively autocatalytic set as a whole, and achieves catalytic closure as a whole. No molecule in a cell reproduces itself, the cell as a whole reproduces.

The more general theory of autocatalytic sets is based on several general ideas (10, 12):

1. Consider a set of monomers, say A and B, making in the simplest case linear polymers, and a reaction graph of all dimers, trimers, Nmers. Count the number of molecular species in this reaction graph.
2. Consider a set of kinds of reactions, for example, in the present case, cleavage and ligation reaction alone. More generally, the set of molecules might not be linear polymers, and the set of reactions might include two substrate two product reactions or higher order reactions.
 - Count the ratio of reactions per molecule as the length of the longest polymer in 1), the Nmer, increases in length.
 - In the case of 1) and 2) above, the ratio of reactions to polymers scales linearly with N, as $N - 2$.
 - If two substrate two product reactions are also considered, the ratio of reactions to molecules increases very much faster.
 - Now suppose that the molecules in the system are not only substrates and products of the reaction in the reaction graph, but may also be catalysts for one or more of the reactions in the reaction graph.
 - If we knew which molecules catalyzed which reactions, we could assess if the system contained a collectively autocatalytic subset. In general, we do not know which molecules catalyze which reactions.
 - For several different simple models of which molecules catalyze which reactions, as the diversity of molecules in the system increases, the diversity of reactions among them which are catalyzed increases rapidly.

Eventually a diversity of molecules is reached in which so many reactions among them are catalyzed that a connected set of catalyzed reactions leading from a founder “food set” to a collectively autocatalytic set arises with probability near 1.0. Molecular reproduction “crystallizes” as a self organized property of the system. This is a phase transition in the “catalyzed reaction subgraph” of the reaction graph, from ones with small unconnected “components, to ones with “giant” connected components, analogous to a similar phase transition in random graphs studied by Erdos and Renyi (16).

This theory has been shown analytically (7), tested for a simple model in which each polymer has a chance, P, of catalyzing each reaction (12), and in which each polymer “matches” sites on substrates whose ligation and cleavage it

may catalyze. An example of such a collectively autocatalytic set is shown in Figure 2.

If this view is right, then molecular reproduction may be far more probable than we have thought. The above analysis leaves out sources of energy to drive the reactions, which might include enclosure in a liposome driven through hydration – dehydration cycles, pyrophosphate, or other sources of energy. It also leaves out an analysis of enclosure or some other means to hold the reacting molecules close enough to one another to react.

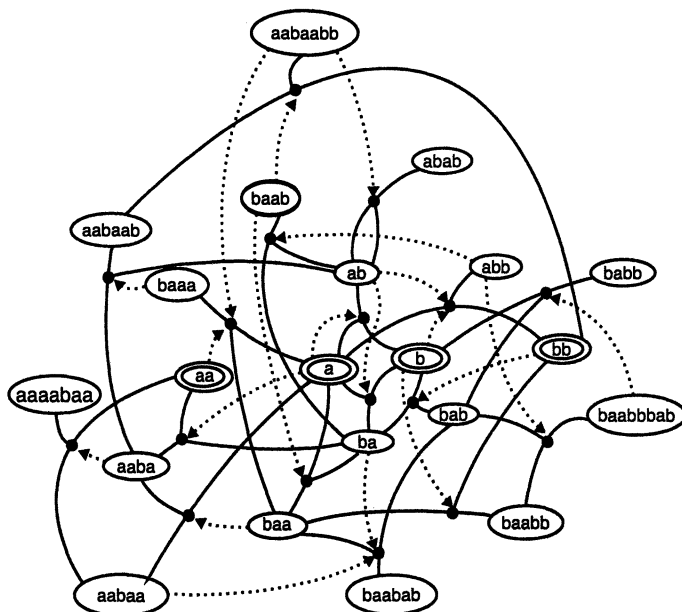


Figure 2. A typical autocatalytic set, built up from a food set, concentric ellipses, consisting in the monomers, a and b, as well as the dimers aa and bb. Catalysis is shown by the dotted lines leading from the catalyst to the reaction box, here reduced to a node, representing each of the ligation reactions. (Reproduced with permission from reference 9. Copyright 2000 Oxford University Press.)

Importantly, it has been shown that such autocatalytic systems can, in principle, evolve by heritable variation. So natural selection can, in principle, act on such systems.

Also, this theory can now be tested using libraries of stochastic DNA, RNA, peptides, and polypeptides. Here, my student Thomas LaBean showed some

years ago that stochastic polypeptides biased to the known ratio of amino acids in evolved proteins form helix and beta sheet structures and molten globules or even better folded structures (17). Luisi and students have recently extended this to fully random polypeptides (18). Thus, in so far as folding modestly well is required for catalytic activity, this property seems abundant among polymers of the standard twenty amino acids. Folding may not be common with other amino acids, of course, and needs to be investigated. The study of the folding properties of random peptides and polypeptides open up an avenue to study structure distribution among such polymers by NMR and other techniques.

One approach to begin to test this theory is to ask the probability distribution among peptides or polypeptides to catalyze specific, or a diversity of, chemical reactions. The existence of catalytic antibodies suggests that this probability may be on the order of one in a million to one in a billion (10). Beyond this, would be the evolution of collectively autocatalytic sets in systems of sufficient diversity. Finally, I note that similar questions can be tested concerning the catalysis of a connected metabolism among small organic molecules and the union of such a metabolism, hopefully including lipids to make bounding membranes, with an autocatalytic set of polymers or other molecular species.

Molecular “Autonomous Agents”

On our march towards increasing molecular complexity, a next step is fundamental. Consider a bacterium swimming up a glucose gradient. Most biologists would say that the bacterium is going to get food. That is, we biologists would use teleological language for the bacterium, but not for a rock. The use of teleological language is, of course, a complex issue I will not discuss here, but humans are described with teleological language and I seek the minimal physical system to which it might reasonably apply. Let me call such a minimal system a “molecular autonomous agent”, meaning that it can act on its own behalf in an environment.

It is, in fact, remarkable that agency has come to exist in the universe. We are all examples of it.

In my book *Investigations* (9), I propose a tentative definition of a molecular autonomous agent: It must reproduce itself. And it must carry out at least one thermodynamic work cycle. Figure 3 shows an hypothetical molecular autonomous agent which couples self reproduction and a chemical work cycle. There are many points to be made about this chemical system. Foremost, it is a legitimate non-equilibrium chemical system linking exergonic and endergonic reactions, does a work cycle as advertised, and reproduces. On this account, agency is a non-equilibrium concept for no work cycle can be performed at equilibrium. The legend of Figure 3 explains the workings of this hypothetical

system. If the appropriate differential equations are written down, the system exhibits a limit cycle oscillation. Further, it is open to natural selection as the constants in those equations are varied.

The inclusion of a work cycle seems to be a central feature of this tentative definition, for work cycles link spontaneous and non-spontaneous (exergonic and endergonic) chemical reactions. The collectively autocatalytic system considered in section II might have been entirely exergonic. If one considers the biosphere as a whole, it is a richly interwoven web of linked exergonic and endergonic reactions building up the enormous chemical complexity of the entire biosphere, the most complex chemical system we know.

I suspect that we will create molecular autonomous agents in the reasonably near future, for molecular reproduction has been achieved experimentally, as have molecular motors. I also suggest that such systems may foretell a technological revolution for they do work cycles, hence can build things, as do cells when they build copies of themselves and do other work. It may be, although I would not insist on it, that molecular autonomous agents, augmented to have a bounding membrane, may be a minimal definition of life. I would note that Schrodinger, in *What is Life*, argued for the necessity for “negentropy”, but not for the requirement for a work cycle.

Propagating Organization of Process

Work cycles in living cells brings up a confusing topic. I wish I could be clearer than I shall be, but hope to bring the main issues out. I think a broad phenomenon is right in front of us, but we lack the language to see it: propagating organization of process (9, 19, 20).

I begin by asking “What is work?” Of course, we all know that work is force acting through a distance. But Atkins, in his book on the Second Law, argues that work is a “thing”, specifically, work is the constrained release of energy into a few degrees of freedom.

As a concrete case, consider a cylinder and a piston, with the working gas hot and compressed in the cylinder head. The random motions of the gas particles exert pressure against the piston which undergoes translational motion down the cylinder in the power stroke. This is precisely the constrained release of the random energy of the gas particles into a few degrees of freedom, the translational motion of the piston.

What, then, are the constraints? Evidently, the cylinder and piston and the location of the piston inside the cylinder, with the working gas confined in the cylinder head.

Now let us ask a new question: Where did the constraints come from? In the current case, it took work to make the cylinder, piston, and assemble the system. Thus, we seem to come to a very interesting cycle of ideas: It takes work to

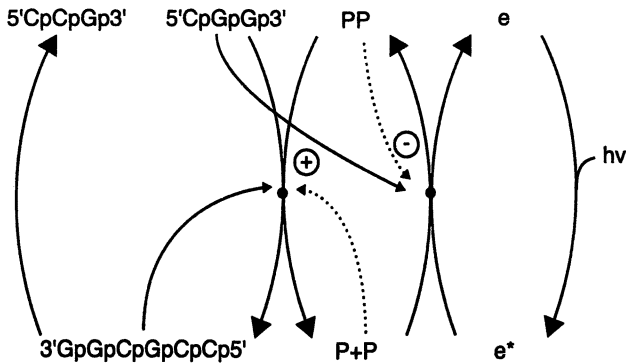


Figure 3. A first hypothetical molecular autonomous agent. The entire system is an open none equilibrium thermodynamic system driven by two sustained sources of food. The sources of food are two single stranded DNA trimers and a photon source, $h\nu$. The two single stranded DNA trimers undergo a ligation reaction to form a second copy of the hexamer. There are two reaction pathways for synthesis of the hexamer and its breakdown back to the trimers. Each pathway is reversible, but due to displacement from equilibrium by the food, tends to flow in a forward direction towards synthesis of the hexamer. The first forward pathway is coupled to the breakdown of pyrophosphate, PP , to two monophosphates, $\text{P} + \text{P}$. The exergonic drop in free energy from the breakdown of PP drives the excess endergonic synthesis, hence excess replication, of the DNA hexamer, compared to the equilibrium otherwise achievable. There is a reverse pathway by which the hexamer breaks down to the trimers that does not couple to PP . However, in the absence of an enzyme to catalyze this return reaction, the reaction is very slow, and the excess replicated DNA hexamer can persist in the system for a long time. PP in turn, is reformed from ligation of $\text{P} + \text{P}$ by an endergonic reaction that is driven by coupling to a photon-excited electron, e^ , which gives up free energy in an exergonic reaction to return to a ground state, while adding that energy to the endergonic synthesis of PP from $\text{P} + \text{P}$. The hexamer catalyzes the reaction leading to its own excess synthesis. One of the trimers catalyzes the reaction leading to the PP resynthesis. The analogue of gears and escapements in a Carnot engine is played by allosteric enhancers and inhibitors that gate the different reactions so they occur reciprocally. Thus, monophosphate, P , activates the hexamer enzyme. Pyrophosphate, PP , inhibits the trimer enzyme. Overall, the autonomous agents couple reproduction and a work cycle. (Reproduced with permission from reference 9. Copyright 2000 Oxford University Press.)*

make constraints, and constraints on the release of energy to make work. (I can think of cases in which it takes no work to make constraints, but these seem to “cheat” by starting with high energy compounds that fall to low energy states like liposomes that then comprise constraints.) So while I hesitate to say that it always takes work to make constraints on the release of energy, it often does.

Now what a cell does is rather astonishing, and hard to pin down. Chemical processes happen that do work to construct constraints on the release of energy, which, when released, does further work that builds a variety of things, including further constraints on the release of energy. This, crudely, is a propagating process. In due course, this propagating process of constraint construction, the constrained release of energy in specific directions, the resulting building of structures, and carrying out of processes, closes upon itself in a set of “tasks” such that the cell constructs a rough copy of itself.

While we all know this is true, we seem not to have a language for it. The closest simple analogy I can think of is a river and river bed, where the river carves the bed, while the bed is a constraint on the flow of the river. The phenomena of propagating processes, with linked constraint construction and constrained release of energy, are right in front of us, but hard to describe so far, and hard to mathematize so far. It is this self propagating organization of processes, upon which the philosopher Immanuel Kant commented over two hundred years ago, that we need to understand more fully, and for which we need to formulate a mathematical framework. Perhaps the reader knows of such a framework already. I confess I do not as yet. Nevertheless, cells carry out a propagating organization of process, overwhelmingly chemical, that remains poorly analyzed. Linked among cells, this propagating organization of process flows through and constructs the biosphere.

The Incapacity to Prestate the Evolution of the Biosphere

The final topic upon which I touch is far from the center of the current conference, but central to the evolution of the biosphere, this overwhelmingly complex chemical non-equilibrium system.

Let me define first a Darwinian adaptation. Were one to ask Darwin what is the function of the heart, he might have responded, “To pump blood”. Now the heart has other causal consequences, such as heart sounds. So already this is interesting, for the function of the heart is a subset of its causal consequences and must be ascertained in the light of the full life cycle of the organism in its selective environment over evolutionary time. Darwin is telling a selection story in ascribing to pumping blood a special role as the function of the heart: he is asserting that hearts exist in the biosphere thanks to this property.

But Darwin also spoke of preadaptations. His brilliant insight was that a part of an organism might have causal consequences, like heart sounds, of no

selective significance in the normal environment, but of potential selective significance in some other environment. The canonical example is the swim bladder of an early fish, filled with both air and water, to maintain neutral buoyancy in a water column. Since the bladder was filled partially with air, it was “preadapted” to evolve into a lung. This is a Darwinian preadaptation. Now such a preadaptation typically gives rise to a novel function in the biosphere, here air breathing. And it may have profound causal consequences, such as the invasion of land by animals.

I now ask a new question: Do you think that you could say, ahead of time, all possible Darwinian preadaptations of all organisms, or just humans? More formally, could you finitely prestate all possible Darwinian preadaptations? I’ve not met anyone who thinks the answer is “Yes”. I do not know how to prove the answer is “No”, but part of the difficulty is that there appears to be no effective procedure to list all possible selective environments. How would we even get started on such a task?

But the implications are striking. First, the incapacity to prestate preadaptations is not slowing down the evolution of the biosphere, where they arise all the time. Second, we cannot even make probability statements about such preadaptations. Consider a fair coin tossed 1000 times. It will come up heads about 500 times. This is the frequency interpretation of probability. But note that it rests on knowing ahead of time all the possible outcomes. We do not know this for the evolution of lungs ahead of time. A related concept of probability derives from Laplace, who noted that if one were confronted by N doors behind one of which was a treasure, but we had no idea of which door, then the probability of finding the treasure was $1/N$. But note that we knew ahead of time that there were N doors. Again, we do not know the analogue of N with respect to Darwinian preadaptations, thus in general we do not seem even to be able to make probability statements about them.

The next implication is that we cannot proceed as Newton taught us to do. We cannot write down the variables, the laws among the variables, the initial and boundary conditions, and solve for the forward evolution of the system. We cannot because we do not yet know what the variables are, we do not know that lungs will arise one day, yet they are among the variables with causal consequences for the further evolution of the biosphere.

In short, we do not know how the biosphere will evolve via such preadaptations. For better or worse, this appears to be a limitation of science itself, for we seem precluded even from attempting to simulate the evolution of this specific biosphere given quantum events and continuous spacetime. So the consequences appear to be radical.

Yet these very consequences bear on the evolution of molecular complexity in the biosphere, for the same preadaptations bring forth novel proteins, and probably small molecules, hence altering the unique trajectory of the universe on the vast chemical reaction graph that we are exploring (9).

Conclusions

I began by noting that I am not a chemist. The central topics of this conference concern the origins of organic molecules, their possible delivery to the protoplanet, their possible synthesis on Earth, and related topics. I have tried to raise five issues, each of which contributes to the emergence of chemical complexity: 1) What is the behavior of a chemical reaction system where the number of atoms is small compared to the vast reaction graph upon which reactions are occurring. I hope it is reasonable to think this is a worthy topic, for here the concept of chemical equilibrium seems ill posed, fluctuations unlikely to damp out, and the detailed occupancy of the graph hard to predict, perhaps even “lawless”, if by law one means a description ahead of time of the regularities of the process. 2) I have outlined alternative theories for the origin of molecular self reproduction, and noted that collectively autocatalytic DNA and peptide systems have been created. The existence of collectively autocatalytic peptide systems demonstrates that molecular reproduction need not be based on DNA or RNA or similar polynucleotides. Further, I have sketched the theory of the emergence of collectively autocatalytic sets as a phase transition in a chemical reaction graph because the catalyzed subgraph grows to a giant component as the diversity of molecular species increases. The theory is now testable using libraries of stochastic DNA, RNA and peptides or polypeptides. 3) I have discussed a new class of non-equilibrium chemical reaction networks that both reproduce and carry out chemical work cycles, that I called “molecular autonomous agents”. Whether the reader accepts that such systems can act on their own behalf, they are an interesting new class of non-equilibrium chemical reaction networks; real cells are such networks, the biosphere is built of such interacting networks, and they hint a technological revolution for they reproduce and can build things. 4) I have given a confused discussion of self propagating process of the kind Kant talked about in the 18th Century. Here it takes work to construct constraints on the release of energy that performs work, in part to construct further constraints on the release of energy. We need to build a theory of such systems, for cells are such systems, and the linking of these processes within and between cells has built the biosphere. 5) I have discussed Darwinian preadaptations, and suggested that we cannot foretell their evolution, hence cannot know ahead of time how the biosphere with its teeming chemical complexity will evolve. I find most of this surprising and I hope it is of interest to the conference.

References

1. Hill, A. R.; Orgel, L. E.; Wu, T., The limits of template-directed synthesis with nucleoside-5'-phosphoro(2-methyl)imidazolides. *Origin of Life and Evolution of the Biosphere* **1993**, *23*, 285-291.

2. Johnston, W. K.; Unrau, P. J.; Lawrence, M. S.; Glasner, M. E.; Bartel, D. P., RNA-catalyzed RNA polymerization: Accurate and general rna-templated primer extension. *Science* **2001**, *292*, 1319-1325.
3. Bachmann, P. A.; Luisi, P. L.; Lang, J., Autocatalytic self-replicating micelles as models for prebiotic structures. *Nature* **1992**, *357*, 57-59.
4. Walde, P.; Wick, R.; Fresta, M.; Mangone, A.; Luisi, P. L., Autopoietic self-reproduction of fatty-acid vesicles. *Journal of the American Chemical Society* **1994**, *116*, 11649-11654.
5. Morowitz, H. J., Personal communication. In 2004.
6. Eschenmoser, A. In *Keynote lecture*, Chembiogenesis 2006, Barcelona, 2006; Barcelona, 2006.
7. Kauffman, S. A., Autocatalytic sets of proteins. *Journal of Theoretical Biology* **1986**, *119*, 1-24.
8. Kauffman, S. A., *At home in the universe The search for laws of self-organization and complexity*. Oxford University Press: New York, 1995; p viii, 321 p.
9. Kauffman, S. A., *Investigations*. Oxford University Press: Oxford; New York, 2000; p xii, 287 p.
10. Kauffman, S. A., *The origins of order Self-organization and selection in evolution*. Oxford University Press: New York, 1993; p xviii, 709.
11. Dyson, F. J., *Origins of life*. Cambridge University Press: Cambridge; New York, 1985; 81 p.
12. Farmer, J. D.; Kauffman, S. A.; Packard, N. H., Autocatalytic replication of polymers. *Physica D* **1986**, *22*, 50-67.
13. Sievers, D.; Von Kiedrowski, G., Self replication of complementary nucleotide-based oligomers. *Nature* **1994**, *369*, 221-224.
14. Lee, D. H.; Granja, J. R.; Martinez, J. A.; Severin, K.; Ghadiri, M. R., A self-replicating peptide. *Nature* **1996**, *382*, 525-528.
15. Lee, D. H.; Severin, K.; Yokobayashi, Y.; Ghadiri, M. R., Emergence of symbiosis in peptide self-replication through a hypercyclic network. *Nature* **1997**, *390*, 591-594.
16. Erdos, P.; Renyi, A., On random graphs *Publ. Math. Debrecen* **1959**, *6*, 290-297.
17. LaBean, T. Examination of folding in random sequence proteins. Ph D Dissertation; University of Pennsylvania, 1993.
18. Chessari, S.; Thomas, R.; Polticelli, F.; Luisi, P. L., The production of de novo folded proteins by a stepwise chain elongation: A model for prebiotic chemical evolution of macromolecular sequences. *Chemistry & Biodiversity* **2006**, *3*, 1202-1210.
19. Kauffman, S.; Logan, T. K.; Este, R.; Goebel, R.; Hobill, D.; Shmulevich, I., Propagating organization: An enquiry. *Biology & Philosophy* 2007, In Press.
20. Kauffman, S.; Clayton, P., On emergence, agency, and organization. *Biology & Philosophy* **2006**, *21*, 501-521.

Part IV: Teaching Chemical Evolution

Chapter 18

Science and the Concept of Evolution: From the Big Bang to the Origin and Evolution of Life

Lori Zaikowski¹, Richard T. Wilkens², and Kurt Fisher³

Departments of ¹Chemistry, ²Biology, and ³Physics, Dowling College,
Oakdale, NY 11769

The common thread of evolution runs through all science disciplines, and the concept of evolution enables students to better understand the nature of the universe and our origins. "Science and the Concept of Evolution" is one of two interdisciplinary science Core courses taken by Dowling College undergraduates as part of their General Education requirements. The course examines basic principles and methods of science by following the concept of evolution from the big bang to the origin and evolution of life. Case studies of leading scientists illustrate how their ideas developed and contributed to the evolution of our understanding of the world. Evidences for physical, chemical, and biological evolution are explored, and students learn to view the evolution of matter and of ideas as a natural process of change over space and time.

Reprinted with permission from *Evolution Education and Outreach* Vol. 1(1).
Copyright Springer. Available online at <http://www.springer.com>.

Introduction

“Science and the Concept of Evolution, NSC 2003C” integrates fundamental concepts in physics, chemistry, and biology to provide students with an interdisciplinary understanding of evolution. The course explores not only the evolution of the universe, solar system, and life on earth, but also the evolution of ideas regarding various realms of the scientific enterprise. The philosophy of science is introduced from the perspective of scientists in each field, and through examples of how their ideas have played out in the “evolution” of our understanding of the solar system model, the sciences of mechanics and electricity, atomic theories, and biological species change. The course provides students with an interwoven mosaic about the evolutionary nature of our world and our understanding of that world. It follows the evolution of physical forces and of chemistry beginning with the first seconds of the universe: from the formation of the simplest elements, to more complex elements and molecules, to prebiotic compounds, and ultimately to the molecular diversity and complexity present in living organisms today. In the process, students learn how science works, how it is used to unravel the mysteries of the universe, and how physics, chemistry, and biology have evolved over time and shaped our worldview.

Dowling College is an independent, coeducational college of more than 7,000 students, approximately 3,500 of which are undergraduates. Students in all majors complete a Core Curriculum to fulfill General Education requirements. The six credit two semester sequence NSC 2003C (Science and the Concept of Evolution) and NSC 2004C (The Science of Natural Systems) fulfills the Natural Sciences portion of the Core Curriculum. NSC 2003C meets for 160 minutes per week, and 14 weeks per semester (typically 80 minutes per class meeting, two days per week). About 25 sections of NSC 2003C are offered each year since the course is taken by virtually all Dowling undergraduates. Most students in the course are non-science majors. Faculty teaching the interdisciplinary NSC Core courses come from a wide variety of disciplinary backgrounds, and must meet the challenge of teaching subject matter that is not in their immediate area of expertise. A composite sample syllabus that lists NSC 2003C course topics as well as laboratories and demonstrations is available in the supplementary materials. A main objective is to impart an integrated overview of science and the concept of evolution. To achieve this integrated picture, principles of the philosophy of science are first discussed in general terms, and then are illustrated with reference to specific theories that form our contemporary view of how the world works. Likewise, when discussing specific scientific theories and how they have evolved, reference is made to the philosophical principles that were operative at the time. This bi-directional reinforcement helps to instill both the scientific principles themselves and the

methods by which they came about. The narrative that follows describes how the course explores the nature of science, the fundamental makeup of the universe, the way in which these fundamental parts are assembled into the totality of the universe, how life on Earth evolved and fits into the cosmic fabric, and how our ideas about the universe have evolved over time.

The Universe Alive and Kicking

The grandest story of all encompasses the origin, makeup and evolution of our universe, which includes life. This is the story that we teach at Dowling College in our general science Core course “Science and the Concept of Evolution.” Indeed, it is a grand story, unified by the majesty of the topic; nonetheless, there is a surfeit of compelling subplots. One subplot is a perfect complement to the overarching story – the way that scientists have come to know the universe in all its splendor and complexity. Educators hotly debate how best to deliver general education; we believe that this course hits many of the right notes. It encompasses topics that speak to the fundamental reality of our existence. Furthermore, it stresses the human endeavor of science. These are exactly the kinds of lessons that are important for every college student to embrace; that is, the universe is large, complex, marvelous, and often knowable. The course emphasizes what we know, how we learned it, and what is left unknown. For students to grasp the concept that scientists have fundamentally explained processes that once seemed unknowable is among the most important messages of this course. Science is alive and dynamic and the universal unknown is the frontier to which scientists set sail as explorers.

Breaking the Universe Into Fundamental Parts: Matter, Force and Time

We argue that to know the universe, students should know its fundamental composition. In this unit, we break the universe into its fundamental building blocks. First, we introduce the concept of the smallest piece of matter. But to do so, we do not simply make a list fundamental particles. Rather we explore the subplot of discovery. How did humans come to know of the fundamental parts of matter? Starting with Democritus’s *átom* and going through a sequence of scientists (Dalton, Thomson, Rutherford, Bohr, Pauli, Fermi) we end with our current state of knowledge: six quarks and six leptons.

Matter is not motionless, not frozen in space and time; it moves, sometimes dramatically. So next, we discuss the three laws that govern the motion of matter, courtesy of Isaac Newton. Of course, matter does not move magically; a

force is responsible. As such, we spend several lectures on the four fundamental forces, paying particular attention to gravity and electromagnetism. These two forces, along with the strong nuclear force, are essential for understanding the next unit, which covers in part, the life and death of stars. Once the concepts of matter and force have been established, we move on to the fundamentals of thermodynamics. No discussion of the universe can be complete without some understanding of both laws. The first law of thermodynamics is absolutely essential to make the following point: nothing in the universe is magical; that is, whenever an object emits or utilizes energy, that energy must come from somewhere. In the next unit, this fundamental concept is used to make an important point about stars – they die. The second law of thermodynamics is no less important. It establishes a sequence of events: order goes to disorder, heat flows from hot to cold bodies, and energy goes from a concentrated form to a less concentrated form with the release of heat. In other words, the second law dictates the arrow of time. Voilà, we have done it! The universe broken down into matter, force and time with a handful of laws that govern them.

Reassembling the Universe

To know a thing is to know more than the fundamental building blocks. After all, if each of a human's 11 trillion cells were presented to you one at a time, you would hardly understand what it means to be a human – so too for the universe. As such, in this unit we aim to reassemble the universe into a coherent entity made up of fundamental building blocks. The book we use for the course, *The Sciences* by Trefil and Hazen (1), has a fascinating approach that is adopted for the first presentation in this unit. Imagine the first person able to form a question (perhaps one of our hominid ancestors) emerging from a slumber and looking up at the night sky. They surely asked an obvious question, "What are those points of light?" Thus, astronomy was born. In this class, the same question is asked of students, only we permit them to use the basic information learned in the previous unit. Thus follows a remarkable logical sequence: stars emit light; light is electromagnetic energy; stars are not magical, thus they must convert some other form of energy into light; stars are not infinite in volume, so they will run out of energy some day; all stars will die; and finally, if all stars die, then all stars were born. Two questions naturally flow from this discussion:

- How are stars born? and
- How do stars die?

The answers to these questions are marvelous in their own right, but they are essential to understanding the origin of life itself, for it is in the forge of

thermonuclear fusion that the elements of life were generated. By detailing the processes of star birth and death, we construct a panoply of stars: main sequence stars (from sun-sized yellow stars to blue giants), red giants, super red giants, white dwarfs, black dwarfs, neutron stars and black holes.

Next, we consider the ways that astronomers measure distances to stars. Triangulation, using trigonometric functions, to measure distance works well for stars nearby. But before powerful telescopes, there were a number of “fuzzy stars” that were far too distant to be measured using this technique (1). Edwin Hubble used Cepheid variables (a special type of dying star that reveals its absolute brightness by the duration of its brightening/dimming cycle) to determine that the so called fuzzy stars were really clusters of stars that were astonishingly far away (1); we now recognize these as galaxies. The nearest galaxy to us is Andromeda, 2.5 million light years away! Hubble helped us realize the immensity of the universe. Indeed, the arrangement of galaxies in the universe has a large-scale structure in which galaxies come in clusters and groupings. Hubble’s discovery of the immensity of the universe vastly changed our sense of the universe, but he was not done surprising us. Using light spectroscopy, Hubble discovered that all galaxies are moving away from us; the farther away the faster they move. Hubble determined that only universal expansion could explain such a result! For a second time, Hubble dramatically changed the way we view the universe.

However, the universe is large (infinite actually) and surprises seem to be the norm rather than the exception. In 1998, Science magazine named the discovery that the universe is not only expanding but that it is doing so at an expanding rate as its “Breakthrough of the Year” (2). At this point in the class, we have established how stars form and die, how they are collected into galaxies, how the galaxies are arranged in space and how they are constantly zooming away from each other at an accelerating rate! Not bad for a unit in a general science class, but we do not finish with this. No; remarkably, using particle accelerators, scientists have determined with great precision what the conditions of the universe were like in the first moments after the Big Bang. For instance, at 10^{-35} seconds after the Big Bang, the strong force froze out and at 10^{-10} seconds all four fundamental forces existed as separate entities. The stunning energy and expansion of the early universe led to an important phenomenon for understanding the origin of life; that is, rapid expansion prevented the formation of heavier elements through fusion. The vast majority of matter in the universe is hydrogen, helium and lithium; everything else is rare. But hydrogen, helium and lithium simply won’t suffice for life. To account for life, we need to explain the origin of heavier elements: nitrogen, oxygen, phosphorus and many others, but especially carbon. Moreover, we need to think about how they got to us here in our solar system.

Life

At this point, a review session examines images from the Hubble telescope. Students marvel at images of planetary nebulae that spew their contents in diametrically opposed jets of gas and at elegant spiral galaxies (among the most beautiful objects in the universe). We finish with images of the deep field survey of galaxies. Few images are more stirring – galaxy upon galaxy upon galaxy piled up one after the other to the edges of universe, each galaxy possessing millions, billions or even trillions of stars. If a goal of general education is to imbue a sense of place and scale in our students, what could be more effective than a deep understanding of the universe? On the other hand, it is not our intention to make them feel small and insignificant. As an antidote to this natural feeling of being miniscule, the following quote is read from Alan Dressler's 1994 book, *Voyage to the Great Attractor* (3).

We continue to take the wrong lesson from what we are now learning. An astronaut who had taken a tethered spacewalk while on a Gemini flight was recently asked whether the experience had changed him. He had been struck, he recalled, by how small and insignificant were the Earth and the human adventure, "like an ant crawling across the Sahara Desert." Exactly. The ant, astronomically outnumbered by the grains of sand, overwhelmed by the size of the inhospitable desert, is nevertheless the greater marvel, by far.

It is time to take stock of the discovery that life is the most complex thing we know of in the Universe, and, as such, most worthy of our admiration. Yes, the Universe dwarfs our world in size and immense power. But the Universe of stars, galaxies, and vast gulfs of space is so very, very simple compared to us and our brethren life forms. If we could but learn to look at the Universe with eyes that are blind to power and size, but keen for subtlety and complexity, then our world would outshine a galaxy of stars. Indeed, we should marvel at the Universe for its majesty, but we must truly be in awe of its greatest achievement – life.

Certainly, if life is the Universe's greatest achievement, it is most worthy to understand its origin and evolution in a general education science class. Moreover, this course enables us to frame that grand story in a way that pure biology courses cannot. Living organisms are made of particles, arranged in atoms to form different elements, which are arranged in a dizzying array of molecules interacting according to their chemical properties. How then did these chemicals originate and how did they come to be on Earth? The first item that we tackle in this last unit is to define life. Like so much in biology, it's more

complex than it seems at first. Trefil and Hazen (*I*) handle the questions by listing characteristics that most known living organisms share:

1. All living things maintain a high degree of order and complexity.
2. All living things are part of a larger system of matter and energy.
3. All life depends on chemical reactions that take place in cells.
4. All known life requires liquid water.
5. Organisms grow and develop.
6. Living things regulate their use of energy and respond to their environment.
7. All things share the same genetic code, which is passed from parent to offspring.
8. All living things are descended from a common ancestor.

The first two items are concepts that directly relate to earlier discussions of the laws of thermodynamics. One should be careful to point out that these two items do not imply that life violates the second law of thermodynamics, but that living systems are open systems, can receive energy, and are thus free to experience localized increases in order. A bit more time is spent with item 3. First, the stunning diversity of life on the planet is described. Next, we discuss the complexity of the shapes, sizes, and the even greater diversity of chemical reactions that take place in living systems. Despite the complexity of life and its biochemistry, every element on the periodic table is not equally represented in the makeup of living organisms. Indeed, no element is more central to the understanding of life than carbon. If there is such great complexity of shape and chemistry in living systems, then there had better be a flexible building block; the ultimate erector set if you will. Carbon is special. Its ability to form stable covalent bonds with four other atoms, including another carbon atom, makes very large, complex molecules possible. The story of the origins of life must, therefore, tackle an even more fundamental question. If life depends on the chemistry of carbon, where did carbon come from? In answering that fundamental question, we also discover the origin of four other elements from that oft-cited neumonic from introductory biology classes, CHiNOPS: carbon, hydrogen, nitrogen, oxygen, phosphorus, and sulfur (hydrogen formed during the first second of The Big Bang), all of which are essential to known life and are found as a fairly large percentage of dry biomass. That is why biologists refer to these as essential macroelements.

There are also a number of microelements that are essential, but in much smaller quantities. These include some heavier elements like iron, iodine and zinc. Where do all of the essential elements come from? In the Reassembling the Universe unit, we examine the processes of star birth and death. Students learn that all main sequence stars the size of our sun and larger eventually undergo helium fusion resulting in the formation of carbon. Larger stars exhibit

fusion layers leading to elements even more massive than carbon, including phosphorus and nitrogen. Indeed, main sequence stars at least eight times larger than our sun will eventually have a core that leads to iron. No amount of pressure in the core on any star can get iron to fuse, so that is the heaviest element formed in the cores of stars. Students can identify and to a large degree explain the processes that lead to the origin of carbon and nearly every other essential element – fusion in star cores. But there are still some outstanding questions the students must ponder. First, some essential elements are more massive than iron, for example iodine. Where do elements heavier than iron come from? Second, how did carbon and all of the other essential elements get to our Solar System?

The answer to both questions is the same – supernova. In Type I supernovae, a white dwarf (a hot carbon/oxygen remnant of sun-sized star) rapidly draws the gas from its binary partner, leading to a rapid accumulation of mass and pressure and, ultimately, the detonation of the former white dwarf (*I*). In Type II supernovae, a large star's iron ash core catastrophically collapses into a neutron core, which rebounds out and smashes into billions of kilometers of in-falling mass. Either way the energy is monstrous. The energy produced in a supernova of either type exceeds the energy emitted at that moment by all of the stars in a galaxy. The energy generated in a supernova is sufficient to fuse every element of the periodic table, including iodine and other heavier bioessential elements. After the supernova, gases seeded with every element on the periodic table are hurled at a significant portion of the speed of light. This means that at some time in the past, a supernova blasted materials to where our solar system now resides. Those gases either formed or added to a nebula, a huge cloud of gas and debris, that eventually led to our Solar System. So, by carefully developing the sequence of events that lead to red giant and ultimately to a supernova, students now know where all elements, including carbon, came from and how they got to where the Solar System currently resides. Though we have not even come close to explaining the origins of life, we have at least explained the origins of the elements that comprise life, and furthermore, how they got to Earth's neighborhood.

It is one thing to place carbon and all other essential elements in a nebula. It is quite another to locate them on a planet. How, then, did these elements wind up on Earth? Astronomers normally invoke some version of the Nebular Hypothesis. In this hypothesis, nebular gases deep in the cloud, dominated by hydrogen and helium begin to gravitationally contract. But rather than simply contracting into a ball, the cloud begins to develop rotational movement. This rotation spews out thin disks of matter. Though thin relative to the central mass and ultimate source of the sun's mass, it is still substantial enough to form localized collections of mass due to gravity. Earth is one of these masses that formed in the disc of our developing sun. Like its three inner solar system

companions, Earth formed as a smallish rocky planet possessing all of the bioessential elements.

At this point in the class we have established how carbon and all elements wound up on Earth. However, for life to form, we need to explain the origins of organic chemicals, and moreover, the presence of chemicals in the atmosphere. Trefil and Hazen (*1*) suggest that we consider what early Earth was like after it formed around our young sun. Though eight distinct planets formed (*sans* Pluto!), there were many, many planetesimals in the early Solar System. These planetesimals ranged from the size of boulders to several kilometers across. Earth is small compared to the sun, but it was large enough to gravitationally entrain many planetesimals. As they smashed into the Earth over and over, the solid Earth became semiliquid and denser materials sank to the core. Over time, Earth cleared its planetary neighborhood of most debris; indeed, that is part of the accepted definition of a planet (*4*). As less energy impacted Earth, the great bombardment ended and it cooled. A crust formed, which trapped gasses underneath. Gases eventually built up pressure and erupted in global volcanoes. If today's volcanoes are any guide, they spewed simple gases including carbon dioxide, hydrogen, methane, ammonia and especially water vapor. As Earth cooled, atmospheric water condensed and fell as rain. It rained and rained and rained. Oceans filled up with rain water. Lightning surely laced this early roiling, charged atmosphere. We must still address a simple question – how did carbon get into organic compounds? By this point we have only established a plausible mechanism for locating simple carbon compounds in the atmosphere, but no organics. We can never go back in time, but we can try and reconstruct what the conditions were like at that time. That, of course, is what Stanley Miller and Harold Urey did in their famous experiments in the 1950s (*5,6*). This experiment was vital in that it showed that the early conditions of Earth could lead to formation of organic molecules. No magic need be invoked, no tricks of modern chemistry introduced, just a simple system of gases, water and heat. There may be other ways that organic compounds could be introduced to early Earth; for instance, meteorites may contain organic compounds that can survive impact on Earth. However it happened, Earth is and surely was rich in organic molecules – a veritable organic soup.

How this soup yielded life is one of the great unresolved mysteries of science. Perhaps it had something to do with the way that phospholipids form hollow balls containing mixtures of organic chemicals, perhaps it has something to do with the way RNA molecules can act as both template or enzyme or perhaps it involves myriad processes that we have yet to uncover. The honest scientific stance is that we do not know the answer. But we remind students to relish the unknown, for it is the unknown that drives scientists to journey with stars and to discover. Once life formed, the grand process of evolutionary biology could play out, with natural selection leading the way. As Charles

Darwin famously said in the end of his book, “There is grandeur in this view of life, with its several powers, having been originally breathed into a few forms or into one; and that, whilst this planet has gone cycling on according to the fixed law of gravity, from so simple a beginning endless forms most beautiful and most wonderful have been, and are being, evolved” (7). We submit that Charles Darwin would be much impressed and deeply moved to see that his version of origins had been moved back to the beginning of time and matter.

The Evolution of Ideas in Science

Our understanding of the universe has evolved over time as new data are collected, new observations are made, and new explanations are proposed. The primary textbook for the course, *The Sciences*, is structured around “great ideas” in science that provide a framework for our understanding of the universe (1). In the context of these core ideas, the text integrates knowledge from every science discipline in describing the origin, evolution, and nature of the universe and life within it. A major goal is to enable students to understand the fundamental concepts and principles of nature that are common threads in all the sciences, and to be able to apply those concepts to future applications of science that they may encounter. Table I lists some of the great ideas in science considered in the course, and described below are examples of how the course traces the evolution of our scientific knowledge regarding chemical change and the structure of matter. These are highlighted here because an understanding of the basic principles of matter and energy is the foundation for comprehending the universe and its evolution.

Chemical Change.

Combustion was the first chemical change to be studied intensively. Aristotle, who gave the first non-supernatural explanation, hypothesized that all flammable material contained earth and fire as constituents. In the 18th century, the phlogiston hypothesis extended Aristotle’s idea to other reactions, and the word “fire” was replaced by the more esoteric term “phlogiston” (Greek word for flame). The escape of phlogiston from matter was postulated as the explanation for the loss of mass observed when most substances are burned. The phlogiston hypothesis ran into serious trouble, however, when it was shown that when a metal is heated until it turns to a powder, the powder weighs more than the metal. Proponents of the phlogiston hypothesis were forced to assume that phlogiston could sometimes have negative weight.

Table I. Evolution of Ideas Across the Sciences

<i>Early Ideas</i>	<i>Middle Progress</i>	<i>Developed Theory</i>	<i>Latest Refinements</i>
Solar System Astronomy			
Geocentric model based on religious beliefs, but explains observed phenomena.	Careful observations (Brahe, Kepler) point to Heliocentric Model first suggested by Copernicus. Telescope confirms model.	9 planets eventually discovered. Discovery of Neptune confirms Newton's theory of universal gravitation. Anomaly in orbit of Mercury resists solution with Newton's laws.	Precession of Mercury's orbit is solved by Einstein's Theory of General Relativity. Theory and observations agree. Pluto is demoted to non-planet status (4).
Mechanics: Motion and Force			
Aristotle thought that constant-speed motion requires a force to maintain it. He also believed that heavier bodies fall faster than lighter ones.	Galileo's experiments refuted Aristotle's theory. Newton built on Galileo's work and quantified it.	Newton's laws of motion and universal gravitation hold for most human-sized objects and speeds <10% lightspeed. For fast, atomic- or galaxy-sized objects, Einsteinian mechanics is necessary.	The universal gravitational constant is hypothesized to change as the universe expands. Black holes are the ultimate condensed matter state.
Chemistry: Chemical Bonds			
Phlogiston theory, Alchemy	Oxidation process discovered (Lavoisier); basic chemical reactions known: acid-base, oxidation-reduction, bonding.	Development of novel chemical syntheses created new materials: dyes, fibers, polymers, plastics, etc.	Ceramics, high temperature superconductors, advanced pharmaceuticals.

Structure of matter: Atomic Theory		
Democritus (~530 BC) suggested that there was an ultimate unit of matter (atom – means “uncuttable”)	Dalton-law of definite proportions; Mendeleev-periodic table; J.J. Thomson-discovery of electron showed existence of subatomic particles; Rutherford-nuclear atom.	Relation between elementary particles and fundamental forces sought. Process of reductionism seeks to find a grand unified theory (GUT); superstring theory, M branes are under active research.
Cosmology		
Supernatural creation	Planets, stars, moons identified; Galaxies and red shift discovered in 20 th century.	Dark matter & dark energy; attempts to explain increased rate of expansion of universe.
Earth Science: Geology		
Earth thought to be 6,000 years old (Bible).	Hutton-Earth is old; Lyell-established geology as a science.	Plate tectonics; seismology probes interior structure of earth; Early atmosphere better understood.
Life Sciences: Evolution of the Theory of Evolution		
Great chain of being (Aristotle again)-all living things are immutable as they were created by God.	Buffon-species not fixed; Hutton-there is time for evolution; Lamarck-inheritance of acquired characteristics; Cuvier- fossils	Discovery of the DNA double helix, RNA; the mechanism of inheritance was detailed; gene sequencing & mapping.

However, scientists evolved new ideas to explain the observed weight changes caused by combustion. Antoine Lavoisier conducted a series of experiments that demolished the phlogiston hypothesis. He showed that heating a metal to form a powder requires a substance from the air. By heating a piece of tin floating on a block of wood, and covered by a glass jar, he showed that one-fifth of the air combined with the tin. When Joseph Priestly discovered oxygen, Lavoisier realized that this was the gas that combined with substances upon heating. Not only did this provide a satisfactory explanation for combustion processes, but it also led to a very important idea that governs all chemical changes: the Law of Conservation of Matter. Subsequent scientists would broaden the principle of Conservation of Matter to develop the Law of Conservation of Energy, and Einstein would put forth the remarkable idea that matter could be converted into energy according the equation $E=mc^2$. Extensions of these great ideas regarding matter and energy include the concept that electromagnetic radiation has not only properties of waves (energy), but also properties of particles (matter); and DeBroglie put forth the extraordinary idea that matter has wave properties. Hence, the overthrow of the phlogiston hypothesis was an impressive chapter in the history of ideas. In its day, there was no more respected concept in all of chemistry, but its demise was caused by and led to the development of new great ideas with far-reaching implications.

Structure of Matter.

Another example of the case study approach used in the course involves the evolution of scientific ideas regarding matter. As far as we know, the earliest concept of an atom dates to Democritus of ancient Greece. His philosophical reasoning led him to conclude that there must be a smallest “un-cuttable” (a-tom) piece of any given substance. At the start of the 19th century, no one had any defensible ideas about the structure of matter or how elements combine to make compounds. The theory that answered these questions came from John Dalton. He reasoned that if only certain specific ratios of substances combine, it must be due to fundamental units of matter, the atoms, which combine in that same ratio. Some of his original concepts were modified by subsequent scientists to account for new observations, but his basic idea led to numerous discoveries that provided a better understanding of the nature of matter.

Although most 19th century scientists accepted the principle that the chemical elements consist of atoms, they knew virtually nothing about the atoms themselves. In 1815 Prout proposed that all atoms consist of multiples of hydrogen atoms. This theory ran into difficulty later in the century when atomic masses were found not to be integer multiples of the mass of a hydrogen atom. In 1869 Dmitri Mendeleev conceived the Periodic Table of the Elements that

enabled chemists to predict the properties of then-unknown elements. Discovery of the electron by J.J. Thomson in 1897 led to the realization that all atoms contain electrons. This was the first important insight into the structure of the atom itself. Thomson subsequently proposed his “plum pudding” model of the atom, but that model could neither predict nor explain observed atomic spectra such as the Balmer spectrum of hydrogen. The groundbreaking alpha particle scattering experiment by Ernest Rutherford in 1911 was the prototype of all present day probing of the atom using particle accelerators. This experiment showed that Thomson’s model was incorrect and it led Rutherford to propose his theory of the “nuclear atom”.

However, the nuclear model of the atom also hit a snag because well-established electromagnetic theory predicted that atoms conforming to this model should collapse. The apparent disparity between observation and theory ushered in the scientific revolution called the “quantum theory of the atom”. In 1913 Neils Bohr proposed the quantum model to explain the hydrogen spectrum, and for the first time there was a theory that precisely predicted the wavelengths of all the hydrogen spectral lines. Bohr found it necessary to invoke quantum postulates that broke sharply from classical physics. The atomic electrons could only occupy discrete quantized energy levels, which meant they could only move in certain “allowed” orbits. Wolfgang Pauli used quantum physics to explain the periodicity of the periodic table and the existence of inert elements, and revealed the principle that underlies the building up of the elements in the periodic table. Scientists today have a good grasp of atomic and molecular structure and bonding, and have learned to “evolve” chemicals through synthesis to suit a variety of purposes. But new frontiers beckon as we now seek to understand supramolecular assembly of molecules into layers, cages, helices, and other geometric possibilities. By establishing the rules by which molecules self-assemble both in nature and in the laboratory flask, we can design new molecular architectures, predict the properties of new supramolecular structures, and contribute to the continuing evolution of chemistry and the structure of matter.

Resources

The corresponding laboratory manual for *The Sciences* uses common lab equipment to give students first-hand experience with the scientific process (8). The labs most relevant to the topics taught in Science and the Concept of Evolution are related to prediction and measurement in science, scientific models and modeling, the acceleration due to gravity, the Laws of Thermodynamics, electromagnetic wavelengths and spectra, stellar evolution, heredity and probability, and natural selection.

The *Voyages Through Time* curriculum series provides textual and visual materials for teachers and students to explore concepts of evolution from the beginnings of the universe to the development of modern technology through six modules: Cosmic Evolution, Planetary Evolution, Origin of Life, Evolution of Life, Hominid Evolution, and Evolution of Technology. The curriculum is directed toward the high school level, but it could be modified for use with non-science majors at the college level or for use with middle school students. The accompanying “Student Reader” books for each of the six modules include journal and magazine articles from the current literature. Throughout the curriculum, students consider three major questions: (1) what is changing?, (2) what are the mechanisms for change?, and (3) what is the rate of change? The major goals of the curriculum are for students to understand that:

“Evolution is the result of cumulative changes over time that occur in all realms of the natural world. Various processes underlie these changes in both the physical universe and in living systems. There are differing time scales and rates of change. There are connections and relationships between the physical universe and the life it hosts. Science is a process of advancing our understanding of the natural world, not a set of final answers or beliefs (9).”

Books

- Chalmers, A.F. *What is This Thing Called Science?*; University of Queensland Press: Saint Lucia, Queensland, 1976.
- Edey, M.A.; Johanson, D.C. *BLUEPRINTS: Solving the Mystery of Evolution*; Penguin Books: New York, NY, 1989.
- Green, B. *The Elegant Universe: Superstrings, Hidden Dimensions, and the Quest for the Ultimate Theory*; Vintage Books: New York, NY, 2000.
- Krauskopf, K.B.; Bieser, A. *The Physical Universe*; McGraw-Hill: New York, NY, 1991.
- Livio, M. *The Accelerating Universe: Infinite Expansion, The Cosmological Constant, and the Beauty of the Cosmos*; John Wiley & Sons, Inc.: New York, NY, 2000.
- SETI Institute. *Voyages Through Time*; Six high school curriculum modules. Learning in Motion, Inc.: Santa Cruz, CA, 2005.
- White, F.D. *Science and the Human Spirit*; Wadsworth Publishing Co.: Belmont, CA, 1989.

VHS and DVD

Creation of the Universe, PBS Home Video # 135, 1990

Evolution (Darwin & Natural Selection), Hawkhill Associates, 125 East Gilman St., Madison, WI 53703.

Evolution: Constant Change and Common Threads, Howard Hughes Medical Institute, 400 Jones Bridge Road, Chevy Chase, MD 20815, 2005. URL <http://www.biointeractive.org> (accessed April 15, 2007).

Powers of Ten, The Films of Charles and Ray Eames, Volume 1, Pyramid Film & Video, Santa Monica, CA, 90404, 1989

Voyages Through Time, Six DVD modules. Learning in Motion, Inc.: Santa Cruz, CA, 2005. URL <http://www.voyagesthroughtime.org> (accessed March 17, 2007).

Acknowledgments

This paper was prepared for a presentation given at the 233rd National Meeting of the American Chemical Society (ACS) in March 2007 at the symposium “*Chemical Evolution I: Chemical Change Across Space and Time*”. The symposium was co-organized by Lori Zaikowski and Jon M. Friedrich, and was co-sponsored by the ACS Divisions of Chemical Education (CHED), Geochemistry, and Nuclear Chemistry and Technology. We thank the following for providing financial support for the symposium, attendees, ACS Symposium Series book “*Chemical Change Across Space and Time*”, and DVD production: CHED, Dowling College, Fordham University, The Meteoritical Society, and the National Science Foundation (Award No. 03-35799).

References

1. Trefil, J.; Hazen, R.M. *The Sciences: An Integrated Approach*; John Wiley and Sons, Inc.: Hoboken, NJ, 2007.
2. Glanz, J. Cosmic Motion Revealed. *Science*. **1998**, *282*, 2156-2157.
3. Dressler, A. *Voyage to the Great Attractor: Exploring Intergalactic Space*; A.A. Knopf: New York, NY, 1994.
4. Resolution 6 from the XXVIth General Assembly in Prague: Definition of a Planet in the Solar System, 2006. International Astronomical Union. URL http://www.iau.org/resolution_at_GA-XXVI.340.0.html (accessed March 17, 2007).
5. Miller, S.L. A production of amino acids under possible primitive Earth conditions. *Science*. **1953**, *117*, 528-529.

6. Miller, S.L.; Urey, H.C. Organic compound synthesis on the primitive Earth. *Science*. **1959**, *130*, 245-251.
7. Darwin, C. *The Origin of Species by Means of Natural Selection: Or the Preservation of Favored Races in the Struggle for Life*; AMS Press: New York, NY, 1972.
8. Stanionis, V.A. *Laboratory Manual for The Sciences: An Integrated Approach*; John Wiley and Sons, Inc.: Hoboken, NJ, 1998.
9. SETI Institute. *Voyages Through Time*; Learning in Motion, Inc.: Santa Cruz, CA, 2005.

Chapter 19

Online Tools for Understanding Galactic Chemical Evolution

Allen Parker and Bradley S. Meyer

Department of Physics and Astronomy, Clemson University,
Clemson, SC 29634-0978

Due to element formation in stars, the abundances of the isotopes in our Galaxy have evolved over time. While study of this evolution can be an excellent classroom activity for illustrating principles of chemistry, astronomy, and nuclear physics, it requires a number of complicated ingredients. We are developing some online tools for investigating these inputs and for demonstrating the chemical evolution of the Galaxy. We recommend that persons interested in these tools subscribe visit www.webnucleo.org for more information.

Introduction

Our Galaxy is a collection of gas and stars nearly 13 billion years in age. Throughout its history, gas has condensed into stars. These stars live their lives in stable configurations by burning nuclear fuel which creates new nuclei (*I*). Once the usable nuclear fuel is exhausted, the star dies and expels its outer layers, thereby enriching the gas between the stars in new isotopes. This gas then can form into new stars, and the cycle repeats. One of the new stars that formed in the Galaxy 4.5 billion years ago is our Sun, and the chemical elements and their isotopes in our Solar System are thus the result of billions of years of Galactic history.

This story of how the Galaxy has enriched itself in the abundance of its isotopes over time is known to astronomers as Galactic chemical evolution. Strictly speaking, Galactic chemical evolution is a misnomer since it is not about the evolution of the chemistry of the Galaxy but rather the evolution of the Galactic abundances of the elements and isotopes. Perhaps the proper term would be Galactic Abundance Evolution. Nevertheless, the term galactic chemical evolution has stuck, and we use it here.

As a pedagogical theme, Galactic chemical evolution is an excellent means of introducing students to the chemical elements and their isotopes, Galactic history and astronomy, element formation in stars, and the interstellar medium. The difficulty is that the ingredients for modeling Galactic chemical evolution at any level above the most superficial are numerous and complex. For example, to follow the evolution of oxygen in the Galaxy, one needs the yield of the oxygen isotopes in various generations of stars, the star formation rate, and a model of the evolution of the gas in the Galaxy with time. Moreover, one needs a good appreciation of the concepts underlying these ingredients. Gathering and explaining the necessary ingredients can be daunting, which limits the usefulness of Galactic chemical evolution as an organizing idea in the classroom.

Because of the complexity of the inputs for studying Galactic chemical evolution, we are developing a number of tools that make these ingredients and the underlying concepts more accessible to educators, students, and the general public. These tools are available over the World Wide Web at the URL

<http://www.webnucleo.org>

This is the web site of the Clemson University nuclear astrophysics research group. Each available tool has background material explaining the underlying concepts as well as tutorials demonstrating correct usage of the tool. Underlying code modules are available for download. A mail list allows users to report bugs, request new features, and to receive announcements regarding new tools.

The Available Tools

In this section, we briefly review some of the available tools, their features, and possible pedagogical uses. Other tools not necessarily related to Galactic chemical evolution are also available, and the interested reader is invited to explore them at [webnucleo.org](http://www.webnucleo.org).

Solar Abundances Tool

Webnucleo's Solar Abundances Online Tool allows an internet user to interactively study the abundance of the chemical elements and their isotopes, that is, the Solar Abundance Distribution (SAD). Users can use default by Anders and Grevesse (2) or upload their own. The tool then allows the user to view, sort, and plot the abundances in various ways. Common plots or tables generated show how the abundance, fractional abundance, or mass fractions of the species vary with atomic number or mass number. Figure 1 is a plot of abundance as a function of the species' mass number, A . From a plot like this we can easily see how the abundances fall off for the more massive species.

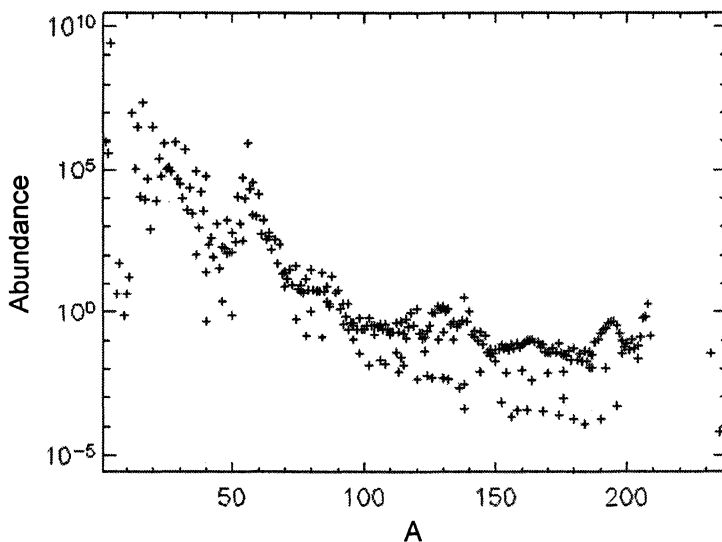


Figure 1. This is a plot of the solar abundance distribution generated by the Solar Abundances Tool. This plot shows the abundance of each species as a function of its mass number, A .

Students can use this tool to explore the variety of elements and isotopes, understand the idea of abundances and mass fractions, compare elemental and isotopic abundances (for example, how much gold is there compared to iron or how much ^{17}O there is compared to ^{16}O), and appreciate the different number of nucleosynthetic processes that have built up the Solar System's supply of isotopes. In a soon to be released update of the tool, users will also be able to convert between the various abundance notations used throughout the scientific literature such as the cosmochemical and logarithmic notations, fractional

abundances, and the mass fractions of the elements. In this way, the language of astrophysicists and chemists can be easily reconciled.

Nuclear Decay Tool

Webnucleo's Nuclear Decay Tool allows an internet user to follow isotopic changes that occur due to α -decay and β -decay. In its current version, the user inputs an initial abundance distribution and a decay interval. The Webnucleo server computes the abundance changes and then emails the user the final results. A soon-to-be-released version of the tool will allow will users to upload their own decay rates.

Students can use this tool to understand radioactive decay, nuclear decay chains, and geological dating via radioactive isotopes (such as the Mg-Al, K-Ar, Rb-Sr, and Pb-Pb systems).

Nuclear Data Tool

Webnucleo's Nuclear Data Tool allows an internet user to explore some of the key properties of nuclei that govern how the species behave in nuclear reactions. These are the atomic number Z , the neutron number N , the mass number A , the mass excess, the ground-state spin, and the nuclear partition function. Students can use the Nuclear Data Tool to explore these quantities and then to study questions such as what reactions among nuclei are energetically possible or even to simply look up needed quantities for their homework.

Galactic Chemical Evolution Machine

Webnucleo's Galactic Chemical Evolution Machine lets users interactively explore the chemical evolution of the Galaxy. With this tool, users may explore in detail the ejecta from a massive star (3) too see how the abundances of the elements are distributed throughout the ejecta. The isotopic yields from a generation of stars can be explored, or one can use these yields to run Galactic chemical evolution models. For example, Figure 2 shows how the isotopes of oxygen change through time as a result of chemical evolution and clearly demonstrates the difference between primary and secondary isotopes. ^{16}O is a primary isotope and increases linearly with time while ^{17}O and ^{18}O are secondary isotopes and vary with the cube of the time. Students can follow the tutorial and the help links in this tool to learn more about this concept and many of the basics of Galactic chemical evolution.

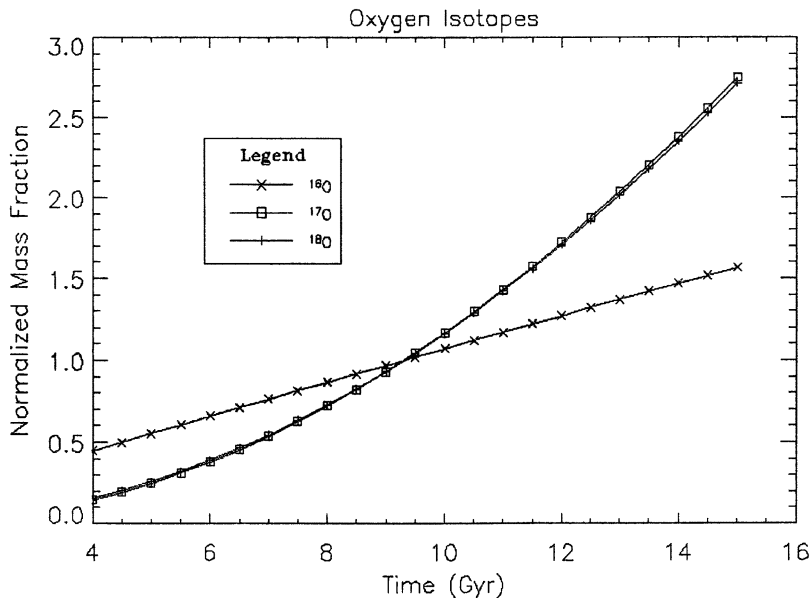


Figure 2. This figure was generated from the Galactic Chemical Evolution Machine. Here we can see how the mass fractions of different isotopes of oxygen vary with time.

Tools Under Development

In addition to the above tools, we are developing other tools related to Galactic chemical evolution. These include a Nuclear Reactions Tool, a Nuclear Network Tool, and a Stellar Ejecta Tool. The Nuclear Reactions Tool will help users calculate nuclear reaction rates and help organize, view, and sort many of the common parameters need for these calculations. The Nuclear Network Tool will provide an easy way to evolve a system of species through time for a given environment's temperature and pressure. The features of the Stellar Ejecta Tool are designed to help a user understand the isotopic anomalies found in primitive meteorites or presolar grains. The Stellar Ejecta Tool will provide an easy way to view the isotopic abundance of a star's ejecta, run a nuclear decay network on this material, and then mix it with a second distribution of isotopic abundances. In this way it can simulate systems such as a late injection of material into the early solar nebula. When these tools are released, we will announce them over the Webnucleo mail list (see below).

The Webnucleo Mail List

Webnucleo.org is a living web site. As we develop, we release new tools or new versions of old tools, and we retire old versions. Our protocol is to announce any such changes via the Webnucleo mail list. This low-volume (typically one to two emails a month) mail list is available to any interested internet user. The mail list is hidden, which means your identity as a subscriber is not available to others.

Subscribing to the Webnucleo mail list is easy. Visit www.webnucleo.org and click on the Mail lists utility link in the upper right corner of the page. Choose the Public List and then enter the fields in the Subscribing to Webnucleo section of the List Info page. You will receive an email requesting confirmation to prevent others from gratuitously subscribing you. Simply reply to this confirmation email. You will now be automatically updated on any new developments at Webnucleo.org.

References

1. Meyer, B. S., this volume.
2. Anders, E.; Grevesse, N. *Geochim. Cosmochim. Acta* **1989**, *53*, 197.
3. Meyer, B. S., Weaver, T. A.; Woosley, S. E. *Meteoritics* **1995**, *30*, 325.

Chapter 20

Spectroscopy and the Cosmos: Applications in the Chemical Sciences

Lori Zaikowski¹, S. Russell Seidel¹, and Jon M. Friedrich^{2,3}

¹Department of Chemistry, Dowling College, Oakdale, NY 11769

²Department of Chemistry, Fordham University, Bronx, NY 10458

³Department of Earth and Planetary Sciences, American Museum of Natural History, New York, NY 10024

Spectroscopy involving the entire range of the electromagnetic spectrum is applied to the study of extraterrestrial phenomena, and laboratory or computer-based analogs can illustrate fundamental principles of chemistry and related spectroscopic methods. Integration of astronomical spectroscopy into courses can facilitate student understanding of fundamental chemical spectroscopic techniques and enable them to see the relevance of these techniques to solving real-world problems related to understanding the solar system and universe. This chapter provides an overview of spectroscopic applications that enable scientists to probe the mysteries of space, suggests implementations of stellar and planetary spectroscopy across the chemistry curriculum, and describes available resources.

Observing the Universe Across the Electromagnetic Spectrum

The electromagnetic spectrum encompasses a nearly incomprehensible range of wavelengths and frequencies from the hundredths of a millimeter gamma ray wavelengths to radiowaves stretching tens of meters in length. With each of these wavelengths, chemical information is carried to the Earth from space: the births and deaths of stars produce x-rays containing information about stellar structure and composition, electronic transitions of elements caught in the Sun's atmosphere reveal their presence and abundance in the visible and ultraviolet (UV) regions, and the steady hum of the cosmic microwave background shows the history and structure of the known universe. As fascinating and complex as these topics and the instruments used to investigate them seem, we can use them to illustrate fundamental chemical principles in the classroom. Coupling these topics with demonstrations or activities involving common chemical instrumentation gives new options for the instructor and may increase the interest level of the learner.

In general, we must split examples of spectroscopy into space- and ground-based observatories or instrumentation. With a few exceptions, the Earth's atmosphere allows only visible and radiowaves to pass; blocking gamma rays, x-rays, UV, and infrared radiation from the Earth's surface. In astronomy, these are known as the Earth's optical and radio windows. Earth-orbiting space observatories are necessary to view the universe in the wavelengths blocked by our atmosphere. It should be remembered that much of the scientific data returned by space observatories is not obtained as photographic images, but with a variety of spectrometers that gather information across the electromagnetic spectrum from gamma rays to radio waves.

Gamma rays, electromagnetic radiation with wavelengths of 5×10^{-13} to 1.4×10^{-10} m, are most often measured in units of keV to MeV in astronomical and nuclear research settings. By comparison, visible light has an energy of only about 1eV. Gamma rays are produced by radioactive decay and through some of the most energetic phenomena in the universe: supernova, neutron stars, pulsars, and black holes. Gamma ray bursts are also intriguing phenomena, but the implications are primarily astrophysical and not chemical in nature. Gamma-ray capable observatories currently in orbit include the High Energy Transient Explorer (HETE-2), the International Gamma-Ray Astrophysics Laboratory (INTEGRAL) of the European Space Agency, and the Swift unmanned orbiting spacecraft managed by NASA. An example of the retrieval of chemical data from gamma ray observatories occurred with the verification of the presence of ^{44}Ti (half life of 67 years) in the remains of a supernova (*1*). This discovery helped to verify astrophysical theories of element-building nuclear processes and theories of supernova structure. Most gamma ray observatories are also capable of detecting photons into the x-ray portion of the electromagnetic spectrum.

X-rays also generally have energies measured in units of keV for astronomical and elemental analyses, and occupy wavelengths between 5×10^{-13} and 1×10^{-8} m. Orbiting x-ray observatories include the Chandra X-ray Observatory, the XMM-Newton, and the recently launched Suzaku (Astro-E2) observatory. X-rays are produced by the intense gravitational interaction of gas falling into such objects as neutron stars and black holes. Another source of x-rays are supernova remnants.

Ultraviolet (UV; wavelengths between ~ 10 nm and 400 nm) and visible light (400 - 700 nm) are often detected together on space observatories because the optics necessary for directing the light are similar, although dedicated UV space observatories also exist. Examples of UV observations include the physical (structure, temperature) and chemical analysis of the interstellar medium. The Far Ultraviolet Spectroscopic Explorer (FUSE) is an example of a dedicated UV space observatory. The best known example of an Earth-orbiting observatory operating in the UV-visible region is the Hubble Space Telescope (HST). Both FUSE and HST contain spectrographs that separate light into its component wavelengths. Since visible light passes through the Earth's atmosphere, Earth-based visible telescopes and spectrometers can be used to identify the composition of the light sources and physical (e.g. velocity) properties of light sources from Doppler shifting of known spectral lines. Most Earth-based telescopes can operate modestly into the UV and IR regions within the aforementioned optical window limitations.

In astrophysical contexts, infrared (IR) electromagnetic radiation is generally referred to in units of μm for astronomical observations. NASA's Spitzer Space Telescope is currently the premier space telescope observing in the infrared. IR astronomy often observes the emissions from dust grains that have absorbed visible light and re-radiated it in the IR region of the spectrum. It also detects the universe's farthest objects whose visible frequencies are red-shifted due to the Doppler Effect and therefore appear in the IR region in our neighborhood of the universe. Brown dwarfs, stellar objects with masses in between planets and stars, and disks of material and possible planets around other stars can also be observed in the IR (2). Observatories capable of operating in the IR use instrumentation very similar to that found in chemical laboratories.

Microwaves occupy wavelengths easily measured in mm to cm lengths. The Submillimeter Wave Astronomy Satellite (SWAS) examined the composition of interstellar clouds by examining water, oxygen, carbon, and carbon monoxide. Following the success of the Cosmic Background Explorer (COBE), the Wilkinson Microwave Anisotropy Probe (WMAP) continues to map the heat (fluctuations) remaining from the Big Bang and relating to the structure of the universe. We should note that although similar in principle, electromagnetic radiation in the microwave region requires detectors very different from those

used in more common laboratory equipment. Microwaves can also be used to examine molecular species in interstellar space from their rotational spectra.

Radiowaves occupy the cm to km wavelengths of the electromagnetic spectrum, and are generally referred to in terms of frequency (MHz and kHz). Exotic radio sources such as radio galaxies, pulsars, and quasars show the diversity of interstellar objects, and radio astronomy has been used to examine galactic rotation (3). Like visible light, radiowaves can be observed from Earth since the portion from ~10 cm to 10 m passes through Earth's atmosphere. Like microwaves, instrumentation for radio astronomy is mostly foreign to the chemical laboratory. However, interferometry, a concept encountered in undergraduate instrumental analysis, can be illustrated with examples of radio astronomy. There are numerous radiotelescopes around the world, with the Arecibo radio telescope and the Very Large Array (VLA) being the best known.

Atomic Emission Spectroscopy (Line Spectra)

One type of spectroscopy that finds use in the field of astrochemistry is atomic emission spectroscopy. This kind of spectroscopy results from an atom of an element (e.g. hydrogen, mercury, etc.) releasing a photon as one of its electrons falls from an excited state, or higher energy level, to either a lower energy excited state or to the ground state. The photon released corresponds to the energy difference between the energy levels and is sometimes, though certainly not always, a quantum of visible light. For the hydrogen atom four visible lines appear, all of which are in the Balmer series, in which the electron transitions from a higher energy level to the second energy level. Line spectra are distinct to their elements and can thus serve as a means of determining which elements are present in a given sample. In essence, they provide a fingerprint of the element (4, 5). It is this last fact that has found much use in the field of astrochemistry, where significant insights into the elemental composition of various astronomical bodies have been made. For instance, such spectra are of particular relevance to interstellar gas clouds that are close to a star. In such clouds, atoms of the elements are put into excited states by the heat from the star and, as they relax, emit their element-specific line spectra. These spectra can then be observed, recorded, and studied via a spectrograph on a terrestrial telescope (6).

Line spectra for multi-electron atoms are more complex than the hydrogen line spectrum, and thus are less easily explained in an explicit fashion at a middle school, high school, or even first year undergraduate level. However, discussions of this topic with respect to the hydrogen atom allow for the instructor to point out many important features of rudimentary quantum mechanics. Among these are the quantized nature of the electrons in atoms, the Bohr model of one-electron atoms, the dual wave-particle nature of light, the

notion of a quantum leap, and the use of Planck's constant in converting wavelength and frequency into photon energy (4, 5). Moreover, these discussions serve as a springboard into topics such as quantum numbers and atomic orbitals, which are later key to understanding chemical bonding.

At a higher level, such as a Physical or Quantum Chemistry course, a similar discussion can be utilized in a brief background sense. Additionally the relevance of line spectra can be put into context with discussions on the topic of one-electron solutions to the Schrodinger equation, as well as more advanced forays into the electronic structure of multi-electron systems.

In terms of a laboratory and / or in-class demonstration setting, the emission spectra of gas tubes with hydrogen, sodium, neon, or mercury may be viewed with inexpensive diffraction gratings to illustrate identification of elements. A demonstration with flame tests of salts can further illustrate the basis of Bohr's atomic theory. Additionally, flame tests are often employed as a part of qualitative inorganic laboratory procedures for the determination of various cations. Such lab activities or demonstrations are appropriate for middle school, high school, and undergraduate chemistry courses.

UV-visible Spectroscopy

Another form of spectroscopy that is common to both astronomy and undergraduate chemistry curricula is that of Ultraviolet-visible absorption spectroscopy (UV-vis.) This type of spectroscopy, much like atomic emission spectroscopy, is based upon electrons transitioning between energy levels in either atoms or molecules. In the case of atoms, it is simply the opposite situation as that of atomic emission spectroscopy. Instead of a photon of energy corresponding to the energy gap between levels being emitted, it is absorbed. This absorption of energy causes the electron to "jump" from a lower to a higher energy level. This results in a subsequent decrease in the intensity of electromagnetic radiation at the frequency of the jump and an absorption line appears in the atom's spectrum. This is the source of "dark-line" absorptions in the field of astronomy, as seen in the spectra of a variety of cosmic phenomena, particularly those of stars (6). Such spectra can be used to elucidate the composition of the lower density outer layers of stars, whose components absorb various lines out of the radiation emitted by the more dense, hotter inner parts of the star. The strengths and identities of the absorption lines can be used as a means of classifying stars according to their temperatures. This is primarily due to the temperature-dependence of absorption efficiency for the various components of the star. Moreover, the spectroscopically-determined metal content of a star is often used as an indicator of the star's age, with a greater metal content generally signifying a younger star (6).

When one applies UV-vis spectroscopy to molecules, a situation similar to that observed for atoms occurs. In the case of molecules, however, the

transitions that are involved are between molecular orbitals. For organic compounds, which are of import to UV-vis applications in astronomical studies, the transitions are generally of an n to π^* or a π to π^* nature. Transitions involving σ and σ^* molecular orbitals are generally out of the readily accessible spectral region of 200 nm to 700 nm for such spectroscopy (7). Sigma (σ) molecular orbitals are those that result from a mathematical combination of atomic orbitals on bonded atoms in which the overlap occurs in a head-to-head manner, whereas pi (π) molecular orbitals are similar but instead result from overlap of a side-to-side fashion (4, 5). Nonbonding (n) molecular orbitals are those that do not partake significantly in bonding. In astronomical studies, the UV spectra of various cosmic entities can be compared to the UV spectra of known organic compounds to determine if the presence of the organic compound is probable (8). Moreover, molecular absorption bands can lead to insights into the composition of such astronomical bodies as stars in a manner similar to that delineated above for atomic absorption lines (6).

In chemistry, UV-vis spectroscopy is also important to transition metal complexes. Once again, a photon is absorbed that corresponds to the energy gap between molecular energy levels, and an electron “jumps” from a lower to a higher level. This model can often be explained both in terms of a simple point-charge model, known as crystal (or ligand) field theory, or a more sophisticated molecular orbital treatment. The latter is a more complex methodology and thus can explain not only the same phenomena as crystal field theory but also other possible transitions, such as both metal-to-ligand and ligand-to-metal charge transfer bands (9).

UV-vis spectroscopy for atoms (“dark line” spectra) can be used in a chemistry classroom to complement the presentation of atomic emission spectra, as discussed previously. As the former is based upon photon absorption and the latter is based upon photon emission, presenting both can be utilized as a tool to show the distinction between the two opposite phenomena, while also elucidating the notion of quantized energy in atomic species (6). Such discussions can be employed in the same context as those delineated above under atomic emission spectroscopy.

Molecular UV-vis spectroscopy is prevalent in the more advanced chemistry curriculum for undergraduates. It appears in Organic Chemistry in the analysis of organic compounds, and it can also be applied to Physical (or Quantum) Chemistry courses in discussions of molecular orbitals, electronic transitions between these orbitals, and also transition selection rules and microstates. It is also relevant to Inorganic Chemistry, as it is investigated in terms of transition metal complex color, crystal field theory, and molecular orbital diagrams and electronic transitions for a variety of inorganic compounds.

In a laboratory setting, students at all undergraduate levels can be exposed to the principles and practices of UV-vis (or at the very least, visible) spectroscopy. Often employed in first year labs are Spectronic-20 instruments. These can be utilized to demonstrate the notions of absorbance, transmittance,

wavelength, and the color wheel. Moreover, these instruments can be used to demonstrate Beer's Law and the construction of calibration curves for the determination of unknowns (7). In Instrumental Analysis, Analytical Chemistry, and Environmental Chemistry courses, multiple laboratories utilizing more sophisticated UV-vis spectrophotometers abound, including those of a Beer's Law and calibration curve nature. In Inorganic Chemistry courses, UV-vis spectrophotometers can also play a substantial role, with investigations into crystal field theory and molecular orbital theory of inorganic compounds being possible (10).

Infrared Spectroscopy

The infrared (IR) region of the electromagnetic spectrum is generally divided into the near- (~ 1 to $5\mu\text{m}$), mid- (5 to $\sim 30\mu\text{m}$) and far- (~ 30 to $\sim 300\mu\text{m}$) infrared. For reference, typical Fourier Transform IR (FTIR) spectrometers in an undergraduate organic chemistry laboratory operate in wavelengths between about 2 and 16 μm . Near-infrared can pass through the Earth's atmosphere, and the observations and instrumentation involved resembles that used by UV-vis telescopes. As we move from the near-IR to the mid-IR, stars become less visible while dust and gas becomes more visible. This allows astronomers to examine structures and compositions of dust surrounding planetary nebulae, and both young and old stars. This is because light from a forming star is absorbed by the surrounding disk (or planet) and re-emitted in the IR frequencies. Moving further into the far IR, stars emit extremely little light, allowing astronomers to focus their examinations on gas and dust cloud structure.

The energies in the IR regions are not as high as those in the UV or visible regions and electronic transitions are not produced from interaction of molecules with IR radiation. Instead, IR spectroscopy can detect small energy differences between the quantized molecular vibrational and rotational states of molecules with a dipole moment. IR radiation in astronomy primarily focuses on the identification of molecular species and observing structures of small particles (dust) and molecules (gas) in various astronomical settings. However, some IR sources include objects with extremely red-shifted electronic transition spectra. The principles involved in the production of these lines can be seen in the preceding sections. In these cases, IR spectroscopy is used to peer into the oldest portions of the universe where sources are traveling quickly away from our own galaxy.

Rotational and vibrational/rotational transitions are the physical properties measurable in the IR. Vibrations can be divided into the classes of stretching and bending. Stretching vibrations can be approximated with the idea of harmonic motion: i.e. a mass attached to a spring. The frequency of a given vibration is determined by the strengths of the bonds involved and the mass of the component atoms, and this approximation holds for the next type of

molecular vibration: bending. Bending-type vibrations include motions best described as scissoring, rocking, and wagging. Far-IR spectra typically represent molecular rotational levels. In the gas phase, such as in the interstellar medium, absorptions by molecules are discrete lines, but when in the solid phase where rotational states are restricted, the lines are broadened into a continuum. The discrete lines of molecules in the gas phase can be used for the identification of molecules, but most often are joined with information from the rotational/vibrational coupling of a molecule. In molecules there are several rotational levels for every vibrational state, so IR spectra are usually a series of closely spaced lines. These combined spectra are most useful for the identification of unknown molecules in space.

Educational Resources

Presented below and summarized in Table I are suggestions and resources for integrating the above topics of cosmic evolution, multiwavelength spectroscopy, atomic line spectra, UV-visible, and IR spectroscopy into specific chemistry courses.

Stellar Evolution

1. The book *Stars and their Spectra* (6) details stellar evolution and classification. The book and the author's website contains a wealth of information that can be utilized to incorporate astrochemical spectroscopy into the chemistry curriculum at all levels. The information is presented in a distinctly logical progression and includes both the basics as well as many detailed descriptions of various spectroscopic phenomena found in extraterrestrial settings. The material is easy to understand, yet still substantive enough to make this a very valuable resource. Among the items discussed are the electromagnetic spectrum; the history of telescopic spectrographs and how astronomical spectra are recorded; and a description of astronomical atoms, ions, molecules, and isotopes. Included are discussions of how one can determine a star's temperature from its electromagnetic spectrum, an explanation of the origin and value of atomic absorption lines from stars, a similar explanation of the origin and value of atomic emission lines from interstellar gas clouds, and a general comparison of atomic absorption and emission lines. It delves into how stars are characterized based on the strengths and identities of their absorption lines and bands. It also describes how the metal content of stars is determined by spectroscopy and is an indicator of the age of a given star.

2. Project CLEA (Contemporary Laboratory Experiments in Astronomy) of Gettysburg College in Pennsylvania has produced a module “Dying Stars and the Birth of the Elements” that is suitable for use at the high school to university level (11). In this computer-based exercise, topics such as x-ray spectral analysis and nucleosynthesis are covered as students direct their own x-ray observatory to examine supernova remnants.
3. The XMM-Newton Education and Public Outreach internet resource is another place educators can obtain materials about nucleosynthesis and related x-ray spectroscopy (12).

Multiwavelength Spectroscopy

Nearly all robotic explorers orbiting the sun or on far off trajectories to other planets use a variety of spectrometers. Individual NASA missions each have readily accessible education pages associated with them and advanced technical descriptions of instruments are generally available for download. Future potential resources can be found by beginning at www.nasa.gov and selecting the Education hyperlink. Some current resources to consider include:

1. *Cool Cosmos*, the Education and Public Outreach section of the Spitzer Space Telescope mission has a section on Multiwavelength Astronomy, where appropriate links are collected and updated. There are activities for students of all levels, K-12 and undergraduates (13).
2. To support its public outreach and education mission, NASA maintains the online *Space Science Education Resource Directory* to provide assistance in locating resources for topics relevant to teaching goals (14).
3. The NASA publication “*Space Based Astronomy: An Educator Guide with Activities for Science, Mathematics, and Technology Education*” is a good general introduction and has activities appropriate for students from grade school to high school (15).
4. For more advanced studies, such as undergraduate research projects, ambitious students may wish to use NASA’s *Planetary Data System* to use actual returned data to conduct independent research or class projects (16).
5. An overview of the electromagnetic spectrum is available at a website developed by Dr. Bill Blair at Johns Hopkins University with the aid of a seed grant from Johns Hopkins University’s Maryland Space Grant Consortium (17). It focuses on the basics of the electromagnetic spectrum, spectroscopy, and specific equipment utilized in astrochemical investigations. It is presented at a level conducive to middle and high school education. There are a variety of links to observatories, satellites, and telescopes prominent in astrochemical studies.

**Table I. Astrochemistry Across the Chemistry Curriculum
Using Spectroscopy**

<i>Topic</i>	<i>Principles Illustrated</i>	<i>Level</i>	<i>Courses</i>	<i>Equipment and resources</i>
Multiwavelength astronomy (12,14,18-21)	x-rays, gamma rays, UV, visible, IR, radio waves	MS HS UGN UGS	GC, IA	Electromagnetic spectrum (11,12,14,15,16,22)
Line spectra (6,20-24)	Atomic theory, ID of elements, absorption vs. emission spectra	HS UGN UGS	GC, PC	Diffraction gratings or hand-held spectrometer, gas tubes, power source (23,25)
Ultraviolet-visible (6)	Chemical composition, temperature, density	MS HS UGN UGS	GC, IO, PC	UV-vis spectrometer (13,25)
Infrared (2,13,21-24,26-29)	ID of molecules, bonding, AIB	UGS	OC, IA, AC	IR spectrometer (13,26)

Abbreviations used: MS is middle school, HS is high school, UGN is undergraduate non-science major, UGS is undergraduate science major, AIB is Aromatic Infrared Bands. GC is General Chemistry, OC is Organic Chemistry, PC is Physical Chemistry, IO is Inorganic Chemistry, IA is Instrumental Analysis, AC is Analytical Chemistry.

UV/visible and Line Spectra

Here we present a few resources available for educators who want to incorporate UV/visible concepts and themes into chemistry courses:

1. An article by Smith et al. (18) describes a “chemical detective” activity appropriate for middle to high school students, where students identify elements from line spectra.
2. An online resource on this topic is available at (30). This webpage was developed by Aeree Chung and Ben Johnson at Columbia University in conjunction with their astronomy lab. The pages give an overview of the electromagnetic spectrum, and outline applications of spectroscopy to astronomical studies. Included are pictorial representations of astronomical observations with brief descriptions, and information on observational instrumentation. Also discussed are the distinctions between continuum,

emission (“line”), and absorption (“dark line”) spectra. This resource is applicable to the middle school through undergraduate level student and teacher.

3. With Science Teaching through Astronomical Roots (STAR) Spectrometers, students can observe line spectra and learn about diffraction gratings. STAR Spectrometers are high-quality, inexpensive visible light spectrometers available from Learning Technologies, Inc. They also have ready-made curricular materials available (25).
4. For an introduction to the UV, students can easily recreate the experiment that yielded initial evidence for the existence of UV radiation. The original experiment was performed by Johann Ritter in 1801 and used silver chloride, but the recreation outlined in (13) can be done using nonhazardous reagents, a prism, and common household items. This exercise is primarily for students of middle school age, but addresses National Science Standards from grades K-12 with appropriate classroom tutorials.

Infrared Resources

There are several resources available for educators who want to incorporate IR ideas and themes into chemistry courses.

1. *Active Astronomy: Classroom Activities for Learning About Infrared Light* consists of five modules where students of middle school to high school levels participate in hands-on experiments to learn about the properties and uses of IR radiation. In addition to worksheets, tests and teacher answer keys, the self-contained modules have compiled parts lists with vendors for the experiments that require easy-to-construct experimental set-ups. The modules can be downloaded from the Educational Materials section (21) and are consistent with national educational standards.
2. The Education and Public Outreach section of the Spitzer Space Telescope mission is known as *Cool Cosmos* (13). It has a wealth of information and links for teachers including details on reproducing how Sir Frederick William Herschel discovered IR radiation, now known as The Herschel Experiment. This is an experiment for younger students, perhaps up to middle school.
3. The Astrochemistry Laboratory at NASA’s Ames Research Center (27) maintains a website containing relevant background information for instructors and details on the information spectroscopy provides about organic molecules in space.
4. There are several books reviewing IR spectroscopy for the instructor’s background information. Mampaso *et al.* have compiled an advanced and up-to-date review appropriately called *Infrared Astronomy* (28). The

information is at a beginning graduate school level, so instructors with any science background can review topics before bringing the topics to the classroom.

The information and examples provided here are meant to give a brief introduction to current topics that allow us to relate spectroscopy in the universe to the chemical sciences. Spectroscopy plays a fundamental role in the identification of elements and molecules and interpreting astrophysical processes. It also provides a basis for teaching theoretical aspects of chemistry that may serve to inspire and engage students at many different educational levels.

Acknowledgments

The authors would like to thank Dr. Lucy M. Ziurys for helpful comments.

References

1. Iyudin, A. F.; Diehl, R.; Bloemen, H.; Hermsen, W.; Lichti, G. G.; Morris, D.; Ryan, J.; Schoenfelder, V.; Steinle, H.; Varendorff, M.; de Vries, C.; Winkler, C. *Astro. Astrophys.* **1994**, *284*, L1-L4.
2. Reid N. and Hawley S.L. *New Light on Dark Stars: Red Dwarfs, Low-Mass Stars, Brown Stars*. 2nd edition. Springer Verlag: Berlin, 2005.
3. Sofue, Y.; V. C. Rubin *Ann. Rev. Astro. Astrophys.* **2001**, *39*, 137-174.
4. Chang, R. *General Chemistry: The Essential Concepts, 4th Ed.*; McGraw Hill: New York, 2006.
5. Hill, J. W.; Petrucci, R. H.; McCreary, T. W.; Perry, S. S. *General Chemistry, 4th Ed.*; Pearson Prentice Hall: New Jersey, 2005.
6. Kaler J.B. *Stars and their Spectra*; Cambridge University Press: Cambridge, UK, 1997.
URL <http://www.astro.uiuc.edu/~kaler/sow/spectra.html>
7. Skoog, D. A.; Holler, F. J.; Nieman, T. A. *Principles of Instrumental Analysis, 5th Ed.*; Thomson Learning, Inc.: United States, 1998.
8. Egan, W. G.; Hilgeman, T. *Nature* **1978**, *273*, 369-370 and references therein.
9. Huheey, J. E.; Keiter, E. A.; Keiter, R. L. *Inorganic Chemistry: Principles of Structure and Reactivity, 4th Ed.*; HarperCollins College Publishers: New York, 1993.
10. Szafran, Z.; Pike, R. M.; Singh, M. M. *Microscale Inorganic Chemistry: A Comprehensive Laboratory Experience*; John Wiley & Sons: New York, 1991.

11. *Contemporary Laboratory Experiences in Astronomy (Project CLEA)*, Department of Physics, Gettysburg College, Gettysburg, PA. URL <http://public.gettysburg.edu/~marschal/clea>
12. *XMM-Newton Education and Public Outreach*, NASA and European Space Agency (ESA), URL <http://xmm.sonoma.edu>
13. *Cool Cosmos*, Education and Public Outreach, Spitzer Space Telescope, NASA, URL <http://www.spitzer.caltech.edu>
14. *Space Science Education Resource Directory*, NASA, URL <http://www.teachspacescience.org>
15. *Space Based Astronomy: An Educator Guide with Activities for Science, Mathematics, and Technology Education*. NASA publication # EG-2001-01-122-HQ.
16. *Planetary Data System*, NASA, URL <http://pds.nasa.gov>
17. Blair, W. P. *Learning from Light Educational Home Page*, URL http://violet.pha.jhu.edu/~wpb/spectroscopy/spec_home.html
18. Smith, D.; Eisenhamer, B.; DeVore, E.; Bianchi, L. *The Science Teacher* **2003**, *70*, 47-51.
19. *Haystack Observatory Education and Outreach*, Massachusetts Institute of Technology (MIT), URL <http://www.haystack.edu>
20. Trefil, J.; Hazen, R.M. *The Sciences: An Integrated Approach*, 5th edition. John Wiley and Sons, Inc.: Hoboken, NJ, 2007; pp 157-176.
21. *Multiwavelength Astronomy*, Infrared Processing and Analysis Center, California Institute of Technology, URL <http://www.ipac.caltech.edu> and URL http://www.ipac.caltech.edu/Outreach/Edu/Spectra/irspectra_index.html
22. *The Electromagnetic Spectrum*, Interactive Multimedia Adventures for Grade School Education Using Remote Sensing (IMAGERS), Goddard Space Flight Center, NASA, URL <http://imagers.gsfc.nasa.gov/ems>
23. Stanionis, V.A. *Laboratory Manual for The Sciences: An Integrated Approach*, 2nd edition. John Wiley and Sons, Inc.: Hoboken, NJ, 1998; pp 123-138.
24. *University of Arizona Alumni Association Astronomy Camp*, URL <http://www.astronomycamp.org/facilities.html>
25. Project STAR Spectrometers. Learning Technologies, Inc. (Somerville, Massachusetts) cardboard (\$9.00) and plastic (\$25.00).
26. *Active Astronomy: Classroom Activities for Learning About Infrared Light*, SOFIA Education and Public Outreach, URL <http://www.sofia.usra.edu>
27. Astrochemistry Laboratory, Ames Research Center, NASA, URL <http://www.astrochem.org>
28. Mampaso A., Prieto M., and Sanchez F. *Infrared Astronomy*. Cambridge University Press: Cambridge, UK, 2003.

29. *Infrared Space Observatory Education and Public Outreach*, European Space Agency (ESA), URL <http://www.iso.vilspa.esa.es> and URL <http://sci.esa.int>
30. Chung, A.; Johnson B. D. *Columbia University Astronomy Tutorial*, URL http://www.astro.columbia.edu/~archung/labs/fall2001/lec04_fall01.html

Chapter 21

Development of Laboratories for Teaching Chemical Principles Using Radio Astronomy

DeWayne T. Halfen^{1,2}, Aldo J. Apponi¹, and Lucy M. Ziurys¹

¹Departments of Chemistry and Astronomy, Arizona Radio Observatory, Steward Observatory, University of Arizona, Tucson, AZ 85721

²NSF Astronomy and Astrophysics Postdoctoral Fellow

Experimental exercises have been developed for undergraduate and graduate chemistry, astronomy, biology, and biochemistry students to teach basic principles in physical chemistry using the interstellar medium as the laboratory. Employing a radio telescope, in this case the Arizona Radio Observatory (ARO) 12m antenna, the physical and chemical properties of interstellar gas are investigated by measuring spectra of molecules such as HCO^+ , HCN, HC_3N , CH_3CN , and SiO in astronomical sources. For example, laboratory exercises have been created for graduate students with life sciences backgrounds that investigate the nature of organic chemistry in interstellar clouds. Additional laboratories are being developed to teach astronomy graduate and undergraduate students about practical aspects of molecular astrophysics and spectroscopy. Basic chemical principles are thus illustrated through an interesting, non-traditional approach.

Introduction

New techniques to illustrate basic chemical principles are valuable tools for the chemistry teacher, regardless of the level of instruction. The use of laboratory exercises exposes students to direct applications of these principles. Because chemistry encompasses a wide variety of fields, the traditional “bench experiments” approach is no longer the only avenue by which to introduce new concepts. Furthermore, the perpetuation of “traditional” labs can make the subject uninteresting

Here we describe a novel approach to the teaching of basic concepts of physical chemistry that falls under the category of chemical evolution. Laboratory exercises have been developed for undergraduate and graduate students that illustrate principles of gas-phase spectroscopy and kinetics using interstellar space as the “laboratory”. Observations at radio telescopes are used to measure high resolution spectra of molecules in a variety of astronomical objects. Not only can principles of spectroscopy be illustrated from these data, but concepts of detailed balance in quantum states, kinetic theory of gases, local thermodynamic equilibrium (LTE), and ion-molecule chemistry can also be taught.

In one laboratory exercise, students use a radio telescope to measure the emission spectra of selected molecules in astronomical sources, such as dense clouds and old stars. Molecular hyperfine structure, classical spectral patterns of linear and symmetric top species, and maser action are investigated. Another laboratory exercise was developed where students measure the rotational spectra of HCO^+ , HCCCN , and CH_3CN in the laboratory, and determine their unique spectroscopic properties. They then use their measurements to identify these molecules in interstellar gas.

Radio Telescopes as Instruments of Chemical Education

Modern teaching laboratories in physical chemistry often use nuclear magnetic resonance (NMR), Fourier transform infrared instruments (FTIR), or ultraviolet-visible light spectrometers to illustrate scientific concepts and methods. Radio telescopes can also be employed in the same manner. However, instead of shining a form of light through a sample in a laboratory, these instruments collect radio waves emitted from gas clouds thousands of light years away. The experiments conducted with a radio telescope involve collecting radiation with optics and detectors, processing the information received through a spectrometer, and analyzing it with a computer interface, similar to any lab system. This information is then analyzed to assess the molecular content and concentrations, as in NMR and mass spectrometry.

Radio telescopes, however, are more complicated than the usual laboratory instrument. Furthermore, the signals of interest are far weaker than those in a laboratory setting by many orders of magnitude, on the order of 10^{-19} Watts/m². Therefore, the sensitivity and stability of the detectors on these telescopes must exceed that of normal laboratory instrumentation. The detection process consequently requires electronics that need to be fine-tuned to function at optimal performance.

Detection of radiation at radio telescopes is done using superconducting mixers, which are kept at 4.2 K with a closed-cycle helium refrigerator. Radiation from the sky, ν_{sky} , is combined inside the mixer with a source of radiation at the telescope called the local oscillator (or ν_{LO}). This technique, called “heterodyne mixing” is needed because signals from space cannot be

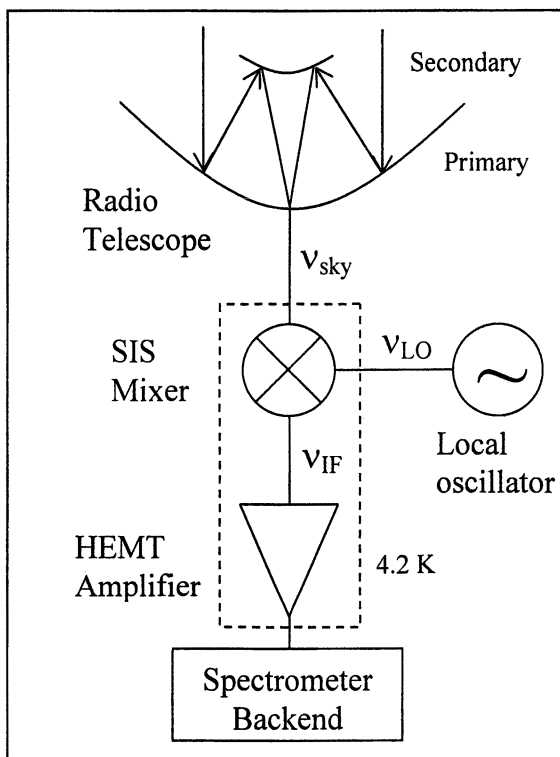


Figure 1. Schematic of the detection system at a radio telescope using an SIS (superconducting-insulating-superconducting) mixer and a HEMT (high electron mobility transistor) amplifier. Here ν_{sky} is the sky frequency, ν_{LO} is the local oscillator frequency, and ν_{IF} is the intermediate frequency.

directly amplified due to a lack of low noise electronics; instead they are transformed to a lower frequency where they can be suitably amplified. The resulting signal, called the intermediate frequency or ν_{IF} , where $\nu_{IF} = \nu_{sky} - \nu_{LO}$, is sent to a spectrometer backend where the data is separated as a function of frequency and stored in a computer. This process is illustrated graphically in Figure 1. Depending on the spectrometer backend, the spectral resolution can range from 30 kHz to 2 MHz and the bandwidth from 4 to 500 MHz. The data is displayed as a spectrum (i.e. signal as a function of frequency) with the intensity axis labeled in units of K, an artifact of early radio astronomy, where the signals were referenced to liquid nitrogen at 77 K. Signal averaging is done with specific data reduction programs that are available at the telescope, such as Unipops or Class, which can also be used to take out baselines and determine the spectral parameters such as line width and intensity.

On the practical side, most modern radio telescopes are under computer control. Tracking of an individual source is done by computer command. The data collected is automatically transferred and stored on computer disks, and the interface between the observer and the telescope is a menu driven system.

The telescope used in the laboratory exercises is the Arizona Radio Observatory 12m telescope on Kitt Peak, Arizona, see Plate 1. This instrument is a single dish radio telescope with a 12m diameter antenna. Because of its large diameter, the telescope can be used to study specific sources in the sky. The solid angle subtended by the telescope, or the beam size θ , is related to the wavelength λ being observed by the relationship, $\theta = 1.2\lambda/D$, where D is the diameter of the antenna. The facility operates at wavelengths of 2 and 3 mm or from 65 to 180 GHz in frequency, and can be run 24 hours a day for 9 months of the year. Sky conditions can limit the use of the telescope, with clouds adding noise and rain, snow, or strong winds halting operations. Observers are allocated telescope time, similar to NMR use. However, due to high demand, a committee reviews the observing proposals for merit, with an emphasis on educational programs. The telescope can be used either on-site or remotely through the Internet, allowing observers from around the world to perform measurements. For the remote observing, users employ the same computer interface used at the telescope.

A General Laboratory on Molecular Astrophysics

During this laboratory exercise, graduate students in astrochemistry and astronomy conducted several experiments involving observations using the 12m telescope. Different molecules were chosen to illustrate various concepts. The first exercise concerned HCCCN, cyanoacetylene. This molecule, a widespread interstellar species, has a simple spectrum with only one line per rotational

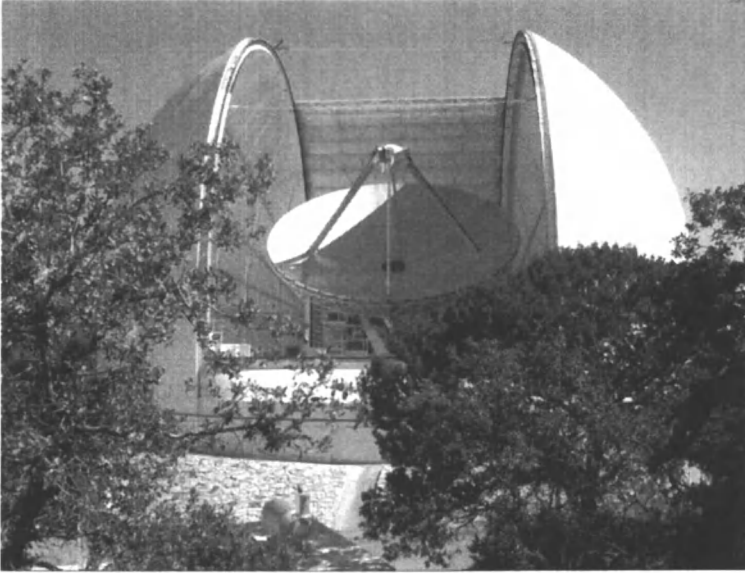


Plate 1. The Arizona Radio Observatory (ARO) 12m telescope on Kitt Peak, Arizona was used for the laboratories. (See page 18 of color inserts.)

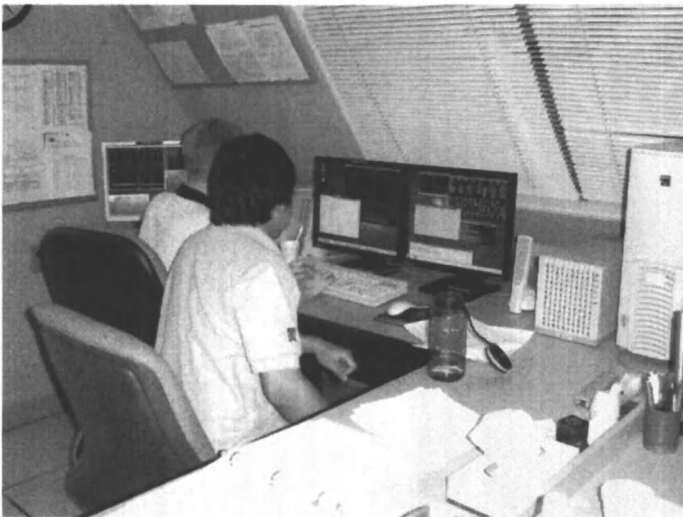


Plate 2. Astronomy graduate students Marc-André Besel and Wiphu Rujopakarn observing at the ARO 12m telescope. Telescope operation and data processing are all conducted via computer interface. (See page 18 of color inserts.)

transition. Hence, the rotational spectrum can be accurately described by two spectroscopic constants B and D , see equation 1.

$$\nu = 2B(J + 1) - 4D(J + 1)^3 \quad (1)$$

Here ν is the transition frequency, B is the rotational constant, D is the centrifugal distortion parameter, and J is the rotational quantum number. Students were first asked to calculate the frequencies of HCCCN based on these constants and equation 1. Three rotational transitions were chosen by the students to be measured at the telescope in the range of 72 to 163 GHz prior to the observations. This task allowed the students to actively participate in planning the observations. These frequencies were then used at the telescope to detect HCCCN towards a dense cloud, W51M, located approximately 23,000

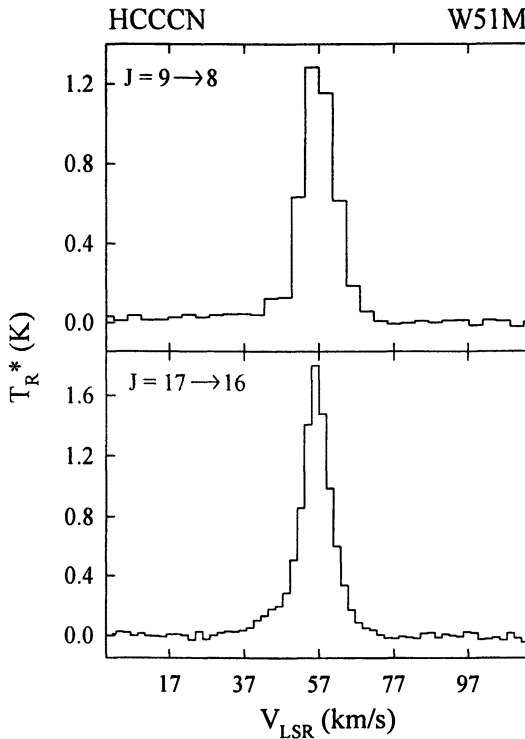


Figure 2. Spectra of the $J = 9 \rightarrow 8$ (top panel) and $J = 17 \rightarrow 16$ (bottom panel) transitions of HCCCN observed towards the molecular cloud W51M. Here T_R^ is the intensity (in K), and V_{LSR} is the source velocity with respect to the local standard of rest, which is directly related to the frequency via the Doppler relationship.*

light years from Earth. All the transitions were readily observable; two are shown in Figure 2. This part of the exercise also gave the students an idea of the overall pattern of the rotational spectrum of a simple linear molecule.

The second exercise concerned a more complex species, CH_3CN . The $J = 8 \rightarrow 7$ transition of this molecule near 147 GHz was observed towards W51M. The frequencies were provided to the students. In contrast to HCCCN, the spectrum of the CH_3CN molecule, or methyl cyanide, has many components per rotational transition. This species is a symmetric top molecule, and its geometry causes the spectrum to be split into multiple components labeled by the quantum number K (I). These K components can range from $K = 0$ up to the value where K equals the rotational quantum number J ; i.e. $K = J$. Thus, the observed $J = 8 \rightarrow 7$ transition can have eight K components from $K = 0$ to $K = 7$. The spectrum of this transition, recorded with the ARO 12m, is displayed in Figure 3. The $K = 7$ component is blended with other emissions, but the other K components are visible. Other species are also present in the data, such as CH_3OCH_3 . The relative intensities of the K components can be used to estimate the temperature

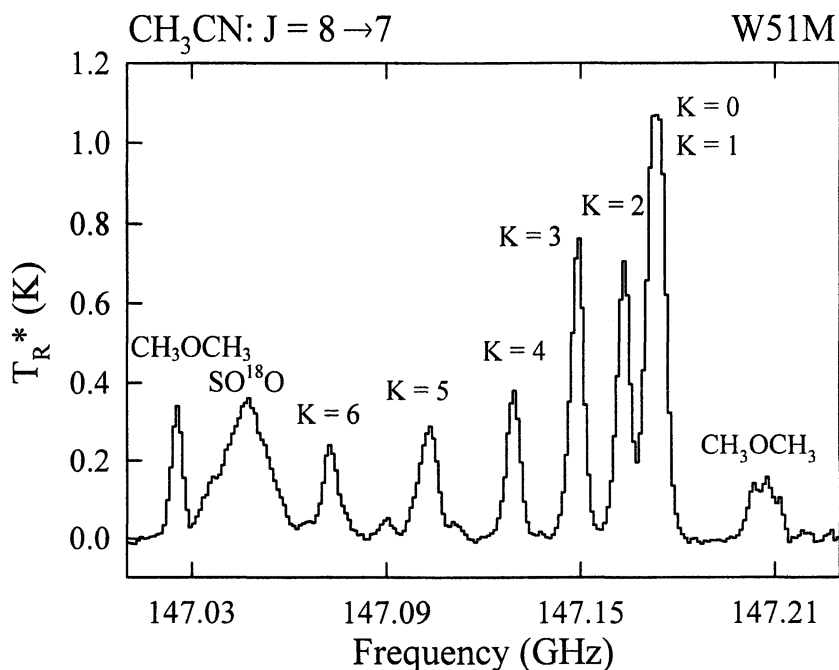


Figure 3. Spectrum of the $J = 8 \rightarrow 7$ transition of CH_3CN observed towards the molecular cloud W51M using the ARO 12m telescope. The components of the symmetric top pattern are labeled with the quantum number K . Features due to CH_3OCH_3 and SO^{18}O are also present in the bandpass.

of the molecular cloud W51M using a simple Boltzmann relationship, see below. CH_3CN is a good thermometer because the K components lie across a range of energies, according to equation 2:

$$E_{\text{rot}} = BJ(J + 1) + (A - B)K^2 \quad (2)$$

where A and B are the rotational constants of CH_3CN . The parameter A is much larger than B ($A = 158,099$ GHz and $B = 9,188.9$ GHz) and thus the second part of equation 2 causes the separation between K components to quadratically increase in energy as K increases. Students were asked to calculate the gas kinetic temperature, T_{kin} , of W51M from the spectrum. The formula used is:

$$\frac{T(K)}{T(K')} = \frac{g(K)}{g(K')} \cdot \frac{J^2 - K^2}{J^2 - K'^2} \exp\left(\frac{-E_{\text{rot}}(K) + E_{\text{rot}}(K')}{kT_{\text{kin}}}\right) \quad (3)$$

where $g(K)$ is a factor accounting for spin statistics in the molecule due to its 3-fold symmetry, $g(K)$ is 2 for $K = 3, 6, 9$, etc. and 1 otherwise, and k is the Boltzmann constant.

The third part of the lab concerned the $J = 1 \rightarrow 0$ transition of HCN near 88.6 GHz. This line was measured towards the cold, dark cloud L673 (2) and the molecular cloud M17-NW. The nitrogen nucleus has a spin of $I(N) = 1$; I is the quantum number defining nuclear spin. An important spectroscopic effect of nuclear spin is quadrupole hyperfine structure. Consequently, the spectrum of the $J = 1 \rightarrow 0$ transition is split into three hyperfine components, indicated by the quantum number F ($F = J + I$), which provides a spectral fingerprint for HCN. In order of increasing frequency, these transitions are labeled: $F = 1 \rightarrow 1$, $F = 1 \rightarrow 2$, and $F = 1 \rightarrow 0$. The intrinsic, or fundamental, intensity of the three hyperfine lines is determined by quantum mechanics, and should be related to the quantity $(2F + 1)$. Hence, the LTE intensity ratio should be on the order of 3:5:1. This ratio is evident in the spectrum of HCN towards M17-NW, see the top panel of Figure 4. The line marked U is an unknown feature. However, physical processes in the interstellar medium can change the observed intensities of the lines from the expected ratio. Opacity, or line trapping, can alter the LTE ratio, and this effect is evident in the observed spectrum of HCN towards L673, as seen in the bottom panel of Figure 5. The observed ratios of the HCN lines are approximately 1.1:1.8:1.0. Line trapping occurs when a species is very abundant and some of the radiation that is emitted by the molecule is continuously reabsorbed by the same species until it is lost to collisions. When such line trapping occurs, the molecule is said to be "optically thick". This effect is described by the equation: $T_{\text{R}} = T_{\text{ex}}(1 - e^{-\tau})$, where T_{R} is the observed intensity, T_{ex} is the excitation temperature, and τ is the optical depth parameter.

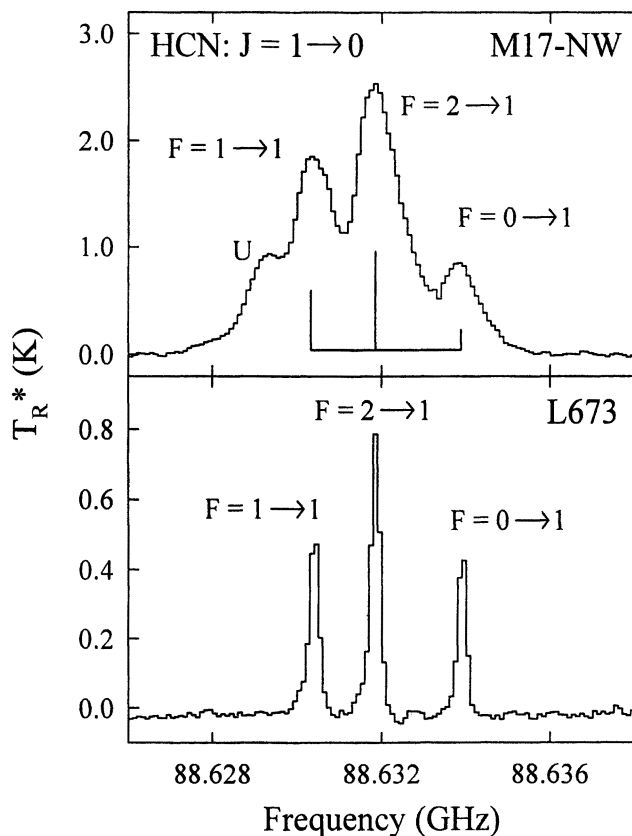


Figure 4. Spectra of the $J = 1 \rightarrow 0$ transition of HCN observed towards the molecular clouds M17-NW (top panel) and L673 (bottom panel) using the ARO 12m telescope. The three quadrupole hyperfine components are labeled with the quantum number F , and their relative intensities (3:5:1) are indicated by the stick spectrum underneath the data in the top panel.

The frequencies of the observed hyperfine components were also used to estimate the quadrupole coupling constant for HCN. The splitting of the three components is related to the value of the quadrupole parameter, eQq , which is associated with the electric field gradient of the electrons across the nucleus with the quadrupole moment (3). The students measured the line frequencies, and calculated eQq using the following equation,

$$E_{eQq} = eQq \frac{\frac{3}{4}C(C+1) - I(I+1)J(J+1)}{2I(2I-1)(2J-1)(2J+3)} \quad (4)$$

where $C = F(F+1) - I(I+1) - J(J+1)$, and $F = J+I$.

Finally, the students were asked to observe the $J = 2 \rightarrow 1$ transition of SiO in its ground and first excited vibrational states, $v = 0$ and $v = 1$, near 86.8 and 86.2 GHz, respectively, towards the star Chi Cygni, or Chi Cyg (4). The resulting spectra are shown in Figure 5. The intensity of the $v = 0$ data is about 0.4 K (top panel); however, the $v = 1$ line (bottom panel) shows much stronger emission near 9 K and a narrower line profile. These transitions were observed to illustrate maser emission in space. (A maser is a laser at microwave wavelengths.) The $J = 2 \rightarrow 1$ transition in $v = 1$ is pumped by infrared radiation emitted by the star, which creates a population inversion. Hence, maser action occurs for this line. The students calculated the vibrational temperature of SiO based on these two transitions. The result is a negative value ($T_{\text{vib}} = -600$ K) – a nonphysical temperature indicating non-thermal emission from the $v = 1$ state.

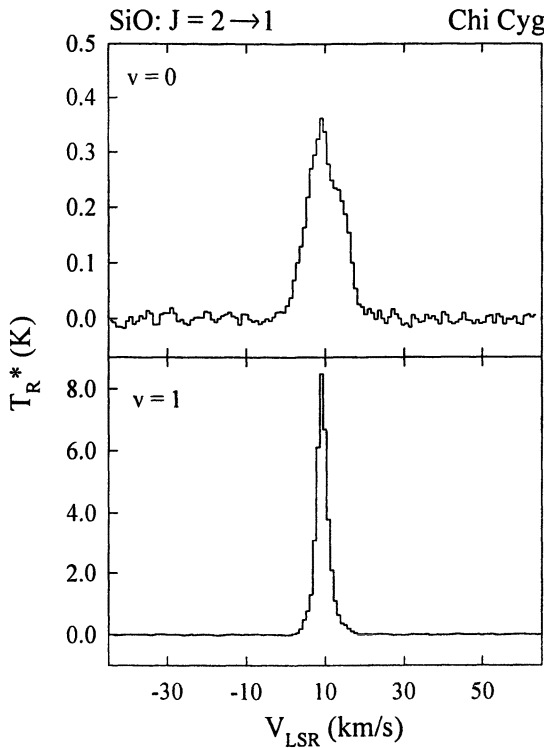


Figure 5. Spectrum of the $J = 2 \rightarrow 1$ transition of SiO observed towards the star Chi Cygnus using the ARO 12m telescope, showing the $v = 0$ transition near 82.8 GHz (top panel), and the $v = 1$ line near 82.2 GHz (bottom panel). The line intensity of the $v = 1$ transition indicates that this feature is a maser.

A handout describing the molecules and sources to be observed, as well as the procedure for the observations, was prepared and given to the students prior to the laboratory. The students analyzed the collected data, and were given accompanying questions and calculations. A picture of some of the students observing at the ARO 12m telescope is given in Plate 2.

A Laboratory in Applying Molecular Spectroscopy for the Detection of Interstellar Molecules

Observations of molecular emission would not be possible without a priori knowledge of the spectral-line transition frequencies. Therefore, an exercise was prepared where students recorded the rotational spectrum of several known interstellar molecules in the laboratory, and took the resulting frequencies and spectroscopic constants to the ARO 12m and observed the same species in the interstellar medium. This laboratory was first developed for a mix of biology and astronomy graduate students. It is currently being remodeled as an exercise for chemistry graduate students taking an introductory spectroscopy course. The students used laboratory spectrometers already in place at the University of Arizona to first record rotational transitions of several molecules. The relatively simple systems HCO^+ and HCCCN were used to demonstrate the steps involved in first identifying a molecule in the laboratory, fitting rotational constants to the measured frequencies, and accurately predicting the complete spectrum.

The spectrum of HCO^+ was investigated initially using a millimeter/submillimeter spectrometer. This species is transient and requires exotic synthesis methods. It has to be produced in the gas phase from the reaction of CO and H_2 in the presence of an AC discharge. For this section, the students were given the rotational constant of HCO^+ , $B = 44,594.4$ MHz (5), and asked to calculate the frequency of the $J = 2 \rightarrow 3$ transition near 267 GHz only using the B value (see equation 1). The spectrum of this transition of HCO^+ was recorded, as shown in the bottom panel of Figure 6, and the calculated frequency was compared to the measured frequency. The difference is due to centrifugal distortion and this effect is taken into account by the constant D , see equation 1. The students then estimated the value of the D parameter and used that value to predict the frequency of the $J = 3 \rightarrow 4$ transition of HCO^+ near 356 GHz, using equation 1. The spectrum of this transition was measured and the frequency recorded. Both lines were then used to determine more accurate values of B and D for HCO^+ .

As a second task, the students conducted measurements with a very high-resolution Fourier transform microwave (FTMW) spectrometer at the University of Arizona. This machine consists of a large resonant cavity created between two spherical mirrors. Molecules are introduced into the cavity in a supersonic

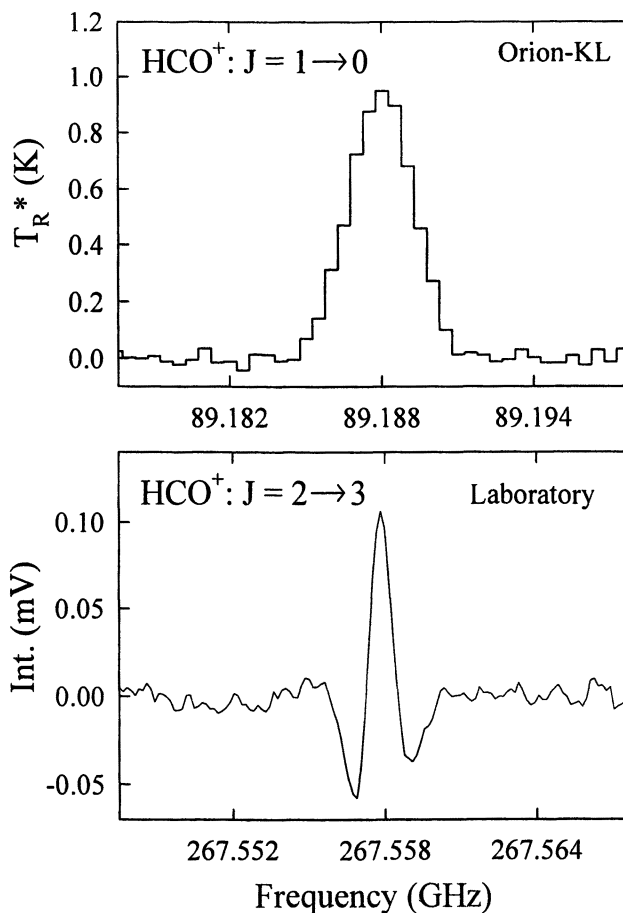


Figure 6. A combined lab/astronomical study of HCO^+ . The $J = 1 \rightarrow 0$ transition near 89 GHz was observed towards the molecular cloud Orion-KL, based in part on the $J = 2 \rightarrow 3$ transition near 267 GHz that previously was recorded in the laboratory.

jet. Microwave pulses are then used to excite these molecules into a higher energy state, and they spontaneously decay over time. The emitted radiation is recorded as a function of time for each transition; i.e. a “free induction decay” (FID). The Fourier transform of the FID results in a frequency spectrum, similar to NMR. Each spectral line in this machine is split into two Doppler components due to the orientation of the supersonic jet source relative to the resonant cavity. A precision of better than 1 part in 10^8 is obtainable from this instrument.

This system was used to measure the spectrum of HCCCN, a highly reactive (sometimes explosive) gas that is not commercially available. Hence, it has to be synthesized by an exotic production method. HCCCN was made from a 0.75%:0.75% gas mixture of acetylene (C_2H_2) and cyanogen (NCCN) highly diluted in argon (98.5%) in the presence of a 900 V DC discharge. This mixture was pre-made for the students. The dilution in argon made it extremely safe. In this exercise, the students measured the two lowest lying rotational transitions ($J = 1 \rightarrow 0$ and $J = 2 \rightarrow 1$) of HCCCN using the FTMW spectrometer. HCCCN was introduced into the reaction chamber and pulses of microwave radiation at two specific frequencies were used to excite the two rotational transitions of interest. First, the $J = 1 \rightarrow 0$ transition near 9 GHz was measured, followed by the $J = 2 \rightarrow 1$ line near 18 GHz. These data were then used to determine the rotational constants, B and D . The $J = 1 \rightarrow 0$ transition for this molecule is additionally split into three components due to electric quadrupole coupling. The splitting of the three lines was used to determine the spectroscopic constant eQq for HCCCN.

The students also measured the $J = 2 \rightarrow 1$ transitions of the rare ^{13}C and ^{15}N isotopic species of HCCCN: $H^{13}CCCN$, $HC^{13}CCN$, $HCC^{13}CN$, and $HCCC^{15}N$ in natural abundance. Despite the small change in mass resulting from using ^{13}C instead of ^{12}C or ^{15}N vs. ^{14}N , the frequency of the transitions and hence the rotational constants will vary considerably with each isotopically-substituted species. These data were consequently used to precisely determine the structure of HCCCN, which is shown in Figure 7. A spectrum of the $J = 2 \rightarrow 1$ transition of $HCC^{13}CN$ is displayed in Figure 8.

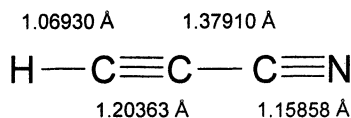


Figure 7. The HCCCN molecule showing the lengths of the four bonds.

Using the spectroscopic parameters for HCO^+ and HCCCN, the students then observed the $J = 1 \rightarrow 0$ transition of HCO^+ and the $J = 9 \rightarrow 8$ transition of HCCCN in the Orion molecular cloud. The spectrum recorded for HCO^+ is displayed in the top panel of Figure 6. These results demonstrated to the students that unusual species present in interstellar gas can be made under extreme conditions for fractions of seconds on Earth.

For the introductory spectroscopy course, the laboratory exercise will include measurements of the spectrum of CH_3CN , methyl cyanide or acetonitrile, using a millimeter/submillimeter spectrometer. The $J = 18 \rightarrow 19$ and $19 \rightarrow 20$ transitions of CH_3CN will be measured near 350 and 368 GHz. As stated earlier, this species is a symmetric top molecule and has several K components per

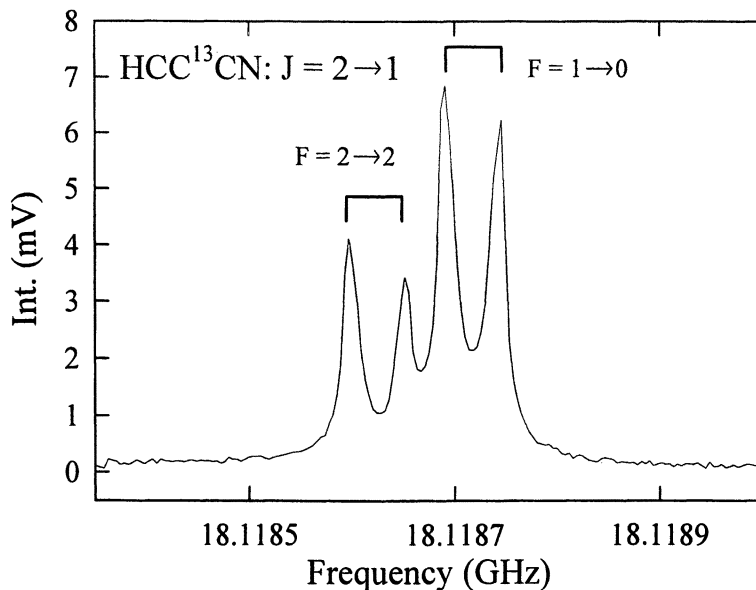


Figure 10. The $J = 2 \rightarrow 1$ transition of HCC^{13}CN near 18 GHz showing two quadrupole hyperfine lines observed in the spectrum. Each component has a double peak profile due to the orientation of the molecular flow with respect to the microwave cavity.

rotational transition. The spacing between the lines starting at $K = 0$ has a ratio of 1:3:5:7, etc. A sufficient frequency range will be scanned to cover up to $K = 10$. With these data, the students will be asked to determine the spectroscopic constants that characterize a symmetric top: B , D_J and D_{JK} , using equation 6.

$$\nu = 2B(J+1) - 4D_J(J+1)^3 - 2D_{JK}(J+1)K^2 \quad (6)$$

Educational Level and Operational Modifications

A modified version of the spectroscopy exercise could be conducted for physical chemistry laboratory courses, and could even be simplified to be used for honors freshman chemistry labs. In order to obtain frequencies that are accessible with radio telescopes, measurements have to be conducted at microwave or millimeter wavelengths. Spectrometers that operate in this range are not readily available to physical chemistry teachers; however, a simple direct

absorption spectrometer can be constructed at microwave wavelengths. Microwave sources and detectors are commercially available. Microwave Gunn oscillator sources and room temperature detectors can be purchased for \$1000 each. A steel or glass cell, optics components, a Welch pump, and a pressure gauge are also needed and can be constructed or bought. Measurements of several known interstellar molecules, such as OCS, N₂O, SO₂, can be conducted with this simple instrument. Isotopic species of these molecules could also be studied in natural abundance for structure determinations.

The astrophysical version could be used for high school physics and astronomy classes for search and discover activities, in a simplified form. For elementary school, the concept of “space chemistry” can be illustrated by the many different types of species observed, such as N₂H⁺, CCH, HC₃N. Atomic emission from hydrogen H α lines also observed at radio telescopes can be used to exemplify the Bohr atom.

Additional Resources

Resources with more information on laboratory rotational spectroscopy and radio astronomy are available. The Ziurys group maintains a website with information on rotational spectroscopy and links to other resources (6). The ARO website features descriptions of the 12m radio telescope and science conducted at millimeter wavelengths (7). Several books are available that describe rotational spectroscopy and radio astronomy in detail (e.g. 1,3,8).

References

1. Townes, C. H.; Schawlow, A. L. *Microwave Spectroscopy*; Dover Publications, Inc.: New York, 1975; p 48.
2. Sandell, G.; Höglund, B.; Kislyakov, A. G. *Astron. & Astrophys.* **1983**, *118*, 306.
3. Gordy, W.; Cook, R. L. *Microwave Molecular Spectra*; John Wiley & Sons: New York, 1984; p 391.
4. Schwartz, P. R.; Bologna, J. M.; Zuckerman, B. *Astrophys. J.* **1982**, *256*, L55.
5. Savage, C.; Ziurys, L. M. *Rev. Sci. Instrum.* **2005**, *76*, 043106.
6. Ziurys Group Research, URL: <http://www.chem.arizona.edu/faculty/ziur/ziur-group.html>
7. Arizona Radio Observatory, URL: <http://aro.as.arizona.edu/>
8. Rohlfs, K.; Wilson, T. L. *Tools of Radio Astronomy*, 4th ed.; Springer-Verlag: Berlin, 2004.

Chapter 22

Chemistry of Life: Chemical Evolution as a Theme for Teaching Undergraduate Chemistry

Bhawani Venkataraman

**The New School for Liberal Arts, Eugene Lang College,
New York, NY 10011**

The course “Chemistry of Life” investigates fundamental concepts in chemistry using chemical evolution as a contextual theme. By examining questions like “Where did the elements of life come from?”, “Why is water an essential ingredient of life?”, “Why does carbon-based life offer complexity?”, and “What is the role of self-assembly in life?”, the course introduces the underlying chemical and physical concepts such as nucleosynthesis, atomic structure, periodic properties, chemical bonding, intermolecular interactions, stereochemistry, energetics, kinetics, self-assembly, and structure-function relationships. Active learning methods are integrated into the course, including computational molecular modeling, visualizations, simulations, experiments, and student papers and presentations.

Introduction

The course Chemistry of Life uses chemical evolution as a thematic focus to teach fundamental principles typically discussed in an introductory level chemistry course. This course is part of the chemistry curriculum taught in the Science, Technology and Society (STS) program at Eugene Lang College, a four-year liberal arts college of The New School in New York City. The objective of the STS program is to support the education of students interested in science-based careers such as environmental and health policy, law, ethics, education, science writing, and journalism. An equally important objective is to support general education. Science faculty in the STS program try to insure that all students, whether majoring in STS or not, have a firm understanding of basic scientific principles, quantitative reasoning, and an appreciation of the process of scientific inquiry. The chemistry curriculum in the STS program consists of two introductory and two intermediate level courses. The Chemistry of Life is the first in this sequence and is intended for students who typically do not have strong backgrounds in science and little or no chemistry background.

The objectives of the course include:

1. Understanding the importance of molecular scale interactions.
2. Understanding the role of the environment in supporting molecular interactions.
3. Understanding how chemistry and the environment can influence macro-scale observations.
4. Understanding fundamental chemical concepts.

There are many successful examples of courses that teach fundamental chemical concepts along with applications of these concepts. The Chemistry of Life course is reversed in that it first engages students through the theme and then teaches underlying chemical principles in order to understand the theme, in this case processes relevant to chemical evolution. The use of themes to teach chemical principles is a format that has been successfully used in modules developed by the NSF funded consortium ChemConnections (1-3).

The Chemistry of Life course incorporates active learning methods, including computational molecular modeling, simulations, experiments, and student papers and presentations. As described below, activities have been designed that use commercial software packages to enable students to visualize chemical and physical processes that influence and support life.

Conceptual Framework, Course Structure, and Assessment of Student Performance

The course is structured around questions relevant to the origin of life on Earth and chemical evolution. Understanding each topic or question requires

knowledge of fundamental chemical concepts. The class also reads chapters from Robert Hazen's book *Genesis – The Scientific Quest for Life's Origins* (4), which describes past and current research on the origins of life. The questions below provide the focus for class discussions, with each question forming the basis for understanding fundamental chemical concepts.

Discussion Questions

What are the elements of life, and where did they come from?

In understanding this question, the class briefly discusses the Big Bang, primarily to emphasize conservation of energy and matter. This leads to discussions of nucleosynthesis and the periodic table, which introduces more detailed discussions of atomic structure, models of the atom, the periodic table, periodic properties, and electron configuration.

What is life?

Recognizing that there is no one accepted definition of life is an interesting challenge for students. The definition "Life is a self-sustained chemical system capable of undergoing Darwinian evolution" is discussed (4). This definition is examined to begin understanding what conditions are required to support life. The role of molecules, energy, and genetic information is introduced, leading to discussions of the role of liquid water, carbon and carbon containing molecules, energy, and information-carrying molecules in life today.

Why is liquid water essential for life?

This question introduces molecular bonding, structure, and geometry. Bonding and geometry are restricted to the Lewis Dot Model and the Valence Shell Electron-Pair Repulsion Model, but a more detailed treatment including quantum mechanics and bonding theories (valence bond theory, molecular orbital theory, hybridization) could be discussed. To understand the relation between bonding and geometry students use Wavefunction's Spartan Student Edition (5) to visualize the three dimensional nature of molecules. This leads to a closer look at the shape of water and how its shape determines its properties. Using molecular models and simulations in Spartan, students investigate electronegativity, polarity, non-covalent interactions, hydrogen bonding,

physical properties such as boiling point, melting point, and solubility, and ionic bonding. These concepts are connected to how the structure of the water molecule determines its properties that are so crucial for life.

Why is life carbon-based?

In conjunction with understanding why liquid water is essential to life, students also investigate the flexibility of carbon in bonding, appreciating that a half-filled valence shell allows a diversity of molecular structures. This also allows introduction of functional groups and stereochemistry. Again Spartan is used to build molecules and investigate the shapes of molecules.

What is the role of energy?

To understand the energetics of chemical processes, the question “How are simple molecules in the atmosphere transformed to larger molecules?” is posed. This question is then discussed through the Urey-Miller experiment (6). Students read the original paper by Miller as well as an article written 50 years later which discusses the historical significance of the experiment (7). Students run a series of simulations using a program called “Origin of Life” (8), which allows the user to change the composition of the atmosphere, the temperature and the level and type of energy source to determine the conditions under which amino acids will be synthesized under pre-biotic conditions as perceived by Miller. The program defines “success” as producing a defined level of aspartic acid in less than 2 million years. The assumption is that if amino acids are formed in two million years that conditions are right for life to take a foothold.

Through these simulations, students appreciate the energetic and kinetic aspects of chemical reactions and why the composition of the atmosphere is critical to the outcome. For example, the class simulates the effect on the yield of amino acids if the atmospheric composition was CO_2 instead of CH_4 or the nitrogen source was N_2 instead of NH_3 . The simulations also allow students to investigate the consequences if the pre-biotic atmosphere contained free O_2 . Through these simulations, basic chemical concepts are discussed including thermodynamics, thermochemistry and bond enthalpies, kinetics, and catalysis.

How do simple building blocks of life become complex systems?

To investigate this question, the class first examines the chemical complexity demonstrated by life today by looking at the structure and function of proteins and nucleic acids and the inter-connectedness of these systems.

Discussions then focus on why it is such a challenge for scientists to understand how the simple building blocks of life could have come together to form proteins and DNA. Students are fascinated by the chemical complexity demonstrated by life, and how their own lives are dependent on molecular level processes. They also begin to appreciate the challenges faced by scientists. The role of self-assembly, which was first introduced in discussions on water and inter-molecular interactions, is also emphasized here in considerations of the secondary structure of proteins and the double-helix of DNA.

Why is it such a challenge to understand how life began?

These questions are addressed through student papers and presentations on chapters from the latter half of Hazen's book (4). Each chapter elaborates on past and current theories of the chemical origins of life, including Bernal's "Clay World", David Deamer's "Lipid World", Sidney Fox's "Protenoid World", Christian De Duve's "Thioester World", Günter Wächtershäuser's "Iron-sulfide World", and Leslie Orgel's "RNA World". The details of these theories are above the level of an introductory undergraduate course, yet students are able to get a sense of the big picture in each by applying the chemistry they have learned. Students become quite involved in the theory they are presenting. They also gain an appreciation of how much still needs to be understood and how far these theories are from being complete descriptions of the origins of life. This project also serves as an assessment of students' ability to apply their newly-learned basic chemical knowledge to understand more complex theories.

Learning Activities

The course makes extensive use of in-class activities that involve computer modeling, visualizations, simulations, and experiments. Activities are done in small groups with questions that focus the activities and gauge student learning. Students also read and discuss Hazen's book in class and conduct research for a paper and in-class presentation. Some of these activities are described below.

Molecular modeling

Wavefunction's Spartan Student Edition (6) is used extensively in this course for building molecules and visualizing molecular shape, polarity, intermolecular interactions, hydrogen bonding, solubility, protein and nucleic acid structure. Spartan exercises are used to investigate the connection between the structure and shape of water and its polarity, intermolecular interactions, and

solvent properties. Some of these activities also connect with simple experiments so that students observe and try to explain the molecular processes involved. Then they perform simulations in Spartan to understand the molecular-scale process, confirming or altering their suggested explanations. An example of this is a simple oil/water/soap activity, followed by a Spartan simulation with clusters of hexane (as a model oil), hexanoic acid (as a model soap) and water to understand the difference between polar, non-polar, and an amphiphile, and how inter-molecular interactions affect solubility and drive self-assembly.

Simulation software

“Origins of Life” is a simulation software that allows students to understand the effect of energy, temperature, and chemical composition of the reaction mixture on the outcome of a chemical reaction (9). The simulation software is based on Stanley Miller’s classic experiment (6). In the simulation software, students change the composition of the atmosphere, the energy source, and the temperature, to maximize the yield of amino acids in the shortest amount of time.

Experiments

Students do simple experiments that demonstrate the principles being discussed such as:

- Investigating ionic bonding and covalent bonding by measuring conductivity of solutions of compounds soluble in water
- Understanding the interaction between hydrophobic, hydrophilic, and amphiphilic systems with water
- Looking at line spectra in discharge tubes to understand the model of the atom, Investigating the effect of the environment on the shape of proteins (9).

Readings

Throughout the semester, the class reads chapters 1 to 10 of Robert Hazen’s book and submit chapter summaries which are discussed in class. The book helps students understand the current state of research, and develop an understanding of the interdisciplinary nature of the research, the process of scientific inquiry, the importance of data and experimental verification of a hypothesis, and the highs and lows of scientific research.

NOVA "Origins" Series (10)

The class begins by viewing the first two parts of the NOVA series "Origins" which depicts the origins of Earth, the hostile environment of early Earth and how researchers try to unravel what may have happened over 4 billion years ago from fossil records, chemical analyses of meteorites, and by simulating conditions in a lab. Students really enjoy this series and often comment on how the videos provide a framework and good introduction for the course. While watching the movies, students answer questions and are advised to write down questions they have. These questions and answers become the basis for a discussion after the movie and introduce the larger questions and ideas that the course tries to address.

Papers and Presentations

At the end of the semester each student submits a paper by expanding a topic or a researcher's work from the last half of the Hazen book. The latter half of this book, which focuses on current theories of origin of life, is quite speculative and open-ended. The purpose of the students' papers is to encourage students to go beyond the book and to develop library research skills. To support this, a session is held with the librarian on how to conduct a search of primary and secondary sources. At the end of the semester students present their papers to the class and are required to use PowerPoint (or other presentation software) for their presentation.

Assessing a Student's Performance

Learning of chemical concepts is assessed through two tests and homework assignments. Many of the questions on the tests require students to connect chemical concepts to issues relevant to chemical evolution or chemical processes important for life. For example, questions look at the possibility of life on Titan and the potential for "successful life" on Titan. This requires students to address this possibility in terms of energy sources, temperature, chemical processes given Titan's atmosphere, and the differences in chemical and physical processes in a liquid methane environment versus water.

During the course of the semester, students write chapter summaries on Hazen's book. In these summaries, students highlight key points in the chapter, discuss what interested them, what surprised them, what bothered them, and what questions they have. The purpose of writing the summaries is to encourage students to question whether they understand what they are reading. These

summaries are discussed in class leading to discussions on the process of scientific inquiry, the importance of experiments and data, and the importance of independent verification.

Over the second half of the semester students begin researching and preparing for their final paper and presentations. Students identify a topic of research described in Hazen's book and are expected to explore this work in more detail than in the book. Students first write a one-page outline and a bibliography, followed by a first draft that is commented on by the instructor. Students submit a final paper at the end of the semester, and present their papers to the class. For the presentations students are required to use PowerPoint or other presentation software packages and are advised to include images and data from the literature in their presentations, rather than text-only slides. One student created models in Spartan to explain the basis of the research she presented.

Writing the paper and preparing for their presentations is a challenging project for students, many of whom are freshman, and it is even challenging for the non-freshman. While some of the sources they read are *Scientific American*, *American Scientist*, or chapters from books like *Vital Dust* (11), *Life's Origin* (12), and *Environmental Evolution* (13), they also identify papers in the primary literature and extract a basic level of understanding. They also read brief reports of work in journals such as *Science*.

Through outlines and drafts that the students write, and through meetings with the instructor, the students begin to develop the confidence and skills to apply what they have learned towards understanding a research topic. In fact, many are quite amazed that they are able to develop some understanding of the work they are researching. Judging from the final papers and presentations, students were indeed able to apply basic chemical concepts in class towards developing some sense of the work they were researching. It was interesting to observe how vested students became in the theory for the origins of life that they were researching. However, given that these are complex theories, supporting students so that their lack of understanding of the details does not frustrate them is challenging for both student and instructor.

Students' comments on a survey handed out at the end of the class suggested that they did get some satisfaction out of this project:

- "My research was challenging because of the complexity of my topic, but I was happy that I could understand at least the basics with my new found understanding of chemistry"
- "I found myself tying the research back to discussions. I was proud of the work and effort put into it".
- "I was able to apply the chemistry but not as much as I was able to learn how to deal with scientific journals and research".

Conclusions

The success of the course in teaching students chemical principles as well as engaging them, is assessed through evaluation tools specifically designed for this course. Students have consistently rated this course highly over the three years that it has been taught. The course changes some students' perception and appreciation of chemistry and their ability to understand and enjoy the subject. Below are some selected comments from students responding to the two questions below.

“What did you think about using the context of the chemistry of early Earth and the origin of life as a way to understand and appreciate chemistry?”

- “It is awesome! It makes a vague discipline like chemistry focus on something specific and fascinating – makes chemistry easier to understand.”
- “A great way to approach a generally dry topic.”
- “It was a very tangible, applicable way to study chemistry.”
- “I think a (at least basic) understanding/appreciation for chemistry is essential to really understanding early earth / origins of life, and understanding where we came from is a good reason to study chemistry.”
- “I think it was helpful to do it this way because this area is so fascinating and it is one where chemistry played a lead role.”

“What did you think of chemistry coming into the class and what do you think about it now?”

- “Chemistry was not my forte; I was a little worried at first; now I love it!”
- “I didn't know anything about it. I now really enjoy looking at the world from a chemical perspective.”
- “I was feeling a bit insecure about being able to understand it that well. But coming to the class and putting it in a context, I feel really comfortable with it.”
- “Coming into the class I dreaded chemistry. Now I appreciate chemistry much more.”
- “I used to think it was too complex for me to understand – but now I think that with this base of ideas I could understand other, more complex things. Also it is a lot more interesting now that I understand it better.”

Judging from students' performance and comments, the course appears to be meeting its objectives in teaching basic chemical concepts and connected to students' interest through the role of chemistry in the origins of life. However, there are some challenges to be aware of. There is a constant struggle between trying to balance the depth to which the course should address basic chemistry and at the same time expanding on the connections between the chemistry and the over-arching theme, which is the draw for many of the students. It is not

clear to the author where this balance lies, and in fact seems to vary with individual classes. A few students comment that there is not enough chemistry, and a few others struggle with the level at which the chemistry is being addressed. For the latter group of students what maintains their interest in the class is the focus on chemical evolution that they seem to find appealing.

The course, Chemistry of Life, appears to be successful in teaching fundamental principles in chemistry through the thematic focus of chemical evolution. Students seem to appreciate the role of chemistry in the origins of life, as well as in their own lives, and feel more confident about their ability to understand chemistry and complex scientific ideas.

Acknowledgements

This work has been supported by a grant from the National Science Foundation's CCLI-A&I program (DUE-05- 10543) and matching grants for equipment from OceanOptics, Inc. and Eugene Lang College, The New School.

References

1. Anthony, S.; Mernitz, H.; Spencer, B.; Gutwill, J.; Kegley, S.; Molinaro, M., The ChemLinks and ModularCHEM Consortia: Using Active and Context-Based Learning to Teach Students How Chemistry is Actually Done. *Journal of Chemical Education* **1998**, *75*, (3), 322.
2. Burke, K. A.; Greenbowe, T.; Lewis, E.; Peace, G. E., The Multi-Initiative Dissemination Project: Active-Learning Strategies for College Chemistry. *Journal of Chemical Education* **2002**, *79*, (6), 699.
3. *ChemConnections*. W. W. Norton: 2003.
URL <http://www.wwnorton.com/college/titles/chemistry/chemx/>
URL <http://www.wwnorton.com/nrl/chemlchemx/>
The ChemConnection series includes a module titled "How Could Life Have Arisen on Earth" that discusses kinetics and thermodynamics in context with processes relevant to chemical evolution.
4. Hazen, R., *Gen-e-sis: The Scientific Quest for Life's Origin*. Joseph Henry Press: Washington, DC, 2005.
5. Wavefunction *Spartan Student Edition*, Wavefunction, Inc.
www.wavefunction.com
6. Miller, S. L., A Production of Amino Acids Under Possible Primitive Earth Conditions. *Science* **1953**, *117*, 528.
7. Bada, J. L.; Lazcano, A., Prebiotic Soup – Revisiting the Miller Experiment. *Science* **2003**, *300*, 745.
8. Bender, F.; Ponnampereuma, C. *Origin of Life*, EME Corporation: 1990.

9. Bowen, R.; Hartung, R.; Gindt, Y., A Simple Protein Purification and Folding Experiment for General Chemistry Laboratory. *Journal of Chemical Education* **2000**, *77*, (11), 1456.
10. NOVA: Origins, 2004, WGBH Educational Foundation, Boston, MA
11. De Duve, C., *Vital Dust: The Origin and Evolution of Life on Earth*. BasicBooks: 1995.
12. Schopf, W., *Life's Origin. The Beginnings of Biological Evolution* University of California: 2002.
13. Margulis, L.; Matthews, C.; Haselton, A., *Environmental Evolution*. The MIT Press: 2000.

Afterword

Richard N. Zare

Department of Chemistry, Stanford University, Stanford, CA 94305

Once upon a time, some four and one-half billion or so years ago, the Earth was a dreadful, horrid place from what we can tell based upon various geological records. Cosmic debris from the formation of the solar system rained down nearly continuously on the Earth causing the oceans to boil, evaporate, and reform. Volcanoes spewed forth foul gases. The atmosphere was a noxious mix of nitrogen, ammonia, water vapor, methane, hydrogen sulfide, hydrogen cyanide, and carbon dioxide, with few traces of oxygen. In such a world nothing could live and nothing did. Then, something happened. Within a half billion years after the cosmic barrage had diminished, life sprang forth on Earth -- simple, one-celled life, but certainly life. For science, the question has always been, "How did life arise from nonlife?" This puzzle, which is central to our existence, remains to this day an unsolved great mystery.

The stage has been set, as can be understood by studying the present volume *Chemical Evolution. Chemical Change Across Space and Time*. We eagerly await the arrival of the players for the production of the next volume *Chemical Evolution: From Origins of Life to Modern Society*. What might we find in this second volume?

As the great chemist Isaac Asimov wrote in *Omni* (1983):

"We can make inspired guesses, but we don't know for certain what physical and chemical properties of the planet's crust, its ocean and its atmosphere made it so conducive to such a sudden appearance of life. We are not certain about the amount and forms of energy that permeated the environment in the planet's early days. Thus the problem that scientists face is how to explain the suddenness in which life appeared on this young (4.6 billion year old) planet earth. In the nineteenth century, scientists first began to accept the concept of biological evolution and to dismiss the possibility that life had been

created in its present complexity by some supernatural agency. That raised the question of how this extraordinary phenomenon called life could possibly have come to be by accident.”

Are we any wiser today than then? It is my hope that the second volume will explore the age-old question about the origin or origins (?) of life. It is a huge question that has engaged the best minds for centuries, It is essentially a chemical question, worthy of the thoughts and efforts of all chemists.

To appreciate the complexity of the issue, just try to define what life is. If we content ourselves with simple definitions, like self-replicating, self-organizing, moving systems, we stumble into problems like whether the stars are alive or whether fire is alive. Surely we ought to do better than Dave Barry’s definition: “Life is anything that dies when you stomp on it.” Yet, this problem is not just a semantic one. To decide whether a virus is alive or not is a truly problematic inquiry, in my estimation. Of course, we can always have recourse to the same definition as for obscenity, namely, I know it when I see it. Still, despite this unsatisfying situation, chemists have a huge role to play in understanding how order can emerge from disorder in an open system. We do know much more than in 1983 when Asimov posed anew this question, but humility is important in understanding the limits of our knowledge as we quest for a solution to this grand cosmological question.

And what does the story of life’s beginnings on Earth reveal about the possibility of life elsewhere in the Universe? Answers to those questions are among the most intriguing and profound that science can ask. I commend the reading of this monograph and the one to follow for all those who join in searching for an understanding of how nonlife can be transformed into life, somewhere, somehow.

Glossary

Abyssal plain Flat or gently sloping areas of the deep ocean floor generally covered with fine-grained sediments.

Achondrite Meteorite from an asteroid that has gone through the process of differentiation.

Adiabatic A term in thermodynamics that describes a process that occurs without exchange of heat.

Aerosol Sub-microscopic dispersions or suspensions of liquid droplets or solid particles in a gas.

AGB see Asymptotic Giant Branch

Alkali-feldspar A feldspar with a chemical composition of or between the endmembers $\text{NaAlSi}_3\text{O}_8$ and KAlSi_3O_8 .

Amphibole A group of chain silicates. The simplest chemical formula for an amphibole is $\text{Ca}_2\text{Mg}_5\text{Si}_8\text{O}_{22}(\text{OH})_2$.

Ankerite A sedimentary rock composed of calcium, iron, magnesium, and manganese carbonates.

Apatite A group of phosphate minerals with the general formula $\text{Ca}_5(\text{PO}_4)_3(\text{X})$ where X is F, Cl, or OH.

Aphelion The point in the elliptical orbit of a planet farthest from the sun.

Archean Terrestrial geologic eon that extends from the Hadean (3.8 Ga) until 2.5 billion years ago.

Asymptotic Giant Branch Stars (AGB) A period of stellar evolution. They are named for their place in a region on the Hertzsprung-Russell Diagram dominated by evolving low to medium-mass stars (0.6-10 solar masses).

Astronomical Unit (AU) An astronomical unit of length equal to the average distance between the Earth and the Sun. $1\text{AU} = 149.6 \times 10^6 \text{ km}$.

AU see Astronomical Unit.

Baryon Subatomic particles made of three quarks. Protons and neutrons are both baryons.

Biotite A common phyllosilicate (sheet silicate) mineral with the general formula $\text{K}(\text{Mg}, \text{Fe})_3\text{AlSi}_3\text{O}_{10}(\text{F}, \text{OH})_2$.

Chalcophile An element that tends to follow sulfur's behavior during geochemical processes. cf. lithophile and siderophile

C Class Star Red giant stars where there is an excess of carbon in the atmosphere. Carbon stars are near the end of their lives.

Centaur An icy asteroid that orbits between Jupiter and Neptune.

Chondrite Meteorite from an undifferentiated planetary body, most likely an asteroid. Unaltered varieties generally contain chondrules or chondrule fragments.

Chondrule Spherical millimeter-sized silicate droplet formed by melting and quenching prior to incorporation into undifferentiated meteorites.

Circumstellar Envelope (CSE) The circumstellar environments around a mass-losing giant star.

Clathrate Well-defined chemical compounds consisting of a caged (trapped) molecular species contained in a lattice of a second type of molecule.

CNO cycle A catalytic fusion cycle that converts H to He in stars.

Corundum An oxide mineral with the formula Al_2O_3 .

CSE see circumstellar envelope.

D Abbreviation for Deuterium (^2H).

dex (decimal exponent) A logarithmic unit used in astronomy. For example, $-0.XX \text{ dex}$ equals $10^{-0.XX}$.

Differentiation Melting and fractionation of a planetary body into layers of different chemical composition. e.g. core, mantle and crust. In this process high-density materials sink and low-density materials float.

Dolomite A sedimentary rock composed of calcium magnesium carbonate.

Dwarf star A star on the main-sequence of the Hertzsprung-Russell diagram. Also known as main-sequence stars. Our Sun is a main-sequence star.

Eccentricity A measure of the departure of an orbit from a circular path.

Endmember A mineral that is at a pure compositional end of a mineral series. Minerals are solid solutions of varying chemical composition rather than having an exact chemical formula. For example, olivine contains *endmembers* fayalite (Fe_2SiO_4) and forsterite (Mg_2SiO_4), but actual olivine compositions are generally charge-balanced solid solutions between these: e.g. $\text{Fe}_{0.75}\text{Mg}_{1.25}\text{SiO}_4$ or $\text{Fe}_{0.10}\text{Mg}_{1.90}\text{SiO}_4$. c.f. olivine, fayalite, forsterite.

Enstatite The Mg-rich pyroxene group endmember mineral with the formula MgSiO_3 .

Fayalite The Fe-rich olivine group endmember mineral with the formula Fe_2SiO_4 .

Feldspar A group of aluminum silicate minerals. Feldspars compose many of the rock-forming minerals found in the Earth's crust.

Ferrosillite The Fe-rich pyroxene group endmember mineral with the formula FeSiO_3 .

Forsterite The Mg-rich olivine group endmember mineral with the formula Mg_2SiO_4 .

Ga A unit of time equal to one billion (10^9) years. In geological or cosmological contexts, one can often assume that "ago" is implied if not explicitly stated.

Garnet A group of silicate minerals with the general formula $\text{X}_3\text{Y}_2(\text{SiO}_4)_3$ where X is a divalent cation and Y is a trivalent cation.

Greenalite An iron-rich phyllosilicate mineral found in banded iron formations.

Hadean Terrestrial geologic eon that extends back to the Earth's formation until about 3.8 billion years ago.

Hematite Oxide mineral with the formula Fe_2O_3 .

Hornblende A general term for an amphibole group chain silicate.

Illite A phyllosilicate (layered silicate) with a structure of parallel silicate tetrahedral sheets. Each sheet has the general formula Si_2O_5 .

Interstellar medium (ISM) The matter (gas and dust) that exists between the stars within a galaxy.

IOM see Insoluble Organic Matter.

Isochron A set of data points on an isochron plot that all fall on a single line and represent a single radiometric age.

ISM see Interstellar Medium.

Kuiper belt An area of the solar system extending from the orbit of Neptune (~30 AU) to 50 AU from the Sun.

Lithophile An element that tends to follow (be concentrated in) the silicate portions of a rock during geochemical processes. cf. calcophile and siderophile.

M_{\odot} Mass of the Sun: 1.99×10^{30} kg.

Ma A unit of time equal to one million (10^6) years. In geological or cosmological contexts, one can often assume that “ago” is implied if not explicitly stated.

M Class Star The most common class of stars. These are red dwarf stars and are relatively small and cool.

Magnetite A ferrimagnetic mineral with chemical formula Fe_3O_4 .

Metallicity A measure of the proportion of elements in a star other than hydrogen or helium. In astronomy, chemical elements other than hydrogen and helium are called metals.

Meteor Light that results from the entry of a meteoroid or micrometeoroid from space into the Earth’s atmosphere.

Meteorite A fragment of a planetary body that reaches the surface of another planetary body.

Meteoroid A fragment dislodged from a planetary body that is traveling in space.

Mineral Naturally occurring inorganic elements or compounds with crystalline structure.

Molecular cloud An interstellar cloud whose density and size permits the formation of molecules.

Monte Carlo method A nondeterministic computational method for simulating the behavior of complex physical and systems.

Montmorillonite A phyllosilicate mineral that typically forms microscopic crystals making a clay. It is the main constituent of the volcanic ash weathering product, bentonite.

Nierite A mineral with the formula Si_3N_4 .

Nova A cataclysmic nuclear explosion.

Nuclear cross section A model used to characterize the probability that a nuclear reaction will occur. Nuclear cross section is measured in units of barns with one barn equal to 10^{-24} cm^2 .

Nucleosynthesis The formation of unstable and stable isotopes in stars.

Olivine A magnesium iron silicate mineral with the common solid solution endmembers forsterite and fayalite.

Osbornite A mineral with the formula TiN.

Parsec (pc) A unit of length used in astronomy that stands for parallax of 1 arcsecond. In more common units: $3.09 \times 10^{13} \text{ km}$ or $2.063 \times 10^5 \text{ AU}$.

Plagioclase A series of minerals within the feldspar family with endmember chemical compositions ranging from $\text{NaAlSi}_3\text{O}_8$ to $\text{CaAl}_2\text{Si}_2\text{O}_8$.

Phyllosilicate A class of minerals with a parallel or layered silicate sheet structure. Mica is a common example.

Photosphere The region where an astronomical object stops being transparent to light. For stars, this is the visible "surface".

Pillow basalts Igneous rocks formed when basaltic lavas flow directly into water before solidifying.

p-process The proton (p) capture process is a nucleosynthetic process responsible for the production of the proton-rich isotopes with masses $A > 100$.

Pyroxene A class of chain silicate minerals with the general formula $XY(\text{Si,Al})_2\text{O}_6$. X and Y can be a wide range of charge-balancing cations (typically Fe, Mg, Ca, Na).

Quartz A silicate mineral having the formula SiO_2 .

R_☉ Radius of the Sun: $6.96 \times 10^8 \text{m}$.

RG see Red Giant Star.

Red Giant Star Red giants are stars of 0.4 to 10 times the mass of the Sun which have exhausted the supply of hydrogen in their cores and switched to fusing hydrogen in a shell outside the core. The Sun is expected to become a red giant in about five billion years.

Retrograde motion Orbital or rotational motion that is clockwise as seen from north of the ecliptic. For example, Triton is in retrograde orbit around Neptune and Venus is in retrograde rotation.

Riebeckite A sodium-rich member of the amphibole mineral group.

r-process The rapid (r) neutron capture process is a nucleosynthetic process where nuclei are bombarded with a large neutron flux to form highly unstable neutron rich nuclei that rapidly decay to form stable nuclei. Most elements heavier than Fe are formed by the r-process.

S Class Star These stars are classified by the presence of zirconium oxide lines, and reside between the Class M stars and Class C stars in spectral type.

Siderite A mineral with the formula FeCO_3 .

Siderophile An element that tends to follow iron's behavior during geochemical processes. Siderophiles are enriched in the Earth's core. cf. calcophile and lithophile.

Silicate A compound containing silicon and oxygen.

Sinoite A mineral with the formula $\text{Si}_2\text{N}_2\text{O}$.

Spinel A group of minerals named after the namesake mineral MgAl_2O_4 . They have the general formula XY_2O_4 where cation X occupies tetrahedral sites and Y cations occupy octahedral sites.

s-process The slow (s) neutron capture process is a nucleosynthetic process where the rate of neutron capture by nuclei is slow relative to the rate of radioactive beta-decay.

Stilpnomelane An iron-rich phyllosilicate mineral often found in association with iron ores.

Stromatolite Lithified sedimentary structures thought to result from the growth or activity of microorganisms.

T Abbreviation for Tritium (^3H).

Titanite A calcium titanium silicate mineral with the formula CaTiSiO_5 . Sometimes called sphene.

TNO see Trans-Neptunian Object.

Trans-Neptunian Object (TNO) Any object in the solar system that orbits the sun at a greater average distance than Neptune.

Troilite The mineral name for iron(II) sulfide: FeS .

Trojan Asteroids that orbit 60° ahead of or behind a larger object. They do not collide with the larger because they orbit within one of the two Lagrangian points of stability.

Turbidite Geological formations formed from underwater avalanches.

Zircon A mineral with the formula ZrSiO_4 .

Indexes

Author Index

- Allamandola, Louis J., 80
Apponi, Aldo J., 363
Bada, J. L., 282
Botta, Oliver, 246
Chalmers, J. H., 282
Clayton, Robert N., 141
Cleaves, H. J., 282
Delano, John W., 293
Ehrenfreund, P., 232
Eldredge, Niles, xvii
Fegley, Bruce, Jr., 187
Ferris, James P., 293
Fisher, Kurt, 326
Friedrich, Jon M., 349
Halfen, DeWayne T., 363
Hazen, Robert M., 2
Kauffman, Stuart A., 310
Kleine, Thorsten, 208
Lazcano, A., 282
Lewis, John S., 130
Lipschutz, Michael E., 153
Lodders, Katharina, 61
Meyer, Bradley S., 39, 343
Miller, S. L., 282
Olive, Keith A., 16
Parker, Allen, 343
Rumble, Douglas, III, 261
Schaefer, Laura, 187
Seidel, S. Russell, 349
Spaans, M., 232
Venkataraman, Bhawani, 378
Wilkins, Richard T., 326
Zaikowski, Lori, 326, 349
Zare, Richard N., 389
Ziurys, Lucy M., 111, 363

Subject Index

A

- α -Aminoisobutyric acid (AIB),
 - abundance in meteorites, 253
- Abiotic production
 - high performance liquid chromatography of derivatized amino acids from spark discharge reactions, 290*f*
 - ozone, 142
 - spark discharge apparatus for experiments, 286, 288
 - syntheses in neutral atmospheres, 286, 289
 - yields of amino acids and small molecules in neutral atmospheres, 287*t*
- Ablative deceleration, meteorites, 159, 162
- Abundance, chemical. *See* Solar system
- Abundance ratios of molecules, circumstellar envelope (CSE), 71, 72*f*
- Acasta rocks, Earth's oldest, 263, 264*f*
- Accretionary phase
 - giant impacts, 224
 - Solar System, 133
 - See also* Hafnium-tungsten chronometry of planetary formation
- Acetonitrile, radio astronomy, 369–370
- Achondrites
 - classifications, 161*f*
 - definition, 391
 - gas retention age, 181
 - igneous, 168
 - numbers of classified falls and finds, 164*t*
 - properties, 156
 - stony meteorites, 136
- Activated nucleotides, ribonucleic acid (RNA) world scenario, 297–298
- Adaptations, Darwinian, of organisms, 321
- "Age" of meteorites
 - cosmic ray exposure (CRE), 178–179, 180*f*
 - gas retention age, 178, 181, 182*f*
 - solidification age, 181, 183–185
 - variety, 177–178, 180*f*
- Ages, oldest rocks on Earth, 263, 264*f*
- Aliphatic hydrocarbons, abundance in Murchison meteorite, 253*t*
- Amino acids
 - enantiomeric excesses in meteoritic, 254
 - meteorites, 257–258
 - prebiotic syntheses, 284–286
 - yields from neutral atmospheres, 287*t*
- Ammonia photolysis, Jupiter, Saturn, Uranus and Neptune, 202–203
- Amphiphiles, self-organization, 8
- Analytical procedures
 - insoluble organic matter (IOM), 250–251
 - soluble organic compounds, 251–252
- Antarctic ice cores, volcanic eruptions, 277, 278*f*
- Archean rocks, discoveries of microstructures, 268–269
- Arizona Radio Observatory (ARO) telescope for laboratory exercises, 366, 367
- See also* Radio astronomy

- Aromatic hydrocarbons, abundance in Murchison meteorite, 253*t*
- Asteroid belt, Solar System, 135
- Asteroids
- carbon chemistry, 242
 - chondritic chemical abundances, 176–177
 - chondritic mineralogic properties, 174
 - evolution, 174–177
 - exogenous delivery of organic matter, 284
 - meteorite-, link, 171–177
 - mineralogy, 171
 - orbits, 172, 173
 - petrographic thin sections in polarized transmitted light, 174, 175
 - source of volatiles for terrestrial planets, 139
 - spectral reflectances, 171–172
- Astrochemistry
- atomic emission spectroscopy, 352–353
 - educational resources, 358*t*
 - infrared resources, 359–360
 - multiwavelength spectroscopy resources, 357
 - stellar evolution resources, 356–357
 - UV/visible and line spectra resources, 358–359
- See also* Molecules in space
- Astronomers, triangulation to measure stars, 330
- Astronomer's periodic table, elements, 15, 84*f*
- Astronomical quantities, sun, 62*t*
- Astronomy
- evolution of ideas, 336*t*
 - ultraviolet-visible spectroscopy, 353–355
- See also* Radio astronomy
- Astrophysics, molecular. *See* Radio astronomy
- Astrospectroscopy, chemistry within molecular clouds, 85
- Asymptotic giant branch (AGB) stars
- complete loss from, 66
 - definition, 391
 - dust grains from, in meteorites, 74–76
 - evolution, 62–64
 - idealized sketch of circumstellar envelopes (CSE), 65*f*
 - mass-loss rates in, by stellar pulsation and grain condensation, 64
 - organic compound production, 255
 - properties, 63*t*
- Ataxites, meteorite classification, 161*f*, 168
- Atmospheres
- extrasolar Earth-like planets, 203–204
- See also* Earth's evolution; Neutral atmospheres; Planetary atmospheres
- Atmospheric chemistry
- impact of volcanic eruptions, 276–279
 - search for proxies, 273
- Atomic emission spectroscopy, astrochemistry, 352–353
- Atomic theory, evolution of ideas, 337*t*
- Australia, stromatolites, 269, 270–272
- Autocatalytic sets. *See* Collectively autocatalytic sets
- B**
- Banded iron formation, sedimentary rocks, 264
- Baryons
- density setting reaction rates, 25
 - neutrons and protons, 17
- See also* WMAP data

Big Bang nucleosynthesis (BBN)
 theory
 basic idea, 18
 comparing light element
 observations with theory, 25–33
 cosmic microwave background
 (CMB), 17–18, 25
 cosmological equations of motion,
 18
 density of baryons and reaction
 rates, 25
 deuterium abundance, 26–27
 elemental abundances, 21
 energy density, 18–19
 formation of deuterium, 19–20
⁴He abundance determinations, 27
 heavier nuclei, 20–21
⁴He mass fraction, 23*f*
³He observations and model, 32–33
 Li observations and model, 28, 30,
 31*f*
 metallicity, 21
 microwave background anisotropy,
 25
 modeling He observations, 28, 29*f*,
 30*f*
 nitrogen and oxygen abundances,
 23*f*
 Nuclear Astrophysics Compilation
 of Reaction Rates (NACRE)
 collaboration, 21, 24
 nuclear network for BBN
 calculations, 22*f*
 predictions of standard, 24*f*
 primordial light element
 abundances by, 34*f*
 primordial mass fraction of ⁴He, 21
 production of elements from, and
 stars, 40, 41*f*
 reactions for tritium and ³He, 20
 Robertson–Walker metric, 18
 space-time metric, 18
 synthesis of light elements, 19
 systematic uncertainties, 27–28,
 29*f*, 30*f*

systematic uncertainty, 31–32
 universe expansion, 330
 Biochemical compounds, prebiotic
 syntheses, 284–286
 Biomolecules, emergence of, 6–7
 Biosphere
 incapacity to prestate evolution of,
 321–322
See also Earth's evolution
 Books, evolution, 340

C

C (carbon) stars
 definition, 392
 elemental abundance classification,
 68
 Calcium-aluminum-rich inclusions
 (CAIs)
 meteorites, 143, 169
 oxygen isotopic record in, 146–147
 oxygen three-isotope diagram from
 Allende CAIs, 129
 oxygen three-isotope diagram
 showing isotopic compositions
 of minerals from Allende CAIs,
 144*f*
 Carbon
 first ionization potential, 149*t*
 meteorite evidence, 149
 pathways between interstellar and
 circumstellar regions, 234*f*
See also Cosmic carbon chemistry
 Carbonaceous chondrites
 abundances of soluble organic
 compounds in Murchison
 meteorite, 253*t*
 analytical protocols and separation
 techniques, 250–251, 251–252
 classification, 248*f*
 enantiomeric excesses in meteoritic
 amino acids, 254
 insoluble organic matter (IOM),
 250–251

- meteorites, 136
- molecular and isotopic
 - characteristics, 251, 252–253
 - organic compounds in, 250–254
 - soluble organic compounds, 251–254
- See also* Extraterrestrial organic chemistry
- Carbonaceous meteorites, carbon chemistry, 241–242
- Carbon burning, stage of stellar burning, 47–48
- Carbon dioxide
 - Mars' atmosphere, 198*t*
 - Venus' atmosphere, 191, 193–194
- Carbon monoxide
 - difference in zero-point energy between ^{12}CO and ^{13}CO , 142
 - photochemical self-shielding, 146
 - ultraviolet photolysis, 145
- Carbon-nitrogen-oxygen (CNO) bi-cycle
 - definition, 392
 - hydrogen burning, 45–46
- Cassini* Saturn orbiter, Titan, 138
- Catalytic chlorine cycle, Venus' atmosphere, 194*t*
- Cauliflower morphology, presolar graphite grains, 75
- Centaur, Solar System, 138–139
- Chapman cycle, Earth's atmosphere, 196, 197*t*
- Chemical abundances. *See* Solar system
- Chemical bonds, evolution of ideas, 336*t*
- Chemical change, evolution of ideas, 335, 338
- Chemical complexity
 - chemical education and future of, 10–11
 - emergence, 323
 - molecular autonomous agents, 318–319
- Chemical composition
 - Jupiter's and Saturn's atmospheres, 199*t*
 - Mars' atmosphere, 198*t*
 - montmorillonites, 302–303
 - terrestrial troposphere, 195*t*
 - Uranus' and Neptune's atmospheres, 201*t*
 - Venus' atmosphere, 192*t*
- Chemical diversity. *See* Solar system
- Chemical education
 - future of chemical
 - complexification, 10–11
 - radio telescopes, 364–366
- Chemical equilibrium abundances, circumstellar molecules, 71, 72*f*
- Chemical evolution
 - astronomer's periodic table of elements, 15
 - available tools, 344–346
 - biomolecules, 6–7
 - emergent events, 6–10
 - Galactic Chemical Evolution Machine, 325*f*, 346, 347*f*
 - natural selection, 9–10
 - online tools, 344–346
 - organized molecular systems, 7–8
 - origin of life, 6–10
 - self-replicating molecular systems, 8–9
 - solar abundances tool, 345–346
 - Solar System, 129
 - teaching, 325
 - tools under development, 347
 - Webnucleo mail list, 348
 - Webnucleo's Nuclear Data Tool, 346
 - Webnucleo's Nuclear Decay Tool, 346
 - See also* Interstellar medium (ISM)
- Chemical origins
 - Big Bang nucleosynthesis (BBN), 17–18
 - cosmic microwave background (CMB), 17–18

- See also* Big Bang nucleosynthesis (BBN) theory
- Chemical principles. *See* Radio astronomy
- Chemistry
 astrochemistry across, curriculum using spectroscopy, 358*t*
 early Earth, 102, 104
 evolution of ideas, 336*t*
See also Systems Chemistry
- Chemistry of Life course
 assessing student's performance, 384–386
 carbon basis of life, 381
 discussion questions, 380–382
 elements of life, 380
 experiments, 383
 introduction, 379
 learning activities, 382–384
 liquid water and life, 380–381
 molecular modeling, 382–383
 NOVA series "Origins", 384
 objectives, 379
 papers and presentations, 384
 readings, 383–384
 role of energy, 381
 simulation software, 383
 students' performance and comments, 386–387
 understanding how life began, 382
- Chlorine cycle, Venus' atmosphere, 194*t*
- Chondrites
 chemical abundances, 176–177
 classification, 161*f*, 169
 class of meteorites, 4
 definition, 392
 gas retention age, 181, 182*f*
 Hf–W evolution of, 214–215
 meteorites, 136
 mineralogic properties, 174, 175
 numbers of classified falls and finds, 164*t*
 silicon-normalized contents of Fe as metal and in FeS vs. Fe in ferromagnesium silicates, 170*f*
 solidification age, 181, 183–185
 unaltered, 4–5
 U–Pb ages of phosphates from ordinary, 184*f*
- Chondrules
 definition, 392
 spherules in meteorites, 136
- Circumstellar chemistry
 abundance ratios of molecules and emitting regions as function of radial distance, 71, 72*f*
 AGB (asymptotic giant branch) stars, 62
 AGB stars by stellar pulsation and grain condensation, 64
 calculated changes in gas chemistry, 66, 67*f*
 circumstellar envelope chemistry (CSE), 68–74
 condensates and condensation temperatures as function of C/O ratio, 69, 70*f*
 dust condensation and thermochemistry, 68–71
 dust grains from AGB stars in meteorites, 74–76
 elemental abundance classification of stars, 66, 68
 giant star evolution, 62–66
 idealized sketch of CSE around AGB star, 65*f*
 mass loss from giant stars, 64
 middle envelope region, 73
 molecules detected in circumstellar shells, 68*t*
 morphology of presolar graphite grains, 75
 outer envelope region, 73–74
 photochemistry of outer envelope region, 73–74
 photosphere and inner CSE, 68–71

- properties of sun and cool AGB stars, 63*t*
- reaction kinetics and dust-gas reactions, 73
- temperatures and densities in circumstellar shell, 69, 71
- useful astronomical quantities, 62*t*
- Circumstellar envelope chemistry (CSE)
 - abundance ratios of molecules and their emitting regions as function of radial distance, 71, 72*f*
 - chemical equilibrium abundances for C-, N-, and O-bearing gases, 71
 - condensates as function of C/O ratio, 69, 70*f*
 - dust condensation and thermochemistry, 68–71
 - middle envelope region, 73
 - outer envelope region, 73–74
 - photochemistry of outer envelope region, 73–74
 - photosphere and inner CSE, 68–71
 - radiation from central star heating dust in, 69
 - reaction kinetics and dust-gas reactions, 73
 - temperature and densities in circumstellar shell, 69, 71
- Circumstellar envelopes (CSE)
 - carbon chemistry, 233, 234*f*, 238
 - clouds of gas, 112, 114
 - definition, 392
 - evolved star CRL 2688, 116
 - processing, 254–255
 - See also* Circumstellar chemistry
- Circumstellar shells, molecules in, 68*t*
- Classification
 - meteorites, 165–169
 - See also* Meteorites
- Clouds
 - dust particles in dense, 83
 - gas phase reactions in, 83
 - infrared spectroscopy of molecular, 85–88, 91
 - planetary systems, 83–84
 - See also* Interstellar medium (ISM)
- Cold Bokkeveld meteorite
 - insoluble organic matter (IOM), 251
 - macromolecular material, 256–257
- Collectively autocatalytic sets
 - origin of molecular reproduction, 314–318
 - See also* Systems Chemistry
- Column density of gas, definition, 189
- Comets
 - carbon chemistry, 241–242
 - comparing interstellar ice components to components of, 90*t*
 - exogenous delivery of organic matter, 284
 - Solar System, 138–139
 - source of volatiles for terrestrial planets, 139
- Competition, natural selection, 10
- Condensates, inner circumstellar envelope (CSE), 68–69, 70*f*
- Constraints, work cycle, 319, 321
- Controversy, first life on Earth, 268–269
- Core formation
 - accretion decreasing with concomitant, 221–222, 224
 - age of moon and W isotope constraints on mechanisms of terrestrial, 224, 227
 - growth curves for Earth, 223*f*
 - Hf–W system dating, 212, 213*f*, 214
 - model ages for Vesta, Mars, Earth and moon, 219–221
 - planetary accretion and, 209–210
 - See also* Hafnium–tungsten chronometry of planetary formation

- Cosmic carbon chemistry
 allotropic forms in space, 233
 circumstellar envelopes, 233, 234*f*, 238
 cycle of, in space, 233, 234*f*
 cycle of birth and death of stars, 236–237
 first stars, 234–237
 formation of elements, 234–237
 from elements to molecules, 237–239
 from interstellar medium to planet formation, 241
 fullerenes, 239, 240*f*
 hyper metal-poor stars (HMPs), 236
 interstellar carbon compounds and abundance, 239
 interstellar clouds, 233, 234*f*, 238
 pathways between interstellar and circumstellar regions, 233, 234*f*
 polycyclic aromatic hydrocarbons (PAHs), 239, 240*f*
 population III stars, 236–237
 relative amount of carbon as function of redshift, 237, 238*f*
 small bodies and extraterrestrial delivery, 241–242
 solar abundances of selected elements, 235*t*
 solar system formation, 233, 234*f*
 synthesis and dispersal of carbon by stars, 235–236
- Cosmic microwave background (CMB)
 backbody radiation in universe, 17–18, 25
See also Big Bang nucleosynthesis (BBN) theory
- Cosmic ray exposure (CRE), "age" of meteorites, 178–179, 180*f*
- Cosmological equations of motion, Big Bang nucleosynthesis, 18
- Cosmology, evolution of ideas, 337*t*
- Craters, meteor forming, 162
- Crust
 first solid on Earth, 263–266
See also Earth's evolution
- Cyanoacetylene (HCCCN)
 Fourier transform microwave (FTMW) spectrometer, 375, 376*f*
 radio astronomy, 366, 368–369
 structure showing bond lengths, 375*f*
See also Radio astronomy
- Cyclical selective processes, Earth mineralogical evolution, 6
- D**
- Darwin
 defining Darwinian adaptation, 321
 preadaptations, 321–322
- Deep-ocean ecosystems, discovery, 7
- Definitions, 391–397
- Deimos, observed and zero-pressure densities, 134*t*
- Densities
 circumstellar shells, 69, 71
 terrestrial bodies, 134*t*
- Deoxyribonucleic acid (DNA), self-replicating system, 9
- Deuterium
 comparing abundance observation with theory, 26–27
 nucleosynthesis chain, 19–20
- Diatomic molecule
 energy levels, 114, 117*f*
 rotational axes, 118*f*
- Dicarboximides, abundance in Murchison meteorite, 253*t*
- Dicarboxylic acids, abundance in Murchison meteorite, 253*t*
- Differentiated meteorites, classification, 167–169
- Differentiation
 chemical, of planet, 209–210

- See also* Hafnium–tungsten chronometry of planetary formation
- Differentiation and outgassing phase, Solar System, 133
- Dowling College, curriculum, 327–328
- Dust, nature of interstellar ice and, 88, 90*f*, 91
- Dust condensation, inner circumstellar envelope, 68–71
- Dust from dead stars. *See* Circumstellar chemistry
- Dust-gas reactions
middle region of circumstellar envelope (CSE), 73
- Dust grains
chemical catalysts, 255
from asymptotic giant branch (AGB) stars in meteorites, 74–76
- DVD, evolution, 341
- Dwarf stars
definition, 393
star evolution, 62
- E**
- Early Earth. *See* Earth's evolution
- Earth
atmosphere, 188, 194–197
Chapman cycle, 196, 197*t*
chemical composition of terrestrial troposphere, 195*t*
core formation ages, 217–221
core formation model ages, 219–221
cyclical selective processes, 6
environments on primitive, 304
FeO contents, 135*t*
granite formation, 5
growth curves for Earth's mantle, 223*f*
interstellar polycyclic aromatic hydrocarbons (PAHs), ices and chemistry of early, 102, 104
major oxygen-bearing species, 196
mineralogical diversity, 5
model age for instantaneous core formation, 220*f*
observed and zero-pressure densities, 134*t*
ozone depletion cycles, 197*t*
photosynthesis, 196
source of N₂, 196
terrestrial stratospheric chemistry, 196
See also Planetary atmospheres
- Earth-like planets
calculated composition of
outgassed atmosphere, 190, 191*f*
extrasolar, 203–204
- Earth science, evolution of ideas, 337*t*
- Earth's evolution
Acasta rocks, 263
argument about nature of Hadean–Archean Earth, 262–263
clues of ancient processes
"proxies", 273
controversy of first life on Earth, 268–269
data on Antarctic ice cores, 277, 278*f*
deducing history of, 262
definitions of quantities describing isotope ratios, 275–276
discovery of anomalous fractionations in sulfur isotopes, 274–275
earliest crust, ocean, life and, 279
first solid crust covering earth, 263–266
geologists and mysteries of ancient Earth, 262
igneous processes, 266
indirect geochemical evidence for liquid water presence, 267–268

- initial oxygenation, 273–279
- liquid water appearance, 266–268
- locations of rock outcrops older than 2.5 Ga (1Ga = 109!), 264*f*
- oldest known rocks on Earth, 263, 264*f*
- oldest known sedimentary rocks, 263–265
- oldest minerals, 265–266
- outline of pillow lavas, 267*f*
- pillow basalts, 266–268
- search for definitive proxies of atmospheric chemistry, 273
- search for surface deposits of anomalous oxygen isotope fractionations, 273–274
- stromatolites throughout geological record, 269, 270, 271, 272
- sulfur aerosols from polar ice-cores, 276*f*
- sulfur isotope anomalous fractionations vs. age, 274*f*
- turbidite sediments, 264–265
- U–Pb isotopic data from oldest zircon crystals, 265*f*
- volcanic eruptions and impact on atmospheric chemistry, 276–279
- zircon crystals, 265
- See also* Chemical evolution
- Ecosystems, discovery of deep-ocean, 7
- Education
 - future of chemical complexification, 10–11
 - spectroscopy exercise, 376–377
 - See also* Chemistry of Life course; Radio astronomy; Resources
- Electromagnetic spectrum
 - atomic emission spectroscopy, 352–353
 - educational resources, 356–360
 - infrared spectroscopy, 355–356
 - line spectra, 352–353
 - observing universe, 350–352
 - UV-visible spectroscopy, 353–355
- Electronic configuration, molecules, 114, 117–119
- Elemental abundance, classification of stars, 66, 68
- Elements
 - astronomer's periodic table of, 15, 84*f*
 - chemical, heavier than lithium by nucleosynthesis in Red Giant stars, 81, 82
 - formation of, in first stars, 234–237
 - from, to molecules, 237–239
 - heaviest, 55–57
 - origin of, on Earth, 332–334
 - proton-capture process, 57
 - rapid "r" process of neutron capture, 56–57
 - slow "s" process of neutron capture, 55–56
 - solar abundances, 235*t*
 - stellar evolution and origin of, 3–4
 - See also* Big Bang nucleosynthesis (BBN) theory; Origin of elements
- Emergence
 - biomolecules, 6–7
 - natural selection, 9–10
 - ordering by process of, 3
 - organized molecular systems, 7–8
 - self-replicating molecular systems, 8–9
- Endogenous synthesis, cycle of stellar birth/death, 105*f*
- Energy, role of, in life, 381
- Energy density, Big Bang nucleosynthesis, 18–19
- Energy levels
 - diatomic molecule, 117*f*
 - polyatomic molecules, 118*f*, 119
 - rotational, 114, 117, 118*f*
- Enstatite (E) chondrites
 - definition, 393
 - meteorites, 136

- Environments
 catalytically active
 montmorillonites, 303–304
 primitive Earth, 304
- Equations of motion, Big Bang
 nucleosynthesis, 18
- Ethane formation, photochemistry on
 giant planets, 202*t*
- Eugene Lang College. *See* Chemistry
 of Life course
- Evolution
 asteroids, 174–177
 books, 340
 chemical change, 335, 338
 courses, 327–328
 Dowling College and curriculum,
 327–328
 educational resources, 356–360
 evolution of ideas, 337*t*
 ideas in science, 335–339
 incapacity to prestate, of biosphere,
 321–322
 mineralogical, and origin of
 planets, 4–6
 resources, 339–341
 solar system, 389–390
 stellar, 356–357
 stellar, and origin of elements, 3–4
 VHS and DVD, 341
See also Chemical evolution;
 Earth's evolution; Universe
- Exogenous delivery, cycle of stellar
 birth/death, 105*f*
- Experiments, Chemistry of Life
 course, 383
- Explosive burning, stage of stellar
 burning, 53–54
- Explosive volcanism, catalytically
 active montmorillonites, 303
- Exposure age, nebula to meteorite,
 155*f*
- Extrasolar Earth-like planets,
 atmospheres, 203–204
- Extraterrestrial organic chemistry
 amino acids, 257–258
 interstellar and circumstellar
 processes, 254–255
 macromolecular materials of
 meteorites, 256–257
 parent body processing, 256–258
 processes for components of
 meteorites, 254
 processing during solar system
 formation, 255–256
 Strecker-cyanohydrin synthesis,
 257, 258*f*
- F**
- FeO contents, terrestrial bodies, 135*t*
- Force, evolution of ideas, 336*t*
- Formation interval, nebula to
 meteorite, 155*f*
- Fossils, microstructures in Archean
 rocks, 268–269
- Fourier transform microwave
 (FTMW) spectroscopy
 cyanoacetylene, 375, 376*f*
 rotational levels of molecules, 120–
 121, 123*f*
 spectrum, 125*f*
- Fuel, stars, 40–42
- Fullerenes
 cosmic carbon chemistry, 239,
 240*f*
 organic compounds from space,
 284
- Fusion crust, meteorites, 162, 163
- Fuzzy stars, universe, 330
- G**
- Galactic Chemical Evolution
 Machine, online tool, 325*f*, 346,
 347*f*
- Galaxy
 chemical evolution, 131
 molecular clouds in, 112, 113

- Galilean family, planetary sub-
nebulae, 137–138
- Gamma rays, observing universe,
350
- Gas abundances, definition, 189
- Gas chemistry, stars, 66, 67*f*
- Gas retention age
"age" of meteorites, 179, 181
nebula to meteorite, 155*f*
- Genetics, self-replicating system, 9
- Geologists, mysteries of ancient Earth,
262
- Geology, evolution of ideas, 337*t*
- Giant planets
ammonia photolysis, 202–203
atmospheres, 200–203
methane photochemistry, 200–202
satellite systems, 137
Solar System, 137
- Giant stars
nucleosynthesis in, 66
organic compound production,
255
- Granite formation, Earth, 5
- Greenberg model, interstellar ice
mantle formation, 103
- H**
- Habitable zones (HZ), definition, 203–
204
- Hadean, definition, 393
- Hadean-Archean Earth, argument
about nature of, 262–263
- Hafnium–tungsten chronometry of
planetary formation
accretion decreasing with
concomitant core formation,
221–222, 224
age of moon on mechanisms of
terrestrial core formation, 224,
227
chemical differentiation of planet,
209–210
- core formation ages vs. degree of
metal-silicate re-equilibration,
225*f*
- core formation model ages of
Vesta, Mars, Earth and moon,
219–221
- extinct ^{128}Hf – ^{182}W system, 210–
214
- giant impacts, 224
- growth curves for Earth, 223*f*
- Hf–W evolution of chondrites,
214–215
- Hf/W ratio in mantle of accreting
planetesimals vs. metal-silicate
re-equilibration during core
formation, 225*f*
- Hf/W ratio of bulk planetary
mantles, 217–218
- Hf–W system dating core
formation, 212, 213*f*, 214
- iron meteorite parent bodies, 215–
217
- melting in interior of planetary
object, 209
- model ages for instantaneous core
formation vs. parent body size,
220*f*
- planetary accretion and core
formation, 209–210
- solar nebula, 209
- tungsten (W) isotope ratios, 212
- Vesta, Mars, Earth and moon, 217–
221
- $^{182}\text{W}/^{184}\text{W}$ ratios of bulk planetary
mantles, 218
- W isotope constraints on
mechanisms of terrestrial core
formation, 224, 227
- W isotope evolution for Earth's
mantle and core, 221–222, 223*f*
- W isotope evolution of Earth's
mantle in two accretion
scenarios, 226*f*
- HCO^+ , molecular spectroscopy, 373–
374

Heavier nuclei, nucleosynthesis, 20–21

Height, definition of pressure scale, 189

Helium
 determination of ^4He mass fraction, 21, 23*f*
 reactions for formation, 20–21
 systematic uncertainties in ^4He abundance, 27–28, 29*f*

Helium burning, stage of stellar burning, 46–47

Hexahedrites, meteorite classification, 161*f*, 168

High resolution laboratory spectroscopy, rotational spectrum, 119–121

Hot desert meteorites, terrestrial age distributions for, 165, 166*f*

Howardites, eucrites, and diogenites (HED) association, meteorites, 168–169

Hubble telescope, immensity of universe, 330

Huygens entry probe, Titan, 138

Hydrogen
 first ionization potential, 149*t*
 meteorite evidence, 150

Hydrogen burning
 carbon-nitrogen-oxygen (CNO) bi-cycle, 45–46
 proton-proton (PP) chains, 43–45
 stage of stellar burning, 42–46

Hydrogen chloride, Venus' atmosphere, 193

Hydrogen cyanide (HCN), radio astronomy, 370–372

Hydrogen fluoride, Venus' atmosphere, 193

Hydrosphere. *See* Earth's evolution

Hydroxycarboxylic acids, abundance in Murchison meteorite, 253*t*

Hyper metal-poor stars (HMPs), early star formation, 236

I

Igneous processes, Earth's oldest rocks and minerals, 266

Infrared (IR) spectroscopy
 astronomy, 355–356
 interstellar ice compositions, 87, 88
 interstellar molecule detection by observational IR, 81
 observing universe, 351
 Orion Constellation, 85–86
 resources, 359–360

Insoluble organic matter (IOM)
 analytical protocol and separation techniques, 250–251
 kerogen, 250
 molecular and isotopic characteristics, 251
See also Meteorites

Interplanetary dust particles (IDPs)
 carbon chemistry, 242
 exogenous delivery of organic matter, 284

Interstellar clouds, carbon chemistry, 233, 234*f*, 238

Interstellar ices
 early Earth, 102, 104
 fluorescence micrograph, 103
 Greenberg model, 103
 high performance liquid chromatography of, residue and extracts from Murchison meteorite, 98–99
 laser desorption mass spectrum, 99–100
 molecular clouds, 85–88, 91
 nature of, and dust, 88, 90*f*, 91
 photochemical evolution, 94–97
 polycyclic aromatic nitrogen heterocycles (PANHs), 101–102

Interstellar medium (ISM)
 astronomer's periodic table of elements, 84*f*
 astrospectroscopy, 85

- attenuation by dust particles in dense clouds, 83
- comparing interstellar ice components to those of several comets, 90*t*
- comparing laboratory analog spectra with spectra from protostar (W33A) embedded in dense molecular cloud, 87, 89*f*
- complex organic production in ices without polycyclic aromatic hydrocarbons (PAHs), 97–100
- complex organic production in ices with PAHs, 100–102
- compounds identified by UV photolysis and warm-up of interstellar ice analogs, 97*f*
- cycle of stellar birth/death, 105*f*
- fluorescence micrograph of droplets from photolysis residue of interstellar/precometary ice analog, 103*f*
- fluorescence micrograph of water insoluble droplets from Murchison meteorite extract, 103*f*
- from, to planet formation, 241
- gas phase reactions in clouds, 83
- Greenberg model of interstellar ice mantle formation and chemical evolution, 103*f*
- high performance liquid chromatography of residue compared to extracts from Murchison meteorite, 99*f*
- history of elements heavier than Li, 81, 82
- ice composition and local conditions, 106
- infrared spectroscopy of molecular clouds, 85–88, 91
- interstellar ice, 85–88, 91
- interstellar ice compositions by infrared (IR) spectra, 87, 88
- interstellar ice photochemical evolution, 94–97
- interstellar PAHs, ices, and chemistry of early Earth, 102, 104
- IR absorption spectra of interstellar clouds, 88*f*
- laser desorption mass spectrum of interstellar ice analog residue, 99–100
- models describing chemistry, 91–92
- nature of interstellar ice and dust, 88, 90*f*, 91
- observational infrared (IR) and radio astronomy, 81
- PAH emission from spiral galaxy, 92
- PAH IR emission features, 93
- photochemical processing of H₂O-rich polar ices, 95–96
- planet formation, 83–85
- polycyclic aromatic hydrocarbons (PAHs), 82, 91, 92, 93
- polycyclic aromatic nitrogen heterocycles (PANHs), 101–102
- processes throughout cloud's lifetime, 91–92
- processing, 254–255
- radio astronomy, 85
- residue after evaporation of volatiles from irradiated ice, 96
- spectral evolution of interstellar ice analog, 94, 95*f*
- types of PAH structures in residue of PAHs UV radiated in water ice, 102*f*
- visible and infrared images of sky toward Orion Constellation, 85–86
- Interstellar molecules, listed by number of atoms, 115*t*
- Io, observed and zero-pressure densities, 134*t*

Iron meteorites, parent bodies, 215–217

Irons

- class of meteorites, 136
- gas retention age, 181
- numbers of classified falls and finds, 164*t*
- properties, 156

Irradiation geometries, molecular clouds, 145–146

Isua, sedimentary rocks, 264

J

Jupiter

- ammonia photolysis, 202–203
- atmosphere, 188
- chemical composition, 199*t*
- Galilean satellites, 137–138
- giant planets, 137
- methane photochemistry, 200–202
- See also* Planetary atmospheres

K

Kerogen, insoluble organic matter (IOM), 250

L

Laboratory

- spectroscopy exercise, 376–377
- See also* Radio astronomy

Laser desorption, interstellar ice analog residue, 99–100

Laws of thermodynamics, origin of life, 332

Life

- discussion questions, 380–382
- Earth and universe, 390
- origin of, in universe, 331–335
- See also* Chemistry of Life course

Life cycle, low mass star, 82

Life on Earth, controversy over first, 268–269

Life sciences, evolution of ideas, 337*t*

Line spectra

- astrochemistry, 352–353
- educational resources, 358–359

Liquid water, first appearance on Earth, 266–268

Lithium

- history of elements heavier than, 81, 82
- model, 28, 30–31
- systematic uncertainties in abundance, 31–32
- systems for observations, 28

Lithosphere. *See* Earth's evolution

Living organisms, debate of stromatolites as evidence, 269, 270–272

Lunar origin, meteorites, 156, 160

M

Macromolecules, complication, 8

Magnesium, meteorite evidence, 150

Mail list, Webnucleo, 348

Mars

- atmosphere, 188, 197–198
- catalytic CO₂ cycle in atmosphere, 198*t*

chemical composition of atmosphere, 198*t*

core formation ages, 217–221

core formation model ages, 219–221

FeO contents, 135*t*

model age for instantaneous core formation, 220*f*

observed and zero-pressure densities, 134*t*

See also Planetary atmospheres

Martian meteorite, fusion crust of Lafayette, 162, 163

- Martian origin, meteorites, 156, 160
- Mechanics, evolution of ideas, 336*t*
- Melting, interior of planetary object, 209
- Mercury
 - atmosphere, 188
 - FeO contents, 135*t*
 - observed and zero-pressure densities, 134*t*
- Metabolism, self-replicating system, 9
- Metabolism first view, origin of life, 315
- Metal ions
 - catalysis of ribonucleic acid (RNA) oligomers, 299
 - template-directed synthesis of RNA, 301
- Metallicity
 - abundance of ^4He as function of, 21, 23*f*
 - definition, 394
- Metal-silicate re-equilibration, accretion and core formation, 222, 223*f*
- Meteor Crator, Flagstaff, Arizona, 162
- Meteorites
 - ablative deceleration, 162
 - achondrites, 156, 161*f*, 164*t*
 - "age", 177–185
 - amino acids, 257–258
 - Antarctica recoveries, 248
 - associations between classes, 167*f*
 - asteroids, 171–177
 - ataxites, 161*f*, 168
 - calcium-aluminum-rich inclusions (CAIs), 143, 144*f*
 - carbon chemistry, 241–242
 - chondrites, 4, 161*f*, 164*t*, 169, 176–177
 - chondritic chemical abundances, 176–177
 - chondritic mineralogic properties, 174
 - classifications, 161*f*, 165–169, 176–177, 247–248
 - collections on Earth, 164–165
 - common types, 157, 158, 159
 - concentrations of cosmic-ray-produced radioactive and stable nuclides during cosmic ray exposure and after, fall to earth, 160*f*
 - cosmic ray exposure (CRE), 178–179
 - crater-forming, 162
 - CRE ages for chondrites, 180*f*
 - definition, 394
 - differentiated meteorites, 167–169
 - dust grains from asymptotic giant branch (AGB) stars in, 74–76
 - enantiomeric excesses in amino acids, 254
 - evolution of asteroids, 174, 176–177
 - fusion crust of Lafayette Martian, 163
 - gas retention age, 179, 181
 - gas retention ages of chondrites, 182*f*
 - general properties, 156, 160, 162, 164–165
 - hexahedrites, 161*f*, 168
 - howardites, eucrites, and diogenites (HED), 168–169
 - igneous achondrites, 168
 - irons, 156, 161*f*, 164*t*
 - large bodies, 170–171
 - Lunar or Martian origin, 156, 160
 - macromolecular material, 256–257
 - mapping Solar System, 167
 - Meteor Crater near Flagstaff, Arizona, 162
 - mineralogy, 171
 - Murchison, 248, 249*f*
 - nebula to, processes, 155*f*
 - numbers of classified falls and finds, 164*t*
 - octahedrites, 161*f*, 168
 - orbits, 172, 173
 - origination, 136

- oxygen, 143, 145–147
 petrographic thin sections in
 polarized transmitted light, 175
 scientific importance, 154, 156
 Shergottites–Nakhilites–Chassigny
 (SNC) association, 168–169
 silicon-normalized contents of Fe
 as metal and in FeS vs. Fe in
 ferromagnesium silicates, 170*f*
 solidification age, 181, 183–185
 spectral reflectances, 171–172
 stony-irons, 156, 161*f*, 164*t*
 Strecker-cyanohydrin synthesis,
 257, 258*f*
 terrestrial age distributions in hot
 deserts, 166*f*
 U–Pb ages of phosphates from
 chondrites, 184*f*
- Methane photochemistry
 ethane formation, 202*t*
 Jupiter, Saturn, Uranus and
 Neptune, 200–202
- Microwaves, observing universe, 351–
 352
- Mineralogical evolution, origin of
 planets, 4–6
- Mineralogy, asteroid-meteorite link,
 171
- Minerals
 carbonaceous chondrite anhydrous
 minerals (CCAM), 129
 definition, 395
 oldest known, on Earth, 265–266
- Models
 evolution of stars, 51, 52*f*
 ³He abundance, 32–33
 ⁴He abundance, 27–28, 29*f*, 30*f*
 lithium abundance, 28, 30–31
 RNA world, 9
- Molecular astrophysics. *See* Radio
 astronomy
- Molecular autonomous agent
 definition, 318
 hypothetical, 320*f*
 molecular reproduction, 319
 work cycle, 319
- Molecular clouds
 complex organic production in ices
 without polycyclic aromatic
 hydrocarbons (PAHs), 97–100
 complex organic production in ices
 with PAHs, 100–102
 definition, 395
 densities, 114
 Galaxy, 112, 113
 high resolution laboratory
 spectroscopy, 119–121, 123*f*
 infrared spectroscopy of, 85–88, 91
 interstellar ice photochemical
 evolution, 94–97
 irradiation geometries, 145–146
 measuring infrared absorption
 spectra, 88
 models describing chemistry, 91–
 92
 processes throughout lifetime, 91–
 92
 spectra of protostar embedded
 within, 87, 89*f*
 star formation, 141–142
 typical searches, 127–128
 See also Interstellar medium (ISM)
- Molecular modeling, Chemistry of
 Life course, 382–383
- Molecular reproduction, origins,
 collectively autocatalytic sets, 314–
 318
- Molecular selection, process, 9–10
- Molecular systems
 emergence of organized, 7–8
 emergence of self-replicating, 8–9
- Molecules
 circumstellar shells, 68*t*
 formation and evolution of
 complex, in space, 254–258
 from elements to, 237–239
 yields of amino acids and small,
 from neutral atmospheres, 287*t*
 See also Extraterrestrial organic
 chemistry

- Molecules in space
- atomic energy levels, 114, 117
 - circumstellar envelope of evolved star CRL 2688, 116
 - circumstellar envelopes, 112, 114
 - densities of molecular clouds, 114
 - detection, 112, 114, 117, 119
 - diagram of direct absorption system, 120*f*
 - direct absorption, 120
 - discharges in reactor flow oven and supersonic jet expansion, 121, 122
 - distribution of molecular clouds in galaxy, 112, 113
 - early study of stars and nebulae, 112
 - energy levels of diatomic molecule, 117*f*
 - Fourier transform microwave (FTMW) spectroscopy, 120–121, 123*f*
 - high resolution laboratory spectroscopy, 119–121
 - known interstellar, by number of atoms, 115*t*
 - millimeter radio telescope, 124
 - molecular rotational levels, 114, 117, 118*f*
 - radio astronomical spectra, 126–127
 - radio astronomy as analytical tool, 123–128
 - rotational energy level diagrams for CO and CH₂OHCHO, 118*f*
 - rotation of polyatomic species, 119
 - schematic of FTMW spectrometer, 123*f*
 - signal-averaging, 126
 - sky frequency, 125
 - spectra towards molecular cloud in Galactic Center, 119*f*
 - spectrum with FTMW spectrometer, 125*f*
 - surprising complexity, 112
 - typical molecular clouds in searches, 127–128
 - unraveling interstellar spectra, 127*f*, 128
- Mono-carboxylic acids, abundance in Murchison meteorite, 253*t*
- Montana montmorillonites, environments producing, 303
- Montmorillonites
- catalysis of ribonucleic acid (RNA) oligomers, 299–300
 - chemical compositions, 302–303
 - definition, 395
 - environments producing catalytically active, 303–304
 - primitive Earth environments, 304
- Moon
- core formation ages, 217–221
 - core formation model ages, 219–221
 - FeO contents, 135*t*
 - model age for instantaneous core formation, 220*f*
 - observed and zero-pressure densities, 134*t*
- Morphology, presolar graphite grains, 75
- Motion, evolution of ideas, 336*t*
- M stars
- definition, 394
 - elemental abundance classification, 66
- Multiwavelength spectroscopy, educational resources, 357
- Murchison meteorite
- α -aminoisobutyric acid (AIB), 253
 - abundances of soluble organic compounds in, 253*t*
 - carbonaceous chondrite in Australia, 248, 249*f*
 - comparing residues from interstellar ice to extract from, 98–99
 - detection of diamino acids, 257–258

enantiomeric excesses in meteoritic amino acids, 254
 fluorescence micrograph, 103
 insoluble organic matter (IOM), 251
 macromolecular material, 256–257

N

Natural selection, emergence of, 9–10

Nebular Hypothesis, elements on Earth, 333–334

Nebular phase, Solar System, 132–133

Neon burning, stage of stellar burning, 48–49

Neptune

ammonia photolysis, 202–203
 atmosphere, 188
 chemical composition of atmosphere, 201*t*
 giant planets, 137
 methane photochemistry, 200–202
 trans-Neptunian objects, 138–139
See also Planetary atmospheres

Neutral atmospheres

abiotic syntheses in, 286, 289
 high performance liquid chromatography of derivatized amino acids from spark discharge reactions, 290*f*
 spark discharge apparatus, 286, 288
 yields of amino acids and small molecules from, 287*t*
See also Atmospheres

N-heteroaromatic compounds,

abundance in Murchison meteorite, 253*t*

Nitrogen

Earth's atmosphere, 196
 element abundances, 21, 23*f*
 first ionization potential, 149*t*
 isotope abundance in Solar System materials, 148*f*

photochemistry in Solar System, 147–149

Nuclear Astrophysics Compilation of Reaction Rates (NACRE) collaboration

abundance predictions, 21, 24

Nuclear burning. *See* Nucleosynthesis in stars

Nuclear Data Tool, Webnucleo, 346

Nuclear Decay Tool, Webnucleo, 346

Nuclear fusion, solar system, 41–42

Nuclear network, Big Bang nucleosynthesis (BBN), 22*f*

Nucleosides, ribonucleic acid (RNA) world scenario, 297–298

Nucleosynthesis in stars

carbon burning, 47–48
 carbon-nitrogen-oxygen (CNO) bi-cycle, 45–46
 definition, 395
 elements heavier than lithium by, 81, 82
 explosive burning, 53–54
 fuel of stars, 40–42
 heaviest elements, 55–57
 helium burning, 46–47
 hydrogen burning, 42–46
 model of star evolution, 52*f*
 nebula to meteorite, 155*f*
 neon burning, 48–49
 oxygen burning, 49–50
 production of elements, 40, 41*f*
 proton-capture "p" process, 57
 proton-proton (PP) chains of hydrogen burning, 43–45
 rapid "r" process of neutron capture, 56–57
 silicon burning, 50–51
 slow "s" process of neutron capture, 55–56
 stages of stellar burning and products, 42–55
 stellar burning lifetimes, 51–53
 supernova classification, 54–55

- Nucleotides, ribonucleic acid (RNA)
world scenario, 297–298
- Number density of gas, definition, 189
- O**
- Oceans, compositional changes, 5
- Octahedrites, meteorite classification,
161*f*, 168
- Onion morphology, presolar graphite
grains, 75
- Online tools
available, 344–346
Galactic Chemical Evolution
Machine, 325*f*, 346, 347*f*
under development, 347
understanding Galaxy, 343–344
Webnucleo mail list, 348
Webnucleo's Nuclear Data Tool,
346
Webnucleo's Nuclear Decay Tool,
346
Webnucleo's Solar Abundances
Online Tool, 345–346
- Orbits, asteroid-meteorite link, 172,
173
- Ordering
process of emergence, 3
Organic chemistry. *See*
Carbonaceous chondrites;
Extraterrestrial organic
chemistry
- Organic matter, exogenous delivery
from space, 284
- Organic production
cycle of stellar birth/death, 105*f*,
236–237
ices without polycyclic aromatic
hydrocarbons (PAHs), 97–100
ices with PAHs, 100–102
- Organic synthesis
geochemical, 7
"home-grown" prebiotic syntheses,
284–286
- Organisms
characteristics of known living,
332
Darwinian preadaptations, 322
debate of stromatolites as evidence
of life, 269, 270–272
- Organization, propagating, of process,
319, 321
- Organized molecular systems,
emergence of, 7–8
- Orgueil meteorite
amino acid analysis, 258
insoluble organic matter (IOM),
251
macromolecular material, 256–257
- Origin of elements
carbon burning, 47–48
carbon-nitrogen-oxygen (CNO)
burning, 45–46
explosive burning, 53–54
fractional abundance of elements in
solar system, 41*f*
fuel of stars, 40–42
further reading, 58
heaviest elements, 55–57
helium burning, 46–47
hydrogen burning, 42–46
model of evolution of star, 52*f*
neon burning, 48–49
nuclear burning, 42
oxygen burning, 49–50
proton-capture "p" process, 57
proton-proton (PP) chains, 43–45
rapid "r" process of neutron
capture, 56–57
silicon burning, 50–51
slow "s" process of neutron
capture, 55–56
stellar burning lifetimes, 51–53
stellar evolution and, 3–4
supernova classification, 54–55
- Origin of life
age-old question, 389–390
chemical evolution and, 6–10
chemistry of early Earth, 283

- deciding on important properties, 294
- interdisciplinary fields of study, 293–294
- laws of thermodynamics, 332
- prebiotic soup theory, 283–284
- ribonucleic acid (RNA) world scenario, 294–295, 304–305
- structures of RNA and DNA, 295*f*
- universe, 331–335
- See also* Chemistry of Life course; Ribonucleic acid (RNA) world scenario
- Origin of planets, mineralogical evolution and, 4–6
- Orion, molecular cloud, 142
- Orion Constellation, visible and infrared images of sky, 85–86
- Oxygen
 - element abundances, 21, 23*f*
 - evolution of oxygenated Earth's atmosphere, 273–279
 - first ionization potential, 149*t*
 - solar system photochemistry, 143, 145–147
 - three-isotope diagram, 129
- Oxygen burning, stage of stellar burning, 49–50
- Oxygen isotopes, varying with time, 325*f*, 347*f*
- Ozone, abiotic production, 142
- Ozone depletion, Earth's atmosphere, 197*t*

- P**

- Parent body processing, meteorites, 256–258
- Pb/Pb method, solidification age, 181, 183
- Periodic table
 - astronomer's, of elements, 15, 84*f*
 - origin of elements, 3–4
- Phobos, observed and zero-pressure densities, 134*t*
- Phospholipid molecules, self-organization, 8
- Photochemical evolution, interstellar ice, 94–97
- Photochemical self-shielding, carbon monoxide, 146
- Photochemistry, outer region of circumstellar envelope (CSE), 73–74
- Photochemistry in early Solar System
 - abiotic production of ozone, 142
 - carbon, 149
 - first ionization potentials of H, C, H, O, 149*t*
 - formation of stars, 141–142
 - hydrogen, 150
 - irradiation geometries of solar nebula, 145–146
 - magnesium, 150
 - nitrogen, 147–149
 - nitrogen isotope abundances in Solar System materials, 148*f*
 - other elements, 149–150
 - oxygen, 143, 145–147
 - oxygen isotopic record in CAIs, 146–147
 - oxygen three-isotope diagram showing isotopic compositions of minerals from Allende CAIs, 144*f*
 - self-shielding of CO consequences, 146
 - silicon, 150
 - statistical mechanical theory, 145
 - sulfur, 150
 - ultraviolet photolysis of carbon monoxide, 145
 - ultraviolet sunlight effects on planetary atmospheres, 142–143
- Photosphere
 - definition, 395
 - inner circumstellar envelope (CSE), 68–71

- Photosynthesis, Earth's atmosphere, 196
- Pillow basalts
 definition, 396
 liquid water on Earth's surface, 266–268
- Planetary accretion, and core formation, 209–210
- Planetary atmospheres
 catalytic chlorine cycle for Venus, 194*t*
 catalytic CO₂ cycle on Mars, 198*t*
 chemical composition of Jupiter and Saturn, 199*t*
 chemical composition of Mars' atmosphere, 198*t*
 chemical composition of terrestrial troposphere, 195*t*
 chemical composition of Uranus and Neptune, 201*t*
 chemical composition of Venus, 192*t*
 definitions, 188–189
 Earth, 194–197
 ethane formation from methane, 202*t*
 extrasolar Earth-like planets, 203–204
 gas giant planets, 200–203
 Mars, 197–198
 methane photochemistry of Jupiter, Saturn, Uranus, and Neptune, 200–202
 NH₃ photolysis on Jupiter, Saturn, Uranus, and Neptune, 202–203
 outgassed atmosphere for Earth-like planet, 190, 191*f*
 ozone depletion cycles in Earth, 197*t*
 physical properties of, 189*t*
 range within solar system, 188
 reaction cycle for N₂ formation in gas giants, 203*t*
 Venus, 190–194
- Planetary mantles, core formation ages, 217–221
- Planetary sub-nebulae, Galilean family, 137–138
- Planetesimals, protoplanetary environment form, 4
- Planet formation
 cycle of stellar birth/death, 105*f*
 from interstellar medium to, 241
 molecular clouds, 83–84
See also Hafnium–tungsten chronometry of planetary formation
- Planets, mineralogical evolution and origin of, 4–6
- Plate tectonics, subduction, 5–6
- Plurality of worlds, Solar System, 131
- Pluto, atmosphere, 188
- Polyatomic molecules, energy levels, 118*f*, 119
- Polycyclic aromatic hydrocarbons (PAHs)
 carbon-rich stars, 82
 complex organic production in ices with, 100–102
 complex organic production in ices without, 97–100
 cosmic carbon chemistry, 239, 240*f*
 distribution of PAH emission from spiral galaxy, 92
 interstellar, of early Earth, 102, 104
 interstellar PAHs, 91
 IR emission spectra from interstellar PAHs, 93
 organic compounds from space, 284
See also Interstellar medium (ISM)
- Polycyclic aromatic nitrogen heterocycles (PANHs), interstellar ice analogs, 101–102
- Preadaptations, Darwinian, of organisms, 322
- Prebiotic soup theory, origin of life, 283–284
- Prebiotic syntheses

- home-grown, 284–286
 - ribonucleic acid (RNA) monomers, 296–297
 - Presolar grains
 - asymptotic giant branch (AGB) stars, 74–76
 - morphology, 75
 - Pressure, definition, 189
 - Pressure scale height, definition, 189
 - Process, propagating organization of, 319, 321
 - Proton-capture process, heaviest elements, 57
 - Proton-proton (PP) chains, hydrogen burning, 43–45
 - Proxies, clues of ancient processes, 273
 - Purine bases, ribonucleic acid (RNA) monomers, 296–297
 - Pyrimidine bases, ribonucleic acid (RNA) monomers, 296–297
- Q**
- Quantum mechanics
 - molecular detection, 112, 114, 117, 119
 - See also* Molecules in space
- R**
- Radiation, central star heating dust in circumstellar envelope, 69
 - Radio astronomy
 - analytical tool, 123–128
 - Arizona Radio Observatory (ARO) on Kitt Peak, Arizona, 366, 367
 - chemical education instruments, 364–366
 - combined lab/astronomical study of HCO^+ , 374*f*
 - cyanoacetylene (HCCCN) showing bond lengths, 375*f*
 - describing rotation spectrum, 368
 - educational level, 376–377
 - graduate students, 367
 - heterodyne mixing, 365–366
 - high electron mobility transistor (HEMT) amplifier, 365*f*
 - interstellar molecule detection, 81
 - $J = 2 \rightarrow 1$ transition of HCC^{13}CN , 376*f*
 - laboratory exercises, 364
 - laboratory for detection of interstellar molecules, 373–376
 - laboratory for molecular astrophysics, 366, 368–373
 - measuring spectrum of HCCCN, 375
 - millimeter, 124
 - molecular clouds, 85
 - operational modifications, 376–377
 - quadrupole parameter, 371
 - schematic of detection system, 365*f*
 - spectra of $J = 1 \rightarrow 0$ transition of HCN towards molecular clouds, 371*f*
 - spectra of $J = 9 \rightarrow 8$ and $J = 17 \rightarrow 16$ transitions of HCCCN towards molecular cloud, 368*f*
 - spectrum of $J = 2 \rightarrow 1$ transition of SiO towards star, 372*f*
 - spectrum of $J = 8 \rightarrow 7$ transition of CH_3CN towards molecular cloud, 369*f*
 - superconducting mixers, 365
 - Radionuclides, decay products of extinct, 184–185
 - Radio telescope, sky frequency, 125
 - Radiowaves, observing universe, 352
 - Rapid "r" neutron capture
 - definition, 396
 - heaviest elements, 56–57
 - Reaction graphs
 - carbon, hydrogen, nitrogen, oxygen, phosphorus, and sulphur (CHNOPS) vast, 311, 313

- hypothetical network of chemical reactions, 312*f*
 - vast and under-populated chemical, 311–314
 - See also* Systems Chemistry
 - Reaction kinetics, middle region of circumstellar envelope (CSE), 73
 - Red giant stars
 - definition, 396
 - elements heavier than lithium by nucleosynthesis in, 81, 82
 - evolution, 62
 - Resources
 - astrochemistry across chemistry curriculum using spectroscopy, 358*t*
 - evolution, 339–341
 - infrared, 359–360
 - multiwavelength spectroscopy, 357
 - stellar evolution, 356–357
 - UV/visible and line spectra, 358–359
 - Ribonucleic acid (RNA)
 - RNA world model, 9, 315
 - self-replicating system, 9, 315
 - Ribonucleic acid (RNA) world scenario
 - adenine formation, 297*f*
 - catalysis of RNA oligomer formation, 299–300
 - catalysis of template-directed synthesis, 301
 - chemical compositions of montmorillonites, 302–303
 - current status, 304–305
 - environments on primitive Earth, 304
 - environments producing catalytically active montmorillonites, 303
 - formation of adenine and pyrimidines by hydrolysis, 296*f*
 - metal ion catalysis for RNA oligomer formation, 299
 - montmorillonite catalysis for RNA oligomer formation, 299–300
 - nucleosides, nucleotides and activated nucleotides, 297–298
 - origins of life, 9, 294–295, 315
 - prebiotic synthesis of RNA monomers, 296–297
 - purine and pyrimidine bases, 296–297
 - pyrimidine formation, 297*f*
 - ribose, 297, 298*f*
 - selectivity in oligomers formed by template-derived catalysis, 301–302
 - Ribose, ribonucleic acid (RNA) world scenario, 297, 298*f*
 - Robertson–Walker metric, Big Bang nucleosynthesis, 18
 - Rocks
 - oldest known, on Earth, 263, 264*f*
 - See also* Earth's evolution
 - Rotational levels
 - energies of molecular, 114, 117, 118*f*
 - Fourier transform microwave (FTMW) spectroscopy, 120–121
 - spectrum with FTMW spectrometer, 125*f*
- S**
- Satellite systems, giant planets, 137
 - Saturn
 - ammonia photolysis, 202–203
 - atmosphere, 188
 - chemical composition, 199*t*
 - giant planets, 137
 - methane photochemistry, 200–202
 - Titan, 138
 - See also* Planetary atmospheres
 - Science
 - books, 340
 - chemical change, 335, 338
 - evolution of ideas, 335–339

- evolution of ideas across sciences, 336*t*, 337*t*
- resources, 339–341
- VHS and DVD, 341
- Science, Technology and Society (STS) program. *See* Chemistry of Life course
- Sedimentary rocks, oldest known, 263–265
- Selection
 - process, 10
 - See also* Natural selection
- Self-organization, phospholipid molecules, 8
- Self-replicating molecular systems
 - competition, 10
 - emergence of, 8–9
- Separation techniques
 - insoluble organic matter (IOM), 250–251
 - soluble organic compounds, 251–252
- Shergottites–Nakhilites–Chassigny (SNC) association, meteorites, 168–169
- Silicon, meteorite evidence, 150
- Silicon burning, stage of stellar burning, 50–51
- Silicon monoxide (SiO), radio astronomy, 372
- Simulation software, Chemistry of Life course, 383
- Sky frequency, radio telescope, 125
- Slow "s" neutron capture
 - definition, 397
 - heaviest elements, 55–56
- Slow s-process elements, asymptotic giant branch (AGB) stars, 62
- Software, Chemistry of Life course, 383
- Solar Abundances Online Tool, Webnucleo, 345–346
- Solar nebula, accretion of Earth, 209
- Solar System
 - accretionary phase, 133
 - asteroid belt, 135
 - asteroids, 139
 - centaurs, 138–139
 - chemical evolution, 129
 - comets, 138–139
 - densities of terrestrial bodies, 134*t*
 - differentiation and outgassing phase, 133
 - early history of, 4
 - FeO contents of terrestrial bodies, 135*t*
 - formation, 234*f*, 389–390
 - fractional abundance of elements, 40, 41*f*
 - Galilean family, 137–138
 - giant planets, 137
 - history of material of, 131–132
 - meteorite connection, 136
 - meteorites mapping, 167
 - nebular phase, 132–133
 - planetary sub-nebulae, 137–138
 - "plurality of worlds", 131
 - processing during, formation, 255–256
 - satellite systems of giant planets, 137
 - sources of volatiles for terrestrial planets, 139
 - terrestrial planet region, 134–135
 - Titan, 138
 - trans-Neptunian objects, 138–139
 - See also* Interstellar medium (ISM); Photochemistry in early Solar System
- Solar system astronomy, evolution of ideas, 336*t*
- Solidification age
 - "age" of meteorites, 181, 183–185
 - nebula to meteorite, 155*f*
- Soluble organic compounds
 - analytical procedures and separation techniques, 251–252
 - enantiomeric excesses in meteoritic amino acids, 254

- molecular and isotopic characteristics, 252–523
- See also* Meteorites
- South Dakota montmorillonites, environments producing, 303
- Space
 - organic compounds from, 284
 - See also* Molecules in space
- Spacecraft missions, extrasolar Earth-like planets, 203–204
- Space-time metric, Big Bang nucleosynthesis, 18
- Spectral reflectance, asteroid-meteorite link, 171–172
- Spectroscopy
 - astrochemistry, 358*t*
 - astrochemistry across chemistry curriculum using, 358*t*
 - atomic emission, 352–353
 - detecting interstellar molecules, 373–376
 - educational resources, 356–360
 - infrared, 355–356
 - line spectra, 352–353, 358–359
 - multiwavelength, 357
 - observing universe, 350–352
 - stellar evolution, 356–357
 - UV-visible, 353–355, 358–359
 - See also* Radio astronomy
- S stars
 - definition, 396
 - elemental abundance classification, 66, 68
- Standard Model physics, Big Bang nucleosynthesis (BBN), 17
- Stars
 - cycle of birth and death, 236–237
 - cycle of stellar birth/death, 105*f*
 - elemental abundance classification of, 66, 68
 - elements heavier than lithium by nucleosynthesis in red giant (RG), 81, 82
 - first, 234–237
 - formation, 141–142, 255–256
 - formation of elements, 234–237
 - fuel of, 40–42
 - fuzzy, 330
 - gas chemistry, 66, 67*f*
 - hyper metal-poor stars (HMPs), 236
 - life cycle of low mass, 82
 - low-mass dwarf, 62
 - model of evolution of, 52*f*
 - population III, 236–237
 - red giant (RG), 62
 - stellar evolution resources, 356–357
 - See also* Circumstellar chemistry; Nucleosynthesis in stars
- Stellar burning
 - lifetimes, 51–53
 - stages, 42–51
 - See also* Nucleosynthesis in stars
- Stellar evolution
 - educational resources, 356–357
 - origin of elements, 3–4
- Stones, class of meteorites, 136
- Stony-irons
 - class of meteorites, 136
 - numbers of classified falls and finds, 164*t*
 - properties, 156
- Stromatolites, geologic record, 269, 270–272
- Structure of matter, evolution of ideas, 337*t*, 338–339
- Student's performance, Chemistry of Life course, 384–386
- Subduction, plate tectonics, 5–6
- Sugar-related compounds, abundance in Murchison meteorite, 253*t*
- Sulfur, meteorite evidence, 150
- Sulfur dioxide, Venus' atmosphere, 193
- Sulfur isotope anomalous fractionations
 - definitions of quantities, 275–276
 - discovery, 274–275
 - ice core record, 278*f*

- plotted vs. age, 274*f*
- production by ultraviolet light, 275
- sulfate aerosols from polar ice-cores, 276
- volcanic eruptions, 276–278
- See also* Earth's evolution
- Sulphonic acids, abundance in Murchison meteorite, 253*t*
- Sun
 - astronomical quantities, 62*t*
 - giant planets, 137
 - properties, 63*t*
- Supernova, elements on Earth, 333
- Supernova classification, stellar burning, 54–55
- Surface deposits, search for anomalous oxygen isotope fractionations, 273–274
- Systems Chemistry
 - carbon, hydrogen, nitrogen, oxygen, phosphorus, and sulphur (CHNOPS) vast reaction graph, 311, 313
 - collective autocatalytic set, 315–318
 - defining chemical "Actual" and "Adjacent Possible", 313
 - emerging area, 311
 - incapacity to prestate evolution of biosphere, 321–322
 - molecular autonomous agents, 318–319, 320*f*
 - molecular reproduction origin, 314–318
 - origin of life views, 314–315
 - propagating organization of process, 319, 321
 - reaction graph, 312*f*
 - topics, 311
 - typical autocatalytic set, 317*f*
 - vast chemical reaction graphs, 311–314
- T
- Teaching
 - chemical evolution, 325
 - See also* Radio astronomy
- Temperatures
 - circumstellar shells, 69, 71
 - planetary atmospheres, 189*t*
- Template-directed synthesis
 - metal ion catalysis of ribonucleic acid (RNA) oligomer, 301
 - selectivity in oligomer formation, 301–302
- Terrestrial age
 - hot desert meteorites, 165, 166*f*
 - nebula to meteorite, 155*f*
- Terrestrial bodies
 - densities, 134*t*
 - FeO contents, 135*t*
- Terrestrial planet region, Solar System, 134–135
- Terrestrial planets, sources of volatiles for, 139
- Thermochemistry, inner circumstellar envelope (CSE), 68–71
- Titan, Solar System, 138
- Tools. *See* Online tools
- Triangulation, measuring distances to stars, 330
- Tritium, reactions for formation, 20
- Tungsten isotopes
 - accretion decreasing with concomitant core formation, 221–222, 224
 - age of moon and, constraints on terrestrial core formation, 224, 227
 - core formation ages vs. metal-silicate re-equilibration, 225*f*
 - evolution for Earth's mantle and core, 223*f*
 - evolution in chondrites, 212, 213*f*
 - evolution of Earth's mantle in different accretion scenarios, 226*f*

- great impacts, 224
 - growth curves for Earth, 223*f*
 - See also* Hafnium–tungsten
chronometry of planetary
formation
 - Turbidite sediments
 - definition, 397
 - sedimentary rocks, 264–265
 - See also* Earth's evolution
- U**
- Ultraviolet photolysis, carbon
monoxide, 145
 - Ultraviolet sunlight
 - effects on planetary atmospheres,
142–143
 - See also* Photochemistry in early
Solar System
 - Ultraviolet/visible spectroscopy
 - astronomy, 353–355
 - educational resources, 358–
359
 - observing universe, 351
 - Universe
 - evolution, 328
 - expansion, 330
 - fundamental parts, 328–329
 - history of, 3
 - life, 331–335
 - life on Earth and elsewhere,
390
 - observing, across electromagnetic
spectrum, 350–352
 - reassembling, 329–330
 - See also* Evolution
 - Uranus
 - ammonia photolysis, 202–203
 - chemical composition of
atmosphere, 201*t*
 - giant planets, 137
 - methane photochemistry, 200–
202
 - See also* Planetary atmospheres

V

- Variation, process, 10
 - Venus
 - atmosphere, 188, 190–194
 - catalytic chlorine cycle in
atmosphere, 194*t*
 - chemical composition of
atmosphere, 192*t*
 - CO₂ conversion, 193–194
 - CO₂ pressure, 191, 193
 - FeO contents, 135*t*
 - hydrogen chloride and HF, 193
 - observed and zero-pressure
densities, 134*t*
 - sulfur dioxide, 193
 - See also* Planetary atmospheres
 - Vessicle first theory, origin of life,
315
 - Vesta
 - core formation ages, 217–221
 - core formation model ages, 219–
221
 - model age for instantaneous core
formation, 220*f*
 - VHS, evolution, 341
 - Volcanic eruptions
 - Antarctic ice cores, 277, 278*f*
 - impact on atmospheric chemistry,
276–279
 - lava from Hawaiian Pu'u'O'o, 266–
267
- W**
- Water, first appearance on Earth, 266–
268
 - Webnucleo
 - mail list, 348
 - online tools, 344–346
 - Western Australia, stromatolites, 269,
270–272
 - WMAP data
 - baryon density determination, 25

- ^3He abundance, 32–33
 - ^4He abundance, 28
 - ^7Li abundance, 30, 32
 - primordial light element abundance
 - predictions, 34*f*
 - Work cycles
 - living cells, 319
 - molecular autonomous agents, 318–319, 320*f*
 - Wyoming-type montmorillonites
 - environments producing, 303
 - primitive Earth environments, 304
- X**
- X-rays, observing universe, 351
- Z**
- Zircon crystals
 - definition, 397
 - oldest minerals on Earth, 265–266

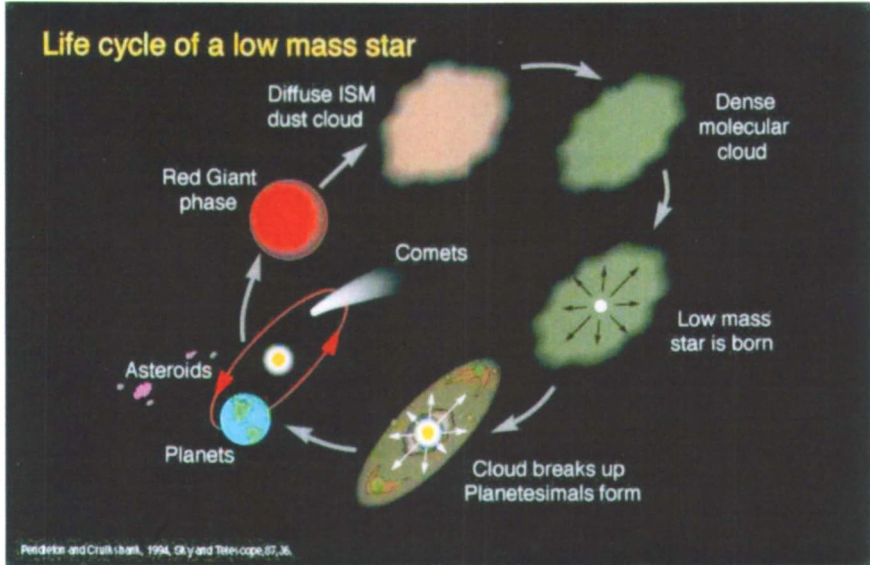


*Plate 5.1. The chemical elements heavier than Lithium are produced by nucleosynthesis in Red Giant stars and injected into the interstellar medium during the Red Giant phase. Once in the interstellar medium, they participate in the chemistry at each stage of this cycle. These objects are not drawn to scale. A Red Giant can swell to sizes that engulf the inner planets of our Solar System. The diffuse ISM can be as vast as the space between the spiral arms of our Galaxy, The Milky Way, while molecular clouds measure from hundreds to hundreds of thousands of light years across. There are many star forming regions in molecular clouds, each several times the size of the Solar System.
Plate reproduced with permission from (12).*

2 - Color inserts

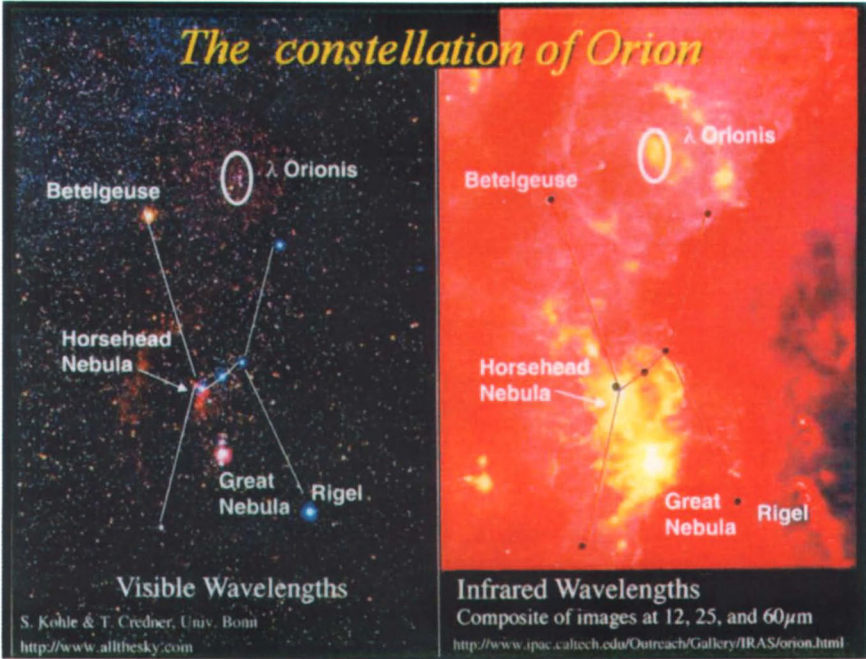


Plate 5.2. Visible and infrared images of the sky toward the Orion Constellation. Left: Visible Image. The white lines indicate the main stars of the well-known constellation. Right: The Infrared Astronomical Satellite IR image of the same region of the sky. The interconnected dark circles indicate the positions of the now invisible constellation stars. The reddish glow is from the dust in this enormous cloud which is many thousands of light years across. The yellow areas correspond to emission from the warmest dust, generally regions illuminated by light from nearby stars. Clouds such as these are the birthplace of stars and planets and are home to complex interstellar molecules. In this case the cloud is behind the stars that make up the constellation. Otherwise this would appear as a dark patch in the night sky. Plate courtesy of Dr. Andrew Mattioda

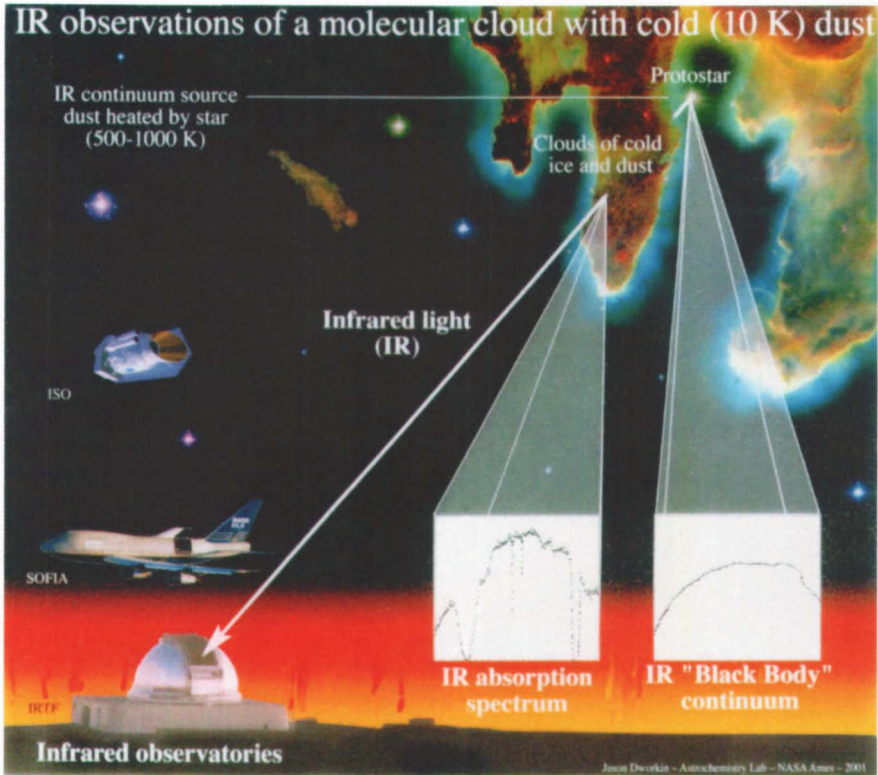


Plate 5.3. An illustration of how one measures the IR absorption spectra of interstellar clouds. A background star (protostar) serves as the IR source, the cloud is the sample, and the telescope gathers the light and sends it to a monochromator or spectrometer. The advent of airborne IR telescopes in the 70's and orbiting telescopes in the 80's made it possible to avoid IR absorptions by atmospheric H_2O , CO_2 , and so on, opening a new window into the Cosmos. Plate courtesy of Dr. Jason Dworkin.

4 - Color inserts

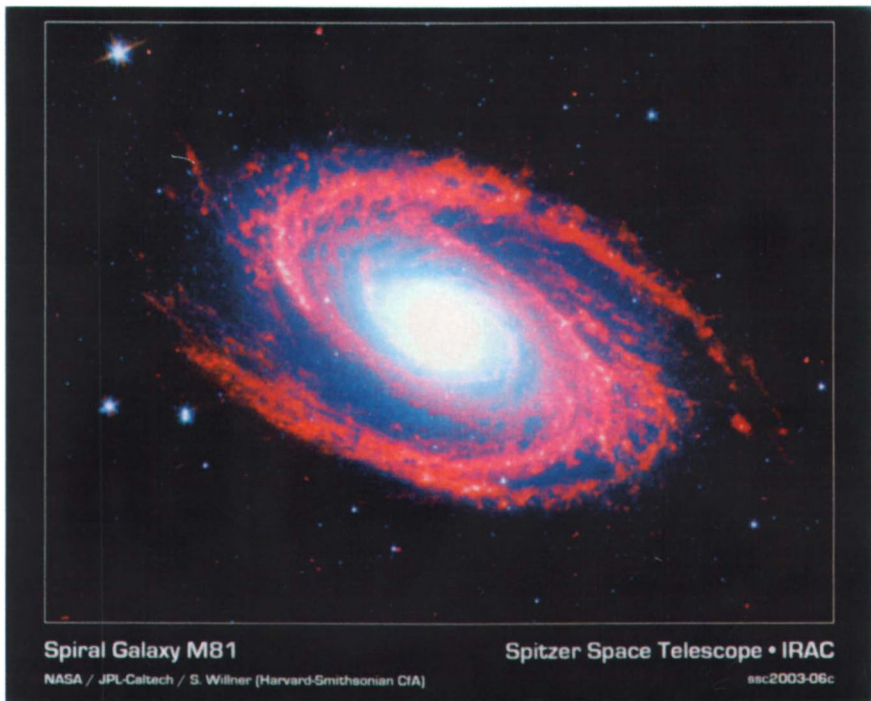


Plate 5.4. Spitzer Space Telescope IR image of M 81. The red color traces the strong PAH emission band between about 7 and 9 μm shown in Plate 5.5.

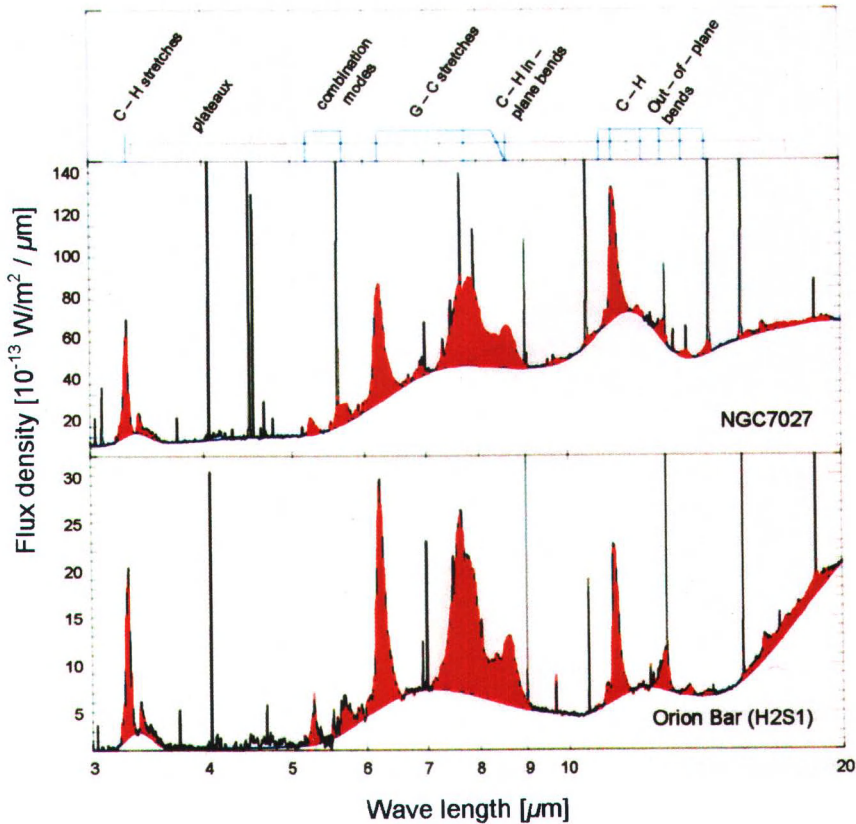


Plate 5.5. Two examples of the IR emission spectra from interstellar PAHs. The upper spectrum is of PAHs that were "freshly" ejected from a Red Giant. The lower spectrum is from the Great Nebula in the Orion molecular cloud (Figure 3, bottom, center, both panels) where it is exposed to the intense UV field from hot, young stars. The red features are all attributed to PAHs. The fundamental vibrations which produce the features are summarized across the top of the figure. The underlying broad structure is thought to arise from overlapping individual bands from PAHs and larger species. The variations between spectra reveal differences in the PAHs present in each object, reflecting the unique chemical history and conditions within the PAH emission region. Plate courtesy of Dr. Els Peeters, see reference (29). PAH structures are shown in Figure 8.

6 - Color inserts

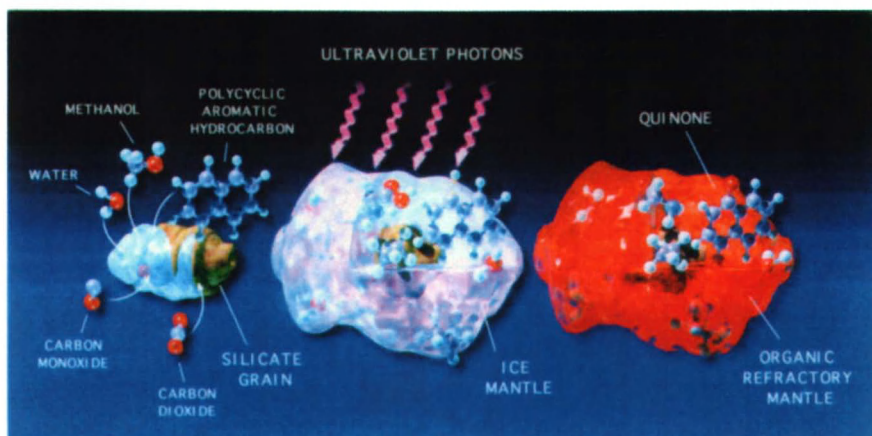


Plate 5.6. The Greenberg model of interstellar ice mantle formation and chemical evolution. The mantle grows by condensation of gas phase species onto the cold dust grains. Simultaneously, surface reactions between these species, ultraviolet radiation and cosmic ray bombardment drive a complex chemistry. These ice-mantled grains are thought to be micron sized at most. Plate reproduced with permission from (37).

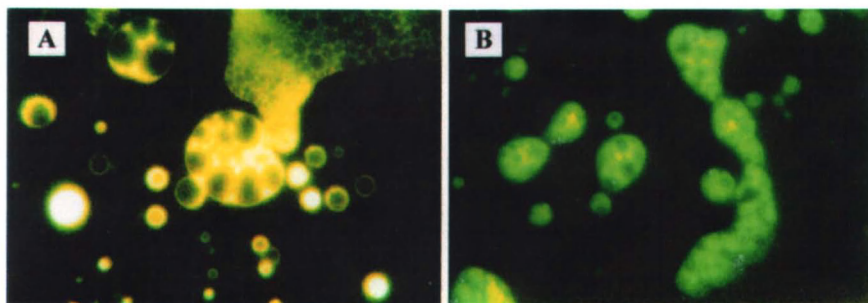


Plate 5.7. (A) Fluorescence micrograph of the water insoluble droplets formed from a Murchison meteorite extract (67) compared to (B) the fluorescent droplets produced from the photolysis residue of the interstellar/precometary ice analog: $H_2O:CH_3OH:NH_3:CO$ (100:50:1:1) at 10 K (40). The similarity between these vesicles is another indication of similarity between the laboratory ice residue and extraterrestrial organics in meteorites.

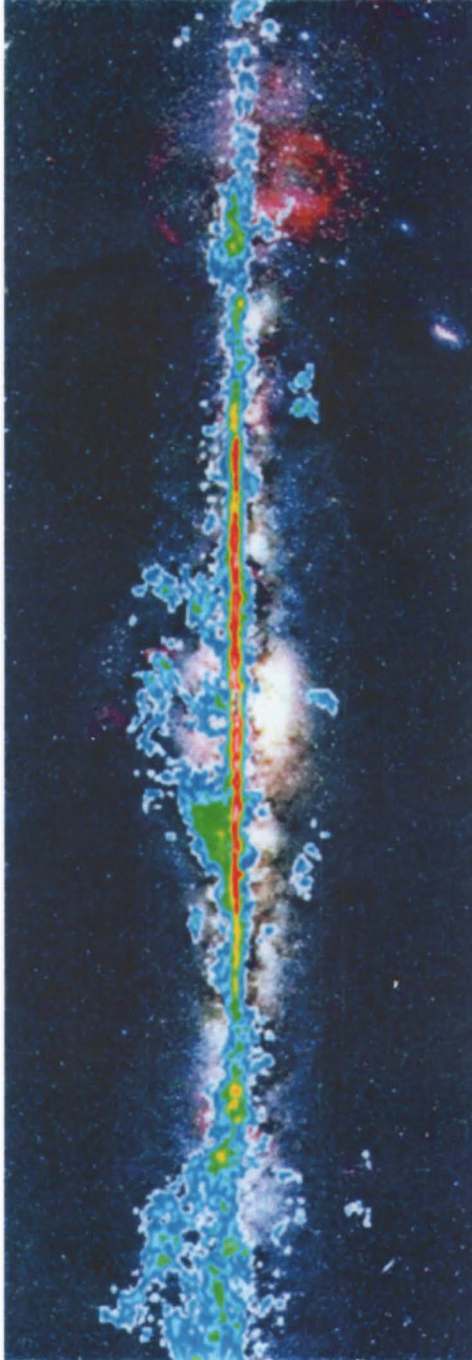


Plate 6.1. The distribution of molecular clouds in our Galaxy, as traced by emission of carbon monoxide at 115 GHz (CO: $J = 1 \rightarrow 0$ transition; colored contour; from Harvard CfA survey), superimposed over an optical image.



Plate 6.2. The circumstellar envelope of the evolved star CRL 2688, showing outflowing material (light blue: HST image) and resulting molecular shell (contours).

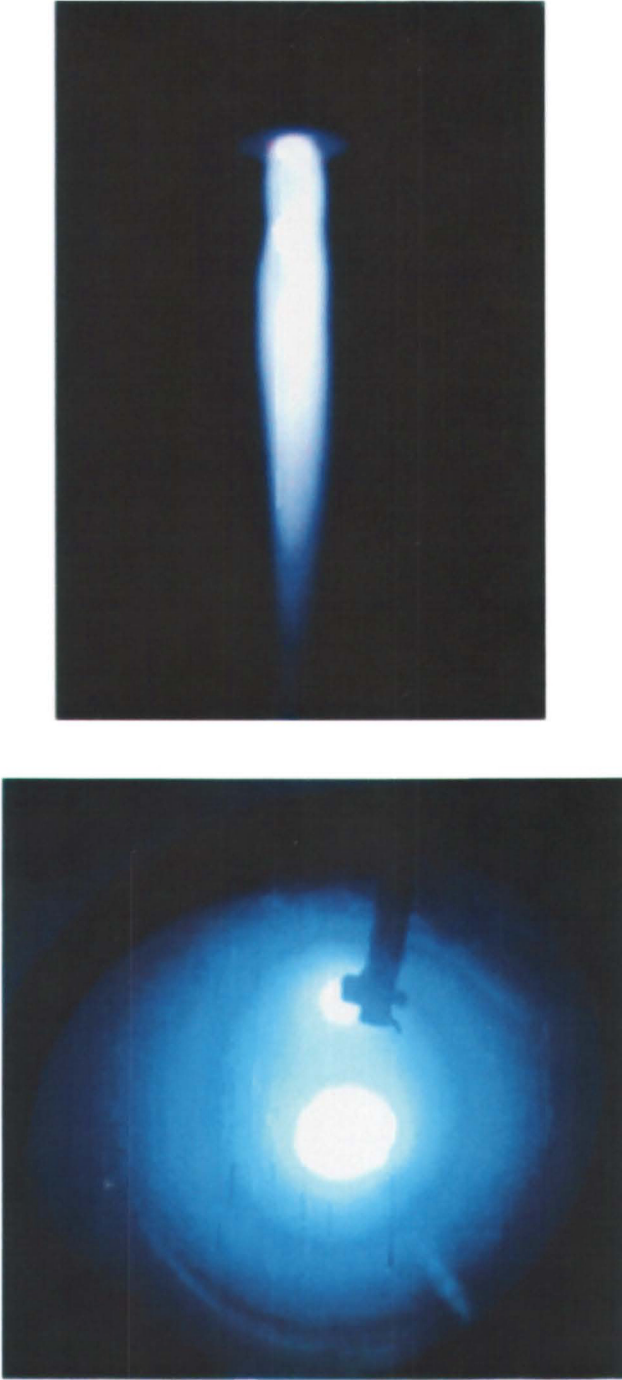


Plate 6.3. Molecular free radicals being created in DC discharges in a reactor flow oven (left) and a supersonic jet expansion (right).

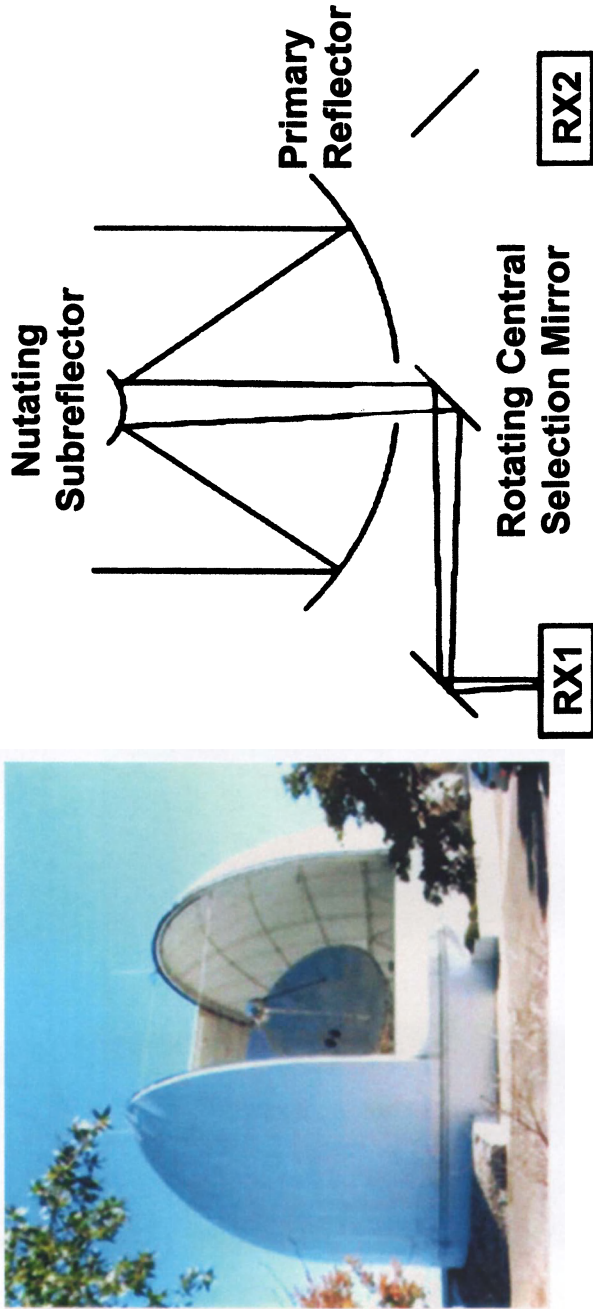


Plate 6.4. A millimeter radio telescope, the 12 m of the Arizona Radio Observatory (left), and its associated optics (right).

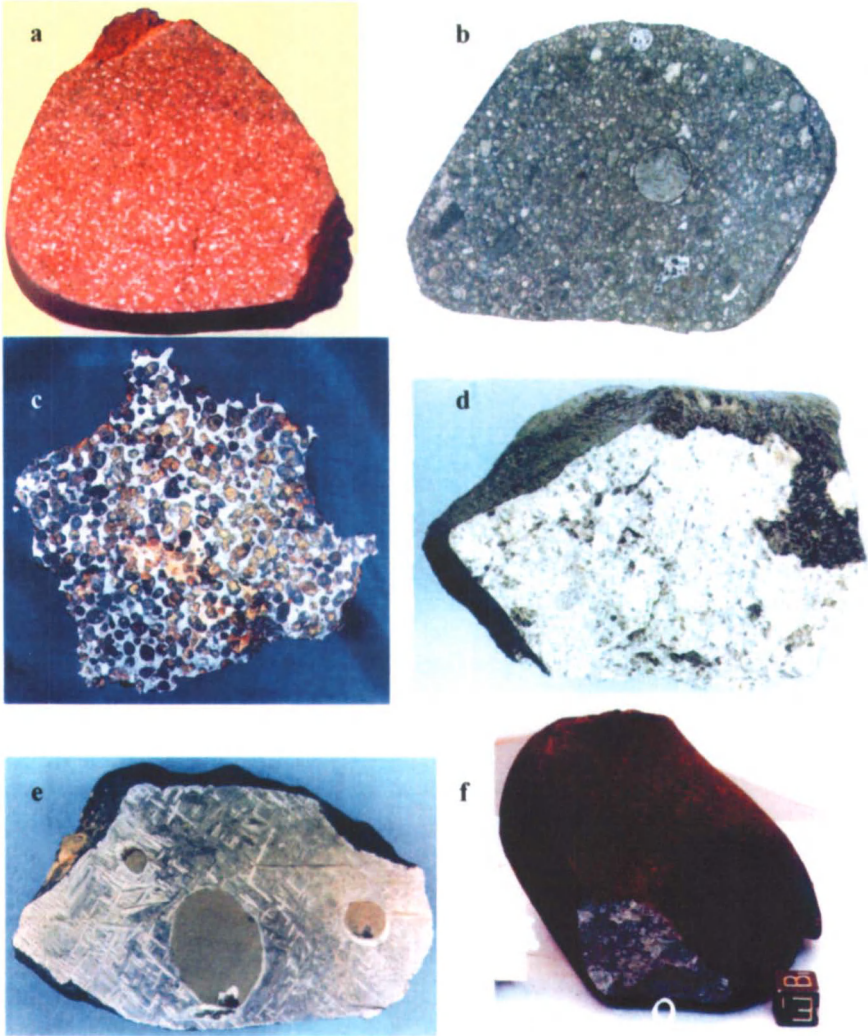


Plate 9.1. Common meteorite types (approximate longest dimensions):
a) Whitman, H5 (6 cm); b) Allende; C3V (8 cm) – note 1 cm chondrule in center, c) Springwater pallasite (18 cm); d) Sioux Co. eucrite (8 cm); e) Sanderson III B medium octahedrite (13 cm) – note large FeS inclusions; f) Noblesville H chondrite – note that the fusion crust is thin and smooth (as it is on most meteorites) and has an usual dark brown color on top which grades to black on the other exposed surfaces (contrast with the Lafayette fusion crust in Plate 2). The broken surface next to the 1-cm cube shows the interior of this gas-rich regolith breccia. (Reproduced with permission from reference 1. Copyright 2006 Elsevier.)

12 - Color inserts

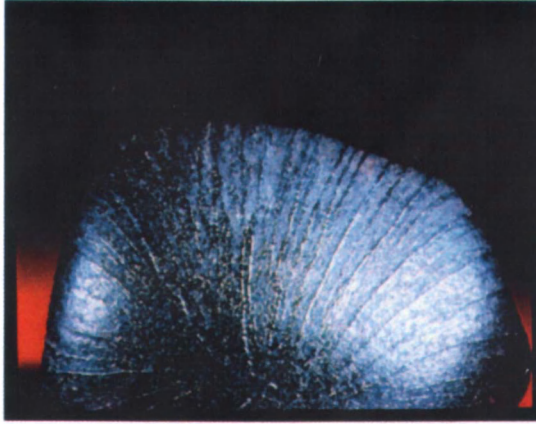


Plate 9.2. Fusion crust of Lafayette Martian meteorite. Lafayette exhibits very delicate, redeposited droplets on its sides, indicating an orientation with its front pointing Earthward late in its atmospheric traversal. (Reproduced with permission from reference 1. Copyright 2006 Elsevier.)

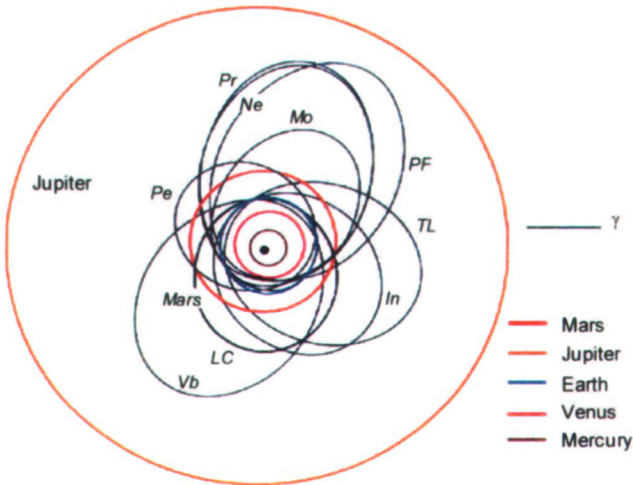


Plate 9.3. Orbits determined from overlapping camera coverage for nine recovered chondrite falls. Pr–Pribram (H5, 7 Apr. 1959); LC–Lost City (H5, 3 Jan. 1970); In–Innisfree (L5, 5 Feb. 1977); Pe–Peekskill (H6, 9 Oct. 1992); TL–Tagish Lake (C, 18 Jan. 2000); Mo–Moravka (H5-6, 6 May 2000); Ne–Neuschwanstein (EL6, 6 Apr. 2002); PF–Park Forest (L5, 26 Mar. 2003); Vb–Villalbeto de la Peña (L6, 4 Jan. 2004). The orbits shown are projections onto the ecliptic plane (orbits of the terrestrial planets and Jupiter in color are included with γ , the vernal equinox). Pribram and Neuschwanstein had identical orbits, but are of different chondritic types. (Reproduced with permission from reference 1. Copyright 2006 Elsevier.)

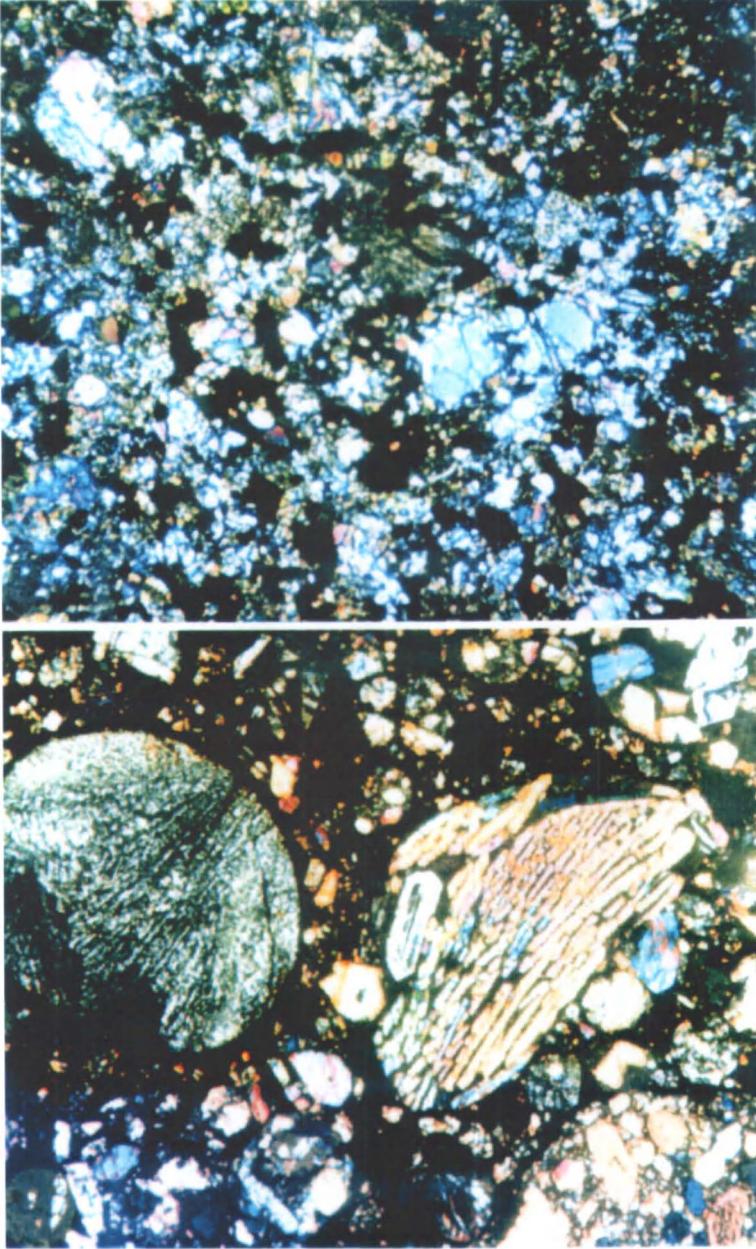


Plate 9.4. Petrographic (2.5 mm wide) thin sections in polarized transmitted light. Partial large chondrules are obvious in the H3 condrite Sharps (left) but barely recognizable in the H6 chondrite Kernouve (right). (Reproduced with permission from reference 1. Copyright 2006 Elsevier.)



Plate 14.1A. Stromatolites growing today on the floor of Shark Bay, Western Australia (Figure 1). The bulbous, top-heavy individual stromatolite in left foreground will eventually join the massive reef to the right by bridging laterally towards other individuals such as the smaller one in center foreground. Largest stromatolites are approximately 0.5 meter in height (underwater photo by author).

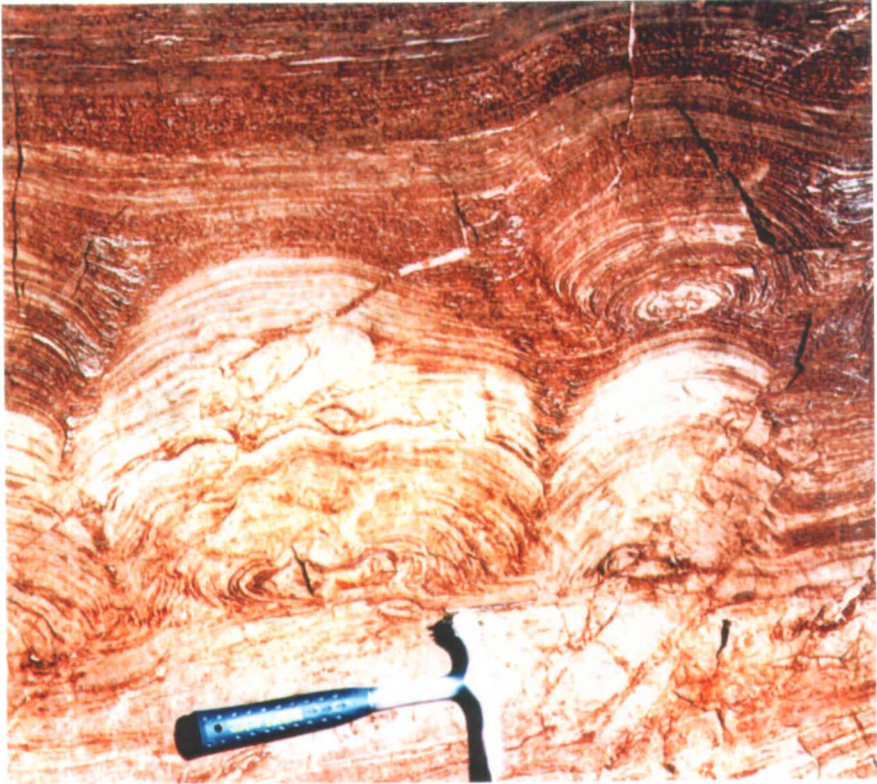


Plate 14.1B. Outcrop cross-section of 1.9 Ga stromatolites exposed in Duck Creek Gorge, Western Australia. Stromatolites nucleate as isolated individuals then grow upward and laterally, bridging to adjacent individuals to form massive reefs. Note new stromatolite growing on a substrate of old stromatolites in upper right. Cross-sections show same bulbous, top-heavy form seen at Shark Bay. Hammer handle 25 cm in length (photo by author).

16 - Color inserts



Plate 14.1C. Outcrop cross-section of 2.7 Ga stromatolites exposed near Redmont, Western Australia. See Plate 1B caption. Hammer handle 35 cm in length (photo by author).

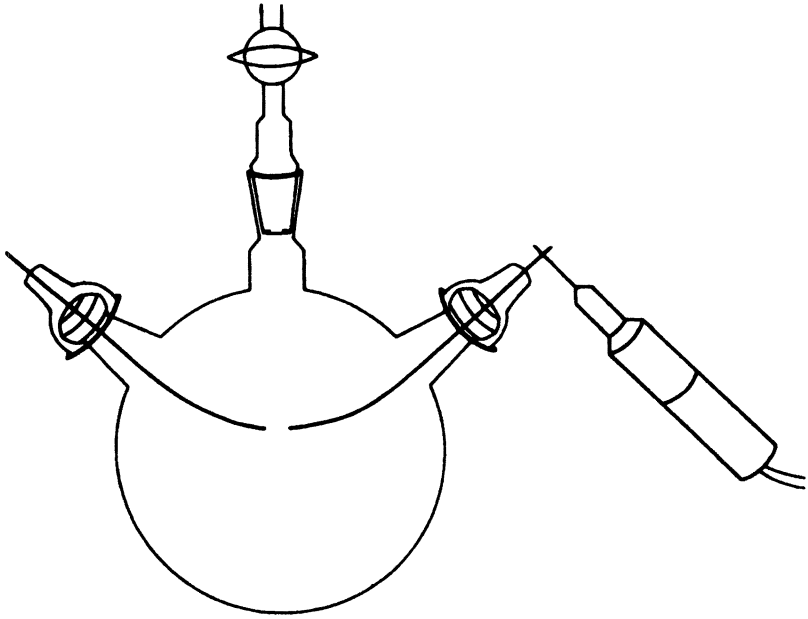


Plate 15.1. Spark discharge apparatus used in these experiments.



Plate 21.1. The Arizona Radio Observatory (ARO) 12m telescope on Kitt Peak, Arizona was used for the laboratories.



Plate 21.2. Astronomy graduate students Marc-André Besel and Wiphu Rujopakarn observing at the ARO 12m telescope. Telescope operation and data processing are all conducted via computer interface